Emerging Topics in Statistics and Biostatistics

Andriëtte Bekker
(Din) Ding-Geng Chen
Johannes T. Ferreira
Editors

Computational and Methodological Statistics and Biostatistics

Contemporary Essays in Advancement

Springer

Emerging Topics in Statistics and Biostatistics

More information about this series at http://www.springer.com/series/16213

Andriëtte Bekker • (Din) Ding-Geng Chen
Johannes T. Ferreira
Editors

Computational and Methodological Statistics and Biostatistics

Contemporary Essays in Advancement

Springer

Editors
Andriëtte Bekker
Department of Statistics
University of Pretoria
Pretoria, South Africa

Johannes T. Ferreira
Department of Statistics
University of Pretoria
Pretoria, South Africa

(Din) Ding-Geng Chen
Department of Statistics
University of Pretoria
Pretoria, South Africa

School of Social Work
and Department of Biostat
Chapel Hill, NC, USA

ISSN 2524-7735 ISSN 2524-7743 (electronic)
Emerging Topics in Statistics and Biostatistics
ISBN 978-3-030-42195-3 ISBN 978-3-030-42196-0 (eBook)
https://doi.org/10.1007/978-3-030-42196-0

To my Bekker family; for your conscious (and unconscious) eternal support throughout my entire life.

Andriëtte Bekker

To my parents and parents-in-law who value higher education, and to my wife, Ke, my son, John D. Chen, and my daughter, Jenny K. Chen, for their love and support.

(Din) Ding-Geng Chen

To my mother and late father, Annalize and Nico, for empowering me in mind and spirit through my past and still into my future.

Johannes T. Ferreira

Preface

In modern times, the field of statistics has sustained itself as the intersection of modelling and learning of data, in both theoretical and applied contexts. Continuous unification of these contexts remains meaningful and relevant to graduate students, academics, and practitioners, by fostering novel ways of developing and reaching insight into the phenomena of random behaviour. The context within which this insight is sought connects closely to modern buzzwords such as big data and machine learning—thereby highlighting the continuous and crucial role that statistics keep playing within learning and understanding data. In a more theoretical sense, postulating methodological frameworks by proposing and deriving shapes and distributions for data remains of certain value by ensuring continuous development and enhancement of theory-based probabilistic models that may serve the said phenomena of random behaviour mathematically. A more applied context calls these theoretical developments to action, with approaches many times requiring computationally challenging environments in which the modelling effort may be enriched with subsequent estimation and hypothesis testing.

Within this context, this contributed volume houses a collection of contemporary essays in statistical advancement on a variety of topics, all of which are rooted in this intersection of theoretical and applied research. The main objective is to unify fundamental methodological research in statistics together with computational aspects of the modern era. Three distinct realms of sustained statistical interest occupy this book: theory and application of statistical distributions, supervised and unsupervised learning, and biostatistics. This book is intended for readers who are interested in consuming contemporary advancements in these domains.

By reflecting on the above, this volume's three main parts provide advancements in their respective fields, with dedicated contributions paving the way for future research and innovation within statistics. The overarching goals of this book include:

1. emphasising cutting-edge research within both theoretical and applied statistics and motivating the value of both;
2. highlighting computational challenges and solutions within these spheres;

3. further stimulating the research within the respective focus area of our discipline of statistics; and finally,
4. continuously unifying these spheres as part of the larger statistical field of both an academic and practical nature.

The editing team has endeavoured to provide a balanced and stimulating contributed book that will appeal to the diverse interests of most readers from a fundamental theoretical as well as applied statistical background. We believe that the topics covered in the book are timely and have high potential to impact and influence in statistics in the three spheres of interest here.

Outline of this Book Volume

This book volume brings together 23 chapters that are organised as follows: Recent Developments in Theory and Applications of Statistical Distributions (*Part I*), Recent Developments in Supervised and Unsupervised Modelling (*Part II*), and Recent Developments in Biostatistics (*Part III*). All the chapter contributions have undergone a thorough and independent review process.

Part I of this book includes nine papers focusing on modern developments in the theory and applications of statistical distribution theory. In Chap. 1, the authors discuss computational aspects of maximum likelihood estimation within a skew distribution paradigm. Ley and Simone provide geostatistical models for modelling earthquake behaviour in Chap. 2. Chapter 3 contains theoretical contributions in a multivariate setting relating to order statistics. In Chap. 4, the authors address variable selection in a regression context based on information theoretic measures Chapter 5 provides a departure from the usual normality assumption in modelling condition numbers of Wishart matrices with applications within a multiple-input multiple-output environment. Geldenhuys and Ehlers provide refreshing contributions within bivariate Polya–Aeppli modelling in Chap. 6. In Chap. 7, Arashi et al. describe and apply a multivariate construction technique with a Dirichlet flavour. Chapter 8 sees a contribution of normal mean–variance mixture using Birnbaum–Saunders distribution and evaluation of risk measures by Naderi et al. Finally, in Part I, Chap. 9 contains new suggestions for modelling of linear combinations of chi-square random variables by Coelho.

Part II comprises seven chapters that highlight contemporary developments in supervised and unsupervised modelling. In Chap. 10, Banerjee discusses conjugate Bayesian approaches within a geostatistical setting for massive data sets. Roozbeh et al. provide an approach for modelling high-dimensional data using improved yet robust estimators in Chap. 11. Chan et al. investigate optimal allocation subject to time censoring in a regression sense in Chap. 12, and Stein et al. explore a copula approach to spatial interpolation of extreme value modelling in Chap. 13. Chapter 14 discusses a scale mixture approach to t-distributed mixture regression, and Samawi writes on improving logistic regression performance by way of extreme ranking in

Chap. 15. Finally, Ge et al. provide insight into the application of spatial statistics in a policy framework for China in Chap. 16.

Part III includes seven chapters that focus on recent contributions within the realm of biostatistics. Chapter 17 includes a thorough and meaningful contribution within novel Bayesian adaptive designs in cancer clinical trials. In Chap. 18, the authors utilise topological data analysis in a computational and statistical sense in a real data application. Chapter 19 provides refreshing contributions within simultaneous variable selection and estimation of longitudinal data, and Chap. 20 also contains contributions of variable selection but within an interval-censored failure time data framework. Manda discusses the modelling of frailty effects in clustered survival data in Chap. 21. Arreola and Wilson apply partitioned GMM models to survey data in Chap. 22, and the book concludes with a contribution from Chen and Lio about a generalised Rayleigh–Exponential–Weibull distribution and its application within interval-censored data in Chap. 23.

Pretoria, South Africa — Andriëtte Bekker
Chapel Hill, NC, USA — (Din) Ding-Geng Chen
Pretoria, South Africa — Johannes T. Ferreira

Acknowledgements

We are deeply grateful to those who have supported in the process of creating this book. We thank the contributors to this book for their enthusiastic involvement and their kindness in sharing their professional knowledge and expertise. We thank all the reviewers for providing thoughtful and in-depth evaluations of the papers contained in this book. We gratefully acknowledge the professional support of Laura Briskman, Saveetha Balasundaram, and Santhamurthy Ramamoorthy from Springer who made the publication of this book a reality.

This volume was made possible through funding provided by the following agencies:

1. NRF-SARChI Research Chair in Computational and Methodological Statistics, UID: 71199;
2. DST-NRF-SAMRC-SARChI Research Chair in Biostatistics, Grant number: 114613;
3. Centre of Excellence in Mathematics and Statistical Science, University of the Witwatersrand, South Africa, ref. nrs. STA19/002 and STA19/003;
4. University Capacity Development Grant, South Africa, ref. nr. UCDP-324;
5. Knowledge, Interchange and Collaboration Grant, National Research Foundation, South Africa, ref. nr. KIC180913358471; and
6. National Research Foundation grant ref. nr. SRUG190308422768 Grant No: 120839

Opinions expressed and conclusions arrived at are those of the author(s) and are not necessarily to be attributed to the NRF.

We welcome readers' comments, including notes on typos or other errors, and look forward to receiving suggestions for improvements to future editions. Please send comments and suggestions to any of the editors.

List of Reviewers

Anis Iranmanesh
Departmen of Statistics, Faculty of Sciences, Islamic Azad University, Mashhad, Iran
Filipe Marques
Departamento de Matemática, Faculdade de Ciências e Tecnologia, Universidade Nova de Lisboa, Lisbon, Portugal
Daniel de Waal
Department of Statistics, Faculty of Natural and Agricultural Sciences, University of Pretoria, Pretoria, South Africa
Mohammad Arashi
Department of Statistics, Faculty of Mathematical Sciences, Shahrood University of Technology, Shahrood, Iran
Mahdi Salehi
Department of Mathematics and Statistics, University of Neyshabur, Neyshabur, Iran
Broderick Oluyede
Department of Statistics, Georgia Southern University, Statesboro, GA, USA
Chien-Tai Lin
Department of Mathematics, Tamkang University, Taipei City, Taiwan
Mahdi Roozbeh
Faculty of Mathematics, Statistics and Computer Sciences, Semnan University, Semnan, Iran
Hossein Baghishani
Department of Statistics, Shahrood University of Technology, Shahrud, Iran
Qingning Zhou
Department of Mathematics and Statistics, University of North Carolina at Charlotte, Charlotte, NC, USA
Peter Bubenik
Department of Mathematics, University of Florida, Gainesville, FL, USA
Freedom Gumedze
Department of Statistics Sciences, University of Cape Town, Cape Town, South Africa
Naushad Ali Mamode Khan
Department of Mathematics, University of Mauritius, Moka, Mauritius
Hassan Doosti
Department of Mathematics and Statistics, Macquarie University, Macquarie Park, NSW, Australia
Tzong-Ru Tsai
College of Business and Management, Tamkang University, Taipei City, Taiwan
Divan Burger
Department of Statistics, Faculty of Natural and Agricultural Sciences, University of Pretoria, Pretoria, South Africa

Hyoung-Moon Kim
College of Commerce and Economics, Konkuk University, Seoul, South Korea
Jan Beirlant
Department of Mathematics (Statistics and Risk Section), Katholieke Universiteit, Leuven, Belgium
Mei-Po Kwan
Department of Geography and Geographic Information Science, University of Illinois at Urbana-Champaign, Champaign, IL, USA
Roy Cerqueti
University of Macerata, Department of Economics and Law, Macerata, Italy
Bernard Omolo
Division of Mathematics and Computer Science, University of South Carolina, Spartanburg, SC, USA
Robert Schall
Department of Mathematical Statistics and Actuarial Science, Bloemfontein, Republic of South Africa
Tsung-I Lin
Department of Applied Mathematics and Institute of Statistics, National Chung Hsing University, Taichung, Taiwan
Elham Mirfarah
Department of Statistics, Faculty of Natural and Agricultural Sciences, University of Pretoria, Pretoria, South Africa
Mehrdad Naderi
Department of Statistics, Faculty of Natural and Agricultural Sciences, University of Pretoria, Pretoria, South Africa

Contents

Editors and Contributors

About the Editors

Professor Andriëtte Bekker is a Professor and the current Head of the Department of Statistics at the Faculty of Natural and Agricultural Sciences, at the University of Pretoria and has been serving in this capacity since 2012. Her expertise lies in Statistical Distribution Theory and comprises the study, development, and expansion of distributions and the addressing of parametric statistical inferential aspects, within the classical as well as the Bayesian framework. She is the academic research leader of the Statistical Theory and Applied Statistics focus area within the Department of Science and Technology/National Research Foundation (DST-NRF), Centre of Excellence in Mathematical and Statistical Sciences. She is also an elected member of the International Statistical Institute and serves on several national and international, educational and academic research boards. She has published more than 80 peer-reviewed papers in fundamental statistical research. She contributes significantly to the human capacity development of Southern Africa through the multitude of students for whom she acts as supervisor and mentor.

Professor (Din) Ding-Geng Chen is a fellow of the American Statistical Association and currently the Wallace H. Kuralt Distinguished Professor at the University of North Carolina at Chapel Hill, USA, and an Extraordinary Professor at University of Pretoria, South Africa. He was a Professor at the University of Rochester and the Karl E. Peace endowed eminent scholar chair in biostatistics at Georgia Southern University. He is also a senior consultant for biopharmaceuticals and government agencies with extensive expertise in clinical trial biostatistics and public health statistics. He has written more than 150 refereed publications and co-authored/co-edited 25 books on clinical trial methodology, meta-analysis, causal inference, and public health statistics.

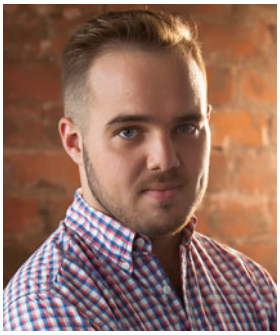

Doctor Johannes T. Ferreira is currently a Senior Lecturer in the Department of Statistics at the University of Pretoria, South Africa, and is a Junior Focus Area Coordinator for the Statistical Theory and Applied Statistics focus area of the Centre of Excellence in Mathematical and Statistical Sciences based at the University of the Witwatersrand in Johannesburg. He regularly publishes in accredited peer-reviewed journals and reviews manuscripts for international journals. He is an ASLP 4.1/4.2 fellow of Future Africa and has been identified as one of the Top 200 South Africans under the age of 35 by the Mail & Guardian newspaper in the Education category in 2016. His ramblings can be found on Twitter with the handle @statisafrican.

Contributors

Fakhereh Alidoost Netherlands E-Science Centre, Amsterdam, The Netherlands

Mohammad Arashi Department of Statistics, Faculty of Mathematical Sciences, Shahrood University of Technology, Shahrood, Iran

Elsa Vazquez Arreola Arizona State University, Tempe, AZ, USA

Olcay Arslan Faculty of Science, Department of Statistics, Ankara University, Ankara, Turkey

Adelchi Azzalini Department of Statistical Sciences, University of Padua, Padua, Italy

Sudipto Banerjee UCLA Department of Biostatistics, University of California, Los Angeles, CA, USA

Andriëtte Bekker Department of Statistics, University of Pretoria, Pretoria, South Africa

Hamparsum Bozdogan The University of Tennessee, Knoxville, TN, USA

Ping Shing Chan Department of Statistics, The Chinese University of Hong Kong, Shatin, N.T., Hong Kong SAR

(Din) Ding-Geng Chen Department of Statistics, University of Pretoria, Pretoria, South Africa

Carlos A. Coelho Mathematics Department (DM) and Centro de Matemática e Aplicações (CMA), Faculdade de Ciências e Tecnologia, NOVA University of Lisbon, Caparica, Portugal

Daniel de Waal Department of Statistics, University of Pretoria, Pretoria, South Africa

René Ehlers Department of Statistics, University of Pretoria, Pretoria, South Africa

Johannes T. Ferreira Department of Statistics, University of Pretoria, Pretoria, South Africa

Wei Gao School of Mathematics and Statistics, Northeast Normal University, Changchun, Jilin, China

Claire Geldenhuys Department of Statistics, University of Pretoria, Pretoria, South Africa

Yong Ge State Key Laboratory of Resources and Environmental Information System, Institute of Geographical Sciences and Natural Resources Research, Chinese Academy of Sciences, Beijing, China

Yeşim Güney Faculty of Science, Department of Statistics, Ankara University, Ankara, Turkey

Nor Aishah Hamzah UM Centre for Data Analytics, Institute of Mathematical Sciences, Faculty of Science, University of Malaya, Kuala Lumpur, Malaysia

Giseon Heo School of Dentistry, Department of Mathematical and Statistical Sciences, University of Alberta, Edmonton, AB, Canada

Shan Hu State Key Laboratory of Resources and Environmental Information System, Institute of Geographical Sciences and Natural Resources Research, Chinese Academy of Sciences, Beijing, China

Ahad Jamalizadeh Department of Statistics, Shahid Bahonar University, Kerman, Iran

Frans Kanfer Department of Statistics, University of Pretoria, Pretoria, South Africa

Peter T. Kim Department of Mathematics & Statistics, University of Guelph, Guelph, ON, Canada

Christine H. Lee Clinical Professor at Department of Pathology and Laboratory Medicine, University of British Columbia, Vancouver, BC, Canada
Department of Microbiology, Royal Jubilee Hospital, Victoria, BC, Canada

J. Jack Lee Department of Biostatistics, The University of Texas MD Anderson Cancer Center, Houston, TX, USA

Christophe Ley Department of Applied Mathematics, Computer Science and Statistics, Ghent University, Ghent, Belgium

Ruitao Lin Department of Biostatistics, The University of Texas MD Anderson Cancer Center, Houston, TX, USA

Tsung-I Lin Institute of Statistics, National Chung Hsing University, Taichung, Taiwan
Department of Public Health, China Medical University, Taichung, Taiwan

Yuhlong Lio Department of Mathematical Sciences, University of South Dakota, Vermilion, SD, USA

Mengxiao Liu State Key Laboratory of Resources and Environmental Information System, Institute of Geographical Sciences and Natural Resources Research, Chinese Academy of Sciences, Beijing, China

Seite Makgai Department of Statistics, University of Pretoria, Pretoria, South Africa

Samuel Manda Biostatistics Research Unit, South African Medical Research Council, Pretoria, South Africa
Department of Statistics, University of Pretoria, Pretoria, South Africa
School of Mathematics, Statistics, and Computer Science, University of KwaZulu-Natal, Pietermaritzburg, South Africa

Sollie Millard Department of Statistics, University of Pretoria, Pretoria, South Africa

Nur Anisah Mohamed UM Centre for Data Analytics, Institute of Mathematical Sciences, Faculty of Science, University of Malaya, Kuala Lumpur, Malaysia

Mehrdad Naderi Department of Statistics, Faculty of Natural & Agricultural Sciences, University of Pretoria, Pretoria, South Africa

Hon Keung Tony Ng Department of Statistical Science, Southern Methodist University, Dallas, TX, USA

Pavel Petrov Data Scientist at Rocky Mountaineer, Vancouver, BC, Canada

Shaun Pinder Methodologist at Statistics Canada, Ottawa, ON, Canada

Mahdi Roozbeh Department of Statistics, Faculty of Mathematics, Statistics and Computer Sciences, Semnan University, Semnan, Iran

Roohollah Roozegar Department of Mathematics, College of Sciences, Yasouj University, Yasouj, Iran

Narayanaswamy Balakrishnan McMaster University, Hamilton, ON, Canada

Stephen T. Rush Senior Statistician at AstraZeneca, Mölndal, Sweden

Mahdi Salehi Department of Mathematics and Statistics, University of Neyshabur, Neyshabur, Iran

Hani M. Samawi Department of Biostatistics, Epidemiology and Environmental Health Sciences, Jiann-Ping Hsu College of Public Health, Georgia Southern University, Statesboro, GA, USA

Rosaria Simone Department of Political Sciences, Università degli Studi di Napoli Federico II, Naples, Italy

Hon Yiu So Department of Statistics and Actuarial Science, University of Waterloo, Waterloo, ON, Canada

Alfred Stein Faculty of Geo-Information Science and Earth Observation (ITC), University of Twente, Enschede, The Netherlands

Jianguo Sun Department of Statistics, University of Missouri, Columbia, MO, USA

Mozghan Taavoni Department of Statistics, Faculty of Mathematical Sciences, Shahrood University of Technology, Shahrood, Iran

Vera van Zoest Department of Information Technology, Uppsala University, Uppsala, Sweden

Wan-Lun Wang Department of Statistics, Graduate Institute of Statistics and Actuarial Science, Feng Chia University, Taichung, Taiwan

Jeffrey R. Wilson Arizona State University, Tempe, AZ, USA

Qiwei Wu Department of Statistics, University of Missouri, Columbia, MO, USA

Hui Zhao School of Mathematics and Statistics & Hubei Key Laboratory of Mathematical Sciences, Central China Normal University, Wuhan, People's Republic of China

Part I
Recent Developments in Theory and Applications of Statistical Distributions

Some Computational Aspects of Maximum Likelihood Estimation of the Skew-*t* Distribution

Adelchi Azzalini and Mahdi Salehi

Abstract Since its introduction, the skew-*t* distribution has received much attention in the literature both for the study of theoretical properties and as a model for data fitting in empirical work. A major motivation for this interest is the high degree of flexibility of the distribution as the parameters span their admissible range, with ample variation of the associated measures of skewness and kurtosis. While this high flexibility allows to adapt a member of the parametric family to a wide range of data patterns, it also implies that parameter estimation is a more delicate operation with respect to less flexible parametric families, given that a small variation of the parameters can have a substantial effect on the selected distribution. In this context, the aim of the present contribution is to deal with some computational aspects of maximum likelihood estimation. A problem of interest is the possible presence of multiple local maxima of the log-likelihood function. Another one, to which most of our attention is dedicated, is the development of a quick and reliable initialization method for the subsequent numerical maximization of the log-likelihood function, both in the univariate and the multivariate context.

1 Background and Aims

1.1 Flexible Distributions: The Skew-t Case

In the context of distribution theory, a central theme is the study of flexible parametric families of probability distributions, that is, families allowing substantial variation of their behaviour when the parameters span their admissible range.

A. Azzalini (✉)
Department of Statistical Sciences, University of Padua, Padua, Italy
e-mail: azzalini@stat.unipd.it

M. Salehi
Department of Mathematics and Statistics, University of Neyshabur, Neyshabur, Iran
e-mail: salehi2sms@gmail.com

A. Bekker et al. (eds.), *Computational and Methodological Statistics and Biostatistics*, Emerging Topics in Statistics and Biostatistics,
https://doi.org/10.1007/978-3-030-42196-0_1

For brevity, we shall refer to this domain with the phrase 'flexible distributions'. The archetypal construction of this logic is represented by the Pearson system of curves for univariate continuous variables. In this formulation, the density function is regulated by four parameters, allowing wide variation of the measures of skewness and kurtosis, hence providing much more flexibility than in the basic case represented by the normal distribution, where only location and scale can be adjusted.

Since Pearson times, flexible distributions have remained a persistent theme of interest in the literature, with a particularly intense activity in recent years. A prominent feature of newer developments is the increased consideration for multivariate distributions, reflecting the current availability in applied work of larger datasets, both in sample size and in dimensionality. In the multivariate setting, the various formulations often feature four blocks of parameters to regulate location, scale, skewness and kurtosis.

While providing powerful tools for data fitting, flexible distributions also pose some challenges when we enter the concrete estimation stage. We shall be working with maximum likelihood estimation (MLE) or variants of it, but qualitatively similar issues exist for other criteria. Explicit expressions of the estimates are out of the question; some numerical optimization procedure is always involved and this process is not so trivial because of the larger number of parameters involved, as compared with fitting simpler parametric models, such as a Gamma or a Beta distribution. Furthermore, in some circumstances, the very flexibility of these parametric families can lead to difficulties: if the data pattern does not aim steadily towards a certain point of the parameter space, there could be two or more such points which constitute comparably valid candidates in terms of log-likelihood or some other estimation criterion. Clearly, these problems are more challenging with small sample size, later denoted n, since the log-likelihood function (possibly tuned by a prior distribution) is relatively more flat, but numerical experience has shown that they can persist even for fairly large n, in certain cases.

The focus of interest in this paper will be the skew-t (ST) distribution introduced by Branco and Dey (2001) and studied in detail by Azzalini and Capitanio (2003); see also Gupta (2003). The main formal constituents and properties of the ST family will be summarized in the next subsection. Here, we recall instead some of the many publications that have provided evidence of the practical usefulness of the ST family, in its univariate and multivariate version, thanks to its capability to adapt to a variety of data patterns. The numerical exploration by Azzalini and Genton (2008), using data of various origins and nature, is an early study in this direction, emphasizing the potential of the distribution as a tool for robust inference. The robustness aspects of ST-based inference has also been discussed by Azzalini and Capitanio (2014, § 4.3.5) and more extensively by Azzalini (2016). On the more applied domain, numerous publications motivated by application problems have further highlighted the ST usefulness, typically with data distributions featuring substantial tailweight and asymmetry. For space reasons, the following list reports only a few of the many publications of this sort, with a preference for early work: Walls (2005) and Pitt (2010) use the ST distribution for modelling log-transformed

returns of film and music industry products as a function of explanatory variables; Meucci (2006) and Adcock (2010) develop methods for optimal portfolio allocation in a financial context, where long tails and asymmetry of returns distribution are standard features; Ghizzoni et al. (2010) use the multivariate ST distributions to model riverflow, jointly at multiple sites; Pyne et al. (2009) present an early model-based clustering formulation using the multivariate ST distributions as the basic component for flow cytometric data analysis.

Given its value in data analysis, but also the above-mentioned possible critical aspects of the log-likelihood function, it seems appropriate to explore the corresponding issues for MLE computation and to develop a methodology which provides good starting points for the numerical maximization of the log-likelihood. After a brief summary of the main facts about the ST distribution in the next subsection, the rest of the paper is dedicated to these issues. Specifically, one section examines qualitatively and numerically various aspects of the ST log-likelihood, while the rest of the paper develops a technique to initialize the numerical search for MLE.

To avoid potential misunderstanding, we underline that the above-indicated program of work does not intend to imply a general inadequacy of the currently available computational resources, which will be recalled in due course. There are, however, critical cases where these resources run into problems, most typically when the data distribution exhibits very long tails. For these challenging situations, an improved methodology is called for.

1.2 The Skew-t Distribution: Basic Facts

Before entering our actual development, we recall some basic facts about the ST parametric family of continuous distributions. In its simplest description, it is obtained as a perturbation of the classical Student's t distribution. For a more specific description, start from the univariate setting, where the components of the family are identified by four parameters. Of these four parameters, the one denoted ξ in the following regulates the location of the distribution; scale is regulated by the positive parameter ω; shape (representing departure from symmetry) is regulated by λ; tail-weight is regulated by ν (with $\nu > 0$), denoted 'degrees of freedom' like for a classical t distribution.

It is convenient to introduce the distribution in the 'standard case', that is, with location $\xi = 0$ and scale $\omega = 1$. In this case, the density function is

$$t(z; \lambda, \nu) = 2\, t(z; \nu)\, T\left(\lambda z \sqrt{\frac{\nu + 1}{\nu + z^2}}; \nu + 1\right), \qquad z \in \mathbb{R}, \tag{1}$$

where

$$t(z;\nu) = \frac{\Gamma\left(\frac{1}{2}(\nu+1)\right)}{\sqrt{\pi\,\nu}\,\Gamma\left(\frac{1}{2}\nu\right)}\left(1+\frac{z^2}{\nu}\right)^{-(\nu+1)/2}, \qquad z \in \mathbb{R}, \tag{2}$$

is the density function of the classical Student's t on ν degrees of freedom and $T(\cdot;\nu)$ denotes its distribution function; note however that in (1) this is evaluated with $\nu+1$ degrees of freedom. Also, note that the symbol t is used for both densities in (1) and (2), which are distinguished by the presence of either one or two parameters.

If Z is a random variable with density function (1), the location and scale transform $Y = \xi + \omega Z$ has density function

$$t_Y(x;\theta) = \omega^{-1}\, t(z;\lambda,\nu), \qquad z = \omega^{-1}(x-\xi), \tag{3}$$

where $\theta = (\xi, \omega, \lambda, \nu)$. In this case, we write $Y \sim \mathrm{ST}(\xi, \omega^2, \lambda, \nu)$, where ω is squared for similarity with the usual notation for normal distributions.

When $\lambda = 0$, we recover the scale-and-location family generated by the t distribution (2). When $\nu \to \infty$, we obtain the skew-normal (SN) distribution with parameters (ξ, ω, λ), which is described for instance by Azzalini and Capitanio (2014, Chap. 2). When $\lambda = 0$ and $\nu \to \infty$, (3) converges to the $\mathrm{N}(\xi, \omega^2)$ distribution.

Some instances of density (1) are displayed in the left panel of Fig. 1. If λ was replaced by $-\lambda$, the densities would be reflected on the opposite side of the vertical axis, since $-Y \sim \mathrm{ST}(-\xi, \omega^2, -\lambda, \nu)$.

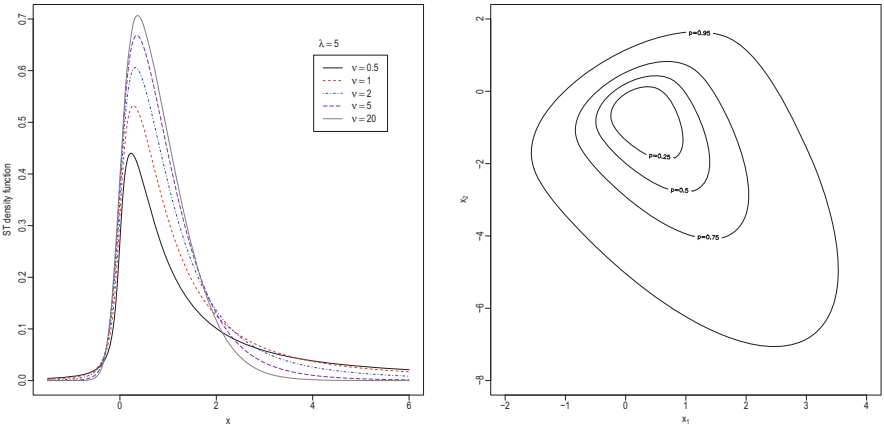

Fig. 1 The left plot displays a set of univariate skew-t density functions when $\lambda = 5$ and ν varying across a range of values; the right plot displays the contour level plot of a bivariate skew-t density

Similarly to the classical t distribution, moments exist when their order is smaller than ν. Under this condition, expressions for the mean value, the variance and the coefficients of skewness and excess kurtosis, namely the standardized third and fourth cumulants, are as follows:

$$\begin{aligned}
\mu &= \mathbb{E}\{Y\} = \xi + \omega\, b_\nu\, \delta, && \text{if } \nu > 1,\\
\sigma^2 &= \mathrm{var}\{Y\} = \omega^2 \left[\frac{\nu}{\nu-2} - (b_\nu\,\delta)^2\right] = \omega^2\sigma_z^2\,, \text{ say}, && \text{if } \nu > 2,\\
\gamma_1 &= \frac{b_\nu\,\delta}{\sigma_z^3}\,\left[\frac{\nu(3-\delta^2)}{\nu-3} - \frac{3\,\nu}{\nu-2} + 2\,(b_\nu\,\delta)^2\right], && \text{if } \nu > 3,\\
\gamma_2 &= \frac{1}{\sigma_z^4}\left[\frac{3\nu^2}{(\nu-2)(\nu-4)} - \frac{4(b_\nu\,\delta)^2\nu(3-\delta^2)}{\nu-3} + \frac{6(b_\nu\,\delta)^2\nu}{\nu-2} - 3(b_\nu\,\delta)^4\right] - 3 \\
& && \text{if } \nu > 4,
\end{aligned}$$

where

$$\delta = \delta(\lambda) = \frac{\lambda}{(1+\lambda^2)^{1/2}} \in (-1,1), \qquad b_\nu = \frac{\sqrt{\nu}\,\Gamma\left(\frac{1}{2}(\nu-1)\right)}{\sqrt{\pi}\,\Gamma\left(\frac{1}{2}\nu\right)} \quad \text{if } \nu > 1. \tag{4}$$

It is visible that, as λ spans the real line, so does the coefficient of skewness γ_1 when $\nu \to 3$ from above. For $\nu \le 3$, γ_1 does not exist; however, at least one of the tails is increasingly heavier as $\nu \to 0$, given the connection with the Student's t. A fairly similar pattern holds for the coefficients of kurtosis γ_2, with the threshold at $\nu = 4$ for its existence. If $\nu \to 4^+$, the range of γ_2 is $[0, \infty)$. The feasible (γ_1, γ_2) space when $\nu > 4$ is displayed in Figure 4.5 of Azzalini and Capitanio (2014). Negative γ_2 values are not achievable, but this does not seem to be a major drawback in most applications.

The multivariate ST density is represented by a perturbation of the classical multivariate t density in d dimensions, namely

$$t_d(z;\bar\Omega,\nu) = \frac{\Gamma((\nu+d)/2)}{(\nu\pi)^{d/2}\,\Gamma(\nu/2)\,\det(\bar\Omega)^{1/2}}\left(1+\frac{Q(z)}{\nu}\right)^{-\frac{\nu+d}{2}}, \quad z \in \mathbb{R}^d\,. \tag{5}$$

where $\bar\Omega$ is a symmetric positive-definite matrix with unit diagonal elements and $Q(z) = z^\top \bar\Omega^{-1} z$. The multivariate version of (1) is then given by

$$t_d(x) = 2\,t_d(z;\bar\Omega,\nu)\;T\left(\alpha^\top z\sqrt{\frac{\nu+d}{\nu+Q(z)}};\,\nu+d\right), \qquad z \in \mathbb{R}^d \tag{6}$$

where α is a d-dimensional vector regulating asymmetry. An instance of density (6) with $d = 2$ is displayed in the right panel of Fig. 1 via contour level curves.

Similarly to the univariate setting, we consider the location and scale transformation of a variable Z with density (6) to $Y = \xi + \omega Z$ where now $\xi \in \mathbb{R}^d$ and ω is a diagonal matrix with positive diagonal elements. For the resulting variable, we use the notation $Y \sim \mathrm{ST}_d(\xi, \Omega, \alpha, \nu)$ where $\Omega = \omega\bar{\Omega}\omega$.

One property required for our later development is that each marginal component of Y is a univariate ST variable, having a density of type (1) whose parameters are extracted from the corresponding components of Y, with the exception of λ for which the marginalization step is slightly more elaborate.

There are many additional properties of the ST distribution which, for space reasons, we do not report here and refer the reader to the quoted literature. A self-contained account is provided by the monograph (Azzalini and Capitanio 2014); see specifically Chapter 4 for the univariate case and Chapter 6 for the multivariate case.

2 On the Likelihood Function of ST Models

2.1 Basic General Aspects

The high flexibility of the ST distribution makes it particularly appealing in a wide range of data fitting problems, more than its companion, the SN distribution. Reliable techniques for implementing connected MLE or other estimation methods are therefore crucial.

From the inference viewpoint, another advantage of the ST over the related SN distribution is the lack of a stationary point at $\lambda = 0$ (or $\alpha = 0$ in the multivariate case), and the implied singularity of the information matrix. This stationary point of the SN is systematic: it occurs for all samples, no matter what n is. This peculiar aspect has been emphasized more than necessary in the literature, considering that it pertains to a single although important value of the parameter. Anyway, no such problem exists under the ST assumption. The lack of a stationary point at the origin was first observed empirically and welcomed as 'a pleasant surprise' by Azzalini and Capitanio (2003), but no theoretical explanation was given. Additional numerical evidence in this direction has been provided by Azzalini and Genton (2008). The theoretical explanation of why the SN and the ST likelihood functions behave differently was finally established by Hallin and Ley (2012).

Another peculiar aspect of the SN likelihood function is the possibility that the maximum of the likelihood function occurs at $\lambda = \pm\infty$, or at $\|\alpha\| \to \infty$ in the multivariate case. Note that this happens without divergence of the likelihood function, but only with divergence of the parameter achieving the maximum. In this respect the SN and the ST model are similar: both of them can lead to this pattern.

Differently from the stationarity point at the origin, the phenomenon of divergent estimates is transient: it occurs mostly with small n, and the probability of its

occurrence decreases very rapidly when n increases. However, when it occurs for the n available data, we must handle it. There are different views among statisticians on whether such divergent values must be retained as valid estimates or they must be rejected as unacceptable. We embrace the latter view, for the reasons put forward by Azzalini and Arellano-Valle (2013), and adopt the maximum penalized likelihood estimate (MPLE) proposed there to prevent the problem. While the motivation for MPLE is primarily for small to moderate n, we use it throughout for consistency.

There is an additional peculiar feature of the ST log-likelihood function, which however we mention only for completeness, rather than for its real relevance. In cases when ν is allowed to span the whole positive half-line, poles of the likelihood function must exist near $\nu = 0$, similarly to the case of a Student's t with unspecified degrees of freedom. This problem has been explored numerically by Azzalini and Capitanio (2003, pp. 384–385), and the indication was that these poles must exist at *very* small values of ν, such as $\hat{\nu} = 0.06$ in one specific instance.

This phenomenon is qualitatively similar to the problem of poles of the likelihood function for a finite mixture of continuous distributions. Even in the simple case of univariate normal components, there always exist n poles on the boundary of the parameter space if the standard deviations of the components are unrestricted; see for instance Day (1969, Section 7). The problem is conceptually interesting, in both settings, but in practice it is easily dealt with in various ways. In the ST setting, the simplest solution is to impose a constraint $\nu > \nu_0 > 0$ where ν_0 is some very small value, such as $\nu_0 = 0.1$ or 0.2. Even if fitted to data, a t or ST density with $\nu < 0.1$ would be an object hard to use in practice.

2.2 Numerical Aspects and Some Illustrations

Since, on the computational side, we shall base our work the `R` package `sn`, described by Azzalini (2019), it is appropriate to describe some key aspects of this package. There exists a comprehensive function for model fitting, called `selm`, but the actual numerical work in case of an ST model is performed by functions `st.mple` and `mst.mple`, in the univariate and the multivariate case, respectively. To numerical efficiency, we shall be using these functions directly, rather than via `selm`. As their names suggest, `st.mple` and `mst.mple` perform MPLE, but they can be used for classical MLE as well, just by omitting the penalty function. The rest of the description refers to `st.mple`, but `mst.mple` follows a similar scheme.

In the univariate case, denote by $\theta = (\xi, \omega, \alpha, \nu)^\top$ the parameters to be estimated, or possibly $\theta = (\beta^\top, \omega, \alpha, \nu)^\top$ when a linear regression model is introduced for the location parameter, in which case β is a vector of p regression coefficients. Denote by $\log L(\theta)$ the log-likelihood function at point θ. If no starting values are supplied, the first operation of `st.mple` is to fit a linear model to the available explanatory variables; this reduces to the constant covariate value 1 if $p = 1$. For the residuals from this linear fit, sample cumulants of order up to four are computed, hence including the sample variance. An inversion from these

values to θ may or may not be possible, depending on whether the third and fourth sample cumulants fall in the feasible region for the ST family. If the inversion is successful, initial values of the parameters are so obtained; if not, the final two components of θ are set at $(\alpha, \nu) = (0, 10)$, retaining the other components from the linear fit. Starting from this point, MLE or MPLE is searched for using a general numerical optimization procedure. The default procedure for performing this step is the `R` function `nlminb`, supplied with the score functions besides the log-likelihood function. We shall refer, comprehensively, to this currently standard procedure as 'method M0'.

In all our numerical work, method M0 uses `st.mple`, and the involved function `nlminb`, with all tuning parameters kept at their default values. The only activated option is the one switching between MPLE and MLE, and even this only for the work of the present section. Later on, we shall always use MPLE, with penalty function `Qpenalty` which implements the method proposed in Azzalini and Arellano-Valle (2013).

We start our numerical work with some illustrations, essentially in graphical form, of the log-likelihood generated by some simulated datasets. The aim is to provide a direct perception, although inevitably limited, of the possible behaviour of the log-likelihood and the ensuing problems which it poses for MLE search and other inferential procedures. Given this aim, we focus on cases which are unusual, in some way or another, rather than on 'plain cases'.

The type of graphical display which we adopt is based on the profile log-likelihood function of (α, ν), denoted $\log L_p(\alpha, \nu)$. This is obtained, for any given (α, ν), by maximizing $\log L(\theta)$ with respect to the remaining parameters. To simplify readability, we transform $\log L_p(\alpha, \nu)$ to the likelihood ratio test statistic, also called 'deviance function':

$$D(\alpha, \nu) = 2\,\{\log L_p(\hat{\alpha}, \hat{\nu}) - \log L_p(\alpha, \nu)\} \tag{7}$$

where $\log L_p(\hat{\alpha}, \hat{\nu})$ is the overall maximum value of the log-likelihood, equivalent to $\log L(\hat{\theta})$. The concept of deviance applies equally to the penalized log-likelihood.

The plots in Fig. 2 displays, in the form of contour level plots, the behaviour of $D(\alpha, \nu)$ for two artificially generated samples, with ν expressed on the logarithmic scale for more convenient readability. Specifically, the top plots refer to a sample of size $n = 50$ drawn from the ST(0, 1, 1, 2); the left plot, refers to the regular log-likelihood, while the right plot refers to the penalized log-likelihood. The plots include marks for points of special interest, as follows:

△ the true parameter point;
○ the point having maximal (penalized) log-likelihood on a 51×51 grid of points spanning the plotted area;
+ the MLE or MPLE point selected by method M0;
∗ the preliminary estimate to be introduced in Sect. 3.2, later denoted M1;
× the MLE or MPLE point selected by method M2 presented later in the text.

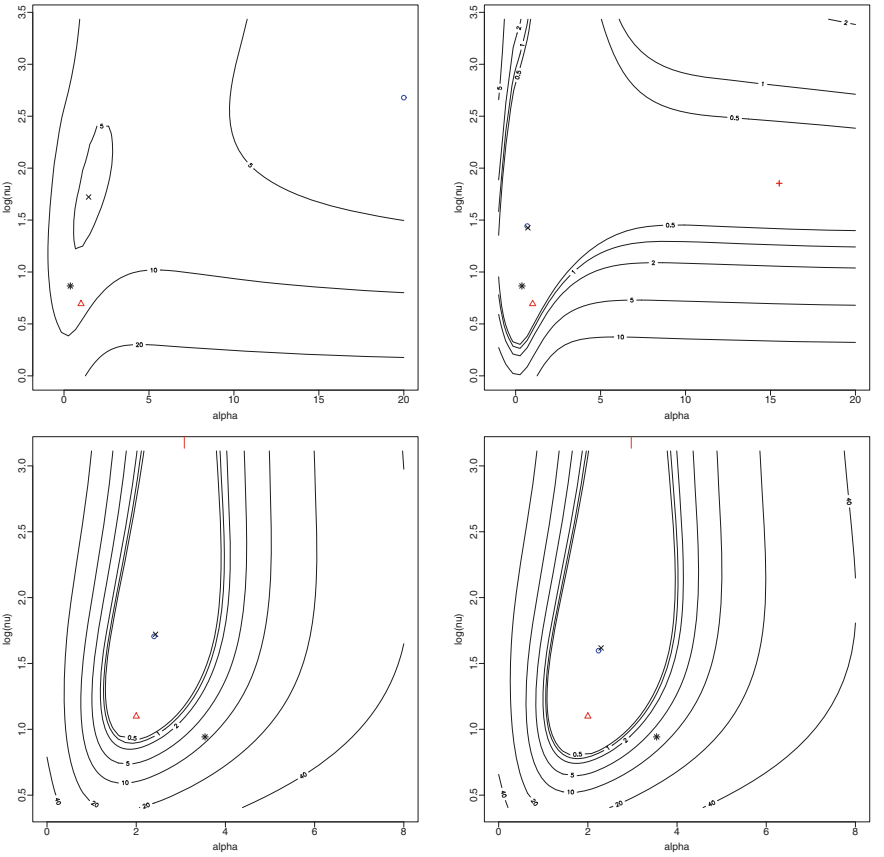

Fig. 2 Contour level plots of the deviance function for simple samples from ST$(0, 1, \alpha, \nu)$ associated to the log-likelihood (on the left side) or to its penalized version (on the right side). The top plots refer to a sample of size $n = 50$ from ST$(0, 1, 1, 2)$; the bottom plots refer to a sample of size $n = 300$ from ST$(0, 1, 2, 3)$. See the text for explanation of the marked points

It will be noticed that the top-left plot does not show a + mark. This is because the MLE point delivered by M0 has $\hat{\alpha} = \hat{\nu} \to \infty$ (actually some huge values representing a numerical 'approximations of infinity'), where $\log L_p \approx -81.85$; consequently the maximum of $\log L_p$ over the plotted area takes place at its margin. Note that the log-likelihood function has a local maximum at about $(\alpha, \nu) = (1.45, 5.6)$, where $\log L_p \approx -84.09$; this local maximum is quite close to the true parameter point, especially so in the light of the limited sample size. There are two messages from this example: one is that the log-likelihood may have more than one maximum; the other is that a local maximum can provide a better choice than the global maximum, at least in some cases.

Given that $\hat{\alpha} = \infty$, consider MPLE estimation in the top-right plot. The maximum of $\log L_p$, marked by ○, is now close to the point $(1.45, 5.6)$, but method

M0 fails to find it, and it picks up the point (15.5, 6.4). This must be due to a poor choice of the initial point for numerical search, given that method M2, which differs only for this initial point, lands on the correct point.

Peculiar behaviours, either of the log-likelihood or of the estimation procedures or both of them, are certainly more frequent when n is small or moderate, but problems can persist even for fairly large n, as illustrated by the bottom two plots of Fig. 2 which refer to a sample of size $n = 300$ from ST(0, 1, 2, 3). In this case, M0 yields $\hat{\alpha} \approx 3$ and $\hat{\nu} \to \infty$, denoted by the vertical ticks below the top side of the plotted area; the associated $\log L_p$ value is -422.5 for the left plot, -424.4 for the right plot. Both these values are lower than the corresponding maximal $\log L_p$ values, -419.8 and -420.8. Again, better initial search points used by method M2 leads to the correct global maxima, at about (2.4, 5.6) and (2.3, 5.0), respectively.

3 On the Choice of Initial Parameters for MLE Search

The aim of this section, which represents the main body of the paper, is to develop a methodology for improving the selection of initial parameter values from where to start the MPLE search via some numerical optimization technique, which should hopefully achieve a higher maximum.

3.1 Preliminary Remarks and the Basic Scheme

We have seen in Sect. 2 the ST log-likelihood function can be problematic; it is then advisable to select carefully the starting point for the MLE search. While contrasting the risk of landing on a local maximum, a connected aspect of interest is to reduce the overall computing time. Here are some preliminary considerations about the stated target.

Since these initial estimates will be refined by a subsequent step of log-likelihood maximization, there is no point in aiming at a very sophisticate method. In addition, we want to keep the involved computing header as light as possible. Therefore, we want a method which is simple and quick to compute; at the same time, it should be reasonably reliable, hopefully avoiding nonsensical outcomes.

Another consideration is that we cannot work with the methods of moments, or some variant of it, as this would impose a condition $\nu > 4$, bearing in mind the constraints recalled in Sect. 1.2. Since some of the most interesting applications of ST-based models deal with very heavy tails, hence with low degrees of freedom, the condition $\nu > 4$ would be unacceptable in many important applications. The implication is that we have to work with quantiles and derived quantities.

To ease exposition, we begin by presenting the logic in the basic case of independent observations from a common univariate distribution $\mathrm{ST}(\xi, \omega^2, \lambda, \nu)$. The first step is to select suitable quantile-based measures of location, scale,

asymmetry and tail-weight. The following list presents a set of reasonable choices; these measures can be equally referred to a probability distribution or to a sample, depending on the interpretation of the terms quantile, quartile and alike.

Location The median is the obvious choice here; denote it by q_2, since it coincides with the second quartile.

Scale A commonly used measure of scale is the semi-interquartile difference, also called quartile deviation, that is

$$d_q = \tfrac{1}{2}(q_3 - q_1)$$

where q_j denotes the jth quartile; see for instance Kotz et al. (2006, vol. 10, p. 6743).

Asymmetry A classical non-parametric measure of asymmetry is the so-called Bowley's measure

$$G = \frac{(q_3 - q_2) - (q_2 - q_1)}{q_3 - q_1} = \frac{q_3 - 2\,q_2 + q_1}{2\,d_q};$$

see Kotz et al. (2006, vol. 12, p. 7771–3). Since the same quantity, up to an inessential difference, had previously been used by Galton, some authors attribute to him its introduction. We shall refer to G as the Galton-Bowley measure.

Kurtosis A relatively more recent proposal is the Moors measure of kurtosis, presented in Moors (1988),

$$M = \frac{(e_7 - e_5) + (e_3 - e_1)}{e_6 - e_2}$$

where e_j denotes the jth octile, for $j = 1, \ldots, 7$. Clearly, $e_{2j} = q_j$ for $j = 1, 2, 3$.

A key property is that d_q is independent of the location of the distribution, and G and M are independent of location and scale.

For any distribution $\mathrm{ST}(\xi, \omega^2, \lambda, \nu)$, the values of $Q = (q_2, d_q, G, M)$ are functions of the parameters $\theta = (\xi, \omega, \lambda, \nu)$. Given a set of observations $y = (y_1, \ldots, y_n)$ drawn from $\mathrm{ST}(\xi, \omega^2, \lambda, \nu)$ under mutual independence condition, we compute sample values of $\tilde{Q} = (\tilde{q}_2, \tilde{d}_q, \tilde{G}, \tilde{M})$ of Q from the sample quantiles and then inversion of the functions connecting θ and Q will yield estimates $\tilde{\theta}$ of the ST parameters. In essence, the logic is similar to the one underlying the method of moments, but with moments replaced by quantiles.

In the following subsection, we discuss how to numerically carry out the inversion from Q to θ. Next, we extend the procedure to settings which include explanatory variables and multivariate observations.

3.2 Inversion of Quantile-Based Measures to ST Parameters

For the inversion of the parameter set $Q = (q_2, d_q, G, M)$ to $\theta = (\xi, \omega, \lambda, \nu)$, the first stage considers only the components (G, M) which are to be mapped to (λ, ν), exploiting the invariance of G and M with respect to location and scale. Hence, at this stage, we can work assuming that $\xi = 0$ and $\omega = 1$.

Start by computing, for any given pair (λ, ν), the set of octiles $e_1, \ldots, e_7$ of ST$(0, 1, \lambda, \nu)$, and from here the corresponding (G, M) values. Operationally, we have computed the ST quantiles using routine `qst` of package `sn`. Only non-negative values of λ need to be considered, because a reversal of the λ sign simply reverses the sign of G, while M is unaffected, thanks to the mirroring property of the ST quantiles when λ is changed to $-\lambda$.

Initially, our numerical exploration of the inversion process examined the contour level plots of G and M as functions of λ and ν, as this appeared to be the more natural approach. Unfortunately, these plots turned out not to be useful, because of the lack of a sufficiently regular pattern of the contour curves. Therefore these plots are not even displayed here.

A more useful display is the one adopted in Fig. 3, where the coordinate axes are now G and M. The shaded area, which is the same in both panels, represents the set of feasible (G, M) points for the ST family. In the first plot, each of the black lines indicates the *locus* of points with constant values of δ, defined by (4), when ν spans the positive half-line; the selected δ values are printed at the top of the shaded area, when feasible without clutter of the labels. The use of δ instead of λ simply yields a better spread of the contour lines with different parameter values, but it is conceptually irrelevant. The second plot of Fig. 3 displays the same admissible region with superimposed a different type of *loci*, namely those corresponding to

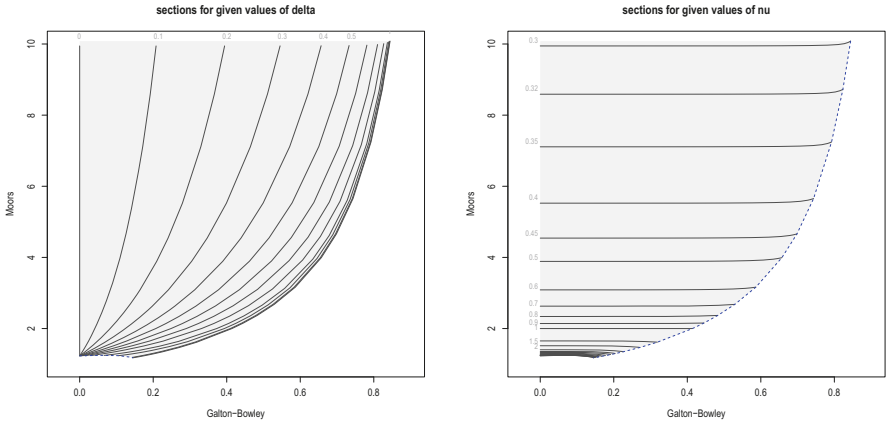

Fig. 3 *Loci* of the (G, M) space for given values of δ as ν varies (left plot) and for given values of ν as δ varies (right plot)

specified values of ν, when δ spans the $[0, 1]$ interval; the selected ν values are printed on the left side of the shaded area.

Details of the numerical calculations are as follows. The Galton-Bowley and the Moors measures have been evaluated over a 13×25 grid of points identified by the selected values

$$\begin{aligned}\delta^* &= (0,\ 0.1,\ 0.2,\ 0.3,\ 0.4,\ 0.5,\ 0.6,\ 0.7,\ 0.8,\ 0.9,\ 0.95,\ 0.99,\ 1),\\ \nu^* &= (0.30,\ 0.32,\ 0.35,\ 0.40,\ 0.45,\ 0.50,\ 0.60,\ 0.70,\ 0.80,\ 0.90,\ 1,\ 1.5,\ 2,\\ &\qquad 3,\ 4,\ 5,\ 7,\ 10,\ 15,\ 20,\ 30,\ 40,\ 50,\ 100,\ \infty)\,.\end{aligned}$$

The G and M values so obtained form the basis of Fig. 3 and subsequent calculations. Note that, while the vectors δ^* and ν^* identify a regular grid of points on the (δ, ν) space, they correspond to a curved grid on the shaded regions of Fig. 3.

Boundary parameter values require a special handling. Specifically, $\delta = 1$ and correspondingly $\lambda = \infty$ identify the Student's t distribution truncated below 0, that is, the square root transformation of the Snedecor's $F(1, \nu)$ distribution; hence, in this case the quantiles are computed as square roots of the $F(1, \nu)$ quantiles. The associated points lie on the right-side boundary of the shaded area. Another special value is $\nu = \infty$ which corresponds to the SN distribution. In this case, function `qsn` of package `sn` has been used; the corresponding points lie on the concave curve in the bottom-left corner of the shaded area.

Conceptually, Fig. 3 represents the key for the inversion from (G, M) to (δ, ν) and equivalently to (λ, ν) since $\lambda = (1 - \delta^2)^{-1/2}\delta$. However, in practical terms, we must devise a mechanism for inversely interpolating the (G, M) values computed at the grid points. Evaluation of this interpolation scheme at the sample values $(\tilde{G}, \tilde{M})$ will yield the desired estimates.

To this end, the second plot indicates the most favourable front for tackling the problem, since its almost horizontal lines show that the Moors measure is very nearly a function of ν only. Denote by M° the value of M when $\delta = 0$. The 25 available values of M° at ν^* are reported in the second column of Table 1; the remaining columns will be explained shortly. From these 25 values, an interpolating spline of $1/\nu$ as a function of M° has been introduced. Use of the $1/\nu$ transformed variable substantially reduces the otherwise extreme curvature of the function. Evaluation of this spline function at the sample value $\tilde{M}$ and conversion into its reciprocal yields an initial estimate $\tilde{\nu}$.

Consider now estimation of δ or equivalently of λ, a task which essentially amounts to approximate the curves in the first plot in Fig. 3. After some numerical exploration, it turned out that a closely interpolating function can be established in the following form:

$$\log\lambda \approx \eta_1^{(\nu)}\, u + \eta_2^{(\nu)}\, u^3 + \eta_3^{(\nu)}\, u^{-3}, \qquad u = \log G. \tag{8}$$

Table 1 Coefficients used for interpolation of the G and M tabulated values

ν^*	$M\big\vert_{\delta=0}$	$\eta_1^{(\nu)}$	$\eta_2^{(\nu)}$	$\eta_3^{(\nu)}$
0.30	9.946	2.213831	−0.315418	−0.007641
0.32	8.588	2.022665	−0.240821	−0.012001
0.35	7.110	1.790767	−0.164193	−0.021492
0.40	5.525	1.506418	−0.090251	−0.047034
0.45	4.543	1.305070	−0.050702	−0.087117
0.50	3.888	1.156260	−0.028013	−0.143526
0.60	3.088	0.952435	−0.005513	−0.307509
0.70	2.630	0.819371	0.004209	−0.536039
0.80	2.339	0.724816	0.008992	−0.818739
0.90	2.142	0.653206	0.011596	−1.142667
1.00	2.000	0.596276	0.013136	−1.495125
1.50	1.652	0.417375	0.015798	−3.365100
2.00	1.517	0.314104	0.016371	−5.011929
3.00	1.403	0.192531	0.016274	−7.304089
4.00	1.354	0.123531	0.015682	−8.676470
5.00	1.327	0.080123	0.014987	−9.546498
7.00	1.298	0.030605	0.013674	−10.561206
10.00	1.277	−0.003627	0.012113	−11.335506
15.00	1.262	−0.024611	0.010334	−11.977601
20.00	1.254	−0.030903	0.009149	−12.343369
30.00	1.247	−0.031385	0.007650	−12.789281
40.00	1.244	−0.027677	0.006721	−13.074983
50.00	1.241	−0.023285	0.006079	−13.284029
100.00	1.237	−0.005288	0.004478	−13.874691
∞	1.233			

where the fitted values of the coefficients $\eta_j^{(\nu)}$ for the selected ν^* values are reported in the last three columns of Table 1, with the exception of $\nu = \infty$. Use of (8) combined with the coefficients of Table 1 allows to find an approximate value of λ for the selected values of ν. If an intermediate value of ν must be considered, such that $\nu_1 < \nu < \nu_2$ where ν_1, ν_2 are two adjacent values of ν^*, a linear interpolation of the corresponding coefficients is performed. More explicitly, a value of $\eta_j^{(\nu)}$ is obtained by linear interpolation of $\eta_j^{(\nu_1)}$ and $\eta_j^{(\nu_2)}$, for $j = 1, 2, 3$; then (8) is applied using these interpolated coefficients. If ν is outside the range of finite ν values in the first column of Table 1, the $\eta_j^{(\nu)}$ values associated with the closest such value of ν are used.

Operationally, we use the just-described scheme with ν set at the value $\tilde{\nu}$ obtained earlier, leading to an estimate $\tilde{\lambda}$ of λ.

Numerical testing of this procedure has been performed as follows. For a number of pairs of values (α, ν), the corresponding octiles and the (G, M) measures have been computed and the proposed procedure has been applied to these measures. The

returned parameter values were satisfactorily close to the original (α, ν) pair, with some inevitable discrepancies due to the approximations involved, but of limited entity. If necessary, a refinement can be obtained by numerical search targeted to minimize a suitable distance between a given pair (G, M) and the analogous values derived from the associated (α, ν) pair. However, this refinement was not felt necessary in the numerical work described later, thanks to the good working of the above-described interpolation scheme.

We are now left with estimation of ξ and ω. Bearing in mind the representation $Y = \xi + \omega Z$ introduced just before (3), ω is naturally estimated by

$$\tilde{\omega} = \frac{q_3 - q_1}{q_3^{\mathrm{ST}} - q_1^{\mathrm{ST}}} \tag{9}$$

where the terms in the numerator are sample quartiles and those in the denominator are quartiles of $Z \sim \mathrm{ST}(0, 1, \tilde{\lambda}, \tilde{\nu})$.

Consideration of $Y = \xi + \omega Z$ again says that an estimate of ξ can be obtained as an adjustment of the sample median q_2 via

$$\tilde{\xi} = q_2 - \tilde{\omega}\, q_2^{\mathrm{ST}} \tag{10}$$

where q_2^{ST} is the median of $Z \sim \mathrm{ST}(0, 1, \tilde{\lambda}, \tilde{\nu})$.

The estimates so produced are marked by an asterisk in the examples of Fig. 2, showing to perform well in those cases, while requiring a negligible computing time compared to MLE.

3.3 Extension to the Regression Case

We want to extend the methodology of Sect. 3.2 to the regression setting where the location parameter varies across observations as a linear function of a set of p, say, explanatory variables, which are assumed to include the constant term, as it is commonly the case. If x_i is the vector of covariates pertaining to the ith subject, observation y_i is now assumed to be drawn from $\mathrm{ST}(\xi_i, \omega, \lambda, \nu)$ where

$$\xi_i = x_i^\top \beta, \qquad i = 1, \ldots, n, \tag{11}$$

for some p-dimensional vector β of unknown parameters; hence now the parameter vector is $\theta = (\beta^\top, \omega, \lambda, \nu)^\top$. The assumption of independently drawn observations is retained.

The direct extension of the median as an estimate of location, which was used in Sect. 3.2, is an estimate of β obtained by median regression, which corresponds to adoption of the least absolute deviations fitting criterion instead of the more familiar least squares. This can also be viewed as a special case of quantile regression, when the quantile level is set at $1/2$. A classical treatment of quantile regression

is Koenker (2005) and corresponding numerical work can be carried out using the `R` package `quantreg`, see Koenker (2018), among other tools.

Use of median regression delivers an estimate $\tilde{\beta}^m$ of β and a vector of residual values, $r_i = y_i - x_i^\top \tilde{\beta}^m$ for $i = 1, \ldots, n$. Ignoring β estimation errors, these residuals are values sampled from $\mathrm{ST}(-m_0, \omega^2, \lambda, \nu)$, where m_0 is a suitable value, examined shortly, which makes the distribution to have 0 median, since this is the target of the median regression criterion. We can then use the same procedure of Sect. 3.2, with the y_i's replaced the r_i's, to estimate ω, λ, ν, given that the value of m_0 is irrelevant at this stage.

The final step is a correction to the vector $\tilde{\beta}^m$ to adjust for the fact that $y_i - x_i^\top \beta$ should have median m_0, that is, the median of $\mathrm{ST}(0, \omega, \lambda, \nu)$, not median 0. This amounts to increase all residuals by a constant value m_0, and this step is accomplished by setting a vector $\tilde{\beta}$ with all components equal to $\tilde{\beta}^m$ except that the intercept term, β_0 say, is estimated by

$$\tilde{\beta}_0 = \tilde{\beta}_0^m - \tilde{\omega}\, q_2^{\mathrm{ST}}$$

similarly to (10).

3.4 Extension to the Multivariate Case

Consider now the case of n independent observations from a multivariate Y variable with density (6), hence $Y \sim \mathrm{ST}_d(\xi, \Omega, \alpha, \nu)$. This case can be combined with the regression setting of Sect. 3.3, so that the d-dimensional location parameter varies for each observation according to

$$\xi_i^\top = x_i^\top \beta, \qquad i = 1, \ldots, n, \tag{12}$$

where now $\beta = (\beta_{\cdot 1}, \ldots, \beta_{\cdot d})$ is a $p \times d$ matrix of parameters. Since we have assumed that the explanatory variables include a constant term, the regression case subsumes the one of identical distribution, when $p = 1$. Hence we deal with the regression case directly, where the ith observation is sampled from $Y_i \sim \mathrm{ST}_d(\xi_i, \Omega, \alpha, \nu)$ and ξ_i is given by (12), for $i = 1, \ldots, n$.

Arrange the observed values in a $n \times d$ matrix $y = (y_{ij})$. Application of the procedure presented in Sects. 3.2 and 3.3 separately to each column of y delivers estimates of d univariate models. Specifically, from the jth column of y, we obtain estimates $\tilde{\theta}_j$ and corresponding 'normalized' residuals $\tilde{z}_{ij}$:

$$\tilde{\theta}_j = (\tilde{\beta}_{\cdot j}^\top, \tilde{\omega}_j, \tilde{\lambda}_j, \tilde{\nu}_j)^\top, \qquad \tilde{z}_{ij} = \tilde{\omega}_j^{-1}(y_{ij} - x_i^\top \tilde{\beta}_{\cdot j})\,. \tag{13}$$

where it must be recalled that the 'normalization' operation uses location and scale parameters, but these do not coincide with the mean and the standard deviation of the underlying random variable.

Since the meaning of expression (12) is to define a set of univariate regression modes with a common design matrix, the vectors $\tilde{\beta}_{\cdot 1}, \ldots, \tilde{\beta}_{\cdot d}$ can simply be arranged in a $p \times d$ matrix $\tilde{\beta}$ which represents an estimate of β.

The set of univariate estimates in (13) provide d estimates for ν, while only one such a value enters the specification of the multivariate ST distribution. We have adopted the median of $\tilde{\nu}_1, \ldots, \tilde{\nu}_d$ as the single required estimate, denoted $\tilde{\nu}$.

The scale quantities $\tilde{\omega}_1, \ldots, \tilde{\omega}_d$ estimate the square roots of the diagonal elements of Ω, but off-diagonal elements require a separate estimation step. What is really required to estimate is the scale-free matrix $\bar{\Omega}$. This is the problem examined next.

If ω is the diagonal matrix formed by the squares roots of $\Omega_{11}, \ldots, \Omega_{dd}$, all variables $\omega^{-1}(Y_i - \xi_i)$ have distribution $\mathrm{ST}_d(0, \bar{\Omega}, \alpha, \nu)$, for $i = 1, \ldots, n$. Denote by $Z = (Z_1, \ldots, Z_d)^\top$ the generic member of this set of variables. We are concerned with the distribution of the products $Z_j Z_k$, but for notational simplicity we focus on the specific product $W = Z_1 Z_2$, since all other products are of similar nature.

We must then examine the distribution of $W = Z_1 Z_2$ when (Z_1, Z_2) is a bivariate ST variable. This looks at first to be a daunting task, but a major simplification is provided by consideration of the perturbation invariance property of symmetry-modulated distributions, of which the ST is an instance. For a precise exposition of this property, see for instance Proposition 1.4 of Azzalini and Capitanio (2014), but in the present case it says that, since W is an even function of (Z_1, Z_2), its distribution does not depend on α, and it coincides with the distribution of the case $\alpha = 0$, that is, the case of a usual bivariate Student's t distribution, with dependence parameter $\bar{\Omega}_{12}$.

Denote by $F_W(w; \rho, \nu)$ the distribution function of the product W of variables (Z_1, Z_2) having bivariate Student's t density (5) in dimension $d = 2$ with ν degrees of freedom and dependence parameter ρ where $|\rho| < 1$. An expression of $F_W(w; \rho, \nu)$ is available in Theorem 1 of Wallgren (1980). Although this expression involves numerical integration, this is not problematic since univariate integration can be performed efficiently and reliably with the `R` function `integrate`.

To estimate Ω_{12}, we search for the value of ρ such that the median of the distribution of W equates its sample value. In practice, we compute the sample values $\tilde{w}_1, \ldots, \tilde{w}_n$ where $\tilde{w}_i = \tilde{z}_{i1}\tilde{z}_{i2}$, using the residuals in (13), and denote their median by $m_{\tilde{w}}$. Then we must numerically solve the non-linear equation

$$F_W(m_{\tilde{w}}; \rho, \tilde{\nu}) = 1/2 \tag{14}$$

with respect to ρ. The Solution of this equation is facilitated by the monotonicity of $F_W(w; \rho, \nu)$ with respect to ρ, ensured by Theorem 2 of Wallgren (1980). The solution of (14) is the estimate $\tilde{\Omega}_{12}$.

Proceeding similarly for other pairs of variables (Z_j, Z_k), all entries of matrix $\bar{\Omega}$ can be estimated; the diagonal elements are all 1. However, it could happen that the matrix so produced is not a positive-definite correlation matrix, because of estimation errors. Furthermore, an even more stringent condition has to be satisfied, namely that

$$\Omega^* = \begin{pmatrix} \bar{\Omega} & \delta \\ \delta^\top & 1 \end{pmatrix} > 0\,. \tag{15}$$

This condition on Ω^* applies to all skew-elliptical distributions, of which the ST is an instance; see Branco and Dey (2001, p. 101) or Azzalini and Capitanio (2014, p. 171).

Denote by $\tilde{\Omega}^*$ the estimate of Ω^* with $\bar{\tilde{\Omega}}$ in the $d \times d$ top-left block obtained by solutions of equations of type (14) and $\tilde{\delta}$ computed by applying $\delta(\tilde{\lambda}_j)$ in (4) to $\tilde{\lambda}_1, \ldots, \tilde{\lambda}_d$. If $\tilde{\Omega}^*$ is positive definite, then we move on to the next step; otherwise, an adjustment is required.

There exist various techniques to adjust a nearly positive-definite matrix to achieve positive-definiteness. Some numerical experimentation has been carried out using procedure `nearPD` of `R` package `Matrix`; see Bates and Maechler (2019). Unfortunately, this did not work well when we used the resulting matrix for the next step, namely computation of the vector

$$\alpha = \left(1 - \delta^\top \bar{\Omega}^{-1} \delta\right)^{-1/2} \bar{\Omega}^{-1} \delta \tag{16}$$

which enters the density function (6); see for instance equation (4) of Azzalini and Capitanio (2003), which is stated for the SN distribution, but it holds also for the ST. The unsatisfactory outcome from `nearPD` for our problem is presumably due to modifications in the relative size of the components of $\tilde{\Omega}^*$, leading to grossly inadequate α vectors, typically having a gigantic norm.

A simpler type of adjustment has therefore been adopted, as follows. If condition (15) does not hold for $\tilde{\Omega}^*$, the off-diagonal elements of the matrix are shrunk by a factor 0.95, possibly repeatedly, until (15) is satisfied. This procedure was quick to compute and it did not cause peculiar outcomes from (16).

Hence, either directly from the initial estimates of $\bar{\Omega}$ and δ or after the adjustment step just described, we obtain valid components satisfying condition (15) and a corresponding vector $\tilde{\alpha}$ from (16). The final step is to introduce scale factors via

$$\tilde{\Omega} = \tilde{\omega}\, \bar{\tilde{\Omega}}\, \tilde{\omega}$$

where $\tilde{\omega} = \mathrm{diag}(\tilde{\omega}_1, \ldots, \tilde{\omega}_d)$. This completes estimation of $(\beta, \Omega, \alpha, \nu)$.

3.5 Simulation Work to Compare Initialization Procedures

Several simulations runs have been performed to examine the performance of the proposed methodology. The computing environment was `R` version 3.6.0. The reference point for these evaluations is the methodology currently in use, as provided by the publicly available version of `R` package `sn` at the time of writing, namely version 1.5-4; see Azzalini (2019). This will be denoted 'the current method' in the following. Since the role of the proposed method is to initialize the numerical MLE search, not the initialization procedure *per se*, we compare the new and the current method with respect to final MLE outcome. However, since the numerical optimization method used after initialization is the same, any variations in the results originate from the different initialization procedures.

We stress again that in a vast number of cases the working of the current method is satisfactory and we are aiming at improvements when dealing with 'awkward samples'. These commonly arise with ST distributions having low degrees of freedom, about $\nu = 1$ or even less, but exceptions exist, such as the second sample in Fig. 2.

The primary aspect of interest is improvement in the quality of data fitting. This is typically expressed as an increase of the maximal achieved log-likelihood, in its penalized form. Another desirable effect is improvement in computing time.

The basic set-up for such numerical experiments is represented by simple random samples, obtained as independent and identically distributed values drawn from a named ST$(\xi, \omega, \lambda, \nu)$. In all cases we set $\xi = 0$ and $\omega = 1$. For the other ingredients, we have selected the following values:

$$\begin{aligned} &\lambda : 0, \quad 2, \quad 8, \\ &\nu : 1, \quad 3, \quad 8, \\ &n : 50, \ 100, \ 250, \ 500 \end{aligned} \tag{17}$$

and, for each combination of these values, $N = 2000$ samples have been drawn.

The smallest examined sample size, $n = 50$, must be regarded as a sort of 'sensible lower bound' for realistic fitting of flexible distributions such as the ST. In this respect, recall the cautionary note of Azzalini and Capitanio (2014, p. 63) about the fitting of a SN distribution with small sample sizes. Since the ST involves an additional parameter, notably one having a strong effect on tail behaviour, that annotation holds *a fortiori* here.

For each of the $3 \times 3 \times 4 \times 2000 = 72,000$ samples so generated, estimation of the parameters $(\xi, \omega, \lambda, \nu)$ has been carried out using the following methods.

M0: this is the current method, which maximizes the penalized log-likelihood using function `st.mple` as described in Sect. 2.2.
M1: preliminary estimates are computed as described in Sect. 3.2;
M2: maximization of the penalized log-likelihood, still using function `st.mple`, but starting from the estimates of M1;

M3: similar to M2, but using a simplified form of M1, where only the location and scale parameters are estimated, setting $\lambda = 0$ and $\nu = 10$.

An exhaustive analysis of the simulation outcome would be far too lengthy and space consuming. As already mentioned, our primary interest is on the differences of maximized log-likelihood. Specifically, if denote by $\log \hat{L}_h$ the maximized value of the penalized log-likelihood using method Mh, we focus on the quantities D_{20}, D_{23} and D_{30}, where $D_{hk} = \log \hat{L}_h - \log \hat{L}_k$. Table 2 reports the observed frequencies of D_{hk} values, grouped in intervals

$$(-\infty, -20],\ (-20, -2],\ (-2, -0.2],\ (-0.2, 0],\ (0, 0.2],\ (0.2, 2],\ (2, 20],\ (20, \infty]$$

crosstabulated either with n or with ν.

We are not concerned with samples having values D_{hk} in the interval $(-0.2, 0.2)$, since these differences are not relevant from an inferential viewpoint; just note that they constitute the majority of cases. As for D_{20}, the fraction of cases falling outside

Table 2 Frequency tables of grouped values of D_{20}, D_{23} and D_{30} crossed with values of n and of ν in case of simple random sampling

Frequencies of $D_{20} \times n$								
n	$(-\infty, -20]$	$(-20, -2]$	$(-2, -0.2]$	$(-0.2, 0]$	$(0, 0.2]$	$(0.2, 2]$	$(2, 20]$	$(20, \infty]$
50	1	0	5	9380	8562	47	3	2
100	0	0	0	9359	8606	31	3	1
250	0	0	0	9235	8730	24	5	6
500	0	0	0	9163	8807	10	8	12
Total	1	0	5	37,137	34,705	112	19	21
Frequencies of $D_{20} \times \nu$								
ν	$(-\infty, -20]$	$(-20, -2]$	$(-2, -0.2]$	$(-0.2, 0]$	$(0, 0.2]$	$(0.2, 2]$	$(2, 20]$	$(20, \infty]$
1	1	0	1	12,903	11,035	21	18	21
3	0	0	2	11,926	12,054	17	1	0
8	0	0	2	12,308	11,616	74	0	0
Frequencies of $D_{23} \times n$								
n	$(-\infty, -20]$	$(-20, -2]$	$(-2, -0.2]$	$(-0.2, 0]$	$(0, 0.2]$	$(0.2, 2]$	$(2, 20]$	$(20, \infty]$
50	1	0	3	9445	8550	1	0	0
100	0	0	0	9324	8676	0	0	0
250	0	0	0	9117	8883	0	0	0
500	0	0	0	9011	8989	0	0	0
Total	1	0	3	36,897	35,098	1	0	0
Frequencies of $D_{30} \times n$								
n	$(-\infty, -20]$	$(-20, -2]$	$(-2, -0.2]$	$(-0.2, 0]$	$(0, 0.2]$	$(0.2, 2]$	$(2, 20]$	$(20, \infty]$
0	0	0	3	8925	9020	47	3	2
100	0	0	0	9075	8890	31	3	1
250	0	0	0	9132	8833	24	5	6
500	0	0	0	9195	8775	10	8	12
Total	0	0	3	36,327	35,518	112	19	21

$(-0.2, 0.2)$ is small, but it is not negligible, and this justifies our efforts to improve over M0. As expected, larger D_{20} values occur more easily when n or ν are small, but sometimes also otherwise. In all but a handful of cases, these larger differences are on the positive sides, confirming the effectiveness of the proposed method for initialization. The general indication is that both methods M2 and M3, and implicitly so M1, improve upon the current method M0.

Visual inspections of individual cases where M1 performs poorly indicates that the problem originates in the sample octiles, on which all the rest depends. Especially with very low n and/or ν, the sample octiles can occasionally happen to behave quite differently from expectations, spoiling everything. Unfortunately, there is no way to get around this problem, which however is sporadic.

Another indication from Table 2 is that M3 is essentially equivalent to M2, in terms of maximized log-likelihood, and in some cases it is even superior, in spite of its simplicity.

Another aspect is considered in Table 3 which reports computing times and their differences as frequencies of time intervals. A value t_k represents the computing time for estimation from a given sample using method Mk, obtained by the first value reported by the `R` function `system.time`. For M2 and M3, t_k includes the time spent for initialization with M1, although this is a very minor fraction of the overall time. Clearly, the samples considered are of quite different nature, especially so for sample size. However, our purpose is solely comparative and, since exactly the same samples are processed by the various methods, the comparison of average computing times is valid. Table 3 shows a clear advantage of M2 over M0 in terms of computing time and also some advantage, but less prominent, over M3.

Additional simulations have been run having the location parameter expressed via a linear regression. Given a vector x formed by n equally spaced points on the interval $(-1, 1)$, design matrices have been built using p transformations $T_j(x)$, inclusive of the constant function $T_0(x) = 1$, as follows:

	$T_0(x)$	$T_1(x)$	$T_2(x)$	$T_3(x)$
case A $(p = 3)$:	1	x	$\sqrt{1+x}$	
case B $(p = 3)$:	1	x	$\sin 3x$	
case C $(p = 4)$:	1	x	$\sin 3x$	$x/(1 + 0.8\,x)$

Computation of $T_j(x)$ over the n values of x yields the columns of the design matrix; the regression parameters $\beta_1, \ldots, \beta_p$ have been set at $\beta_j = 1$ for all js. For each of the A, B, C design matrices, and for each parameter combinations in (17), $N = 2000$ have been generated, similarly to the case of simple random samples.

In Table 4, we summarize results only for case C, as the other cases are quite similar. The distribution of D_{20} in the top two sub-tables still indicate a superiority of M2 over M0, although less pronounced than for simple samples. The lower portion of the table indicates a slight superiority of M3 over M2, reinforcing the similar indication from Table 2.

Table 3 Frequency table of computing time and their differences in the case of simple random samples

	$(-\infty, -0.25]$	$(-0.25, -0.1]$	$(-0.1, -0.05]$	$(-0.05, 0]$	$(0, 0.05]$	$(0.05, 0.1]$	$(0.1, 0.25]$	$(0.25, \infty]$
t_0	0	0	0	0	39,561	21,049	10,815	575
t_1	0	0	0	0	71,998	0	2	0
t_2	0	0	0	0	49,086	20,047	2866	1
t_3	0	0	0	0	44,178	21,880	5942	0
$t_2 - t_0$	163	2010	4629	51,101	13,790	294	13	0
$t_2 - t_3$	0	30	1148	50,694	19,679	438	11	0
$t_3 - t_0$	121	1487	2783	46,038	21,451	116	4	0

The values of t_2 and t_3 include the time t_1 for their initialization

In the two subtables of Table 4 about D_{20}, note that there are 160 samples where M0 goes completely wrong. All these samples were generated with $\nu = 1$, a fact which is not surprising considering the initial parameter selection of `st.mple`, in its standard working described at the beginning of Sect. 2.2. Since that initial selection is based on a least-squares fit of the regression parameters, this step clashes with the non-existence of moments when the underlying ST distribution has $\nu = 1$ degrees of freedom. Not only the regression parameters are poorly fitted, but the ensuing residuals are spoiled, affecting also the initial fit of the other parameters.

A set of simulations has also been run in the bivariate case, hence sampling from density (6) with $d = 2$. The scale matrix and the shape vector have been set to

$$\Omega = \begin{pmatrix} 1 & 1/2 \\ 1/2 & 1 \end{pmatrix}, \qquad \alpha = \lambda \begin{pmatrix} 1 \\ 2 \end{pmatrix}$$

Table 4 Frequency tables of grouped values of D_{20}, D_{23} and D_{30} crossed with values of n and of ν in case of a linear regression setting with $p = 4$ explanatory variables

Frequencies of $D_{20} \times n$								
n	$(-\infty, -20]$	$(-20, -2]$	$(-2, -0.2]$	$(-0.2, 0]$	$(0, 0.2]$	$(0.2, 2]$	$(2, 20]$	$(20, \infty]$
50	0	138	278	8480	8772	195	94	43
100	0	15	44	8829	8984	75	19	34
250	0	0	1	9029	8902	23	9	36
500	0	0	0	9326	8597	14	16	47
Total	0	153	323	35,664	35,255	307	138	160
Frequencies of $D_{20} \times \nu$								
ν	$(-\infty, -20]$	$(-20, -2]$	$(-2, -0.2]$	$(-0.2, 0]$	$(0, 0.2]$	$(0.2, 2]$	$(2, 20]$	$(20, \infty]$
1	0	118	188	12,967	10,291	156	120	160
3	0	23	88	11,074	12,759	44	12	0
8	0	12	47	11,623	12,205	107	6	0
Frequencies of $D_{23} \times n$								
n	$(-\infty, -20]$	$(-20, -2]$	$(-2, -0.2]$	$(-0.2, 0]$	$(0, 0.2]$	$(0.2, 2]$	$(2, 20]$	$(20, \infty]$
50	0	177	329	8413	8864	167	50	0
100	0	18	43	8802	9096	37	4	0
250	0	0	3	8899	9096	2	0	0
500	0	0	0	9066	8934	0	0	0
Total	0	195	375	35,180	35,990	206	54	0
Frequencies of $D_{30} \times n$								
n	$(-\infty, -20]$	$(-20, -2]$	$(-2, -0.2]$	$(-0.2, 0]$	$(0, 0.2]$	$(0.2, 2]$	$(2, 20]$	$(20, \infty]$
50	0	32	117	8856	8641	200	111	43
100	0	3	26	9069	8783	63	22	34
250	0	0	1	9160	8770	24	9	36
500	0	0	0	9188	8735	14	16	47
Total	0	35	144	36,273	34,929	301	158	160

where λ spans the values given in (17). Also n and ν have been set like in (17), with the exception that $n = 50$ has been not included, considering that 50 data points would constitute a too small sample in the present context. On the whole, $3^3 \times 2000 = 54,000$ bivariate samples have then been generated. They have been processed by function `mst.mple` of package `sn` and the initialization method of Sect. 3.4, with obvious modifications of the meaning of notation M0 to M3.

The summary output of the simulations is presented in Table 5. There is a clear winner this time, since M3 is constantly superior to the others. Between M0 and M2, the latter is still preferable for $\nu = 1$, but not otherwise.

The almost constant superiority of M3 over M2 is quite surprising, given the qualitatively different indication emerging in the univariate case. This rather surprising effect must be connected to transformation (16), as it has also been indicated by direct examination of a number of individual cases: a moderate estimation error even of a single λ_j component, and consequently of δ_j, transforms into a poor estimate of α. It so happens that the conservative choice $\alpha = 0$ of M3 avoids problems and can be, in its simplicity, more effective.

Table 5 Frequency tables of grouped values of D_{20}, D_{23} and D_{30} crossed with values of n and of ν in the bivariate case

Frequencies of $D_{20} \times n$								
n	$(-\infty, -20]$	$(-20, -2]$	$(-2, -0.2]$	$(-0.2, 0]$	$(0, 0.2]$	$(0.2, 2]$	$(2, 20]$	$(20, \infty]$
100	28	71	238	9410	8169	61	9	14
250	8	8	29	9613	8326	7	1	8
500	0	3	4	9330	8657	1	1	4
Total	36	82	271	28,353	25,152	69	11	26
Frequencies of $D_{20} \times \nu$								
ν	$(-\infty, -20]$	$(-20, -2]$	$(-2, -0.2]$	$(-0.2, 0]$	$(0, 0.2]$	$(0.2, 2]$	$(2, 20]$	$(20, \infty]$
1	1	3	8	8368	9578	14	2	26
3	12	14	61	9814	8094	5	0	0
8	23	65	202	10,171	7480	50	9	0
Frequencies of $D_{23} \times n$								
n	$(-\infty, -20]$	$(-20, -2]$	$(-2, -0.2]$	$(-0.2, 0]$	$(0, 0.2]$	$(0.2, 2]$	$(2, 20]$	$(20, \infty]$
100	28	71	232	9607	8006	50	6	0
250	8	8	29	9747	8205	3	0	0
500	0	3	4	9611	8382	0	0	0
Total	36	82	265	28,965	24,593	53	6	0
Frequencies of $D_{30} \times n$								
n	$(-\infty, -20]$	$(-20, -2]$	$(-2, -0.2]$	$(-0.2, 0]$	$(0, 0.2]$	$(0.2, 2]$	$(2, 20]$	$(20, \infty]$
100	0	0	25	8924	8998	36	3	14
250	0	0	2	9035	8946	8	1	8
500	0	0	0	8839	9155	1	1	4
Total	0	0	27	26,798	27,099	45	5	26

3.6 Conclusions

The overall indication of the simulation work is that the proposed preliminary estimates work quite effectively, providing an improved initialization of the numerical MPLE search. The primary aspect is that higher log-likelihood values are usually achieved, compared to the currently standard method, M0, sometimes by a remarkable margin. Another positive aspect is the saving in the overall computing time.

Of the two variant forms of the new initialization, leading to methods M2 and M3, the latter has emerged as clearly superior in the multivariate case, but no such clear-cut conclusion can be drawn in the univariate setting, with indications somewhat more favourable for M2. In this case, it is advisable to consider both variants of the preliminary estimation and carry out two numerical searches. Having to choose between them, the quick route is to take the one with higher log-likelihood. However, direct inspection of both outcomes must be recommended, including exploration of the profile log-likelihood surface.

Surely, it would have been ideal to identify a universally superior method, to be adopted for all situations, but this type of simplification still eludes us.

References

Adcock, C. J. (2010). Asset pricing and portfolio selection based on the multivariate extended skew-Student-*t* distribution. *Annals of Operations Research, 176*(1), 221–234. https://doi.org/10.1007/s10479-009-0586-4.

Azzalini, A. (2016). Flexible distributions as an approach to robustness: The skew-*t* case. In C. Agostinelli, A. Basu, P. Filzmoser, & D. Mukherjee (Eds.), *Recent advances in robust statistics: Theory and applications* (Chap. 1, pp. 1–16). New Delhi: Springer. https://doi.org/10.1007/978-81-322-3643-6.

Azzalini, A. (2019). *The R package* `sn`*: The skew-normal and related distributions such as the skew-t (version 1.5-4)*. Università di Padova, Italia. https://cran.r-project.org/package=sn; http://azzalini.stat.unipd.it/SN

Azzalini, A., & Arellano-Valle, R. B. (2013). Maximum penalized likelihood estimation for skew-normal and skew-*t* distributions. *Journal of Statistical Planning and Inference, 143*(2), 419–433. https://doi.org/10.1016/j.jspi.2012.06.022. Retrieved June 30, 2012.

Azzalini, A., & Capitanio, A. (2003). Distributions generated by perturbation of symmetry with emphasis on a multivariate skew *t* distribution. *Journal of the Royal Statistical Society: Series B, 65*(2), 367–389. https://doi.org/10.1111/1467-9868.00391. Full version of the paper at `arXiv.org:0911.2342`.

Azzalini, A., & Capitanio, A. (2014). *The skew-normal and related families*. *IMS monographs*. Cambridge: Cambridge University Press. http://www.cambridge.org/9781107029279

Azzalini, A., & Genton, M. G. (2008). Robust likelihood methods based on the skew-*t* and related distributions. *International Statistical Review, 76*, 106–129. https://doi.org/10.1111/j.1751-5823.2007.00016.x.

Bates, D., & Maechler, M. (2019). *Matrix: Sparse and dense matrix classes and methods*. https://CRAN.R-project.org/package=Matrix. R package version 1.2-17.

Branco, M. D., & Dey, D. K. (2001). A general class of multivariate skew-elliptical distributions. *Journal of Multivariate Analysis, 79*(1), 99–113.

Day, N. E. (1969). Estimating the components of a mixture of normal distributions. *Biometrika, 56*, 463–474.

Ghizzoni, T., Roth, G., & Rudari, R. (2010). Multivariate skew-*t* approach to the design of accumulation risk scenarios for the flooding hazard. *Advances in Water Resources, 33*(10, Sp. Iss. SI), 1243–1255. https://doi.org/10.1016/j.advwatres.2010.08.003.

Gupta, A. K. (2003). Multivariate skew *t*-distribution. *Statistics, 37*(4), 359–363. https://doi.org/10.1080/715019247.

Hallin, M., & Ley, C. (2012). Skew-symmetric distributions and Fisher information – A tale of two densities. *Bernoulli, 18*, 747–763. https://doi.org/10.3150/12-BEJ346. http://arxiv.org/pdf/1207.0282.

Koenker, R. (2005). *Quantile regression*. *Econometric society monographs*. Cambridge: Cambridge University Press.

Koenker, R. (2018). *quantreg: Quantile regression*. https://CRAN.R-project.org/package=quantreg. R package version 5.38.

Kotz, S., Read, C. B., Balakrishnan, N., & Vidakovic, B. (Eds.). (2006). *Encyclopedia of statistical sciences* (2nd ed.). New York: Wiley.

Meucci, A. (2006). Beyond Black-Litterman: Views on non-normal markets. *Risk Magazine, 19*(2), 87–92.

Moors, J. J. A. (1988). A quantile alternative for kurtosis. *The Statistician, 37*, 25–32.

Pitt, I. L. (2010). Superstar effects on royalty income in a performing rights organization. *Journal of Cultural Economics, 34*, 219–236. https://doi.org/10.1007/s10824-010-9123-1.

Pyne, S., Hu, X., Wang, K., Rossin, E., Lin, T. I., Maier, L. M., et al. (2009). Automated high-dimensional flow cytometric data analysis. *PNAS, 106*(21), 8519–8524. https://doi.org/10.1073/pnas.0903028106.

Wallgren, C. M. (1980). The distribution of the product of two correlated *t* variates. *Journal of the American Statistical Association, 75*, 996–1000. https://doi.org/10.1080/01621459.1980.10477585.

Walls, W. D. (2005). Modeling heavy tails and skewness in film returns. *Applied Financial Economics, 15*(17), 1181–1188. https://doi.org/10.1080/0960310050391040. http://www.tandf.co.uk/journals

Modelling Earthquakes: Characterizing Magnitudes and Inter-Arrival Times

Christophe Ley and Rosaria Simone

Abstract Statistical modelling of earthquakes is a challenging and delicate topic: research activity is vivid in this respect, and tailored to an improved understanding of the seismic phenomena and of their dynamics over time and space in all its shades. By surfing on some of the available literature, a critical investigation of the probability distributions best fitting earthquake sizes and inter-arrival times is performed, by using data on the Pacific Ring of Fire as illustrative example. As a by-product of our analysis, new ideas about adequate modelling of earthquake sizes and inter-event times together with the location of the earthquakes are advanced, which in turn could pave the way to further developments in a directional perspective.

1 Introduction

Earthquakes modelling is a challenging topic, yet its comprehension is crucial if we wish to improve our understanding of the phenomenon and of its dynamics over time and space. Finding the best probability distribution to model the various phenomena of the earthquakes is therefore an important task, and the devoted statistical literature is huge. Nevertheless, research directions narrow down mainly to three different topics: earthquake sizes (in terms of magnitude, for instance, or other measurement units), inter-arrival times and location. Our critical overview will focus on the first two problems. Indeed, an effective modelling of earthquake strengths within statistical seismology is required to deal with measurements of the *seismic hazard and risk*, thus assessing the probability of a major shock in a future time period in order to enhance both civil engineering and geophysics efforts

C. Ley (✉)
Department of Applied Mathematics, Computer Science and Statistics, Ghent University, Ghent, Belgium
e-mail: christophe.ley@ugent.be

R. Simone
Department of Political Sciences, Università degli Studi di Napoli Federico II, Naples, Italy

A. Bekker et al. (eds.), *Computational and Methodological Statistics and Biostatistics*, Emerging Topics in Statistics and Biostatistics,
https://doi.org/10.1007/978-3-030-42196-0_2

to prevent damages and understand earth-dynamics: according to Betbeder-Matibet (2008, Part 3), seismic hazard analysis concerns mainly the latter subject, whereas seismic risk addresses the former issues on earthquakes' impact on the territory. In both cases, the main challenge is to understand the tail behaviour of earthquake sizes and, as a consequence, a quite large time span should be considered (or large areas).

Let us first focus on earthquake sizes. Power-law models are very popular in these endeavours. Departing from the Gutenberg-Richter law, many research efforts are continuously addressed to the proposal of candidate size distributions for seismic events. Our critical overview tests classical proposals and discusses advantages and pitfalls of several alternatives: Pareto, tapered Pareto, truncated Gamma, and log-normal. Specifically, when dealing with deviations from the power law, an interesting scenario is opened when comparing the log-normal to power-laws. Evidence from our comparative overview suggests that a composite Pareto-Log-Normal model could provide an adequate fit to earthquake sizes. Indeed, model selection between a Pareto and a tapered Pareto model requires a careful analysis, since large shocks in the data are in small number and few deviations from that might change the results. Several datasets have been investigated and support this claim, referring to different geographical areas.

For inter-event times, instead, several candidate models have been proposed in the literature with reference to different geographical areas. Despite the wide range of models, it can be noticed that the Generalized Gamma model offers a universal framework after rescaling (Corral 2004). This distribution is a versatile tool allowing for both a scale-invariant part and an exponential taper, that features several other sub-models, for instance the Gamma and the Weibull. Our comparative analysis of model fits advances that indeed inter-event times obey to a unifying scheme that foresees the Generalized Gamma as an adequate leading model.

Our results from the present chapter pave the way to the next natural research step: the joint modelling of inter-arrival times and earthquake sizes together with the location on the surface of the earth where the earthquake took place. The addition of the location places the problem within a directional perspective. We shall briefly outline our idea of how to address this issue in future research.

The present chapter is organized as follows. In Sect. 2 we describe the data used throughout this chapter for our comparison of models. Section 3 then deals with the sizes of earthquakes, while Sect. 4 is concerned with inter-arrival times. In each section, we describe, discuss and compare the most used models from the literature, and propose alternative options. Conclusions and an outlook on future research are provided in Sect. 5.

2 The Pacific Ring of Fire

For illustrative purposes, we shall consider data referring to the Pacific Ring of Fire. This is a belt of active volcanoes that runs along the Pacific coasts from Oceania, Asia and the American continents, see Fig. 1. Data are taken from the Northern

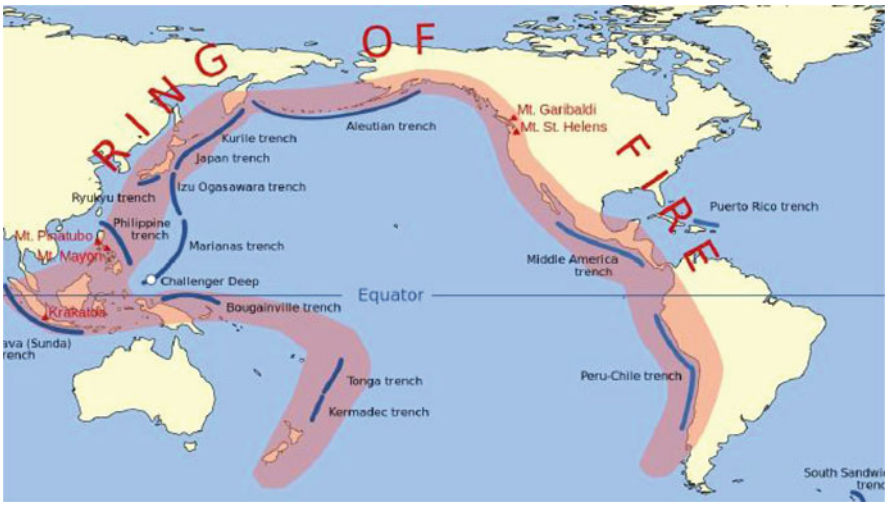

Fig. 1 Illustration of the Pacific Ring of Fire (image taken from Wikipedia)

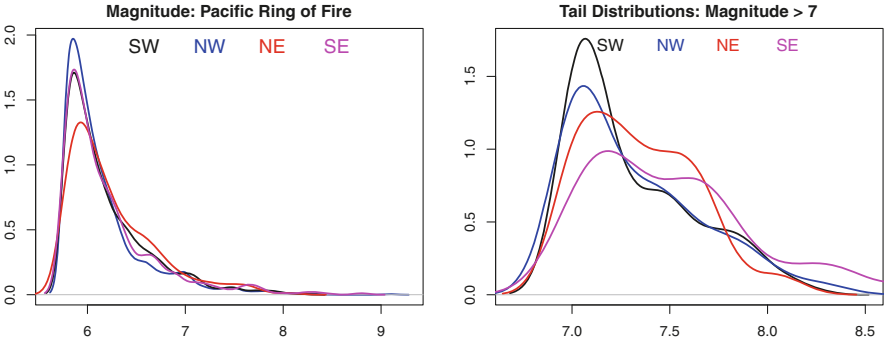

Fig. 2 Kernel density plots of earthquakes' magnitude exceeding the threshold of 5.8 (left panel) and with a focus on the tail distributions (right panel).

California Earthquake Data Center (NCEDC 2014) and have been downloaded from http://www.ncedc.org/anss/catalog-search.html.

Given that the faults have different seismic behaviour (see, e.g., Fig. 2), we will split the area in four corners: South-West (SW), South-East (SE), North-West (NW) and North-East (NE). The partition has been obtained using the tool https://mynasadata.larc.nasa.gov/latitudelongitude-finder/ that allows drawing a map of a polygon for which latitude and longitude are returned at its corners. Figure 2 displays kernel density plots of magnitudes of seismic events that exceed the threshold of 5.8 on the Richter scale, according to the above-mentioned division into four zones, at a depth that does not exceed 70 km. The reason we focus on this set of data is multifold: first, seismic hazard is mainly concerned with strong and

Table 1 Number of earthquakes in the SW area of the Pacific Ring of Fire above increasing thresholds, for the period from January 1st, 1967 to August 31st, 2017

Magnitude threshold	5.8	6.3	6.8	7	7.5	7.8	8
Number of events	1920	617	207	139	43	18	5

shallow earthquakes. Secondly, we do not deal with the issue of classification of elements of an earthquake sequence into main events, foreshocks and aftershocks: then, such magnitude constraint mitigates possible dependences among events. Last, it is a common practice to set a lower threshold for magnitude when the analysis of earthquake catalogs is concerned to take into account the incompleteness problem. Indeed, seismic detection devices are sensitive only to events that occur with a magnitude greater than a certain value, and thus they might not be able to monitor the weakest seismic activity. This is a prominent issue in studies concerning the economic impact of earthquakes (see Ficcadenti and Cerqueti 2017, for instance), and the development of statistical methods to assess the completeness of a catalog is a quite vivid topic in the literature (see Rydelk and Selwyn Sacks 1989; Schorlemmer et al. 2010, for instance). Nevertheless, the analysis hereafter pursued focuses on strong seismic events, thus the completeness of the used catalogues in the chosen time window can be safely claimed.

Throughout this chapter, we will mainly focus on the SW area of the Pacific Ring of Fire (latitude ranging from −42.740 to 0 and longitude ranging from 100 E to 180 E). The sample consists of $n = 1921$ seismic events occurring from January 1st, 1967 to August 31st, 2017. Table 1 reports the number of larger events (tails) for increasing thresholds.

Data analysis has been performed in the `R` environment, by using standard optimization and graphical tools. In addition, libraries `gendist` and `actuar`, available on the official CRAN repository, have been considered as far as composite models' estimation is concerned (Dutang et al. 2008; Abu Bakar 2015).

3 Modelling Earthquake Sizes

As underlined in Kagan and Schoenberg (2001) and firstly advanced by Vere-Jones et al. (2001), an effective modelling of the size or strength of earthquakes within statistical seismology requires dealing with measurements of both the seismic hazard and risk. In what follows, we shall present and discuss various options to model earthquake sizes. On the basis of our dataset we shall furthermore compare the fitting abilities of the distinct models.

3.1 The Gutenberg-Richter Law and the Exponential Distribution

The very first result you come across when digging into the statistics of earthquakes is the Gutenberg-Richter law (Gutenberg and Richter 1941), derived from the empirical observation that the number $N(m)$ of earthquakes with magnitude m exceeding a given threshold $\bar{m} \in \mathbb{R}_0^+$ is exponentially distributed, see Utsu (1999) for a comprehensive discussion. This law thus assumes that the magnitude size follows the (lower) truncated exponential distribution, with density $f(x; \lambda, \bar{m})$ and distribution function $F(x; \lambda, \bar{m})$ respectively given by:

$$f(x; \lambda, \bar{m}) = \lambda \exp\big(-\lambda(x-\bar{m})\big), \quad F(x; \lambda, \bar{m}) = 1-\exp\big(-\lambda(x-\bar{m})\big), \quad x > \bar{m}, \qquad (.1)$$

with scale parameter $\lambda \in \mathbb{R}_0^+$. In other words, on the log-scale the magnitude-frequency relation is of linear type, with slope that is approximately unitary and intercept related to the seismic activity of the region (Utsu 1999). The left panel of Fig. 3 shows evidence for the Gutenberg-Richter law for the SW corner of the Pacific Ring of Fire, on a doubly logarithmic scale as customarily.

Here we have set the threshold at the magnitude $\bar{m} = 5.8$ since seismic hazard analysis is mainly concerned with larger events. It is worth mentioning that such a threshold has to be set also when considering smaller and moderate earthquakes because of the limited sensitivity of the seismographic measurements.

However, the exponential distribution is not the best suited to express the earthquake sizes. Indeed, the size of earthquakes is a system that manifests a scale invariance property:

$$f(c\,x) = c^k\, f(x) \propto f(x), \qquad (2)$$

and this property is not warranted by the exponential law. Thus, alternative proposals ought to be looked at.

3.2 The Gutenberg-Richter Law Revisited and the Power-Law Distributions

In addition to the mentioned fact that the exponential law cannot satisfy the scale invariance property (2), magnitude is not a proper physical unit. For this reason, it is acknowledged that the most suited measure of earthquake size is the scalar seismic moment M, measured in Newton-meters (somehow related to the energy release (Utsu 1999)), related to magnitude m by a relation of the type:

$$m \approx \frac{2}{3}\log_{10}(M) - 6. \qquad (3)$$

This choice implies that the Gutenberg-Richter law should be based on a power-law distribution.

3.2.1 The Pareto Distribution

Let $\bar{M}$ be the seismic moment corresponding to the chosen magnitude truncation point $\bar{m}$ (here, $\bar{m} = 5.8$). The arguably most popular power-law distribution is the Pareto model (Pareto 1897) with density and distribution functions given respectively by:

$$f_P(x;\beta,\bar{M}) = \frac{\beta}{\bar{M}}\left(\frac{\bar{M}}{x}\right)^{\beta+1}, \qquad F_P(x;\beta,\bar{M}) = 1-\left(\frac{\bar{M}}{x}\right)^{\beta}, \qquad x \geq \bar{M}, \tag{4}$$

with scale parameter $\beta \in \mathbb{R}_0^+$. Then, the scale invariance requirement is fulfilled. However, even if this choice is practical and flexible (the tails of several distributions have a power law decay), this model has serious pitfalls. One is obvious, and it is the poor fit achieved for larger events which are overpredicted by the Pareto model (see the right panel of Fig. 3). Furthermore, this choice is difficult to support from a physical point of view because it entails an infinite mean value for the seismic moment when $\beta \leq 1$, thus mismatching the required finiteness of the seismic moment: see Sornette and Sornette (1999) for a discussion on this topic, among other results.

3.2.2 The Tapered Pareto Distribution

The inadequacy of the baseline Pareto model has led scholars to search for more performing distributions. Among the solutions that have been advanced, the most natural one is to truncate the distribution from above. This choice is not that

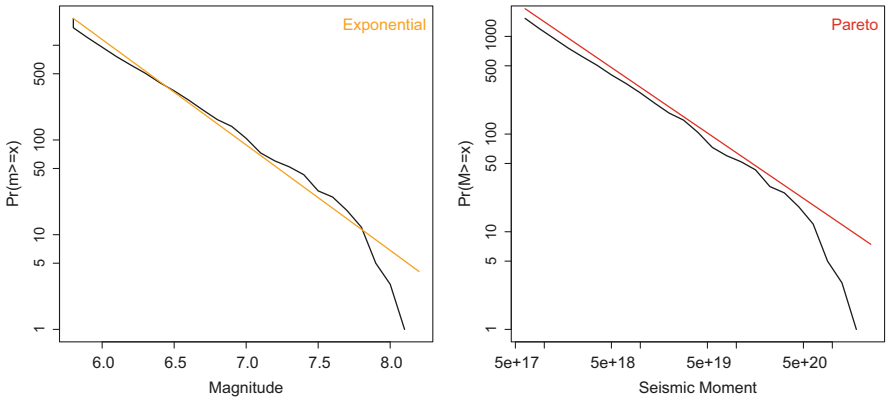

Fig. 3 Gutenberg-Richter law for the SW corner of the Pacific Ring of Fire: in terms of moment magnitude (left) and in terms of scalar seismic moment (right)

satisfactory because it contradicts both some physical principles of dissipative energy and the fact that every measurement is accompanied by error (Kagan 1993), so it is not conceivable that an earthquake of size slightly larger than the chosen hard cutoff has zero probability of occurrence (Lomnitz-Adler and Lomnitz 1979). These considerations motivate the modification of the Gutenberg-Richter law with the introduction of a soft cutoff θ, leading to the so-called tapered Pareto distribution, obtained with the application of an exponential smoother to the distribution function (Vere-Jones et al. 2001; Kagan and Schoenberg 2001):

$$f_{TAP}(x;\beta,\theta,\bar{M}) = \left(\frac{\bar{M}}{x}\right)^{\beta} \exp\left(\frac{\bar{M}-x}{\theta}\right)\left(\frac{\beta}{x}+\frac{1}{\theta}\right), \qquad x \geq \bar{M}, \tag{5}$$

$$F_{TAP}(x;\beta,\theta,\bar{M}) = 1-\left(\frac{\bar{M}}{x}\right)^{\beta} \exp\left(\frac{\bar{M}-x}{\theta}\right), \qquad x \geq \bar{M}. \tag{6}$$

The additional positive parameter θ is called the *corner moment* and governs the transition from a linear to an exponential decay for large shocks; the shape parameter β, instead, drives the decrease in frequency with seismic moments. For the sake of completeness, it is worth to mention that Vilfredo Pareto introduced both the Pareto distribution and its tapered version in his seminal work (Pareto 1897).

3.2.3 Parameter Estimation and Comparison

It is widely acknowledged by scientists and scholars in the fields of statistical seismology that the shape parameter β in both the Pareto and tapered Pareto distributions is easily estimable and it can be set as globally constant for certain classes of earthquakes of shallow events, like those related to subduction and those occurring in continental (estimated magnitude about 8), as well as in oceanic regions (estimated magnitude in the range $(5.8, 7.2)$). In particular, customarily it is assumed that $\hat{\beta} \in (0.6, 0.7)$, or slightly higher in certain cases: see Kagan and Schoenberg (2001) and references therein for a discussion on the topics. Given such a universality property, one usually considers a benchmark value for β (for instance, $\beta = 0.67$), and focuses, for the tapered Pareto, on the estimation of θ rather than pursuing joint estimation of parameters (Kagan and Schoenberg 2001). This practice is advantageous mostly because the estimation of the upper cutoff θ is tricky, depending mainly on the largest events (so all asymptotic results might be unreliable given the small sample size). Specifically, in order to deal with such issue, it is advisable to consider a large time span and wide geographical zones.

We consider maximum likelihood methods for estimating the parameters of both models (β for the Pareto and (β, θ) for its tapered version) in both situations when β is fixed to a certain value and not fixed. For data from the SW corner of the Pacific Ring of Fire, we plot the fit of both models in Fig. 4 in terms of complementary cumulative distribution function on log-log scale. The table reported along with Fig. 4 provides the parameter estimates and the value of the log-likelihood: for the

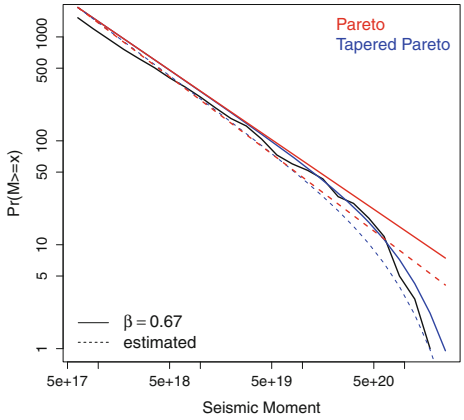

	$\hat{\beta}$	$\hat{\theta}$	$\hat{m}$	Loglik
		$\beta = 0.67$ fixed		
Pareto	0.67			-83826.55
Tap. Pareto	0.67	$1.2 \cdot 10^{21}$	8	-83820.45
		β estimated		
Pareto	0.74			-83816.85
Tap. Pareto	0.73	$1.7 \cdot 10^{21}$	8.08	-83813.30

Fig. 4 Pareto and tapered Pareto model for the SW corner of the Pacific Ring of Fire: results from joint estimation of parameters are displayed with dashed lines. The scale parameter β is set to 0.67 and both models are estimated conditional on this value

tapered Pareto model, we report also the magnitude value $\hat{m}$ corresponding to the estimated cutoff $\hat{\theta}$. We clearly see that the tapered Pareto provides a better fit than the Pareto distribution, and this both when β is fixed to 0.67 or estimated. This underpins the announced superiority of the tapered Pareto model.

3.3 Criticism on the Tapered Pareto Distribution

The good performance of the tapered Pareto model for earthquakes' seismic moment is not a universal rule. For instance, evidence is found against the tapered Pareto model in some data catalogs after the Sumatra earthquake in 2004 (Slifka et al. 2000). Specifically, in that case it is found that the best fitting performances are those granted by a truncated version of the Gamma distribution, which had already been considered for earthquake sizes in Sornette and Sornette (1999), Kagan (1997), and Kagan and Knopoff (1984).

Specifically, a Gamma distribution truncated at $\bar{M}$, with $\bar{M} \geq 0$, has probability density function given by:

$$f_{TG}(x; \tilde{\beta}, \theta, \bar{M}) = \frac{1}{\theta\, \Gamma(-\tilde{\beta}, \frac{\bar{M}}{\theta})} \left(\frac{\theta}{x}\right)^{1+\tilde{\beta}} \exp\left(-\frac{x}{\theta}\right), \qquad \bar{M} \leq x \leq \infty \tag{7}$$

with $\tilde{\beta} \in \mathbb{R}, \theta > 0$, and $\Gamma(\cdot, \cdot)$ denoting the upper incomplete Gamma function with possibly negative shape parameter, defined $\forall a \neq 0, a \neq -k, k \in \mathbb{N}$, for $x > 0$, as

$$\Gamma(a, x) = x^a \sum_{n=0}^{\infty} \frac{(-1)^n x^n}{n!(a+n)} \tag{8}$$

and satisfying

$$\Gamma(a+1, x) = a\Gamma(a, x) + x^a \exp(-x). \tag{9}$$

This model has both probabilistic and physical background as it arises when minimizing the Kullback-Leibler divergence with respect to the Pareto model (see Sornette and Sornette (1999) and references therein), and corresponds to the branching model under a subcritical regime (*cascade mechanism*). Nevertheless, in some sense the tapered Pareto distribution and the truncated Gamma are not that far apart. Indeed, it has been noticed in Slifka et al. (2000) that the tapered Pareto arises as a mixture of two truncated Gamma distributions:

$$f_{TAP}(x; \beta, \theta, \bar{M}) = p\, f_{TG}(x; \beta, \theta, \bar{M}) + (1-p)\, f_{TG}(x; \beta-1, \theta, \bar{M}), \qquad x \geq \bar{M}, \tag{10}$$

with

$$p = \beta\, \Gamma\left(-\beta, \frac{\bar{M}}{\theta}\right)\left(\frac{\bar{M}}{\theta}\right)^{\beta} \exp\left(\frac{\bar{M}}{\theta}\right), \qquad 1-p = \Gamma\left(1-\beta, \frac{\bar{M}}{\theta}\right)\left(\frac{\bar{M}}{\theta}\right)^{\beta} \exp\left(\frac{\bar{M}}{\theta}\right) \tag{11}$$

Via the properties of the incomplete Gamma, we can see that indeed the mixture of truncated Gamma distributions defining the tapered Pareto model is well-defined, since identity (9) for $x = \frac{\bar{M}}{\theta}$ reduces to:

$$\Gamma\left(1-\beta, \frac{\bar{M}}{\theta}\right) + \beta\Gamma\left(-\beta, \frac{\bar{M}}{\theta}\right) = \left(\frac{\theta}{\bar{M}}\right)^{-\beta} \exp\left(-\frac{\bar{M}}{\theta}\right), \tag{12}$$

and thus the mixing weights for (10) sum up to 1.

However, despite this theoretical match, the truncated Gamma model is somewhat more involved for estimation purposes because the normalizing constant depends on the incomplete Gamma function with possibly negative shape parameter. For this reason, the truncated Gamma distribution is not considered in our comparative analysis.

3.4 Power-Law or Log-Normal Distribution?

In the previous section, we discussed in how far the tapered Pareto model is a better choice to model earthquake sizes as it overcomes the tail rigidity of the Pareto model. However, estimation of the soft cutoff θ for tapered Pareto models is not stable as it requires a reasonable amount of data in the tail.

The literature has wondered in several directions about the identification of alternative good models for earthquake sizes. For instance, sometimes also the log-normal distribution with probability density function

$$f_{LogN}(x;\mu,\sigma) = \frac{1}{\sqrt{2\pi}\,\sigma\,x}\exp\left(-\left(\frac{\log(x)-\mu}{\sqrt{2}\sigma}\right)^2\right), \quad x>0, \mu\in\mathbb{R}, \sigma\in\mathbb{R}_0^+, \tag{13}$$

has been mistaken for a power law distribution (see Mitzenmacher (2003) for a comparative overview), and this is due to the fact that, taken on logarithmic scale and if σ is sufficiently large, the quadratic term in the logarithm of the density function becomes negligible, which then becomes approximately linear in $\log(x)$.

Indeed, the log-normal fit to earthquake size distributions has found support in the literature (Kagan 1969; Lomnitz 1964). In order to check its potential suitability, we apply the log-normal model on seismic moment data for the SW corner of the Pacific Ring of Fire and use the Bayesian Information Criterion (BIC) to assess fitting performances. As can be appreciated from Fig. 5 and Table 2, the fit implied by the log-normal improves when increasing the lower threshold, since the

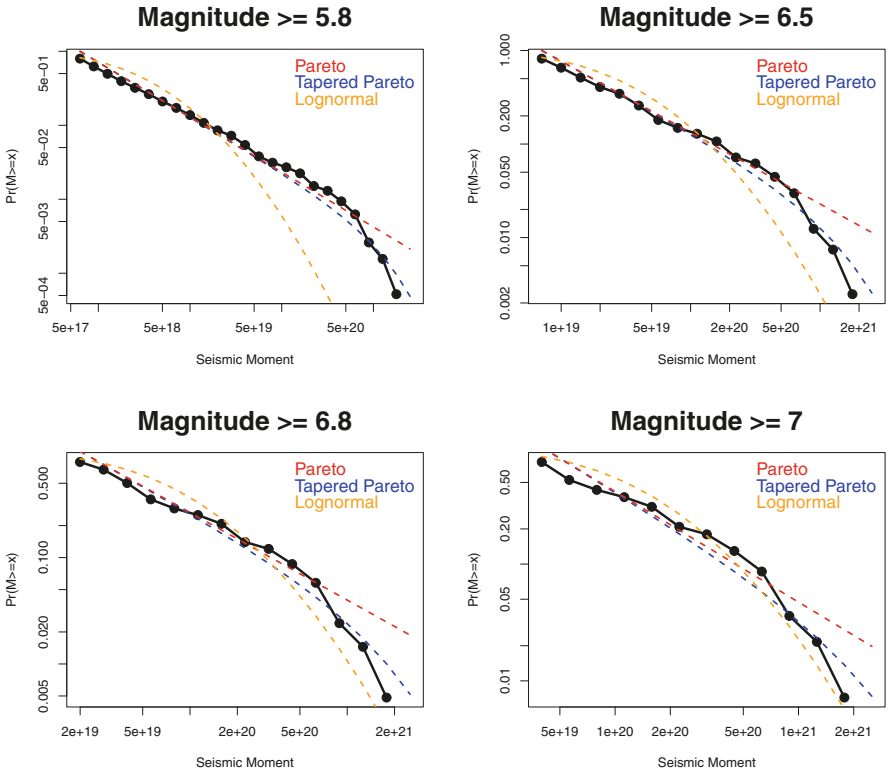

Fig. 5 SW corner of the Pacific Ring of Fire: fitting performances of earthquake sizes for competing models when varying the lower threshold

Table 2 SW corner of the Pacific Ring of Fire: (rounded) Bayesian Information Criterion (BIC) of competing models for earthquake sizes when varying the lower threshold

	$m \geq 5.8$	$m \geq 6.5$	$m \geq 6.8$	$m \geq 7$
Pareto	167,641	37,069	19,400	13,138
Tapered Pareto	167,634	37,062	19,396	13,135
Log-normal	169,614	37,404	19,565	13,267

difference in BIC with respect to the tapered Pareto model decreases. Hence the log-normal seems to be a valid choice, which we further investigate here.

Since the log-normal fit is sometimes mistaken to be of power-law type, and since it achieves a good fit when enlarging the upper cutoff, the idea fostered is to set up a procedure that (1) automatically checks if the power law model holds over the log-normal alternative in the tail, and (2) switches regime when the log-normal behaviour is supported by the data in the tail. In order to address this comparative test, we briefly recall a debate between (singly) truncated normal and exponential distributions, as if we were not working on the log-scale of seismic moments but directly on magnitudes.

The singly truncated normal distribution (STN) is an *increasing failure rate* distribution: it is a member of the *non-steep* class of the full exponential family, with sufficient statistic $T(x) = (x, -x^2)$ and Laplace transform (del Castillo 1994)

$$L_T(\theta_1, \theta_2) = \int_0^\infty \exp\left(\theta_1 x - \theta_2 x^2\right) dx, \quad (\theta_1, \theta_2) \in D, \tag{14}$$

where

$$D = (\mathbb{R} \times \mathbb{R}^+) \cup \mathbb{R}^- \times \{0\}. \tag{15}$$

Let us elaborate on two well-known particular situations:

- If $(\theta_1, \theta_2) \in Int(D) = \mathbb{R} \times \mathbb{R}^+$, and we set $\theta_1 = \frac{\mu}{\sigma^2}$, $\theta_2 = \frac{1}{2\sigma^2}$, then the truncated normal distribution arises (we denote by Φ the cumulative distribution function of the standard normal distribution):

$$f(x; \theta_1, \theta_2) = \left(\sqrt{2\pi}\sigma\, \Phi\left(\frac{\mu}{\sigma}\right)\right)^{-1} \exp\left(-\frac{(x-\mu)^2}{2\sigma^2}\right), \; x > 0; \tag{16}$$

- If (θ_1, θ_2) is on the border of D, which is $\mathbb{R}^- \times \{0\}$, then the exponential model arises:

$$f(x; \theta, 0) = -\theta \exp\left(\theta\, x\right), \quad \theta < 0, \; 0 < x < \infty. \tag{17}$$

It can be proved (Hollander and Proschan 1972) that the likelihood equations for the STN model resort to the following identity for the coefficient of variation c:

$$c^2 = C^2(\gamma), \qquad \gamma = -\frac{\theta_1}{2\sqrt{\theta_2}}, \tag{18}$$

where

$$C(x) = \frac{-xh(x) + x^2 + 0.5}{(h(x) - x)^2} - 1, \qquad h(x) = \frac{\exp(-x^2)}{2\sqrt{\pi}\left(1 - \Phi(\sqrt{2}\,x)\right)}. \tag{19}$$

The coefficient of variation for the singly truncated normal satisfies $c < 1$, whereas $c = 1$ on the border (in case the exponential is the reference model). Thus, the lower c, the larger evidence against the null of the hypothesis testing problem $\mathcal{H}_0$:*Exponential* against $\mathcal{H}_1$:*STN*. Thus, the critical region will be of the form $CR(\alpha) : C(\gamma) < k_\alpha$, for critical values k_α to be obtained numerically given the distribution of $C(\gamma)$ under the null. One of the strategies[1] proposed in del Castillo and Puig (1999) is based on the fact that the LRT statistic for this hypothesis testing problem can be written as a function of γ, say $W(\gamma)$: then, an estimate $\hat{\gamma}$ of γ can be obtained numerically by equating $W(\gamma)$ to the α-quantile of its asymptotic distribution, which is a 50:50 mixture of a degenerate mass at 0 and a χ^2_1 for a given significance level α (≈ 2.706 for $\alpha = 0.05$). Then, $\kappa_\alpha = \sqrt{C(\hat{\gamma})}$, with $C(\gamma)$ defined in (19), is the approximated lower tail percentage point of the model coefficient of variation under the null.

This is a UMPU test for exponentiality against STN (del Castillo and Puig 1999), which has been used to settle a debate on the distribution of city sizes (Malevergne et al. 2011). For earthquake sizes, this test can be applied for the tail distribution of the seismic moment to test the Pareto against the log-normal model. For illustrative purposes and for the SW corner of the Pacific Ring of Fire, we consider seismic moments values t lying in $[D_5, D_9]$[2] and the tail of seismic moments M such that $M \geq t$. For such data, we test the Exponential against the STN model on the transformed sample $\log\left(\frac{M}{t}\right)$, $M \geq t$. Results for the derived model with log-normal tails are displayed in Fig. 6 for one special value of t and summarized in Table 3 for all considered situations. In this table, n stands for the size of the sub-sample $M \geq t$ for each t and $m(t)$ denotes the magnitude corresponding to seismic moment t; the sample coefficient of variation c and the approximated κ_α are also reported. As we see, the null hypothesis is rejected in the majority of the cases, showing that the log-normal clearly improves on the basic Pareto distribution in the tails of earthquake sizes.

[1] Some other methods are proposed in del Castillo and Puig (1999) to speed up the convergence of the LRT distribution to its asymptotic distribution.

[2] Here, D_i denotes the ith decile of the seismic moments distribution.

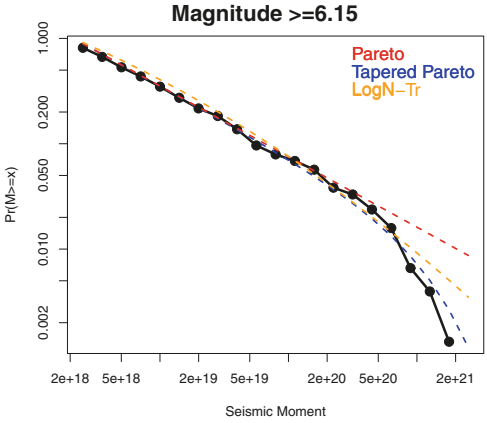

Fig. 6 Pareto, tapered Pareto and truncated log-normal models fitting the tails of seismic moments (expressed in magnitude $m \geq 6.15$) of the SW corner of the Pacific Ring of Fire

Table 3 Testing the exponentiality against the STN on tails of log-transformed seismic moments of the SW corner of the Pacific Ring of Fire

$m(t)$	n	$\kappa_{0.05}$	c	Reject $\mathcal{H}_0$?
6.15	758	0.9413	0.8966	TRUE
6.25	617	0.9351	0.8904	TRUE
6.35	506	0.9285	0.8962	TRUE
6.45	403	0.9201	0.8752	TRUE
6.5	403	0.9201	0.9906	FALSE
6.55	330	0.9120	0.8842	TRUE
6.65	264	0.9020	0.8772	TRUE
6.75	207	0.8898	0.8486	TRUE
6.8	207	0.8898	0.9693	FALSE
6.85	164	0.8769	0.8252	TRUE
6.9	164	0.8769	0.9452	FALSE
6.95	139	0.8668	0.8868	FALSE
7.05	104	0.8473	0.8406	TRUE
7.1	104	0.8473	0.9768	FALSE

3.5 A New Proposal: Composite Models

The evidence collected in the previous sections suggests that composite models might be a good modelling framework to deal with earthquake sizes: see Dominicy and Sinner (2017) for a concise introduction to the topic, here recalled briefly. Let $f_1(x)$ and $f_2(x)$ be two probability distributions over the positive real halfline, with cumulative distribution functions $F_1(x)$ and $F_2(x)$, respectively. Then the density of the composite model is defined as

$$f(x) = \begin{cases} c\, f_1^{\star}(x), & 0 < x \leq u \\ (1-c)\, f_2^{\star}(x), & u < x < \infty, \end{cases} \tag{20}$$

where

$$f_1^\star(x) = \frac{f_1(x)}{F_1(u)}, \qquad f_2^\star(x) = \frac{f_2(x)}{1 - F_2(u)} \tag{21}$$

For instance, the log-normal-Pareto composite model is very popular for actuarial data (Cooray and Ananda 2005).

Now, given the fact that the tails of earthquake sizes can be log-normal distributed, but the cut-off is data driven, the above strategy can be applied to identify the best option for a Pareto-log-normal composite model. The next section will shed light on the fitting abilities of this new model compared to the aforementioned models.

3.6 Full Comparative Analysis

For the SW corner of the Pacific Ring of Fire, Fig. 7 compares the fitting abilities of the Pareto, tapered Pareto and log-normal models to the Pareto-log-normal composite model. It is obvious both visually and numerically that this composite model improves on the other proposals.

Similar evidence can be checked also on a more complex dataset, taken from the Kaggle repository (https://www.kaggle.com/usgs/earthquake-database), and which concerns significant earthquakes occurring all over the globe in the period 1965–2016, with magnitude 5.5 or higher. Here we consider the sub-sample of $n = 9358$ shallow earthquakes (depth ≤ 70 km) with magnitude $m \geq 5.8$; see Fig. 8. Again the composite model yields the best fit.

We thus conclude that, for earthquake sizes, the composite Pareto-log-normal model is the best choice as probability distribution.

Model	BIC
Pareto	167660.7
Tap. Pareto	167648.5
Truncated Log-normal	167710.1
Pareto-LogN$^{(u=6.15)}$	**167546.2**

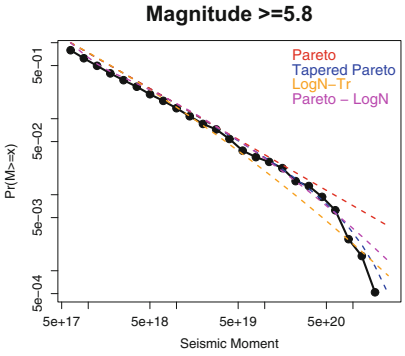

Fig. 7 Fitting results of competing models for the SW corner of the Pacific Ring of Fire

Model	BIC:
Pareto	815511.6
Tap. Pareto	815507
Pareto-LogN $^{(u=6.15)}$	815013.5

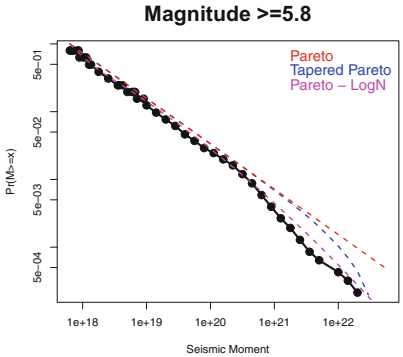

Fig. 8 Fitting results of competing models for the Kaggle dataset on significant earthquakes

4 Modelling Inter-Arrival Times

In this section, we undertake the analysis of inter-arrival times (IAT, for short) of seismic events. Again we shall focus only on shallow earthquakes (depth within 70 km) with magnitude exceeding the threshold $m \geq 5.8$. After a concise review of the state of the art on the topic, we challenge the Generalized Gamma model (Stacy 1962) as general reference model for earthquake inter-arrival times, with possible sub-specification at different geographical areas. We shall discuss performances of the main competing models on the sample of data for the Pacific Ring of Fire.

4.1 The State of the Art

For small events, it is acknowledged that a Poisson process is a good choice if after- and foreshocks are removed. For larger events, instead, empirical evidence has suggested temporal models allowing for a long-term clustering. Several models were tested to assess the distribution of inter-events of the selected earthquakes. The most popular distributions arising in geostatistics in the framework of earthquakes' IAT modelling are:

- the Gamma distribution, for example for a study in the Taiwan region (Chen et al. 2013):
- the log-normal distribution, for example for a study of earthquakes occurred in Japan and Greece (Musson et al. 2002);
- the tapered Pareto distribution, for example for modelling seismic events in Southern California (Schoenberg et al. 2009). These findings provided new insights in the understanding of the phenomenon, starting from formal assessment of the adequacy of the Pareto model to fit distance in time and in space

between a seismic event and the sequence of its aftershock (see references in Schoenberg et al. 2009).

In Schoenberg et al. (2009), the authors conclude their analysis by claiming that *Further study is needed to determine whether similar results are obtained with other catalogs and in other seismic zones*. Indeed, it is of foremost importance to characterize earthquakes' statistical distributions regardless of the data under examination. Stemming from this principle, we pursue a comparative analysis on the behaviour of competing models by adding an overarching model: the generalized Gamma distribution. This proposal has already appeared in the literature as a universal distribution for rescaled recurrence times (see Corral 2004 and references therein), but, to the best of our knowledge, no extensive comparative analysis of this model with respect to other state of the art models has been pursued so far.

4.2 The Generalized Gamma Model

The goal of this very short section is to present the Generalized Gamma model (Stacy 1962) with density

$$f_{GG}(x;a,b,s) = \frac{b\,x^{a-1}}{s^a\,\Gamma(\frac{a}{b})}\,\exp\left(-\left(\frac{x}{s}\right)^b\right).$$

This distribution is a versatile tool allowing for both a scale-invariant part and an exponential taper, and it features several other sub-models, for instance the Gamma and the Weibull for specific parameter values (see Fig. 9). Its fitting abilities for IAT will be evaluated in the next section with respect to model sub-specifications and alternative candidates.

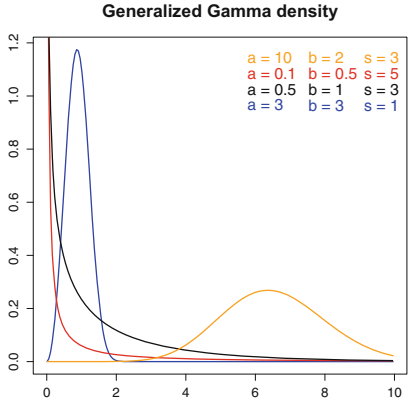

- Weibull ($a = b$):

$$f_W(x;a,s) = \frac{a\,x^{a-1}}{s^a}\,\exp\left(-\left(\frac{x}{s}\right)^a\right)$$

- Gamma ($b = 1$):

$$f_G(x;a,s) = \frac{x^{a-1}}{s^a\Gamma(a)}\,\exp\left(-\frac{x}{s}\right)$$

Fig. 9 Generalized Gamma probability density functions for specific parameters, and submodels

Table 4 Comparison of the competing models for modelling inter-arrival times of earthquakes in the Pacific Ring of Fire

BIC	S-W	N-W	N-E	S-E	pv: K-S test	S-W	N-W	N-E	S-E
Tap. Pareto	11,330.35	9894.62	4855.66	3584.17	Tap. Pareto	0.010	0.005	0.557	0.133
Gen. Gamma	11,431.94	10,021.52	4910.34	3629.69	Gen. Gamma	0.409	0.235	0.090	0.522
Log-normal	12,061.30	10,721.48	5247.76	3765.94	Log-normal	$\star$	$\star$	$\star$	$\star$
Gamma	11,430.28	10,026.10	4913.08	3626.20	Gamma	0.082	0.017	0.020	0.459
Weibull	11,511.90	10,143.08	4952.76	3658.86	Weibull	$\star$	$\star$	0.006	0.005
n	1920	1656	579	455	n				

Left: BIC values, Right: p-values associated with the Kolmogorov-Smirnov goodness-of-fit test ($\star$: p-value $< 10^{-10}$)

4.3 Comparison of the Generalized Gamma Distribution to State-of-the-Art Models

For the chosen competing models, we will check goodness-of-fit on inter-event times measured in days since the last occurrence, and this for all four regions of the Pacific Ring of Fire. In the same spirit as Schoenberg et al. (2009), the comparative analysis will be based on QQ-plots, the Kolmogorov-Smirnov goodness-of-fit test and the BIC. Specifically, for earthquakes data in the chosen time windows, we see that the tapered Pareto model gives dominant goodness-of-fit in terms of the BIC (Table 4, left), and that the Generalized Gamma is, in general, the second to best (if one considers its sub-specifications). Regarding the KS test, the Generalized Gamma yields the largest p-values and would be the preferable model from that perspective (Table 4, right). Figure 10 displays the QQ-plot of the selected distributions fitted to inter-arrival times of seismic events in the given time windows for the Pacific Ring of Fire. Both the tapered Pareto and Generalized Gamma lead to the best visual fit, underlining that these two distributions ought to be chosen for modelling IATs, at least for the Pacific Ring of Fire. However, given that the tapered Pareto is sometimes only weakly supported by the KS test, we suggest that the Generalized Gamma model should be chosen as the generating model for the inter-arrival times in general.

In the spirit of Nishenko (1991); Panagiotopoulos (1995), we conclude this section by reporting the estimated probability, under a given model, for an earthquake of magnitude greater than a certain threshold to occur within a month (p_{30}) and within a year (p_{365}) from the last event: see Table 5. Inter-event times have been recomputed on each sub-sample of observations determined by a magnitude threshold. Standard maximum likelihood estimation has been implemented in the `R` environment: for the tails samples ($m \geq 7, m \geq 7.5$), initial values should be chosen carefully, and in certain cases, it is advisable to trim data from below (by eliminating the lowest 5% of the distribution, for instance; see also Schoenberg et al. 2009).

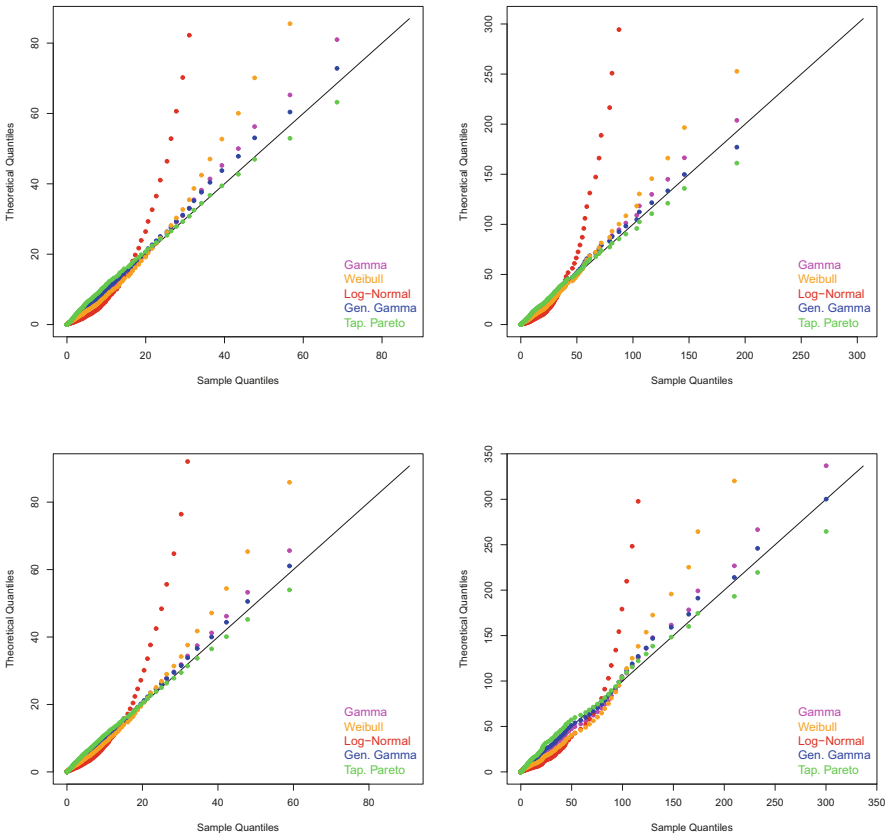

Fig. 10 QQ-plots of the competing distributions for the inter-arrival times in the North-West corner (top left), North-East corner (top right), South-West corner (bottom-left), and South-East corner (bottom-right) of the Pacific Ring of Fire

5 Conclusions and Future Development Plan

We have discussed and compared various probability distributions for modelling earthquake sizes and inter-arrival times. We have found that, for earthquake sizes, the composite Pareto-log-normal model is the best choice, while for inter-arrival times the Generalized Gamma distribution is the safest option. Of course, we should keep in mind that these conclusions are drawn on the basis of data from the Pacific Ring of Fire, and a large-scale comparison should be done. This will be achieved in future work, but we hope to have stimulated interest in these probability distributions for seismological research purposes.

We conclude this chapter by presenting the next and more challenging issue that we will address, namely the combination of earthquake size and/or IAT with the location on the earth where the earthquake took place. As a starting point, we may

Table 5 The Pacific Ring of Fire: probability of occurrence within 30 days (p_{30}) and within 1 year (p_{365}) of an earthquake of size exceeding a given threshold, assuming different model specifications

	$m \geq 5.8$			$m \geq 6.5$			$m \geq 7$			$m \geq 7.5$		
	BIC	p_{30}	p_{365}	BIC	p_{30}	p_{365}	BIC	p_{30}	p_{365}	BIC	p_{30}	p_{365}
South-West corner												
Tap. Pareto	11,330.35	0.933	1	3555.99	0.550	0.99	1529.03	0.331	0.873	543.50	0.244	0.602
Gen. Gamma	11,431.93	0.923	1	3605.27	0.590	0.997	1532.64	0.369	0.906	588.082	0.279	0.663
Log-normal	12,061.32	0.860	0.984	3769.01	0.665	0.920	1606.93	0.498	0.831	582.78	0.390	0.696
Gamma	11,430.29	0.922	1	3603.20	0.608	0.994	1539.41	0.398	0.907	555.71	0.284	0.686
Weibull	11,511.91	0.914	0.999	3631.61	0.629	0.985	1552.65	0.406	0.895	562.07	0.276	0.695
South-East corner												
Tap. Pareto	3584.18	0.608	0.998	1016.25	0.330	0.808	448.80	0.179	0.561	238.47	0.127	0.377
Gen. Gamma	3629.69	0.650	0.996	1033.59	0.374	0.806	455.83	0.217	0.588	246.40	0.10	0.448
Log-normal	3765.94	0.723	0.92	1076.62	0.496	0.784	470.44	0.299	0.654	248.26	0.119	0.497
Gamma	3626.20	0.668	0.992	1031.30	0.386	0.823	452.70	0.217	0.608	242.13	0.106	0.404
Weibull	3658.86	0.70	0.976	1041.82	0.403	0.824	455.12	0.204	0.627	242.96	0.089	0.408
North-West corner												
Tap. Pareto	9894.62	0.905	1	2694.17	0.422	0.987	1242.79	0.247	0.816	453.98	0.188	0.560
Gen. Gamma	10,021.10	0.894	1	2714.25	0.487	0.989	1255.50	0.311	0.857	462.53	0.222	0.585
Log-normal	10,721.48	0.832	0.971	2856.58	0.586	0.888	1313.70	0.421	0.793	484.82	0.322	0.653
Gamma	10,026.09	0.895	0.999	2714.77	0.509	0.981	1252.95	0.321	0.862	461.54	0.224	0.625
Weibull	10,143.08	0.889	0.998	2736.12	0.522	0.969	1260.47	0.316	0.859	465.51	0.202	0.632
North-East corner												
Tap. Pareto	4868.34	0.628	0.999	1697.27	0.269	0.943	639.24	0.186	0.579	234.48	0.190	0.413
Gen. Gamma	4922.95	0.652	0.999	1715.74	0.286	0.941	848.52	0.180	0.648	248.51	0.220	0.589
Log-normal	5261.40	0.686	0.931	1774.11	0.377	0.862	673.67	0.252	0.679	256.36	0.304	0.583
Gamma	4925.93	0.672	0.994	1712.13	0.294	0.936	645.46	0.178	0.671	242.37	0.198	0.516
Weibull	4965.80	0.683	0.997	1714.64	0.289	0.934	647	0.164	0.680	245.47	0.174	0.519

consider the Abe-Ley proposal for circular-linear data (Abe and Ley 2017), defined for $\theta \in [-\pi, \pi), x \in [0, \infty)$ by:

$$f(x,\theta) = \frac{\big(1+\lambda\ \sin(\theta-\mu)\big)}{2\pi\ \cosh(\kappa)}\ \frac{a\,x^{a-1}}{s^a}\ \exp\left(-\left(\frac{x}{s}\right)^a\big(1+\tanh(k)\ \cos(\theta-\mu)\big)\right) \tag{22}$$

where $\mu \in [-\pi, \pi)$ is the location parameter on the circle, $\kappa \geq 0$ the circular concentration, $\lambda \in (-1, 1)$ regulates circular skewness, and a, s are the shape parameters as in the classical Weibull distribution. The Abe-Ley model has originally been termed WeiSSVM because it is a combination of the linear Weibull distribution and the circular sine-skewed von Mises distribution, see Abe and Ley (2017) for details. This model has already been proven to be a versatile and effective tool for a broad set of applications (Lagona et al. 2015; Sadeghianpourhamami et al. 2019; Cremers et al. 2019), due to easiness of parameter interpretation and estimation. We intend to propose an extension of this model for spherical-linear data, where now the non-linear parameter θ no longer takes values on the unit circle, but rather on the unit sphere. With this model, we shall be able to model earthquake size, IAT and location, which would definitely lead to new means of analysing earthquake data. In particular, we will then use as linear parts the composite Pareto-log-normal model and the Generalized Gamma distribution, based on the results of the comparative analysis done in this chapter.

Acknowledgements Both authors thank two anonymous reviewers for their helpful comments. Christophe Ley thanks the Fonds Wetenschappelijk Onderzoek (FWO) for financial support via the Krediet aan Navorsers grant with reference number 1510391N.

References

Abe, T., & Ley, C. (2017). A tractable, parsimonious and flexible model for cylindrical data, with applications. *Econometrics and Statistics, 4*, 91–104.

Abu Bakar, S. A. (2015). gendist: Generated probability distribution models. R package version 1.0. https://CRAN.R-project.org/package=gendist

Betbeder-Matibet, J. (2008). Seismic engineering. *Wiley Online Library*. https://doi.org/10.1002/9780470611135. Online ISBN:9780470611135.

Chen, C.-H., Wang, J.-P., Wu, Y.-M., Chan, C.-H., & Chang, C.-H. (2013). A study of earthquake inter-occurrence times distribution models in Taiwan. *Natural Hazards, 69*, 1335–1350.

Cooray K., & Ananda M. M. A. (2005). Modeling actuarial data with a composite lognormal-Pareto model. *Scandinavian Actuarial Journal, 5*, 321–334.

Corral, A. (2004). Long-term clustering, scaling, and universality in the temporal occurrence of earthquakes. *Physical Review Letters, 92*, 108501.

Cremers, J., Pennings, H. J. M., & Ley, C. (2019). *Regression models for cylindrical data in psychology*. Multivariate Behavioral Research, in press.

del Castillo, J. (1994). The singly truncated normal distribution, a non-steep exponential family. *Journal of the Royal Statistical Society Series A, 46*, 57–66.

del Castillo, J., & Puig, P. (1999). The best test of exponentiality against singly truncated normal alternatives. *Journal of the American Statistical Association, 94*, 529–532.

Dominicy, Y., & Sinner, C. (2017). Distributions and composite models for size-type data. In T. Hokimoto (Ed.), *Advances in statistical methodologies and their applications to real problems*. London: IntechOpen. https://doi.org/10.5772/66443.

Dutang, C., Goulet, V., & Pigeon, M. (2008). actuar: An R package for actuarial science. *Journal of Statistical Software, 25*(7), 1–37. http://www.jstatsoft.org/v25/i07

Ficcadenti, V., & Cerqueti, R. (2017). Earthquakes economic costs through rank-size laws. *Journal of Statistical Mechanics: Theory and Experiments, 2017*, 083401.

Gutenberg, B., & Richter, C. F. (1941). Seismicity of the Earth. *Geological Society of America Special Papers, 34*, 1–131.

Hollander, M., & Proschan, F. (1972). Testing whether new is better than used. *Annals of Mathematical Statistics, 43*, 1136–1146.

Kagan, Y. Y. (1969). A study of the energy of the seismoacoustic pulses arising during bursts in a coal bed. *Izvestiya Physics of the Solid Earth*, 85–91 (English translation).

Kagan, Y. Y. (1993). Statistics of characteristic earthquakes. *Bulletin of the Seismological Society of America, 83*, 7–24.

Kagan, Y. Y. (1997). Seismic moment-frequency relation for shallow earthquakes: Regional comparison. *Journal of Geophysical Research, 102*, 2835–2852.

Kagan, Y. Y., & Knopoff, L. (1984). A stochastic model of earthquake occurrence. In *Proceedings of the 8th International Conference on Earthquake Engineering* (Vol. 1, pp. 295–302).

Kagan, Y. Y., & Schoenberg, F. (2001). Estimation of the upper cutoff parameter for the tapered Pareto distribution. *Journal of Applied Probability, 38A*, 168–185.

Lagona, F., Picone, M., & Maruotti, A. (2015). A hidden Markov model for the analysis of cylindrical time series. *Environmetrics, 26*, 534–544.

Lomnitz, C. (1964). Estimation problems in earthquake series. *Tectonophysics, 1*, 130–144.

Lomnitz-Adler, J., & Lomnitz, C. (1979). A modified form of the Gutenberg-Richter magnitude-frequency relation. *Bulletin of the Seismological Society of America, 69*, 1209–1214.

Malevergne, Y., Pisarenko, V., & Sornette, D. (2011). Testing the Pareto against the lognormal distribution with the uniformly most powerful unbiased test applied to the distribution of cities. *Physical Review E, 83*, 036111.

Mitzenmacher, M. (2003). A brief history of generative models for power law and lognormal distributions. *Internet Mathematics, 1*, 226–251.

Musson, R. M. W., Tsapanos, T., & Nakas, C. T. (2002). A power-law function for earthquake interarrival time and magnitude. *Bulletin of the Seismological Society of America, 92*, 1783–1794.

NCEDC (2014). Northern California Earthquake Data Center. UC Berkeley Seismological Laboratory. https://doi.org/10.7932/NCEDC.

Nishenko, S. P. (1991). Circum Pacific seismic potential. *Pageoph, 135*, 169–259.

Panagiotopoulos, D. C. (1995). Long-term earthquake prediction in Central America and Caribbean Sea based on the time- and magnitude-predictable model. *Bulletin of the Seismological Society of America, 85*, 1190–1201.

Pareto, V. (1897). Cours d'Économie Politique, Tome Second, Lausanne, F. Rouge, quoted by Pareto, V. (1964), Oeuvres Complètes, published by de Giovanni Busino, Genève, Droz, vol II.

Rydelk, P. A., & Sacks, I. S. (1989). Testing the completeness of earthquake catalogues and the hypothesis of self-similarity. *Nature, 337*, 251–253.

Sadeghianpourhamami, N., Benoit, D. F., Deschrijver, D., & Develder, C. (2019). Bayesian cylindrical data modeling using Abe-Ley mixtures. *Applied Mathematical Modelling, 68*, 629–642.

Schoenberg, F. P., Barr, C., & Seo, J. (2009). The distribution of Voronoi cells generated by Southern California earthquake epicenters. *Environmetrics, 20*, 159–171.

Schorlemmer, D., Mele, F., & Marzocchi, W. (2010). A completeness analysis of the National Seismic Network of Italy. *Journal of Geophysical Research 115*, B04308.

Slifka, M. K., Whitton, J. L., Sierra, I., & Corral, A. (2000). Deviation from power law of the global seismic moment distribution. *Scientific Reports, 7*, 40045. https://doi.org/10.1038/srep40045.

Sornette, D., & Sornette, A. (1999). General theory of the modified Gutenberg-Richter law for large seismic moment. *Bulletin of the Seismological Society of America, 89*, 1121–1130.

Stacy, E. W. (1962). A generalization of the Gamma distribution. *Annals of Mathematical Statistics, 33*, 1187–1192.

Utsu, T. (1999). Representation and analysis of the earthquake size distribution: A historical review and some new approaches. *Pure and Applied Geophysics, 155*, 509–535.

Vere-Jones, D., Robinson, R., & Yang W. Z. (2001). Remarks on the accelerated moment release model: Problems of model formulation, simulation and estimation. *Geophysical Journal International, 144*, 517–531.

Multivariate Order Statistics Induced by Ordering Linear Combinations of Components of Multivariate Elliptical Random Vectors

Ahad Jamalizadeh, Roohollah Roozegar, Narayanaswamy Balakrishnan, and Mehrdad Naderi

Abstract In this chapter, by considering a np-dimensional random vector $\left(\mathbf{X}_1^\top, \ldots, \mathbf{X}_n^\top\right)^\top$, $\mathbf{X}_i \in \mathbb{R}^p$, $i = 1, \ldots, n$, having a multivariate elliptical distribution, we derive the exact distribution of multivariate order statistics induced by ordering linear combinations of the components. These induced multivariate order statistics are often referred to as the concomitant vectors corresponding to order statistics from multivariate elliptical distribution. Specifically, we derive a mixture representation for the distribution of the rth concomitant vector, and also for the joint distribution of the rth order statistic and its concomitant vector. We show that these distributions are indeed mixtures of multivariate unified skew-elliptical distributions. The important special cases of multivariate normal and multivariate student-t distributions are discussed in detail. Finally, the usefulness of the established results is illustrated with a real dataset.

A. Jamalizadeh (✉)
Department of Statistics, Shahid Bahonar University, Kerman, Iran
e-mail: a.jamalizadeh@uk.ac.ir

R. Roozegar
Department of Mathematics, College of Sciences, Yasouj University, Yasouj, Iran
e-mail: roozegar@yu.ac.ir

N. Balakrishnan
McMaster University, Hamilton, ON, Canada
e-mail: bala@mcmaster.ca

M. Naderi
Department of Statistics, Faculty of Natural & Agricultural Sciences, University of Pretoria, Pretoria, South Africa
e-mail: m.naderi@up.ac.za

A. Bekker et al. (eds.), *Computational and Methodological Statistics and Biostatistics*, Emerging Topics in Statistics and Biostatistics,
https://doi.org/10.1007/978-3-030-42196-0_3

1 Introduction

Let $\mathbf{X}_1, \ldots, \mathbf{X}_n$ be a set of n independent and identically distributed p-dimensional absolutely continuous random vectors. Over the past few decades, several papers have appeared in which efforts have been made to generalize the concept of order statistics from the univariate case to the multivariate case. All these works can be subsumed by an ordering induced, where we consider the random vectors $\mathbf{X}_i$'s as concomitants, by an univariate auxiliary random variable. This auxiliary random variable might be one of the components or a linear combination of the components. In this regard, David (1973) was the first to introduce the concept of multivariate order statistics in the case when the multivariate data are ordered by one of its components. The behavior of these induced multivariate order statistics is of interest in many practical situations (see David 1982; Bhattacharya 1984). Balakrishnan (1993) and Song and Deddens (1993) computed the moments of multivariate order statistics induced by an ordering of linear combinations of the components of a multivariate normal distribution. Finally, Arnold et al. (2009) introduced a general form for the distribution of the rth multivariate order statistic via multivariate concomitants.

It is important to mention here that all the above mentioned works are based on independent and identically distributed (i.i.d.) samples. But, this assumption may not be realistic in the some situations. In this chapter, we generalize these results for the case when the joint distribution of the random vectors $\mathbf{X}_1, \ldots, \mathbf{X}_n$ follows a general structure as

$$\begin{pmatrix} \mathbf{X}_1 \\ \vdots \\ \mathbf{X}_n \end{pmatrix} \sim EC_{np}\left(\boldsymbol{\mu} = \begin{pmatrix} \boldsymbol{\mu}_1 \\ \vdots \\ \boldsymbol{\mu}_n \end{pmatrix}, \boldsymbol{\Sigma} = \begin{pmatrix} \boldsymbol{\Sigma}_{11} & \cdots & \boldsymbol{\Sigma}_{1n} \\ \vdots & \ddots & \vdots \\ \boldsymbol{\Sigma}_{n1} & \cdots & \boldsymbol{\Sigma}_{nn} \end{pmatrix}, h^{(np)}\right), \tag{1}$$

the $(n \times p)$-dimensional elliptical distribution with location parameter $\boldsymbol{\mu}$, scale parameter $\boldsymbol{\Sigma}$ and density generator $h^{(n)}$. The class of elliptically distributions is a rich family of symmetric distributions which contain most important distributions like normal, student-t, Cauchy, Laplace and logistic distributions.

So, the main objective of this chapter is to present an exact distribution for the rth multivariate order statistic induced by ordering linear combinations of the components when the random vectors $\mathbf{X}_1, \ldots, \mathbf{X}_n$ follow the distribution presented in (1). We also derive the joint distribution of the rth order statistic and its concomitant vector in this case. We show that these distributions are indeed mixtures of multivariate unified skew-elliptical (SUE) distributions and use them to discuss some properties.

2 Preliminaries

An n-dimensional random vector $\mathbf{X}$ is said to have an elliptically contoured (EC) distribution with location vector $\boldsymbol{\mu} \in \mathbb{R}^n$, non-negative definite dispersion matrix $\boldsymbol{\Sigma} \in \mathbb{R}^{n\times n}$ and characteristic generator $\varphi^{(n)}$ if the centered random vector $\mathbf{X}-\boldsymbol{\mu}$ has characteristic function of the form $\varphi^{(n)}_{\mathbf{X}-\boldsymbol{\mu}}(\mathbf{t}) = \varphi^{(n)}\left(\mathbf{t}^\top \boldsymbol{\Sigma}\mathbf{t}\right)$, for $\mathbf{t} \in \mathbb{R}^n$. Moreover, if the probability density function (pdf) of $\mathbf{X}$ exists, it is of the form

$$f_{EC_n}\left(\mathbf{x}\,;\boldsymbol{\mu},\boldsymbol{\Sigma},h^{(n)}\right) = |\boldsymbol{\Sigma}|^{-\frac{1}{2}}\, h^{(n)}\left((\mathbf{x}-\boldsymbol{\mu})^\top \boldsymbol{\Sigma}^{-1}(\mathbf{x}-\boldsymbol{\mu})\right),\quad \mathbf{x}\in\mathbb{R}^n, \tag{2}$$

when $h^{(n)}$ is the density generator function. In this case, we use the notation $\mathbf{X} \sim EC_n\left(\boldsymbol{\mu},\boldsymbol{\Sigma},h^{(n)}\right)$. For more details, see Kelker (1970), Cambanis et al. (1981) and Fang et al. (1990).

Over the past two decades, several authors have proposed different forms of univariate and multivariate skew elliptical distributions to accommodate both asymmetry and heavy tails. Interested readers may refer to Azzalini (1985), Henze (1986), Azzalini and Dalla Valle (1996), Arnold and Beaver (2002) and Genton (2004). A unification of different forms of skew-elliptical distributions has been presented by Arellano-Valle and Azzalini (2006) in the following way.

Let $\mathbf{U}$ and $\mathbf{V}$ be two m and n dimensional random vectors, respectively, and

$$\begin{pmatrix}\mathbf{U}\\ \mathbf{V}\end{pmatrix} \sim EC_{m+n}\left(\begin{pmatrix}\boldsymbol{\eta}\\ \boldsymbol{\xi}\end{pmatrix},\begin{pmatrix}\boldsymbol{\Gamma} & \boldsymbol{\Lambda}^\top\\ \boldsymbol{\Lambda} & \boldsymbol{\Omega}\end{pmatrix},h^{(m+n)}\right). \tag{3}$$

The n-dimensional random vector $\mathbf{X}$ is then said to have the multivariate unified skew-elliptical (SUE) distribution with parameter $\boldsymbol{\theta} = (\boldsymbol{\xi},\boldsymbol{\eta},\boldsymbol{\Omega},\boldsymbol{\Gamma},\boldsymbol{\Lambda})$, denoted by $\mathbf{X} \sim SUE_{n,m}\left(\boldsymbol{\xi},\boldsymbol{\eta},\boldsymbol{\Omega},\boldsymbol{\Gamma},\boldsymbol{\Lambda},h^{(m+n)}\right)$ or simply by $\mathbf{X} \sim SUE_{n,m}\left(\boldsymbol{\theta},h^{(m+n)}\right)$, if

$$\mathbf{X} \overset{d}{=} \mathbf{V} \mid (\mathbf{U} > \mathbf{0}), \tag{4}$$

where $\boldsymbol{\xi} \in \mathbb{R}^n$ and $\boldsymbol{\eta} \in \mathbb{R}^m$ are location vectors, $\boldsymbol{\Omega} \in \mathbb{R}^{n\times n}$ and $\boldsymbol{\Gamma} \in \mathbb{R}^{m\times m}$ are dispersion matrices, $\boldsymbol{\Lambda} \in \mathbb{R}^{n\times m}$ is a skewness/shape matrix and $h^{(m+n)}$ is the density generator function. The pdf of $\mathbf{X}$ takes on the form (see Arellano-Valle and Genton 2010 or Arellano-Valle and Azzalini 2006)

$$\begin{aligned} &g_{SUE_{n,m}}\left(\mathbf{x};\boldsymbol{\theta},h^{(m+n)}\right) \\ &= \frac{f_{EC_n}\left(\mathbf{x};\boldsymbol{\xi},\boldsymbol{\Omega},h^{(n)}\right)}{F_{EC_m}\left(\boldsymbol{\eta};\boldsymbol{\Gamma},h^{(m)}\right)} \times F_{EC_m}\left(\boldsymbol{\eta}+\boldsymbol{\Lambda}^\top\boldsymbol{\Omega}^{-1}(\mathbf{x}-\boldsymbol{\xi})\,;\boldsymbol{\Gamma}-\boldsymbol{\Lambda}^\top\boldsymbol{\Omega}^{-1}\boldsymbol{\Lambda},h^{(m)}_{w(\mathbf{x})}\right),\ \mathbf{x}\in\mathbb{R}^n, \end{aligned} \tag{5}$$

where $F_{EC_m}\left(\cdot;\boldsymbol{\Gamma},h^{(m)}\right)$ denotes the cdf of $EC_m\left(\mathbf{0},\boldsymbol{\Gamma},h^{(m)}\right)$ and $w(\mathbf{x}) = (\mathbf{x}-\boldsymbol{\xi})^\top\boldsymbol{\Omega}^{-1}(\mathbf{x}-\boldsymbol{\xi})$. Furthermore, we can generate the SUE distribution by using the convolution approach, utilizing the stochastic representation

$$\mathbf{X} \stackrel{d}{=} \boldsymbol{\xi} + \boldsymbol{\Lambda}\boldsymbol{\Gamma}^{-1}\mathbf{X}_{0\boldsymbol{\eta}} + \mathbf{X}_1, \tag{6}$$

where $\mathbf{X}_1 \sim EC_n\left(\mathbf{0}, \boldsymbol{\Omega} - \boldsymbol{\Lambda}\boldsymbol{\Gamma}^{-1}\boldsymbol{\Lambda}^\top, h^{(n)}\right)$ and $\mathbf{X}_{0\boldsymbol{\eta}} \sim TEC_m\left(-\boldsymbol{\eta}; \mathbf{0}, \boldsymbol{\Gamma}, h^{(m)}\right)$, with $TEC_m(\mathbf{c}; \boldsymbol{\mu}, \boldsymbol{\Sigma})$ representing the multivariate elliptical variable with components truncated below $\mathbf{c}$. From (6), we can easily derive the first moment of SUE distribution, as presented in the following lemma.

Lemma 1 *If* $\mathbf{X} \sim SUE_{n,m}\left(\boldsymbol{\xi}, \boldsymbol{\eta}, \boldsymbol{\Omega}, \boldsymbol{\Gamma}, \boldsymbol{\Lambda}, h^{(m+n)}\right)$, *then we have*

$$E(\mathbf{X}) = \boldsymbol{\xi} + \boldsymbol{\Lambda}\boldsymbol{\Gamma}^{-1}E\left(\mathbf{X}_{0\boldsymbol{\eta}}\right). \tag{7}$$

The marginal and conditional distributions of the SUE distribution have been presented by Jamalizadeh and Balakrishnan (2012) in terms of the parametrization in (5) as follows.

Suppose $\mathbf{X}_1$ and $\mathbf{X}_2$ are two random vectors of dimensions n_1 and $n - n_1$, respectively, such that

$$\begin{pmatrix}\mathbf{X}_1\\ \mathbf{X}_2\end{pmatrix} \sim SUE_{n,m}\left(\boldsymbol{\xi}, \boldsymbol{\eta}, \boldsymbol{\Omega}, \boldsymbol{\Gamma}, \boldsymbol{\Lambda}, h^{(m+n)}\right).$$

Corresponding to $\mathbf{X}_1$ and $\mathbf{X}_2$, let us consider the following partitions of $\boldsymbol{\xi}$, $\boldsymbol{\Omega}$ and $\boldsymbol{\Lambda}$ with the dimensions matching suitably:

$$\boldsymbol{\xi} = \begin{pmatrix}\boldsymbol{\xi}_1\\ \boldsymbol{\xi}_2\end{pmatrix}, \quad \boldsymbol{\Omega} = \begin{pmatrix}\boldsymbol{\Omega}_{11} & \boldsymbol{\Omega}_{12}\\ \boldsymbol{\Omega}_{21} & \boldsymbol{\Omega}_{22}\end{pmatrix} \quad \text{and} \quad \boldsymbol{\Lambda} = \begin{pmatrix}\boldsymbol{\Lambda}_1\\ \boldsymbol{\Lambda}_2\end{pmatrix}.$$

Lemma 2 *We then have*

(i) $\mathbf{X}_1 \sim SUE_{n_1,m}\left(\boldsymbol{\xi}_1, \boldsymbol{\eta}, \boldsymbol{\Omega}_{11}, \boldsymbol{\Gamma}, \boldsymbol{\Lambda}_1, h^{(m+n_1)}\right)$.
(ii) For $\mathbf{x}_1 \in \mathbb{R}^{n_1}$,

$$\mathbf{X}_2 \mid (\mathbf{X}_1 = \mathbf{x}_1) \sim SUE_{n-n_1,m}\left(\boldsymbol{\xi}^{2.1}(\mathbf{x}_1), \boldsymbol{\eta}^{2.1}(\mathbf{x}_1), \boldsymbol{\Omega}^{22.1}, \boldsymbol{\Gamma}^{2.1}, \boldsymbol{\Lambda}^{2.1}, h^{(m+n-n_1)}_{q(\mathbf{x}_1)}\right),$$

where

$$\boldsymbol{\xi}^{2.1}(\mathbf{x}_1) = \boldsymbol{\xi}_2 + \boldsymbol{\Omega}_{21}\boldsymbol{\Omega}_{11}^{-1}\left(\mathbf{x}_1 - \boldsymbol{\xi}_1\right), \quad \boldsymbol{\eta}^{2.1}(\mathbf{x}_1) = \boldsymbol{\eta} + \boldsymbol{\Lambda}_1^\top\boldsymbol{\Omega}_{11}^{-1}\left(\mathbf{x}_1 - \boldsymbol{\xi}_1\right),$$
$$\boldsymbol{\Omega}^{22.1} = \boldsymbol{\Omega}_{22} - \boldsymbol{\Omega}_{21}\boldsymbol{\Omega}_{11}^{-1}\boldsymbol{\Omega}_{12}, \quad \boldsymbol{\Gamma}^{2.1} = \boldsymbol{\Gamma} - \boldsymbol{\Lambda}_1^\top\boldsymbol{\Omega}_{11}^{-1}\boldsymbol{\Lambda}_1, \quad \boldsymbol{\Lambda}^{2.1} = \boldsymbol{\Lambda}_2 - \boldsymbol{\Omega}_{21}\boldsymbol{\Omega}_{11}^{-1}\boldsymbol{\Lambda}_1$$

and $q(\mathbf{x}_1) = \left(\mathbf{x}_1 - \boldsymbol{\xi}_1\right)^\top \boldsymbol{\Omega}_{11}^{-1}\left(\mathbf{x}_1 - \boldsymbol{\xi}_1\right)$.

For a proof, one may refer to Aghamohammadi et al. (2012).

2.1 Two Special cases

An important special case of SUE distribution is the multivariate unified skew-normal distribution (SUN). Specifically, if the density generator function in (5) is $h^{(m+n)}(u) = (2\pi)^{-(m+n)/2} \exp(-u/2)$ $(u \geq 0)$, we obtain the SUN distribution, denoted by $\mathbf{X} \sim SUN_{n,m}(\boldsymbol{\theta})$, with pdf (see Arellano-Valle and Azzalini 2006)

$$g_{SUN_{n,m}}(\mathbf{x};\boldsymbol{\theta}) = \frac{\phi_n(\mathbf{x};\boldsymbol{\xi},\boldsymbol{\Omega})}{\Phi_m(\boldsymbol{\eta};\boldsymbol{\Gamma})} \times \Phi_m\left(\boldsymbol{\eta} + \boldsymbol{\Lambda}^\top \boldsymbol{\Omega}^{-1}(\mathbf{x}-\boldsymbol{\xi}); \boldsymbol{\Gamma} - \boldsymbol{\Lambda}^\top \boldsymbol{\Omega}^{-1}\boldsymbol{\Lambda}\right),$$

where $\phi_n(\cdot;\boldsymbol{\xi},\boldsymbol{\Omega})$ denotes the pdf of $N_n(\boldsymbol{\xi},\boldsymbol{\Omega})$ and $\Phi_m(\cdot;\boldsymbol{\Gamma})$ denotes the cdf of $N_m(\mathbf{0},\boldsymbol{\Gamma})$.

Another important special case of SUE distribution is the multivariate unified skew-t (SUT) distribution. Specifically, if $h^{(m+n)}(u) = \frac{\Gamma\left(\frac{\nu+m+n}{2}\right)}{\Gamma\left(\frac{\nu}{2}\right)(\nu\pi)^{\frac{m+n}{2}}}\left(1+\frac{u}{\nu}\right)^{-(\nu+m+n)/2}$, we obtain the multivariate unified skew-t (SUT) distribution, denoted by $\mathbf{Y} \sim SUT_{n,m}(\boldsymbol{\theta},\nu)$, with pdf

$$g_{SUT_{n,m}}(\mathbf{x};\boldsymbol{\theta},\nu) = \frac{t_n(\mathbf{x};\boldsymbol{\xi},\boldsymbol{\Omega},\nu)}{T_m(\boldsymbol{\eta};\boldsymbol{\Gamma},\nu)}$$
$$\times T_m\left(\boldsymbol{\eta}+\boldsymbol{\Lambda}^\top\boldsymbol{\Omega}^{-1}(\mathbf{x}-\boldsymbol{\xi}); \frac{\nu+(\mathbf{x}-\boldsymbol{\xi})^\top\boldsymbol{\Omega}^{-1}(\mathbf{x}-\boldsymbol{\xi})}{\nu+n}\left(\boldsymbol{\Gamma}-\boldsymbol{\Lambda}^\top\boldsymbol{\Omega}^{-1}\boldsymbol{\Lambda}\right), \nu+n\right),$$

where $t_n(\cdot;\boldsymbol{\xi},\boldsymbol{\Omega},\nu)$ denotes the pdf of multivariate student-t distribution with location vector $\boldsymbol{\xi}$, dispersion matrix $\boldsymbol{\Omega}$ and degrees of freedom ν, and $T_m(\cdot;\boldsymbol{\Gamma},\nu)$ denotes the corresponding cdf of $t_m(\cdot;\mathbf{0},\boldsymbol{\Gamma},\nu)$.

Using the results in Lemma 2, we can obtain the marginal and conditional distributions of SUT distribution as presented in the following corollary.

Corollary 1 *Let*

$$\begin{pmatrix}\mathbf{X}_1\\ \mathbf{X}_2\end{pmatrix} \sim SUT_{n,m}(\boldsymbol{\xi},\boldsymbol{\eta},\boldsymbol{\Omega},\boldsymbol{\Gamma},\boldsymbol{\Lambda},\nu).$$

Then, we have:

(i) $\mathbf{X}_1 \sim SUT_{n_1,m}\left(\boldsymbol{\xi}_1,\boldsymbol{\eta},\boldsymbol{\Omega}_{11},\boldsymbol{\Gamma},\boldsymbol{\Lambda}_1,\nu\right)$.
(ii) For $\mathbf{x}_1 \in \mathbb{R}^{n_1}$,

$$\mathbf{X}_2 \mid (\mathbf{X}_1 = \mathbf{x}_1) \sim SUT_{n-n_1,m}\left(\boldsymbol{\theta}^{2.1}(\mathbf{x}_1), \nu+n_1\right),$$

where $\boldsymbol{\theta}^{2.1}(\mathbf{x}_1) = \left(\boldsymbol{\xi}^{2.1}(\mathbf{x}_1), \boldsymbol{\eta}^{2.1}(\mathbf{x}_1), \boldsymbol{\Omega}^{22.1}(\mathbf{x}_1), \boldsymbol{\Gamma}^{2.1}(\mathbf{x}_1), \boldsymbol{\Lambda}^{2.1}(\mathbf{x}_1)\right)$ *with* $\boldsymbol{\xi}^{2.1}(\mathbf{x}_1)$ *and* $\boldsymbol{\eta}^{2.1}(\mathbf{x}_1)$ *are as in Lemma 2, and*

$$\boldsymbol{\Omega}^{22.1}(\mathbf{x}_1) = \frac{\nu + q_1(\mathbf{x}_1)}{\nu + n_1}\boldsymbol{\Omega}^{22.1}, \quad \boldsymbol{\Gamma}^{2.1}(\mathbf{x}_1) = \frac{\nu + q_1(\mathbf{x}_1)}{\nu + n_1}\boldsymbol{\Gamma}^{2.1},$$
$$\boldsymbol{\Lambda}^{2.1}(\mathbf{x}_1) = \frac{\nu + q_1(\mathbf{x}_1)}{\nu + n_1}\boldsymbol{\Lambda}^{2.1}.$$

The moments of multivariate truncated normal and student-t distributions have been derived by many authors. In particular, Ho et al. (2012) derived these moments in a matrix form. In the following lemma, we present their results in the left truncated case, which we need for the derivations in subsequent sections.

Lemma 3 *Let* $\mathbf{X} \sim \mathbf{T}N_p(\mathbf{0}, \boldsymbol{\Sigma}; \mathbf{X} > \mathbf{a})$ *and* $\mathbf{Y} \sim \mathbf{T}t_p(\mathbf{0}, \boldsymbol{\Sigma}, \boldsymbol{\nu}; \mathbf{Y} > \mathbf{a})$, *and the vector* $\mathbf{a}$ *and the* $m \times m$ *positive definite matrix* $\boldsymbol{\Sigma}$ *be partitioned, for* $i = 1, \ldots, m$, *as*

$$\begin{pmatrix} a_i \\ \mathbf{a}_{-i} \end{pmatrix}, \quad \begin{pmatrix} \sigma_{ii} & \boldsymbol{\sigma}_{-ii}^{\top} \\ \boldsymbol{\sigma}_{-ii} & \boldsymbol{\Sigma}_{-i-i} \end{pmatrix}. \tag{8}$$

Then, we have

$$E(\mathbf{X}) = \frac{1}{\Phi_m(-\mathbf{a}; \boldsymbol{\Sigma})}\boldsymbol{\Sigma}\mathbf{q}^N(\boldsymbol{a}; \boldsymbol{\Sigma}), \quad E(\mathbf{Y}) = \frac{\sqrt{\frac{\nu}{\nu-2}}}{T_m(-\mathbf{a}; \boldsymbol{\Sigma}, \boldsymbol{\nu})}\boldsymbol{\Sigma}\boldsymbol{q}^t(\mathbf{a}; \boldsymbol{\Sigma}, \boldsymbol{\nu}),$$

where $\mathbf{q}^N(\mathbf{a}; \boldsymbol{\Sigma})$ *and* $\mathbf{q}^t(\mathbf{a}; \boldsymbol{\Sigma}, \boldsymbol{\nu})$ *are two* $p \times 1$ *vectors whose* i*th elements are*

$$q_i^N(\mathbf{a}; \boldsymbol{\Sigma}) = \phi(a_i; \sigma_{ii})\,\Phi_{m-1}\left(\frac{\boldsymbol{\sigma}_{-ii}}{\sigma_{ii}}a_i - \mathbf{a}_{-i}; \boldsymbol{\Sigma}_{-i|i}\right),$$

$$q_i^t(\mathbf{a}; \boldsymbol{\Sigma}, \boldsymbol{\nu}) = t\left(a_i\sqrt{\frac{\nu-2}{\nu}}; \sigma_{ii}, \nu-2\right) T_{m-1}\left(\frac{\boldsymbol{\sigma}_{-ii}}{\sigma_{ii}}a_i - \mathbf{a}_{-i}; \boldsymbol{\Sigma}_{-i|i}\,\frac{\nu + \frac{a_i^2}{\sigma_{ii}}}{\nu-1}, \nu-1\right),$$

with $\boldsymbol{\Sigma}_{-i|i} = \boldsymbol{\Sigma}_{-i-i} - \frac{\boldsymbol{\sigma}_{-ii}\boldsymbol{\sigma}_{-ii}^{\top}}{\sigma_{ii}}$.

By using the results in Lemma 3 and the convolution representation in (6), we can derive the first moments of SUN and SUT distributions as presented in the following theorem.

Theorem 1 *Let* $\mathbf{X} \sim SUN_{n,m}(\boldsymbol{\xi}, \boldsymbol{\eta}, \boldsymbol{\Omega}, \boldsymbol{\Gamma}, \boldsymbol{\Lambda})$ *and* $\mathbf{Y} \sim SUT_{n,m}(\boldsymbol{\theta}, \nu)$. *Then, we have*

$$E(\mathbf{X}) = \boldsymbol{\xi} + \frac{\boldsymbol{\Lambda}\mathbf{q}^N(-\boldsymbol{\eta}; \boldsymbol{\Gamma})}{\Phi_m(\boldsymbol{\eta}; \boldsymbol{\Gamma})}, \quad E(\mathbf{Y}) = \boldsymbol{\xi} + \frac{\boldsymbol{\Lambda}\mathbf{q}^t(-\boldsymbol{\eta}; \boldsymbol{\Gamma}, \boldsymbol{\nu})}{T_m(\boldsymbol{\eta}; \boldsymbol{\Gamma}, \boldsymbol{\nu})}.$$

3 Concomitant Vector of Order Statistics

Let $\mathbf{X}_1, \ldots, \mathbf{X}_n$ be random vectors of the same dimension p having elliptical distribution in (1), and let for $i = 1, 2, \ldots, n$, $Y_i = \mathbf{a}^\top \mathbf{X}_i$ be a linear combination of these vectors, where $\mathbf{a} = \left(a_1, \ldots, a_p\right)^\top \in R^p$ and $\mathbf{a} \neq \mathbf{0} = (0, \ldots, 0)^\top$. Further, let $\mathbf{Y}_{(n)} = \left(Y_{(1)}, \ldots, Y_{(n)}\right)^\top$, with $Y_{(1)} < \cdots < Y_{(n)}$, denote the vector of order statistics arising from $\mathbf{Y} = (Y_1, \ldots, Y_n)^\top$, and $\mathbf{X}_{[r]}$ denote the vector of concomitants corresponding to the rth order statistic $Y_{(r)}$.

In this section, we establish a mixture representation for the distribution of $\mathbf{X}_{[r]}$ in terms of univariate SUE distribution. For this purpose, we shall first introduce the following notation. Let $1 \leq r \leq n$ be an integer, and for integers $1 \leq j_1 < \cdots < j_{r-1} \leq n-1$, let $\mathbf{S}_{j_1 \ldots j_{r-1}} = \operatorname{diag}(s_1, \ldots, s_{n-1})$ be a $(n-1) \times (n-1)$ diagonal matrix where

$$s_i = \begin{cases} 1 & i = j_1, \ldots, j_{r-1} \\ -1 & \text{otherwise.} \end{cases}$$

In the special cases, we have $\mathbf{S}_{j_1 \cdots j_{n-1}} = \mathbf{I}_{n-1}$ and $\mathbf{S}_{j_0} = -\mathbf{I}_{n-1}$. Furthermore, let, for $i = 1, \ldots, n$, the random vector $\mathbf{Y} = (Y_1, \ldots, Y_n)^\top$ be partitioned as

$$\mathbf{Y} = \begin{pmatrix} Y_i \\ \mathbf{Y}_{-i} \end{pmatrix},$$

where we use the notation $\mathbf{Y}_{-i}$ for the vector obtained from $\mathbf{Y}$ by deleting its ith component.

Now, let us introduce the following partitions for $\boldsymbol{\mu}_{\mathbf{Y}}$, $\boldsymbol{\Sigma}_{\mathbf{YY}}$ and $\boldsymbol{\Sigma}_{\mathbf{YX}_i}$:

$$\boldsymbol{\mu}_{\mathbf{Y}} = \begin{pmatrix} \mu_{Y_i} \\ \boldsymbol{\mu}_{\mathbf{Y}_{-i}} \end{pmatrix}, \quad \boldsymbol{\Sigma}_{\mathbf{YY}} = \begin{pmatrix} \sigma_{Y_i Y_i} & \boldsymbol{\sigma}^\top_{\mathbf{Y}_{-i} Y_i} \\ \boldsymbol{\sigma}_{\mathbf{Y}_{-i} Y_i} & \boldsymbol{\Sigma}_{\mathbf{Y}_{-i} \mathbf{Y}_{-i}} \end{pmatrix}, \quad \boldsymbol{\Sigma}_{\mathbf{YX}_i} = \begin{pmatrix} \boldsymbol{\sigma}_{Y_i \mathbf{X}_i} \\ \boldsymbol{\sigma}_{\mathbf{Y}_{-i} \mathbf{X}_i} \end{pmatrix}.$$

We now derive the exact distribution of $\mathbf{X}_{[r]}$, for $r = 1, 2, \ldots, n$, in the following theorem.

Theorem 2 *The cdf of* $\mathbf{X}_{[r]}$, *for* $r = 1, 2, \ldots, n$ *and* $\mathbf{t} \in \mathbb{R}^p$, *is given by*

$$F_{[r]}\left(\mathbf{t}; \boldsymbol{\mu}, \boldsymbol{\Sigma}, h^{(np)}\right) = \sum_{i=1}^{n} \sum_{\substack{j_1 < \cdots < j_{r-1} \\ 1 \leq j_k \leq n-1}} \pi_{i j_1, \ldots, j_{r-1}} G_{SUE_{p,n-1}}\left(\mathbf{t}; \boldsymbol{\theta}_{i j_1, \ldots, j_{r-1}}, h^{(p+n-1)}\right),$$

where $G_{SUE_{p,n-1}}\left(\cdot; \boldsymbol{\theta}, h^{(p+n-1)}\right)$ *denotes the cdf of* $SUE_{p,n-1}\left(\boldsymbol{\theta}, h^{(p+n-1)}\right)$, *and the mixing probabilities are*

$$\pi_{ij_1,\ldots,j_{r-1}} = F_{EC_{n-1}}\left(\boldsymbol{\eta}_{ij_1,\ldots,j_{r-1}}; \boldsymbol{\Gamma}_{ij_1,\ldots,j_{r-1}}, h^{(n-1)}\right)$$

and

$$\boldsymbol{\theta}_{ij_1,\ldots,j_{r-1}} = \left(\boldsymbol{\xi}_i, \boldsymbol{\eta}_{ij_1,\ldots,j_{r-1}}, \boldsymbol{\Omega}_i, \boldsymbol{\Gamma}_{ij_1,\ldots,j_{r-1}}, \boldsymbol{\Lambda}_{ij_1,\ldots,j_{r-1}}\right),$$

where

$$\boldsymbol{\xi}_i = \boldsymbol{\mu}_{\mathbf{X}_i}, \quad \boldsymbol{\eta}_{ij_1,\ldots,j_{r-1}} = \mathbf{S}_{j_1\ldots j_{r-1}}\left(\mathbf{1}_{n-1}\mu_{Y_i} - \boldsymbol{\mu}_{\mathbf{Y}_{-i}}\right), \quad \boldsymbol{\Omega}_i = \boldsymbol{\Sigma}_{\mathbf{X}_i\mathbf{X}_i},$$

$$\boldsymbol{\Lambda}_{ij_1,\ldots,j_{r-1}} = \left[\mathbf{S}_{j_1\ldots j_{r-1}}\left(\mathbf{1}_{n-1}\boldsymbol{\sigma}_{Y_i\mathbf{X}_i} - \boldsymbol{\Sigma}_{\mathbf{Y}_{-i}\mathbf{X}_i}\right)\right]^\top,$$

$$\boldsymbol{\Gamma}_{ij_1,\ldots,j_{r-1}} = \mathbf{S}_{j_1\ldots j_{r-1}}\left(\sigma_{Y_iY_i}\mathbf{1}_{n-1}\mathbf{1}_{n-1}^\top - \mathbf{1}_{n-1}\boldsymbol{\sigma}_{\mathbf{Y}_{-i}Y_i}^\top - \boldsymbol{\sigma}_{\mathbf{Y}_{-i}Y_i}\mathbf{1}_{n-1}^\top + \boldsymbol{\Sigma}_{\mathbf{Y}_{-i}\mathbf{Y}_{-i}}\right)\mathbf{S}_{j_1\ldots j_{r-1}}^\top.$$

Proof See Appendix. □

For $i = 1, 2, \ldots, n$, let $\boldsymbol{\theta}_i = \left(\boldsymbol{\xi}_i, \boldsymbol{\eta}_i, \boldsymbol{\Omega}_i, \boldsymbol{\Gamma}_i, \boldsymbol{\Lambda}_i\right)$, where

$$\begin{aligned}
&\boldsymbol{\xi}_i = \boldsymbol{\mu}_{\mathbf{X}_i}, \quad \boldsymbol{\eta}_i = \left(\mathbf{1}_{n-1}\mu_{Y_i} - \boldsymbol{\mu}_{\mathbf{Y}_{-i}}\right), \quad \boldsymbol{\Omega}_i = \boldsymbol{\Sigma}_{\mathbf{X}_i\mathbf{X}_i}, \\
&\boldsymbol{\Lambda}_i = \left(\mathbf{1}_{n-1}\boldsymbol{\sigma}_{Y_i\mathbf{X}_i} - \boldsymbol{\Sigma}_{\mathbf{Y}_{-i}\mathbf{X}_i}\right)^\top, \\
&\boldsymbol{\Gamma}_i = \left(\sigma_{Y_iY_i}\mathbf{1}_{n-1}\mathbf{1}_{n-1}^\top - \mathbf{1}_{n-1}\boldsymbol{\sigma}_{\mathbf{Y}_{-i}Y_i}^\top - \boldsymbol{\sigma}_{\mathbf{Y}_{-i}Y_i}\mathbf{1}_{n-1}^\top + \boldsymbol{\Sigma}_{\mathbf{Y}_{-i}\mathbf{Y}_{-i}}\right).
\end{aligned} \tag{9}$$

Then, we obtain the following result.

Corollary 2 *The cdf of* $\mathbf{X}_{[n]}$ *and* $\mathbf{X}_{[1]}$, $\mathbf{t} \in \mathbb{R}^p$, *are given by*

$$F_{[n]}\left(\mathbf{t}; \boldsymbol{\mu}, \boldsymbol{\Sigma}, h^{(np)}\right) = \sum_{i=1}^{n}\pi_i G_{SUE_{p,n-1}}\left(\mathbf{t}; \boldsymbol{\theta}_i, h^{(p+n-1)}\right),$$

$$F_{[1]}\left(\mathbf{t}; \boldsymbol{\mu}, \boldsymbol{\Sigma}, h^{(np)}\right) = \sum_{i=1}^{n}\pi_i' G_{SUE_{p,n-1}}\left(\mathbf{t}; \boldsymbol{\theta}_i', h^{(p+n-1)}\right),$$

where

$$\pi_i = F_{EC_{n-1}}\left(\boldsymbol{\eta}_i; \boldsymbol{\Gamma}_i, h^{(n-1)}\right), \ \pi_i' = F_{EC_{n-1}}\left(-\boldsymbol{\eta}_i; \boldsymbol{\Gamma}_i, h^{(n-1)}\right),$$

$$\boldsymbol{\theta}_i' = \left(\boldsymbol{\xi}_i, -\boldsymbol{\eta}_i, \boldsymbol{\Omega}_i, \boldsymbol{\Gamma}_i, -\boldsymbol{\Lambda}_i\right).$$

Proof In Part (i), $\mathbf{S}_{j_1\ldots j_{n-1}} = \mathbf{I}_{n-1}$ and in Part (ii), $\mathbf{S}_{j_0} = -\mathbf{I}_{n-1}$, and so the proof follows directly from Theorem 2. □

3.1 An Exchangeable Case

Now, we focus on an exchangeable case when in (1), for $i, j = 1, \ldots, n$, and $i \neq j$, we have

$$\boldsymbol{\mu}_{\mathbf{X}_i} = \boldsymbol{\mu}_{\mathbf{X}}, \ \boldsymbol{\Sigma}_{\mathbf{X}_i\mathbf{X}_i} = \boldsymbol{\Sigma}_1 \ \text{ and } \ \boldsymbol{\Sigma}_{\mathbf{X}_i\mathbf{X}_j} = \boldsymbol{\Sigma}_2. \tag{10}$$

In what follows, $\mathbf{J}_{n-1}$ denotes the vector $\left(\mathbf{1}_{r-1}^{\top}, -\mathbf{1}_{n-r}^{\top}\right)^{\top}$. From the mixture form in Theorem 2, we can simply obtain the exact distribution of $\mathbf{X}_{[r]}$ for this special exchangeable case as follows.

Corollary 3 *In the exchangeable case as in (10), we have, for* $r = 1, 2, \ldots, n$,

$$\mathbf{X}_{[r]} \sim SUE_{p,n-1}\left(\boldsymbol{\mu}_{\mathbf{X}}, \mathbf{0}, \boldsymbol{\Sigma}_1, \boldsymbol{\Gamma}^*, \boldsymbol{\Lambda}^*, h^{(p+n-1)}\right),$$

where

$$\boldsymbol{\Gamma}^* = \left[\mathbf{a}^{\top}\left(\boldsymbol{\Sigma}_1 - \boldsymbol{\Sigma}_2\right)\mathbf{a}\right]\left(\mathbf{J}_{n-1}\mathbf{J}_{n-1}^{\top} + \mathbf{I}_{n-1}\right), \quad \boldsymbol{\Lambda}^* = \left[\mathbf{J}_{n-1}\mathbf{a}^{\top}\left(\boldsymbol{\Sigma}_1 - \boldsymbol{\Sigma}_2\right)\right]^{\top}.$$

Proof We can show in this special case that

$$\begin{aligned}
\boldsymbol{\sigma}_{Y_i\mathbf{X}_i} &= \mathbf{a}^{\top}\boldsymbol{\Sigma}_1, \quad \boldsymbol{\Sigma}_{\mathbf{Y}_{-i}\mathbf{X}_i} = \mathbf{1}_{n-1}\mathbf{a}^{\top}\boldsymbol{\Sigma}_2, \\
\sigma_{Y_iY_i} &= \mathbf{a}^{\top}\boldsymbol{\Sigma}_1\mathbf{a}, \quad \boldsymbol{\sigma}_{\mathbf{Y}_{-i}Y_i} = \mathbf{1}_{n-1}\mathbf{a}^{\top}\boldsymbol{\Sigma}_2\mathbf{a}, \\
\boldsymbol{\Sigma}_{\mathbf{Y}_{-i}\mathbf{Y}_{-i}} &= \mathbf{a}^{\top}\boldsymbol{\Sigma}_2\mathbf{a}\left(\mathbf{1}_{n-1}\mathbf{1}_{n-1}^{\top}\right) + \left(\mathbf{a}^{\top}\boldsymbol{\Sigma}_1\mathbf{a} - \mathbf{a}^{\top}\boldsymbol{\Sigma}_2\mathbf{a}\right)\mathbf{I}_{n-1},
\end{aligned}$$

and so the required result can be obtained by some simple algebraic calculations. □

The following result is an immediate consequence of Corollary 3.

Corollary 4 *Let in (10),* $\boldsymbol{\Sigma}_2 = \mathbf{0}$ *and* $\boldsymbol{\Sigma}_1 = \boldsymbol{\Sigma}$, *then we have*

$$\mathbf{X}_{[r]} \sim SUE_{p,n-1}\left(\boldsymbol{\mu}, \mathbf{0}, \boldsymbol{\Sigma}, \boldsymbol{\Gamma}', \boldsymbol{\Lambda}', h^{(p+n-1)}\right),$$

where $\boldsymbol{\Gamma}' = \boldsymbol{a}^{\top}\boldsymbol{\Sigma}\boldsymbol{a}\left(\boldsymbol{J}_{n-1}\boldsymbol{J}_{n-1}^{\top} + \boldsymbol{I}_{n-1}\right)$, $\boldsymbol{\Lambda}' = \left[\boldsymbol{J}_{n-1}\boldsymbol{a}^{\top}\boldsymbol{\Sigma}\right]^{\top}$.

3.2 Multivariate Normal Case

In the special case of the multivariate normal distribution, from the general mixture form in Theorem 2, we get the following corollary.

Corollary 5 *If* $\begin{pmatrix} \boldsymbol{X}_1 \\ \vdots \\ \boldsymbol{X}_n \end{pmatrix} \sim N_{np}\left(\boldsymbol{\mu} = \begin{pmatrix} \boldsymbol{\mu}_1 \\ \vdots \\ \boldsymbol{\mu}_n \end{pmatrix}, \boldsymbol{\Sigma} = \begin{pmatrix} \boldsymbol{\Sigma}_{11} & \cdots & \boldsymbol{\Sigma}_{1n} \\ \vdots & \ddots & \vdots \\ \boldsymbol{\Sigma}_{n1} & \cdots & \boldsymbol{\Sigma}_{nn} \end{pmatrix}\right)$, *then the cdf of* $\boldsymbol{X}_{[r]}$, *for* $\boldsymbol{t} \in \mathbb{R}^p$, *is given by*

$$F_{[r]}(\boldsymbol{t}; \boldsymbol{\mu}, \boldsymbol{\Sigma}) = \sum_{i=1}^{n} \sum_{\substack{j_1 < \cdots < j_{r-1} \\ 1 \le j_k \le n-1}} \pi_{ij_1,\ldots,j_{r-1}} G_{SUN_{p,n-1}}\left(\boldsymbol{t}; \boldsymbol{\theta}_{ij_1,\ldots,j_{r-1}}\right),$$

where $G_{SUN_{p,n-1}}(\cdot; \boldsymbol{\theta})$ *denotes the cdf of* $SUN_{p,n-1}(\boldsymbol{\theta})$, *and the mixing probabilities are*

$$\pi_{ij_1,\ldots,j_{r-1}} = \Phi_{n-1}\left(\boldsymbol{\eta}_{ij_1,\ldots,j_{r-1}}; \boldsymbol{\Gamma}_{ij_1,\ldots,j_{r-1}}\right),$$

and $\boldsymbol{\theta}_{ij_1,\ldots,j_{r-1}}$ *is as given in Theorem 2.*

In addition, upon using the mean of $SUN_{n,m}(\boldsymbol{\theta})$ presented in Theorem 1, the mean of $\boldsymbol{X}_{[r]}$ can be readily obtained as

$$E\left(\boldsymbol{X}_{[r]}\right) = \sum_{i=1}^{n} \sum_{\substack{j_1 < \cdots < j_{r-1} \\ 1 \le j_k \le n-1}} \pi_{ij_1,\ldots,j_{r-1}} \boldsymbol{\mu}_{ij_1,\ldots,j_{r-1}}, \tag{11}$$

where $\boldsymbol{\mu}_{ij_1,\ldots,j_{r-1}}$ denotes the mean of $SUN_{p,n-1}\left(\boldsymbol{\theta}_{ij_1,\ldots,j_{r-1}}\right)$.

3.3 Multivariate Student-t Case

In the case of multivariate student-t distribution, we can easily obtain the exact distribution of $\boldsymbol{X}_{[r]}$ as follows.

Corollary 6 *If* $\begin{pmatrix} \boldsymbol{X}_1 \\ \vdots \\ \boldsymbol{X}_n \end{pmatrix} \sim t_{np}(\boldsymbol{\mu}, \boldsymbol{\Sigma}, \nu)$, *then the cdf of* $\boldsymbol{X}_{[r]}$, *for* $\boldsymbol{t} \in \mathbb{R}^p$, *is given by*

$$F_{[r]}(\boldsymbol{t}; \boldsymbol{\mu}, \boldsymbol{\Sigma}) = \sum_{i=1}^{n} \sum_{\substack{j_1 < \cdots < j_{r-1} \\ 1 \le j_k \le n-1}} \pi_{ij_1,\cdots,j_{r-1}} G_{SUT_{p,n-1}}\left(\boldsymbol{t}; \boldsymbol{\theta}_{ij_1,\cdots,j_{r-1}}, \nu\right),$$

where $G_{SUT_{p,n-1}}(\cdot; \boldsymbol{\theta}, \nu)$ *denotes the cdf and pdf of* $SUT_{p,n-1}(\boldsymbol{\theta}, \nu)$ *and the mixing probabilities are*

$$\pi_{ij_1,\ldots,j_{r-1}} = T_{n-1}\left(\boldsymbol{\eta}_{ij_1,\ldots,j_{r-1}}; \boldsymbol{\Gamma}_{ij_1,\ldots,j_{r-1}}, \nu\right),$$

and $\boldsymbol{\theta}_{ij_1,\cdots,j_{r-1}}$ *is as defined in Theorem 2.*

By using the mixture representation in Corollary 6 and the mean of $SUT_{n,m}(\boldsymbol{\theta}, \nu)$ presented in Theorem 1, the mean of $\boldsymbol{X}_{[r]}$ is readily obtained as

$$E\left(\boldsymbol{X}_{[r]}\right) = \sum_{i=1}^{n} \sum_{\substack{j_1<\cdots<j_{r-1} \\ 1\le j_k\le n-1}} \pi_{ij_1,\ldots,j_{r-1}} \boldsymbol{\mu}^t_{ij_1,\ldots,j_{r-1}}, \tag{12}$$

where $\boldsymbol{\mu}^t_{ij_1,\ldots,j_{r-1}}$ denotes the mean of $SUT_{p,n-1}\left(\boldsymbol{\theta}_{ij_1,\ldots,j_{r-1}}, \nu\right)$.

4 Joint Distribution of $\left(\boldsymbol{X}_{[r]}, \boldsymbol{Y}_{(r)}\right)^\top$

We now derive the exact joint distribution of $\left(\boldsymbol{X}_{[r]}, Y_{(r)}\right)^\top$, for $r = 1, \ldots, n$, and show that this distribution is indeed a mixture of unified skew-elliptical distributions.

Theorem 3 *The joint cdf of* $\left(\boldsymbol{X}_{[r]}, Y_{(r)}\right)^\top$, *for* $\boldsymbol{t} = \left(\boldsymbol{t}_1^\top, t_2\right)^\top \in \mathbb{R}^{p+1}$, *is given by*

$$F_{[r],(r)}\left(\boldsymbol{t}; \boldsymbol{\mu}, \boldsymbol{\Sigma}, h^{(np)}\right) = \sum_{i=1}^{n} \sum_{\substack{j_1<\cdots<j_{r-1} \\ 1\le j_k\le n-1}} \pi_{ij_1,\ldots,j_{r-1}} G_{SUE_{p+1,n-1}}\left(\boldsymbol{t}; \boldsymbol{\theta}^*_{i,j_1,\ldots,j_{r-1}}, h^{(p+n)}\right),$$

where, for $i = 1, \ldots, n$ *and* $1 \le j_1 < \cdots < j_{r-1} \le n-1$, *the mixing probabilities* $\pi_{ij_1,\ldots,j_{r-1}}$ *are as given in Theorem 2, and*

$$\boldsymbol{\theta}^*_{ij_1,\ldots,j_{r-1}} = \left(\boldsymbol{\xi}^*_i, \boldsymbol{\eta}_{ij_1,\ldots,j_{r-1}}, \boldsymbol{\Omega}^*_i, \boldsymbol{\Gamma}_{ij_1,\ldots,j_{r-1}}, \boldsymbol{\Lambda}^*_{ij_1,\ldots,j_{r-1}}\right),$$

with

$$\boldsymbol{\xi}^*_i = \begin{pmatrix} \mu_{\boldsymbol{X}_i} \\ \mu_{Y_i} \end{pmatrix}, \quad \boldsymbol{\Omega}^*_i = \begin{pmatrix} \boldsymbol{\Sigma}_{\boldsymbol{X}_i\boldsymbol{X}_i} & \boldsymbol{\sigma}_{\boldsymbol{X}_i Y_i} \\ \boldsymbol{\sigma}^\top_{\boldsymbol{X}_i Y_i} & \sigma_{Y_i Y_i} \end{pmatrix},$$

$$\boldsymbol{\Lambda}^*_{ij_1,\ldots,j_{r-1}} = \begin{pmatrix} \left[\mathbf{S}_{ij_1,\cdots,j_{r-1}}\left(\mathbf{1}_{n-1}\boldsymbol{\sigma}_{Y_i\boldsymbol{X}_i} - \boldsymbol{\Sigma}_{\boldsymbol{Y}_{-i}\boldsymbol{X}_i}\right)\right]^\top \\ \left[\mathbf{S}_{ij_1,\cdots,j_{r-1}}\left(\mathbf{1}_{n-1}\boldsymbol{\sigma}_{Y_i Y_i} - \boldsymbol{\sigma}_{\boldsymbol{Y}_{-i}Y_i}\right)\right]^\top \end{pmatrix}.$$

Proof This theorem can be proved by proceeding exactly as done in Theorem 2. □

From Lemma 2, we can easily derive the conditional distribution of $\boldsymbol{X}_{[r]}$, given $Y_{(r)}$, as presented in the following corollary.

Corollary 7 *The conditional distribution of* $\mathbf{X}_{[r]}$, *given* $Y_{(r)} = t_2$, *for* $r = 1, \ldots, n$ *and* $t_2 \in \mathbb{R}$, *is given by*

$$F_{\mathbf{X}_{[r]}|\, Y_{(r)}=t_2}\left(\mathbf{t}_1; \boldsymbol{\mu}, \boldsymbol{\Sigma}, h^{(np)}\right)$$
$$= \sum_{i=1}^{n} \sum_{\substack{j_1<\cdots<j_{r-1} \\ 1\le j_k\le n-1}} \pi^{e}_{ij_1,\cdots,j_{r-1}} G_{SUE_{p,n-1}}\left(\mathbf{t}_1; \boldsymbol{\theta}^{1.2}_{ij_1,\cdots,j_{r-1}}(t_2), h^{(p+n-1)}_{u_i(t_2)}\right), \ \mathbf{t}_1 \in \mathbb{R}^p,$$

where

$$\boldsymbol{\theta}^{1.2}_{ij_1,\cdots,j_{r-1}}(t_2) = \left(\boldsymbol{\xi}^{1.2}_{i}(t_2), \boldsymbol{\eta}^{1.2}_{ij_1,\cdots,j_{r-1}}(t_2), \boldsymbol{\Omega}^{1.2}_{i}, \boldsymbol{\Gamma}^{1.2}_{ij_1,\cdots,j_{r-1}}, \boldsymbol{\Lambda}^{1.2}_{ij_1,\cdots,j_{r-1}}\right),$$

with

$$\boldsymbol{\xi}^{1.2}_{i}(t_2) = \mu_{\mathbf{X}_i} + \boldsymbol{\sigma}_{\mathbf{X}_i Y_i}\frac{t_2-\mu_{Y_i}}{\sigma_{Y_iY_i}},$$

$$\boldsymbol{\eta}^{1.2}_{ij_1,\cdots,j_{r-1}}(t_2) = \boldsymbol{\eta}_{ij_1,\cdots,j_{r-1}} + \left[\mathbf{S}_{ij_1,\cdots,j_{r-1}}\left(\mathbf{1}_{n-1}\sigma_{Y_iY_i} - \boldsymbol{\sigma}_{\mathbf{Y}_{-i}Y_i}\right)\right]\frac{t_2-\mu_{Y_i}}{\sigma_{Y_iY_i}},$$

$$\boldsymbol{\Omega}^{1.2}_{i} = \boldsymbol{\Sigma}_{\mathbf{X}_i\mathbf{X}_i} - \frac{\boldsymbol{\sigma}_{\mathbf{X}_iY_i}\boldsymbol{\sigma}^{T}_{\mathbf{X}_iY_i}}{\sigma_{Y_iY_i}},$$

$$\boldsymbol{\Gamma}^{1.2}_{ij_1,\cdots,j_{r-1}} = \boldsymbol{\Gamma}_{ij_1,\cdots,j_{r-1}} - \frac{\left[\mathbf{S}_{ij_1,\cdots,j_{r-1}}\left(\mathbf{1}_{n-1}\sigma_{Y_iY_i}-\boldsymbol{\sigma}_{\mathbf{Y}_{-i}Y_i}\right)\right]\left[\mathbf{S}_{ij_1,\cdots,j_{r-1}}\left(\mathbf{1}_{n-1}\sigma_{Y_iY_i}-\boldsymbol{\sigma}_{\mathbf{Y}_{-i}Y_i}\right)\right]^T}{\sigma_{Y_iY_i}},$$

$$\boldsymbol{\Lambda}^{1.2}_{ij_1,\cdots,j_{r-1}} = \left[\mathbf{S}_{ij_1,\cdots,j_{r-1}}\left(\mathbf{1}_{n-1}\boldsymbol{\sigma}_{Y_i\mathbf{X}_i} - \boldsymbol{\Sigma}_{\mathbf{Y}_{-i}\mathbf{X}_i}\right)\right]^T - \frac{\boldsymbol{\sigma}_{\mathbf{X}_iY_i}}{\sigma_{Y_iY_i}}\left[\mathbf{S}_{ij_1,\cdots,j_{r-1}}\left(\mathbf{1}_{n-1}\sigma_{Y_iY_i} - \boldsymbol{\sigma}_{\mathbf{Y}_{-i}Y_i}\right)\right]^T$$

and

$$u_i(t_2) = \frac{\left(t_2-\mu_{Y_i}\right)^2}{\sigma_{Y_iY_i}},$$

and the mixing probabilities $\pi^{e}_{ij_1,\cdots,j_{r-1}}$ *are*

$$\frac{\pi_{ij_1,\cdots,j_{r-1}} g_{SUE_{1,n-1}}\left(t_2;\boldsymbol{\theta}^{'}_{ij_1,\cdots,j_{r-1}}, h^{(n)}\right)}{\sum_{i=1}^{n}\sum_{\substack{j_1<\cdots<j_{r-1}\\ 1\le j_k\le n-1}} \pi_{ij_1,\cdots,j_{r-1}} g_{SUE_{1,n-1}}\left(t_2;\boldsymbol{\theta}^{'}_{ij_1,\cdots,j_{r-1}}, h^{(n)}\right)},$$

where

$$\boldsymbol{\theta}^{'}_{ij_1,\cdots,j_{r-1}} = \left(\mu_{Y_i}, \boldsymbol{\eta}_{ij_1,\cdots,j_{r-1}}, \sigma_{Y_iY_i}, \boldsymbol{\Gamma}_{ij_1,\cdots,j_{r-1}}, \boldsymbol{\Lambda}^{'}_{ij_1,\cdots,j_{r-1}}\right),$$

with

$$\boldsymbol{\Lambda}^{'}_{ij_1,\cdots,j_{r-1}} = \left[\mathbf{S}_{ij_1,\cdots,j_{r-1}}\left(\mathbf{1}_{n-1}\sigma_{Y_iY_i} - \boldsymbol{\sigma}_{\mathbf{Y}_{-i}Y_i}\right)\right]^T.$$

4.1 Multivariate Normal Case

As an immediate consequence, we obtain the following corollary when $\left(\boldsymbol{X}_1^{\top},\ldots,\boldsymbol{X}_n^{\top}\right)^{\top}$ follows a multivariate normal distribution.

Corollary 8 *If* $\begin{pmatrix}\mathbf{X}_1\\ \vdots\\ \mathbf{X}_n\end{pmatrix} \sim N_{np}(\boldsymbol{\mu},\boldsymbol{\Sigma})$, *then the conditional distribution of* $\mathbf{X}_{[r]}$, *given* $Y_{(r)} = t_2$, *for* $t_2 \in \mathbb{R}$, *is given by*

$$F_{\mathbf{X}_{[r]}|\ Y_{(r)}=t_2}(\mathbf{t}_1;\boldsymbol{\mu},\boldsymbol{\Sigma}) = \sum_{i=1}^{n}\sum_{\substack{j_1<\cdots<j_{r-1}\\ 1\le j_k\le n-1}} \pi^{n}_{ij_1,\cdots,j_{r-1}} G_{SUN_{p,n-1}}\left(\mathbf{t}_1;\boldsymbol{\theta}^{1.2}_{ij_1,\cdots,j_{r-1}}(t_2)\right),\ \mathbf{t}_1\in\mathbb{R}^p,$$

where the mixing probabilities are

$$\pi^{n}_{ij_1,\cdots,j_{r-1}} = \frac{\pi_{ij_1,\cdots,j_{r-1}} g_{SUN_{1,n-1}}\left(t_2;\boldsymbol{\theta}^{'}_{ij_1,\cdots,j_{r-1}}\right)}{\sum_{i=1}^{n}\sum_{\substack{j_1<\cdots<j_{r-1}\\ 1\le j_k\le n-1}} \pi_{ij_1,\cdots,j_{r-1}} g_{SUN_{1,n-1}}\left(t_2;\boldsymbol{\theta}^{'}_{ij_1,\cdots,j_{r-1}}\right)},$$

and $\boldsymbol{\theta}^{1.2}_{ij_1,\cdots,j_{r-1}}(t_2)$ *and* $\boldsymbol{\theta}^{'}_{ij_1,\cdots,j_{r-1}}$ *are as given in Corollary 7.*

The conditional mean of $\mathbf{X}_{[r]}$, given $Y_{(r)}$ can be easily deduced, using the mean of $SUN_{n,m}(\boldsymbol{\theta})$ presented in Theorem 1 as

$$E\left(\mathbf{X}_{[r]} \mid Y_{(r)} = t_2\right) = \sum_{i=1}^{n} \sum_{\substack{j_1<\cdots<j_{r-1} \\ 1\le j_k\le n-1}} \pi^{n}_{ij_1,\cdots,j_{r-1}} \boldsymbol{\mu}_{ij_1,\cdots,j_{r-1}}(t_2), \tag{13}$$

where $\boldsymbol{\mu}_{ij_1,\cdots,j_{r-1}}(t_2)$ denotes the mean of $SUN_{p,n-1}\left(\boldsymbol{\theta}^{1.2}_{ij_1,\cdots,j_{r-1}}(t_2)\right)$.

4.2 Multivariate Student-t Case

Corollary 9 *If* $\begin{pmatrix} \mathbf{X}_1 \\ \vdots \\ \mathbf{X}_n \end{pmatrix} \sim t_{np}(\boldsymbol{\mu}, \boldsymbol{\Sigma}, \nu)$, *then the conditional distribution of* $\mathbf{X}_{[r]}$, *given* $Y_{(r)} = t_2$ *for* $t_2 \in \mathbb{R}$, *is given by*

$$F_{\mathbf{X}_{[r]}\mid Y_{(r)}=t_2}(\mathbf{t}_1; \boldsymbol{\mu}, \boldsymbol{\Sigma}, \nu) = \sum_{i=1}^{n} \sum_{\substack{j_1<\cdots<j_{r-1} \\ 1\le j_k\le n-1}} \pi^{t}_{ij_1,\cdots,j_{r-1}} G_{SUT_{p,n-1}}\left(\mathbf{t}_1; \boldsymbol{\theta}^{*1.2}_{ij_1,\cdots,j_{r-1}}(t_2), \nu+1\right), \ \mathbf{t}_1 \in \mathbb{R}^p,$$

where the mixing probabilities are

$$\pi^{t}_{ij_1,\cdots,j_{r-1}} = \frac{\pi_{ij_1,\cdots,j_{r-1}} g_{SUT_{1,n-1}}\left(t_2; \boldsymbol{\theta}'_{ij_1,\cdots,j_{r-1}}, \nu\right)}{\sum_{i=1}^{n} \sum_{\substack{j_1<\cdots<j_{r-1} \\ 1\le j_k\le n-1}} \pi_{ij_1,\cdots,j_{r-1}} g_{SUT_{1,n-1}}\left(t_2; \boldsymbol{\theta}'_{ij_1,\cdots,j_{r-1}}, \nu\right)},$$

and

$$\boldsymbol{\theta}^{*1.2}_{ij_1,\cdots,j_{r-1}}(t_2) = \left(\boldsymbol{\xi}^{1.2}_{i}(t_2), \boldsymbol{\eta}^{1.2}_{ij_1,\cdots,j_{r-1}}(t_2), \boldsymbol{\Omega}^{1.2}_{i}(t_2), \boldsymbol{\Gamma}^{1.2}_{ij_1,\cdots,j_{r-1}}(t_2), \boldsymbol{\Lambda}^{1.2}_{ij_1,\cdots,j_{r-1}}(t_2)\right),$$

with $\boldsymbol{\xi}^{1.2}_{i}(t_2)$ *and* $\boldsymbol{\eta}^{1.2}_{ij_1,\cdots,j_{r-1}}(t_2)$ *being as in Corollary 7, and*

$$\boldsymbol{\Omega}^{1.2}_{i}(t_2) = \boldsymbol{\Omega}^{1.2}_{i} \frac{\nu + u_i(t_2)}{\nu+1},$$

$$\boldsymbol{\Gamma}^{1.2}_{ij_1,\cdots,j_{r-1}}(t_2) = \boldsymbol{\Gamma}^{1.2}_{ij_1,\cdots,j_{r-1}} \frac{\nu + u_i(t_2)}{\nu+1},$$

$$\boldsymbol{\Lambda}^{1.2}_{ij_1,\cdots,j_{r-1}}(t_2) = \boldsymbol{\Lambda}^{1.2}_{ij_1,\cdots,j_{r-1}} \frac{\nu + u_i(t_2)}{\nu+1}.$$

In a similar manner, the conditional mean of $\mathbf{X}_{[r]}$, given $Y_{(r)}$ is given by

$$E\left(\mathbf{X}_{[r]} \mid Y_{(r)} = t_2\right) = \sum_{i=1}^{n} \sum_{\substack{j_1<\cdots<j_{r-1} \\ 1\le j_k\le n-1}} \pi^{t}_{ij_1,\cdots,j_{r-1}} \boldsymbol{\mu}^{*}_{ij_1,\cdots,j_{r-1}}(t_2)\,, \tag{14}$$

where $\boldsymbol{\mu}^{*}_{ij_1,\cdots,j_{r-1}}(t_2)$ denotes the mean of $SUT_{p,n-1}\left(\boldsymbol{\theta}^{*1.2}_{ij_1,\cdots,j_{r-1}}(t_2), \nu\right)$.

5 Illustrative Example

To illustrate the results derived in the preceding sections, we consider a real dataset from Johnson and Wichern (2007) (the data are presented in Table 1). This dataset gives the mineral content of three bones obtained by photon absorptiometry from 25 older women. Measurements were recorded on three bones (radius, humerus and ulna) on the dominant and non-dominant sides. Let us specifically denote

Table 1 Mineral content in bones

Subject	Dominant radius	Radius	Dominant humerus	Humerus	Dominant ulna	Ulna
1	1.103	1.052	2.139	2.238	0.873	0.872
2	0.842	0.859	1.873	1.741	0.590	0.744
3	0.925	0.873	1.887	1.809	0.767	0.713
4	0.857	0.744	1.739	1.547	0.706	0.674
5	0.795	0.809	1.734	1.715	0.549	0.654
6	0.787	0.779	1.509	1.474	0.782	0.571
7	0.933	0.880	1.695	1.656	0.737	0.803
8	0.799	0.851	1.740	1.777	0.618	0.682
9	0.945	0.876	1.811	1.759	0.853	0.777
10	0.921	0.906	1.954	2.009	0.823	0.765
11	0.792	0.825	1.624	1.657	0.686	0.668
12	0.815	0.751	2.204	1.846	0.678	0.546
13	0.755	0.724	1.508	1.458	0.662	0.595
14	0.880	0.866	1.786	1.811	0.810	0.819
15	0.900	0.838	1.902	1.606	0.723	0.677
16	0.764	0.757	1.743	1.794	0.586	0.541
17	0.733	0.748	1.863	1.869	0.672	0.752
18	0.932	0.898	2.028	2.032	0.836	0.805
19	0.856	0.786	1.390	1.324	0.578	0.610
20	0.890	0.950	2.187	2.087	0.758	0.718
21	0.688	0.532	1.650	1.378	0.533	0.482
22	0.940	0.850	2.334	2.225	0.757	0.731
23	0.493	0.616	1.037	1.268	0.546	0.615
24	0.835	0.752	1.509	1.422	0.618	0.664
25	0.915	0.936	1.971	1.869	0.869	0.868

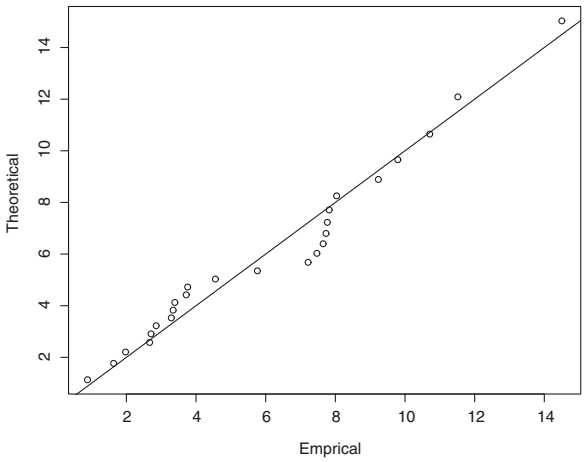

Fig. 1 The chi-squared Q-Q plot for the six-dimensional data

X_{11} : mineral content in dominant side of Radius bone,

X_{12} : mineral content in non-dominant side of Radius bone,

X_{21} : mineral content in dominant side of Humerus bone,

X_{22} : mineral content in non-dominant side of Humerus bone,

X_{31} : mineral content in dominant side of Ulna bone,

X_{32} : mineral content in non-dominant side of Ulna bone,

and $\boldsymbol{X}_i = (X_{i1}, X_{i2})^\top$, $i = 1, 2, 3$. We first calculate the generalized Shapiro–Wilk statistic (Villasenor-Alva and Gonzalez-Estrada 2009) and the E-statistic (energy) (Szekely and Rizzo 2005) to evaluate the joint normality of $\left(\boldsymbol{X}_1^\top,\ \boldsymbol{X}_2^\top,\ \boldsymbol{X}_3^\top\right)^\top$. We found the corresponding p-values to be 0.7801 and 0.1952, respectively. These p-values, as well as the chi-squared Q-Q plot shown in Fig. 1, support the joint normality assumption on these variables.

We, therefore, assume that $\left(\boldsymbol{X}_1^\top,\ \boldsymbol{X}_2^\top,\ \boldsymbol{X}_3^\top\right)^\top \sim N_6\left(\hat{\boldsymbol{\mu}}, \hat{\boldsymbol{\Sigma}}\right)$, where $\hat{\boldsymbol{\mu}}$ and $\hat{\boldsymbol{\Sigma}}$ are the MLEs of the mean vector and the covariance matrix, given by

$$\hat{\boldsymbol{\mu}} = \begin{pmatrix} \hat{\mu}_{X_{11}} \\ \hat{\mu}_{X_{12}} \\ \hat{\mu}_{X_{21}} \\ \hat{\mu}_{X_{22}} \\ \hat{\mu}_{X_{31}} \\ \hat{\mu}_{X_{32}} \end{pmatrix} = \begin{pmatrix} 0.8438 \\ 0.8183 \\ 1.7927 \\ 1.7348 \\ 0.7044 \\ 0.6938 \end{pmatrix}, \quad \hat{\boldsymbol{\Sigma}}_{XX} = \begin{pmatrix} 0.0125 & 0.0100 & 0.0215 & 0.0193 & 0.0088 & 0.0076 \\ & 0.0110 & 0.0178 & 0.0203 & 0.0082 & 0.0086 \\ & & 0.0771 & 0.0641 & 0.0162 & 0.0123 \\ & & & 0.0667 & 0.0170 & 0.0161 \\ & & & & 0.0111 & 0.0077 \\ & & & & & 0.0102 \end{pmatrix}.$$

Let $Y_i = X_{i1} + X_{i2}$, and suppose we are interested in finding the best (nonlinear) prediction (under square error loss) of the mineral content in dominant and non-

dominant sides of a bone where for this bone the sum of mineral content in both sides is less than that of other bones, i.e., we are interested in $E\left(\boldsymbol{X}_{[1]}\right)$.

From (11), the estimated mean of $\boldsymbol{X}_{[1]}$ can be determined as

$$\hat{E}\left(\boldsymbol{X}_{[1]}\right) = \sum_{i=1}^{3} \hat{\pi}_i \, \hat{\boldsymbol{\mu}}_i,$$

where $\hat{\boldsymbol{\mu}}_i$ denotes the mean of $SUN_{2,2}\left(\hat{\boldsymbol{\theta}}_i\right)$, with $\hat{\boldsymbol{\mu}}_i = \left(\hat{\boldsymbol{\xi}}_i, \hat{\boldsymbol{\eta}}_i, \hat{\boldsymbol{\Omega}}_i, \hat{\boldsymbol{\Gamma}}_i, \hat{\boldsymbol{\Lambda}}_i\right)$. Then, we find

$$\hat{\mu}_{Y_1} = 1.6621, \ \hat{\mu}_{Y_2} = 3.5275, \ \hat{\mu}_{Y_3} = 1.3982,$$

$$\hat{\boldsymbol{\xi}_1} = \begin{pmatrix} 0.8438 \\ 0.8183 \end{pmatrix}, \ \hat{\boldsymbol{\xi}_2} = \begin{pmatrix} 1.7927 \\ 1.7348 \end{pmatrix}, \ \hat{\boldsymbol{\xi}_3} = \begin{pmatrix} 0.7044 \\ 0.6938 \end{pmatrix},$$

$$\hat{\boldsymbol{\eta}_1} = \begin{pmatrix} 1.8654 \\ -0.2639 \end{pmatrix}, \ \hat{\boldsymbol{\eta}_2} = \begin{pmatrix} -1.8654 \\ -2.1293 \end{pmatrix}, \ \hat{\boldsymbol{\eta}_3} = \begin{pmatrix} 0.2639 \\ 2.1293 \end{pmatrix}$$

$$\hat{\boldsymbol{\Omega}_1} = \begin{bmatrix} 0.0125 & 0.0100 \\ 0.0100 & 0.0110 \end{bmatrix}, \ \hat{\boldsymbol{\Omega}_2} = \begin{bmatrix} 0.0771 & 0.0641 \\ 0.0641 & 0.0667 \end{bmatrix}, \ \hat{\boldsymbol{\Omega}_3} = \begin{bmatrix} 0.0111 & 0.0077 \\ 0.0077 & 0.0102 \end{bmatrix},$$

$$\hat{\boldsymbol{\lambda}_1} = \begin{bmatrix} 0.0183 & 0.0171 \\ -0.0061 & -0.0042 \end{bmatrix}, \ \hat{\boldsymbol{\lambda}_2} = \begin{bmatrix} -0.1019 & -0.0912 \\ -0.1127 & -0.0977 \end{bmatrix}, \ \hat{\boldsymbol{\lambda}_3} = \begin{bmatrix} -0.0018 & -0.0017 \\ 0.0144 & 0.0105 \end{bmatrix},$$

$$\hat{\boldsymbol{\Gamma}}_1 = \begin{bmatrix} 0.1577 & -0.007 \\ -0.007 & 0.0138 \end{bmatrix}, \ \hat{\boldsymbol{\Gamma}}_2 = \begin{bmatrix} 0.1577 & 0.1647 \\ 0.1647 & 0.1855 \end{bmatrix}, \ \hat{\boldsymbol{\Gamma}}_3 = \begin{bmatrix} 0.0138 & 0.0208 \\ 0.0208 & 0.1855 \end{bmatrix},$$

and

$$\hat{\pi}_1 = 0.012337, \ \hat{\pi}_2 = 0.000000297, \ \hat{\pi}_3 = 0.9876627,$$

$$\hat{\boldsymbol{\mu}}_1 = \begin{pmatrix} 0.709155 \\ 0.721094 \end{pmatrix}, \ \hat{\boldsymbol{\mu}}_2 = \begin{pmatrix} 0.4427732 \\ 0.5553359 \end{pmatrix}, \ \hat{\boldsymbol{\mu}}_3 = \begin{pmatrix} 0.7039037 \\ 0.6933313 \end{pmatrix}.$$

Therefore, we find

$$\hat{E}\left(\boldsymbol{X}_{[1]}\right) = \begin{pmatrix} 0.7039685 \\ 0.6936738 \end{pmatrix}.$$

Next, suppose we are interested in finding the best (nonlinear) prediction (under square error loss) of the mineral content in the dominant and non-dominant sides of a bone where for this bone the sum of mineral content in both sides is minimum in comparison with the other bones and its value is 1.5, i.e., we are interested in $E\left(\boldsymbol{X}_{[1]} \middle| Y_{(1)} = 1.5\right)$.

From (13), the estimated conditional expectation can be determined as

$$\hat{E}\left(\boldsymbol{X}_{[1]}\,|Y_{(1)}=1.5\right)=\sum_{i=1}^{3}\hat{\pi}_i^n\,\hat{\boldsymbol{\mu}}_i\,(1.5)\,,$$

where

$$\hat{\pi}_1^n=0.01336501,\ \hat{\pi}_2^n=2.731107e-09,\ \hat{\pi}_3^n=0.986635,$$

$$\hat{\boldsymbol{\mu}}_1\,(1.5)=\begin{pmatrix}0.4944770\\0.5225139\end{pmatrix},\ \hat{\boldsymbol{\mu}}_2\,(1.5)=\begin{pmatrix}-4.101705\\-3.583772\end{pmatrix},\ \hat{\boldsymbol{\mu}}_3\,(1.5)=\begin{pmatrix}0.7554106\\0.7423744\end{pmatrix},$$

so that we find

$$\hat{E}\left(\boldsymbol{X}_{[1]}\,|Y_{(1)}=1.5\right)=\begin{pmatrix}0.7519232\\0.7394359\end{pmatrix}.$$

6 Conclusion

In this chapter, we have derived the exact distribution of multivariate order statistics induced by ordering linear combinations of the components when the random vectors $\boldsymbol{X}_1,\ldots,\boldsymbol{X}_n$ follow a multivariate elliptical distribution. We also derive the joint distribution of the rth order statistic and its concomitant vector in this case. The class of multivariate normal and student-t distributions have been discussed in detail as special cases. Finally, we illustrate the usefulness of the established results by a real dataset.

Appendix

Proof of Theorem 2

Proof The cdf of $\mathbf{X}_{[r]}$ is

$$F_{[r]}\left(\mathbf{t};\boldsymbol{\mu},\boldsymbol{\Sigma},h^{(np)}\right)=\Pr\left(\mathbf{X}_{[r]}\le\mathbf{t}\right)=\sum_{i=1}^{n}\Pr\left(\mathbf{X}_i\le\mathbf{t}\,,Y_{(r)}=Y_i\right).\tag{15}$$

Let us consider the ith term on the RHS of (15), and express it as

$$\Pr\left(\mathbf{X}_i\le\mathbf{t}\,,Y_{(r)}=Y_i\right)$$

$$= \sum_{\substack{j_1<\cdots<j_{r-1} \\ 1\le j_k\le n-1}} \Pr\left(\mathbf{X}_i \le \mathbf{t}\,, \mathbf{S}_{j_1\cdots j_{r-1}}\,(\mathbf{1}_{n-1}Y_i - \mathbf{Y}_{-i}) > \mathbf{0}\right)$$

$$= \sum_{\substack{j_1<\cdots<j_{r-1} \\ 1\le j_k\le n-1}} \Pr\left(\mathbf{X}_i \le \mathbf{t} \,\middle|\, \mathbf{S}_{j_1\cdots j_{r-1}}\,(\mathbf{1}_{n-1}Y_i - \mathbf{Y}_{-i}) > \mathbf{0}\right)$$

$$\Pr\left(\mathbf{S}_{j_1\cdots j_{r-1}}\,(\mathbf{1}_{n-1}Y_i - \mathbf{Y}_{-i}) > \mathbf{0}\right),$$

for $i = 1, \ldots, n$. Now,

$$\Pr\left(\mathbf{S}_{j_1\cdots j_{r-1}}\,(\mathbf{1}_{n-1}Y_i - \mathbf{Y}_{-i}) > \mathbf{0}\right) = \pi_{ij_1,\ldots,j_{r-1}},$$

and since

$$\begin{pmatrix} \mathbf{S}_{j_1\cdots j_{r-1}}\,(\mathbf{1}_{n-1}Y_i - \mathbf{Y}_{i(-1)}) \\ \mathbf{X}_i \end{pmatrix}$$

$$\sim EC_{n(p+1)-1}\left(\begin{pmatrix} \boldsymbol{\eta}_{i,j_1,\ldots,j_{r-1}} \\ \boldsymbol{\xi}_i \end{pmatrix}, \begin{pmatrix} \boldsymbol{\Gamma}_{i,j_1,\ldots,j_{r-1}} & \boldsymbol{\lambda}_{i,j_1,\cdots,j_{r-1}} \\ \boldsymbol{\lambda}^{\top}_{i,j_1,\ldots,j_{r-1}} & \boldsymbol{\Omega}_i \end{pmatrix}, h^{(p+n-1)}\right),$$

we obtain, by (4),

$$\Pr\left(\mathbf{X}_i \le \mathbf{t} \,\middle|\, \mathbf{S}_{j_1\cdots j_{r-1}}\,(\mathbf{1}_{n-1}Y_i - \mathbf{Y}_{-i}) > \mathbf{0}\right) = G_{SUE_{p,n-1}}\left(t; \boldsymbol{\theta}_{i,j_1,\ldots,j_{r-1}}, h^{(p+n-1)}\right),$$

which readily yields the required mixture representation for the cdf. □

Program Code

The program of Q-Q plot and the p-values of energy and generalized Shapiro–Wilk tests.

```
\library(foreign)
\library(energy)
\library(mvnormtest)
\mvnorm.etest(Data)
\library(mvShapiroTest)
\mvShapiro.Test(Data)
\n=nrow(Data)
\D=c()
\Sigma.hat=((n-1)/n*cov(Data))
\Mean.hat=colMeans(Data)
```

(continued)

```
\for(i in 1:n){D[i]=t(Data[i,]-Mean.hat)
     %*%solve(Sigma.hat)%*%(Data[i,]-Mean.hat)}
\Q=(1:n-0.5)/n
\Theoretical=qchisq(Q,df=6)
\Emprical=sort(D)
\plot(Emprical,Theoretical)
\abline(a=0,b=1)
\Mean.hat
\round(Sigma.hat,4)
\mvnorm.etest(Data, R = 999)
\mvnorm.e(Data)
\normal.e(Data)
\mvnorm.etest
```

References

Aghamohammadi, S. Z., Jamalizadeh, A., Farnoosh, R., & Balakrishnan, N. (2012). Prediction based on linear combinations of order statistics and bivariate concomitants in the case of multivariate elliptical distributions. *Journal of Statistical Computation and Simulation, 84*, 1079–1098.

Arellano-Valle, R. B., & Azzalini, A. (2006). On the unification of families of skew-normal distributions. *Scandinavian Journal of Statistics, 33*, 561–574.

Arellano-Valle, R. B., & Genton, M. G. (2010). Multivariate unified skew-elliptical distributions. *Chilean Journal of Statistics, 1*, 17–33.

Arnold, B. C., & Beaver, R. J. (2002). Skew multivariate models related to hidden truncation and/or selective reporting (with discussion). *Test, 11*, 7–54.

Arnold, B. C., Castillo, E., & Sarabia, J. M. (2009). Multivariate order statistics via multivariate concomitants. *Journal of Multivariate Analysis, 100*, 946–951.

Azzalini, A. (1985). A class of distributions which includes the normal ones. *Scandinavian Journal of Statistics, 12*, 171–178.

Azzalini, A., & Dalla Valle, A. (1996). The multivariate skew-normal distribution. *Biometrika, 74*, 715–729.

Balakrishnan, N. (1993). Multivariate normal distribution and multivariate order statistics induced by ordering linear combinations. *Statistics and Probability Letters, 23*, 239–242.

Bhattacharya, P. K. (1984). Induced order statistics: Theory and applications. In P. R. Krishnaiah & P. K. Sen (Eds.), *Handbook of statistics* (Vol. 4, pp. 383–403). Amsterdam: North-Holland.

Cambanis, S., Huang, S., & Simons, G. (1981). On the theory of elliptically contoured distributions. *Journal of Multivariate Analysis, 11*, 368–385.

David, H. A. (1973). Concomitants of order statistics. *Bulletin of International Statistical Institute, 45*, 295–300.

David, H. A. (1982). Concomitants of order statistics: Theory and applications. In J. Tiago de Oliveira (Ed.), *Some recent advances in statistics* (pp. 89–100). New York: Academic Press.

Fang, K. T., Kotz, S., & Ng, K. W. (1990). *Symmetric multivariate and related distributions*. London: Chapman & Hall.

Genton, M. G. (2004). *Skew-elliptical distributions and their applications: A journey beyond normality*. Boca Raton: CRC Press.

Henze, N. A. (1986). A probabilistic representation of the skew-normal distribution. *Scandinavian Journal of Statistics, 13*, 271–275.

Ho, H. J., Lin, T. I., Chen, H. Y., & Wang, W. L. (2012). Some results on the truncated multivariate t distribution. *Journal of Statistical Planning and Inference, 142*, 25–40.

Jamalizadeh, A., & Balakrishnan, N. (2012). Concomitants of order statistics from multivariate elliptical distributions. *Journal of Statistical Planning and Inference, 142*, 397–409.

Johnson, R. A., & Wichern, D. W. (2007). *Applied multivariate statistical analysis* (6th ed.). Upper Saddle River: Pearson.

Kelker, D. (1970). Distribution theory of spherical distributions and a location scale parameter generalization. *Sankhya, A 32*, 419–430.

Song, R., & Deddens, J. A. (1993). A note on moments of variables summing to normal order statistics. *Statistics and Probability Letters, 17*, 337–341.

Szekely, G. J., & Rizzo, M. L. (2005). A new test for multivariate normality. *Journal of Multivariate Analysis, 93*, 58–80.

Villasenor-Alva, J. A., & Gonzalez-Estrada, E. (2009). A generalization of Shapiro-Wilk's test for multivariate normality. *Communications in Statistics-Theory and Methods, 38*, 1870–1883.

Variable Selection in Heteroscedastic Regression Models Under General Skew-t Distributional Models Using Information Complexity

Yeşim Güney, Olcay Arslan, and Hamparsum Bozdogan

Abstract In this paper we study several competing models under general class of skew-t distributions. Namely. we consider joint location and scale model (JLSM) under Student's t and under skew-t distributions, respectively. Similarly, we consider the extension of JLSM to joint location-scale and skewness model (JLSSM) under skew-t distribution in heteroscedastic regression models for subset selection of variables and to deal with heavy-tailedness, and skewness in a data set. To this end, for the first time, we introduce and develop the information-theoretic measure of complexity (ICOMP) criterion in such problems to select the best subset of predictor variables. We provide the computational forms of the celebrated Fisher information and the inverse Fisher information matrices for these models to be used in ICOMP. A large-scale Monte Carlo simulation study is carried out to study the performance of ICOMP in such complicated models. In addition, a real example is provided on a real benchmark data set to select the best subset of the predictors under these three competing models without knowing the true structure and the distributional form of the regression model. Our approach shows the flexibility and versatility of our approach for model selection in complex models.

1 Introduction

The normal distribution is a common continuous probability model which is used almost always to analyze data set in many statistical applications. However, when the data exhibits very high skewness and heavy or tick tails, it is no longer that normal probability model is a good choice in models complex data structures.

Y. Güney · O. Arslan (✉)
Faculty of Science, Department of Statistics, Ankara University, Ankara, Turkey
e-mail: ydone@ankara.edu.tr; oarslan@ankara.edu.tr

H. Bozdogan
The University of Tennessee, Knoxville, TN, USA
e-mail: bozdogan@utk.edu

A. Bekker et al. (eds.), *Computational and Methodological Statistics and Biostatistics*, Emerging Topics in Statistics and Biostatistics,
https://doi.org/10.1007/978-3-030-42196-0_4

In the literature, therefore, joint location and scale models (JLSMs) have been popular for modelling complex data sets. In particular, there are several research works focused on JLSM to model data sets involving heteroscedasticity. In reviewing the literature, for example, we see that Park (1966) proposed a log-linear model for the scale parameter and described the Gaussian model using a two-stage process to estimate the parameters. Harvey (1976) investigated the maximum likelihood (ML) estimation of the location and suggested a likelihood ratio test for heteroscedasticity. Aitkin (1987) offered to model variance heterogeneity in normal regression analysis and provided ML estimation for a JLSM. However, since the normal distribution is not suitable for modeling heavy-tailed data sets, alternative distributions, such as t-distribution is used by Lange et al. (1989). Further, Taylor and Verbyla (2004) proposed the JLSM of the t-distribution for modeling heteroscedastic data sets that are symmetric and heavy-tailed. For the multivariate data sets, Lin and Wang (2009) proposed a t-based joint modeling of mean-scale covariance for the analysis of longitudinal data and demonstrated its robustness through several real examples. Later, Lin and Wang (2011) investigated Bayesian inference for the JLSM under the t distribution for longitudinal data.

If we are dealing with asymmetric data sets, modeling such data sets with a symmetric distribution may result in wrong statistical inferences. Therefore, for such data sets skew distributional models would be more appropriate to be used for general modeling purposes. Although there are several skew distributions that can be used as alternative to the symmetric distributions for modeling skew and/or heavy-tailed data sets, Azzalini type skew normal and skew-t distributions (Azzalini 1985, 2003), and their variants are the most popular skew distributions used in literature. For this reason, the JLSM of Azzalini type skew distributions have also been considered for modeling heteroscedasticity of skew data sets. For example, Li and Wu (2014) studied the JLSM of the skew normal distribution, Wu et al. (2013) obtained the ML estimators of the JLSM of the skew-t-normal distribution and Wu (2014) proposed a method for parameter estimation in the JLSM of the skew-t-normal distribution. Although, all of the skew distributions mentioned above have a parameter controlling skewness, the proposed joint models only involve modeling location and scale parameters not the skewness parameter. The first attempt to model skewness parameter along with the location and scale parameters is given by Li et al. (2017). In their paper, joint location, scale and skewness model (JLSSM) of the skew-normal distribution is only considered. Later, many researchers have proposed modeling the skewness parameters to understand the source of variability in skewness.

When we deal with JLSM, the location, and scale parameters are expressed with models involving unknown parameters and explanatory variables. One of our tasks is to estimate the unknown parameters. Similarly, if we have joint location-scale and skewness model (JLSSM), beside the location and scale parameters the skewness parameter is also expressed with a model involving some explanatory variables along with other unknown parameters. In general, all of the unknown parameters in these models need to be estimated. It is experienced that in applications a large number of explanatory variables are usually introduced at the initial stage of the model

to learn possible modeling biases. However, including unnecessary explanatory variables can degrade the efficiency of the resulting estimation procedure and yields less accurate predictions. On the other hand, omitting an important explanatory variable may produce biased parameter estimates and prediction results. Therefore, selecting significant explanatory variables in JLSM and JLSSM is a challenging problem. To handle this problem, many researchers have turned their attentions to the problem of variable selection in these models, but they have only considered selecting explanatory variables in location and scale models. For example, Wang and Zhang (2009) proposed only variable selection of the mean explanation variable criterion based on the extended quasi-likelihood for joint generalized linear models with structured dispersions. Zhang and Wang (2011) proposed a simultaneous variable selection criterion for selecting both the mean model and variance model in a special class of heteroscedastic linear models. Wu and Li (2012) proposed a unified procedure simultaneously to select significant variables in mean and dispersion model under the inverse Gaussian distribution. Wu et al. (2012) proposed a unified procedure, which can simultaneously select significant variables in the joint mean and variance models using the Box–Cox transformation. Wu et al. (2013) proposed a unified penalized likelihood method, which can simultaneously perform parameter estimation and variable selection in JLSM under skew-normal distribution. Wu (2014) proposed a parameter estimation and variable selection method based on the penalized likelihood in JLSM under the skew-t-normal distribution. Zhao and Zhang (2015) developed an efficient penalized likelihood-based method in JLSM under the Student t-distribution. Later, Wu et al. (2016) developed a unified penalized t-type pseudo-likelihood method to simultaneously select significant variables for the mean and dispersion models in the t-type joint generalized linear model. In these studies, the variable selection is considered for only location and scale models. Although, selecting significant variables in the skewness model to determine the source of variability in skewness is as important as that in the location and scale models, few number of research have been carried out to study variable selection in JLSSM. Recently, Li et al. (2017) and Wu et al. (2017) have considered variable selection in JLSSM under the skew-normal distribution and skew-t-normal distribution, respectively. In both papers, they have used the penalized maximum likelihood method to carry out the parameter estimation and variable selection, simultaneously. However, since a JLSSM involves three different models with different sets of unknown parameters and the related explanatory variables, the penalized likelihood methods usually become computationally very intensive due to the large number of unknown parameters that need to be either estimated or chosen.

In addition to the previous studies, in this paper our objectives are twofold. One of these objectives is to use the JLSSM of the skew-t distribution as an alternative to the JLSSM under the skew-normal distribution if robustness against non-normality or outliers is a concern. Since Student's t distribution and its Azzalini type skew extension (Azzalini 2003) are very popular among researchers for modeling data sets with heavy-tails and asymmetric features, in this paper we will use Azzalini type skew-t distribution. Our second objective is to carry out variable selection in

the JLSSM under the skew-t distribution using a computationally efficient model selection method for variable selection in both JLSM and JLSSM. To be more specific, in this paper, for the first time, we will introduce and use the information-theoretic measure of complexity (ICOMP) criterion developed by Bozdogan (1990, 2000, 2003, 2004) to select the important subsets of explanatory variables in three models related to the location, scale and skewness parameters of the JLSSM under the skew-t distribution. Since the ICOMP is based on the covariance matrix of the parameter estimates or the estimated inverse Fisher information matrix (IFIM) of the estimators under consideration, we first derive these matrices for the three models. Then, we provide the analytical forms of ICOMP criterion to select the important explanatory variables in the JLSSM under the skew-t distribution. After establishing parameter estimation and proposed variable selection procedure, we carry out a large-scale Monte Carlo simulation study to study the performance of the information criterion. A real benchmark data example is also shown to assess the finite sample performance of the proposed JLSSM and variable selection procedure.

The rest of the paper is organized as follows. In Sect. 2, we develop the heteroscedastic regression models under the general skew-t distributions for the JLSM under Student's t distribution, JLSM and JLSSM under skew-t distributions. We present the implementation of ML estimation of the parameters of interest. Moreover, we also derive the Fisher information matrices (FIMs) and the inverse Fisher information matrices (IFIMs) needed to score ICOMP. In Sect. 3, we introduce and derive ICOMP for JLSM under Student's t and skew-t distributions and JLSSM under skew-t distribution. Section 4 presents our results from a large-scale Monte Carlo simulation to study the performance of proposed criterion. In Sect. 5, we illustrate the subset selection of variables on a real benchmark data set. Finally, Sect. 6 concludes the paper.

2 Heteroscedastic Regression Models Under General Skew-t Distributions

In this section, we present the JLSM and JLSSM based on the Student's t and the skew-t distributions and provide the parameter estimates of each of the models for the heteroscedastic regression for variable selection.

2.1 Model 1-JLSM: Under Student's t Distribution

It is common for observations to come from a population that has a heavy-tailed distribution. Student's t distribution is one of the basic models for describing heavy-tailed data, which is common in a variety of applications.

Let $y_i \in \mathbb{R}$, for $i = 1, 2, \ldots, n$, be independently distributed random variables and assume that for each i, y_i has the student t distribution ($y_i \sim t\left(\mu_i, \sigma_i^2, \nu\right)$) with the following probability density function (pdf)

$$f(y_i; \mu_i, \sigma_i, \nu) = \frac{c_\nu}{\sigma_i}\left(\nu + \frac{(y_i - \mu_i)^2}{\sigma_i^2}\right)^{-\frac{\nu+1}{2}} \tag{1}$$

where $\mu_i \in \mathbb{R}$ and $\sigma_i > 0$ are the location and scale parameters, respectively. Here ν is the degrees of freedom that can be seen as a robustness parameter and down weights the effect of the outliers. As ν tends to infinity, this model reduces the JLSM under normal distribution. In this study, the parameter ν is regarded as known and we take $\nu = 3$ to achieve the robustness (see Lange et al. 1989; Arslan and Genç 2003). Figure 1 shows the plots of the pdf of the Student t distribution for different degrees of the freedom.

Now, let us consider the JLSM of the student t distribution given by

$$\begin{cases} y_i \sim t\left(\mu_i, \sigma_i^2, \nu\right) \\ \mu_i = \boldsymbol{x}_i^T \boldsymbol{\beta} \\ \log \sigma_i^2 = \boldsymbol{z}_i^T \boldsymbol{\gamma} \\ i = 1, 2, \ldots, n \end{cases} \tag{2}$$

where $\boldsymbol{x}_i = \left[x_{i1}, x_{i2}, \ldots, x_{ip}\right]^T$ and $\boldsymbol{z}_i = \left[z_{i1}, z_{i2}, \ldots, z_{iq}\right]^T$ are the observed covariates corresponding to the response y_i, and $\boldsymbol{\beta} = \left[\beta_1, \beta_2, \ldots, \beta_p\right]^T \in \mathbb{R}^p$ and $\boldsymbol{\gamma} = \left[\gamma_1, \gamma_2, \ldots, \gamma_q\right]^T \in \mathbb{R}^q$ are the unknown parameter vectors in the location and scale models, respectively. We will assume that $n > p + q$. Note that, although we use two different sets of explanatory variables to model location and scale

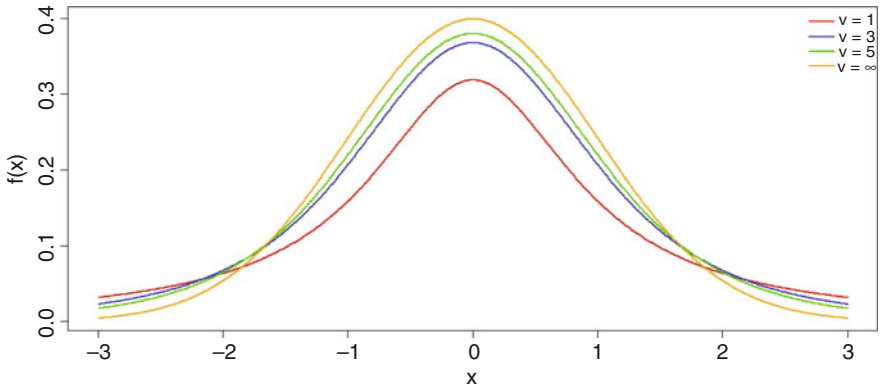

Fig. 1 Pdf of the Student t distribution for different values of the degrees of freedom ν

parameters, there may be only one set of explanatory variables to model location and scale parameters in some problems.

In this model the first major problem is to estimate the unknown parameter vectors $\boldsymbol{\beta}$ and $\boldsymbol{\gamma}$. We will use the maximum likelihood (ML) estimation method to estimate the unknown parameters. Let $\boldsymbol{\theta} = (\theta_1, \theta_2, \ldots, \theta_{s_1}) = (\boldsymbol{\beta}^T, \boldsymbol{\gamma}^T)$ with $s_1 = p+q$ be the combined vector of unknown parameters that need to be estimated. Given independent observations $y_1, y_2, \ldots, y_n$ the log likelihood function of $\boldsymbol{\theta}$ corresponding to the JLSM of the student t distribution can be written as follows

$$\begin{aligned}\ell(\boldsymbol{\theta}|\, y, \boldsymbol{x}, \boldsymbol{z}) &= n\log(c_\nu) - \frac{1}{2}\sum_{i=1}^{n}\log\sigma_i^2 - \frac{\nu+1}{2}\sum_{i=1}^{n}\log\left(\nu + \frac{(y_i-\mu_i)^2}{\sigma_i^2}\right)\\ &= n\log(c_\nu) - \frac{1}{2}\sum_{i=1}^{n}\boldsymbol{z}_i^T\boldsymbol{\gamma}\\ &\quad -\frac{\nu+1}{2}\sum_{i=1}^{n}\log\left(\nu + \frac{\left(y_i - \boldsymbol{x}_i^T\boldsymbol{\beta}\right)^2}{\boldsymbol{e}^{\boldsymbol{z}_i^T\boldsymbol{\gamma}}}\right), \end{aligned} \tag{3}$$

where $c_\nu = \frac{\Gamma\left(\frac{\nu+1}{2}\right)\nu^{\nu/2}}{\sqrt{\pi}\Gamma\left(\frac{\nu}{2}\right)}$ and $(\boldsymbol{x}_i, \boldsymbol{z}_i)$, for $i = 1, 2, \ldots, n$ are the corresponding explanatory variables. The ML estimate of $\boldsymbol{\theta}$ can be obtained by setting the score function $\boldsymbol{S}(\boldsymbol{\theta})$ to zero and solving the score equations. The components of the score function $\boldsymbol{S}(\boldsymbol{\theta}) = (\boldsymbol{S}_{\boldsymbol{\beta}}^T, \boldsymbol{S}_{\boldsymbol{\beta}}^T)^T$ are:

$$\boldsymbol{S}_{\boldsymbol{\beta}} = \sum_{i=1}^{n}\omega_i\frac{\boldsymbol{x}_i\left(y_i - \boldsymbol{x}_i^T\boldsymbol{\beta}\right)}{\boldsymbol{e}^{\boldsymbol{z}_i^T\boldsymbol{\gamma}}}, \tag{4}$$

$$\boldsymbol{S}_{\boldsymbol{\gamma}} = \frac{1}{2}\sum_{i=1}^{n}\left(\omega_i\frac{\left(y_i - \boldsymbol{x}_i^T\boldsymbol{\beta}\right)^2}{\boldsymbol{e}^{\boldsymbol{z}_i^T\boldsymbol{\gamma}}} - 1\right)\boldsymbol{z}_i. \tag{5}$$

Here $\omega_i = \frac{\nu+1}{\nu+\frac{\left(y_i-\boldsymbol{x}_i^T\boldsymbol{\beta}\right)^2}{\boldsymbol{e}^{\boldsymbol{z}_i^T\boldsymbol{\gamma}}}}$ is a weight for the ith point in the ith subject. Since ω_i decreases with increasing $\frac{\left(y_i-\boldsymbol{x}_i^T\boldsymbol{\beta}\right)^2}{\boldsymbol{e}^{\boldsymbol{z}_i^T\boldsymbol{\gamma}}}$ when $\nu < \infty$, the ML estimations of the parameters are robust in the sense that outliers are downweighted.

For the sake of simplicity, let $\boldsymbol{X} = [\boldsymbol{x_1}, \boldsymbol{x_2}, \ldots, \boldsymbol{x_p}]$ with $rank(\boldsymbol{X}) = p$, $\boldsymbol{y} = [y_1, y_2, \ldots, y_n]^T$, $\boldsymbol{R} = diag\left\{\frac{1}{\sigma_i^2}\right\}_{i=1}^{n}$ and $\boldsymbol{W} = diag\{\omega_i\}_{i=1}^{n}$ be diagonal $(n \times n)$ matrices. Then we get the following equation for the ML estimate of $\boldsymbol{\beta}$

$$\widehat{\boldsymbol{\beta}} = \left(\boldsymbol{X}^T\widehat{\boldsymbol{R}}\widehat{\boldsymbol{W}}\boldsymbol{X}\right)^{-1}\left(\boldsymbol{X}^T\widehat{\boldsymbol{R}}\widehat{\boldsymbol{W}}\boldsymbol{y}\right), \tag{6}$$

provided that $\left(\boldsymbol{X}^T\widehat{\boldsymbol{R}}\widehat{\boldsymbol{W}}\boldsymbol{X}\right)^{-1}$ exists.

To obtain the estimate of the scale parameter vector $\boldsymbol{\gamma}$, we need to solve the following equation

$$\boldsymbol{Z}^T\,(\widehat{\boldsymbol{r}} - \mathbf{1}_{n\times n}) = \mathbf{0}, \tag{7}$$

where $\boldsymbol{Z} = [\boldsymbol{z_1}, \boldsymbol{z_2}, \ldots, \boldsymbol{z_q}]$ with $rank(\boldsymbol{Z}) = q$, $\boldsymbol{r}$ is the vector of length n with ith element $\omega_i u_i^2$, $u_i = \frac{(y_i-\mu_i)}{\sigma_i}$, and $\mathbf{1}_{n\times n} = [1, 1, \ldots, 1]^T$.

Equations (4) and (5) are clearly non-linear equations, which means that there is not a straightforward solution. Thus, iterative procedures such as the Newton-Raphson or Fisher-scoring methods have been considered in the literature (Taylor and Verbyla 2004) in order to obtain the ML estimates of $\boldsymbol{\beta}$ and $\boldsymbol{\gamma}$.

The covariance matrix of the ML estimators of the parameters can be obtained by using the inverse of the following FIM

$$\mathcal{F}_{JLSM\text{-}t} = \begin{bmatrix} \frac{\nu+1}{\nu+3}(\boldsymbol{X}^T\boldsymbol{R}\boldsymbol{X}) & \mathbf{0} \\ \mathbf{0} & \frac{\nu}{2(\nu+3)}\boldsymbol{Z}^T\boldsymbol{R}\boldsymbol{R}\boldsymbol{Z} \end{bmatrix} \tag{8}$$

(Taylor and Verbyla 2004). Then the estimated IFIM, that is, the celebrated Cramer-Rao lower bound matrix is given by

$$\widehat{\mathcal{F}}^{-1}_{JLSM\text{-}t} = \begin{bmatrix} \frac{\nu+3}{\nu+1}(\boldsymbol{X}^T\widehat{\boldsymbol{R}}\boldsymbol{X})^{-1} & \mathbf{0} \\ \mathbf{0} & \frac{2(\nu+3)}{\nu}(\boldsymbol{Z}^T\widehat{\boldsymbol{R}}\widehat{\boldsymbol{R}}\boldsymbol{Z})^{-1} \end{bmatrix}. \tag{9}$$

2.2 Model 2-JLSM: Under Skew-t Distribution

In addition to heavy tailedness, there can be a presence of high skewness in the data. To accommodate skewness and heavy tailed data together, the construction of flexible parametric skew distributions has received considerable attention in recent years. Numerous authors have developed various classes of these distributions. In this study, we will use the skew-t distribution, which is proposed by Azzalini (2003). To provide a wide and flexible family of modeling data that account for skewness and heavy tail, Azzalini (2003) have proposed skew-t distribution by introducing a generalization of the Student's t distribution.

Let $y_i \in \mathbb{R}$, for $i = 1, 2, \ldots, n$, be independently distributed random variables and assume that for each i, y_i has the skew-t distribution ($y_i \sim St\,(\mu_i, \sigma_i, \lambda i, \nu)$) with the following pdf

$$f_{St,\nu}(y_i; \mu_i, \sigma_i, \lambda_i, \nu) = \frac{2}{\sigma_i} t_\nu\,(y_{i0}, \nu)\; T_{\nu+1}\left(\lambda y_{i0}\sqrt{\frac{\nu+1}{\nu + y_{i0}^2}}\right) \tag{10}$$

where $\mu_i \in \mathbb{R}$, $\sigma_i > 0$ and $\lambda_i \in \mathbb{R}$ are the location, scale and skewness parameters, respectively. Here $y_{i0} = {}^{(y_i-\mu_i)}/_{\sigma_i}$, $t_\nu\,(\cdot)$ denotes the pdf of Student t distribution

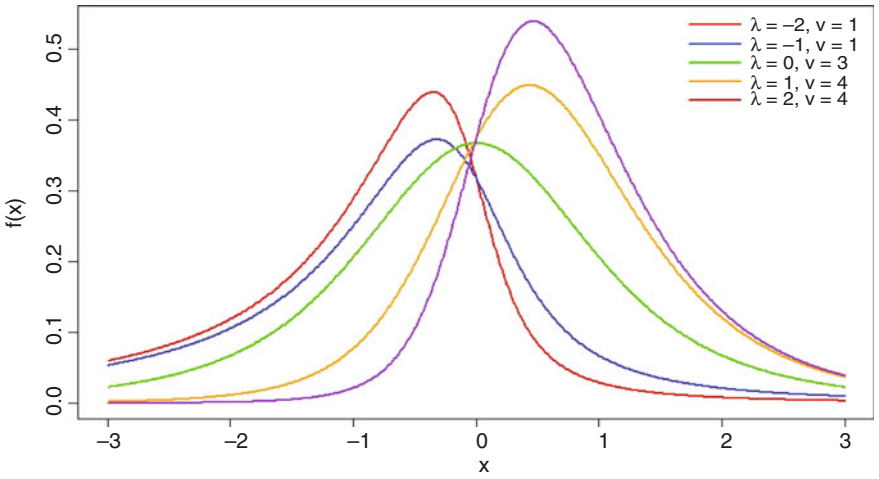

Fig. 2 Pdf of the skew t distribution for different values of the skewness parameter λ and the degrees of freedom ν

with ν degrees of freedom and $T_{\nu+1}(\cdot)$ denotes the cumulative distribution function (cdf) of Student t distribution with $\nu + 1$ degrees of freedom (Azzalini 2003). Figure 2 shows the plots of the pdf of the skew-t distribution for different values of λ and ν.

Similar to the Student's t distribution case, the JLSM under skew-t distribution is defined as follows.

$$\begin{cases} y_i \sim St\left(\mu_i, \sigma_i^2, \lambda, \nu\right) \\ \mu_i = \boldsymbol{x}_i^T \boldsymbol{\beta} \\ \log \sigma_i^2 = \boldsymbol{z}_i^T \boldsymbol{\gamma} \\ i = 1, 2, \ldots, n \end{cases} \tag{11}$$

Note that, the skewness parameter λ has no variability in this model. When λ is equal to zero, this model reduces the JLSM of Student t distribution. Moreover when $\lambda = 0$ and $\nu \to \infty$, this model reduces the JLSM of normal distribution. Here we will assume that $n > p + q + 1$. Similar to Student's t distribution case, the parameter ν is taken 3 to achieve the robustness and regarded as known.

We first obtain the ML estimates of the parameters of JLSM of skew-t distribution. Let $\boldsymbol{\theta} = (\theta_1, \theta_2, \ldots, \theta_{s_2}) = (\boldsymbol{\beta}^T, \boldsymbol{\gamma}^T)$ with $s_2 = p + q + 1$ be the combined vector of unknown parameters. Given independent observations $y_1, y_2, \ldots, y_n$ the log likelihood function of $\boldsymbol{\theta}$ corresponding to the JLSM of the skew t distribution can be written as follows.

$$\ell\left(\boldsymbol{\theta} | \, y, \boldsymbol{x}, \boldsymbol{z}\right) = n \log\left(c_\nu\right) - \frac{1}{2} \sum_{i=1}^{n} \boldsymbol{z}_i^T \boldsymbol{\gamma} - \frac{\nu + 1}{2} \sum_{i=1}^{n} \log\left(\nu + \frac{\left(y_i - \boldsymbol{x}_i^T \boldsymbol{\beta}\right)^2}{\boldsymbol{e}^{\boldsymbol{z}_i^T \boldsymbol{\gamma}}}\right)$$

$$+\sum_{i=1}^{n}\log T_{\nu+1}\left(\lambda u_i\sqrt{\frac{\nu+1}{\nu+\frac{\left(y_i-\boldsymbol{x}_i^T\boldsymbol{\beta}\right)^2}{e^{z_i^T\boldsymbol{\gamma}}}}}\right), \tag{12}$$

where $u_i = \frac{(y_i-\mu_i)}{\sigma_i}$ as defined in Sect. 2.1. The components of the score function $\boldsymbol{S}(\boldsymbol{\theta}) = (\boldsymbol{S}_{\boldsymbol{\beta}}^T, \boldsymbol{S}_{\boldsymbol{\gamma}}^T, \boldsymbol{S}_{\lambda}^T)^T$ are given by

$$\boldsymbol{S}_{\boldsymbol{\beta}} = \sum_{i=1}^{n}\omega_i\frac{\boldsymbol{x}_i\left(y_i-\boldsymbol{x}_i^T\boldsymbol{\beta}\right)}{e^{z_i^T\boldsymbol{\gamma}}} - \frac{\nu}{\nu+1}\sum_{i=1}^{n}\lambda\frac{t_{\nu+1}\left(t_i\sqrt{\omega_i}\right)}{T_{\nu+1}\left(t_i\sqrt{\omega_i}\right)}\frac{\omega_i^{3/2}}{e^{\frac{1}{2}z_i^T\boldsymbol{\gamma}}}\boldsymbol{x}_i, \tag{13}$$

$$\begin{aligned}\boldsymbol{S}_{\boldsymbol{\gamma}} = {} & \frac{1}{2}\sum_{i=1}^{n}\left(\omega_i\frac{\left(y_i-\boldsymbol{x}_i^T\boldsymbol{\beta}\right)^2}{e^{z_i^T\boldsymbol{\gamma}}}-1\right)z_i \\ & -\frac{\nu}{2(\nu+1)}\sum_{i=1}^{n}\frac{\lambda}{e^{\frac{1}{2}z_i^T\boldsymbol{\gamma}}}\frac{t_{\nu+1}\left(t_i\sqrt{\omega_i}\right)}{T_{\nu+1}\left(t_i\sqrt{\omega_i}\right)}\boldsymbol{x}_i z_i\omega_i^{3/2},\end{aligned} \tag{14}$$

$$\boldsymbol{S}_{\lambda} = \sum_{i=1}^{n}\frac{t_{\nu+1}\left(t_i\sqrt{\omega_i}\right)}{T_{\nu+1}\left(t_i\sqrt{\omega_i}\right)}\frac{\left(y_i-\boldsymbol{x}_i^T\boldsymbol{\beta}\right)}{e^{\frac{1}{2}z_i^T\boldsymbol{\gamma}}}\sqrt{\omega_i}. \tag{15}$$

Setting Eq. (13) to zero and solving the equation gives the following equation for $\widehat{\boldsymbol{\beta}}$

$$\widehat{\boldsymbol{\beta}} = \left(\boldsymbol{X}^T\widehat{\boldsymbol{R}}\widehat{\boldsymbol{W}}\boldsymbol{X}\right)^{-1}\left(\boldsymbol{X}^T\widehat{\boldsymbol{R}}\widehat{\boldsymbol{W}}\boldsymbol{y}-\boldsymbol{X}^T\widehat{\boldsymbol{P}}\widehat{\boldsymbol{W}}^{3/2}\widehat{\boldsymbol{\delta}}\right). \tag{16}$$

Here $\boldsymbol{P} = diag\left\{\frac{\lambda}{\sigma_i}\right\}_{i=1}^{n}$ and $\boldsymbol{W^{3/2}} = diag\left\{\omega_i^{3/2}\right\}_{i=1}^{n}$ are diagonal $(n\times n)$ matrices. $\boldsymbol{\delta}$ is the vector of length n with ith element $\delta_i = \frac{\nu}{\nu+1}\frac{t_{\nu+1}(\lambda u_i\sqrt{\omega_i})}{T_{\nu+1}(\lambda u_i\sqrt{\omega_i})}$. It is observed that unlike $\widehat{\boldsymbol{\beta}}$ given in Eq. (6), the estimating equation here includes $\boldsymbol{\delta}$ vector whose elements are extra weights and $\boldsymbol{P}$ matrix which is based on the skewness parameter. The ML estimates of $\boldsymbol{\gamma}$ and λ can be obtained by setting Eqs. (14) and (15) to zero and solving them iteratively. In the JLSM under skew-t distribution case, the ML estimators of the parameters reduce to the ML estimators for Student's t distribution when λ is equal to zero.

In addition, denoting the second partial derivatives of the log likelihood function by $\boldsymbol{S}_{\boldsymbol{\beta\beta}}, \boldsymbol{S}_{\boldsymbol{\beta\gamma}}, \boldsymbol{S}_{\boldsymbol{\beta}\lambda}, \boldsymbol{S}_{\boldsymbol{\gamma\beta}}, \boldsymbol{S}_{\boldsymbol{\gamma\gamma}}, \boldsymbol{S}_{\boldsymbol{\gamma}\lambda}, \boldsymbol{S}_{\lambda\boldsymbol{\beta}}, \boldsymbol{S}_{\lambda\boldsymbol{\gamma}}, \boldsymbol{S}_{\lambda\lambda}$ in what follows, the FIM is defined as

$$\mathcal{F}_{JLSM\text{-}St}\left(\boldsymbol{\beta},\boldsymbol{\gamma},\lambda\right)=-E\begin{bmatrix}\boldsymbol{S}_{\boldsymbol{\beta\beta}} & \boldsymbol{S}_{\boldsymbol{\beta\gamma}} & \boldsymbol{S}_{\boldsymbol{\beta}\lambda}\\ \boldsymbol{S}_{\boldsymbol{\gamma\beta}} & \boldsymbol{S}_{\boldsymbol{\gamma\gamma}} & \boldsymbol{S}_{\boldsymbol{\gamma}\lambda}\\ \boldsymbol{S}_{\lambda\boldsymbol{\beta}} & \boldsymbol{S}_{\lambda\boldsymbol{\gamma}} & \boldsymbol{S}_{\lambda\lambda}\end{bmatrix}. \tag{17}$$

The elements of the FIM are obtained from the equations given in the Appendix. A major difficulty is that some of the elements of the FIM given in Eq. (17) have no closed analytical form. Therefore, we can use the observed FIM which can be derived using following equation to obtain the approximate covariance matrix of the ML estimators.

$$\mathcal{F}_{obs,JLSM\text{-}St}\left(\boldsymbol{\beta},\boldsymbol{\gamma},\lambda\right)=-\begin{bmatrix}\boldsymbol{S}_{\boldsymbol{\beta\beta}} & \boldsymbol{S}_{\boldsymbol{\beta\gamma}} & \boldsymbol{S}_{\boldsymbol{\beta}\lambda}\\ \boldsymbol{S}_{\boldsymbol{\gamma\beta}} & \boldsymbol{S}_{\boldsymbol{\gamma\gamma}} & \boldsymbol{S}_{\boldsymbol{\gamma}\lambda}\\ \boldsymbol{S}_{\lambda\boldsymbol{\beta}} & \boldsymbol{S}_{\lambda\boldsymbol{\gamma}} & \boldsymbol{S}_{\lambda\lambda}\end{bmatrix}_{\boldsymbol{\beta}=\widehat{\boldsymbol{\beta}},\boldsymbol{\gamma}=\widehat{\boldsymbol{\gamma}},\lambda=\widehat{\lambda}}. \tag{18}$$

2.3 Model-3 JLSSM: Under Skew-t Distribution

JLSMs of Student's t and skew-t distributions are limited in addressing only the heteroscedasticity. However, the skewness parameter is at least as important as the other parameters to model the data and it may be different for each observation and depend on some of the covariates. Because of this case, modeling the skewness may also be required. Since our main concern is to provide the best modeling of all parameters and to obtain the best modeling of the data, we also consider the skewness model in addition to location and scale. For this purpose, JLSM under skew-t distribution can be extended to JLSSM under skew-t distribution in order to allow modeling the skewness of the data. In this subsection, we consider the JLSSM under skew-t distribution to take into account the variability of skewness parameter.

Let $y_i \in \mathbb{R}$, for $i = 1, 2, \ldots, n$, be independently distributed with $St\left(\mu, \sigma, \lambda, \nu\right)$ In some cases, in addition to μ and σ^2, the skewness parameter λ may also be different for each y_i, $i = 1, 2, \ldots, n$, and may also be related to a number of variables. Then, the JLSSM under skew-t distribution is defined as follows.

$$\begin{cases} y_i \sim St\left(\mu_i, \sigma_i^2, \lambda_i, \nu\right) \\ \quad \mu_i = \boldsymbol{x}_i^T\boldsymbol{\beta} \\ \quad \log\sigma_i^2 = \boldsymbol{z}_i^T\boldsymbol{\gamma} \\ \quad \lambda_i = \boldsymbol{v}_i^T\boldsymbol{\alpha} \\ \quad i = 1, 2, \ldots, n \end{cases} \tag{19}$$

where $\boldsymbol{v}_i = [v_{i1}, v_{i2}, \ldots, v_{ir}]^T$ denote the observed covariates and $\boldsymbol{\alpha} = [\alpha_1, \alpha_2, \ldots, \alpha_r]^T \in \mathbb{R}^r$ is the unknown parameter vector in the skewness model. We will assume that $n > p + q + r$.

It is important to stress that the JLSSM under skew-t distribution includes the previous models given in Eqs. (2) and (11) as special cases. If the skewness

parameter does not have variability, then JLSSM under skew-t distribution reduces to the JLSM under skew-t distribution. If the skewness parameter is equal to zero, the model reduces the JLSM under Student t distribution. In addition when $\nu \to \infty$, the JLSSM under skew-t distribution reduces the JLSSM under skew-normal distribution. The advantage of the JLSSM under skew-t distribution is that it may give a better fit for heavy-tailed and/or asymmetric data sets.

We next obtain the ML estimates of the parameters of the JLSSM of skew-t distribution. Here, in addition to the parameters of the location and scale models, we also need to estimate the parameter vector of skewness model. Let $\boldsymbol{\theta} = (\theta_1, \theta_2, \ldots, \theta_{s_3}) = (\boldsymbol{\beta}^T, \boldsymbol{\gamma}^T, \boldsymbol{\alpha}^T)$ with $s_3 = p + q + r$ be the combined vector of unknown parameters. Given independent observations $y_1, y_2, \ldots, y_n$ the log likelihood function of $\boldsymbol{\theta}$ corresponding to the JLSSM of the skew t distribution can be written as follows.

$$\ell(\boldsymbol{\theta} | \, y, \boldsymbol{x}, \boldsymbol{z}, \boldsymbol{v}) = n \log(c_\nu) - \frac{1}{2}\sum_{i=1}^{n} \boldsymbol{z}_i^T \boldsymbol{\gamma} - \frac{\nu+1}{2}\sum_{i=1}^{n} \log\left(\nu + \frac{\left(y_i - \boldsymbol{x}_i^T\boldsymbol{\beta}\right)^2}{e^{\boldsymbol{z}_i^T\boldsymbol{\gamma}}}\right) + \sum_{i=1}^{n} \log T_{\nu+1}\left(\boldsymbol{v}_i^T \boldsymbol{\alpha} u_i \sqrt{\frac{\nu+1}{\nu + \frac{\left(y_i - \boldsymbol{x}_i^T\boldsymbol{\beta}\right)^2}{e^{\boldsymbol{z}_i^T\boldsymbol{\gamma}}}}}\right). \tag{20}$$

The components of the score function $\boldsymbol{S}(\boldsymbol{\theta}) = (\boldsymbol{S}_{\boldsymbol{\beta}}^T, \boldsymbol{S}_{\boldsymbol{\gamma}}^T, \boldsymbol{S}_{\boldsymbol{\alpha}}^T)^T$ are given by

$$\boldsymbol{S}_{\boldsymbol{\beta}} = \sum_{i=1}^{n} \omega_i \frac{\boldsymbol{x}_i\left(y_i - \boldsymbol{x}_i^T\boldsymbol{\beta}\right)}{e^{\boldsymbol{z}_i^T\boldsymbol{\gamma}}} - \frac{\nu}{\nu+1}\sum_{i=1}^{n} \boldsymbol{v}_i^T\boldsymbol{\alpha}\frac{t_{\nu+1}\left(t_i\sqrt{\omega_i}\right)}{T_{\nu+1}\left(t_i\sqrt{\omega_i}\right)}\frac{\omega_i^{3/2}}{e^{\frac{1}{2}\boldsymbol{z}_i^T\boldsymbol{\gamma}}}\boldsymbol{x}_i, \tag{21}$$

$$\boldsymbol{S}_{\boldsymbol{\gamma}} = \frac{1}{2}\sum_{i=1}^{n}\left(\omega_i \frac{\left(y_i - \boldsymbol{x}_i^T\boldsymbol{\beta}\right)^2}{e^{\boldsymbol{z}_i^T\boldsymbol{\gamma}}} - 1\right)\boldsymbol{z}_i - \frac{\nu}{2(\nu+1)}\sum_{i=1}^{n}\frac{\boldsymbol{v}_i^T\boldsymbol{\alpha}}{e^{\frac{1}{2}\boldsymbol{z}_i^T\boldsymbol{\gamma}}}\frac{t_{\nu+1}\left(t_i\sqrt{\omega_i}\right)}{T_{\nu+1}\left(t_i\sqrt{\omega_i}\right)}\boldsymbol{x}_i\boldsymbol{z}_i\omega_i^{3/2}, \tag{22}$$

$$\boldsymbol{S}_{\boldsymbol{\alpha}} = \sum_{i=1}^{n}\frac{t_{\nu+1}\left(t_i\sqrt{\omega_i}\right)}{T_{\nu+1}\left(t_i\sqrt{\omega_i}\right)}\frac{\left(y_i - \boldsymbol{x}_i^T\boldsymbol{\beta}\right)}{e^{\frac{1}{2}\boldsymbol{z}_i^T\boldsymbol{\gamma}}}\sqrt{\omega_i}. \tag{23}$$

Setting Eq. (21) to zero and solving the equation give the following equation for $\widehat{\boldsymbol{\beta}}$

$$\widehat{\boldsymbol{\beta}} = \left(\boldsymbol{X}^T\widehat{\boldsymbol{R}}\widehat{\boldsymbol{W}}\boldsymbol{X}\right)^{-1}\left(\boldsymbol{X}^T\widehat{\boldsymbol{R}}\widehat{\boldsymbol{W}}\boldsymbol{y} - \boldsymbol{X}^T\widehat{\boldsymbol{P}^*}\widehat{\boldsymbol{W}}^{3/2}\widehat{\boldsymbol{\delta}}\right). \tag{24}$$

Here $\boldsymbol{R}$, $\boldsymbol{W}$, $\boldsymbol{W^{3/2}}$ and $\boldsymbol{\delta}$ are defined previously for the ML estimate of $\boldsymbol{\beta}$ for the JLSM under the skew-t distribution. $\boldsymbol{P^*} = diag\left\{\frac{\lambda_i}{\sigma_i}\right\}_{i=1}^{n}$ is a diagonal $(n \times n)$ matrix.

The ML estimates of $\boldsymbol{\gamma}$ and $\boldsymbol{\alpha}$ can be obtained by setting Eqs. (22) and (23) to zero and solving them simultaneously. Iterative procedures are used to obtain the ML estimates of the parameters as mentioned before in previous sections.

The expected FIM is defined as

$$\mathcal{F}_{JLSSM\text{-}St}(\boldsymbol{\beta}, \boldsymbol{\gamma}, \lambda) = -E\begin{bmatrix} \boldsymbol{S_{\beta\beta}} & \boldsymbol{S_{\beta\gamma}} & \boldsymbol{S_{\beta\alpha}} \\ \boldsymbol{S_{\gamma\beta}} & \boldsymbol{S_{\gamma\gamma}} & \boldsymbol{S_{\gamma\alpha}} \\ \boldsymbol{S_{\alpha\beta}} & \boldsymbol{S_{\alpha\gamma}} & \boldsymbol{S_{\alpha\alpha}} \end{bmatrix}. \tag{25}$$

As in JLSM under skew-t distribution, some of the elements of the FIM given in Eq. (25) have no closed analytical form. So, we use the following observed FIM

$$\mathcal{F}_{obs,JLSSM\text{-}St}(\boldsymbol{\beta}, \boldsymbol{\gamma}, \lambda) = -\begin{bmatrix} \boldsymbol{S_{\beta\beta}} & \boldsymbol{S_{\beta\gamma}} & \boldsymbol{S_{\beta\alpha}} \\ \boldsymbol{S_{\gamma\beta}} & \boldsymbol{S_{\gamma\gamma}} & \boldsymbol{S_{\gamma\alpha}} \\ \boldsymbol{S_{\alpha\beta}} & \boldsymbol{S_{\alpha\gamma}} & \boldsymbol{S_{\alpha\alpha}} \end{bmatrix}_{\boldsymbol{\beta}=\widehat{\boldsymbol{\beta}},\boldsymbol{\gamma}=\widehat{\boldsymbol{\gamma}},\boldsymbol{\alpha}=\widehat{\boldsymbol{\alpha}}}. \tag{26}$$

whose elements given in the Appendix.

3 Derived Forms of ICOMP for Variable Selection

Model selection criteria are generally introduced to balance between the ability of a model to fit the data set and the complexity of the model to achieve the fidelity in the data. In this context, model complexity interpretation is critical in defining model selection criteria. There are different definitions of model complexity in the literature. For example, Akaike (1973) in his AIC defines the complexity of a model in terms of the number of free parameters estimated in a model. On the other hand, Bozdogan defined his ICOMP criterion based on a generalization of the covariance complexity index introduced by Van Emden (1971). His rationale was to measure model complexity with both the number of free model parameters and the interdependency of the parameter estimates at the same time, which is different from counting and penalizing the number of parameters. Therefore, ICOMP provides a more flexible form than AIC-type criteria. In contrast to AIC, ICOMP uses the entropic structural complexity of random vectors via a generalization of the information-based covariance complexity index of Van Emden (1971). The penalization of the covariance matrix of the coefficients is carried out with the concept of maximal covariance complexity which is defined as:

Definition 1 A maximal information-theoretic measure of complexity of a covariance matrix Σ of a multivariate normal distribution is

$$C_1(\Sigma) = \frac{s}{2}\log\left[\frac{tr(\Sigma)}{s}\right] - \frac{1}{2}\log|\Sigma| \tag{27}$$

Bozdogan (1988, 1990).

ICOMP uses (-2) times the maximized log-likelihood to measure the lack of fit of the model and the maximal information-theoretic measure of complexity $C_1(.)$ of the covariance matrix to measure the complexity of the model. It can be seen from Eq. (27) that unlike other criteria, the penalty term in ICOMP is not only based on the number of parameters used by the model, but also depends on the covariance matrix of the coefficients.

Based this Bozdogan (1994, 1997, 2000, 2004) defines his information-theoretic measure of complexity (ICOMP) ("I" for information and "COMP" for complexity) given by

$$ICOMP = -2\log L\left(\widehat{\boldsymbol{\theta}}\right) + 2C_1\left(\widehat{\Sigma}_{\text{model}}\right), \tag{28}$$

where $\widehat{\boldsymbol{\theta}}$ is the ML estimator of the parameter vector under the model whose covariance matrix is denoted by $\widehat{\Sigma}_{\text{model}} = \widehat{Cov}\left(\widehat{\theta}\right)$. $C_1(.)$ represents a real-valued complexity measure of $\widehat{\Sigma}_{\text{model}}$. $\widehat{\Sigma}_{\text{model}}$ can be obtained in several ways since it is the estimated covariance matrix of the model parameters. Here, we use the celebrated Cramer-Rao lower bound matrix, which is equal to the inverse of estimated IFIM of the model. Therefore, the most general form of ICOMP, referred to as ICOMP(IFIM), is defined by

$$ICOMP(IFIM) = -2\log L\left(\widehat{\boldsymbol{\theta}}\right) + 2C_1\left(\widehat{\mathcal{F}}^{-1}\right), \tag{29}$$

where C_1 denotes the maximal information complexity of $\widehat{\mathcal{F}}^{-1}$, the estimated IFIM. The best model according to the criterion is the one that gives the minimum value ICOMP among the competing the models. For more details on ICOMP, we refer the readers to Bozdogan (1994, 1997, 2000, 2004), Bozdogan and Haughton (1998), and others.

3.1 ICOMP for Model-1 JLSM Under Student's t Distribution

ICOMP for the JLSM under Student's t distribution is defined as

$$ICOMP_{JLSM\text{-}t} = -2\log L\left(\widehat{\boldsymbol{\theta}}\right) + 2C_1\left(\widehat{\mathcal{F}}^{-1}_{JLSM\text{-}t}\right), \tag{30}$$

where $L\left(\widehat{\boldsymbol{\theta}}\right)$ is the maximized likelihood function, $\widehat{\boldsymbol{\theta}}$ is the ML estimate of the parameter vector $\boldsymbol{\theta}$. To derive the complexity term of ICOMP for JLSM under

Student's t distribution, we need the determinant and trace of $\widehat{\mathcal{F}}^{-1}_{JLSM\text{-}t}$. After some work, we obtain the following.

$$tr\left(\widehat{\mathcal{F}}^{-1}_{JLSM\text{-}t}\right) = \frac{\nu+3}{\nu+1} tr\left(\left(\boldsymbol{X}^T\widehat{\boldsymbol{R}}\boldsymbol{X}\right)^{-1}\right) + \frac{2(\nu+3)}{\nu} tr\left(\left(\boldsymbol{Z}^T\widehat{\boldsymbol{R}}\widehat{\boldsymbol{R}}\boldsymbol{Z}\right)^{-1}\right), \tag{31}$$

$$\left|\widehat{\mathcal{F}}^{-1}_{JLSM\text{-}t}\right| = \frac{(\nu+3)^p}{(\nu+1)^p}\left|\left(\boldsymbol{X}^T\widehat{\boldsymbol{R}}\boldsymbol{X}\right)^{-1}\right| + 2^q\left(\frac{\nu+3}{\nu}\right)^q\left|\left(\boldsymbol{Z}^T\widehat{\boldsymbol{R}}\widehat{\boldsymbol{R}}\boldsymbol{Z}\right)^{-1}\right|. \tag{32}$$

For the JLSM under Student's t distribution, the ICOMP penalty term defined in Eq. (27) can be expressed as

$$C_1\left(\widehat{\mathcal{F}}^{-1}_{JLSM\text{-}t}\right) = \frac{s_1}{2}\log\left(\frac{\frac{\nu+3}{\nu+1}tr\left(\left(\boldsymbol{X}^T\widehat{\boldsymbol{R}}\boldsymbol{X}\right)^{-1}\right) + 2\left(\frac{\upsilon+3}{\upsilon}\right)tr\left(\left(\boldsymbol{Z}^T\widehat{\boldsymbol{R}}\widehat{\boldsymbol{R}}\boldsymbol{Z}\right)^{-1}\right)}{s_1}\right)$$
$$-\frac{1}{2}\log\left(\left|\frac{(\nu+3)^p}{(\nu+1)^p}\left(\boldsymbol{X}^T\widehat{\boldsymbol{R}}\boldsymbol{X}\right)^{-1}\right| + 2^q\left(\frac{\upsilon+3}{\upsilon}\right)^q\left|\left(\boldsymbol{Z}^T\widehat{\boldsymbol{R}}\widehat{\boldsymbol{R}}\boldsymbol{Z}\right)^{-1}\right|\right) \tag{33}$$

where $s_1 = p + q$ is the number of the free model parameters. In the special case, when $\nu \to \infty$ $ICOMP_{JLSM\text{-}t}$ reduces to ICOMP for JLSM under normal distribution.

3.2 ICOMP for Model-2 JLSM Under Skew-t Distribution

In a similar manner, ICOMP for the JLSM under skew-t distribution defined in Eq. (11) can be obtained as

$$ICOMP_{JLSM\text{-}St} = -2\log L\left(\widehat{\boldsymbol{\theta}}\right) + 2C_1\left(\widehat{\mathcal{F}}^{-1}_{JLSM\text{-}St}\right), \tag{34}$$

where $L\left(\widehat{\boldsymbol{\theta}}\right)$ is the maximized likelihood function, $\widehat{\boldsymbol{\theta}}$ is the ML estimate of the parameter vector $\boldsymbol{\theta}$. To derive ICOMP for the JLSM under skew-t distribution, we need the IFIM. Since the inverse of the expected FIM given in Eq. (17) is difficult to obtain for the JLSM under skew-t. However, it suffices to use the complexity of the observed IFIM in our numerical examples. Also note that, when $\lambda = 0$, then $ICOMP_{JLSM\text{-}St}$ reduces $ICOMP_{JLSM-t}$ given in Eq. (30).

3.3 ICOMP for Model-3 JLSSM Under Skew-t Distribution

In this subsection, we derive ICOMP for JLSSM under skew-t distribution, which has a similar derivation to $ICOMP_{JLSM\text{-}St}$ defined as

$$ICOMP_{JLSSM\text{-}St} = -2\log L\left(\widehat{\boldsymbol{\theta}}\right) + 2C_1\left(\widehat{\mathcal{F}}^{-1}_{JLSSM\text{-}St}\right), \tag{35}$$

where $L\left(\widehat{\boldsymbol{\theta}}\right)$ is the maximized likelihood function, $\widehat{\boldsymbol{\theta}}$ is the ML estimate of the parameter vector $\boldsymbol{\theta}$. To derive ICOMP for the JLSSM under skew-t distribution, we need the IFIM. Similar to JLSM under skew-t distribution, since it is not possible to obtain an analytical forms of the expected FIM given in Eq. (25), we will use the observed FIM given in Eq. (26) in our numerical examples. If λ has no variability, then $ICOMP_{JLSSM\text{-}St}$ reduces to $ICOMP_{JLSM\text{-}St}$ given in Eq. (34).

4 Monte Carlo Simulation Study

In this section, we conduct a large-scale Monte Carlo simulation study to illustrate the performance of the model selection criteria described in Sect. 3. We simulate data from JLSM under Student's t, JLSM and JLSSM under skew-t distribution presented in Sect. 2:

Model 1

$$\begin{cases} y_i \sim t\left(\mu_i, \sigma_i^2, \nu\right) \\ \mu_i = \boldsymbol{x}_i^T\boldsymbol{\beta} \\ \log\sigma_i^2 = \boldsymbol{z}_i^T\boldsymbol{\gamma} \\ i = 1, 2, \ldots, n \end{cases} \tag{36}$$

Here we set the true values of the location parameter to $\boldsymbol{\beta} = [1, 1, 0, 0]^T$ and the scale parameter to $\boldsymbol{\gamma} = [1, 0, 1]^T$.

Model 2

$$\begin{cases} y_i \sim St\left(\mu_i, \sigma_i^2, \lambda, \nu\right) \\ \mu_i = \boldsymbol{x}_i^T\boldsymbol{\beta} \\ \log\sigma_i^2 = \boldsymbol{z}_i^T\boldsymbol{\gamma} \\ i = 1, 2, \ldots, n \end{cases} \tag{37}$$

For the true coefficients, we use $\boldsymbol{\beta} = [1, 1, 0, 0]^T$, the scale parameter to $\boldsymbol{\gamma} = [1, 0, 1]^T$, and $\lambda = 0.1, 0.5$, and 0.9.

Model 3

$$\begin{cases} y_i \sim St\left(\mu_i, \sigma_i^2, \lambda | i, \nu\right) \\ \mu_i = \boldsymbol{x}_i^T \boldsymbol{\beta} \\ \log \sigma_i^2 = \boldsymbol{z}_i^T \boldsymbol{\gamma} \\ \lambda_i = \boldsymbol{v}_i^T \boldsymbol{\alpha} \\ i = 1, 2, \ldots, n \end{cases} \tag{38}$$

For the true coefficients, we use $\boldsymbol{\beta} = [1, 1, 0, 0]^T$, the scale parameter to $\boldsymbol{\gamma} = [1, 0, 1]^T$, and $\boldsymbol{\alpha} = [2, 3, 0]^T$.

Note that throughout the Monte Carlo simulation study and the real data example, we have fixed the degrees of freedom of the Student's t and skew-t distributions to 3, since the small values are suggested for the sake of robustness in the literature (e.g., see Lange et al. 1989; Arslan and Genç 2003).

First, we generate the covariates, $\boldsymbol{x}_i$, $\boldsymbol{z}_i$ (and $\boldsymbol{v}_i$ for JLSSM), from uniform distribution, $U(-1, 1)$. Then, y_i is generated according to Models 1–3. For the sample size, we consider the following sample sizes $n = 30, 50$, and 100. The number of replications of the simulation is set to 100. We count the frequency of the true model chosen by the information criteria to determine their hit ratios.

To highlight the differences between these three models, we give Figs. 3 and 4. For these figures, we take the sample size $n = 100$.

Figure 3 shows the three dimension scatter plots of the data from JLSMs of student t and skew t distributions to show the differences between Models 1 and 2. To obtain the scatter plot we consider the dimensions of the location and scale models as $p = q = 1$. Here we generate the covariates, $\boldsymbol{x}_i$ and $\boldsymbol{z}_i$ from uniform

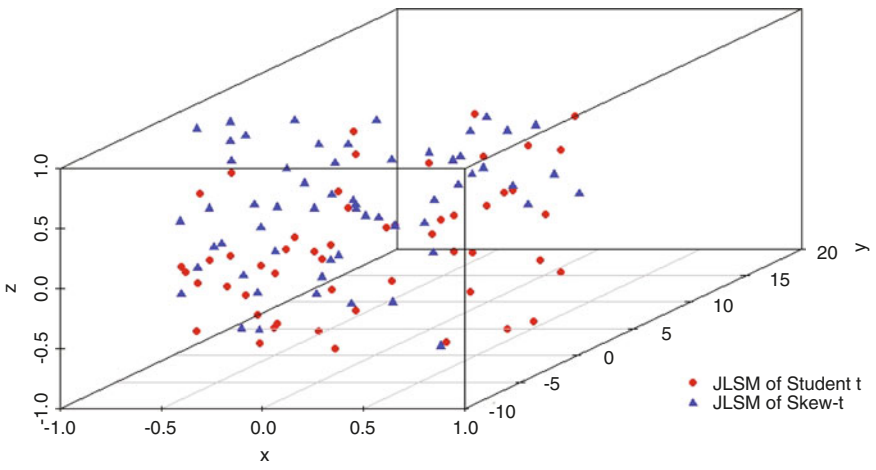

Fig. 3 Scatter plot of the data sets generated from JLSMs under the student t and skew-t distributions

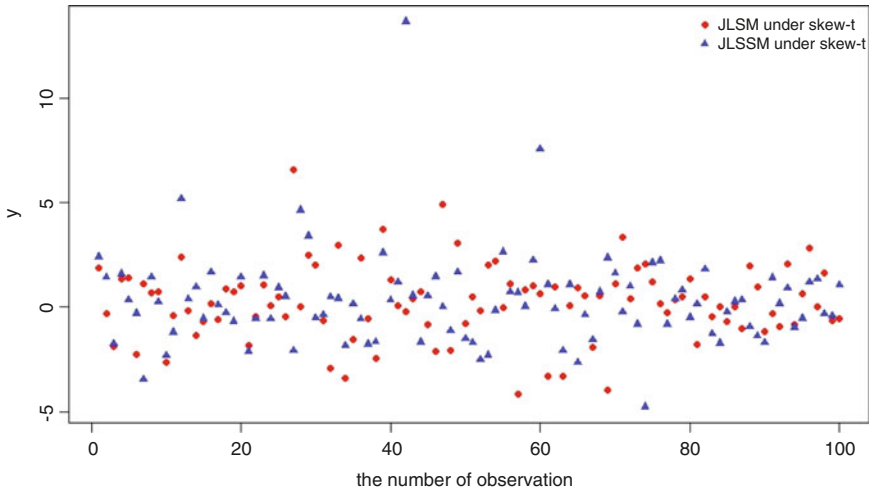

Fig. 4 Data sets generated from Models 2 and 3

Table 1 Simulation results for JLSM under Student t Distribution

n	Criteria	Location		Scale		Skewness	CPU
		CF	MSE	CF	MSE	MSE	
30	**ICOMP**$_{JLSM\text{-}t}$	83	0.185	84	0.193	–	1019
	ICOMP$_{JLSM\text{-}St}$	82	0.191	82	0.198	0.066	1032
	ICOMP$_{JLSSM\text{-}St}$	80	0.199	79	0.201	0.054	1147
50	**ICOMP**$_{JLSM\text{-}t}$	85	0.075	87	0.071	–	1095
	ICOMP$_{JLSM\text{-}St}$	83	0.081	84	0.080	0.022	1100
	ICOMP$_{JLSSM\text{-}St}$	82	0.086	80	0.085	0.025	1208
100	**ICOMP**$_{JLSM\text{-}t}$	89	0.014	90	0.012	–	1158
	ICOMP$_{JLSM\text{-}St}$	86	0.019	85	0.016	0.015	1169
	ICOMP$_{JLSSM\text{-}St}$	85	0.020	82	0.023	0.019	1271

The criteria shown in bold are the criteria for the model in which the data set is generated

distribution, $U(-1, 1)$ as in the simulation study and we take the true values of parameters as $\beta = 1$, the scale parameter to $\gamma = 1$, and $\nu = 3$ for both of the models. We take $\lambda = 1$ for the JLSM of skew-t distribution.

Figure 4 shows the data generated from JLSM and JLSSM of skew t distribution to display the differences between Models 2 and 3. Here we generate the covariates, $\boldsymbol{x}_i$, z_i (and $\boldsymbol{v}_i$ for JLSSM) from uniform distribution, $U(-1, 1)$ as in the simulation study and we take the true values of parameters of the JLSM and JLSSM of skew- t distribution as given in Models 2–3. In Model 2, we take $\lambda = 0.5$.

Our simulation results based on 100 replications are summarized in Tables 1, 2, 3, 4, and 5. In these tables, we give the frequencies of selecting the correct model, the MSE values of the parameter estimates and the average computation time (CPU) (seconds) for each model selection criterion. The MSE values are calculated by:

Table 2 Simulation results for JLSM under St distribution with $\lambda = 0.1$

n	Criteria	Location		Scale		Skewness	CPU
		CF	MSE	CF	MSE	MSE	
30	$ICOMP_{JLSM\text{-}t}$	72	0.192	74	0.156	–	1021
	$\mathbf{ICOMP}_{JLSM\text{-}St}$	86	0.196	85	0.177	0.047	1103
	$ICOMP_{JLSSM\text{-}St}$	83	0.212	83	0.296	0.039	1132
50	$ICOMP_{JLSM\text{-}t}$	76	0.152	75	0.124	–	1123
	$\mathbf{ICOMP}_{JLSM\text{-}St}$	89	0.081	88	0.078	0.034	1139
	$ICOMP_{JLSSM\text{-}St}$	86	0.099	86	0.087	0.028	1212
100	$ICOMP_{JLSM\text{-}t}$	78	0.078	77	0.097	–	1162
	$\mathbf{ICOMP}_{JLSM\text{-}St}$	90	0.024	91	0.017	0.012	1175
	$ICOMP_{JLSSM\text{-}St}$	89	0.052	89	0.038	0.015	1295

The criteria shown in bold are the criteria for the model in which the data set is generated

Table 3 Simulation results for JLSM under St distribution with $\lambda = 0.5$

n	Criteria	Location		Scale		Skewness	CPU
		CF	MSE	CF	MSE	MSE	
30	$ICOMP_{JLSM\text{-}t}$	67	0.146	71	0.190	–	1064
	$\mathbf{ICOMP}_{JLSM\text{-}St}$	85	0.111	87	0.147	0.088	1178
	$ICOMP_{JLSSM\text{-}St}$	81	0.132	82	0.183	0.093	1183
50	$ICOMP_{JLSM\text{-}t}$	70	0.062	74	0.063	–	1128
	$\mathbf{ICOMP}_{JLSM\text{-}St}$	88	0.038	89	0.027	0.041	1179
	$ICOMP_{JLSSM\text{-}St}$	84	0.043	84	0.031	0.045	1229
100	$ICOMP_{JLSM\text{-}t}$	74	0.027	76	0.025	–	1186
	$\mathbf{ICOMP}_{JLSM\text{-}St}$	90	0.019	92	0.012	0.021	1214
	$ICOMP_{JLSSM\text{-}St}$	88	0.025	87	0.018	0.033	1312

The criteria shown in bold are the criteria for the model in which the data set is generated

Table 4 Simulation results for JLSM under St distribution with $\lambda = 0.9$

n	Criteria	Location		Scale		Skewness	CPU
		CF	MSE	CF	MSE	MSE	
30	$ICOMP_{JLSM\text{-}t}$	64	0.253	61	0.295	–	1092
	$\mathbf{ICOMP}_{JLSM\text{-}St}$	83	0.198	84	0.277	0.077	1120
	$ICOMP_{JLSSM\text{-}St}$	80	0.247	81	0.284	0.061	1203
50	$ICOMP_{JLSM\text{-}t}$	67	0.095	64	0.096	–	1146
	$\mathbf{ICOMP}_{JLSM\text{-}St}$	86	0.089	85	0.078	0.058	1155
	$ICOMP_{JLSSM\text{-}St}$	82	0.090	83	0.083	0.032	1246
100	$ICOMP_{JLSM\text{-}t}$	70	0.371	68	0.323	–	1204
	$\mathbf{ICOMP}_{JLSM\text{-}St}$	88	0.036	90	0.045	0.013	1257
	$ICOMP_{JLSSM\text{-}St}$	85	0.055	86	0.062	0.015	1355

The criteria shown in bold are the criteria for the model in which the data set is generated

Table 5 Simulation results for JLSSM under St distribution

n	Criteria	Location		Scale		Skewness		CPU
		CF	MSE	CF	MSE	CF	MSE	
30	$ICOMP_{JLSM\text{-}t}$	75	0.215	66	0.284	–	–	1098
	$ICOMP_{JLSM\text{-}St}$	78	0.202	76	0.213	–	0.079	1132
	$ICOMP_{JLSSM\text{-}St}$	82	0.177	80	0.185	82	0.075	1227
50	$ICOMP_{JLSM\text{-}t}$	76	0.142	73	0.156	–	–	1158
	$ICOMP_{JLSM\text{-}St}$	81	0.128	79	0.125	–	0.042	1180
	$ICOMP_{JLSSM\text{-}St}$	88	0.104	85	0.116	84	0.039	1269
100	$ICOMP_{JLSM\text{-}t}$	79	0.087	78	0.036	–	–	1215
	$ICOMP_{JLSM\text{-}St}$	83	0.026	80	0.028	–	0.018	1278
	$ICOMP_{JLSSM\text{-}St}$	92	0.021	88	0.014	85	0.014	1384

The criteria shown in bold are the criteria for the model in which the data set is generated

$$
\begin{aligned}
MSE_{\boldsymbol{\beta}} &= \left(\boldsymbol{\beta} - \widehat{\boldsymbol{\beta}}\right)^T \mathbf{X}^T \mathbf{X} \left(\boldsymbol{\beta} - \widehat{\boldsymbol{\beta}}\right) \\
MSE_{\boldsymbol{\gamma}} &= \frac{1}{4} \left(\boldsymbol{\gamma} - \widehat{\boldsymbol{\gamma}}\right)^T \mathbf{Z}^T \mathbf{Z} \left(\boldsymbol{\gamma} - \widehat{\boldsymbol{\gamma}}\right) \\
MSE_{\boldsymbol{\alpha}} &= \left(\boldsymbol{\alpha} - \widehat{\boldsymbol{\alpha}}\right)^T \mathbf{V}^T \mathbf{V} \left(\boldsymbol{\alpha} - \widehat{\boldsymbol{\alpha}}\right) \\
MSE_{\lambda} &= \left(\lambda - \widehat{\lambda}\right)^2
\end{aligned} \tag{39}
$$

The results in Tables 1, 2, 3, 4, and 5 show that as the sample size increases, the frequency of choosing the correct model of the information complexity criteria and the averaged computational times also increase. Looking at Table 1, we observe that $ICOMP_{JLSM-t}$ chooses the correct model when the data is generated from JLSM under indeed Student's t distribution. Performances of $ICOMP_{JLSM-St}$ and $ICOMP_{JLSSM-St}$, are in the same order of magnitude of $ICOMP_{JLSM-t}$, but a bit less, since the true data generation was done under the Student's-t distribution and with no skewness.

Tables 2, 3, and 4 show the results for the data generated from JLSM under skew-t distribution with different values of λ. From these results, obviously $ICOMP_{JLSM-St}$ chooses the correct model followed by $ICOMP_{JLSSM-St}$. $ICOMP_{JLSM-t}$ does not perform well and does not take into account the presence of skewness since the data was generated from skew-t distribution although there is no variability in the skewness, it also tries to select the variables, which have an effect on skewness parameter. Further, we note that the performance of $ICOMP_{JLSM-t}$ decreases as the skewness increases since it does not take into account the skewness of the data. Inspecting the results in Table 5, we observe that $ICOMP_{JLSSM-St}$ is able to select correct model more than the others do in the presence of skewness. To summarize our results, we observe that $ICOMP_{JLSSM-St}$ has reasonable performance in all Monte Carlo simulation scenarios. This is encouraging, since in the literature, AIC, or AIC-type model selection criteria do not have the provision

of capturing skew behavior of the data due to the fact that these criteria penalize the number of parameters, which is necessary but not sufficient. On the other hand, ICOMP captures the model complexity better and is much robust criterion.

In a future study, we will generate the covariates, $\boldsymbol{x}_i$, $\boldsymbol{z}_i$ (and $\boldsymbol{v}_i$ for JLSSM), from other distributions other than the uniform distribution, $U(-1, 1)$, and study the performance of our proposed approach.

5 A Real Benchmark Data Example

In this section, we provide a real data example using a well-known benchmark data set to choose the best subset of variables using the three competing models without knowing the distributional property of this data set with our proposed approach. We consider Australian Institute of Sport (AIS) data given in Cook and Weisberg (1994). AIS data was also analyzed by Azzalini and Dalla-Valle (1996), Azzalini (2003, 2005), among others. This data set includes 100 females and 102 males with 13 variables. We use only the 8 variables of this data set for space considerations to carry out $2^8 = 256$ possible subset of predictors, instead of $2^{13} = 8192$ possible subsets of predictors to illustrate our proposed approach. The names of the variables of 8 variables chosen are given in Table 6.

Plot of the distribution of y for the AIS data set is shown in Fig. 5.

We consider the models given in Eqs. (2), (11), and (19) to model this data set and to carry out variable selection under each of these models using ICOMP developed in Sect. 4. For comparative purposes we also score the classic AIC (Akaike 1973) on the AIS dataset. Our results are summarized in Table 7.

From Table 7, we note that $\text{AIC}_{\text{JLSM}-\text{t}}$ and $\text{ICOMP}_{\text{JLSM}-\text{t}}$ criteria chose the common variables x_1, x_4, x_5 and x_8 in location model and x_8 in scale model when the JLSM under Student's t is fitted. When the JLSM under skew-t distribution is fitted to this data set, the selection of the variables has changed. $\text{AIC}_{\text{JLSM}-\text{St}}$ and $\text{ICOMP}_{\text{JLSM}-\text{St}}$ criteria commonly chose the variables x_1, x_4, x_7 and x_8 in location model and variables x_1 and x_8 in scale model. In the case of modeling the skewness, while the location model chosen by $\text{AIC}_{\text{JLSSM}-\text{St}}$ is changed, $\text{ICOMP}_{\text{JLSSM}-\text{St}}$ chooses the same location model. In addition, it is seen that the selected scale models change by modeling the skewness for both criteria. Both criteria commonly select

Table 6 Variables of AIS dataset

y:	lbm (lean body mass)
x_1:	rcc (red blood cell count)
x_2:	wcc (while blood cell count)
x_3:	hc (hematocrit)
x_4:	hg (hemoglobin concentration)
x_5:	fe (plasma ferritins)
x_6:	bmi (body mass index)
x_7:	sff (sum of skin folds)
x_8:	bfat (percent body fat)

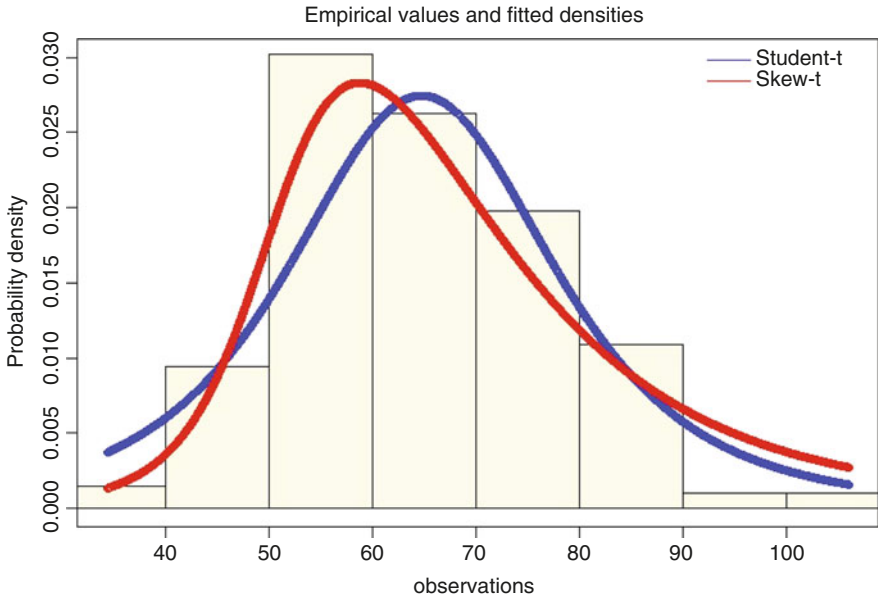

Fig. 5 Plot of the distribution of y for the AIS data set

Table 7 Variable selection in JLSM-t, JLSM-St and JLSSM-St for AIS data

Criterion	Criterion value	Location	Scale	Skewness
$AIC_{JLSM\text{-}t}$	1338.793	$\{x_1, x_4, x_5, x_6, x_8\}$	$\{x_8\}$	–
$AIC_{JLSM\text{-}St}$	1329.856	$\{x_1, x_4, x_6, x_7, x_8\}$	$\{x_1, x_8\}$	–
$AIC_{JLSSM\text{-}St}$	1240.793	$\{x_1, x_4, x_5, x_6, x_7, x_8\}$	$\{x_5, x_8\}$	$\{x_1, x_7, x_8\}$
$ICOMP_{JLSM\text{-}t}$	1304.789	$\{x_1, x_4, x_5, x_7, x_8\}$	$\{x_5, x_8\}$	–
$ICOMP_{JLSM\text{-}St}$	1283.483	$\{x_1, x_4, x_5, x_7, x_8\}$	$\{x_1, x_5, x_8\}$	–
$ICOMP_{JLSSM\text{-}St}$	**1209.709**	$\{x_1, x_4, x_5, x_7, x_8\}$	$\{x_7, x_8\}$	$\{x_1, x_4, x_8\}$

The minimum criteria value which indicate the best criterion is given in bold

the variables x_1 and x_8 in the skewness model. The skewness model selected by $AIC_{JLSSM-St}$ criterion also includes variable x_7, while the $ICOMP_{JLSSM-St}$ also selects variable x_4. We can report the skewness in variable x_4 and x_7 to determine which variable has the largest skewness. Our results have close connections with the results given in Li et al. (2017). According to the common variables chosen by $AIC_{JLSSM-St}$ and $ICOMP_{JLSSM-St}$, the group of variables, which have significant effect on the location, scale and the skewness on y (bmi) are respectively x_1, x_4, x_7 and x_8 (on location of y), x_8 (on scale of y), x_1, and x_8 (on skewness of y). On the other hand, variables x_2 and x_3 have no significant impact on location, scale and skewness of the response y. From criteria values, we select the model chosen by $ICOMP_{JLSSM-St}$. In this manner, in general, we can isolate, which predictor variables are affecting on the location (mean), scale and skewness of the response

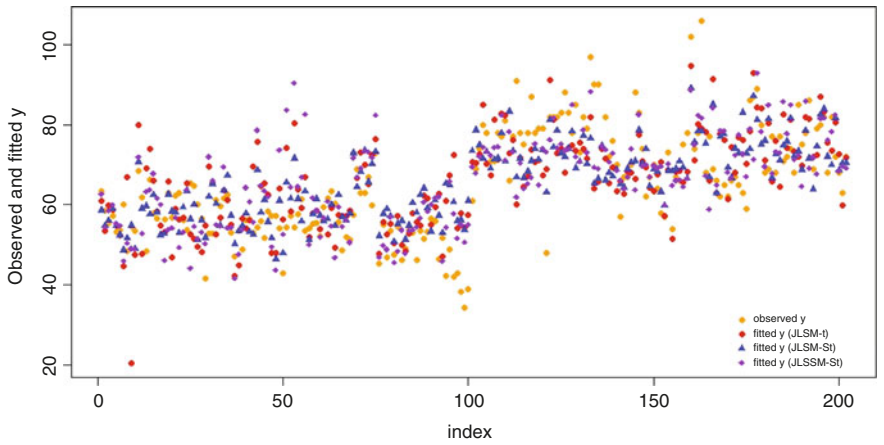

Fig. 6 Observed and fitted y values for AIS data obtained from the models given in Table 7

variable y. Further, we provide the index plot of observed and the fitted y's in Fig. 6. This plot reveals the robustness of all the models based on the Student t and the skew t distributions in terms of outliers.

6 Conclusion

In this paper, we considered the model selection in JLSM under Student's t, JLSM and JLSSM under Azzalini type skew-t distributions by introducing and developing information-theoretic measure of complexity (ICOMP) criterion. We used ICOMP to select the variables, which have an effect on location, scale and skewness of the heteroscedastic, skew datasets with heavy tails. With our numerical examples and the results, we illustrated that $\text{ICOMP}_{\text{JLSSM}-\text{St}}$ yields better performance overall, and hence it can be considered as a criterion of choice to be used to model data on location, scale and skewness with heteroscedasticity. As a conclusion, it is suggested that the proposed forms of ICOMP can be used to determine the significant variables in JLSM under Student's t, JLSM and JLSSM under skew-t distribution models.

Note that, throughout this study, we fixed the degrees of freedom parameter to 3 for the Student t and the skew t distributions for the sake of robustness as suggested in the literature (see Lange et al. 1989; Arslan and Genç 2003). However, the degrees of freedom parameter can also be estimated by forming the score function associated with the degrees of freedom parameter and solving the likelihood equations obtained from the score functions as given by Taylor and Verbyla (2004). Further research work will be carried out on other real data sets and Monte Carlo simulation protocols to study the performance of the proposed approach when the degrees of freedom parameter is unknown. The results will be reported elsewhere.

Acknowledgements This paper is based on the results of the Ph.D. thesis of the first author in the Department of Statistics at Ankara University, Ankara, Turkey. The authors thank the anonymous referee and the editors for their careful reading of this work. Their valuable suggestions have greatly improved our work.

Appendix

For the sake of simplicity, let define $u_i = \frac{(y_i - x_i^T \boldsymbol{\beta})}{e^{z_i^T \boldsymbol{\gamma}/2}}$ and $\varphi_i = \frac{t_{\nu+1}\left(\lambda u_i \sqrt{\omega_i}\right)}{T_{\nu+1}\left(\lambda u_i \sqrt{\omega_i}\right)}$. By taking the second derivatives of the log-likelihood function given in Eq. (12) with respect to the parameters, the elements of observed FIM for JLSM of skew-t distribution are obtained as follows.

$$\boldsymbol{S}_{\boldsymbol{\beta}\boldsymbol{\beta}} = \sum_{i=1}^{n} \frac{\boldsymbol{S}_{uu}}{e^{z_i^T \boldsymbol{\gamma}}} \boldsymbol{x}_i \boldsymbol{x}_i^T, \tag{40}$$

$$\boldsymbol{S}_{\boldsymbol{\gamma}\boldsymbol{\gamma}} = \frac{1}{4} \sum_{i=1}^{n} \frac{1}{e^{z_i^T \boldsymbol{\gamma}}} \left(1 + u_i^2 \boldsymbol{S}_{uu} + 2u_i \left(-u_i \omega_i + \frac{\lambda \nu}{\nu + 1} \omega_i^{3/2} \varphi_i\right)\right) \boldsymbol{z}_i \boldsymbol{z}_i^T, \tag{41}$$

$$\boldsymbol{S}_{\lambda\lambda} = -\sum_{i=1}^{n} u_i \omega_i^{1/2} \left(\frac{(\nu + 2)\, \lambda u_i^2 \varphi_i}{\nu + u_i^2 + \lambda^2 u_i^2} + u_i \omega_i^{1/2} \varphi_i^2\right), \tag{42}$$

$$\boldsymbol{S}_{\boldsymbol{\beta}\boldsymbol{\gamma}} = \frac{1}{2} \sum_{i=1}^{n} \frac{1}{e^{z_i^T \boldsymbol{\gamma}/2}} \left(1 + u_i^2 \boldsymbol{S}_{uu} + 2u_i \left(-u_i \omega_i + \frac{\lambda \nu}{\nu + 1} \omega_i^{3/2} \varphi_i\right)\right) \boldsymbol{x}_i \boldsymbol{z}_i^T, \tag{43}$$

$$\boldsymbol{S}_{\boldsymbol{\beta}\lambda} = \frac{\nu}{2\,(\nu + 1)} \sum_{i=1}^{n} \frac{\omega_i^{1/2}}{e^{z_i^T \boldsymbol{\gamma}/2}} \left(\varphi_i + \lambda \left(\frac{(\nu + 2)\, \lambda u_i^2 \varphi_i}{\nu + u_i^2 + \lambda^2 u_i^2} + u_i \omega_i^{1/2} \varphi_i^2\right)\right) \boldsymbol{x}_i, \tag{44}$$

$$\boldsymbol{S}_{\boldsymbol{\gamma}\lambda} = \frac{\nu}{2\,(\nu + 1)} \sum_{i=1}^{n} \frac{u_i}{e^{z_i^T \boldsymbol{\gamma}/2}} \left(\varphi_i + \lambda \left(\frac{(\nu + 2)\, \lambda u_i^2 \varphi_i}{\nu + u_i^2 + \lambda^2 u_i^2} + u_i \omega_i^{1/2} \varphi_i^2\right)\right) \boldsymbol{z}_i. \tag{45}$$

Here $\boldsymbol{S}_{uu}$ shows the second derivative of the log-likelihood function of the JLSM of skew-t distribution given in (12) with respect to u_i. It can be written as follows.

$$\begin{aligned} \boldsymbol{S}_{uu}(\boldsymbol{\beta}, \boldsymbol{\gamma}, \lambda) = {} & \frac{2\omega_i^2 u_i^2}{\nu + 1} - \omega_i - \frac{3\lambda\nu\omega_i^2 u_i \varphi_i}{(\nu + 1)^2} \\ & - \frac{\lambda\nu\omega_i^{3/2}}{\nu + 1} \left(\frac{\nu\,(\nu + 2)\, \lambda^2 u_i \varphi_i}{\left(\nu + u_i^2 + \lambda^2 u_i^2\right)\left(\nu + u_i^2\right)} + \frac{\lambda\nu\omega_i^{1/2} \varphi_i^2}{\nu + u_i^2}\right) \end{aligned} \tag{46}$$

Let define $\psi_i = \frac{t_{\nu+1}\left(\boldsymbol{v}_i^T\boldsymbol{\alpha}u_i\sqrt{\omega_i}\right)}{T_{\nu+1}\left(\boldsymbol{v}_i^T\boldsymbol{\alpha}u_i\sqrt{\omega_i}\right)}$. Similar to the JLSM of skew-t distribution case, by taking the derivatives of the log-likelihood function given in (20) the elements of observed FIM for JLSSM of skew-t distribution are obtained as follows.

$$\boldsymbol{S}_{\boldsymbol{\beta}\boldsymbol{\beta}} = \sum_{i=1}^{n} \frac{\boldsymbol{S}_{uu}^*}{e^{\boldsymbol{z}_i^T\boldsymbol{\gamma}}}\boldsymbol{x}_i\boldsymbol{x}_i^T, \tag{47}$$

$$\boldsymbol{S}_{\boldsymbol{\gamma}\boldsymbol{\gamma}} = \frac{1}{4}\sum_{i=1}^{n} \frac{1}{e^{\boldsymbol{z}_i^T\boldsymbol{\gamma}}}\left(1 + u_i^2\boldsymbol{S}_{uu}^* + 2u_i\left(-u_i\omega_i + \frac{\nu}{\nu+1}\left(\boldsymbol{v}_i^T\boldsymbol{\alpha}\right)\omega_i^{3/2}\psi_i\right)\right)\boldsymbol{z}_i\boldsymbol{z}_i^T, \tag{48}$$

$$\boldsymbol{S}_{\alpha\alpha} = -\sum_{i=1}^{n} u_i\omega_i^{1/2}\left(\frac{(\nu+2)\left(\boldsymbol{v}_i^T\boldsymbol{\alpha}\right)u_i^2\varphi_i}{\nu + u_i^2 + \left(\boldsymbol{v}_i^T\boldsymbol{\alpha}\right)^2 u_i^2} + u_i\omega_i^{1/2}\psi_i^2\right)\boldsymbol{v}_i\boldsymbol{v}_i^T, \tag{49}$$

$$\boldsymbol{S}_{\boldsymbol{\beta}\boldsymbol{\gamma}} = \frac{1}{2}\sum_{i=1}^{n} \frac{1}{e^{\boldsymbol{z}_i^T\boldsymbol{\gamma}/2}}\left(1 + u_i^2\boldsymbol{S}_{uu}^* + 2u_i\left(-u_i\omega_i + \frac{\nu}{\nu+1}\left(\boldsymbol{v}_i^T\boldsymbol{\alpha}\right)\omega_i^{3/2}\psi_i\right)\right)\boldsymbol{x}_i\boldsymbol{z}_i^T, \tag{50}$$

$$\boldsymbol{S}_{\boldsymbol{\beta}\boldsymbol{\alpha}} = \frac{\nu}{2(\nu+1)}\sum_{i=1}^{n} \frac{\omega_i^{1/2}}{e^{\boldsymbol{z}_i^T\boldsymbol{\gamma}/2}}\left(\psi_i + \boldsymbol{v}_i^T\boldsymbol{\alpha}\left(\frac{(\nu+2)\left(\boldsymbol{v}_i^T\boldsymbol{\alpha}\right)u_i^2\varphi_i}{\nu + u_i^2 + \left(\boldsymbol{v}_i^T\boldsymbol{\alpha}\right)^2 u_i^2} + u_i\omega_i^{1/2}\psi_i^2\right)\right)\boldsymbol{x}_i\boldsymbol{v}_i^T, \tag{51}$$

$$\boldsymbol{S}_{\boldsymbol{\gamma}\boldsymbol{\alpha}} = \frac{\nu}{2(\nu+1)}\sum_{i=1}^{n} \frac{u_i}{e^{\boldsymbol{z}_i^T\boldsymbol{\gamma}/2}}\left(\psi_i + \boldsymbol{v}_i^T\boldsymbol{\alpha}\left(\frac{(\nu+2)\left(\boldsymbol{v}_i^T\boldsymbol{\alpha}\right)u_i^2\varphi_i}{\nu + u_i^2 + \left(\boldsymbol{v}_i^T\boldsymbol{\alpha}\right)^2 u_i^2} + u_i\omega_i^{1/2}\psi_i^2\right)\right)\boldsymbol{z}_i\boldsymbol{v}_i^T, \tag{52}$$

where $\boldsymbol{S}_{uu}^*$ represents the second derivative of the log-likelihood function of the JLSSM of skew-t distribution given in (20) with respect to u_i. It can be written as follows.

$$\begin{aligned}\boldsymbol{S}_{uu}^*(\boldsymbol{\beta},\boldsymbol{\gamma},\boldsymbol{\alpha}) = {} & \frac{2\omega_i^2u_i^2}{\nu+1} - \omega_i - \frac{3\nu\left(\boldsymbol{v}_i^T\boldsymbol{\alpha}\right)\omega_i^{5/2}u_i\psi_i}{(\nu+1)^2} \\ & - \frac{\nu^2(\nu+2)\left(\boldsymbol{v}_i^T\boldsymbol{\alpha}\right)^3\omega_i^{3/2}u_i\varphi_i}{(\nu+1)\left(\nu+u_i^2\right)\left(\nu + u_i^2 + \left(\boldsymbol{v}_i^T\boldsymbol{\alpha}\right)^2u_i^2\right)} \\ & - \frac{\nu^2\left(\boldsymbol{v}_i^T\boldsymbol{\alpha}\right)^2\omega_i^2\psi_i^2}{(\nu+1)\left(\nu+u_i^2\right)}\end{aligned} \tag{53}$$

The AIS data can be obtained from the R package "sn".

References

Aitkin, M. (1987). Modelling variance heterogeneity in normal regression using GLIM. *Journal of the Royal Statistical Society. Series C (Applied Statistics), 36*, 332–339.

Akaike, H. (1973). Information theory and extension of the maximum likelihood principle. In B. N. Petrov & F. Csáki (Eds.), *Second International Symposium on Information Theory* (pp. 267–281). Budapest: Académiai Kiadó.

Arslan, O., Genç, A. I. (2003). Robust location and scale estimation based on the univariate generalized t (GT) distribution. *Communications in Statistics: Theory and Methods, 32*(8), 1505–1525.

Azzalini, A. (1985). A class of distributions which includes the normal ones. *Scandinavian Journal of Statistics, 12*, 171–178.

Azzalini, A. (2005). The skew-normal distribution and related multivariate families. *Scandinavian Journal of Statistics, 32*(2), 159–188.

Azzalini, A., & Capitanio, A. (2003). Distributions generated by perturbation of symmetry with emphasis on a multivariate skew t distribution. *Journal of Royal Statistical Society, Series B, 65*, 367–389.

Azzalini, A., & Dalla-Valle, A. (1996). The multivariate skew-normal distribution. *Biometrika, 83*, 715–726.

Bozdogan, H. (1988). ICOMP: A new model selection criterion. In H. H. Bock (Ed.), *Classification and related methods of data analysis* (pp. 599–608). Amsterdam: North-Holland.

Bozdogan, H. (1990). On the information-based measure of covariance complexity and its application to the evaluation of multivariate linear models. *Communications in Statistics, Theory and Methods, 19*, 221–278.

Bozdogan, H. (1994). Mixture-model cluster analysis using model selection criteria and a new informational measure of complexity. In H. Bozdogan (Ed.), *Multivariate statistical modeling*. Proceedings of the First US/Japan Conference on the Frontiers of Statistical Modeling: An Informational Approach (Vol. 2, pp. 69–113). Dordrecht: Kluwer Academic Publishers.

Bozdogan, H. (1997, October). Empirical econometric modeling of food consumption using a new informational complexity approach. Invited world title award winning paper in the *Journal of Applied Econometrics, 12*, 563–592 (with Peter M. Bearse, and Alan M. Schlottmann). This paper is also published in the book: Magnus, J. R., & Morgan, M. S. (1997). *Methodology & tacit knowledge: Two experiments in econometrics* (pp. 153–182). Chichester: Wiley.

Bozdogan, H. (2000). Akaike's information criterion and recent developments in information complexity. *Journal of Mathematical Psychology, 44*(1), 62–91.

Bozdogan, H. (2003). Intelligent statistical data mining with information complexity and genetic algorithms. In *Statistical data mining and knowledge discovery*. Joint International Summer School JISS-2003 (Vol. II). Universidade de Lisboa, Lisbon.

Bozdogan, H. (2004). Intelligent statistical data mining with information complexity and genetic algorithms. In H. Bozdogan (Ed.), *Statistical data mining and knowledge discovery* (pp. 47–88). Boca Raton: Chapman and Hall/CRC.

Bozdogan, H., & Haughton, D. (1998). Informational complexity criteria for regression models. *Computational Statistics and Data Analysis, 28*, 51–76.

Cook, R. D., & Weisberg, S. (1994). *An introduction to regression graphics*. New York: Wiley.

Harvey, A. C. (1976). Estimating regression models with multiplicative heteroscedasticity. *Econometrica, 44*, 460–465.

Lange, K. L., Little, R. J. A., & Taylor, J. M. G. (1989). Robust statistical modeling using the t distribution. *Journal of the American Statistical Association, 84*, 881–896.

Li, H., Wu, L., & Ma, T. (2017). Variable selection in joint location, scale and skewness models of the skew normal distribution. *Journal of Systems Science and Complexity, 30*(3), 694–709.

Li, H. Q., & Wu, L. C. (2014). Joint modelling of location and scale parameters of the skew-normal distribution. *Applied Mathematics-A Journal of Chinese Universities, 29*(3), 265–272.

Lin, T. I., & Wang, Y. J. (2009). A robust approach to joint modeling of mean and scale covariance for longitudinal data. *Journal of Statistical Planning and Inference, 139*(9), 3013–3026.

Lin, T. I., & Wang, W. L. (2011). Bayesian inference in joint modelling of location and scale parameters of the t distribution for longitudinal data. *Journal of Statistical Planning and Inference, 141*(4), 1543–1553.

Park, R. E. (1966). Estimation with heteroscedastic error terms. *Econometrica, 34*, 888.

Taylor, J. T., & Verbyla, A. P. (2004). Joint modelling of location and scale parameters of the t distribution. *Statistical Modelling, 4*, 91–112.

Van Emden, M. H. (1971). *An analysis of complexity*. Mathematical Centre Tracts, 35. Mathematisch Centrum: Amsterdam.

Wang, D. R., & Zhang, Z. Z. (2009). Variable selection in joint generalized linear models. *Chinese Journal of Applied Probability and Statistics, 25*, 245–256.

Wu, L. C. (2014). Variable selection in joint location and scale models of the skew-t-normal distribution. *Communications in Statistics - Simulation and Computation, 43*(3), 615–630.

Wu, L. C., & Li, H. Q. (2012). Variable selection for joint mean and dispersion models of the inverse Gaussian distribution. *Metrika, 75*, 795–808.

Wu, L. C., Ma, T., & Zhan, J. (2013). Maximum likelihood estimation for joint location, scale and skewness models of the StN distribution. *Applied Mathematics A Journal of Chinese Universities(Ser.A), 4*, 6.

Wu, L., Tian, G. L., Zhang, Y. Q., & Ma, T. (2017). Variable selection in joint location, scale and skewness models with a skew-t-normal distribution. *Statistics and Its Interface, 10*(2), 217–227.

Wu, L. C., Zhang, Z. Z., Tian, G. L., & Xu, D. K. (2016). A robust variable selection to t-type joint generalized linear models via penalized t-type pseudo-likelihood. *Communications in Statistics - Simulation and Computation, 45*(7), 2320–2337

Wu, L. C., Zhang, Z. Z., & Xu, D. K. (2012). Variable selection in joint mean and variance models of Box-Cox transformation. *Journal of Applied Statistics, 39*, 2543–2555.

Wu, L. C., Zhang, Z. Z., & Xu, D. K. (2013). Variable selection in joint location and scale models of the skew-normal distribution. *Journal of Statistical Computation and Simulation, 83*, 1266–1278.

Zhang, Z. Z., & Wang, D. R. (2011). Simultaneous variable selection for heteroscedastic regression models. *Science China Mathematics, 54*, 515–530.

Zhao, W., & Zhang, R. (2015). Variable selection of varying dispersion student-t regression models. *Journal of Systems Science and Complexity, 28*(4), 961–977.

Weighted Condition Number Distributions Emanating from Complex Noncentral Wishart Type Matrices

Johannes T. Ferreira and Andriëtte Bekker

Abstract This chapter investigates an analytical characterisation of MIMO (multiple input multiple output) statistics; in particular that of the condition number. The channel propagation matrix is assumed to be complex matrix variate elliptically distributed; this assumption allows the analysis of the condition number in broad generality. The complex matrix variate elliptical class includes, amongst others, the complex matrix variate normal-, t-, and slash distributions as special cases. Specifically, the probability density function (pdf), moment generating function (mgf), and cumulative distribution function (cdf) of the condition number of a dual noncentral Wishart type matrix is derived, and studied for the known complex noncentral matrix variate normal, as well as for the previously unstudied complex noncentral matrix variate t- and slash case. This dual setting is of interest stemming from a practical consideration; viz. dual-branch systems which are equipped with two transmit- and receive antennas. A numerical- and comparative study supports the analytical expressions.

1 Introduction

Since the 1980s, authors have investigated the stochastic behaviour of the condition number of a random matrix in detail. How does it behave, how can limiting probabilities of the condition number be determined, how can it be interpreted in context of random matrices? Particularly, the distribution of the condition number of a random matrix has been shown to be of interest in the design and analysis of MIMO (multiple input multiple output) systems. Usually defined as the ratio between the largest and smallest eigenvalue of the Wishart form of the MIMO propagation channel, this measure reflects the spread of the eigenvalues and provides an inherent sense of the multipath richness of the channel. As

J. T. Ferreira (✉) · A. Bekker
Department of Statistics, University of Pretoria, Pretoria, South Africa
e-mail: johan.ferreira@up.ac.za; andriette.bekker@up.ac.za

A. Bekker et al. (eds.), *Computational and Methodological Statistics and Biostatistics*, Emerging Topics in Statistics and Biostatistics,
https://doi.org/10.1007/978-3-030-42196-0_5

such, the study of random matrices, their Wishart form and their corresponding eigenvalue behaviour are of sustained interest. The underlying probability density structure for the channel propagation matrix is usually assumed to be that of the complex matrix variate normal distribution. However, Ferreira et al. (2020) and Ferreira and Bekker (2019) questioned this complex normal assumption and observed superior performance of some performance measures within the MIMO arena when assuming alternative members emanating from an underlying complex elliptical model. The authors also utilised a weighted representation of the complex matrix variate elliptical model to create a platform where practitioners can access previously unconsidered models. Ferreira and Bekker (2019) investigated and illustrated the value of assuming an underlying complex elliptical assumption under rank-1 assumption of the noncentrality matrix within the MIMO paradigm. In fact, De Souza and Yacoub (2008) mentioned that the Rayleigh probability density function (pdf) is usually derived based on the assumption that from the central limit theorem for large number of partial waves, the resultant process can be decomposed into two orthogonal zero-mean and equal-standard deviation Gaussian random processes. This is an approximation and the restriction of complex Gaussian may be unnecessarily restrictive—it is not always a large number of interfering signals. Thus a more general assumption than that of complex normal may not be that far from reality, see also Ollila et al. (2011) and Choi et al. (2007).

Many papers have appeared which provide valuable insight into the structure and behaviour of the condition number of a random matrix under the complex matrix variate normal assumption. The contribution of Edelman (1988) may be considered a pioneering starting point in these analyses of condition numbers with an emphasis specifically within numerical analysis of large random matrices. Edelman and Sutton (2005) studied the tail behaviour of the distributions of condition numbers, and Chen and Dongarra (2005) further investigated the behaviour of condition numbers emanating for Gaussian random matrices (see also Ratnarajah et al. 2004). Matthaiou et al. (2009) described the usefulness of the condition number in a MIMO setting, which Matthaiou et al. (2010) explored further. Zhong et al. (2011) considered the Demmel condition number in particular, where Dharmawansa et al. (2013) also provide some refreshing contributions in this regard. More recently, condition numbers from random matrices have also been studied by Movassagh and Edelman (2015) and Shakil and Ahsanullah (2017).

In particular, this chapter focusses on the dual matrix setting; this interest stems from a practical consideration—viz. dual-branch systems which are equipped with two transmit- and arbitrary m number of receive antennas. Therefore this chapter extends the work of Matthaiou et al. (2009) to arbitrary degrees of freedom for the complex Wishart case; and similar interest in this dual structure with arbitrary degrees of freedom has also been studied in Movassagh and Edelman (2015). This chapter therefore provides a methodology for the practitioner within the MIMO environment to potentially consider the distribution of the condition number which emanates from a complex noncentral Wishart type matrix; built from members from the complex matrix variate elliptical class.

This paper is outlined as follows: in Sect. 2 the channel propagation matrix $\mathbf{X}$ within the MIMO design is assumed to be complex matrix variate elliptically distributed for a $m \times 2$ channel—whereafter emphasis is placed on deriving certain statistical properties such as the Wishart type distribution $\mathbf{W} = \mathbf{\Sigma}^{-1}\mathbf{X}^H\mathbf{X}$ ($\mathbf{X}^H$ denotes the conjugate-transpose of matrix $\mathbf{X}$, and $\mathbf{\Sigma}$ denotes the row covariance matrix) and the corresponding joint distribution of the eigenvalues. The complex matrix variate t- and slash distributions are of particular interest. In Sect. 3, specific distributional characteristics of the condition number of $\mathbf{W}$ is studied; with particular focus cases. Section 4 contains some numerical examples and discussions and Sect. 5 concludes the paper.

2 Dual Complex Noncentral Wishart Type Construction

Let $\mathbf{X} : m \times 2$ have a complex noncentral matrix variate elliptical distribution with the following (pdf) ($tr\mathbf{X}$ indicates the trace of matrix $\mathbf{X}$, and $\mathbb{R}^+$ denotes the positive real line):

$$f(\mathbf{X}) = h\left[-tr\mathbf{\Sigma}^{-1}(\mathbf{X}-\mathbf{M})(\mathbf{X}-\mathbf{M})^H\right] \tag{1}$$

denoted as $\mathbf{X} \sim CE_{m,2}(\mathbf{M}, \mathbf{\Sigma} \otimes \mathbf{I}_2, h)$, with density generator $h : \mathbb{R}^+ \to \mathbb{R}^+$, row covariance matrix $\mathbf{\Sigma} : m \times m$, and where $\mathbf{I}_2$ denotes a 2×2 identity matrix. Bekker et al. (2018) and Ferreira and Bekker (2019) have illustrated the above complex noncentral matrix variate elliptical pdf as a scale mixture (in other words, *weighted*) of complex matrix variate normal distributions:

$$f(\mathbf{X}) = \int_{\mathbb{R}^+} \mathcal{W}(t) f_{CN_{m,2}(\mathbf{M}, t^{-1}\mathbf{\Sigma}\otimes\mathbf{I}_2)}(\mathbf{X}|t)dt \tag{2}$$

where $f_{CN_{m,2}(\mathbf{M}, t^{-1}\mathbf{\Sigma}\otimes\mathbf{I}_2)}(\mathbf{X}|t)$ is the pdf of a complex matrix variate normal distribution with mean $\mathbf{M}$ and covariance structure $t^{-1}\mathbf{\Sigma}\otimes\mathbf{I}_2$ (denoted $CN_{m,2}(\mathbf{M}, t^{-1}\mathbf{\Sigma}\otimes\mathbf{I}_2)$) and $\mathcal{W}(t)$ is a weight function depending only on t.

Consider $\tilde{\mathbf{W}} = \mathbf{X}^H\mathbf{X}$. It has pdf

$$\begin{aligned}
&f(\tilde{\mathbf{W}}) \\
&= \int_{\mathbb{R}^+} \exp\left(-\mathrm{tr}t\mathbf{\Sigma}^{-1}\mathbf{M}\mathbf{M}^H\right) {}_0\tilde{F}_1\left(2; t^2\mathbf{\Sigma}^{-1}\mathbf{M}\mathbf{M}^H\mathbf{\Sigma}^{-1}\tilde{\mathbf{W}}\right) \frac{\det\left(t^{-1}\mathbf{\Sigma}\right)^{-2}}{\tilde{\Gamma}_2(2)} \\
&\quad \times \exp\left(-\mathrm{tr}t\mathbf{\Sigma}^{-1}\tilde{\mathbf{W}}\right)\mathcal{W}(t)\,dt \\
&= \int_{\mathbb{R}^+} \frac{t^4}{\tilde{\Gamma}_2(2)} \exp\left(-\mathrm{tr}t\mathbf{\Omega}\right) {}_0\tilde{F}_1\left(2; t^2\mathbf{\Omega}\mathbf{\Sigma}^{-1}\tilde{\mathbf{W}}\right) \det(\mathbf{\Sigma})^{-2} \exp\left(-tr t\mathbf{\Sigma}^{-1}\tilde{\mathbf{W}}\right)\mathcal{W}(t)\,dt \\
&= \int_{\mathbb{R}^+} f\left(\tilde{\mathbf{W}}|t\right)\mathcal{W}(t)\,dt
\end{aligned} \tag{3}$$

where $\boldsymbol{\Omega} = \boldsymbol{\Sigma}^{-1}\mathbf{M}\mathbf{M}^H$, $\tilde{\Gamma}_2(2)$ denotes the complex gamma function (see Ferreira and Bekker 2019), and ${}_0\tilde{F}_1(\cdot;\cdot)$ is the complex hypergeometric function of complex matrix argument (see also James 1964).

Remark 1 If $\mathbf{M} = \mathbf{0}$ is substituted into (3) then the pdf of $\tilde{\mathbf{W}}$ is given by

$$\begin{aligned} f(\tilde{\mathbf{W}}) &= \frac{1}{\tilde{\Gamma}_2(2)\det(\boldsymbol{\Sigma})^2}\int_{\mathbb{R}^+} t^4 \exp\left(-trt\boldsymbol{\Sigma}^{-1}\tilde{\mathbf{W}}\right)\mathcal{W}(t)\,dt \\ &= \frac{\mathcal{G}\left(\tilde{\mathbf{W}}\right)}{\tilde{\Gamma}_2(2)\det(\boldsymbol{\Sigma})^2} \end{aligned}$$

where $\mathcal{G}(\tilde{\mathbf{W}}) = \int_{\mathbb{R}^+} t^4 \exp(-trt\boldsymbol{\Sigma}^{-1}\tilde{\mathbf{W}})\mathcal{W}(t)dt$. This is the pdf of a dual complex central matrix variate elliptical distribution with covariance structure $t^{-1}\boldsymbol{\Sigma}\otimes\mathbf{I}_2$ (see Eq. 6 p. 3 of Ferreira et al. 2020). ■

Consider now the following transformation $\mathbf{W} = \boldsymbol{\Sigma}^{-1}\tilde{\mathbf{W}}$, with Jacobian $J(\tilde{\mathbf{W}} \to \mathbf{W}) = \det(\boldsymbol{\Sigma})^2$; then

$$\begin{aligned} & f(\mathbf{W}) \\ &= \int_{\mathbb{R}^+} \frac{t^4}{\tilde{\Gamma}_2(2)} \exp(-\mathrm{tr}t\boldsymbol{\Omega})\,{}_0\tilde{F}_1\left(2; t^2\boldsymbol{\Omega}\mathbf{W}\right)\exp(-\mathrm{tr}t\mathbf{W})\,\mathcal{W}(t)\,dt \qquad (4) \\ &= \int_{\mathbb{R}^+} \frac{t^4}{\tilde{\Gamma}_2(2)} \exp(-t\,\mathrm{tr}(\boldsymbol{\Omega}+\mathbf{W}))\,{}_0\tilde{F}_1\left(2; t^2\boldsymbol{\Omega}\mathbf{W}\right)\mathcal{W}(t)\,dt \\ &= \int_{\mathbb{R}^+} f(\mathbf{W}|t)\,\mathcal{W}(t)\,dt. \end{aligned}$$

The following remarks describes some special cases of the pdf (4) of $\mathbf{W}$.

Remark 2 If $\mathbf{X}$ follows a complex matrix variate normal distribution, then:

$$\mathcal{W}(t) = \delta(t-1) \qquad (5)$$

where $\delta(\cdot)$ is the dirac-delta function. Substituting this weight (5) into (4) gives the pdf of $\mathbf{W}$ as

$$f(\mathbf{W}) = \int_{\mathbb{R}^+} \frac{t^4}{\tilde{\Gamma}_2(2)} \exp(-t\,\mathrm{tr}(\boldsymbol{\Omega}+\mathbf{W}))_0\tilde{F}_1\left(2; t^2\boldsymbol{\Omega}\mathbf{W}\right)\delta(t-1)\,dt.$$

Let $x = t - 1$, then $t = x + 1$ and $dx = dt$:

$$f(\mathbf{W}) = \int_{\mathbb{R}^+} \frac{(x+1)^4}{\tilde{\Gamma}_2(2)} \exp(-t\mathrm{tr}(\mathbf{\Omega} + \mathbf{W}))_0\tilde{F}_1\left(2; (x+1)^2\mathbf{\Omega}\mathbf{W}\right)\delta(x)\,dx$$
$$= \frac{1}{\tilde{\Gamma}_2(2)} \exp(-t\mathrm{tr}(\mathbf{\Omega} + \mathbf{W}))_0\tilde{F}_1(2; \mathbf{\Omega}\mathbf{W})$$

using the properties of the dirac-delta function, and reflects the result of James (1964). ■

Remark 3 If $\mathbf{X}$ follows a complex matrix variate t distribution with $v > 0$ degrees of freedom, then:

$$\mathcal{W}(t) = \frac{(tv)^v \exp(-tv)}{t\Gamma(v)} \tag{6}$$

where $\Gamma(\cdot)$ denotes the usual gamma function. Substituting this weight (6) into (4) gives the pdf of $\mathbf{W}$ as

$$f(\mathbf{W}) = \int_{\mathbb{R}^+} \frac{t^4}{\tilde{\Gamma}_2(2)} \exp(-t\mathrm{tr}(\mathbf{\Omega} + \mathbf{W}))_0\tilde{F}_1\left(2; t^2\mathbf{\Omega}\mathbf{W}\right)\frac{(tv)^v \exp(-tv)}{t\Gamma(v)}dt$$
$$= \frac{v^v}{\Gamma(v)\tilde{\Gamma}_2(2)} \int_{\mathbb{R}^+} t^{4+v-1} \exp(-t(\mathrm{tr}(\mathbf{\Omega} + \mathbf{W}) + v))_0\tilde{F}_1\left(2; t^2\mathbf{\Omega}\mathbf{W}\right)dt.$$

■

Remark 4 If $\mathbf{X}$ follows a complex matrix variate slash distribution with $b > 0$, then (see Lachos and Labra 2014):

$$\mathcal{W}(t) = bt^{b-1}. \tag{7}$$

Substituting this weight (7) into (4) gives the pdf of $\mathbf{W}$ as

$$f(\mathbf{W}) = \int_0^1 \frac{t^4}{\tilde{\Gamma}_2(2)} \exp(-t\mathrm{tr}(\mathbf{\Omega} + \mathbf{W}))_0\tilde{F}_1\left(2; t^2\mathbf{\Omega}\mathbf{W}\right)bt^{b-1}dt$$
$$= \frac{b}{\tilde{\Gamma}_2(2)} \int_0^1 t^{b+3} \exp(-t(\mathrm{tr}(\mathbf{\Omega} + \mathbf{W})))_0\tilde{F}_1\left(2; t^2\mathbf{\Omega}\mathbf{W}\right)dt.$$

■

Next, the joint pdf of the eigenvalues of $\mathbf{W}$ if $\mathbf{X}$ follows a complex matrix variate elliptical distribution is given. Let $w_1 > w_2 > 0$ denote the real ordered eigenvalues of $\mathbf{W}$ (thus $\boldsymbol{\omega} = \mathbf{diag}(w_1, w_2)$), and let $\mathbf{\Lambda} = \mathbf{diag}\left(\lambda_1, \lambda_2\right)$ where $\lambda_1 > \lambda_2 > 0$ denote the real ordered eigenvalues of $\mathbf{\Omega}$. From Eq. 93, p. 488 in James (1964), the

pdf for the joint eigenvalues $\boldsymbol{\omega}$ is given by

$$f(\boldsymbol{\omega}) = \frac{\pi^{2(2-1)}}{\tilde{\Gamma}_2(2)} \left[\prod_{i<j}^{2} (w_i - w_j)^2 \right] \int_{\mathbb{U}(2)} f\left(\mathbf{U}\mathbf{W}\mathbf{U}^H\right) d\mathbf{U}$$

where $\mathbb{U}(2)$ denotes the unitary space of dimension 2. Using (4) and after some simplification:

$$\begin{aligned}
& f(\boldsymbol{\omega}) \\
&= \frac{\pi^{2(2-1)}}{\tilde{\Gamma}_2(2)} (w_1 - w_2)^2 \int_{\mathbb{U}(2)} \int_{\mathbb{R}^+} \frac{t^4}{\tilde{\Gamma}_2(2)} \exp\left(-t \operatorname{tr}\left(\boldsymbol{\Omega} + \mathbf{U}\mathbf{W}\mathbf{U}^H\right)\right) \\
&\quad \times {}_0\tilde{F}_1\left(2; t^2 \boldsymbol{\Omega}\, \mathbf{U}\mathbf{W}\mathbf{U}^H\right) \mathcal{W}(t)\, dt\, d\mathbf{U} \\
&= \frac{\pi^2}{\tilde{\Gamma}_2(2)\,\tilde{\Gamma}_2(2)} (w_1 - w_2)^2 \int_{\mathbb{R}^+} t^4 \exp(-t \operatorname{tr}\boldsymbol{\Omega}) \int_{\mathbb{U}(2)} \exp\left(-t \operatorname{tr}\mathbf{U}\mathbf{W}\mathbf{U}^H\right) \\
&\quad \times {}_0\tilde{F}_1\left(2; t^2 \boldsymbol{\Omega}\, \mathbf{U}\mathbf{W}\mathbf{U}^H\right) d\mathbf{U} \mathcal{W}(t)\, dt \\
&= (w_1 - w_2)^2 \int_{\mathbb{R}^+} t^4 \exp(-t \operatorname{tr}\boldsymbol{\Omega}) \exp(-t \operatorname{tr}\boldsymbol{\omega}) \int_{\mathbb{U}(2)} {}_0\tilde{F}_1\left(2; t^2 \boldsymbol{\Omega}\, \mathbf{U}\mathbf{W}\mathbf{U}^H\right) d\mathbf{U} \mathcal{W}(t)\, dt \\
&= (w_1 - w_2)^2 \int_{\mathbb{R}^+} t^4 \exp\left(-t \sum_{i=1}^{2} (\lambda_i + w_i)\right) {}_0\tilde{F}_1(2; t\boldsymbol{\Lambda}, t\boldsymbol{\omega}) \mathcal{W}(t)\, dt \qquad (8)
\end{aligned}$$

by using the definition of complex multivariate gamma function (Eq. 83, p. 487), and the splitting formula (Eq. 92, p. 488) in James (1964).

Remark 5 See that ${}_0\tilde{F}_1(2; t\boldsymbol{\Lambda}, t\boldsymbol{\omega})$ above can be written as follows:

$$\begin{aligned}
{}_0\tilde{F}_1(2; t\boldsymbol{\Lambda}, t\boldsymbol{\omega}) &= \frac{\det\left({}_0F_1\left(1; t^2 w_i \lambda_j\right)\right)}{(t\lambda_1 - t\lambda_2)(tw_1 - tw_2)} \\
&= \frac{\det\left({}_0F_1\left(1; t^2 w_i \lambda_j\right)\right)}{t^2(\lambda_1 - \lambda_2)(w_1 - w_2)}.
\end{aligned}$$

where ${}_0F_1(\cdot;\cdot)$ denotes the confluent hypergeometric function of scalar argument; and by using Eq. 4.8 p. 239 of Gross and Richards (1989). Note that ${}_0F_1(s+1; x) = s! x^{-\frac{s}{2}} I_s\left(2\sqrt{x}\right)$, where $I_s(\cdot)$ is the s^{th} order modified Bessel function of the first kind. Then

$$\begin{aligned}
\det\left({}_0F_1\left(1; t^2 w_i \lambda_j\right)\right) &= \det\left(I_0\left(2t\sqrt{w_i \lambda_j}\right)\right) \\
&= \begin{vmatrix} I_0\left(2t\sqrt{w_1\lambda_1}\right) & I_0\left(2t\sqrt{w_1\lambda_2}\right) \\ I_0\left(2t\sqrt{w_2\lambda_1}\right) & I_0\left(2t\sqrt{w_2\lambda_2}\right) \end{vmatrix} \\
&= I_0\left(2t\sqrt{w_1\lambda_1}\right) I_0\left(2t\sqrt{w_2\lambda_2}\right) - I_0\left(2t\sqrt{w_1\lambda_2}\right) I_0\left(2t\sqrt{w_2\lambda_1}\right).
\end{aligned}$$

This particular Bessel function of the first kind has series expansion (see Eq. 8.447.1, p. 919 of Gradshteyn and Ryzhik 2014):

$$I_0(x) = \sum_{k=0}^{\infty} \left(\frac{1}{k!}\right)^2 \left(\frac{x}{2}\right)^{2k}.$$

Then follows that

$$\begin{aligned}
\det\left({}_0F_1\left(1; t^2 w_i \lambda_j\right)\right) &= \sum_{k=0}^{\infty}\sum_{n=0}^{\infty} \left(\frac{1}{k!n!}\right)^2 \left[\frac{2t\sqrt{w_1\lambda_1}}{2}\right]^{2k} \left[\frac{2t\sqrt{w_2\lambda_2}}{2}\right]^{2n} \\
&\quad - \sum_{k=0}^{\infty}\sum_{n=0}^{\infty} \left(\frac{1}{k!n!}\right)^2 \left[\frac{2t\sqrt{w_1\lambda_2}}{2}\right]^{2k} \left[\frac{2t\sqrt{w_2\lambda_1}}{2}\right]^{2n} \\
&= \sum_{k=0}^{\infty}\sum_{n=0}^{\infty} \frac{t^{2k+2n}}{(k!n!)^2} \left[w_1^k \lambda_1^k w_2^n \lambda_2^n - w_1^k \lambda_2^k w_2^n \lambda_1^n\right] \\
&= \sum_{k=0}^{\infty}\sum_{n=0}^{\infty} \frac{t^{2k+2n}}{(k!n!)^2} (w_1 w_2)^{k+n} \left[\lambda_1^k \lambda_2^n - \lambda_2^k \lambda_1^n\right].
\end{aligned}$$

Finally,

$${}_0\tilde{F}_1(2; t\boldsymbol{\Lambda}, t\boldsymbol{\omega}) = \sum_{k=0}^{\infty}\sum_{n=0}^{\infty} \frac{t^{2k+2n} (w_1 w_2)^{k+n} \left[\lambda_1^k \lambda_2^n - \lambda_2^k \lambda_1^n\right]}{(k!n!)^2 t^2 (\lambda_1 - \lambda_2)(w_1 - w_2)} \tag{9}$$

■

Using (9) and substituting into (8) we have

$$\begin{aligned}
f(\boldsymbol{\omega}) &= (w_1 - w_2)^2 \int_{\mathbb{R}^+} t^4 \exp\left(-t \sum_{i=1}^{2} (\lambda_i + w_i)\right) \\
&\quad \times \sum_{k=0}^{\infty}\sum_{n=0}^{\infty} \frac{t^{2k+2n} (w_1 w_2)^{k+n} \left[\lambda_1^k \lambda_2^n - \lambda_2^k \lambda_1^n\right]}{(k!n!)^2 t^2 (\lambda_1 - \lambda_2)(w_1 - w_2)} \mathcal{W}(t)\, dt \\
&= (w_1 - w_2)^2 \sum_{k=0}^{\infty}\sum_{n=0}^{\infty} \frac{(w_1 w_2)^{k+n} \left[\lambda_1^k \lambda_2^n - \lambda_2^k \lambda_1^n\right]}{(k!n!)^2 (\lambda_1 - \lambda_2)(w_1 - w_2)} \\
&\quad \times \int_{\mathbb{R}^+} t^{2k+2n+2} \exp\left(-t \sum_{i=1}^{2} (\lambda_i + w_i)\right) \mathcal{W}(t)\, dt
\end{aligned} \tag{10}$$

which gives the joint pdf of the eigenvalues of $\mathbf{W}$ if $\mathbf{X}$ follows a complex matrix variate elliptical distribution. The following remarks describes some special cases of (10).

Remark 6 If $\mathbf{X}$ follows a complex matrix variate normal distribution, then we substitute the weight (5) into (10) which gives the joint pdf of the eigenvalues of $\mathbf{W}$ as:

$$
\begin{aligned}
& f(\boldsymbol{\omega}) \\
&= (w_1 - w_2)^2 \int_{\mathbb{R}^+} t^4 \exp\left(-t \sum_{i=1}^{2} (\lambda_i + w_i)\right) {}_0\tilde{F}_1\left(2; t\boldsymbol{\Lambda}, t\boldsymbol{\omega}\right) \delta(t-1)\, dt \\
&= (w_1 - w_2)^2 \exp\left(-\sum_{i=1}^{2} (\lambda_i + w_i)\right) {}_0\tilde{F}_1\left(2; \boldsymbol{\Lambda}, \boldsymbol{\omega}\right) \\
&= (w_1 - w_2)^2 \sum_{k=0}^{\infty} \sum_{n=0}^{\infty} \frac{(w_1 w_2)^{k+n} \left[\lambda_1^k \lambda_2^n - \lambda_2^k \lambda_1^n\right]}{(k!n!)^2 (\lambda_1 - \lambda_2)(w_1 - w_2)} \exp\left(-\sum_{i=1}^{2} (\lambda_i + w_i)\right)
\end{aligned}
$$

which reflects Eq. 1, p. 1213 of Matthaiou et al. (2009). ■

Remark 7 If $\mathbf{X}$ follows a complex matrix variate t distribution with v degrees of freedom, then the weight (6) is substituted into (10) which gives the joint pdf of the eigenvalues of $\mathbf{W}$ as

$$
\begin{aligned}
& f(\boldsymbol{\omega}) \\
&= (w_1 - w_2)^2 \int_{\mathbb{R}^+} t^4 \exp\left(-t \sum_{i=1}^{2} (\lambda_i + w_i)\right) {}_0\tilde{F}_1\left(2; t\boldsymbol{\Lambda}, t\boldsymbol{\omega}\right) \frac{(tv)^v \exp(-tv)}{t\Gamma(v)} dt \\
&= \frac{v^v}{\Gamma(v)} (w_1 - w_2)^2 \int_{\mathbb{R}^+} t^{4+v-1} \exp\left(-t \left(\sum_{i=1}^{2} (\lambda_i + w_i) + v\right)\right) {}_0\tilde{F}_1\left(2; t\boldsymbol{\Lambda}, t\boldsymbol{\omega}\right) dt \\
&= \frac{v^v}{\Gamma(v)} (w_1 - w_2)^2 \int_{\mathbb{R}^+} t^{v+3} \exp\left(-t \left(\sum_{i=1}^{2} (\lambda_i + w_i) + v\right)\right) \\
&\quad \times \sum_{k=0}^{\infty} \sum_{n=0}^{\infty} \frac{t^{2k+2n} (w_1 w_2)^{k+n} \left[\lambda_1^k \lambda_2^n - \lambda_2^k \lambda_1^n\right]}{(k!n!)^2 t^2 (\lambda_1 - \lambda_2)(w_1 - w_2)} dt \\
&= \frac{v^v (w_1 - w_2)^2}{\Gamma(v)(\lambda_1 - \lambda_2)(w_1 - w_2)} \sum_{k=0}^{\infty} \sum_{n=0}^{\infty} \frac{\left[\lambda_1^k \lambda_2^n - \lambda_2^k \lambda_1^n\right] (w_1 w_2)^{k+n}}{(k!n!)^2} \\
&\quad \times \int_{\mathbb{R}^+} t^{v+2k+2n+1} \exp\left(-t \left(\sum_{i=1}^{2} (\lambda_i + w_i) + v\right)\right) dt
\end{aligned}
$$

$$= \frac{v^v (w_1 - w_2)}{\Gamma(v)(\lambda_1 - \lambda_2)} \sum_{k=0}^{\infty}\sum_{n=0}^{\infty} \frac{\left[\lambda_1^k \lambda_2^n - \lambda_2^k \lambda_1^n\right](w_1 w_2)^{k+n} \Gamma(v + 2k + 2n + 2)}{(k!n!)^2 (\lambda_1 + \lambda_2 + w_1 + w_2 + v)^{v+2k+2n+2}}$$

using the gamma integral (Eq. 3.381.4, p. 346 of Gradshteyn and Ryzhik 2014). ■

Remark 8 If $\mathbf{X}$ follows a complex matrix variate slash distribution, then the weight (7) is substituted into (10) which gives the joint pdf of the eigenvalues of $\mathbf{W}$ as

$$\begin{aligned}
& f(\boldsymbol{\omega}) \\
&= (w_1 - w_2)^2 \int_0^1 t^4 \exp\left(-t \sum_{i=1}^{2} (\lambda_i + w_i)\right) {}_0\tilde{F}_1(2; t\boldsymbol{\Lambda}, t\boldsymbol{\omega})\, b t^{b-1} dt \\
&= b(w_1 - w_2)^2 \int_0^1 t^{b+3} \exp\left(-t \left(\sum_{i=1}^{2} (\lambda_i + w_i)\right)\right) \\
&\quad \times \sum_{k=0}^{\infty}\sum_{n=0}^{\infty} \frac{t^{2k+2n} (w_1 w_2)^{k+n} \left[\lambda_1^k \lambda_2^n - \lambda_2^k \lambda_1^n\right]}{(k!n!)^2 t^2 (\lambda_1 - \lambda_2)(w_1 - w_2)} dt \\
&= \frac{b(w_1 - w_2)^2}{(\lambda_1 - \lambda_2)(w_1 - w_2)} \sum_{k=0}^{\infty}\sum_{n=0}^{\infty} \frac{\left[\lambda_1^k \lambda_2^n - \lambda_2^k \lambda_1^n\right](w_1 w_2)^{k+n}}{(k!n!)^2} \\
&\quad \times \int_0^1 t^{b+2k+2n+1} \exp\left(-t \left(\sum_{i=1}^{2} (\lambda_i + w_i)\right)\right) dt \\
&= \frac{b(w_1 - w_2)}{(\lambda_1 - \lambda_2)} \sum_{k=0}^{\infty}\sum_{n=0}^{\infty} \frac{\left[\lambda_1^k \lambda_2^n - \lambda_2^k \lambda_1^n\right](w_1 w_2)^{k+n}}{(k!n!)^2} \\
&\quad \times \frac{\gamma\left(2k + 2n + b + 2, \sum_{i=1}^{2} (\lambda_i + w_i)\right)}{\left(\sum_{i=1}^{2} (\lambda_i + w_i)\right)^{2k+2n+b+2}}
\end{aligned}$$

where $\gamma(\cdot, \cdot)$ denotes the lower incomplete gamma function (see Eq. 8.350.1, p. 899 Gradshteyn and Ryzhik 2014 and using Eq. 3.381.1, p. 346 of Gradshteyn and Ryzhik 2014). ■

3 Condition Number

In this section, certain statistical characteristics of the condition number emanating from (4) and using (10) is derived.

Define the condition number as $z = \frac{w_1}{w_2}$, where w_1 and w_2 are the real ordered eigenvalues of $\mathbf{W}$ (see (4)). Consider the joint transformation to $z = \frac{w_1}{w_2}$ and $w_2 =$

w_2. The Jacobian is given by $J\left((w_1, w_2) \to (z, w_2)\right) = w_2$. Then

$$f_Z(z) = \int_0^\infty f(zw_2, w_2)\, w_2 dw_2$$

using (10). See that $w_1 - w_2 = w_2(z-1)$, and $w_1 + w_2 = w_2(z+1)$. Then from (8) and (10) it follows that

$$f_Z(z) = \int_0^\infty w_2 (w_2(z-1))^2 \int_{\mathbb{R}^+} t^4 \exp\left(-t(\lambda_1+\lambda_2)\right) \times \exp\left(-t(w_2(z+1))\right) {}_0\tilde{F}_1\left(2; t\boldsymbol{\Lambda}, t\boldsymbol{\omega}'\right) \mathcal{W}(t)\, dt dw_2$$

where $\boldsymbol{\omega}' = (zw_2, w_2)$. Using (9) leaves

$$\begin{aligned}
& f_Z(z) \\
&= \sum_{k=0}^\infty \sum_{n=0}^\infty \int_{\mathbb{R}^+} \frac{t^{2k+2n}}{(k!n!)^2} \frac{t^2 \exp\left(-t(\lambda_1+\lambda_2)\right)(z-1)z^k}{(\lambda_1-\lambda_2)} \left[\lambda_1^k\lambda_2^n - \lambda_2^k\lambda_1^n\right] \\
&\quad \times \int_0^\infty w_2^{k+n+2} \exp\left(-w_2(t(z+1))\right) dw_2 \mathcal{W}(t)\, dt \\
&= \sum_{k=0}^\infty \sum_{n=0}^\infty \int_{\mathbb{R}^+} \frac{t^{2k+2n}}{(k!n!)^2} \frac{t^2 \exp\left(-t(\lambda_1+\lambda_2)\right)(z-1)z^k}{(\lambda_1-\lambda_2)} \left[\lambda_1^k\lambda_2^n - \lambda_2^k\lambda_1^n\right] \\
&\quad \times \frac{\Gamma(k+n+3)}{(t(z+1))^{k+n+3}} \mathcal{W}(t)\, dt \\
&= \sum_{k=0}^\infty \sum_{n=0}^\infty \frac{z^k(z-1)\Gamma(k+n+3)}{(k!n!)^2(\lambda_1-\lambda_2)(z+1)^{k+n+3}} \left[\lambda_1^k\lambda_2^n - \lambda_2^k\lambda_1^n\right] \\
&\quad \times \int_{\mathbb{R}^+} t^{k+n-1} \exp\left(-t(\lambda_1+\lambda_2)\right) \mathcal{W}(t)\, dt \\
&= \sum_{k=0}^\infty \sum_{n=0}^\infty \frac{z^k(z-1)\Gamma(k+n+3)}{(k!n!)^2(\lambda_1-\lambda_2)(z+1)^{k+n+3}} \left[\lambda_1^k\lambda_2^n - \lambda_2^k\lambda_1^n\right] \kappa(t) \qquad (11)
\end{aligned}$$

where $\kappa(t) = \int_{\mathbb{R}^+} t^{k+n-1} \exp\left(-t(\lambda_1+\lambda_2)\right) \mathcal{W}(t)\, dt$, and leaves the final result.

The following remarks describes some special cases of (11).

Remark 9 If $\mathbf{X}$ follows a complex matrix variate normal distribution, then the weight (5) is substituted into (11) which gives the pdf of the condition number of $\mathbf{W}$ as

$$
\begin{aligned}
& f_Z(z) \qquad (12)\\
&= \sum_{k=0}^{\infty}\sum_{n=0}^{\infty} \frac{z^k (z-1)\,\Gamma(k+n+3)}{(k!n!)^2 (\lambda_1-\lambda_2)(z+1)^{k+n+3}} \left[\lambda_1^k\lambda_2^n - \lambda_2^k\lambda_1^n\right]\\
&\quad \times \int_{\mathbb{R}^+} t^{k+n-1} \exp(-t(\lambda_1+\lambda_2))\delta(t-1)\,dt\\
&= \sum_{k=0}^{\infty}\sum_{n=0}^{\infty} \frac{z^k (z-1)\,\Gamma(k+n+3)\exp(-(\lambda_1+\lambda_2))}{(k!n!)^2 (\lambda_1-\lambda_2)(z+1)^{k+n+3}} \left[\lambda_1^k\lambda_2^n - \lambda_2^k\lambda_1^n\right]
\end{aligned}
$$

which reflects Eq. 7, p. 1214 by Matthaiou et al. (2009). ■

Remark 10 If $\mathbf{X}$ follows a complex matrix variate t distribution with v degrees of freedom, then the weight (6) is substituted into (11) which gives the pdf of the condition number of $\mathbf{W}$ as

$$
\begin{aligned}
& f_Z(z) \qquad (13)\\
&= \frac{v^v}{\Gamma(v)} \sum_{k=0}^{\infty}\sum_{n=0}^{\infty} \frac{z^k (z-1)\,\Gamma(k+n+3)\left[\lambda_1^k\lambda_2^n - \lambda_2^k\lambda_1^n\right]}{(k!n!)^2 (\lambda_1-\lambda_2)(z+1)^{k+n+3}} \frac{\Gamma(k+n+v-1)}{(\lambda_1+\lambda_2+v)^{k+n+v-1}}
\end{aligned}
$$

since

$$
\begin{aligned}
\kappa(t) &= \int_{\mathbb{R}^+} t^{k+n-1} \exp(-t(\lambda_1+\lambda_2))\mathcal{W}(t)\,dt\\
&= \int_{\mathbb{R}^+} t^{k+n-1} \exp(-t(\lambda_1+\lambda_2)) \frac{(tv)^v \exp(-tv)}{t\Gamma(v)} dt\\
&= \frac{v^v}{\Gamma(v)} \int_{\mathbb{R}^+} t^{k+n+v-2} \exp(-t(\lambda_1+\lambda_2+v))dt\\
&= \frac{v^v}{\Gamma(v)} \frac{\Gamma(k+n+v-1)}{(\lambda_1+\lambda_2+v)^{k+n+v-1}} \qquad (14)
\end{aligned}
$$

by using Eq. 3.381.4, p. 346 of Gradshteyn and Ryzhik (2014). ■

Remark 11 If $\mathbf{X}$ follows a complex matrix variate slash distribution, then the weight (7) is substituted into (11) which gives the pdf of the condition number of $\mathbf{W}$ as

$$
\begin{aligned}
& f_Z(z) \qquad (15)\\
&= \sum_{k=0}^{\infty}\sum_{n=0}^{\infty} \frac{z^k (z-1)\,\Gamma(k+n+3)}{(k!n!)^2 (\lambda_1-\lambda_2)(z+1)^{k+n+3}} \left[\lambda_1^k\lambda_2^n - \lambda_2^k\lambda_1^n\right]\kappa(t)\\
&= b\sum_{k=0}^{\infty}\sum_{n=0}^{\infty} \frac{z^k (z-1)\,\Gamma(k+n+3)\left[\lambda_1^k\lambda_2^n - \lambda_2^k\lambda_1^n\right]}{(k!n!)^2 (\lambda_1-\lambda_2)(z+1)^{k+n+3}} \frac{\gamma(k+n+b-1, \lambda_1+\lambda_2)}{(\lambda_1+\lambda_2)^{k+n+b-1}}
\end{aligned}
$$

since

$$\begin{aligned}\kappa(t) &= \int_0^1 t^{k+n-1} \exp(-t(\lambda_1+\lambda_2))\mathcal{W}(t)\,dt \\ &= \int_0^1 t^{k+n-1} \exp(-t(\lambda_1+\lambda_2))bt^{b-1}dt \\ &= b\int_0^1 t^{k+n+b-2} \exp(-t(\lambda_1+\lambda_2))dt \\ &= b\frac{\gamma(k+n+b-1,\lambda_1+\lambda_2)}{(\lambda_1+\lambda_2)^{k+n+b-1}} \end{aligned} \tag{16}$$

by using Eq. 3.381.1, p. 346 of Gradshteyn and Ryzhik 2014). ■

Dharmawansa et al. (2013) also studied the moment generating function (mgf) of the condition number and illustrated that it is meaningful within the discipline of random matrix theory. The mgf pertaining to (11) under the complex matrix variate elliptical assumption of $\mathbf{X}$ is now derived:

$$\begin{aligned} & M_Z(r) \\ &= E(\exp(rZ)) \\ &= \int_0^\infty \exp(rz)\, f_Z(z)\,dz \\ &= \int_0^\infty \exp(rz) \sum_{k=0}^\infty \sum_{n=0}^\infty \frac{z^k(z-1)\Gamma(k+n+3)}{(k!n!)^2(\lambda_1-\lambda_2)(z+1)^{k+n+3}} \left[\lambda_1^k\lambda_2^n - \lambda_2^k\lambda_1^n\right]\kappa(t)\,dz \\ &= \sum_{k=0}^\infty \sum_{n=0}^\infty \frac{\Gamma(k+n+3)}{(k!n!)^2(\lambda_1-\lambda_2)} \left[\lambda_1^k\lambda_2^n - \lambda_2^k\lambda_1^n\right]\kappa(t) \\ &\quad \times \int_0^\infty \exp(rz)\, z^k(z-1)(z+1)^{-(k+n+3)}\,dz \end{aligned}$$

where

$$\begin{aligned} & \int_0^\infty \exp(rz)\, z^k(z-1)(z+1)^{-(k+n+3)}\,dz \\ &= \int_0^\infty \exp(rz)\, z^{k+1}(z+1)^{-(k+n+3)}\,dz - \int_0^\infty e^{rz} z^k (z+1)^{-(k+n+3)}\,dz \\ &= \sum_{m=0}^\infty \frac{r^m}{m!}\left[\int_0^\infty z^m z^{k+1}(z+1)^{-(k+n+3)}\,dz - \int_0^\infty z^m z^k (z+1)^{-(k+n+3)}\,dz\right] \end{aligned}$$

by using the series expansion of the exponential function. Recognising the last two integrals effectively as the kernel of a beta type II distribution (or beta prime distribution) with parameters $k+1$ and $n+2$, and k and $n+2$ respectively:

$$\begin{aligned}
&\sum_{m=0}^{\infty} \frac{r^m}{m!} \left[B(k+1, n+2) \int_0^{\infty} z^m \frac{z^{k+1}(z+1)^{-(k+n+3)}}{B(k+1, n+2)} dz \right. \\
&\qquad \left. - B(k+1, n+2) \int_0^{\infty} z^m \frac{z^{k}(z+1)^{-(k+n+3)}}{B(k+1, n+2)} dz \right] \\
&= \sum_{m=0}^{\infty} \frac{r^m}{m!} \left[B(k+1, n+2) \frac{B(k+1+m, n+2-m)}{B(k+1, n+2)} \right. \\
&\qquad \left. - B(k, n+2) \frac{B(k+m, n+2-m)}{B(k, n+2)} \right] \\
&= \sum_{m=0}^{\infty} \frac{r^m}{m!} \left[B(k+1+m, n+2-m) - B(k+m, n+2-m) \right]
\end{aligned}$$

where $B(\cdot, \cdot)$ denotes the beta function and using the identity for the moments of a beta type II distribution (see p. 248 in Johnston et al. 1994). This leaves the mgf of (11) as

$$\begin{aligned}
M_Z(r) = &\sum_{m=0}^{\infty} \sum_{k=0}^{\infty} \sum_{n=0}^{\infty} \frac{r^m \Gamma(k+n+3)}{m!(k!n!)^2(\lambda_1 - \lambda_2)} \left[\lambda_1^k \lambda_2^n - \lambda_2^k \lambda_1^n \right] \\
&\times \left[B(k+1+m, n+2-m) - B(k+m, n+2-m) \right] \kappa(t) .
\end{aligned} \tag{17}$$

The following remarks describes some special cases of (17).

Remark 12 If $\mathbf{X}$ follows a complex matrix variate normal distribution, then the weight (5) is substituted into (17) which gives the mgf of the condition number of $\mathbf{W}$ as

$$\begin{aligned}
M_Z(r) = &\sum_{m=0}^{\infty} \sum_{k=0}^{\infty} \sum_{n=0}^{\infty} \frac{r^m \Gamma(k+n+3)}{m!(k!n!)^2(\lambda_1 - \lambda_2)} \left[\lambda_1^k \lambda_2^n - \lambda_2^k \lambda_1^n \right] \exp(-(\lambda_1 + \lambda_2)) \\
&\times \left[B(k+1+m, n+2-m) - B(k+m, n+2-m) \right] .
\end{aligned}$$

■

Remark 13 If $\mathbf{X}$ follows a complex matrix variate t distribution with v degrees of freedom, then the weight (6) is substituted into (17) which gives the mgf of the condition number of $\mathbf{W}$ as

$$M_Z(r) = \frac{v^v}{\Gamma(v)} \sum_{m=0}^{\infty} \sum_{k=0}^{\infty} \sum_{n=0}^{\infty} \frac{r^m \Gamma(k+n+3)\Gamma(k+n+v-1)}{m!\,(k!n!)^2 (\lambda_1-\lambda_2)(\lambda_1+\lambda_2+v)^{k+n+v-1}}$$
$$\times \left[\lambda_1^k \lambda_2^n - \lambda_2^k \lambda_1^n\right] [B(k+1+m, n+2-m) - B(k+m, n+2-m)]$$

using (14). ■

Remark 14 If $\mathbf{X}$ follows a complex matrix variate slash distribution, then the weight (7) is substituted into (17) which gives the mgf of the condition number of $\mathbf{W}$ as

$$M_Z(r) = b \sum_{m=0}^{\infty} \sum_{k=0}^{\infty} \sum_{n=0}^{\infty} \frac{r^m \Gamma(k+n+3)\gamma(k+n+b-1, \lambda_1+\lambda_2)}{m!\,(k!n!)^2 (\lambda_1-\lambda_2)(\lambda_1+\lambda_2)^{k+n+b-1}}$$
$$\times \left[\lambda_1^k \lambda_2^n - \lambda_2^k \lambda_1^n\right] [B(k+1+m, n+2-m) - B(k+m, n+2-m)]$$

using (16). ■

Next the cumulative distribution function (cdf) of the condition number z (see (11)) under the complex matrix variate elliptical assumption of $\mathbf{X}$ is also derived and studied:

$$F_Z(x) = \int_1^x f(z)\,dz$$
$$= \sum_{k=0}^{\infty} \sum_{n=0}^{\infty} \frac{\Gamma(k+n+3)}{(k!n!)^2(\lambda_1-\lambda_2)} \left[\lambda_1^k \lambda_2^n - \lambda_2^k \lambda_1^n\right] \kappa(t) \int_1^x \frac{z^k (z-1)}{(z+1)^{k+n+3}} dz$$
$$= \sum_{k=0}^{\infty} \sum_{n=0}^{\infty} \frac{\Gamma(k+n+3)}{(k!n!)^2(\lambda_1-\lambda_2)} \left[\lambda_1^k \lambda_2^n - \lambda_2^k \lambda_1^n\right] \kappa(t) \int_1^x \frac{z^{k+1} - z^k}{(z+1)^{k+n+3}} dz$$

where

$$\int_1^x \frac{z^{k+1} - z^k}{(z+1)^{k+n+3}} dz = \int_1^x \frac{z^{k+1}}{(z+1)^{k+n+3}} dz - \int_1^x \frac{z^k}{(z+1)^{k+n+3}} dz$$
$$= \int_0^x \frac{z^{k+1}}{(z+1)^{k+n+3}} dz - \int_0^1 \frac{z^{k+1}}{(z+1)^{k+n+3}} dz$$
$$- \int_0^x \frac{z^k}{(z+1)^{k+n+3}} dz + \int_0^1 \frac{z^k}{(z+1)^{k+n+3}} dz$$
$$= D_1^{k+1,k+n+3}(x) - D_1^{k,k+n+3}(x)$$

using Result 3.194.1, p. 315 from Gradshteyn and Ryzhik (2014); where

$$D_1^{p,q}(x) = \left(\frac{x^{p+1}}{p+1}\right) {}_2F_1(q, p+1; p+2; -x) - \left(\frac{1}{p+1}\right) {}_2F_1(q, p+1; p+2; -1)$$

and ${}_2F_1(\cdot)$ is the Gauss hypergeometric function. Therefore

$$\begin{aligned} & F_Z(x) \qquad (18) \\ &= \sum_{k=0}^{\infty}\sum_{n=0}^{\infty} \frac{\Gamma(k+n+3)}{(k!n!)^2(\lambda_1-\lambda_2)} \left[\lambda_1^k\lambda_2^n - \lambda_2^k\lambda_1^n\right] \left[D_1^{k+1,k+n+3}(x) - D_1^{k,k+n+3}(x)\right] \kappa(t). \end{aligned}$$

The following remarks describes some special cases of (18).

Remark 15 If $\mathbf{X}$ follows a complex matrix variate normal distribution, then the weight (5) is substituted into (11) which gives the cdf of the condition number of $\mathbf{W}$ as

$$\begin{aligned} & F_Z(x) \qquad (19) \\ &= \sum_{k=0}^{\infty}\sum_{n=0}^{\infty} \frac{\Gamma(k+n+3)\exp(-(\lambda_1+\lambda_2))}{(k!n!)^2(\lambda_1-\lambda_2)} \left[\lambda_1^k\lambda_2^n - \lambda_2^k\lambda_1^n\right] \qquad (20) \\ &\quad \times \left[D_1^{k+1,k+n+3}(x) - D_1^{k,k+n+3}(x)\right] \end{aligned}$$

which reflects Eq. 11, p. 1214 of Matthaiou et al. (2009). ■

Remark 16 If $\mathbf{X}$ follows a complex matrix variate t distribution with v degrees of freedom, then the weight (6) is substituted into (11) which gives the cdf of the condition number of $\mathbf{W}$ as

$$\begin{aligned} F_Z(x) = {} & \frac{v^v}{\Gamma(v)} \sum_{k=0}^{\infty}\sum_{n=0}^{\infty} \frac{\Gamma(k+n+3)\Gamma(k+n+v-1)}{(k!n!)^2(\lambda_1-\lambda_2)} \frac{\left[\lambda_1^k\lambda_2^n - \lambda_2^k\lambda_1^n\right]}{(\lambda_1+\lambda_2+v)^{k+n+v-1}} \\ & \times \left[D_1^{k+1,k+n+3}(x) - D_1^{k,k+n+3}(x)\right]. \qquad (21) \end{aligned}$$

using (14). ■

Remark 17 If $\mathbf{X}$ follows a complex matrix variate slash distribution, then the weight (7) is substituted into (11) which gives the cdf of the condition number of $\mathbf{W}$ as

$$\begin{aligned} F_Z(x) = {} & b \sum_{k=0}^{\infty}\sum_{n=0}^{\infty} \frac{\Gamma(k+n+3)\left[\lambda_1^k\lambda_2^n - \lambda_2^k\lambda_1^n\right]}{(k!n!)^2(\lambda_1-\lambda_2)} \frac{\gamma(k+n+b-1, \lambda_1+\lambda_2)}{(\lambda_1+\lambda_2)^{k+n+b-1}} \\ & \times \left[D_1^{k+1,k+n+3}(x) - D_1^{k,k+n+3}(x)\right] \qquad (22) \end{aligned}$$

using (16). ■

4 Numerical Experiments

In this section, analytical results are presented to illustrate the contribution of the derived results. As in Matthaiou et al. (2009), the eigenvalues of the noncentrality matrix is considered as $\mathbf{\Lambda} = \mathbf{diag}\left(\lambda_1, \lambda_2\right) = (7.0336, 5.6155)$.

4.1 Truncation Error of Infinite Sums

The infinite double summation in (18) has the potential of causing high computational complexity; however, Table 1 shows that even by considering a truncated finite subset of terms, convergence of values for $F_Z(z)$ for both the normal-, t, and slash cases (illustrated here for $v = 5$ and $b = 5$) is reached by truncating the expressions at 30 odd terms. In Table 1, T indicates the truncation value.

4.2 Percentiles

Certain percentiles of the distribution of $F_Z(z)$ are obtained numerically by solving the equation $F_Z(x) = \alpha$. In particular, upper percentiles are computed for the normal case (see (19)) and for the t case (see (21)) for different values of v in Table 2; whereas the same is computed for the normal- and for the slash case (see (22)) for different values of b in Table 3. These values highlight the computational use of these results as they act as potential critical values for testing hypothesis regarding test statistics pertaining to the condition number emanating from an underlying complex matrix variate normal-, t, or slash distribution.

Table 1 Truncated value for infinite sums of cdfs (19), (21), and (22)

$F_Z(x)$	$T = 25$	$T = 30$	$T = 35$
Normal(20)	0.978848	0.978849	0.978849
t (20)	0.957192	0.959675	0.960013
Slash(20)	0.960977	0.960977	0.960977
Normal(25)	0.985299	0.985299	0.985299
t (25)	0.967068	0.969552	0.969890
Slash(25)	0.971377	0.971377	0.971377
Normal(30)	0.988947	0.988947	0.988947
t (30)	0.973128	0.975612	0.975950
Slash(30)	0.977594	0.977594	0.977594

Table 2 Percentiles of cdfs (19) and for (21) for different v

α	$t(2)$	$t(5)$	$t(10)$	Normal
0.90	13.2197	10.2197	9.28070	8.33532
0.95	24.5197	16.9027	14.4340	12.1904
0.975	46.7810	29.0380	23.2610	18.1116
0.99	114.016	64.0161	47.0161	32.0468

Table 3 Percentiles of cdfs (19) and for (22) for different b

α	Slash(2)	Slash(5)	Slash(10)	Normal
0.90	15.2007	10.6284	9.3784	8.33532
0.95	27.5108	16.9511	14.3011	12.1904
0.975	51.2501	27.7173	22.1173	18.1116
0.99	122.0683	59.2771	45.3121	32.0468

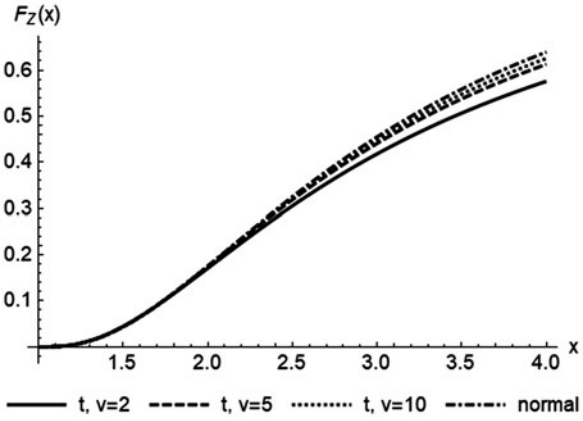

Fig. 1 Cdfs (19) and (21) for different values of v, lower tail

4.3 *Illustration of cdfs*

Figures 1, 2, and 3 illustrate the cdfs (19) and (21) for $v = 2, 5, 10$ respectively; and Figs. 4, 5, and 6 illustrate the cdfs (19) and (22) for different values of $b = 2, 5, 10$ respectively. It is clear that (21) tends to the normal case as the value of v increases; similar behaviour is observed from (22). These figures highlight the value which an underlying complex matrix variate elliptical assumption could provide the practitioner having the engineering expertise within the MIMO arena with. This elliptical platform allows theoretical and practical access to previously unconsidered models (such as the underlying complex matrix variate t) that could potentially yield improved fits to experimental data.

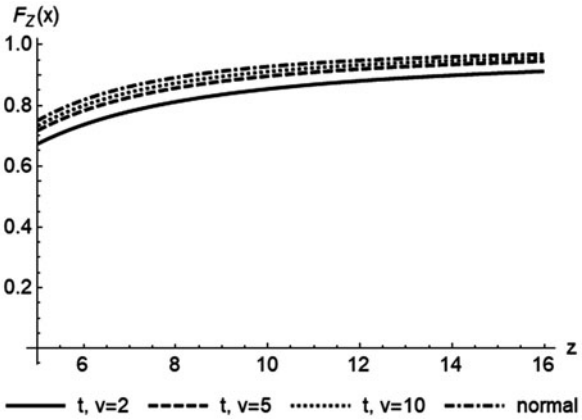

Fig. 2 Cdfs (19) and (21) for different values of v, mid section

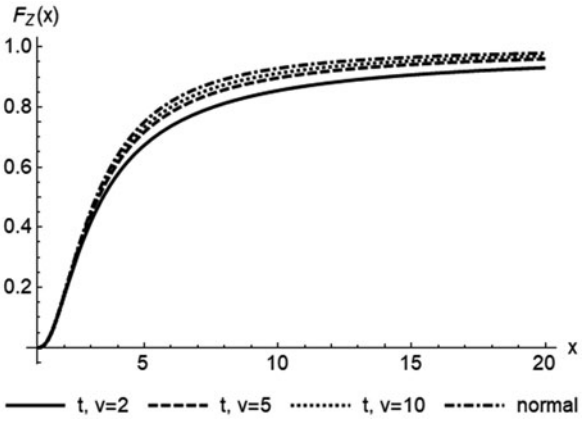

Fig. 3 Cdfs (19) and (21) for different values of v, complete

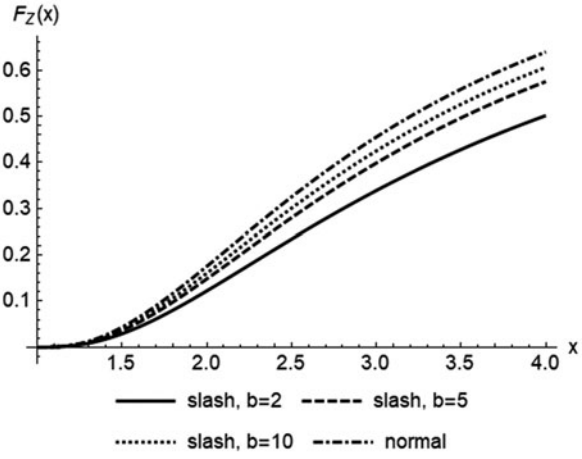

Fig. 4 Cdfs (19) and (22) for different values of b, lower tail

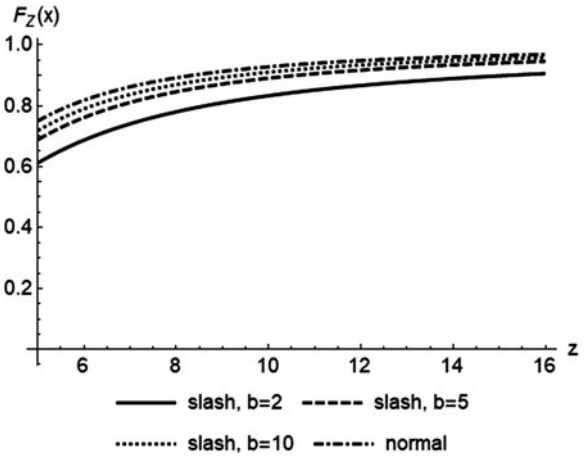

Fig. 5 Cdfs (19) and (22) for different values of b, mid section

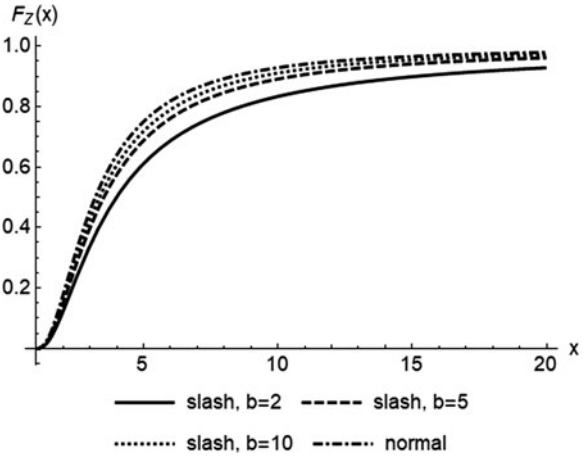

Fig. 6 Cdfs (19) and (22) for different values of b, complete

5 Concluding Remarks

In this paper the dual branch MIMO channel propagation matrix $\mathbf{X}$ is assumed to be complex matrix variate elliptically distributed with a noncentrality matrix $\mathbf{M}$. The distribution of $\mathbf{W} = \mathbf{\Sigma}^{-1}\mathbf{X}^H\mathbf{X}$ was explored together with the joint distribution of the eigenvalues. This generalisation allows the user the flexibility to assume an alternative underlying distribution for $\mathbf{X}$; in particular, this chapter focussed on the complex matrix variate t distribution. The stochastic nature of the condition number of $\mathbf{W}$ was of particular interest and its characteristics were studied and accompanied by a numerical investigation. This assumption of an underlying complex matrix variate elliptical distribution allows the analysis of the condition number and other related MIMO performance measures in broad generality.

Acknowledgements The authors would like to hereby acknowledge the support of the StatDisT group at the Department of Statistics, University of Pretoria, and also to the two reviewers for valuable comments that improved this chapter. The authors would also like to thank Dr. Prathapasinghe Dharmawansa and Prof. Mohammad Arashi for valuable discussions about the work in its early stages. This work is based upon research supported by the National Research Foundation, South Africa (ref. SRUG190308422768 grant nr. 120839 and SARChI Research Chair UID:71199) and the Research Development Programme at the University of Pretoria grant nr. 296/2019.

References

Bekker, A., Arashi, M., & Ferreira, J. (2018). New bivariate gamma types with MIMO application. *Communications in Statistics: Theory and Methods, 48*(3), 596–615 (2018). https://doi.org/10.1080/03610926.2017.1417428

Chen, Z., & Dongarra, J. (2005). Condition numbers of gaussian random matrices. *SIAM Journal of Matrix Analysis and Application, 27*(3), 603–620.

Choi, S.H., Smith, P., Allen, B., Malik, W.Q., & Shafi, M. (2007). Severely fading MIMO channels: Models and mutual information. In *2007 IEEE international conference on communications* (pp. 4628–4633). Piscataway, NJ: IEEE.

De Souza, R., & Yacoub, M. (2008). Bivariate Nakagami-m distribution with arbitrary correlation and fading parameters. *IEEE Transactions on Wireless Communications, 7*(12), 5227–5232 (2008).

Dharmawansa, P., McKay, M., & Chen, Y. (2013). Distributions of Demmel and related condition numbers. *SIAM Journal of Matrix Analysis and Application, 34*(1), 257–279.

Edelman, A. (1998). Eigenvalues and condition numbers of random matrices. *SIAM Journal of Matrix Analysis and Application, 9*(4), 543–560.

Edelman, A., & Sutton, B. (2005). Tails of condition number distributions. *SIAM Journal on Matrix Analysis and Applications, 27*(2), 547–560.

Ferreira, J., & Bekker, A. (2019). A unified complex noncentral Wishart type distribution inspired by massive MIMO systems. *Journal of Statistical Distributions and Applications, 6*(1), 4.

Ferreira, J., Bekker, A., & Arashi, M. (2020). Advances in Wishart type modeling for channel capacity. *REVStat Statistical Journal* (in press).

Gradshteyn, I., & Ryzhik, I. (2014). *Table of integrals, series, and products* (7th ed). London: Academic Press.

Gross, K., & Richards, D. (1989). Total positivity, spherical series, and hypergeometric functions of matrix argument. *Journal of Approximation Theory, 59*(2), 224–246.

James, A. (1964). Distributions of matrix variate and latent roots derived from normal samples. *Annals of Mathematical Statistics, 35*, 475–501.

Johnston, N., Kotz, S., & Balakrishnan, N. (1994). *Continuous univariate distributions* (Vol. 2). New York, NY: Wiley.

Lachos, V.H., & Labra, F.V. (2014). Multivariate skew-normal/independent distributions: Properties and inference. *Pro Mathematica, 28*(56), 11–53.

Matthaiou, M., Laurenson, D., & Wang, C. (2009). On analytical derivations of the condition number distributions of dual non-central Wishart matrices. *IEEE Transactions on Wireless Communications, 8*(3), 1212–1217.

Matthaiou, M., McKay, M., Smith, P., & Nossek, J. (2010). On the condition number distribution of complex Wishart matrices. *IEEE Transactions on Communications, 58*(6), 1705–1716.

Movassagh, R., & Edelman, A. (2015). Condition numbers of indefinite rank 2 ghost Wishart matrices. *Linear Algebra and Its Applications, 483*, 342–351.

Ollila, E., Eriksson, J., & Koivunen, V. (2011). Complex elliptically symmetric random variables—generation, characterisation, and circularity tests. *IEEE Transactions on Signal Processing, 59*(1), 58–69.

Ratnarajah, T., Vaillancourt, R., & Alvo, M. (2004). Eigenvalues and condition numbers of complex random matrices. *SIAM Journal on Matrix Analysis and Applications, 26*(2), 441–456.

Shakil, M., & Ahsanullah, M. (2017). Some inferences on the distribution of the Demmel condition number of complex wishart matrices. *Special Matrices, 5*(1), 127–138.

Zhong, C., McKay, M., Ratnarajah, T., & Wong, K. (2011). Distribution of the Demmel condition number of Wishart matrices. *IEEE Transactions on Communications, 59*(9), 1309–1319.

Weighted Type II Bivariate Pólya-Aeppli Distributions

Claire Geldenhuys and René Ehlers

Abstract In this chapter we extend the existing theory of the Type II bivariate Pólya-Aeppli distribution, a compound Poisson distribution with a bivariate geometric compounding distribution, to the weighted case for two different weight functions. The weight functions address different cases of dispersion of data which allows for more flexible distributions that can be fitted to bivariate count-valued data. We derive the probability generating and probability mass functions, the marginal and conditional distributions and some properties of the distributions. Graphical displays comparing the dispersion of these new distributions are also included. Method of moments estimation of model parameters is discussed and we use real and simulated data to compare the fit of the existing Type II bivariate Pólya-Aeppli and newly proposed weighted Type II bivariate Pólya-Aeppli distributions to the data. Finally the theory is also extended to the multivariate case.

1 Introduction

The Pólya-Aeppli distribution was first introduced by Anscombe (1950). He credited the first derivation of the distribution to G. Pólya in 1930, who based it off of a thesis published by A. Aeppli in 1924. The distribution was henceforth known as the Pólya-Aeppli distribution or as a compound Poisson geometric distribution, due to the fact that the distribution arises from a compound Poisson distribution with a geometric compounding random variable.

The univariate Pólya-Aeppli distribution as derived and discussed in Johnson et al. (2005) is a widely used distribution in risk theory for estimating ruin probability as well as many other applications using count-valued data. The property of over-dispersion makes this distribution more appropriate for modelling certain count-valued data than the equi-dispersed Poisson distribution.

C. Geldenhuys (✉) · R. Ehlers
Department of Statistics, University of Pretoria, Pretoria, South Africa
e-mail: rene.ehlers@up.ac.za

A. Bekker et al. (eds.), *Computational and Methodological Statistics and Biostatistics*, Emerging Topics in Statistics and Biostatistics,
https://doi.org/10.1007/978-3-030-42196-0_6

Weighted distributions was first introduced by Fisher (1934) and it is well known from Patil and Ord (1976) and Patil (2002) as well as various other statistical literature that a random variable Y^w with probability mass function $f^w(y)$ is referred to as the weighted version of a random variable Y with probability mass function $f(y)$, if Y is non-negative and is observed with a probability proportional to the non-negative weight function $w(y)$. The distribution of the observed sample is then given by $f^w(y) = \frac{w(y)f(y)}{E(w(Y))}$, where $E(w(Y))$ is the normalizing factor, provided that $E(w(Y))$ exists. In the referenced statistical literature, weighted distributions are applied with the purpose of finding the true distribution when data points from a sampling framework do not have equal probabilities of being observed within the sample.

The weighted univariate Pólya-Aeppli distribution along with its properties and Fisher indexes of dispersion for a variety of different weight functions was first derived by Minkova and Balakrishnan (2013). In their paper, weighted distributions was utilized to allow for distributions with increased flexibility when fitted to over-dispersed univariate data.

Minkova and Balakrishnan (2014a,b) also introduced the Type I bivariate Pólya-Aeppli distribution which is a compound bivariate Poisson distribution with geometric compounding distribution, as well as the Type II bivariate Pólya-Aeppli distribution which arises when we have a compound Poisson distribution with a bivariate geometric compounding distribution. Both the Type I and Type II bivariate Pólya-Aeppli distributions are over-dispersed with respect to the bivariate Poisson distribution. In their paper Minkova and Balakrishnan (2014a) derived various properties of the Type II bivariate Pólya-Aeppli distribution including the probability generating function, probability mass function through use of recursive relations and conditional distribution.

Qin et al. (2017) derived and compared the method of moments and maximum likelihood estimation of the model parameters of the Type II bivariate Pólya-Aeppli distribution.

In this chapter our main focus will be the extension of the theory to include the weighted Type II bivariate Pólya-Aeppli distribution. We will utilize weighted distributions in the same manner as Minkova and Balakrishnan (2013), with the purpose of finding distributions with increased flexibility when fitted to over-dispersed bivariate data. Two weight functions are considered which allows for over and under-dispersion with respect to the Type II bivariate Pólya-Aeppli distribution. This gives a set of distributions that are more flexible with respect to the bivariate Poisson distribution. The distributions are also extended to the multivariate case.

The existing results of the Type II bivariate Pólya-Aeppli distribution, as well as the multivariate extension are given in Sect. 2 together with an alternative and simpler method to derive the probability mass functions. In Sections 3 and 4 the weighted Type II bivariate Pólya-Aeppli distributions Case I and Case II are respectively derived, as well as the Fisher indexes of dispersion and the extension to the multivariate cases. The method of moments estimates are also derived for the weighted distributions and the marginal and conditional distributions are given. In Sect. 5 a simulation study is used to compare properties of the estimates of the three Type II bivariate Pólya-Aeppli distributions. Bootstrap methods are used to compare

the confidence intervals of the model parameters. The distributions are also fitted to real and simulated data. Some concluding remarks are given in Sect. 6.

2 Type II Bivariate Pólya-Aeppli Distribution

This distribution and its properties was first derived by Minkova and Balakrishnan (2014a) and is a compound Poisson distribution with a bivariate geometric distribution (see Kocherlakota and Kocherlakota 1992) as the compounding distribution.

Let $X = (X_1, X_2)$ have a bivariate geometric distribution with a *pgf* given by

$$\psi_1(s_1, s_2) = \frac{\theta}{1 - \theta_1 s_1 - \theta_2 s_2}, \tag{1}$$

where $0 < \theta_1, \theta_2 < 1$, $\theta = 1 - \theta_1 - \theta_2 \neq 0$, $x_1, x_2 = 0, 1, 2 \ldots$ and we denote $\rho_1 = \frac{\theta_1}{1-\theta_2}$ and $\rho_2 = \frac{\theta_2}{1-\theta_1}$. Also let $Y \sim Poi(\lambda)$ be a random variable with *pgf* given by

$$\psi_2(s) = e^{-\lambda(1-s)}, \tag{2}$$

and define (N_1, N_2) such that $N_1 = \sum_{i=1}^{Y} X_{1i}$ and $N_2 = \sum_{j=1}^{Y} X_{2j}$. The joint distribution of (N_1, N_2) is then said be a Type II bivariate Pólya-Aeppli distribution denoted as $(N_1, N_2) \sim BivPA_{II}(\lambda, \theta_1, \theta_2)$. From (1) and (2) the *pgf* of the distribution follows as

$$\begin{aligned} \psi_{N_1,N_2}(s_1, s_2) &= \psi_2(\psi_1(s_1, s_2)) \\ &= e^{-\lambda\left(1 - \frac{\theta}{(1-\theta_1 s_1 - \theta_2 s_2)}\right)}. \end{aligned} \tag{3}$$

From Minkova and Balakrishnan (2014a), $N_1 \sim PA(\lambda\rho_1, \rho_1)$ and $N_2 \sim PA(\lambda\rho_2, \rho_2)$ and the expected values are $E(N_1) = \frac{\lambda\theta_1}{\theta}$, $E(N_2) = \frac{\lambda\theta_2}{\theta}$ and $E(N_1 N_2) = \frac{\lambda\theta_1\theta_2}{\theta^2}(2 + \lambda)$. The variances are $Var(N_1) = \frac{\lambda\theta_1(1+\theta_1-\theta_2)}{\theta^2}$ and $Var(N_2) = \frac{\lambda\theta_2(1+\theta_2-\theta_1)}{\theta^2}$, and the covariance and correlation between N_1 and N_2 are

$$\begin{aligned} Cov(N_1, N_2) &= E(N_1 N_2) - E(N_1) E(N_2) = \frac{2\lambda\theta_1\theta_2}{\theta^2} \\ Corr(N_1, N_2) \equiv R &= 2\sqrt{\frac{\theta_1\theta_2}{(1 + \theta_1 - \theta_2)(1 + \theta_2 - \theta_1)}}. \end{aligned} \tag{4}$$

In order to measure the variability of the data, Minkova and Balakrishnan (2014a) introduced the theoretical bivariate Fisher index of dispersion, given by

$$FI_2(N_1, N_2) = \left[\frac{Var(N_1)}{E(N_1)} + \frac{Var(N_2)}{E(N_2)} - 2R\frac{Cov(N_1, N_2)}{\sqrt{E(N_1)}\sqrt{E(N_2)}}\right]\frac{1}{1-R^2} \quad . \tag{5}$$

Calculating this for $(N_1, N_2) \sim BivPA_{II}(\lambda, \theta_1, \theta_2)$ gives

$$\begin{aligned} FI_2(N_1, N_2) = &\frac{2}{(1-\rho_1)(1-\rho_2)} \\ &\times \frac{(1+\rho_1)(1+\rho_2)(1-\rho_1\rho_2) - 4\rho_1\rho_2\sqrt{\left(1-\rho_1^2\right)\left(1-\rho_2^2\right)}}{(1+\rho_1)(1+\rho_2) - 4\rho_1\rho_2}. \end{aligned} \tag{6}$$

For the special case $\rho_1 = \rho_2 = \rho$ it follows that

$$FI_2(N_1, N_2) = \frac{2(1+\rho)}{(1-\rho)} > 2.$$

Since the bivariate Fisher index of dispersion is equal to 2 for the bivariate Poisson distribution, this implies that for $\rho_1 = \rho_2 = \rho$ the Type II bivariate Pólya-Aeppli distribution is over-dispersed with respect to the bivariate Poisson distribution and equi-dispersed with respect to the Type I bivariate Pólya-Aeppli distribution (see Minkova and Balakrishnan 2014a).

Minkova and Balakrishnan (2014a) derived the *pmf* of the Type II bivariate Pólya-Aeppli distribution using recursive formulas. In addition they derived the *pmf* of the multivariate extension of the distribution by expanding the *pgf* in powers of $s_1, \ldots, s_k$, however this does not allow for a closed form expression of the *pmf*. In the following two subsections we use an alternative approach for the derivation of the *pmf* of the bivariate and multivariate distributions respectively, using Laguerre polynomials in a similar manner as was first done for the univariate Pólya-Aeppli distribution in Galliher et al. (1959). This methodology is not only much simpler and more elegant compared to the use of recursive formulas, but also allows for a closed form expression of the *pmf* in the multivariate case. Results for the marginal and conditional distributions, including the conditional expected values can be found in Minkova and Balakrishnan (2014a). The method of moments estimates for the parameters of the bivariate distribution as derived by Qin et al. (2017) are

$$\hat{\theta}_1 = \frac{\bar{X}}{\left(\hat{\lambda} + \bar{X} + \bar{Y}\right)} \qquad \hat{\theta}_2 = \frac{\bar{Y}}{\left(\hat{\lambda} + \bar{X} + \bar{Y}\right)} \qquad \textit{and} \quad \hat{\lambda} = \frac{2\bar{X}\bar{Y}}{m_{1,1} - \bar{X}\bar{Y}}.$$

2.1 Joint Probability Mass Function

Theorem 1 *The pmf of* $(N_1, N_2) \sim BivPA_{II}(\lambda, \theta_1, \theta_2)$ *is*

$$f(0,0) = e^{-\lambda(1-\theta)}$$

$$f(i,j) = \frac{\lambda\theta}{(i+j)} \binom{i+j}{j} \theta_1^i \theta_2^j \tag{7}$$
$$\times L_{i+j-1}^1(-\lambda\theta)\, f(0,0)\,,\ i,j = 0,1,\ldots,\ (i,j) \neq (0,0)$$

where $L_n^\alpha(x)$ is the generalized Laguerre polynomial of degree n, defined in the Appendix (see Bayin 2013).

Proof For the initial value it is known that $f(0,0) = \psi_{N_1,N_2}(0,0)$ (see Kocherlakota and Kocherlakota 1992). It follows from the *pgf* in (3) that

$$f(0,0) = e^{-\lambda(1-\theta)}.$$

If we let $x = -\lambda\theta$ and $z_1 = \theta_1 s_1$ and $z_2 = \theta_2 s_2$, then we can write the *pgf* in (3) as

$$\psi_{N_1,N_2}(s_1,s_2) = \sum_{i=0}^{\infty}\sum_{j=0}^{\infty} P(N_1 = i, N_2 = j)\, s_1^i s_2^j$$
$$= e^{-\lambda(1-\theta)} e^{\left(\frac{x(z_1+z_2)}{z_1+z_2-1}\right)}.$$

Differentiating $\psi_{N_1,N_2}(s_1,s_2)$ partially with respect to z_1 and using results (A1), (A2), (A3), and (A5) from the Appendix, we see that

$$\frac{\partial \psi_{N_1,N_2}(s_1,s_2)}{\partial z_1} = \frac{\lambda\theta}{(1-(z_1+z_2))^2} e^{\left(\frac{x(z_1+z_2)}{z_1+z_2-1}\right)} f(0,0)$$
$$= \lambda\theta \sum_{i=0}^{\infty} L_i^1(x)\,(z_1+z_2)^i\, f(0,0)$$
$$= \lambda\theta \sum_{i=0}^{\infty}\sum_{j=0}^{i} \binom{i}{j} L_i^1(x)\, z_1^{i-j} z_2^j f(0,0)$$
$$= \lambda\theta \sum_{j=0}^{\infty}\sum_{i=j}^{\infty} \binom{i}{j} L_i^1(x)\, z_1^{i-j} z_2^j f(0,0)$$
$$= \lambda\theta \sum_{i=0}^{\infty}\sum_{j=0}^{\infty} \binom{i+j}{j} L_{i+j}^1(x)\, z_1^i z_2^j f(0,0)$$
$$= \sum_{i=1}^{\infty}\sum_{j=0}^{\infty} \left[\lambda\theta \binom{i+j-1}{j} L_{i+j-1}^1(x)\, f(0,0)\right] z_1^{i-1} z_2^j$$

Additionally from the definition of a *pgf*

$$\frac{\partial \psi_{N_1,N_2}(s_1,s_2)}{\partial z_1} = \sum_{i=1}^{\infty}\sum_{j=0}^{\infty} i \frac{P\left(N_1=i,N_2=j\right)}{\theta_1^i\theta_2^j} z_1^{i-1} z_2^j.$$

The result for $i = 1, 2, \ldots$ and $j = 0, 1, 2, \ldots$ follows by setting

$$i\frac{P\left(N_1=i,N_2=j\right)}{\theta_1^i\theta_2^j} = \lambda\theta \binom{i+j-1}{i} L_{i+j-1}^1(x)\, f(0,0)$$

and solving for $P\left(N_1=i,N_2=j\right)$. The result for $P\left(N_1=i,N_2=j\right)$, $i = 0, 1, 2, \ldots$ and $j = 1, 2, \ldots$ follows similarly by differentiating $\partial\psi_{N_1,N_2}(s_1,s_2)$ partially with respect to z_2. □

Remark 2.1 Using (A6) in the Appendix, it can be shown that the last expression in (7) is equivalent to

$$f(i,j) = \binom{i+j}{j}\theta_1^i\theta_2^j \sum_{m=1}^{i+j} \binom{i+j-1}{m-1} \frac{(\lambda\theta)^m}{m!} f(0,0).$$

This is the result obtained by Minkova and Balakrishnan (2014a).

2.2 Multivariate Extension

A multivariate extension of the Type II bivariate Pólya-Aeppli distribution was introduced in Minkova and Balakrishnan (2014a). In this chapter we will also consider the multivariate extension, but we will give an alternative and simplified approach for deriving the *pmf* using Laguerre polynomials, which gives a closed form expression of the *pmf*.

Let $X = (X_1, \ldots, X_k)$ have a multivariate geometric distribution with *pgf* given by

$$\psi_1(s_1,\ldots,s_k) = \frac{\theta}{1-\theta_1 s_1 - \ldots - \theta_k s_k},$$

where $0 < \theta_1, \ldots, \theta_k < 1$ and $\theta = 1-\theta_1-\ldots-\theta_k \neq 0$. Let $Y \sim Poi(\lambda)$ and define $(N_1, \ldots, N_k)$ such that $N_i = \sum_{m_i=1}^{Y} X_{im_i}$ for $i = 1, \ldots, k$. The joint distribution of $(N_1, \ldots, N_k)$ is then said be a Type II multivariate Pólya-Aeppli distribution

denoted as $(N_1, \ldots, N_k) \sim MVPA_{II}(\lambda, \theta_1, \ldots, \theta_k)$. The *pgf* of the distribution is

$$\begin{aligned}\psi_{N_1,\ldots,N_k}(s_1, \ldots, s_k) &= \psi_2\left(\psi_1(s_1, \ldots, s_k)\right) \\ &= e^{-\lambda\left(1-\frac{\theta}{(1-\theta_1 s_1-\ldots-\theta_k s_k)}\right)}.\end{aligned} \tag{8}$$

From Minkova and Balakrishnan (2014a) it is known that $N_i \sim PA(\lambda\rho_i, \rho_i)$ for $i = 1, \ldots, k$, and it follows that the expected values are $E(N_i) = \frac{\lambda\theta_i}{\theta}$ and $E\left(N_i N_j\right) = \frac{\lambda\theta_i\theta_j}{\theta^2}(2+\lambda)$, where $i = 1, \ldots, k$, $j = 1, \ldots, k, i \neq j$. The variances are $Var(N_i) = \frac{\lambda\theta_i(\theta+2\theta_i)}{\theta^2}$ and the covariance and correlation are $Cov(N_i, N_j) = E\left(N_i N_j\right) - E(N_i)E\left(N_j\right) = \frac{2\lambda\theta_i\theta_j}{\theta^2}$ and $Corr(N_i, N_j) = 2\sqrt{\frac{\theta_i\theta_j}{(\theta+2\theta_i)(\theta+2\theta_j)}}$.

Theorem 2 *The pmf of* $(N_1, \ldots, N_k) \sim MVPA_{II}(\lambda, \theta_1, \ldots, \theta_k)$ *is*

$$\begin{aligned}f(0, \ldots, 0) &= e^{-\lambda(1-\theta)} \\ f(n_1, \ldots, n_k) &= \lambda\theta\frac{(n_1+\cdots+n_k-1)!}{n_1!\cdots n_k!}\theta_1^{n_1}\cdots\theta_k^{n_k} \\ &\quad \times L^1_{n_1+\cdots+n_k-1}(-\lambda\theta)\, f(0, \ldots, 0), \\ &\quad n_1, \ldots, n_k = 0, 1, \ldots, \ (n_1, \ldots, n_k) \neq (0, \ldots, 0)\end{aligned}$$

where $L_n^{\alpha}(x)$ *is the generalized Laguerre polynomial of degree n.*

Proof The proof is similar to that of Theorem 1. Since $f(0, \ldots, 0) = \psi_{N_1,\ldots,N_k}(0, \ldots, 0)$, it follows from the *pgf* in (8) that

$$f(0, \ldots, 0) = e^{-\lambda(1-\theta)}.$$

If we let $x = -\lambda\theta$ and $z_i = \theta_i s_i$ for $i = 1, \ldots, k$, then the *pgf* in (8) can be written as

$$\begin{aligned}\psi_{N_1,\ldots,N_k}(s_1, \ldots, s_k) &= \sum_{n_1=0}^{\infty}\cdots\sum_{n_k=0}^{\infty} P(N_1 = n_1, \ldots, N_k = n_k)\, s_1^{n_1}\ldots s_k^{n_k} \\ &= e^{-\lambda(1-\theta)}e^{\left(\frac{x(z_1+\cdots+z_k)}{z_1+\cdots+z_k-1}\right)}.\end{aligned}$$

Differentiating $\psi_{N_1,\ldots,N_k}(s_1, \ldots, s_2)$ with respect to z_1 and using results (A1), (A2), (A3), and (A5) from the Appendix, we see that

$$\frac{\partial \psi_{N_1,\ldots,N_k}(s_1,\ldots,s_k)}{\partial z_1}$$

$$= \frac{\lambda\theta}{(1-(z_1+\cdots+z_k))^2} e^{\left(\frac{x(z_1+\cdots+z_k)}{z_1+\cdots+z_{k-1}}\right)} f(0,\ldots,0)$$

$$= \lambda\theta \sum_{n_1=0}^{\infty} L_{n_1}^1(x)(z_1+\cdots+z_k)^{n_1} f(0,\ldots,0)$$

$$= \lambda\theta \sum_{n_1=0}^{\infty} \sum_{n_2=0}^{n_1} \cdots \sum_{n_k=0}^{n_{k-1}} \binom{n_1}{n_2} \cdots \binom{n_{k-1}}{n_k} L_{n_1}^1(x) z_1^{n_1-n_2} \cdots z_{k-1}^{n_{k-1}-n_k} z_k^{n_k} f(0,\ldots,0)$$

$$= \lambda\theta \sum_{n_1=0}^{\infty} \sum_{n_2=0}^{\infty} \cdots \sum_{n_k=0}^{\infty} \binom{n_1+n_2+\cdots+n_k}{n_2+\cdots+n_k} \cdots \binom{n_{k-1}+n_k}{n_k}$$

$$\times L_{n_1+n_2+\cdots+n_k}^1(x) z_1^{n_1} \cdots z_k^{n_k} f(0,\ldots,0)$$

$$= \sum_{n_1=0}^{\infty} \cdots \sum_{n_k=0}^{\infty} \left[\lambda\theta \frac{(n_1+\cdots+n_k)!}{n_1!\cdots n_k!} L_{n_1+\cdots+n_k}^1(x) f(0,\ldots,0)\right] z_1^{n_1} \cdots z_k^{n_k}$$

$$= \sum_{n_1=1}^{\infty} \cdots \sum_{n_k=0}^{\infty} \left[\lambda\theta \frac{(n_1+\cdots+n_k-1)!}{(n_1-1)!\cdots n_k!} L_{n_1+\cdots+n_k-1}^1(x) f(0,\ldots,0)\right] z_1^{n_1-1} \cdots z_k^{n_k}$$

and additionally it can be shown that

$$\frac{\partial \psi_{N_1,\ldots,N_k}(s_1,\ldots,s_k)}{\partial z_1} = \sum_{n_1=1}^{\infty} \cdots \sum_{n_k=0}^{\infty} n_1 \frac{P(N_1=n_1,\ldots,N_k=n_k)}{\theta_1^{n_1}\cdots\theta_k^{n_k}} z_1^{n_1-1} \cdots z_k^{n_k}.$$

Similar results can be derived by differentiating with respect to z_i for $i = 2,\ldots,k$. From these results it follows that for $n_1,\ldots,n_k = 0,1,\ldots,$ and $(n_1,\ldots,n_k) \neq (0,\ldots,0)$ where $k = 2,3,\ldots,$ that

$$\begin{aligned} f(n_1,\ldots,n_k) &= \lambda\theta \frac{(n_1+\cdots+n_k-1)!}{n_1!\cdots n_k!} \theta_1^{n_1}\cdots\theta_k^{n_k} \\ &\quad \times L_{n_1+\cdots+n_k-1}^1(-\lambda\theta) f(0,\ldots,0). \end{aligned} \tag{9}$$

□

Remark 2.2 Using (A6) in the Appendix, it can be shown that the expression in (9) is equivalent to

$$f(n_1, \ldots, n_k) = \frac{(n_1 + \cdots + n_k)!}{n_1! \cdots n_k!} \theta_1^{n_1} \cdots \theta_k^{n_k} \times \sum_{m=1}^{n_1+\cdots+n_k} \binom{n_1 + \cdots + n_k - 1}{m-1} \frac{(\lambda\theta)^m}{m!} f(0, \ldots, 0).$$

which is a closed form expression of the *pmf*.

3 Weighted Type II Bivariate Pólya-Aeppli Distribution Case I

In Minkova and Balakrishnan (2013), the weighted univariate Pólya-Aeppli distribution was obtained by applying the weights to the Poisson random variable, where the weighted Poisson distribution is a generalization of the Poisson distribution.

In Sects. 3 and 4 we apply two different non-negative weight functions to $Y \sim Poi(\lambda)$, namely $w(y) = y$ and $w(y) = \frac{1}{y+1}$, where $y = 0, 1, \ldots$. The weighted univariate Pólya-Aeppli distributions with these two weights are under and over-dispersed with respect to the univariate Pólya-Aeppli distribution, therefore we chose to also apply these two weights in the bivariate case in order to create two models that are under and over-dispersed with respect to the Type II bivariate Pólya-Aeppli distribution.

Let $X = (X_1, X_2)$ have a bivariate geometric distribution with a *pgf* given by

$$\psi_1(s_1, s_2) = \frac{\theta}{1 - \theta_1 s_1 - \theta_2 s_2}, \tag{10}$$

where $0 < \theta_1, \theta_2 < 1$ and $\theta = 1 - \theta_1 - \theta_2 \neq 0$. Let Y^w be the weighted version of $Y \sim Poi(\lambda)$, with a non-negative weight function $w(y) = y$, $y = 0, 1, \ldots$. It then follows that Y^w has a shifted Poisson distribution $Y^w - 1 \sim Poi(\lambda)$ and the *pgf* of Y^w is

$$\psi_2^w(s) = E\left(s^{Y^w}\right) = s e^{-\lambda(1-s)}. \tag{11}$$

Define $\left(N_1^w, N_2^w\right)$ as $N_1^w = \sum_{i=1}^{Y^w} X_{1i}$ and $N_2^w = \sum_{j=1}^{Y^w} X_{2j}$. The joint distribution of $\left(N_1^w, N_2^w\right)$ is then said to be a weighted Type II bivariate Pólya-Aeppli distribution Case I, denoted as $(N_1^w, N_2^w) \sim WBivPA_{II}^{(1)}(\lambda, \theta_1, \theta_2)$. Using (10) and (11) the *pgf* of the distribution is expressed as

$$\begin{aligned} \psi_{N_1^w, N_2^w}(s_1, s_2) &= \psi_2^w(\psi_1(s_1, s_2)) \\ &= \frac{\theta}{1 - \theta_1 s_1 - \theta_2 s_2} e^{-\lambda\left(1 - \frac{\theta}{1-\theta_1 s_1 - \theta_2 s_2}\right)}. \end{aligned} \tag{12}$$

The expected values of $(N_1^w, N_2^w) \sim WBivPA_{II}^{(1)}(\lambda, \theta_1, \theta_2)$ are $E\left(N_1^w\right) = \frac{\theta_1(1+\lambda)}{\theta}$, $E\left(N_2^w\right) = \frac{\theta_2(1+\lambda)}{\theta}$ and $E\left(N_1^w N_2^w\right) = \frac{\theta_1\theta_2(\lambda+1)^2+\theta_1\theta_2(2\lambda+1)}{\theta^2}$. The variances are $Var\left(N_1^w\right) = \frac{(1+\theta_1-\theta_2)\theta_1\lambda+(1-\theta_2)\theta_1}{\theta^2}$ and $Var\left(N_2^w\right) = \frac{(1+\theta_2-\theta_1)\theta_2\lambda+(1-\theta_1)\theta_2}{\theta^2}$ and the covariance and correlation are $Cov\left(N_1^w, N_2^w\right) = \frac{(2\lambda+1)\theta_1\theta_2}{\theta^2}$ and

$$Corr(N_1^w, N_2^w) = (2\lambda + 1) \times \sqrt{\frac{\theta_1\theta_2}{[(1+\theta_1-\theta_2)\lambda + (1-\theta_2)][(1+\theta_2-\theta_1)\lambda + (1-\theta_1)]}}.$$

As λ tends toward infinity, the correlation will tend towards the following limit

$$\lim_{\lambda\to\infty} Corr(N_1^w, N_2^w) = 2\sqrt{\frac{\theta_1\theta_2}{(1+\theta_1-\theta_2)(1+\theta_2-\theta_1)}},$$

which is the same as (4), the correlation for $(N_1, N_2) \sim BivPA_{II}(\lambda, \theta_1, \theta_2)$.

The expression for the Fisher index of $(N_1^w, N_2^w) \sim WBivPA_{II}^{(1)}(\lambda, \theta_1, \theta_2)$ can be calculated using (5) and will be studied graphically in Sect. 5 for different values of the parameters. It can be shown that as λ tends towards infinity, $FI_2(N_1^w, N_2^w)$ will tend towards the following limit

$$\lim_{\lambda\to\infty} FI_2(N_1^w, N_2^w) = FI_2(N_1, N_2) \tag{13}$$

where $FI_2(N_1, N_2)$ is the Fisher Index of $(N_1, N_2) \sim BivPA_{II}(\lambda, \theta_1, \theta_2)$ given in (6).

3.1 Joint Probability Mass Function

Theorem 3 *The pmf of* $(N_1^w, N_2^w) \sim WBivPA_{II}^{(1)}(\lambda, \theta_1, \theta_2)$ *is*

$$f^w(i,j) = \theta \binom{i+j}{j} \theta_1^i \theta_2^j L_{i+j}^0(-\lambda\theta)\, e^{-\lambda(1-\theta)},\ i, j = 0, 1, \ldots, \tag{14}$$

where $L_n^\alpha(x)$ *is the generalized Laguerre polynomial of degree n.*

Proof If we let $x = -\lambda\theta$ and $z_1 = \theta_1 s_1$ and $z_2 = \theta_2 s_2$, and using results (A1), (A2), (A3), and (A5) from the Appendix, we can write the *pgf* in (12) as

$$\begin{aligned}
\psi_{N_1^w,N_2^w}(s_1,s_2) &= \frac{\theta}{(1-z_1-z_2)} e^{\left(\frac{x(z_1+z_2)}{z_1+z_2-1}\right)} e^{-\lambda(1-\theta)} \\
&= \theta \sum_{i=0}^{\infty} L_i^0(x)(z_1+z_2)^i e^{-\lambda(1-\theta)} \\
&= \theta \sum_{i=0}^{\infty} \sum_{j=0}^{i} \binom{i}{j} L_i^0(x) z_1^{i-j} z_2^j e^{-\lambda(1-\theta)} \\
&= \theta \sum_{j=0}^{\infty} \sum_{i=j}^{\infty} \binom{i}{j} L_i^0(x) z_1^{i-j} z_2^j e^{-\lambda(1-\theta)} \\
&= \theta \sum_{i=0}^{\infty} \sum_{j=0}^{\infty} \binom{i+j}{j} L_{i+j}^0(x) z_1^i z_2^j e^{-\lambda(1-\theta)} \\
&= \sum_{i=0}^{\infty} \sum_{j=0}^{\infty} \left[\theta \binom{i+j}{j} \theta_1^i \theta_2^j L_{i+j}^0(x) e^{-\lambda(1-\theta)}\right] s_1^i s_2^j.
\end{aligned}$$

and from the definition of a *pgf*

$$\psi_{N_1^w,N_2^w}(s_1,s_2) = \sum_{i=0}^{\infty} \sum_{j=0}^{\infty} P\left(N_1^w = i, N_2^w = j\right) s_1^i s_2^j.$$

Therefore by setting

$$P\left(N_1^w = i, N_2^w = j\right) = \theta \binom{i+j}{j} \theta_1^i \theta_2^j L_{i+j}^0(x) e^{-\lambda(1-\theta)}$$

the result follows. □

Remark 3.1 Using (A6) in the Appendix, it can be shown that the expression in (14) is equivalent to

$$f^w(i,j) = \binom{i+j}{j} \theta_1^i \theta_2^j \sum_{m=0}^{i+j} \binom{i+j}{m} \frac{\lambda^m \theta^{m+1}}{m!} e^{-\lambda(1-\theta)}.$$

3.2 Marginal and Conditional Distributions

The derivation for the marginal distribution is similar to the derivation for the joint *pmf* in Sect. 3.1 and the derivation for the conditional distribution and conditional

expected value is similar to the derivation of these properties for the Type II bivariate Pólya-Aeppli distribution in Minkova and Balakrishnan (2014a), so we will only give these results here.

If $(N_1^w, N_2^w) \sim WBivPA_{II}^{(1)}(\lambda, \theta_1, \theta_2)$, then the marginal *pmf* for N_1^w is given by

$$P\left(N_1^w = i\right) = e^{-\lambda\rho_1}\left(1-\rho_1\right)\rho_1^i L_i^0\left(-\lambda\left(1-\rho_1\right)\right) \quad i = 0, 1, \ldots$$

where $L_n^{\alpha}(x)$ is the generalized Laguerre polynomial of degree n. The marginal *pmf* of N_2^w follows similarly. The conditional *pgf* of N_2^w given N_1^w is

$$\psi_{N_2^w|(N_1^w=i)}(s_2) = \left(\frac{1-\theta_2}{1-\theta_2 s_2}\right)^{i+1} \frac{\sum_{m=0}^{\infty}\binom{m+i}{m}\frac{\lambda^m\theta^m}{m!}\frac{1}{(1-\theta_2 s_2)^m}}{\sum_{m=0}^{\infty}\binom{m+i}{m}\frac{\lambda^m\theta^m}{m!}\frac{1}{(1-\theta_2)^m}} \quad i = 0, 1, \ldots$$

and the conditional mean of N_2^w given N_1^w is

$$E\left[N_2^w|N_1^w = i\right] = \frac{\theta_2}{(1-\theta_2)}\left[(i+1) + \frac{\sum_{m=1}^{\infty} m\binom{m+i}{m}\frac{\lambda^m\theta^m}{m!}\frac{1}{(1-\theta_2)^m}}{\sum_{m=0}^{\infty}\binom{m+i}{m}\frac{\lambda^m\theta^m}{m!}\frac{1}{(1-\theta_2)^m}}\right] \quad i = 0, 1, \ldots$$

The conditional mean of N_1^w given N_2^w follows similarly.

3.3 Method of Moments Estimates

In order to calculate the method of moments parameter estimates for $(N_1^w, N_2^w) \sim WBivPA_{II}^{(1)}(\lambda, \theta_1, \theta_2)$, we denote the joint moments of the random variable N_1^w and N_2^w by

$$\mu'_{r,s} = E\left(N_1^{w(r)}, N_2^{w(s)}\right) \quad r, s = 0, 1, 2, \ldots,$$

where $\mu'_{1,0} = E\left(N_1^w\right) = \frac{\theta_1(1+\lambda)}{\theta}$, $\mu'_{0,1} = E\left(N_2^w\right) = \frac{\theta_2(1+\lambda)}{\theta}$ and $\mu'_{1,1} = E\left(N_1^w, N_2^w\right) = \frac{\theta_1\theta_2(\lambda+1)^2+\theta_1\theta_2(2\lambda+1)}{\theta^2}$ are the population moments. Equating the first sample moments $\bar{X}^w$ and $\bar{Y}^w$ to the population moments, the moment estimates for the parameters θ_1 and θ_2 are

$$\hat{\theta}_1 = \frac{\bar{X}^w}{\left(\lambda + \bar{X}^w + \bar{Y}^w + 1\right)} \quad and \quad \hat{\theta}_2 = \frac{\bar{Y}^w}{\left(\lambda + \bar{X}^w + \bar{Y}^w + 1\right)}.$$

To find the moment estimate for λ, we equate the mixed sample moment $m_{1,1}^w$ to the population moment $\mu_{1,1}^{'}$, which gives

$$\left(\hat{\lambda}^2 + 2\hat{\lambda} + 1\right)\overline{n}_1^w \overline{n}_2^w - \hat{\lambda}^2 \overline{n}_1^w \overline{n}_2^w = \left(\hat{\lambda} + 1\right)^2 \left(m_{1,1}^w - \bar{X}^w \bar{Y}^w\right).$$

Solving this for $\hat{\lambda}$ gives

$$\hat{\lambda} = \frac{1}{\sqrt{\frac{\bar{X}^w \bar{Y}^w}{\left(2\bar{X}^w \bar{Y}^w - m_{1,1}^w\right)}} - 1}.$$

3.4 Multivariate Extension

The weighted Type II bivariate Pólya-Aeppli distribution Case I can naturally be extended to the multivariate case and we will give the newly proposed results of this distribution here.

Let $X = (X_1, \ldots, X_k)$ have a multivariate geometric distribution with *pgf*

$$\psi_1(s_1, \ldots, s_k) = \frac{\theta}{1 - \theta_1 s_1 - \ldots - \theta_k s_k},$$

where $0 < \theta_1, \ldots, \theta_k < 1$, $\theta = 1 - \theta_1 - \ldots - \theta_k \neq 0$ and Y^w is the weighted version of $Y \sim Poi(\lambda)$, with a non-negative weight function $w(y) = y$ and *pgf* given by (11). Define $\left(N_1^w, \ldots, N_k^w\right)$ as $N_i^w = \sum_{m_i=1}^{Y^w} X_{im_i}$ for $i = 1, \ldots, k$. The joint distribution of $\left(N_1^w, \ldots, N_k^w\right)$ is then said to be a weighted Type II multivariate Pólya-Aeppli distribution Case I, denoted as $(N_1^w, \ldots, N_k^w) \sim WMVPA_{II}^{(1)}(\lambda, \theta_1, \ldots, \theta_k)$. Extending the *pgf* in (12), we can express the *pgf* of the distribution as

$$\begin{aligned}\psi_{N_1^w,\ldots,N_k^w}(s_1, \ldots, s_k) &= \psi_2^w\left(\psi_1(s_1, \ldots, s_k)\right) \\ &= \frac{\theta}{1 - \theta_1 s_1 - \ldots - \theta_k s_k} e^{-\lambda\left(1 - \frac{\theta}{(1 - \theta_1 s_1 - \ldots - \theta_k s_k)}\right)}.\end{aligned} \tag{15}$$

The expected values of $(N_1^w, \ldots, N_k^w) \sim WMVPA_{II}^{(1)}(\lambda, \theta_1, \ldots, \theta_k)$ are $E\left(N_i^w\right) = \frac{\theta_i(1+\lambda)}{\theta}$ and $E\left(N_i^w N_j^w\right) = \frac{\theta_i\theta_j(\lambda+1)^2 + \theta_i\theta_j(2\lambda+1)}{\theta^2}$, where $i = 1, \ldots, k$,

$j = 1, \ldots, k,\ i \neq j$. The variances are $Var\left(N_i^w\right) = \frac{(\theta+2\theta_i)\theta_i\lambda+(\theta+\theta_i)\theta_i}{\theta^2}$ and the covariance and correlation are $Cov\left(N_i^w, N_j^w\right) = \frac{(2\lambda+1)\theta_i\theta_j}{\theta^2}$ and $Corr(N_i^w, N_j^w) = (2\lambda+1) \times \sqrt{\frac{\theta_i\theta_j}{[(\theta+2\theta_i)\lambda+(\theta+\theta_i)]\left[(\theta+2\theta_j)\lambda+(\theta+\theta_j)\right]}}$.

Theorem 4 *The pmf of* $(N_1^w, \ldots, N_k^w) \sim WMVPA_{II}^{(1)}(\lambda, \theta_1, \ldots, \theta_k)$ *is*

$$f^w(n_1, \ldots, n_k) = \theta \frac{(n_1 + \cdots + n_k)!}{n_1! \cdots n_k!} \theta_1^{n_1} \cdots \theta_k^{n_k} \times L_{n_1+\cdots+n_k}^0(-\lambda\theta)\, e^{-\lambda(1-\theta)},\ n_1, \ldots, n_k = 0, 1, \ldots,$$

where $L_n^\alpha(x)$ *is the generalized Laguerre polynomial of degree n.*

Proof Similar to Theorem 3, if we let $x = -\lambda\theta$ and $z_i = \theta_i s_i$ for $i = 1, \ldots, k$, and using results (A1), (A2), (A3), and (A5) from the Appendix, we can write the *pgf* in (15) as

$$\begin{aligned}
&\psi_{N_1^w,\ldots,N_k^w}(s_1, \ldots, s_k) \\
&= \frac{\theta}{(1 - z_1 - \cdots - z_k)} e^{\left(\frac{x(z_1+\cdots+z_k)}{z_1+\cdots+z_k-1}\right)} e^{-\lambda(1-\theta)} \\
&= \theta \sum_{n_1=0}^{\infty} L_{n_1}^0(x)\,(z_1 + \cdots + z_k)^{n_1}\, e^{-\lambda(1-\theta)} \\
&= \theta \sum_{n_1=n_2}^{\infty} \sum_{n_2=n_3}^{\infty} \cdots \sum_{n_k=0}^{\infty} \binom{n_1}{n_2} \cdots \binom{n_{k-1}}{n_k} L_{n_1}^0(x)\, z_1^{n_1-n_2} \cdots z_{k-1}^{n_{k-1}-n_k} z_k^{n_k} e^{-\lambda(1-\theta)} \\
&= \theta \sum_{n_1=0}^{\infty} \sum_{n_2=0}^{\infty} \cdots \sum_{n_k=0}^{\infty} \binom{n_1 + n_2 + \cdots + n_k}{n_2 + \cdots + n_k} \cdots \binom{n_{k-1} + n_k}{n_k} \\
&\times L_{n_1+n_2+\cdots+n_k}^0(x)\, z_1^{n_1} \cdots z_k^{n_k} e^{-\lambda(1-\theta)} \\
&= \theta \sum_{n_1=0}^{\infty} \cdots \sum_{n_k=0}^{\infty} \frac{(n_1 + \cdots + n_k)!}{n_1! \cdots n_k!} L_{n_1+\cdots+n_k}^0(x)\, z_1^{n_1} \cdots z_k^{n_k} e^{-\lambda(1-\theta)} \\
&= \sum_{n_1=0}^{\infty} \cdots \sum_{n_k=0}^{\infty} \left[\theta \frac{(n_1 + \cdots + n_k)!}{n_1! \cdots n_k!} \theta_1^{n_1} \cdots \theta_k^{n_k} L_{n_1+\cdots+n_k}^0(x)\, e^{-\lambda(1-\theta)}\right] s_1^{n_1} \cdots s_k^{n_k}
\end{aligned}$$

and

$$\psi_{N_1^w,\ldots,N_k^w}(s_1,\ldots,s_k)=\sum_{n_1=0}^{\infty}\cdots\sum_{n_k=0}^{\infty}P\left(N_1^w=n_1,\ldots,N_k^w=n_k\right)s_1^{n_1}\cdots s_k^{n_k}.$$

Therefore it follows that for $n_1,\ldots,n_k=0,1,\ldots$ the *pmf* is

$$f^w\left(n_1,\ldots,n_k\right)=\theta\frac{(n_1+\cdots+n_k)!}{n_1!\cdots n_k!}\theta_1^{n_1}\cdots\theta_k^{n_k}L_{n_1+\cdots+n_k}^0\left(-\lambda\theta\right)e^{-\lambda(1-\theta)}. \quad (16)$$

□

Remark 3.3 Using (A6) in the Appendix, it can be shown that the expression in (16) is equivalent to

$$\begin{aligned}f\left(n_1,\ldots,n_k\right)&=\frac{(n_1+\cdots+n_k)!}{n_1!\cdots n_k!}\theta_1^{n_1}\cdots\theta_k^{n_k}\\&\times\sum_{m=1}^{n_1+\cdots+n_k}\binom{n_1+\cdots+n_k-1}{m-1}\frac{(\lambda\theta)^m}{m!}f\left(0,\ldots,0\right).\end{aligned}$$

4 Weighted Type II Bivariate Pólya-Aeppli Distribution Case II

Let $X=(X_1,X_2)$ have a bivariate geometric distribution with a *pgf* given by

$$\psi_1\left(s_1,s_2\right)=\frac{\theta}{1-\theta_1s_1-\theta_2s_2}, \quad (17)$$

where $0<\theta_1,\theta_2<1$ and $\theta=1-\theta_1-\theta_2\neq 0$. Let Y^w be the weighted version of $Y\sim Poi(\lambda)$ with a non-negative weight function $w(y)=\frac{1}{y+1}$, $y=0,1,\ldots,$. The *pgf* of Y^w is

$$\psi_2^w(s)=\frac{e^{-\lambda}}{\left(1-e^{-\lambda}\right)}\frac{\left(e^{s\lambda}-1\right)}{s}. \quad (18)$$

Define $\left(N_1^w,N_2^w\right)$ as $N_1^w=\sum_{i=1}^{Y^w}X_{1i}$ and $N_2^w=\sum_{j=1}^{Y^w}X_{2j}$. The joint distribution of $\left(N_1^w,N_2^w\right)$ is then said to be a weighted Type II bivariate Pólya-Aeppli distribution Case II, denoted as $(N_1^w,N_2^w)\sim WBivPA_{II}^{(2)}(\lambda,\theta_1,\theta_2)$. From (17) and (18) the *pgf* of the distribution follows as

$$\begin{aligned}\psi_{N_1^w,N_2^w}(s_1,s_2)&=\psi_2^w\left(\psi_1\left(s_1,s_2\right)\right)\\&=\frac{e^{-\lambda}}{\left(1-e^{-\lambda}\right)}\frac{(1-\theta_1s_1-\theta_2s_2)}{\theta}\left(e^{\frac{\lambda\theta}{1-\theta_1s_1-\theta_2s_2}}-1\right).\end{aligned} \quad (19)$$

The expected values of $(N_1^w, N_2^w) \sim WBivPA_{II}^{(2)}(\lambda, \theta_1, \theta_2)$ are $E\left(N_1^w\right) = \frac{(\lambda-1+e^{-\lambda})\theta_1}{(1-e^{-\lambda})\theta}$, $E\left(N_2^w\right) = \frac{(\lambda-1+e^{-\lambda})\theta_2}{(1-e^{-\lambda})\theta}$ and $E\left(N_1^w N_2^w\right) = \frac{\lambda^2\theta_1\theta_2}{(1-e^{-\lambda})\theta^2}$. The variances are $Var\left(N_1^w\right) = \frac{(\lambda-1+e^{-\lambda})(1-e^{-\lambda})(1-\theta_2)\theta_1-(\lambda-1+e^{-\lambda})\lambda\theta_1^2+(1-e^{-\lambda})\lambda^2\theta_1^2}{(1-e^{-\lambda})^2\theta^2}$ and $Var\left(N_2^w\right) = \frac{(\lambda-1+e^{-\lambda})(1-e^{-\lambda})(1-\theta_1)\theta_2-(\lambda-1+e^{-\lambda})\lambda\theta_2^2+(1-e^{-\lambda})\lambda^2\theta_2^2}{(1-e^{-\lambda})^2\theta^2}$. The covariance is $Cov\left(N_1^w, N_2^w\right) = \frac{\lambda^2\theta_1\theta_2(1-e^{-\lambda})-(\lambda-1+e^{-\lambda})^2\theta_1\theta_2}{(1-e^{-\lambda})^2\theta^2}$. The correlation can be calculated using these results. As λ tends toward infinity, the correlation will tend towards the following limit

$$\lim_{\lambda\to\infty} Corr(N_1^w, N_2^w) = 2\sqrt{\frac{\theta_1\theta_2}{(1+\theta_1-\theta_2)(1+\theta_2-\theta_1)}}$$

which is the same as (4), the correlation for $(N_1, N_2) \sim BivPA_{II}(\lambda, \theta_1, \theta_2)$. The expression for the Fisher index of $(N_1^w, N_2^w) \sim WBivPA_{II}^{(2)}(\lambda, \theta_1, \theta_2)$ can be calculated using (5) and will be studied graphically in Sect. 5 for different values of the parameters. It can be shown that as λ tends towards infinity, $FI_2(N_1^w, N_2^w)$ will tend towards the following limit

$$\lim_{\lambda\to\infty} FI_2(N_1^w, N_2^w) = FI_2(N_1, N_2) \tag{20}$$

where $FI_2(N_1, N_2)$ is the Fisher Index of $(N_1, N_2) \sim BivPA_{II}(\lambda, \theta_1, \theta_2)$ given in (6).

4.1 Joint Probability Mass Function

Theorem 5 *The pmf of* $(N_1^w, N_2^w) \sim WBivPA_{II}^{(2)}(\lambda, \theta_1, \theta_2)$ *is*

$$\begin{aligned}
f^w(0,0) &= \frac{e^{-\lambda}}{\left(1-e^{-\lambda}\right)}\frac{\left(e^{\lambda\theta}-1\right)}{\theta} \\
f^w(1,0) &= \frac{e^{-\lambda}}{\left(1-e^{-\lambda}\right)}\frac{\theta_1}{\theta}\left[(\lambda\theta-1)e^{\lambda\theta}+1\right] \\
f^w(0,1) &= \frac{e^{-\lambda}}{\left(1-e^{-\lambda}\right)}\frac{\theta_2}{\theta}\left[(\lambda\theta-1)e^{\lambda\theta}+1\right] \\
f^w(i,j) &= \frac{\lambda^2\theta e^{-\lambda(1-\theta)}}{\left(1-e^{-\lambda}\right)(i+j)(i+j-1)}\binom{i+j}{j}\theta_1^i\theta_2^j L_{i+j-2}^2(-\lambda\theta), \\
&\qquad i,j = 0,1,\ldots,\ (i,j)\neq(0,0), (i,j)\neq(1,0), (i,j)\neq(0,1).
\end{aligned} \tag{21}$$

where $L_n^{\alpha}(x)$ *is the generalized Laguerre polynomial of degree* n.

Proof For the initial value we know that $f^w(0,0) = \psi_{N_1^w,N_2^w}(0,0)$ and it follows from the *pgf* in (19) that

$$f^w(0,0) = \frac{e^{-\lambda}}{\left(1-e^{-\lambda}\right)} \frac{\left(e^{\lambda\theta}-1\right)}{\theta}.$$

In order to calculate $f^w(1,0)$, we can rewrite the *pgf* in (19) as

$$\psi_{N_1^w,N_2^w}(s_1,s_2) = \frac{e^{-\lambda}}{\left(1-e^{-\lambda}\right)} \sum_{k=1}^{\infty} \frac{\lambda^k \theta^{k-1}}{k!\left(1-\theta_1 s_1-\theta_2 s_2\right)^{k-1}}.$$

It then follows from the above and (A4) in the Appendix that

$$\psi^{(1,0)}_{N_1^w,N_2^w}(s_1,s_2) = \frac{\partial \psi_{N_1^w,N_2^w}(s_1,s_2)}{\partial s_1} = \frac{e^{-\lambda}}{\left(1-e^{-\lambda}\right)} \sum_{k=1}^{\infty} \frac{\theta_1 (k-1)\lambda^k \theta^{k-1}}{k!\left(1-\theta_1 s_1-\theta_2 s_2\right)^k}$$

and

$$\begin{aligned} f^w(1,0) = \psi^{(1,0)}_{N_1^w,N_2^w}(s_1,s_2)\Big|_{s_1=0,s_2=0} &= \frac{e^{-\lambda}}{\left(1-e^{-\lambda}\right)} \sum_{k=1}^{\infty} \frac{\theta_1 (k-1)\lambda^k \theta^{k-1}}{k!} \\ &= \frac{e^{-\lambda}}{\left(1-e^{-\lambda}\right)} \frac{\theta_1}{\theta} \left[(\lambda\theta-1)e^{\lambda\theta}+1\right]. \end{aligned}$$

The result for $f^w(0,1)$ follows similarly. The result for $f^w(1,1)$ is calculated as

$$\psi^{(1,1)}_{N_1^w,N_2^w}(s_1,s_2) = \frac{\partial^2 \psi_{N_1^w,N_2^w}(s_1,s_2)}{\partial s_1 \partial s_2} = \frac{e^{-\lambda}}{\left(1-e^{-\lambda}\right)} \sum_{k=2}^{\infty} \frac{\theta_1\theta_2 k (k-1)\lambda^k \theta^{k-1}}{k!\left(1-\theta_1 s_1-\theta_2 s_2\right)^{k+1}}$$

and

$$\begin{aligned} f^w(1,1) = \psi^{(1,1)}_{N_1^w,N_2^w}(s_1,s_2)\Big|_{s_1=0,s_2=0} &= \frac{e^{-\lambda}}{\left(1-e^{-\lambda}\right)} \sum_{k=2}^{\infty} \frac{\theta_1\theta_2\lambda^k \theta^{k-1}}{(k-2)!} \\ &= \frac{e^{-\lambda(1-\theta)}}{\left(1-e^{-\lambda}\right)} \theta_1\theta_2\lambda^2\theta. \end{aligned}$$

If we let $x = -\lambda\theta$ and $z_1 = \theta_1 s_1$ and $z_2 = \theta_2 s_2$, then we can write the *pgf* in (19) as

$$\begin{aligned}\psi_{N_1^w,N_2^w}(s_1,s_2) &= \sum_{i=0}^{\infty}\sum_{j=0}^{\infty} P\left(N_1^w = i, N_2^w = j\right) s_1^i s_2^j \\ &= \frac{(1-z_1-z_2)}{\theta\left(1-e^{-\lambda}\right)}\left[e^{-\lambda(1-\theta)}e^{\left(\frac{x(z_1+z_2)}{z_1+z_2-1}\right)} - e^{-\lambda}\right].\end{aligned}$$

Finding the second derivative of $\psi_{N_1^w,N_2^w}(s_1,s_2)$ with respect to z_1 and using results (A1), (A2), (A3), and (A5) from the Appendix, we see that

$$\begin{aligned}\frac{\partial^2\psi_{N_1^w,N_2^w}(s_1,s_2)}{\partial z_1^2} &= \frac{\lambda^2\theta e^{-\lambda(1-\theta)}}{\left(1-e^{-\lambda}\right)(1-z_1-z_2)^3}e^{\left(\frac{x(z_1+z_2)}{z_1+z_2-1}\right)} \\ &= \frac{\lambda^2\theta e^{-\lambda(1-\theta)}}{\left(1-e^{-\lambda}\right)}\sum_{i=0}^{\infty} L_i^2(x)(z_1+z_2)^i \\ &= \frac{\lambda^2\theta e^{-\lambda(1-\theta)}}{\left(1-e^{-\lambda}\right)}\sum_{i=0}^{\infty}\sum_{j=0}^{i}\binom{i}{j} L_i^2(x) z_1^{i-j} z_2^j \\ &= \frac{\lambda^2\theta e^{-\lambda(1-\theta)}}{\left(1-e^{-\lambda}\right)}\sum_{j=0}^{\infty}\sum_{i=j}^{\infty}\binom{i}{j} L_i^2(x) z_1^{i-j} z_2^j \\ &= \frac{\lambda^2\theta e^{-\lambda(1-\theta)}}{\left(1-e^{-\lambda}\right)}\sum_{j=0}^{\infty}\sum_{i=0}^{\infty}\binom{i+j}{j} L_{i+j}^2(x) z_1^i z_2^j \\ &= \frac{\lambda^2\theta e^{-\lambda(1-\theta)}}{\left(1-e^{-\lambda}\right)}\sum_{i=2}^{\infty}\sum_{j=0}^{\infty}\binom{i+j-2}{j} L_{i+j-2}^2(x) z_1^{i-2} z_2^j\end{aligned}$$

Additionally from the definition of a *pgf*

$$\frac{\partial^2\psi_{N_1^w,N_2^w}(s_1,s_2)}{\partial z_1^2} = \sum_{i=2}^{\infty}\sum_{j=0}^{\infty} i(i-1)\frac{P\left(N_1^w = i, N_2^w = j\right)}{\theta_1^i\theta_2^j} z_1^{i-2} z_2^j.$$

The result follows for $i = 2, 3, \ldots$ and $j = 0, 1, \ldots$, by setting

$$\frac{\lambda^2\theta e^{-\lambda(1-\theta)}}{\left(1-e^{-\lambda}\right)}\binom{i+j-2}{j} L_{i+j-2}^2(x) = i(i-1)\frac{P\left(N_1^w = i, N_2^w = j\right)}{\theta_1^i\theta_2^j}.$$

The result for $i = 0, 1, \ldots$, and $j = 2, 3, \ldots$ follows similarly by finding the second derivative of $\psi_{N_1^w,N_2^w}(s_1,s_2)$ with respect to z_2. □

Remark 4.1 Using (A6) in the Appendix, it can be shown that the last expression in (21) is equivalent to

$$f^w(i,j) = \frac{e^{-\lambda(1-\theta)}}{\left(1-e^{-\lambda}\right)} \binom{i+j}{j} \theta_1^i \theta_2^j \sum_{m=2}^{i+j} \binom{i+j-2}{m-2} \frac{\lambda^m \theta^{m-1}}{m!}.$$

4.2 Marginal and Conditional Distributions

As in Sect. 3.2, we will only give the results for the marginal and conditional distributions and conditional expected value here.

If $(N_1^w, N_2^w) \sim WBivPA_{II}^{(2)}(\lambda, \theta_1, \theta_2)$, then the marginal *pmf* for N_1^w is given by

$$P\left(N_1^w = 0\right) = \frac{e^{-\lambda}}{\left(1-e^{-\lambda}\right)} \frac{1}{(1-\rho_1)} \left(e^{\lambda(1-\rho_1)} - 1\right)$$

$$P\left(N_1^w = 1\right) = \frac{e^{-\lambda}}{\left(1-e^{-\lambda}\right)} \frac{\rho_1}{(1-\rho_1)} \left[\left(\lambda\left(1-\rho_1\right) - 1\right) e^{\lambda(1-\rho_1)} + 1\right]$$

$$P\left(N_1^w = i\right) = \frac{e^{-\lambda\rho_1}}{\left(1-e^{-\lambda}\right)} \frac{\lambda^2 (1-\rho_1)\, \rho_1^i}{i\,(i-1)} L_{i-2}^2\left(-\lambda\left(1-\rho_1\right)\right) \qquad i = 2, 3, \ldots$$

where $L_n^{\alpha}(x)$ is the generalized Laguerre polynomial of degree n. The marginal *pmf* of N_2^w follows similarly. The conditional *pgf* of N_2^w given N_1^w is

$$\psi_{N_2^w|(N_1^w=0)}(s_2) = \left(\frac{1-\theta_2 s_2}{1-\theta_2}\right) e^{\left(-\frac{\lambda\theta}{1-\theta_2}\right)\left(1-\frac{1-\theta_2}{1-\theta_2 s_2}\right)}$$

$$\psi_{N_2^w|(N_1^w=1)}(s_2) = \frac{\sum_{m=2}^{\infty} \frac{\lambda^m \theta^m}{m!} \frac{(m-1)}{(1-\theta_2 s_2)^m}}{\sum_{m=2}^{\infty} \frac{\lambda^m \theta^m}{m!} \frac{(m-1)}{(1-\theta_2)^m}}$$

$$\psi_{N_2^w|(N_1^w=i)}(s_2) = \left(\frac{1-\theta_2}{1-\theta_2 s_2}\right)^{i-1} \frac{\sum_{m=2}^{\infty} \binom{m+i-2}{m-2} \frac{\lambda^m \theta^m}{m!} \frac{1}{(1-\theta_2 s_2)^m}}{\sum_{m=2}^{\infty} \binom{m+i-2}{m-2} \frac{\lambda^m \theta^m}{m!} \frac{1}{(1-\theta_2)^m}} \qquad i = 2, 3, \ldots$$

The conditional *pgf* of N_1^w given N_2^w follows similarly and the conditional expected value of N_2^w given N_1^w is

$$E\left[N_2^w|N_1^w=0\right]=\frac{\theta_2}{(1-\theta_2)}\left(\lambda-1-\frac{\lambda\theta_1}{1-\theta_2}\right)$$

$$E\left[N_2^w|N_1^w=1\right]=\frac{\theta_2}{(1-\theta_2)}\frac{\sum_{m=2}^{\infty}\frac{\lambda^m\theta^m}{m!}\frac{m(m-1)}{(1-\theta_2)^m}}{\sum_{m=2}^{\infty}\frac{\lambda^m\theta^m}{m!}\frac{(m-1)}{(1-\theta_2)^m}}$$

$$E\left[N_2^w|N_1^w=i\right]=\frac{\theta_2}{(1-\theta_2)}\left[(i-1)+\frac{\sum_{m=2}^{\infty}m\binom{m+i-2}{m-2}\frac{\lambda^m\theta^m}{m!}\frac{1}{(1-\theta_2)^m}}{\sum_{m=2}^{\infty}\binom{m+i-2}{m-2}\frac{\lambda^m\theta^m}{m!}\frac{1}{(1-\theta_2)^m}}\right]$$

$$i=2,3,\ldots$$

The conditional expected value of N_1^w given N_2^w follows similarly.

4.3 Method of Moments Estimates

In order to calculate the method of moments parameter estimates for $(N_1^w, N_2^w) \sim WBivPA_{II}^{(2)}(\lambda,\theta_1,\theta_2)$, we denote the joint moments of the random variables N_1^w and N_2^w by

$$\mu'_{r,s}=E\left(N_1^{w(r)},N_2^{w(s)}\right)\quad r,s=0,1,2,\ldots,$$

where $\mu'_{1,0}=E\left(N_1^w\right)=\frac{(\lambda-1+e^{-\lambda})\theta_1}{(1-e^{-\lambda})\theta}$, $\mu'_{0,1}=E\left(N_2^w\right)=\frac{(\lambda-1+e^{-\lambda})\theta_2}{(1-e^{-\lambda})\theta}$ and $\mu'_{1,1}=E\left(N_1^w,N_2^w\right)=\frac{\lambda^2\theta_1\theta_2}{(1-e^{-\lambda})\theta^2}$ are the population moments. Equating the first sample moments $\bar{X}^w$ and $\bar{Y}^w$ to the population moments, the moment estimates for the parameters θ_1 and θ_2 are

$$\hat{\theta}_1=\frac{\left(\frac{\lambda}{(1-e^{-\lambda})}-1\right)\bar{X}^w}{\left(\frac{\lambda}{(1-e^{-\lambda})}+\bar{X}^w-1\right)\left(\frac{\lambda}{(1-e^{-\lambda})}+\bar{Y}^w-1\right)-\bar{X}^w\bar{Y}^w}$$

$$\hat{\theta}_2=\frac{\left(\frac{\lambda}{(1-e^{-\lambda})}-1\right)\bar{Y}^w}{\left(\frac{\lambda}{(1-e^{-\lambda})}+\bar{X}^w-1\right)\left(\frac{\lambda}{(1-e^{-\lambda})}+\bar{Y}^w-1\right)-\bar{X}^w\bar{Y}^w}.$$

To find the moment estimate for λ, we equate the mixed sample moment $m_{1,1}^w$ to the population moment $\mu'_{1,1}$, which gives

$$
\begin{aligned}
m_{1,1}^{w} &= \frac{\lambda^2 \hat{\theta}_1 \hat{\theta}_2}{\left(1-e^{-\lambda}\right)\hat{\theta}^2} \\
\hat{\lambda} &= \frac{\left(1-e^{-\hat{\lambda}}\right)\sqrt{m_{1,1}^{w}}}{\sqrt{m_{1,1}^{w}} - \sqrt{\left(1-e^{-\hat{\lambda}}\right)\bar{X}^{w}\bar{Y}^{w}}}.
\end{aligned} \tag{22}
$$

An explicit expression for the estimator of λ is not available, therefore the estimate of λ is obtained iteratively using the Newton Rhapson method where

$$
\hat{\lambda}_{i+1} = \hat{\lambda}_i - \frac{f\left(\hat{\lambda_i}\right)}{f'\left(\hat{\lambda_i}\right)} \tag{23}
$$

From (22) we find that

$$
\frac{\hat{\lambda}^2\left(1-e^{-\hat{\lambda}}\right)\bar{X}^{w}\bar{Y}^{w}}{\left(\hat{\lambda}-1+e^{-\hat{\lambda}}\right)^2} - m_{1,1}^{w} = 0,
$$

therefore

$$
\begin{aligned}
f\left(\hat{\lambda}\right) &= \frac{\hat{\lambda}^2\left(1-e^{-\hat{\lambda}}\right)\bar{X}^{w}\bar{Y}^{w}}{\left(\hat{\lambda}-1+e^{-\hat{\lambda}}\right)^2} - m_{1,1}^{w}, \\
f'\left(\hat{\lambda}\right) &= \frac{2\hat{\lambda}\left(1-e^{-\hat{\lambda}}\right)\bar{X}^{w}\bar{Y}^{w} + \hat{\lambda}^2 e^{-\hat{\lambda}}\bar{X}^{w}\bar{Y}^{w} - 2\hat{\lambda}^2\left(1-e^{-\hat{\lambda}}\right)^2\bar{X}^{w}\bar{Y}^{w}}{\left(\hat{\lambda}-1+e^{-\hat{\lambda}}\right)^2}.
\end{aligned} \tag{24}
$$

Therefore from (23) and (24) the recursion formula is

$$
\hat{\lambda}_{i+1} = \hat{\lambda}_i - \frac{\hat{\lambda_i}^2\left(1-e^{-\hat{\lambda_i}}\right)\bar{X}^{w}\bar{Y}^{w} - m_{1,1}^{w}\left(\hat{\lambda_i}-1+e^{-\hat{\lambda_i}}\right)^2}{2\hat{\lambda_i}\left(1-e^{-\hat{\lambda_i}}\right)\bar{X}^{w}\bar{Y}^{w} + \hat{\lambda_i}^2 e^{-\hat{\lambda_i}}\bar{X}^{w}\bar{Y}^{w} - 2\hat{\lambda_i}^2\left(1-e^{-\hat{\lambda_i}}\right)^2\bar{X}^{w}\bar{Y}^{w}}
$$

where $i = 0, 1, \ldots,$ and choosing the moment estimate for λ from the Type II bivariate Pólya-Aeppli distribution as a starting value for $\hat{\lambda}_i$, and selecting a stopping value such that $\hat{\lambda}_{i+j} - \hat{\lambda}_{i+j-1} < \varepsilon$, where $j = 0, 1, \ldots,$ and $\varepsilon = 0.001$ as the stopping value.

4.4 Multivariate Extension

The weighted Type II bivariate Pólya-Aeppli distribution Case II can naturally be extended to the multivariate case and we will give the newly proposed results of this distribution here.

Let $X = (X_1, \ldots, X_k)$ have a multivariate geometric distribution with *pgf*

$$\psi_1(s_1, \ldots, s_k) = \frac{\theta}{1 - \theta_1 s_1 - \ldots - \theta_k s_k},$$

where $0 < \theta_1, \ldots, \theta_k < 1$, $\theta = 1 - \theta_1 - \ldots - \theta_k \neq 0$ and Y^w is the weighted version of $Y \sim Poi(\lambda)$, a non-negative weight function $w(y) = \frac{1}{y+1}$ and *pgf* given by (18). Define $\left(N_1^w, \ldots, N_k^w\right)$ as $N_i^w = \sum_{m_i=1}^{Y^w} X_{im_i}$ for $i = 1, \ldots, k$. The joint distribution of $\left(N_1^w, \ldots, N_k^w\right)$ is then said to be a weighted Type II multivariate Pólya-Aeppli distribution Case II, denoted as $(N_1^w, \ldots, N_k^w) \sim WMVPA_{II}^{(2)}(\lambda, \theta_1, \ldots, \theta_k)$. Extending the *pgf* in (19), the *pgf* of the distribution is

$$\begin{aligned}\psi_{N_1^w, N_2^w}(s_1, s_2) &= \psi_2^w\left(\psi_1(s_1, s_2)\right) \\ &= \frac{e^{-\lambda}}{\left(1 - e^{-\lambda}\right)} \frac{(1 - \theta_1 s_1 - \ldots - \theta_k s_k)}{\theta} \left(e^{\frac{\lambda\theta}{1-\theta_1 s_1 - \ldots - \theta_k s_k}} - 1\right). \end{aligned} \tag{25}$$

The expected values of $(N_1^w, \ldots, N_k^w) \sim WMVPA_{II}^{(2)}(\lambda, \theta_1, \ldots, \theta_k)$ are $E\left(N_i^w\right) = \frac{(\lambda - 1 + e^{-\lambda})\theta_i}{(1-e^{-\lambda})\theta}$ and $E\left(N_i^w N_j^w\right) = \frac{\lambda^2 \theta_i \theta_j}{(1-e^{-\lambda})\theta^2}$, where $i = 1, \ldots, k$, $j = 1, \ldots, k$, $i \neq j$. The variances are $Var\left(N_i^w\right) = \frac{(\lambda - 1 + e^{-\lambda})(1-e^{-\lambda})(\theta + \theta_i)\theta_i - (\lambda - 1 + e^{-\lambda})\lambda\theta_i^2 + (1-e^{-\lambda})\lambda^2\theta_i^2}{(1-e^{-\lambda})^2\theta^2}$ and the covariance is $Cov\left(N_i^w, N_j^w\right) = \frac{(\lambda - 1 + e^{-\lambda})\theta_i\theta_j + \lambda\theta_i\theta_j}{\theta^2}$. The correlation can be calculated using these results.

Theorem 6 *The pmf of* $(N_1^w, \ldots, N_k^w) \sim WMVPA_{II}^{(2)}(\lambda, \theta_1, \ldots, \theta_k)$ *is*

$$f^w(0, \ldots, 0) = \frac{e^{-\lambda}}{\left(1 - e^{-\lambda}\right)} \frac{\left(e^{\lambda\theta} - 1\right)}{\theta}$$

$$f^w(0, \ldots, 1) = \frac{e^{-\lambda}}{\left(1 - e^{-\lambda}\right)} \frac{\theta_k}{\theta} \left[(\lambda\theta - 1)e^{\lambda\theta} + 1\right]$$

$$f^w(n_1, \ldots, n_k) = \frac{\lambda^2 \theta e^{-\lambda(1-\theta)}}{\left(1 - e^{-\lambda}\right)} \frac{(n_1 + \cdots + n_k - 2)!}{n_1! \cdots n_k!} \theta_1^{n_1} \cdots \theta_k^{n_k} L_{n_1+\cdots+n_k-2}^2(-\lambda\theta),$$

$$n_1, \ldots, n_k = 0, 1, \ldots, \ (n_1, \ldots, n_k) \neq (0, \ldots, 0),$$

$$(n_1, \ldots, n_k) \neq (0, \ldots, 1)$$

where $L_n^{\alpha}(x)$ *is the generalized Laguerre polynomial of degree* n.

Proof Similar to the bivariate case, for the initial value we know that $f^w(0,\ldots,0) = \psi_{N_1^w,\ldots,N_k^w}(0,\ldots,0)$, so it follows from the *pgf* in (25) that

$$f^w(0,\ldots,0) = \frac{e^{-\lambda}}{\left(1-e^{-\lambda}\right)}\frac{\left(e^{\lambda\theta}-1\right)}{\theta}.$$

In order to calculate $f^w(0,\ldots,1)$, we can rewrite the *pgf* in (25) as

$$\begin{aligned}
&\psi_{N_1^w,\ldots,N_k^w}(s_1,\ldots,s_k)\\
&= \frac{e^{-\lambda}}{\left(1-e^{-\lambda}\right)}\frac{(1-\theta_1 s_1-\cdots-\theta_k s_k)}{\theta}\left[\sum_{i=0}^{\infty}\left(\frac{\lambda\theta}{1-\theta_1 s_1-\cdots-\theta_k s_k}\right)^i\frac{1}{i!}-1\right]\\
&= \frac{e^{-\lambda}}{\left(1-e^{-\lambda}\right)}\sum_{i=1}^{\infty}\frac{\lambda^i\theta^{i-1}}{i!\,(1-\theta_1 s_1-\cdots-\theta_k s_k)^{i-1}}.
\end{aligned}$$

Then if $k = 1, 2, \ldots,$ it follows from (A4) in the Appendix, that

$$\begin{aligned}
\psi^{(0,\ldots,1)}_{N_1^w,\ldots,N_k^w}(s_1,\ldots,s_k) &= \frac{\partial\psi_{N_1^w,\ldots,N_k^w}(s_1,\ldots,s_k)}{\partial s_k}\\
&= \frac{e^{-\lambda}}{\left(1-e^{-\lambda}\right)}\sum_{i=1}^{\infty}\frac{\theta_k\,(i-1)\,\lambda^i\theta^{i-1}}{i!\,(1-\theta_1 s_1-\cdots-\theta_k s_k)^i}
\end{aligned}$$

and

$$\begin{aligned}
f^w(0,\ldots,1) &= \psi^{(0,\ldots,1)}_{N_1^w,\ldots,N_k^w}(s_1,\ldots,s_k)\Big|_{s_1=0,\ldots,s_k=0}\\
&= \frac{e^{-\lambda}}{\left(1-e^{-\lambda}\right)}\sum_{i=1}^{\infty}\frac{\theta_k\,(i-1)\,\lambda^i\theta^{i-1}}{i!}\\
&= \frac{e^{-\lambda}}{\left(1-e^{-\lambda}\right)}\frac{\theta_k}{\theta}\left[\sum_{i=1}^{\infty}\frac{\lambda^i\theta^i}{(i-1)!}-\sum_{i=1}^{\infty}\frac{\lambda^i\theta^i}{i!}\right]\\
&= \frac{e^{-\lambda}}{\left(1-e^{-\lambda}\right)}\frac{\theta_k}{\theta}\left[\sum_{i=0}^{\infty}\frac{\lambda^{i+1}\theta^{i+1}}{i!}-\sum_{i=0}^{\infty}\frac{\lambda^i\theta^i}{i!}+1\right]\\
&= \frac{e^{-\lambda}}{\left(1-e^{-\lambda}\right)}\frac{\theta_k}{\theta}\left[(\lambda\theta-1)\sum_{i=0}^{\infty}\frac{\lambda^i\theta^i}{i!}+1\right]\\
&= \frac{e^{-\lambda}}{\left(1-e^{-\lambda}\right)}\frac{\theta_k}{\theta}\left[(\lambda\theta-1)\,e^{\lambda\theta}+1\right].
\end{aligned}$$

If we let $x = -\lambda\theta$ and $z_1 = \theta_1 s_1$ and $z_k = \theta_k s_k$, then the *pgf* in (25) can be expressed as

$$\begin{aligned}
\psi_{N_1^w,\ldots,N_k^w}(s_1,\ldots,s_k) &= \sum_{n_1=0}^{\infty}\cdots\sum_{n_k=0}^{\infty} P\left(N_1^w = n_1,\ldots,N_k^w = n_k\right) s_1^{n_1}\cdots s_k^{n_k} \\
&= \frac{(1-\theta_1 s_1 - \cdots - \theta_k s_k)}{\theta\left(1-e^{-\lambda}\right)}\left[e^{-\lambda\left(1-\frac{\theta}{1-\theta_1 s_1-\cdots-\theta_k s_k}\right)} - e^{-\lambda}\right] \\
&= \frac{(1-\theta_1 s_1 - \cdots - \theta_k s_k)}{\theta\left(1-e^{-\lambda}\right)}\left[e^{-\lambda\left(1-\theta+\theta-\frac{\theta}{1-\theta_1 s_1-\cdots-\theta_k s_k}\right)} - e^{-\lambda}\right] \\
&= \frac{(1-z_1 - \cdots - z_k)}{\theta\left(1-e^{-\lambda}\right)}\left[e^{-\lambda(1-\theta)}e^{\left(\frac{x(z_1+\cdots+z_k)}{z_1+\cdots+z_k-1}\right)} - e^{-\lambda}\right].
\end{aligned}$$

Finding the second derivative of $\psi_{N_1^w,\ldots,N_k^w}(s_1,\ldots,s_k)$ with respect to z_1 and using results (A1), (A2), (A3), and (A5) from the Appendix, it follows that

$$\begin{aligned}
&\frac{\partial^2\psi_{N_1^w,\ldots,N_k^w}(s_1,\ldots,s_k)}{\partial z_1^2} \\
&= \frac{\lambda^2\theta e^{-\lambda(1-\theta)}}{\left(1-e^{-\lambda}\right)(1-z_1-\cdots-z_k)^3} e^{\left(\frac{x(z_1+\cdots+z_k)}{z_1+\cdots+z_k-1}\right)} \\
&= \frac{\lambda^2\theta e^{-\lambda(1-\theta)}}{\left(1-e^{-\lambda}\right)}\sum_{n_1=0}^{\infty} L_{n_1}^2(x)(z_1+\cdots+z_k)^{n_1} \\
&= \frac{\lambda^2\theta e^{-\lambda(1-\theta)}}{\left(1-e^{-\lambda}\right)}\sum_{n_1=n_2}^{\infty}\sum_{n_2=n_3}^{\infty}\cdots\sum_{n_k=0}^{\infty}\binom{n_1}{n_2}\cdots\binom{n_{k-1}}{n_k} L_{n_1}^2(x) z_1^{n_1-n_2}\cdots z_{k-1}^{n_{k-1}-n_k} z_k^{n_k} \\
&= \frac{\lambda^2\theta e^{-\lambda(1-\theta)}}{\left(1-e^{-\lambda}\right)}\sum_{n_1=0}^{\infty}\sum_{n_2=0}^{\infty}\cdots\sum_{n_k=0}^{\infty}\binom{n_1+n_2+\cdots+n_k}{n_2+\cdots+n_k}\cdots\binom{n_{k-1}+n_k}{n_k} \\
&\times L_{n_1+n_2+\cdots+n_k}^2(x) z_1^{n_1}\cdots z_k^{n_k} \\
&= \sum_{n_1=0}^{\infty}\cdots\sum_{n_k=0}^{\infty}\left[\frac{\lambda^2\theta e^{-\lambda(1-\theta)}}{\left(1-e^{-\lambda}\right)}\frac{(n_1+\cdots+n_k)!}{n_1!\cdots n_k!} L_{n_1+\cdots+n_k}^2(x)\right] z_1^{n_1}\cdots z_k^{n_k} \\
&= \sum_{n_1=2}^{\infty}\cdots\sum_{n_k=0}^{\infty}\left[\frac{\lambda^2\theta e^{-\lambda(1-\theta)}}{\left(1-e^{-\lambda}\right)}\frac{(n_1+\cdots+n_k-2)!}{(n_1-2)!\cdots n_k!} L_{n_1+\cdots+n_k-2}^2(x)\right] z_1^{n_1-2}\cdots z_k^{n_k}
\end{aligned}$$

and additionally it can be shown that

$$\frac{\partial^2 \psi_{N_1^w,\ldots,N_k^w}(s_1,\ldots,s_k)}{\partial z_1^2} = \sum_{n_1=2}^{\infty}\cdots\sum_{n_k=0}^{\infty} n_1\,(n_1-1) \times \frac{P\left(N_1^w=n_1,\ldots,N_k^w=n_k\right)}{\theta_1^{n_1}\ldots\theta_k^{n_k}} z_1^{n_1-2}\cdots z_k^{n_k}.$$

When using (A4) in the Appendix, we can see that

$$\psi^{(1,\ldots,1)}_{N_1^w,\ldots,N_k^w}(s_1,\ldots,s_k) = \frac{\partial^k \psi_{N_1^w,\ldots,N_k^w}(s_1,\ldots,s_k)}{\partial s_1\cdots\partial s_k} = \frac{e^{-\lambda}}{\left(1-e^{-\lambda}\right)}\sum_{i=2}^{\infty}\frac{\theta_1\cdots\theta_k\,(i+k-2)\cdots(i-1)\,\lambda^i\theta^{i-1}}{i!\,(1-\theta_1 s_1-\cdots-\theta_k s_k)^{i+(k+1)-2}}$$

and

$$\begin{aligned} f^w(1,\ldots,1) &= \psi^{(1,\ldots,1)}_{N_1^w,\ldots,N_k^w}(s_1,\ldots,s_k)\Big|_{s_1=0,\ldots,s_k=0} \\ &= \frac{e^{-\lambda}}{\left(1-e^{-\lambda}\right)}\sum_{i=2}^{\infty}\frac{\theta_1\cdots\theta_k\,(i+k-2)\cdots(i-1)\,\lambda^i\theta^{i-1}}{i!} \\ &= \frac{e^{-\lambda}}{\left(1-e^{-\lambda}\right)}\theta_1\cdots\theta_k\sum_{i=0}^{\infty}\frac{(i+k)\cdots(i+3)\,\lambda^{i+2}\theta^{i+1}}{i!} \\ &= \frac{e^{-\lambda}}{\left(1-e^{-\lambda}\right)}k!\theta_1\cdots\theta_k\left(\sum_{m=2}^{k}\binom{k-2}{m-2}\frac{\lambda^m\theta^{m-1}}{m!}\right)\sum_{i=0}^{\infty}\frac{\lambda^i\theta^i}{i!} \\ &= \frac{e^{-\lambda(1-\theta)}}{\left(1-e^{-\lambda}\right)}k!\theta_1\cdots\theta_k\sum_{m=2}^{k}\binom{k-2}{m-2}\frac{\lambda^m\theta^{m-1}}{m!}. \end{aligned}$$

Similar results can be derived by differentiating with respect to z_i for $i=2,\ldots,k$. Therefore it follows that for $n_1,\ldots,n_k = 0,1,\ldots,$ $(n_1,\ldots,n_k)\neq(0,\ldots,0)$, $(n_1,\ldots,n_k)\neq(0,\ldots,1)$ the *pmf* is

$$f^w(n_1,\ldots,n_k) = \frac{\lambda^2\theta e^{-\lambda(1-\theta)}}{\left(1-e^{-\lambda}\right)}\frac{(n_1+\cdots+n_k-2)!}{n_1!\cdots n_k!}\theta_1^{n_1}\cdots\theta_k^{n_k} \times L^2_{n_1+\cdots+n_k-2}(-\lambda\theta) \tag{26}$$

□

Remark 4.3 Using (A6) in the Appendix, it can be shown that the expression in (26) is equivalent to

$$f^{w}(n_1,\ldots,n_k) = \frac{e^{-\lambda(1-\theta)}}{\left(1-e^{-\lambda}\right)}\frac{(n_1+\cdots+n_k)!}{n_1!\cdots n_k!}\theta_1^{n_1}\cdots\theta_k^{n_k} \times \sum_{m=2}^{n_1+\cdots+n_k}\binom{n_1+\cdots+n_k-2}{m-2}\frac{\lambda^m\theta^{m-1}}{m!}.$$

5 Simulation Study

5.1 Comparison of Fisher Indexes of Dispersion and Properties

In this subsection the Type II and weighted Type II bivariate Pólya-Aeppli Case I and Case II distributions are graphically studied with the purpose of investigating and comparing the effect of a change in the parameters of the distributions on the Fisher indexes of dispersion. In all cases the theoretical results derived in this chapter are used to create the graphs.

The graphs in Figs. 1 and 2 depict the Fisher indexes of dispersion of the three bivariate distributions. In both graphs we use $\lambda = 2, \theta_1 = 0.3$ and $\theta_2 = 0.2$ as reference parameters and vary only one of the parameters, while keeping all others constant. We observe how the Fisher indexes of dispersion change for varying values of θ_1 in Fig. 1, and λ in Fig. 2.

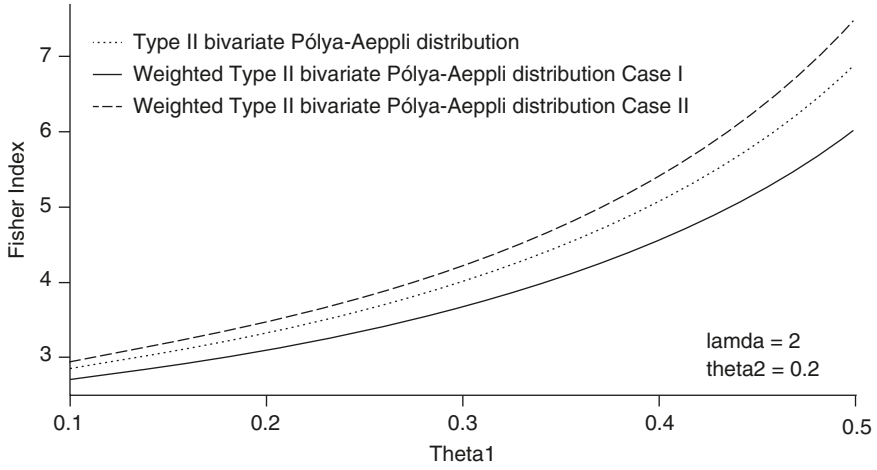

Fig. 1 Fisher indexes of the Type II bivariate Pólya-Aeppli distribution and weighted Type II bivariate Pólya-Aeppli Case I and Case II distributions with parameters $\lambda = 2, \theta_2 = 0.2$

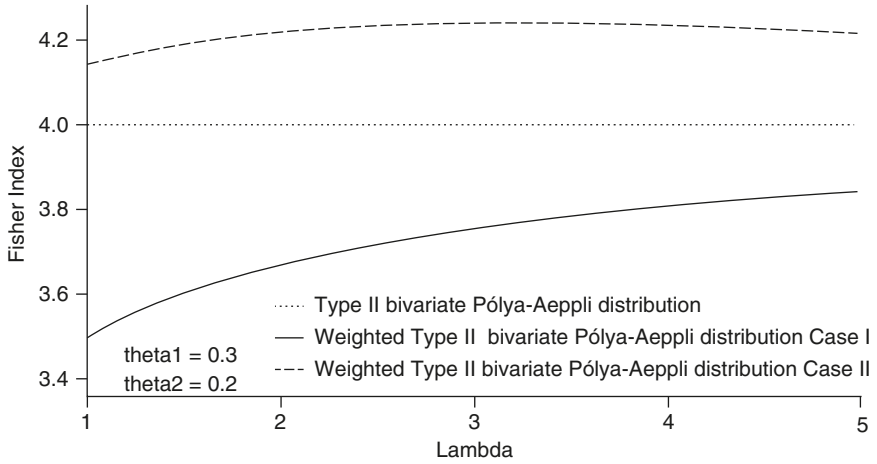

Fig. 2 Fisher indexes of the Type II bivariate Pólya-Aeppli distribution and weighted Type II bivariate Pólya-Aeppli Case I and Case II distributions with parameters $\theta_1 = 0.3, \theta_2 = 0.2$

Table 1 Properties of the Type II bivariate Pólya-Aeppli and weighted Type II bivariate Pólya-Aeppli Case I and Case II distributions (reference parameters: $\lambda = 2, \theta_1 = 0.3, \theta_2 = 0.2$)

	$E\left(N_1^{(w)}\right)$	$E\left(N_2^{(w)}\right)$	$Var\left(N_1^{(w)}\right)$	$Var\left(N_2^{(w)}\right)$
$(N_1, N_2) \sim BivPA_{II}(\lambda, \theta_1, \theta_2)$	1.2	0.8	2.64	1.44
$(N_1^w, N_2^w) \sim WBivPA_{II}^{(1)}(\lambda, \theta_1, \theta_2)$	1.8	1.2	3.6	2
$(N_1^w, N_2^w) \sim WBivPA_{II}^{(2)}(\lambda, \theta_1, \theta_2)$	0.79	0.53	1.83	1

For increasing values of θ_1, the Fisher indexes of dispersion of all the distributions follow an upward trend. Increasing values of θ_2 will have similar effects on the dispersion of the distributions.

For increasing values of λ, the Type II bivariate Pólya-Aeppli distribution has a constant Fisher index of dispersion as can be seen in (13). The dispersion of the weighted Type II Case I distribution follows an upward trend, whilst the weighted Type II Case II distribution initially has a slight upward trend before sloping gradually downwards. From (13) and (20) the Fisher indexes of both weighted bivariate distributions approaches the Fisher index of the Type II bivariate Pólya-Aeppli distribution as λ becomes very large.

The weighted Type II bivariate Pólya-Aeppli Case I and Case II distributions are respectively under and over-dispersed with respect to the Type II bivariate Pólya-Aeppli distribution, except in the case of very large values of λ, for which all distributions tend towards equi-dispersion. Table 1 gives the expected values and variances of the random variables for the three Type II bivariate Pólya-Aeppli distributions with the same parameters $\lambda = 2, \theta_1 = 0.3$ and $\theta_2 = 0.2$.

Compared to the Type II bivariate Pólya-Aeppli distribution, the weighted Case I distribution is shifted towards larger values of both random variables and the variances for both variables are also larger. Conversely both random variables of

the weighted Case II distribution is shifted towards smaller values and has smaller variances, compared to the Type II bivariate distribution.

From the Fisher indexes in Figs. 1 and 2 and the marginal properties of the variables it follows that the weighted Case I and Case II distributions will fit some data better than the Type II bivariate distribution. This is studied in the next subsection.

5.2 Success Rates of Moment Estimates

The success rate of an estimator is the proportion of samples for which an estimate can be calculated. For example, for the Type II bivariate Pólya-Aeppli distribution the moment estimate of λ is $\hat{\lambda} = \dfrac{2\bar{X}\bar{Y}}{m_{1,1} - \bar{X}\bar{Y}}$. If the sample covariance is negative, $\hat{\lambda}$ will be negative and the parameters cannot be estimated.

Tables 2 and 3 give the average percentage success rates of the moment estimates for sample sizes $s = 50$ and $s = 100$ and parameter values of $\lambda = 2, 8$ and $\theta_1, \theta_2 = 0.1, 0.2, 0.3, 0.4$. The success rates are calculated by simulating 100 samples each of size s from each of the three bivariate distributions and calculating the percentage of samples for which the moment estimates could be calculated.

From these tables it follows that for a larger sample and larger values of all the parameters, better success rates are observed.

5.3 Comparison of Moment Estimates

In Sect. 5.3 the mean, bias and MSE of the method of moments estimates are compared for the Type II bivariate Pólya-Aeppli and weighted Type II bivariate Pólya-Aeppli Case I and Case II distributions. Samples of sizes 100, 200 and 500 were simulated from these distributions, all with parameters $\lambda = 8$, $\theta_1 = 0.4$, $\theta_2 = 0.4$, see Algorithm 1.

Algorithm 1

(1) Simulate a dataset from the Type II bivariate Pólya-Aeppli distribution ($\lambda = 8, \theta_1 = 0.4, \theta_2 = 0.4$) and calculate the moment estimates $\left(\hat{\lambda}, \hat{\theta_1}, \hat{\theta_2}\right)$.

(2) Simulate 1000 samples from the $BivPA_{II}(\hat{\lambda}, \hat{\theta_1}, \hat{\theta_2})$ distribution and calculate the moment estimates, $(\lambda^*, \theta_1^*, \theta_2^*)$ for each sample.

(3) The quantile bootstrap estimates are then used to find the 95% confidence intervals for the parameters.

Table 2 Average success rates (%) for $\lambda = 2$

		θ_1											
		0.1			0.2			0.3			0.4		
$\lambda = 2$	$s = 50$	Type II	Case I	Case II	Type II	Case I	Case II	Type II	Case I	Case II	Type II	Case I	Case II
θ_2	0.1	84.79	64.80	78.94	–	–	–	–	–	–	–	–	–
	0.2	94.67	81.90	89.36	99.29	93.03	93.19	–	–	–	–	–	–
	0.3	98.37	90.12	92.51	99.95	96.42	92.78	100	98.04	91.74	–	–	–
	0.4	99.58	94.14	93.17	99.99	97.87	91.87	100	99.92	90.70	100	99.29	99.82
		θ_1											
		0.1			0.2			0.3			0.4		
$\lambda = 2$	$s = 100$	Type II	Case I	Case II	Type II	Case I	Case II	Type II	Case I	Case II	Type II	Case I	Case II
θ_2	0.1	94.09	80.42	89.26	–	–	–	–	–	–	–	–	–
	0.2	99.09	92.46	93.39	99.98	97.92	92.59	–	–	–	–	–	–
	0.3	99.89	96.56	93.01	100	99.11	91.10	100	99.67	90.14	–	–	–
	0.4	99.99	98.35	92.08	100	99.60	90.35	100	99.84	89.61	100	99.95	99.159

Table 3 Average success rates (%) for $\lambda = 8$

		θ_1											
		0.1			0.2			0.3			0.4		
$\lambda = 8$	$s = 50$	Type II	Case I	Case II	Type II	Case I	Case II	Type II	Case I	Case II	Type II	Case I	Case II
θ_2	0.1	90.15	89.46	91.41	–	–	–	–	–	–	–	–	–
	0.2	97.26	96.69	97.74	99.75	99.67	99.81	–	–	–	–	–	–
	0.3	99.30	99.02	99.44	99.98	99.97	99.98	99.99	99.99	100	–	–	–
	0.4	99.85	99.81	99.89	100	99.99	100	100	100	100	100	100	100

		θ_1											
		0.1			0.2			0.3			0.4		
$\lambda = 8$	$s = 100$	Type II	Case I	Case II	Type II	Case I	Case II	Type II	Case I	Case II	Type II	Case I	Case II
θ_2	0.1	97.00	96.20	97.44	–	–	–	–	–	–	–	–	–
	0.2	99.69	99.60	99.78	99.99	99.99	100	–	–	–	–	–	–
	0.3	99.98	99.96	99.99	100	100	100	100	100	100	–	–	–
	0.4	99.99	99.99	99.96	100	100	100	100	100	100	100	100	100

From Sect. 5.2 these parameter values consistently give a 100% success rate for method of moments estimation. The results for the estimates of the three bivariate distributions are given in Tables 4, 5, and 6.

Although the moment estimates for all distributions are asymptotically unbiased, the weighted Type II bivariate Pólya-Aeppli distribution Case II consistently provides parameter estimates with the smallest bias and MSE.

Table 4 The Type II bivariate Pólya-Aeppli distribution method of moments estimates

Sample size	λ (mean, bias, MSE)	θ_1 (mean, bias, MSE)	θ_2 (mean, bias, MSE)
100	(8.349, 0.349, 2.298)	(0.397, −0.003, 0.000)	(0.396, −0.004, 0.000)
200	(8.141, 0.141, 0.959)	(0.399, −0.001, 0.000)	(0.399, −0.001, 0.000)
500	(8.066, 0.066, 0.389)	(0.399, −0.001, 0.000)	(0.399, −0.001, 0.000)

Table 5 The weighted Type II bivariate Pólya-Aeppli distribution Case I method of moments estimates

Sample size	λ (mean, bias, MSE)	θ_1 (mean, bias, MSE)	θ_2 (mean, bias, MSE)
100	(8.414, 0.414, 3.131)	(0.397, −0.003, 0.000)	(0.396, −0.004, 0.0003)
200	(8.236, 0.236, 1.464)	(0.398, −0.002, 0.000)	(0.398, −0.002, 0.000)
500	(8.082, 0.082, 0.585)	(0.399, −0.001, 0.000)	(0.399, −0.001, 0.000)

Table 6 The weighted Type II bivariate Pólya-Aeppli distribution Case II method of moments estimates

Sample size	λ (mean, bias, MSE)	θ_1 (mean, bias, MSE)	θ_2 (mean, bias, MSE)
100	(8.243, 0.243, 1.421)	(0.398, −0.002, 0.000)	(0.397, −0.003, 0.000)
200	(8.093, 0.093, 0.645)	(0.399, −0.001, 0.000)	(0.399, −0.001, 0.000)
500	(8.031, 0.031, 0.261)	(0.400, −0.000, 0.000)	(0.400, −0.000, 0.000)

5.4 Confidence Intervals

Subsequently the bootstrap confidence intervals are constructed for the estimates of the parameters in Sect. 5.3. This is done using the parametric bootstrap approach as follows: This process is repeated for the two weighted versions of the Type II bivariate Pólya-Aeppli distribution and the results are given in Tables 7, 8, and 9.

Of the three bivariate distributions considered, the weighted Type II bivariate Pólya-Aeppli distribution Case II consistently provides the narrowest confidence intervals for all sample sizes.

Table 7 Type II bivariate Pólya-Aeppli distribution

	Coverage probability			Average width of CI		
Sample size	λ	θ_1	θ_2	λ	θ_1	θ_2
100	0.945	0.943	0.941	5.970	0.063	0.063
200	0.948	0.948	0.948	3.980	0.044	0.044
500	0.961	0.943	0.953	2.444	0.027	0.027

Table 8 Weighted Type II bivariate Pólya-Aeppli distribution Case I

	Coverage probability			Average width of CI		
Sample size	λ	θ_1	θ_2	λ	θ_1	θ_2
100	0.937	0.938	0.939	7.159	0.066	0.066
200	0.937	0.927	0.930	4.776	0.045	0.045
500	0.942	0.953	0.942	2.923	0.028	0.028

Table 9 Weighted Type II bivariate Pólya-Aeppli distribution Case II

	Coverage probability			Average width of CI		
Sample size	λ	θ_1	θ_2	λ	θ_1	θ_2
100	0.948	0.947	0.946	4.781	0.060	0.060
200	0.952	0.953	0.958	3.214	0.042	0.042
500	0.950	0.960	0.949	1.982	0.026	0.026

Table 10 Observed frequencies of accidents of 122 railway men during two time periods

	0	1	2	3	4	5	6	7	Total
0	21	14	8	1	0	0	0	0	44
1	17	12	8	3	1	0	0	1	42
2	6	9	2	2	2	0	0	0	21
3	1	1	3	3	1	0	0	0	9
4	1	3	0	0	0	0	0	0	4
5	0	0	0	2	0	0	0	0	2
Total	46	39	21	11	4	0	0	1	122

5.5 Illustrative Example

Table 10 gives the dataset of frequencies of accidents by 122 railway men during two periods (Hamdan 1972). In this subsection the performance of the different models is shown using this dataset. The three bivariate distributions considered thus far, are fitted to the data, and the method of moments parameter estimates are computed for each of the distributions.

Due to the small expected frequencies in some cells, the observed and expected frequencies for the different distributions are given in a 3×3 contingency table of combined cells in Table 11. Table 12 gives the method of moments estimates together with the chi-square goodness of fit test statistic and the p-values for the test.

Table 11 Observed and expected frequencies of accidents of 122 railway men during two time periods

		0	1	2+	Total
0	Observed	21	14	9	44
	Type II	23.57	14.18	9.46	47.21
	Case I	23.36	14.30	9.48	47.14
	Case II	23.72	14.09	9.46	47.27
1	Observed	17	12	13	42
	Type II	14.18	12.34	11.37	37.89
	Case I	14.30	12.38	11.34	38.02
	Case II	14.09	12.30	11.40	37.79
2+	Observed	8	13	15	36
	Type II	9.47	11.37	16.06	36.90
	Case I	9.48	11.34	16.02	36.84
	Case II	9.46	11.40	16.08	36.94
Total	Observed	46	39	37	122
	Type II	47.22	37.89	36.89	122
	Case I	47.14	38.02	36.84	122
	Case II	47.27	37.79	36.94	122

Table 12 Method of moments estimates, χ^2 test statistics and p-values

	λ	θ_1	θ_2	χ^2	p-value
Type II bivariate Pólya-Aeppli distribution	6.135	0.134	0.134	1.640	0.896
Weighted Type II bivariate Pólya-Aeppli distribution Case I	4.586	0.143	0.143	1.572	0.905
Weighted Type II bivariate Pólya-Aeppli distribution Case II	7.582	0.127	0.127	1.693	0.890

Although all three distributions provide a good fit, the weighted Case I distribution has a slightly better fit.

5.6 Simulated Example

In this subsection a comparison of the fit of the three bivariate distributions is done by making use of a dataset simulated from a weighted Type II bivariate Pólya-Aeppli distribution Case II with parameters $\lambda = 3$, $\theta_1 = \theta_2 = 0.3$. Method of moments estimates were calculated for the distributions and the observed and expected frequencies are given in a contingency table in Table 13.

The parameter estimates, chi-square goodness of fit test statistics and corresponding p-values are given in Table 14. In this case the weighted Type II bivariate Pólya-Aeppli distribution Case II is the only distribution that provides a good fit at a 0.05 significance level.

Remark All simulations, figures and results in this section were obtained using RStudio (2016).

Table 13 Observed frequencies of simulated data and expected frequencies for different distributions fitted to the data

		0	1	2	3	4+	Total
0	Observed	323	65	29	12	11	440
	Type II	291.39	76.79	32.78	13.55	8.98	423.49
	Case I	248.66	95.97	36.89	14.12	8.69	404.33
	Case II	296.59	74.62	32.24	13.45	9.01	425.91
1	Observed	64	51	38	24	11	188
	Type II	74.12	63.28	39.24	21.09	19.08	216.81
	Case I	92.63	71.20	40.90	20.81	17.88	243.42
	Case II	72.02	62.23	38.95	21.10	19.24	213.54
2	Observed	25	33	33	19	22	132
	Type II	30.54	37.87	30.54	20.12	24.05	143.12
	Case I	34.36	39.48	30.13	19.11	22.17	145.25
	Case II	30.03	37.60	30.55	20.24	24.31	142.73
3	Observed	14	18	26	17	31	106
	Type II	12.18	19.65	19.42	15.11	23.38	89.74
	Case I	12.70	19.39	18.45	14.00	21.48	86.02
	Case II	12.10	19.66	19.53	15.25	23.66	90.20
4+	Observed	5	18	33	32	46	134
	Type II	7.63	16.70	21.67	21.68	59.16	126.84
	Case I	7.39	15.65	19.97	19.90	58.07	120.98
	Case II	7.65	16.83	21.90	21.94	59.30	127.62
Total	Observed	431	185	159	104	121	1000
	Type II	415.86	214.29	143.65	91.55	134.65	1000
	Case I	395.74	241.69	146.34	87.94	128.29	1000
	Case II	418.39	210.94	143.17	91.98	135.52	1000

Table 14 Method of moments estimates, χ^2 test statistics and p-values

	λ	θ_1	θ_2	χ^2	p-value
Type II bivariate PA distribution	2.126	0.285	0.295	36.124	0.021
Weighted Type II bivariate PA distribution Case I	0.322	0.339	0.351	84.313	<0.0001
Weighted Type II bivariate PA distribution Case II	3.243	0.272	0.281	32.56 7	0.051

6 Summary and Conclusion

In this chapter we introduced and studied two new distributions, the weighted Type II bivariate Pólya-Aeppli distribution under two different weight functions and also extended both distributions to the multivariate case. In addition we proposed a greatly simplified methodology for obtaining the probability mass function of the Type II bivariate Pólya-Aeppli distribution and used this in the derivation of the results for the weighted distributions.

For the two new distributions, we observed that the weighted Type II bivariate Pólya-Aeppli distribution Case I is under-dispersed with respect to the Type II bivariate Pólya-Aeppli distribution, while the weighted Type II bivariate Pólya-Aeppli distribution Case II is over-dispersed with respect to the Type II bivariate Pólya-Aeppli distribution. These new bivariate distributions can therefore be fitted to count-valued data that displays this dispersion. The examples discussed in this chapter illustrate how the weighted distributions provide a better fit to the data.

Using method of moments estimates, the Type II bivariate Pólya-Aeppli distribution Case II consistently provides parameter estimates with the smallest bias and MSE and with the narrowest confidence intervals compared to the other two bivariate distributions.

All of this implies that the weighted Type II bivariate Pólya-Aeppli distributions Case I and Case II provides models of greatly increased flexibility not only with respect to the Type II bivariate Pólya-Aeppli distribution but also the bivariate Poisson distribution.

Appendix

The following well known mathematical results are used throughout this chapter and referred to within the relevant sections.

$$\sum_{k=0}^{\infty} \binom{k+\beta}{k} z^k = \frac{1}{(1-z)^{\beta+1}} \tag{A1}$$

$$\sum_{i=0}^{\infty} \sum_{k=i}^{\infty} a_{i.k} = \sum_{k=0}^{\infty} \sum_{i=0}^{k} a_{i.k} \tag{A2}$$

$$\sum_{i=0}^{\infty} \sum_{k=0}^{\infty} a_{i.k} = \sum_{k=0}^{\infty} \sum_{i=0}^{\infty} a_{i.k} \tag{A3}$$

Probability Generating Function

The probability generating function of a discrete random variable as discussed in Kocherlakota and Kocherlakota (1992) is unique and has a one to one relationship for a given probability mass function. One way in which the probability mass function can be obtained from the probability generating function is by using the fact that the probability generating function can be differentiated with respect to s_1 and s_2 any number of times and evaluated at (0, 0). Consequently we have

$$f(x,y) = \frac{1}{x!y!} \frac{\partial^{x+y} \psi(s_1, s_2)}{\partial s_1^x \partial s_2^y} \bigg|_{s_1=0, s_2=0}. \tag{A4}$$

Additionally we can express the expected values of X and Y as

$$E\left(X^r, Y^s\right) = \frac{\partial^{r+s} \psi(s_1, s_2)}{\partial s_1^r \partial s_2^s} \bigg|_{s_1=1, s_2=1} \qquad r, s = 0, 1, 2, \ldots$$

Laguerre Polynomials

Laguerre and associated Laguerre polynomials, discussed in Bayin (2013) are used throughout this chapter to simplify the calculation of the probability mass functions of the various distributions and weighted distributions. The generating function of the associated Laguerre polynomials is

$$\frac{1}{(1-z)^{\alpha+1}} e^{\left(\frac{xz}{z-1}\right)} = \sum_{m=0}^{\infty} L_m^{\alpha}(x) z^m \tag{A5}$$

and the final form of the associated Laguerre polynomials is

$$L_n^{\alpha}(x) = \sum_{m=0}^{n} (-1)^m \binom{n+\alpha}{n-m} \frac{x^m}{m!}, \tag{A6}$$

where $\alpha \geq 0$. The associated Laguerre polynomial reduces to the Laguerre polynomial for $\alpha = 0$.

Remark Detailed derivations of all the mathematical results given in this chapter can be obtained from the first author.

Acknowledgements We express our sincere thanks to Andriëtte Bekker for many helpful conversations. This work is based on the research supported in part by the National Research Foundation of South Africa (Grant ref. CPRR160403161466 nr. 105840) and the SARChI Research Chair (UID 71199). Opinions expressed and conclusions arrived at are those of the authors and are not necessarily to be attributed to the NRF.

References

Anscombe, F. J. (1950). Sampling theory of the negative binomial and logarithmic series distributions. *Biometrika, 37*(3/4), 358–382.

Bayin, S. S. (2013). *Essentials of mathematical methods in science and engineering*. London: Wiley.

Fisher, R. A. (1934). The effect of methods of ascertainment upon the estimation of frequencies. *Annals of eugenics, 6*(1), 13–25.

Galliher, H., Morse, P. M., & Simond, M. (1959). Dynamics of two classes of continuous-review inventory systems. *Operations Research, 7(3)*, 362–384.

Hamdan, M. A. (1972). Estimation in the truncated bivariate Poisson distribution. *Technometrics, 14*(1), 37–45.

Johnson, N. L., Kemp, A. W., & Kotz, S. (2005). *Univariate discrete distributions* (Vol. 444). London: Wiley.

Kocherlakota, S., & Kocherlakota, K. (1992). *Bivariate discrete distributions*. Statistics: A Series of Textbooks and Monographs. Boca Raton, FL: CRC Press.

Minkova, L. D., & Balakrishnan, N. (2013). Compound weighted Poisson distributions. *Metrika, 76*(4), 543–558.

Minkova, L. D., & Balakrishnan, N. (2014a). Type II bivariate Pólya–Aeppli distribution. *Statistics & Probability Letters, 88*, 40–49.

Minkova, L. D., & Balakrishnan, N. (2014b). On a bivariate Pólya-Aeppli distribution. *Communications in Statistics-Theory and Methods, 43*(23), 5026–5038.

Patil, G. P. (2002). *Weighted distributions*. London: Wiley.

Patil, G. P., & Ord, J. K. (1976). On size-biased sampling and related form-invariant weighted distributions. *Sankhyā: The Indian Journal of Statistics, Series B, 38*(1), 48–61.

Qin, Y., Liu, K., Al-Jarallah, R., & Balakrishnan, N. (2017). Inference for Type II bivariate Pólya–Aeppli distribution. *Communications in Statistics-Simulation and Computation, 46*(8), 5981–5990.

RStudio. (2016). *RStudio: Integrated development environment for R*. Boston, MA: RStudio. http://www.rstudio.com/

Constructing Multivariate Distributions via the Dirichlet Generator

Mohammad Arashi, Andriëtte Bekker, Daniel de Waal, and Seite Makgai

Abstract There exist several endeavours proposing a new family of extended distributions using the beta-generating technique. This is a well-known mechanism in developing flexible distributions, by embedding the cumulative distribution function (cdf) of a baseline distribution within the beta distribution that acts as a generator. Univariate beta-generated distributions offer many fruitful and tractable properties, and have applications in hydrology, biology and environmental sciences amongst other fields. In the univariate cases, this extension works well, however, for multivariate cases the beta distribution generator delivers complex expressions. In this chapter the proposed extension from the univariate to the multivariate domain addresses the need of flexible multivariate distributions that can model a wide range of multivariate data. This new family of multivariate distributions, whose marginals are beta-generated distributed, is constructed with the function $H(x_1, \ldots, x_p) = F\left(G_1(x_1), G_2(x_2), \ldots, G_p(x_p)\right)$, where $G_i(x_i)$ are the cdfs of the gamma (baseline) distribution and $F(\cdot)$ as the cdf of the Dirichlet distribution. Hence as a main example, a general model having the support $[0, 1]^p$ (for p variates), using the Dirichlet as the generator, is developed together with some distributional properties, such as the moment generating function. The proposed Dirichlet-generated distributions can be applied to compositional data. The parameters of the model are estimated by using the maximum likelihood method. The effectiveness and prominence of the proposed family is illustrated through analyzing simulated as well as two real datasets. A new model testing technique is introduced to evaluate the performance of the multivariate models.

M. Arashi
Department of Statistics, Faculty of Mathematical Sciences, Shahrood University of Technology, Shahrood, Iran

A. Bekker · D. de Waal · S. Makgai (✉)
Department of Statistics, University of Pretoria, Pretoria, South Africa
e-mail: andriette.bekker@up.ac.za; deWaalDJ@ufs.ac.za; seite.makgai@up.ac.za

A. Bekker et al. (eds.), *Computational and Methodological Statistics and Biostatistics*, Emerging Topics in Statistics and Biostatistics,
https://doi.org/10.1007/978-3-030-42196-0_7

1 Introduction

In many of the problems of interest to scientists, data consists of proportions and thus are subject to non-negativity and unit-sum constraints. Examples of such data can be found when analyzing rock compositions, household budgets, pollution components to name a few. Datasets such as these are known as compositional datasets and arise naturally in a great variety of disciplines such as biology, medicine, chemistry, economics, psychology, environmetrics, psychology and many others. The most widely studied distribution on the simplex is the Dirichlet distribution (Balakrishnan and Nevzorov 2003). Various generalizations of the Dirichlet distribution are proposed in literature, for example see Connor and Mosimann (1969), Barndorff and Jorgensen (1991), Ehlers (2011), Thomas and Jacob (2006), Epaillard and Bouguila (2019) and Favaro et al. (2011). For an extensive review see Ng et al. (2011) and Kotz et al. (2000). In particular, the Liouville distribution has been widely studied (see Gupta et al. (1997)). Specifically, a flexible Dirichlet was proposed by Ongaro and Migliorati (2013), by extending the basis of gamma independent random variables which generates the Dirichlet distribution. The Dirichlet prior is widely used in estimating discrete distributions and functionals of discrete distributions, and in fact the Dirichlet distribution is the conjugate prior of the categorical distribution and multinomial distribution.

In this chapter we propose a general multivariate construction methodology using the Dirichlet probability density function (pdf) as the generator. This Dirichlet-generated class serves as good alternatives to the Dirichlet and generalized Dirichlet distributions for the statistical representation of specific proportional data. This class is an evolution from the univariate framework describes below into a multivariate setting:

$$H(x) = \int_0^{G(x)} f(y)dy, \tag{1}$$

with pdf

$$h(x) = f\left(G(x)\right) g(x), \tag{2}$$

where $G(\cdot)$ is a continuous cumulative distribution function (cdf) and $f(\cdot)$ is the pdf of a random variable with support $[0, 1]$. By introducing extra parameters in $f(\cdot)$ and $G(\cdot)$ the resulting distribution provides greater flexibility in adapting modality and skewness. Eugene et al. (2002) was the first to introduce the family of beta-generated normal distribution with $f(y) = y^{\alpha-1}(1-y)^{\beta-1}/B(\alpha, \beta)$ as the pdf of the well-known beta distribution, where $B(\alpha, \beta) = \Gamma(\alpha)\Gamma(\beta)/\Gamma(\alpha+\beta)$ denotes the classical beta function and $\Gamma(\alpha) = \int_0^\infty v^{\alpha-1}e^{-v}dv$ is the gamma function defined for all $\alpha > 0$. The resulting cdf and pdf are respectively

$$H(x) = \frac{1}{B(\alpha, \beta)} \int_0^{G(x)} y^{\alpha-1}(1-y)^{\beta-1} dy \tag{3}$$

and

$$h(x) = \frac{1}{B(\alpha, \beta)} g(x) G^{\alpha-1}(x)[1-G(x)]^{\beta-1}, \tag{4}$$

where $\alpha > 0, \beta > 0$, and $g(\cdot)$ and $G(\cdot)$ are the pdf and cdf respectively. The beta distribution $f(\cdot)$ is referred to as the generator and $G(\cdot)$ as the baseline distribution. Another development of (4) is based on the ith order statistic in a random sample of n from a distribution $G(\cdot)$ with pdf $\{n!/[(i-1)!(n-i)!]\} g(x) G^{i-1}(x)[1 - G(x)]^{n-1}$ where (Jones 2004) extended the pdf of the ith order statistic by allowing $a = i$ and $b = n + 1 - i$ which is the pdf in (4). Note that the relation $X = G^{-1}(F(\cdot))$ with $F(\cdot)$ being a beta-distributed random variable, can be used to simulate X values. It is clear that special choices of the baseline model $G(\cdot)$ yield specific models generated by the classic beta distribution. In recent years, several scholars have shown great interest in defining new generalized classes of univariate continuous distributions by using this "mother technique" (see (1)) to generate new models. The interested reader is referred to Elgarhy et al. (2016) (and the references therein), Makgai et al. (2017), Alexander et a. (2012), Barreto et al. (2010), Nadarajah and Kotz (2006), Zografos and Balakrishnan (2009), Mameli (2015) and Nassar et al. (2019) for related studies, amongst others.

Mimicking the same construction methodology (1), three classes of extended bivariate distributions with the beta as generator, can be obtained as follows:

- Builder 1:

$$H(x_1, x_2) = \frac{1}{B(\alpha, \beta)} \int_0^{G(x_1)G(x_2)} y^{\alpha-1}(1-y)^{\beta-1} dy \tag{5}$$

- Builder 2:

$$H(x_1, x_2) = \frac{1}{B(\alpha, \beta)} \int_0^{G_1(x_1)G_2(x_2)} y^{\alpha-1}(1-y)^{\beta-1} dy \tag{6}$$

- Builder 3:

$$H(x_1, x_2) = \frac{1}{B(\alpha, \beta)} \int_0^{G^*(x_1,x_2)} y^{\alpha-1}(1-y)^{\beta-1} dy \tag{7}$$

where $G_i(\cdot), i = 1, 2$, can be any cdf of a baseline univariate distrbution and $G^*(\cdot, \cdot)$ is the cdf of the baseline bivariate distribution, $\alpha > 0, \beta > 0$.

From Builder 1, the pdf has the form

$$\begin{aligned} h(x_1, x_2) = {} & \frac{1}{B(\alpha, \beta)} G^{\alpha-1}(x_1) G^{\alpha-1}(x_2)[1-G(x_1)]^{\beta-1}[1-G(x_2)]^{\beta-1} \\ & \times [g(x_1)G(x_2) + G(x_1)g(x_2)], \end{aligned} \tag{8}$$

where $g(\cdot)$ is the pdf relative to the cdf $G(\cdot)$. In this case only one cdf contributes as baseline to develop the bivariate distribution and is a special case of Builders 2 and 3. The advantage of Builder 1 compared to Builder 2, is that it has fewer number of parameters. Makgai et al. (2019) proposed Builder 3 and studied the properties and dependence structure of the class formed along with multivariate beta-generated distribution. Samanthi and Sepanski (2019) employed copulas to construct a bivariate extension of beta-generated distributions.

From completely a different viewpoint, Sarabia et al. (2014) formed a bivariate distribution (see also Ristić et al. (2018)), using the (Olkin and Liu 2003) beta pdf as generator:

$$h(x_1, x_2) = \frac{1}{B(\alpha, \beta, \gamma)} g_1(x_1) g_2(x_2) \times \frac{G_1^{\alpha-1}(x_1) G_2^{\beta-1}(x_2)[1 - G_1(x_1)]^{\beta+\gamma-1}[1 - G_2(x_2)]^{\alpha+\gamma-1}}{[1 - G_1(x_1)G_2(x_2)]^{\alpha+\beta+\gamma}}. \tag{9}$$

However, the purpose of this study is not to study Builders 1–3, but to propose a general multivariate construction methodology using the Dirichlet pdf as the generator, with the baseline as the product of independent cdfs. This range of baseline distributions can be the exponential, Weibull, gamma, Fréchet, etc. Suppose that $G(\cdot)$ belongs to the Pareto class, then $H(\cdot)$ is referred to as the Dirichlet-Pareto distribution function. The introduction of the Dirichlet distribution as the generating distribution $F(\cdot)$, creates the opportunity to apply a wide range of multivariate distributions. In this context, Sect. 2 provides the basic elements of the construction, that will be described in Sect. 3, with specific emphasis on the Dirichlet-Gamma distribution. In Sect. 4 some properties of the newly proposed multivariate distribution are discussed. To illustrate the effectiveness of the latter model, the well-known Dirichlet distribution is compared to the Dirichlet-Gamma distribution via a simulation studies and an analysis of real datasets using different measures. Finally, some conclusions are given in Sect. 5.

2 Ingredients

In this section, the basic notation and definitions (ingredients) underlying the construction that will described in Sect. 3, are recalled. A random vector $\boldsymbol{Y} = (Y_1, \ldots, Y_p) \in \mathcal{R}^p$ is said to have Dirichlet distribution (or standard Dirichlet) with parameters $\boldsymbol{\alpha} = (\alpha_1, \cdots, \alpha_p; \alpha_{p+1})$ for $\alpha_i > 0, i = 1, \ldots, p+1,\ p \geq 2.$, if the pdf is given by

$$f(\boldsymbol{y}) = \frac{\Gamma(\alpha_+)}{\Gamma(\alpha_1) \cdots \Gamma(\alpha_{p+1})} y_1^{\alpha_1-1} \cdots y_p^{\alpha_p-1} \left(1 - \sum_{i=1}^{p} y_i\right)^{\alpha_{p+1}-1},$$

where $y_i > 0, i = 1, \ldots, p, \sum_{i=1}^{p} y_i < 1$, use $\alpha_+ = \sum_{i=1}^{p+1} \alpha_i$.

For convenience, denote $Y_{p+1} = 1 - \sum_{i=1}^{p} Y_i, \boldsymbol{Y}^{'} = (Y_1, \ldots, Y_p; Y_{p+1}) = (\boldsymbol{Y}; Y_{p+1})$ and write the above Dirichlet distribution as $\boldsymbol{Y} \sim Dir(\boldsymbol{\alpha})$, or simply $\boldsymbol{Y}^{'} \sim Dir(\boldsymbol{\alpha})$ with the understanding that $\boldsymbol{Y} \in \boldsymbol{\Omega}_p$ and $\boldsymbol{Y}^{'} \in \mathcal{S}_{p+1}$ where

$$\boldsymbol{\Omega}_p = \left\{ (y_1, \ldots, y_p) \in \mathcal{R}^p : \sum_{i=1}^{p} y_i < 1, y_i > 0, i = 1, \ldots, p \right\},$$

$$\boldsymbol{S}_{p+1} = \left\{ (y_1, \ldots, y_{p+1}) \in \mathcal{R}^{p+1} : \sum_{i=1}^{p+1} y_i = 1, y_i > 0, i = 1, \ldots, p+1 \right\}.$$

For any $\boldsymbol{\alpha}$ with $\alpha_i > 0, i = 1, \ldots, p+1$ and $y_{p+1} = 1 - \sum_{i=1}^{p} y_i$, the Dirichlet integral is:

$$\int_{\boldsymbol{\Omega}_p} \prod_{i=1}^{p+1} y_i^{\alpha_i - 1} d\,\boldsymbol{y} = \int \cdots \int_{\boldsymbol{\Omega}_p} \prod_{i=1}^{p+1} y_i^{\alpha_i - 1} dy_1 \cdots dy_p = B(\boldsymbol{\alpha}) = \frac{\prod_{i=1}^{p+1} \Gamma(\alpha_i)}{\Gamma(\alpha_+)}. \tag{10}$$

De Groot (1970) and Kotz et al. (2000) provide detailed discussions on the properties of the Dirichlet distribution.

Assume the baseline distributions to be Gamma(θ_i, β_i), $i = 1, \ldots, p$, with cdfs

$$G_i(x_i) = \frac{1}{\theta_i^{\beta_i} \Gamma(\beta_i)} \int_0^{x_i} e^{-\frac{t}{\theta_i}} t^{\beta_i - 1} dt, \quad \theta_i, \beta_i > 0, \ i = 1, \cdots, p, \tag{11}$$

for this chapter. The gamma distribution, which belongs to the exponential class, is a flexible distribution model with shape parameter β, that may offer a good fit to some sets of data.

3 Recipe

The construction methodology for the proposed model is as follows:

- Builder 4:

$$H(x_1, \ldots, x_p) = \int_0^{G_1(x_1)} \cdots \int_0^{G_p(x_p)} \frac{1}{B(\boldsymbol{\alpha})} y_1^{\alpha_1 - 1} \cdots y_p^{\alpha_p - 1} \left(1 - \sum_{i=1}^{p} y_i\right)^{\alpha_{p+1} - 1} d\,\boldsymbol{y} \tag{12}$$

where $G_i(\cdot), i = 1, \ldots, p$, can be any cdf.

Let the joint pdf of $G_i(\cdot), i = 1, \ldots, p$, be the Dirichlet pdf given by

$$
\begin{aligned}
& f(G_1, \ldots, G_p) \\
&= \frac{1}{B(\boldsymbol{\alpha})} G_1^{\alpha_1 - 1}(x_1) \ldots G_{p+1}^{\alpha_{p+1} - 1}(x_{p+1}), \quad 0 < G_i(\cdot) < 1, \sum_{i=1}^{p+1} G_i = 1 \\
&= \frac{1}{B(\boldsymbol{\alpha})} G_1^{\alpha_1 - 1}(x_1) \ldots G_p^{\alpha_p - 1}(x_p) \left(1 - \sum_{i=1}^{p} G_i(x_i)\right)^{\alpha_{p+1} - 1}, 0 < \sum_{i=1}^{p} G_i(x_i) < 1,
\end{aligned} \tag{13}
$$

i.e. the Dirichlet combines the marginals $G_i(\cdot), i = 1, \ldots, p$, with parameters $\boldsymbol{\alpha} = (\alpha_1, \cdots, \alpha_p; \alpha_{p+1})$ for $\alpha_i > 0, i = 1, \ldots, p+1$.

Then, according to (1), the joint generated distribution, namely the Dirichlet-Gamma (DG) has pdf

$$
h(\boldsymbol{x}) = \frac{1}{B(\boldsymbol{\alpha})} \left(1 - \sum_{i=1}^{p} G_i(x_i)\right)^{\alpha_{p+1} - 1} \prod_{i=1}^{p} g_i(x_i) G_i^{\alpha_i - 1}(x_i), \tag{14}
$$

for $\mathcal{R}^p$, $0 < \sum_{i=1}^{p} G_i(x_i) < 1$ and the parameters $\alpha_i, \theta_i, \beta_i$,$i = 1, \cdots, p$, are restricted to take those values for which (14) is non-negative, enote (14) as $\boldsymbol{X} \sim DG(\boldsymbol{\alpha}, \boldsymbol{\theta}, \boldsymbol{\beta})$.

Then, the marginal pdf of $X_i, i = 1, \ldots, p$, has the form

$$
h_i(x_i) = \frac{1}{B(\alpha_i, \alpha_+ - \alpha_i)} g_i(x_i) G_i^{\alpha_i - 1}(x_i) \left(1 - G_i(x_i)\right)^{\alpha_+ - \alpha_i - 1}, \tag{15}
$$

this is useful for determining the moments of $X_i, i = 1, \ldots, p,$.

Although the baseline cdf 's $G_i(\cdot)$ could be presented by several distributions in this chapter, the case where $g_i(\cdot)$ is the pdf Gamma(θ_i, β_i), $i = 1, \cdots, p$ is considered.

4 Properties

Firstly an expression for the product moments will be derived, followed by the moment generating function (mgf) of the $DG(\boldsymbol{\alpha}, \boldsymbol{\theta}, \boldsymbol{\beta})$ distribution. For this purpose, the following lemma is derived.

Lemma 1

$$
\mathcal{I}(\zeta) = \int \cdots \int_{\boldsymbol{\Omega}_p} \prod_{i=1}^{p} u_i^{\alpha_i - 1} \left(1 - \sum_{i=1}^{p} u_i\right)^{\zeta} d\boldsymbol{u} \tag{16}
$$

where $\boldsymbol{u} = (u_1, \ldots, u_p)$. *Then*

$$\mathcal{I}(\zeta) = \prod_{i=1}^{p-1} B\left(\alpha_i, \sum_{j=i+1}^{p} \alpha_j + \zeta + 1\right) B\left(\alpha_p, \zeta + 1\right). \tag{17}$$

Proof

$$\begin{aligned}\mathcal{I}(\zeta) &= \int_{\mathbf{\Omega}_p} \prod_{i=1}^{p} u_i^{\alpha_i - 1} \left(1 - \sum_{i=1}^{p} u_i\right)^{\zeta} \prod_{i=1}^{p} du_i \\ &= \int_{\mathbf{\Omega}_p} u_1^{\alpha_1 - 1} \prod_{i=2}^{p} u_i^{\alpha_i - 1} (1 - u_1)^{\zeta} \\ &\quad \times \left(1 - \sum_{i=1}^{p} \frac{u_i}{1 - u_1}\right)^{\zeta} \prod_{i=1}^{p} du_i.\end{aligned}$$

Now apply the transformation $v_i = \frac{u_i}{1-u_1}$, for $i = 2, \cdots, p$, with $J(u_2, \cdots, u_p \to v_2, \cdots, v_p) = (1 - u_1)^{p-1}$ to obtain

$$u_2 = v_2(1 - u_1), \quad \prod_{i=2}^{p} u_i^{\alpha_i - 1} = (1 - u_1)^{\sum_{i=2}^{p} \alpha_i - (p-1)} \prod_{i=2}^{p} v_i^{\alpha_i - 1}.$$

Hence this results in

$$\begin{aligned}\mathcal{I}(\zeta) &= \int_0^1 u_1^{\alpha_1 - 1} (1 - u_1)^{\zeta + \sum_{i=2}^{p} \alpha_i} du_1 \\ &\quad \times \int_{\mathbf{\Omega}^{p-1}} \prod_{i=2}^{p} v_i^{\alpha_i - 1} \left(1 - \sum_{i=2}^{p} v_i\right)^{\zeta} \prod_{i=2}^{p} dv_i \\ &= B\left(\alpha_1, \sum_{i=2}^{p} \alpha_i + \zeta + 1\right) \\ &\quad \times \int_{\mathbf{\Omega}^{p-1}} v_2^{\alpha_2 - 1} \prod_{i=3}^{p} v_i^{\alpha_i - 1} (1 - v_2)^{\zeta} \left(1 - \sum_{i=3}^{p} \frac{v_i}{1 - v_2}\right)^{\zeta} \prod_{i=2}^{p} dv_i.\end{aligned}$$

At this stage making the transformation $w_i = \frac{v_i}{1-v_2}$ once more, for $i = 3, \cdots, p$, with Jacobian equal to $(1 - v_2)^{p-2}$, it follows that

$$\begin{aligned}\mathcal{I}(\zeta) &= B\left(\alpha_1, \sum_{i=2}^{p} \alpha_i + \zeta + 1\right) B\left(\alpha_2, \sum_{i=3}^{p} \alpha_i + \zeta + 1\right) \\ &\quad \times \int_{\mathbf{\Omega}^{p-2}} \prod_{i=3}^{p} w_i^{\alpha_i - 1} \left(1 - \sum_{i=3}^{p} w_i\right)^{\zeta} \prod_{i=3}^{p} dw_i.\end{aligned}$$

Continuing this procedure, finally yields (17). □

The following result for the product moment is stated, assuming the pdf (14), holds.

Theorem 1 *Let n_i, $i = 1, \ldots, n_p$ are positive integer values. Then, the product moments of $\boldsymbol{X} \sim DG(\boldsymbol{\alpha}, \boldsymbol{\theta}, \boldsymbol{\beta})$ admit the following explicit form*

$$\mathcal{E} = E\left[\prod_{i=1}^{p} X_i^{n_i}\right] = \left(\prod_{i=1}^{p} \frac{\theta_i^{n_i}\Gamma(n_i+\beta_i)}{\Gamma(\beta_i)}\right) \times \left(\prod_{i=1}^{p-1} B\left(\alpha_i, \sum_{j=i+1}^{p} \alpha_j + \frac{\alpha_{p+1}-1}{p} + 1\right)\right) B\left(\alpha_p, \frac{\alpha_{p+1}-1}{p} + 1\right).$$

Proof From (14), for $\boldsymbol{X} = (X_1, \ldots, X_p)$, it follows that

$$\begin{aligned}
\mathcal{E} &= \int\limits_{\mathcal{R}^p, \sum_{j=1}^{p} G_j(x_j)<1} \frac{1}{B(\boldsymbol{\alpha})} \prod_{i=1}^{p} x_i^{n_i} \left(1 - \sum_{j=1}^{p} G_j(x_j)\right)^{\alpha_{p+1}-1} \\
&\quad \times \prod_{j=1}^{p} g_j(x_j) G_j^{\alpha_j - 1}(x_j) d\boldsymbol{x} \\
&= \frac{1}{B(\boldsymbol{\alpha})} \int\limits_{\mathcal{R}^p, \sum_{j=1}^{p} G_j(x_j)<1} \prod_{i=1}^{p} \frac{\theta_i^{n_i}\Gamma(n_i+\beta_i)}{\Gamma(\beta_i)} G_i^{\alpha_i-1}(x_i) \left(1 - \sum_{i=1}^{p} G_i(x_i)\right)^{\frac{(\alpha_{p+1}-1)}{p}} \\
&\quad \times \frac{1}{\theta_i^{n_i+\beta_i}\Gamma(n_i+\beta_i)} e^{-\frac{x_i}{\theta_i}} x_i^{n_i+\beta_i-1} d\boldsymbol{x} \\
&= E\left\{\prod_{i=1}^{p} \frac{\theta_i^{n_i}\Gamma(n_i+\beta_i)}{\Gamma(\beta_i)} G_i^{\alpha_i-1}(V_i) \left(1 - \sum_{i=1}^{p} G_i(V_i)\right)^{\frac{(\alpha_{p+1}-1)}{p}}\right\}
\end{aligned}$$

where $V_i \sim Gamma(\theta_i, n_i + \beta_i)$. Using the fact that $G_i(V_i) \equiv U_i \sim U(0,1)$, it follows that

$$\begin{aligned}
\mathcal{E} &= \prod_{i=1}^{p} \frac{\theta_i^{n_i}\Gamma(n_i+\beta_i)}{\Gamma(\beta_i)} E\left\{\prod_{i=1}^{p} U_i^{\alpha_i-1} \left(1 - \sum_{i=1}^{p} U_i\right)^{\frac{(\alpha_{p+1}-1)}{p}}\right\} \\
&= \prod_{i=1}^{p} \frac{\theta_i^{n_i}\Gamma(n_i+\beta_i)}{\Gamma(\beta_i)} \int\limits_{\boldsymbol{\Omega}_p} \prod_{i=1}^{p} u_i^{\alpha_i-1} \left(1 - \sum_{i=1}^{p} u_i\right)^{\frac{(\alpha_{p+1}-1)}{p}} d\boldsymbol{u}.
\end{aligned}$$

The theorem is completed by applying the Lemma for $\mathcal{I}\left(\frac{\alpha_{p+1}-1}{p}\right)$. ■

Theorem 2 *The moment generating function (mgf) of* $\boldsymbol{X} \sim DG(\boldsymbol{\alpha}, \boldsymbol{\theta}, \boldsymbol{\beta})$ *is given by*

$$M_{\boldsymbol{X}}(\boldsymbol{t}) = \frac{1}{B(\boldsymbol{\alpha})} \sum_{m=0}^{\infty} \frac{1}{m!} \sum_{n_1+n_2+\cdots+n_p=m} \frac{m!}{n_1!n_2!\cdots n_p!} \prod_{i=1}^{p} (t_i)^{n_i}$$
$$\times \left(\prod_{i=1}^{p} \frac{\theta_i^{n_i} \Gamma(n_i + \beta_i)}{\Gamma(\beta_i)} \right) \prod_{i=1}^{p-1} B\left(\alpha_i, \sum_{j=i+1}^{p} \alpha_j + \frac{\alpha_{p+1} - 1}{p} + 1 \right)$$
$$B\left(\alpha_p, \frac{\alpha_{p+1} - 1}{p} + 1 \right)$$

where, $\boldsymbol{t} = (t_1, \ldots, t_p)$, $\boldsymbol{x} = (x_1, \ldots, x_p)$ $\boldsymbol{\theta} = (\theta_1, \cdots, \theta_p)$ *and* $\boldsymbol{\beta} = (\beta_1, \cdots, \beta_p)$.

Proof It follows that

$$\begin{aligned}
M_{\boldsymbol{X}}(\boldsymbol{t}) &= E\left[e^{\boldsymbol{t}\boldsymbol{X}^\top} \right] \\
&= \int_{\mathcal{R}^p, \sum_{j=1}^{p} G_j(x_j) < 1} e^{\boldsymbol{t}\boldsymbol{x}^\top} h(\boldsymbol{x}) d\boldsymbol{x} \\
&= \int_{\mathcal{R}^p, \sum_{j=1}^{p} G_j(x_j) < 1} \sum_{m=0}^{\infty} \frac{1}{m!} (\boldsymbol{t}\boldsymbol{x}^\top)^m h(\boldsymbol{x}) d\boldsymbol{x} \\
&= \int_{\mathcal{R}^p, \sum_{j=1}^{p} G_j(x_j) < 1} \sum_{m=0}^{\infty} \frac{1}{m!} \sum_{n_1+n_2+\cdots+n_p=m} \frac{m!}{n_1!n_2!\cdots n_p!} \prod_{i=1}^{p} (t_i x_i)^{n_i} h(\boldsymbol{x}) d\boldsymbol{x} \\
&= \frac{1}{B(\boldsymbol{\alpha})} \sum_{m=0}^{\infty} \frac{1}{m!} \sum_{n_1+n_2+\cdots+n_p=m} \frac{m!}{n_1!n_2!\cdots n_p!} \prod_{i=1}^{p} (t_i)^{n_i} E\left[\prod_{i=1}^{p} X_i^{n_i} \right]
\end{aligned}$$

where $\top$ denotes transpose of vector.

The result follows by Theorem 1. ∎

5 The Proof of the Pudding Is...

The basic construction of the $DG(\boldsymbol{\alpha}, \boldsymbol{\theta}, \boldsymbol{\beta})$ model entails embedding the cdf of a gamma distribution within the pdf of the Dirichlet distribution, that acts as a generator. The exact generation procedure for the Dirichlet-Gamma random variates is given as Algorithm 1 follows:

Algorithm 1

Step 1: Generate independent gamma random variables $W_1, W_2, \ldots, W_{p+1}$ where $W_i \sim Gamma(\alpha_i, 1)$ for $\alpha_i > 0, i = 1, 2, \ldots, p+1$;

Step 2: Set $Y_i = \frac{W_i}{\sum_{j=1}^{p} W_j}$ for $i = 1, 2, \ldots, p$;

Step 3: Return $(Y_1, Y_2, \ldots, Y_p)$ and let $(Y_1, Y_2, \cdots, Y_p) \equiv (G_1(x_1), G_2(x_2), \ldots, G_p(x_p))$ with $\sum_{i=1}^{p} G_i(x_i) < 1$, where $G_i(x_i)$ is the cdf of the gamma distribution;

Step 4: Set $X_i = G_i^{-1}(y_i)$ for $i = 1, 2, \ldots, p$;

Step 5: Return $(X_1, X_2, \cdots, X_p)$ where $X \sim DG(\boldsymbol{\alpha}, \boldsymbol{\theta}, \boldsymbol{\beta})$ for parameters $\alpha_i, \theta_j, \beta_j > 0, i = 1, 2, \ldots, p+1; j = 1, 2, \ldots, p$.

5.1 Model Presentation

In Figs. 1, 2, 3, 4, 5, and 6, various pdfs and contour plots of (14) for different values of $(\boldsymbol{\alpha}, \boldsymbol{\theta}, \boldsymbol{\beta})$ are provided. A 1000 simulated Dirichlet-Gamma values accompany the graphs.

5.2 Simulation Study 1

Suppose N vector observations $\boldsymbol{X}_1, \ldots, \boldsymbol{X}_N$ of dimension $(p-1) \times 1$ are drawn independently and identically from the $DG(\boldsymbol{\alpha}, \boldsymbol{\theta}, \boldsymbol{\beta})$ distribution. Therefore, the log-likelihood of $\boldsymbol{\psi} = (\boldsymbol{\alpha}, \boldsymbol{\theta}, \boldsymbol{\beta})$ based on the observed data $\{\boldsymbol{X}_i\}_{i=1}^{N}$ from (14) is

$$l(\boldsymbol{\psi}) = \sum_{i=1}^{N} \log h(\boldsymbol{x}; \boldsymbol{\psi}).$$

The above simulation Algorithm 1 is used to generate samples of size 100, 500 and 1000. Using 1000 trials for each group of fixed parameters, 1000 ML estimates of the model parameters (using the optim procedure in R software) is obtained.

To investigate the estimation accuracies, calculate the mean, bias and mean square error (MSE), defined as

$$\text{Bias} = \frac{1}{1000} \sum_{k=1}^{1000} \widehat{\psi}_k - \psi_{true} \quad \text{and} \quad \text{MSE} = \frac{1}{1000} \sum_{k=1}^{1000} \left(\widehat{\psi}_k - \psi_{true}\right)^2,$$

are calculated, where $\widehat{\psi}_k$ denotes the ML estimate of ψ_{true} (a specific parameter) at the kth replication. The detailed numerical results are reported in Tables 1, 2, and 3.

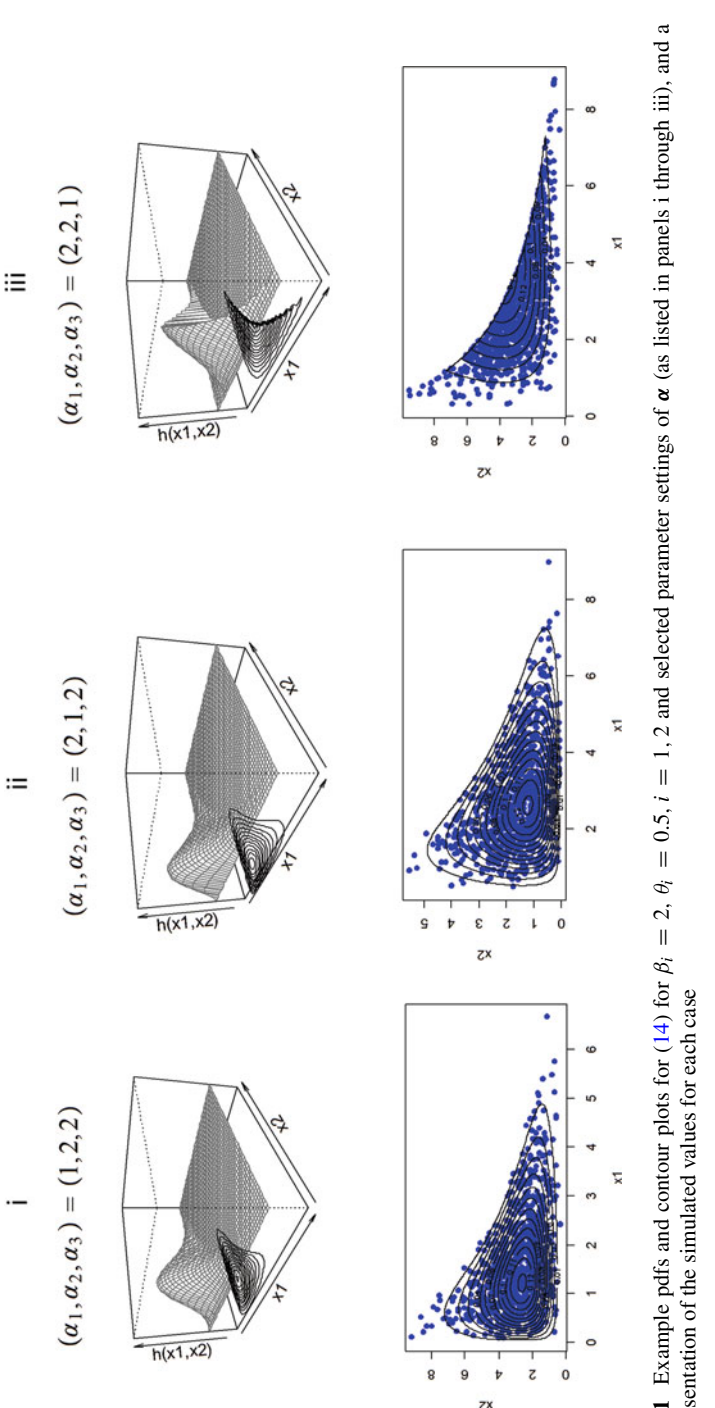

Fig. 1 Example pdfs and contour plots for (14) for $\beta_i = 2$, $\theta_i = 0.5$, $i = 1, 2$ and selected parameter settings of $\boldsymbol{\alpha}$ (as listed in panels i through iii), and a representation of the simulated values for each case

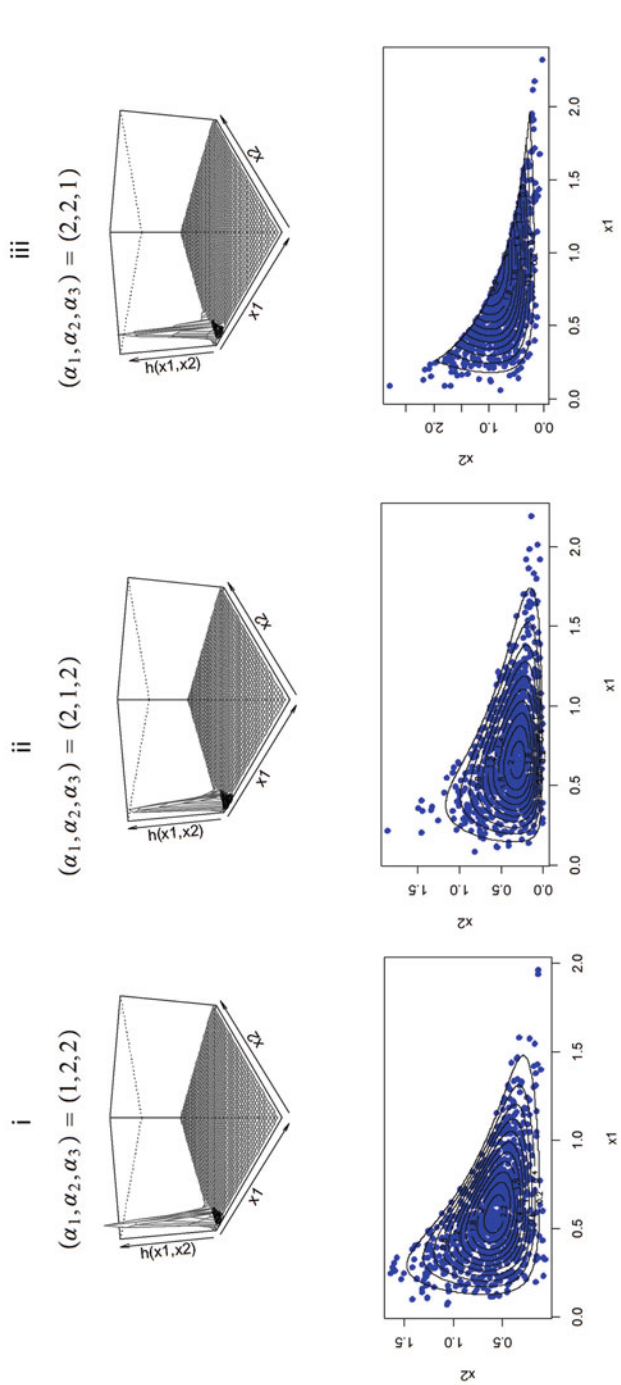

Fig. 2 Example pdfs and contour plots for (14) for $\beta_i = 2$, $\theta_i = 2$, $i = 1, 2$ and selected parameter settings of $\boldsymbol{\alpha}$ (as listed in panels i through iii), and a representation of the simulated values for each case. (The cdf (11) in this case simplifies to the χ^2 distribution)

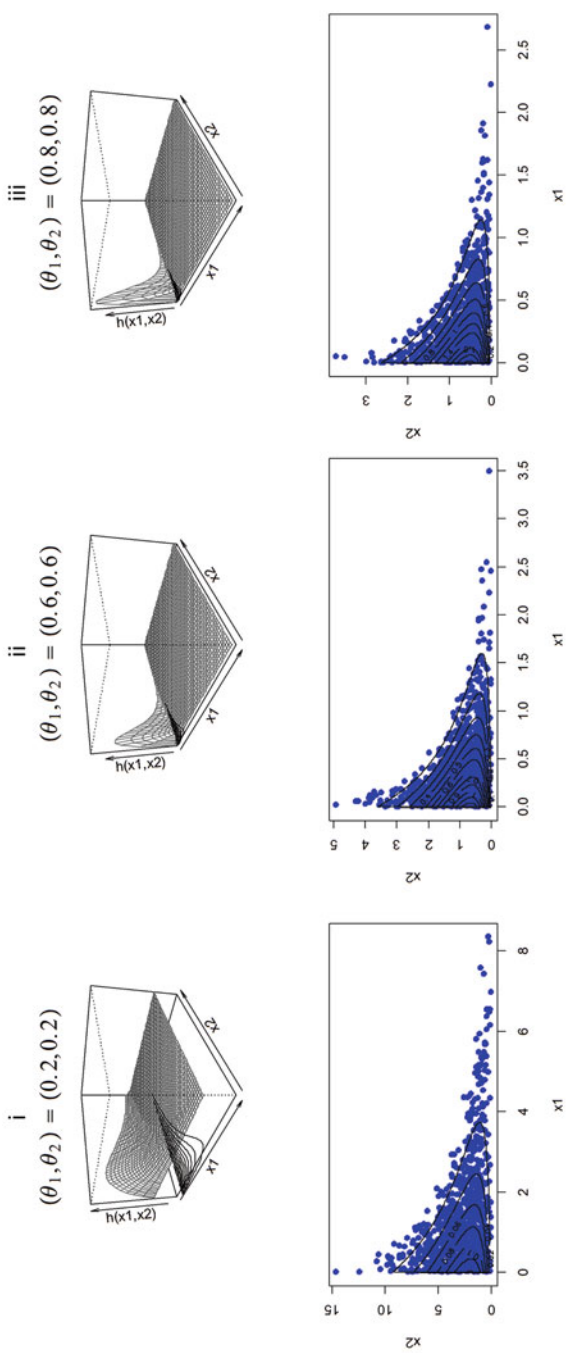

Fig. 3 Example pdfs and contour plots for (14) for $\beta_i = 1, i = 1, 2, \boldsymbol{\alpha} = (1, 2, 2)$ and selected parameter setting of $\boldsymbol{\theta}$ (as listed in panels i through iii), and a representation of the simulated values for each case

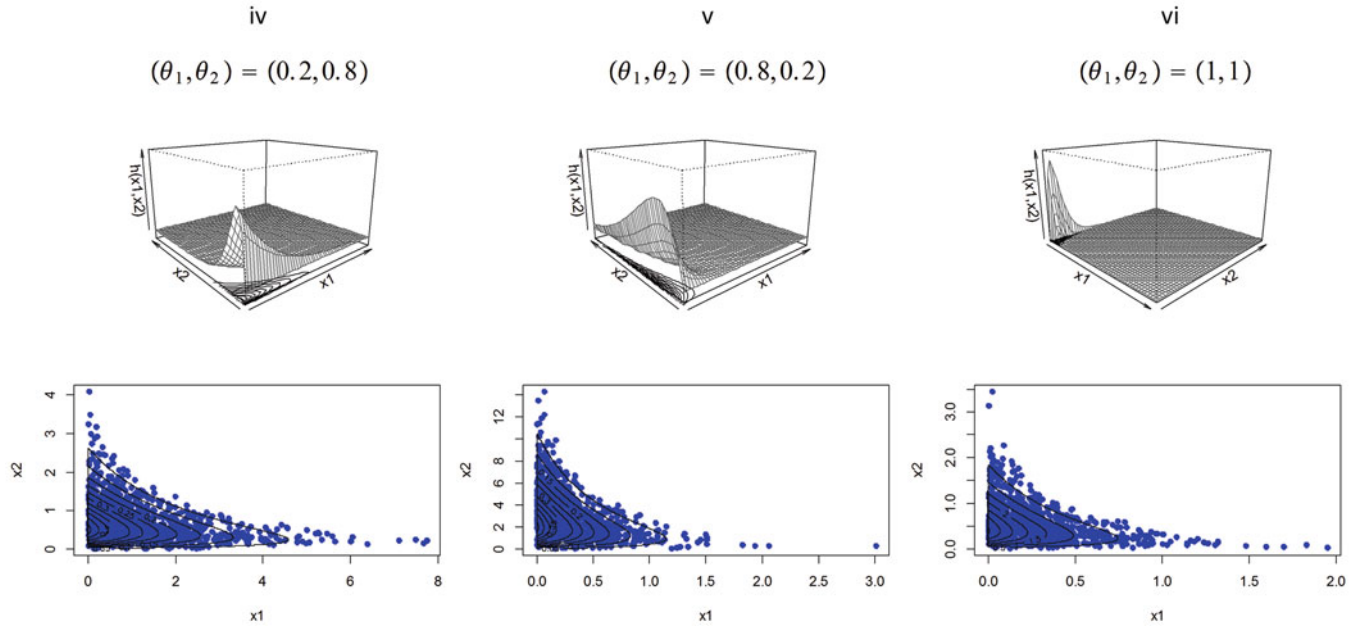

Fig. 4 Example pdfs and contour plots for (14) for $\beta_i = 1, i = 1, 2, \boldsymbol{\alpha} = (1, 2, 2)$ and selected parameter setting of $\boldsymbol{\theta}$ (as listed in panels iv through vi), and a representation of the simulated values for each case

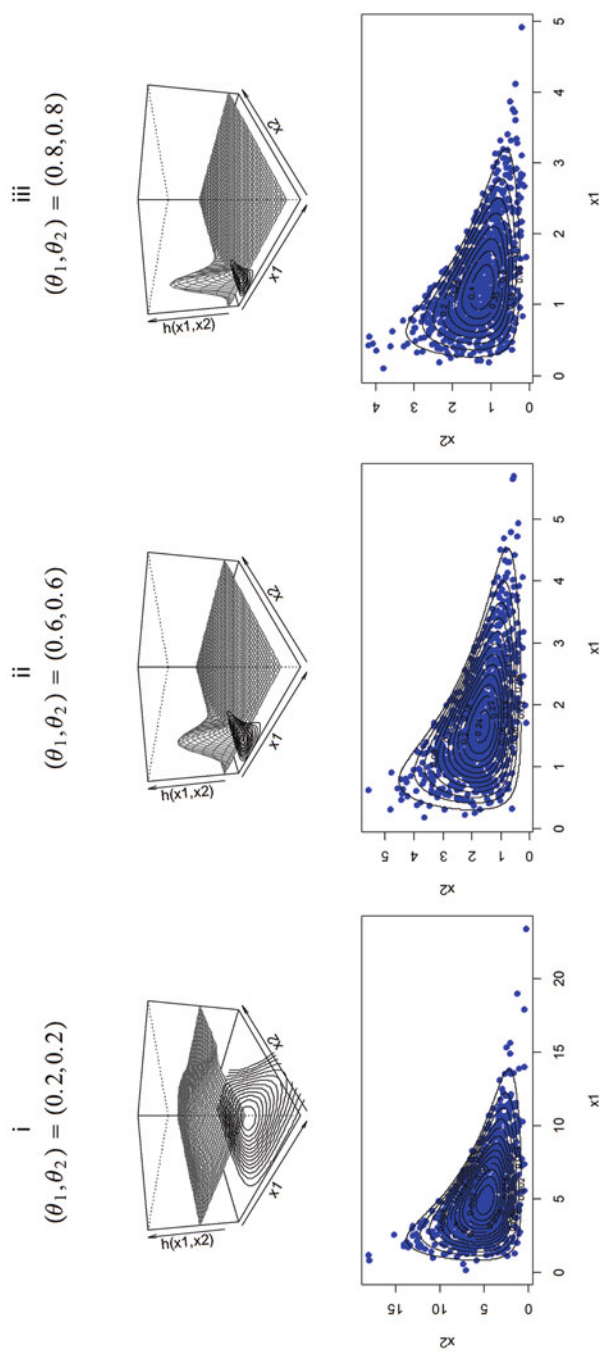

Fig. 5 Example pdfs and contour plots for (14) for $\alpha_i = 2, i = 1, 2, 3$, $\beta_j = 1.8, j = 1, 2$ and selected parameter settings of $\boldsymbol{\theta}$ (as listed in panels i through iii), and a representation of the simulated values for each case

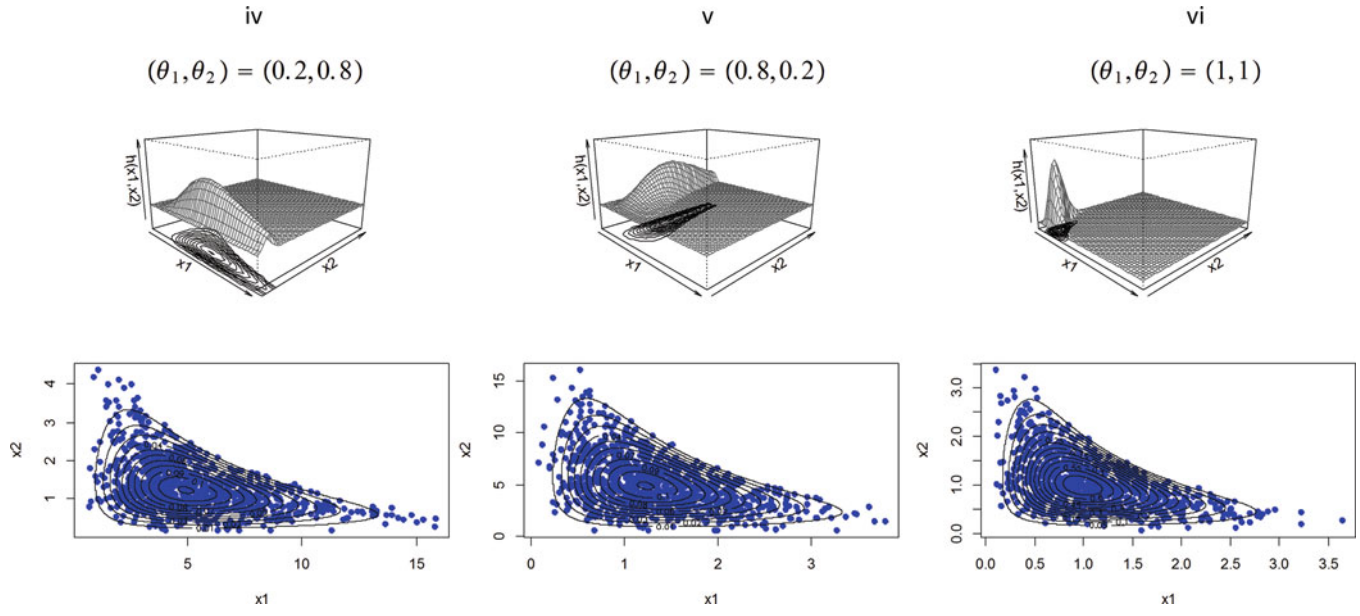

Fig. 6 Example pdfs and contour plots for (14) for $\alpha_i = 2$, $i = 1, 2, 3$, $\beta_j = 1.8$, $j = 1, 2$ and selected parameter settings of $\boldsymbol{\theta}$ (as listed in panels iv through vi), and a representation of the simulated values for each case

Table 1 Results for $n = 100$ and $\boldsymbol{\psi} = (\alpha_1, \alpha_2, \alpha_3, \beta_1, \beta_2, \theta_1, \theta_2) = (2, 2, 3, 1.5, 2.8, 1.1, 1.2)$

$n = 100$	$\widehat{\alpha}_1$	$\widehat{\alpha}_2$	$\widehat{\alpha}_3$	$\widehat{\beta}_1$	$\widehat{\beta}_2$	$\widehat{\theta}_1$	$\widehat{\theta}_2$
Mean	2.158	2.123	2.861	1.604	2.975	1.222	1.307
Bias	0.158	0.123	−0.139	0.104	0.175	0.122	0.107
MSE	0.861	0.711	0.688	0.297	0.723	0.144	0.137
CP asymptotic CI	0.945	0.943	0.961	0.949	0.946	0.927	0.945
CP bootstrapped CI	0.967	0.964	0.966	0.965	0.971	0.965	0.968
Length of asymptotic CI	3.585	3.273	3.206	2.098	3.263	1.406	1.391
Length of bootstrapped CI	2.876	2.604	5.897	2.839	4.894	1.975	1.762

Table 2 Results for $n = 500$ and $\boldsymbol{\psi} = (\alpha_1, \alpha_2, \alpha_3, \beta_1, \beta_2, \theta_1, \theta_2) = (2, 2, 3, 1.5, 2.8, 1.1, 1.2)$

$n = 500$	$\widehat{\alpha}_1$	$\widehat{\alpha}_2$	$\widehat{\alpha}_3$	$\widehat{\beta}_1$	$\widehat{\beta}_2$	$\widehat{\theta}_1$	$\widehat{\theta}_2$
Mean	2.018	2.025	2.928	1.535	2.851	1.138	1.234
Bias	0.018	0.025	−0.072	0.035	0.051	0.038	0.034
MSE	0.182	0.161	0.111	0.054	0.156	0.028	0.027
CP asymptotic CI	0.946	0.939	0.948	0.950	0.938	0.940	0.937
CP bootstrapped CI	0.974	0.974	0.975	0.975	0.975	0.975	0.974
Length of asymptotic CI	1.670	1.571	1.278	0.903	1.537	0.635	0.627
Length of bootstrapped CI	2.124	1.951	2.848	1.478	2.755	1.207	1.341

Table 3 Results for $n = 1000$ and $\boldsymbol{\psi} = (\alpha_1, \alpha_2, \alpha_3, \beta_1, \beta_2, \theta_1, \theta_2) = (2, 2, 3, 1.5, 2.8, 1.1, 1.2)$

$n = 1000$	$\widehat{\alpha}_1$	$\widehat{\alpha}_2$	$\widehat{\alpha}_3$	$\widehat{\beta}_1$	$\widehat{\beta}_2$	$\widehat{\theta}_1$	$\widehat{\theta}_2$
Mean	1.999	2.005	2.963	1.526	2.837	1.125	1.224
Bias	−0.001	0.005	−0.038	0.026	0.037	0.025	0.024
MSE	0.099	0.082	0.059	0.032	0.083	0.016	0.015
CP asymptotic CI	0.946	0.944	0.942	0.937	0.938	0.927	0.935
CP bootstrapped CI	0.975	0.975	0.975	0.975	0.975	0.975	0.975
Length of asymptotic CI	1.237	1.125	0.941	0.690	1.118	0.488	0.478
Length of bootstrapped CI	2.010	2.020	2.847	1.456	2.754	1.237	1.270

For a large sample size the asymptotic distribution of the ML estimates can be used to construct asymptotic confidence intervals. The asymptotic distribution of the ML estimate of ψ is

$$\frac{\widehat{\psi} - \psi}{\sqrt{Var\left(\widehat{\psi}\right)}} \sim N\left(0, 1\right).$$

Confidence intervals (CI) for the model parameters by implementing the parametric bootstrap method are also provided. Tables 1, 2, and 3 reflect also the coverage probabilities (CP) and average lengths of the intervals based on these two methods.

It can be observed that the bias and MSE of the $\boldsymbol{DG}(\boldsymbol{\alpha}, \boldsymbol{\theta}, \boldsymbol{\beta})$ distribution tend to decrease toward zero by increasing sample size (n), showing empirically the consistency of the ML estimates. The MSE of the estimates of $\widehat{\boldsymbol{\beta}}$ is higher than $\widehat{\boldsymbol{\theta}}$, as one would expect from the shape parameter of the gamma baselines. As the sample size changes from 100 to 1000, the average length of confidence intervals do decrease.

5.3 *Simulation Study 2*

A model testing technique, referred to in this chapter as the empirical estimator of the cdf of a multivariate distribution, is proposed in analysing the performances of the two competing models, namely the Dirichlet (D) and Dirichlet-Gamma (DG). The technique compares the empirical cdfs of the observed and simulated datasets. The following steps (Algorithm 2) are taken in order to assess the competence of the models.

The advantage of this technique, is that one can also use the empirical cdfs to rank the simulated data. Ranking data makes it possible to calculate more accurate distances between the observed data points and the simulated points. Figure 7 illustrates an observed dataset (in black) and simulated points from the simulated artificial datasets Dirichlet (in blue) and the Dirichlet-Gamma (in red). The challenge lies in choosing the correct simulated point to calculate the distances. The solution that is proposed in this chapter is to rank the simulated data from

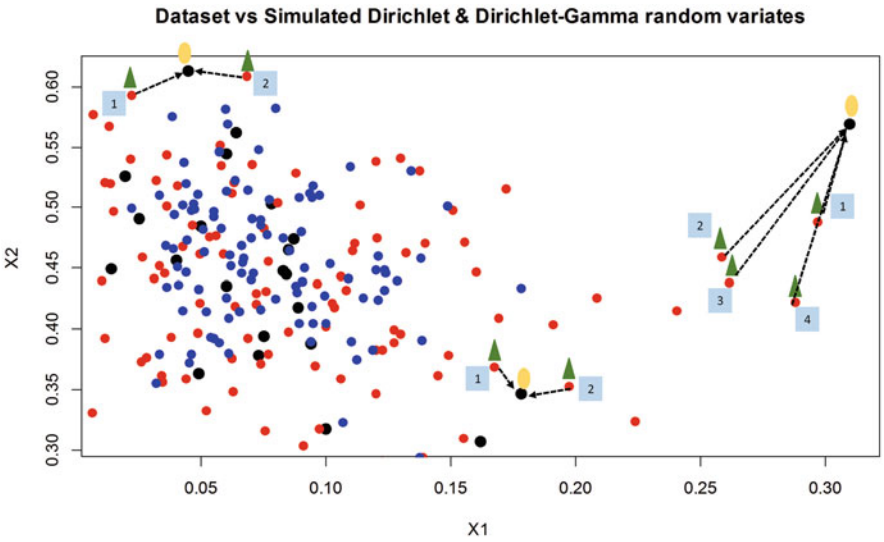

Fig. 7 Observed data versus the simulated data from Dirichlet and Dirichlet-Gamma models

Algorithm 2

Step 1: From the observed dataset $x_{n\times p}$, calculate the empirical cdf
$\widehat{F(\mathbf{x})} = P\left(X_1 \le x_1, X_2 \le x_2, \cdots, X_p \le x_p\right) = \frac{1}{n}\sum_{i=1}^{p} I\left(x_i \le x\right)$,
where $I(\cdot)$ is the indicator function;

Step 2: Obtain the parameter estimates for the two competing models, D and DG distributions and simulate artificial datasets;
$x_D^* = \left(x_1^*, x_2^*, \cdots, x_p^*\right)$ and $x_{DG}^* = \left(x_1^*, x_2^*, \cdots, x_p^*\right)$ of sizes $d > n$.

Step 3: Calculate the empirical cdfs for each simulated artificial dataset
$\widehat{F(\mathbf{x}^*)} = P\left(X_1^* \le x_1, X_2^* \le x_2, \cdots, X_p^* \le x_p\right) = \frac{1}{d}\sum_{i=1}^{p} I\left(x_i^* \le x\right)$;

Step 4: Repeat step 2–3 m times, and for each simulation, compute Kolmogorov-Smirnov (KS) distances between the empirical cdf (as computed in step 1) and the empirical cdfs of the competing models (as computed in step 3) where KS measure is defined in this case as $KS = \max\left|\widehat{F(\mathbf{x}^*)} - \widehat{F(\mathbf{x})}\right|$

Step 5: Compute the average KS distances over the m simulated artificial datasets;

Step 6: Compare the KS distances of the DG to the KS distance of the D in terms of the ratio $\frac{KS of DG}{KS of D}$.

the two competing models according to their calculated empirical cdfs respectively. The distances (as shown with the arrows) between the observed (in black) and the simulated data points can be more accurately calculated based on the quantile positions.

In this chapter for the implementation of this technique, the focus is on the ratio of the KS distances between the two competing models. To test this model testing technique, generate a "observed" dataset from a Dirichlet distribution and analyse the performance of the Dirichlet-Gamma through the steps. Since the KS distances vary from simulation to simulation, samples of sizes $d = 100, 1000, 10{,}000$ are generated from the obtained parameter estimates for Dirichlet and Dirichlet-Gamma from the observed, where KS distances are calculated for each simulated dataset group.

1. Generate an artificial dataset from the Dirichlet distribution with parameters $(\alpha_1, \alpha_2, \alpha_3) = (2, 2, 3)$ and assume it as the observed data;
2. Using this observed dataset, obtain parameter estimates for the Dirichlet and Dirichlet-Gamma distributions;
3. From the obtained parameter estimates simulate datasets of sizes $d = 100, 1000, 10{,}000$. Calculate the empirical cdfs for each simulation, as seen in step 3 of Algorithm 2;

4. Calculate the KS distances between the empirical cdf and the cdfs of the two competing models, for each group;
5. Repeat steps (3–4) a 100 times and compute the average KS distance for the two models.
6. Represent the KS distance of the Dirichlet-Gamma and Dirichlet as a ratio $\frac{KSofDG}{KSofD}$ for each simulated group of $d = 100, 1000, 10{,}000$.

It is observed in Fig. 8 that the Dirichlet-Gamma distribution is flexible enough to model Dirichlet distributed variables. The KS distance of the Dirichlet-Gamma is seen to be smaller for all simulated groups.

5.4 Simulation Study 3

A further simulation study is carried out to illustrate the flexibility of the Dirichlet-Gamma when outliers are present within a dataset. Suppose that two non-Dirichlet artificial compositional datasets, where outliers are present, are generated, using Algorithm 3.

Algorithm 3

Step 1: Generate n random variates $W_i \sim Weibull\,(k_i, \lambda_i)$ for $i = 1, 2, 3$.

Step 2: Define random variables $Y = (Y_1, Y_2, Y_3)$, where $Y_i = \frac{W_i}{\sum_{i=1}^{3} W_i}$, $i = 1, 2, 3$.

and generate artificial dataset $y = (y_1, y_2, y_3)$

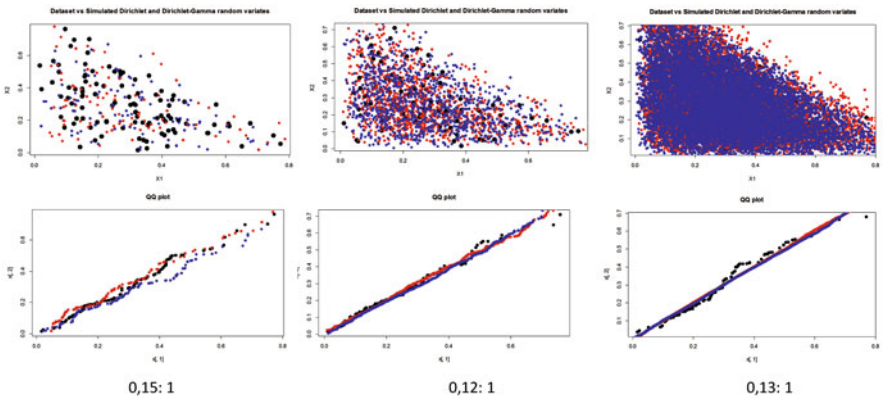

Fig. 8 Performance of the Dirichlet-Gamma on a generated "observed" Dirichlet dataset

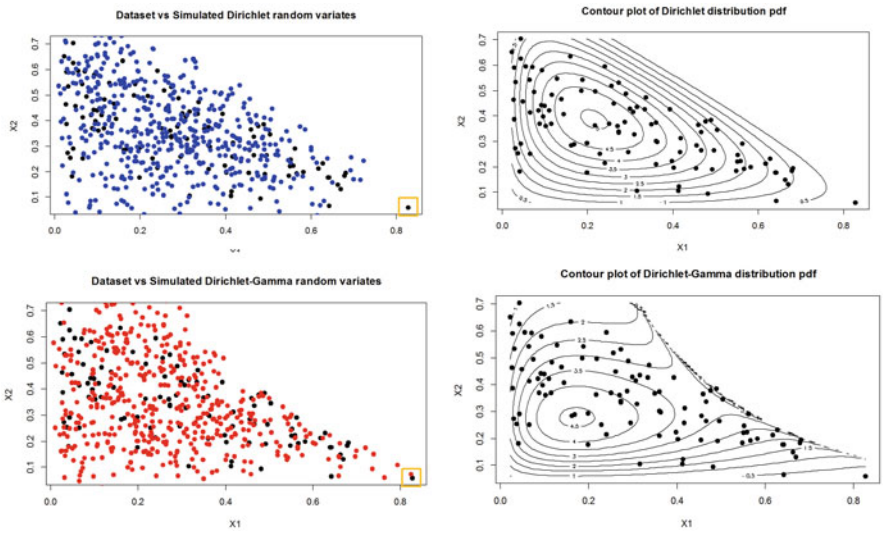

Fig. 9 Contour plots of simulated Gamma and Dirichlet-Gamma datasets on a non-Dirichlet artificial dataset 1

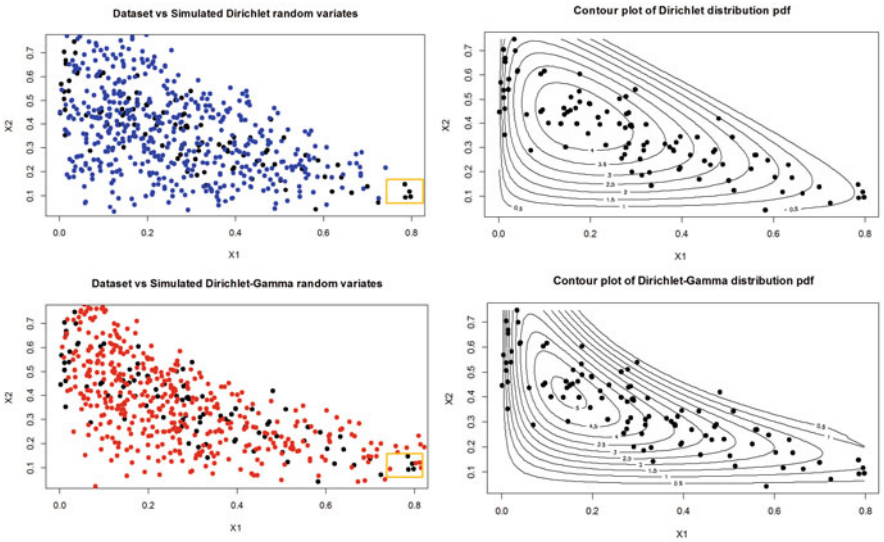

Fig. 10 Contour plots of simulated Gamma and Dirichlet-Gamma datasets on a non-Dirichlet artificial dataset 2

The construction of random variables Y_1, Y_2, Y_3 yields a compositional dataset with a negative correlation. The initial values for the Dirichlet and Dirichlet-Gamma used in the R package *optim* are obtained through a grid search. Figures 9 and 10 illustrates the flexibility of the Dirichlet-Gamma over ousstliers.

5.5 Real Data Analysis

To investigate the performance of the Dirichlet-Gamma distribution with respect to the Dirichlet distribution, different goodness-of-fit measures will be used to evaluate the models as candidates for the different datasets, namely the Q-Q plot, the Akaike information criterion (AIC, Akaike (1998)) and the Bayesian information criterion (BIC, Schwarz (1978)), with the last 2 measures defined as

$$\text{AIC} = 2m - 2l_{max} \quad \text{and} \quad \text{BIC} = m \log N - 2l_{max},$$

where m is the number of free parameters and l_{max} is the maximized log-likelihood value. Models with lower values of AIC and BIC are considered more preferable.

5.5.1 EXAMPLE 1-Pekin Ducklings Dataset

As first illustration, the Serum-protein data of white Pekin ducklings are considered (see Mosimann (1962)). To illustrate the performance of the Dirichlet-Gamma model with respect to extreme outlying observations, observation 20 of the dataset was perturbated. The blood serum proportions (pre-albumin, albumin and globulin) in 3-week-old Pekin ducklings were reported with correlation matrix:

$$\begin{bmatrix} 1 & -0.108 & -0.557 \\ -0.108 & 1 & -0.766 \\ -0.557 & -0.766 & 1 \end{bmatrix}.$$

Using randomly chosen initial parameter values $(\alpha_1, \alpha_2, \alpha_3) = (6.856, 2.392, 1)$ and $(\alpha_1, \alpha_2, \alpha_3, \beta_1, \theta_1, \beta_2, \theta_2) = (2.016, 2.757, 3.318, 0.559, 0.826, 1.569, 1.876)$ to obtain the ML estimates of the Dirichlet and Dirichlet-Gamma respectively with the optim package in R. The simulated Dirichlet and Dirichlet-gamma random variates are obtained using the ML estimates. Figure 11 shows the Q-Q plots on distances to origin of observed and Dirichlet simulated data.

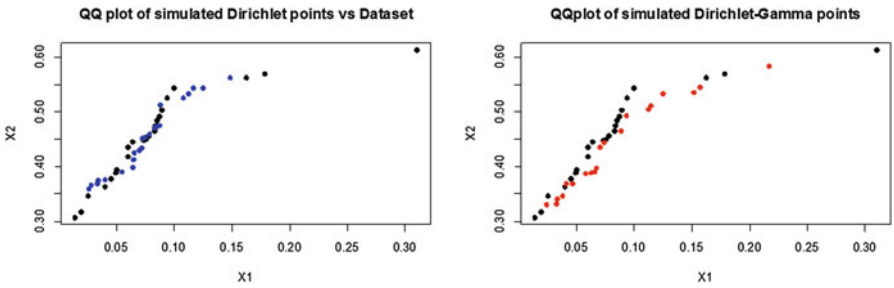

Fig. 11 Q-Q plots on distances to origin of observed and Dirichlet and Dirichlet-Gamma simulated data

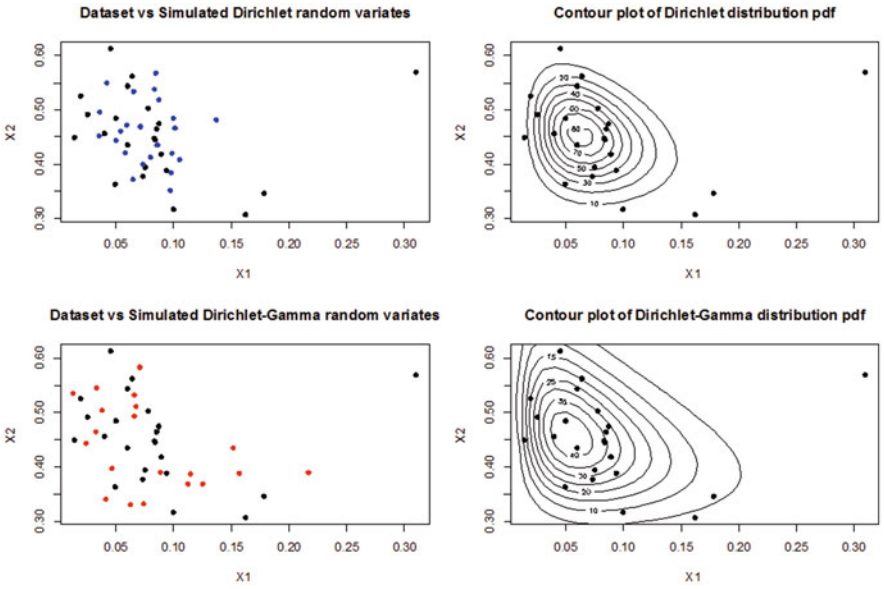

Fig. 12 Scatter plots and contour plots of the observed data versus the simulated data

Table 4 Parameter estimates and the performance summary for the Pekin duckling dataset

	ML estimates									
Model	$\widehat{\alpha}_1$	$\widehat{\alpha}_2$	$\widehat{\alpha}_3$	$\widehat{\beta}_1$	$\widehat{\beta}_2$	$\widehat{\theta}_1$	$\widehat{\theta}_2$	*ll*	AIC	BIC
Dirichlet	4.786	28.798	30.653	n/a	n/a	n/a	n/a	−79.797	165.594	169.0015
DG	2.173	2.466	13.998	0.971	1.383	6.711	8.537	−63.205	140.409	148.358

Figure 12 shows the observed data (black dots) versus simulated data from the Dirichlet distribution (blue dots), accompanied by a contour plot. It is clear that the Dirichlet distribution does not cover all the data points well. Similarly, the red dots show the simulated Dirichlet–Gamma values with a contour plot (second row on Fig. 12). The results presented in Fig. 12, illustrates that the Dirichlet-Gamma distribution provides a dataset closer to the observed data compared to the Dirichlet distribution. The Dirichlet-Gamma covers the outlier while the Dirichlet model could not detect it. Table 4 shows a summary of the ML fittings (note Log-likelihood is indicated as *ll* in the tables).

Using the model testing technique as described by Algorithm 2, it is observed that the KS distance is smaller in the case of the proposed Dirichlet-Gamma model versus the Dirichlet model (see Fig. 13).

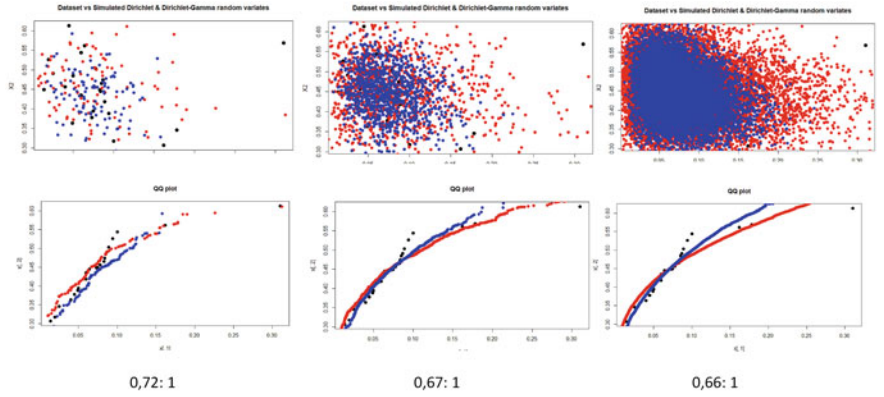

Fig. 13 Performance of Dirichlet–Gamma: Gamma based on the empirical estimator of the cdf of a multivariate distribution

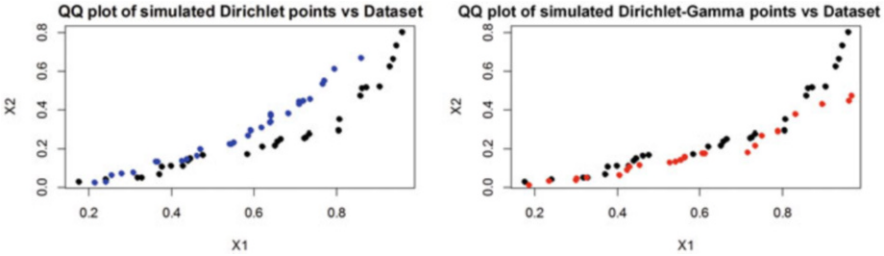

Fig. 14 Q-Q plots on distances to origin of observed and Dirichlet and Dirichlet-Gamma simulated data

5.5.2 EXAMPLE 2-White Cells Dataset

Three kind of white cells (granulocytes, lymphocytes, monocytes) found in 30 blood samples are recorded in this dataset. The inputs result in 30 pairs of 3-part compositions of the white cells, where each portion was determined through time-consuming microscopic and automatic image analysis. The correlation matrix is given as

$$\begin{bmatrix} 1 & -0.832 & -0.405 \\ -0.832 & 1 & -0.170 \\ -0.405 & -0.170 & 1 \end{bmatrix}.$$

The Dirichlet and the Dirichlet-Gamma distributions are tested to see if they are suitable contenders of this dataset. Using randomly chosen initial parameter values $(\alpha_1, \alpha_2, \alpha_3) = (1, 1, 1)$ and $(\alpha_1, \alpha_2, \alpha_3, \beta_1, \theta_1, \beta_2, \theta_2) = (2, 3, 7, 1, 1.5, 0.5, 1)$ in this case. The Q-Q plots, scatter plots and contour plots are presented in Figs. 14 and 15, together with the summary of the results (see Table 5) when fitting the

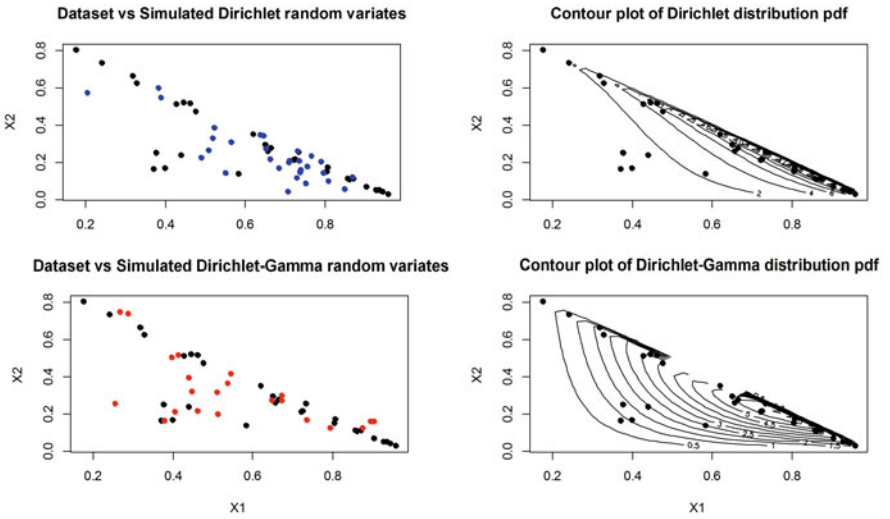

Fig. 15 Scatter plots and contour plots of the observed data versus the simulated data

Table 5 Parameter estimates and the performance summary for the white cells dataset

	ML estimates									
Model	$\widehat{\alpha}_1$	$\widehat{\alpha}_2$	$\widehat{\alpha}_3$	$\widehat{\beta}_1$	$\widehat{\beta}_2$	$\widehat{\theta}_1$	$\widehat{\theta}_2$	ll	AIC	BIC
Dirichlet	3.208	1.455	0.593	n/a	n/a	n/a	n/a	−51.410	108.820	113.023
DG	25.389	4.370	1.142	0.199	0.479	0.483	0.065	−30.155	74.310	84.118

Dirichlet and the Dirichlet-Gamma to this dataset. It is observed that the Dirichlet-Gamma outperforms the Dirichlet model.

6 Conclusion

This chapter's broader target was to show that the "mother technique" (see 3) can still generate novel progeny. A unique contribution is made by introducing a constructive methodology for families of multivariate distributions through the model $H(\boldsymbol{x}) = F(G(\boldsymbol{x}))$ with $\boldsymbol{x}$ a vector; $G(\boldsymbol{x})$ a vector of independent Gamma cdfs referred to as baseline distributions and F a multivariate pdf such as the Dirichlet with negative correlations between variables. Simulation studies and two real life cases are investigated to illustrate the value added of this construction, using several performance measures. A new model testing technique based on the empirical estimator of the cdf, is introduced to evaluate the performance of multivariate models. It flows naturally that instead of the gamma baseline distributions any other family of distributions could be used, similarly a more general structure for the generator could be the Dirichlet-hyper-geometric function type I distribution

(Nagar et al. 2009). To accommodate for positive correlation structure in the data, the authors consider the Dirichlet type III distribution (see Ehlers (2011)) or the Liouville distribution of the second kind (Gupta et al. (1997), Bouguila (2011)) in a follow-up paper. Note that, in contrast with the Dirichlet and like the generalized Dirichlet, the covariance can be positive or negative. The builder would be of the form:

- Builder 5:

$$H(x_1, \ldots, x_p) = \int_0^{G_1(x_1)} \cdots \int_0^{G_p(x_p)} C \prod_{i=1}^{p} y_i^{\alpha_i - 1} q\left(\sum_{i=1}^{p} y_i\right) d\boldsymbol{y}$$

  where $G_i(\cdot), i = 1, \ldots, p$, can be any cdf, C the normalizing constant of the pdf of the generator and $q(\cdot)$ a measurable positive real valued function defined on the interval $(0, 1)$ such that $\int_0^1 q(\tau)\, \tau^{s-1} d\tau$ exists for all $s > 0$.

This new approach to construct multivariate distributions expands the body of knowledge within the distribution theory domain.

Acknowledgements We express our sincere thanks to Mehrdad Naderi for many helpful conversations. This work is based on the research supported in part by the National Research Foundation of South Africa (Grant ref. SRUG190308422768 nr. 120839 and grant ref. IFR170227223754 nr. 109214). Opinions expressed and conclusions arrived at are those of the authors and are not necessarily to be attributed to the NRF. The authors would like to thank the reviewers for their valuable contributions.

Appendix

Code with comments for this chapter is available from the corresponding author.

References

Akaike, H. (1998). Information theory and an extension of the maximum likelihood principle. In *Selected papers of Hirotugu Akaike* (pp. 199–213). Berlin: Springer.

Alexander, C., Cordeiro, G. M., & Ortega, E. M. M. (2012). Generalized beta-generated distributions. *Computational Statistics and Data Analysis, 56*, 1880–1897.

Balakrishnan, N., Nevzorov, V. B. (2003). *A primer on statistical distributions*. New York: John Wiley & Sons.

Barndorff-Nielsen, O. E., & Jorgensen, B. (1991). Some parametric models on the simplex. *Journal of Multivariate Analysis, 39*, 106–116.

Barreto-Souza, W., Santos, A. H. S., & Cordeiro, G. M. (2010). The beta generalized-exponential distribution. *Journal of Statistical Computation and Simulation, 80*(2), 159–172.

Bouguila, N. (2011). Count data modeling and classification using finite mixtures of distributions. *IEEE Transactions On Neural Networks, 22*(2), 186–197.

Connor, J. R., & Mosimann, J. E. (1969). Concepts of independence for proportions with a generalization of the Dirichlet distribution. *Journal of the American Statistical Association, 64*, 194–206.

De Groot, M. H. (1970). *Optimal statistical decisions*. New York: McGraw-Hill.

Ehlers, R. (2011). *Bimatrix variate distributions of Wishart ratios with application*. Unpublished dissertation, University of Pretoria.

Elgarhy, M., Hassan, A. S., & Rashed, M. (2016). Garhy-generated family of distributions with application. *Mathematical Theory and Modeling, 6*(2), 1–15.

Epaillard, A., & Bouguila, N. (2019). Data-free metrics for Dirichlet and generalized Dirichlet mixture-based HMMs – A practical study. *Pattern Recognition, 8*, 207–219.

Eugene, N., Lee, C., & Famoye, F (2002). Beta-normal distribution and its applications. *Communications in Statistics—Theory and Methods, 31*(4), 497–512.

Favaro, S., Hadjicharalambous, G., & Prunster, I. (2011). On a class of distributions on the simplex. *Journal of Statistical Planning and Inference, 141*, 2987–3004.

Gupta, R. D., & Richards, D. St. P. (1997). Multivariate Liouville distributions, V. In N. L. Johnson, N. Balakrishnan (Eds.), *Advances in the theory and practice of statistics: A volume in honour of Samuel Kotz* (pp. 377–396). New York: Wiley.

Jones, M. C. (2004). Families of distributions arising from distributions of order statistics. *Test, 13*(1), 1–43.

Kotz, S., Balakrishnan, N., & Johnson, N.L. (2000). *Continuous multivariate distributions* (2nd ed., Vol. 1). New York: John Wiley & Sons.

Makgai, S. L., Bekker, A., Ferreira, J. T., & Arashi, M. (2017). New results from a beta-Pareto class. *South African Statistical Journal, 51*, 345–360.

Makgai, S. L., Visagie, J., Bekker, A., & De Waal, D. (2019). Contributions to the class of beta-generated distributions, submitted to Communications in Statistics-Theory and Methods.

Mameli, V. (2015). The Kumaraswamy skew-normal distribution. *Statistics & Probability Letters, 104*, 75–81.

Mosimann, J. E. (1962). On the compound multinomial distribution, the multivariate β-distribution, and correlations among proportions. *Biometrika, 49*, 65–82.

Nadarajah, S., & Kotz, S. (2006). The beta exponential distribution. *Reliab Eng Syst Safe, 91*, 689–697.

Nagar, D. K., Bran-Cardona, P. A., & Gupta, A. K. (2009). Multivariate generalization of the hypergeometric function type I distribution. *Acta Applicandae Mathematicae, 105*, 111–122.

Nassar, M., Kumar, D., Cordeiro, G. M., & Afify, A. Z. (2019). The Marshall Olkin alpha power family of distributions with applications. *Journal of Computational and Applied Mathematics, 351*, 41–53.

Ng, K. W., Tian, G., & Tang, M. (2011). *Dirichlet and related distributions. Theory, methods and applications*. New York: John Wiley & Sons.

Olkin, I., & Liu, R. (2003). A bivariate beta distribution. *Statistics & Probability Letters, 62*, 407–412.

Ongaro, A, S., & Migliorati, S. (2013). A generalization of the Dirichlet distribution. *Journal of Multivariate Analysis, 114*, 412–426.

Ristić, M. M., Popović, B. V., Zografos, K., & Balakrishnan, N. (2018). Discrimination among bivariate beta-generated distributions. *Statistics, 52*(2), 303–320.

Samanthi, R. G. M., & Sepanski, J. (2019). A bivariate extension of the beta generated distribution derived from copulas. *Communications in Statistics-Theory and Methods, 48*(5), 1043–1059.

Sarabia, J. M., Prieto, F., & Jordá, V. (2014). Bivariate beta-generated distributions with applications to well-being data. *Journal of Statistical Distributions and Applications, 1*, 1–15.

Schwarz, G. (1978). Estimating the dimension of a model. *The Annals of Statistics, 6*(2), 461–464.

Thomas, S., & Jacob, J. (2006). A generalized Dirichlet model. *Statistics and Probability Letters, 76*, 1761–1767.

Zografos, K., & Balakrishnan, N. (2009). On families of beta- and generalized gamma-generated distributions and associated inference. *Statistical Methodology, 6*, 344–362.

Evaluating Risk Measures Using the Normal Mean-Variance Birnbaum-Saunders Distribution

Mehrdad Naderi, Ahad Jamalizadeh, Wan-Lun Wang, and Tsung-I Lin

Abstract Despite the widespread use and attractive properties of the normal and Student's t distributions for modeling financial risks, it is widely believed that the normal-inverse Gaussian, skew-normal and skew-t distributions can be promising alternatives for describing the asymmetric features of asset returns. In this article, we propose a new benchmark model for quantifying the risk of financial assets based on the normal mean-variance Birnbaum-Saunders (NMVBS) distribution. The theoretical formulae of some popular risk measures based on the NMVBS distribution are exactly derived. Numerical evaluation of risks of some selected stock market returns reveals that the proposed method may outperform some existing approaches.

M. Naderi
Department of Statistics, Faculty of Natural & Agricultural Sciences, University of Pretoria, Pretoria, South Africa
e-mail: m.naderi@up.ac.za

A. Jamalizadeh
Department of Statistics, Faculty of Mathematics and Computer, Shahid Bahonar University of Kerman, Kerman, Iran

Mahani Mathematical Research Center, Shahid Bahonar University of Kerman, Kerman, Iran
e-mail: a.jamalizadeh@uk.ac.ir

W.-L. Wang
Department of Statistics, Graduate Institute of Statistics and Actuarial Science, Feng Chia University, Taichung, Taiwan
e-mail: wlunwang@fcu.edu.tw

T.-I. Lin (✉)
Institute of Statistics, National Chung Hsing University, Taichung, Taiwan

Department of Public Health, China Medical University, Taichung, Taiwan
e-mail: tilin@nchu.edu.tw

A. Bekker et al. (eds.), *Computational and Methodological Statistics and Biostatistics*, Emerging Topics in Statistics and Biostatistics,
https://doi.org/10.1007/978-3-030-42196-0_8

1 Introduction

The fat tails and skewed features are often present in economic and financial data streams such as the employment rates, stock asset returns, and so on. Some asymmetric distributions have been recently exploited and found to be effective in describing the skewness and fatness of the tails embodied in these kinds of data. For example, Vernic (2006) studied the skew-normal (SN; Azzalini (1985)) distribution as an alternative to the classical normal one for modeling insurance risks. Eling (2012, 2014) empirically identified the SN and skew-t (ST; Azzalini and Capitaino (2003)) as promising benchmark models for analyzing the actuarial loss and asset returns of insurance companies. Lee and McLachlan (2013) presented several finite mixtures of asymmetric distributions in providing more accurate forecast of value at risk (VaR) estimation. Adcock et al. (2015) highlighted the usefulness, flexibility and tractability of the SN distribution in the areas of finance and actuarial science. Shushi (2017) derived the general forms of risk measures under the family of skew-elliptical distributions. Barndorff-Nielsen (1997) introduced another class of skewed and heavy-tailed distributions, namely the generalized hyperbolic (GH) distribution, which includes the normal, Student's t, hyperbolic, variance gamma (VG), normal inverse Gaussian (NIG), and generalized hyperbolic skew-t (GHST) distributions, to name just a few, as special cases.

McNeil et al. (2005) defined the GH distribution as a normal mean-variance (NMV) mixture representation, where the mixing variable has a generalized inverse Gaussian (GIG) distribution (Good 1953). Recently, the GH family of distributions have been considered to be a good platform for adequately modeling financial risks. Aas and Haff (2006) demonstrated the superiority of the NIG and GHST distributions in modeling skew financial data. Hu and Kercheval (2007) studied the VaR for a portfolio of assets based on the advantage of the GH distributions that are closed under linear transformation. Konlack Socgnia and Wilcox (2014) discussed the calibrations of the GH distribution and its subclasses (Hyperbolic, VG, NIG and GHST) for the daily log-returns of seven of the most liquid mining stocks listed on the Johannesburg Stocks Exchange. The authors found that the GH distribution can provide a slightly better fit of these data as compared to four subclass competitors, but not all estimated GH parameters are statistically significant due to a non-identifiability problem.

As a parsimonious variant of the GH distribution, Pourmousa et al. (2015) proposed the normal mean-variance Birnbaum-Saunders (NMVBS) distribution, defined as the NMV mixture where the mixing variable has a Birnbaum-Saunders (BS) distribution. Unlike the GH distribution which suffers from non-identifiability problems, the NMVBS distribution has several desirable properties such as the assurance of identifiability and of having closed-form expressions for all parameter estimators under the expectation maximization (EM) based estimation. As also demonstrated by Pourmousa et al. (2015), the NMVBS model may offer a better fit than other skew distributions for some benchmark datasets. The superiority of the NMVBS distribution is largely attributable to the fact that it takes wider ranges

of skewness and kurtosis as compared with the ST and skew-t-normal (Ho et al. 2012; Lin et al. 2014) distributions, see Table 1 of Naderi et al. (2017).

A risk measure, which is taken by a single value for the degree of overall uncertainty associated with the random variable representing the risk at hand, can be thought of as a function mapping a payoff distribution to the real line. VaR is one of the most widely employed measures to characterize the downside risk of a financial investment. Given at a confidence level, VaR can be viewed as the minimum loss expected on a portfolio of assets over a certain period of time. Another commonly employed risk measure with coherence property (Artzner et al. 1999) is the so-called tail value at risk (TVaR). It can be interpreted as the mean of the worst losses given the loss will exceed a particular value, obtained as the quantile of a risk random variable. The aim of this article is to derive the closed-form expressions of VaR and TVaR as well as related measures for the NMVBS random risks and investigate its practical applications in evaluating financial losses.

The rest of the article is structured as follows. Section 2 briefly outlines some main properties of the NMVBS distribution such as the moment generating function and the closure property with respect to the affine transformation. In Sect. 3, we provide analytical formulae for some important risk measures under the assumption of the NMVBS distribution for capital assets. Section 4 illustrates the prominence of the NMVBS distribution in estimating financial risks for stock returns in four selected international equity markets and results are compared with several alternative models. Section 5 concludes with several remarks and possible directions for future research.

2 The Normal Mean-Variance Birnbaum-Saunders Distribution

For the sake of completeness, we review the NMV and GIG distributions firstly. Following McNeil et al. (2005), a d-dimensional random vector $\boldsymbol{X}$ is said to have the NMV distribution if it can be stochastically expressed as

$$\boldsymbol{X} = \boldsymbol{\mu} + W\boldsymbol{\lambda} + W^{1/2}\boldsymbol{Z}, \tag{1}$$

where both $\boldsymbol{\mu}$ and $\boldsymbol{\lambda} \in \mathbb{R}^d$, $\boldsymbol{Z}$ is distributed as the multivariate normal distribution with zero mean vector and covariance matrix $\boldsymbol{\Sigma}$, and W is a non-negative random variable with the distribution function $H(\cdot; \boldsymbol{\theta})$ and independent of $\boldsymbol{Z}$. Under this parameterization, the GH family of distributions are closed under conditioning, marginalization and affine transformations.

If the mixing variable W in (1) is chosen to has a GIG distribution, denoted by $W \sim GIG(\kappa, \chi, \psi)$, with probability density function (pdf)

$$f_{GIG}(w;\kappa,\chi,\psi)=\left(\frac{\psi}{\chi}\right)^{\kappa/2}\frac{w^{\kappa-1}}{2K_{\kappa}(\sqrt{\psi\chi})}\exp\left\{\frac{-1}{2}\left(w^{-1}\chi+w\psi\right)\right\},\quad w>0,$$

where $K_a(\cdot)$ denotes the modified Bessel function of the third kind with order a, then the random vector $\boldsymbol{X}$ follows the GH distribution. The pdf of a d-dimensional random vector $\boldsymbol{X}$ is given by

$$f_{GH_d}(\boldsymbol{x};\boldsymbol{\mu},\boldsymbol{\lambda},\boldsymbol{\Sigma},\kappa,\chi,\psi)=C\frac{K_{d/2-\kappa}\left\{\sqrt{(\psi+\boldsymbol{\lambda}^{\top}\boldsymbol{\Sigma}^{-1}\boldsymbol{\lambda})(\chi+\boldsymbol{\delta}(\boldsymbol{x};\boldsymbol{\mu},\boldsymbol{\Sigma}))}\right\}}{\left\{\sqrt{(\psi+\boldsymbol{\lambda}^{\top}\boldsymbol{\Sigma}^{-1}\boldsymbol{\lambda})(\chi+\boldsymbol{\delta}(\boldsymbol{x};\boldsymbol{\mu},\boldsymbol{\Sigma}))}\right\}^{d/2-\kappa}}\times\exp\left\{(\boldsymbol{x}-\boldsymbol{\mu})^{\top}\boldsymbol{\Sigma}^{-1}\boldsymbol{\lambda}\right\},$$

where $C=(\psi/\chi)^{\frac{\kappa}{2}}(\psi+\boldsymbol{\lambda}^{\top}\boldsymbol{\Sigma}^{-1}\boldsymbol{\lambda})^{d/2-\kappa}(2\pi)^{-d/2}|\boldsymbol{\Sigma}|^{-1/2}/K_{\kappa}(\sqrt{\psi\chi})$ is the normalizing constant and $\boldsymbol{\delta}(\boldsymbol{x};\boldsymbol{\mu},\boldsymbol{\Sigma})=(\boldsymbol{x}-\boldsymbol{\mu})^{\top}\boldsymbol{\Sigma}^{-1}(\boldsymbol{x}-\boldsymbol{\mu})$ is the squared Mahalanobis distance between $\boldsymbol{x}$ and $\boldsymbol{\mu}$.

A non-negative random variable W is said to follow the BS distribution (Birnbaum and Saunders 1969), denoted by $W\sim BS(\alpha,\beta)$, if its cumulative distribution function (cdf) is

$$F(w;\alpha,\beta)=\Phi\left[\frac{1}{\alpha}\left\{\sqrt{\frac{w}{\beta}}-\sqrt{\frac{\beta}{w}}\right\}\right],\quad w>0,\ \alpha>0,\ \beta>0,$$

where $\Phi(\cdot)$ is the cdf of the standard normal distribution, and α and β are the shape and scale parameters, respectively. The BS distribution is positively skewed and is related to the normal model through the following stochastic representation:

$$W=\frac{\beta}{4}\left\{\alpha Z+\sqrt{(\alpha Z)^2+4}\right\}^2,$$

where $Z\sim N(0,1)$. Following Desmond (1986), the BS distribution can be written as a mixture of two equally weighted GIG distributions. Therefore, the pdf of W takes the form of

$$f_{BS}(w;\alpha,\beta)=\frac{1}{2}f_{GIG}\left(w;\frac{1}{2},\frac{\beta}{\alpha^2},\frac{1}{\beta\alpha^2}\right)+\frac{1}{2}f_{GIG}\left(w;\frac{-1}{2},\frac{\beta}{\alpha^2},\frac{1}{\beta\alpha^2}\right).\qquad(2)$$

Proposition 1 *If $W\sim BS(\alpha,\beta)$, the moment generating function (mgf) of W is*

$$M_W(t)=\frac{1}{2}\left(\frac{1}{\sqrt{1-2\alpha^2\beta t}}+1\right)\exp\left\{\frac{1-\sqrt{1-2\alpha^2\beta t}}{\alpha^2}\right\}.\qquad(3)$$

Proof From (2), we can obtain the mgf of W as

$$
\begin{aligned}
M_W(t) &= \frac{1}{2}\Big(M_{W_1}(t) + M_{W_2}(t)\Big) \\
&= \frac{1}{2}\Bigg\{\big(1-2\alpha^2\beta t\big)^{1/4}\frac{K_{0.5}(\alpha^{-2}\sqrt{1-2\alpha^2\beta t})}{K_{0.5}(\alpha^{-2})} \\
&\quad +\big(1-2\alpha^2\beta t\big)^{-1/4}\frac{K_{-0.5}(\alpha^{-2}\sqrt{1-2\alpha^2\beta t})}{K_{-0.5}(\alpha^{-2})}\Bigg\},
\end{aligned}
$$

where $M_{W_1}(t)$ and $M_{W_2}(t)$ are the mgfs of $W_1 \sim GIG(0.5, \beta/\alpha^2, 1/(\beta\alpha^2))$ and $W_2 \sim GIG(-0.5, \beta/\alpha^2, 1/(\beta\alpha^2))$, respectively. Making use the relations of Bessel function $K_\kappa(x) = K_{-\kappa}(x)$ and $K_{0.5}(x) = \sqrt{\pi/2}x^{-0.5}\exp\{-x\}$, it completes the proof. □

The multivariate NMVBS distribution introduced by Pourmousa et al. (2015) is emerged by setting $W \sim BS(\alpha, 1)$ in (1), denoted by $\boldsymbol{X} \sim NMVBS_d(\boldsymbol{\mu}, \boldsymbol{\lambda}, \boldsymbol{\Sigma}, \alpha)$. When $d = 1$, we write $X \sim NMVBS(\mu, \lambda, \sigma^2, \alpha)$ for the univariate case. By Proposition 3.2 of Pourmousa et al. (2015), the cdf of the NMVBS distribution can be expressed by a mixture of two GH cdfs:

$$
\begin{aligned}
F_X(\boldsymbol{x}; \boldsymbol{\mu}, \boldsymbol{\lambda}, \boldsymbol{\Sigma}, \alpha) &= \frac{1}{2}F_{GH_d}\left(\boldsymbol{x}; \boldsymbol{\mu}, \boldsymbol{\lambda}, \boldsymbol{\Sigma}, 0.5, \alpha^{-2}, \alpha^{-2}\right) \\
&\quad +\frac{1}{2}F_{GH_d}\left(\mathbf{x}; \boldsymbol{\mu}, \boldsymbol{\lambda}, \boldsymbol{\Sigma}, -0.5, \alpha^{-2}, \alpha^{-2}\right). \qquad (4)
\end{aligned}
$$

It follows from Pourmousa et al. (2015) that the multivariate NMVBS distribution is closed under affine transformations. Forming a portfolio of dependent risks $\boldsymbol{X} \sim NMVBS_d(\boldsymbol{\mu}, \boldsymbol{\lambda}, \boldsymbol{\Sigma}, \alpha)$, it is easy to show that the weighted sum $Z = \boldsymbol{\pi}^\top \boldsymbol{X}$ is distributed as $NMVBS(\boldsymbol{\pi}^\top\boldsymbol{\mu}, \boldsymbol{\pi}^\top\boldsymbol{\lambda}, \boldsymbol{\pi}^\top\boldsymbol{\Sigma}\boldsymbol{\pi}, \alpha)$. That is, all portfolios share the same asymmetry parameter α. Once we have estimated the NMVBS density, the marginal distribution of a linear portfolio is automatically obtained. Consequently, we establish the following theorem, which is useful to drive several important measures with the underlying NMVBS risks.

Theorem 1 *The mgf of* $X \sim \text{NMVBS}(\mu, \lambda, \sigma^2, \alpha)$ *is*

$$
M_X(t) = \frac{1}{2}\left(\frac{1}{\sqrt{1-2t\lambda\alpha^2-t^2\alpha^2\sigma^2}}+1\right)\exp\left\{\alpha^{-2}\big(1-\sqrt{1-2t\lambda\alpha^2-t^2\alpha^2\sigma^2}\big)+t\mu\right\}.
$$

Proof From (1), we can obtain the mgf of X straightforwardly

$$
\begin{aligned}
M_X(t) &= E\Big\{E(X|W)\Big\} = E\left[\exp\left\{t\mu + t\lambda W + \frac{W}{2}t^2\sigma^2\right\}\right] \\
&= \exp\{t\mu\}M_W\left(t\lambda + \frac{1}{2}t^2\sigma^2\right).
\end{aligned}
$$

Finally, the desired result can be obtained by substituting $t\lambda + \frac{1}{2}t^2\sigma^2$ in (3). □

3 Risk Measure for NMVBS Distribution

The risk evaluation is an important task for investors who hold varying amounts of the risky asset in their portfolios. Thus the risk measures and their theories play a critical role in estimating financial losses. Among the several purposes of the risk measure, the most important ones in practice are determination of risk capital and capital adequacy, management tool and insurance premiums (McNeil et al. 2005). Toward this end, the most modern measures of the risk in a portfolio rely on statistical methods. By Theorem 1, we can calculate different risk measures under the assumption that the asset returns are distributed as NMVBS distributions. The risk measures considered here include the probability of shortfall (PS), probability of outperformance (PO), target shortfall (TS), and a tail value at risk (TVaR), which is the commonly used risk measure and can be treated as a special case of the TS measure. Furthermore, we drive the Esscher premium and the entropic measures of the risks for the NMVBS distribution.

Let $\mathbb{E}\big[x_q - X\big]_+^n$ be the n-th order lower partial moment of the random variable X with respect to the $x_q \in \mathbb{R}$. More specifically,

$$\mathbb{E}\big[x_q - X\big]_+^n = \int_{-\infty}^{x_q} (x_q - x)^n f_X(x;\theta)\, dx,$$

where x_q is a target separating gains and losses, and $f_X(\cdot;\theta)$ is the pdf of X parameterized with θ. The reference point x_q can be specified as a fixed target, e.g., a given income poverty line which applies to all households equally, or as a moving target, i.e., the target is not fixed but depends on the household-specific distribution of the random variable (Brogan and Stidham 2008). The explicit formulae for evaluating the PS and PO for the univariate NMVBS random variable are collected in the following proposition.

Proposition 2 *Let $X \sim NMVBS(\mu, \lambda, \sigma^2, \alpha)$. The probability of X that falls short or outperforms a target level x_p can be obtained, respectively, by*

$$PS(x_q, \mu, \lambda, \sigma^2, \alpha) = \mathbb{E}\big[x_q - X\big]_+^0 = F_X(z_q; \beta, \alpha),$$

and

$$PO(x_q, \mu, \lambda, \sigma^2, \alpha) = 1 - \mathbb{E}\big[x_q - X\big]_+^0 = 1 - F_X(z_q; \beta, \alpha),$$

where $z_q = (x_q - \mu)/\sigma$, $\beta = \lambda/\sigma$, and $F_X(z_q; \beta, \alpha)$ is the standardized cdf of the NMVBS distribution, namely $F_X(z_q; \beta, \alpha) = F_X(z_q; 0, \beta, 1, \alpha)$.

Proof The proof is straightforward and hence is omitted. □

Note that there are no closed expressions for the PS and PO of the NMVBS random variable. From (4), the cdf of the NMVBS distribution is a mixture of two GH cdfs.

Therefore, the two risks can be easily evaluated by implementing `ghyp` R package (Breymann and Luthi 2009).

The TS risk measure is defined as the first-order lower partial moment with respect to the threshold $x_q \in \mathbb{R}$. The next theorem provides a way of calculating the TS when X has the NMVBS distribution.

Theorem 2 *Let $X \sim NMVBS(\mu, \lambda, \sigma^2, \alpha)$. The TS of X takes the form of*

$$\begin{aligned} TS_X(x_q, \mu, \lambda, \sigma^2, \alpha) &= x_q PS(x_q, \mu, \lambda, \sigma^2, \alpha) - E_W\big[(\mu + W\lambda)\Phi(z_q; W\beta, W)\big] \\ &\quad + \frac{\sigma}{2}\Bigg\{ f_{GH}\big(z_q; \beta, 0.5, \alpha^{-2}, \alpha^{-2}\big) + \Big(\frac{\alpha^{-2} + z_q}{\alpha^{-2} + \beta^2}\Big) \\ &\quad \times f_{GH}\big(z_q; \beta, -0.5, \alpha^{-2}, \alpha^{-2}\big)\Bigg\}, \end{aligned}$$

where $z_q = \frac{x_q - \mu}{\sigma}$, $f_{GH}\big(z_q; \beta, \kappa, \chi, \psi\big) = f_{GH}\big(z_q; 0, \beta, 1, \kappa, \chi, \psi\big)$ and $W \sim BS(\alpha, 1)$.

Proof The TS of random variable X is defined as

$$\begin{aligned} TS(x_q, \mu, \lambda, \sigma^2, \alpha) &= \mathbb{E}\big[x_q - X\big]_+^1 \\ &= \int_{-\infty}^{x_q} (x_q - x) f_X(x; \mu, \lambda, \sigma^2, \alpha)\, dx \\ &= x_q PS(x_q, \mu, \lambda, \sigma^2, \alpha) - \int_{-\infty}^{x_q} x f_X(x; \mu, \lambda, \sigma^2, \alpha)\, dx. \end{aligned}$$

By (1), the above integral can be rearranged as

$$\begin{aligned} &\int_{-\infty}^{x_q} x f_X(x; \mu, \lambda, \sigma^2, \alpha)\, dx \\ &= \int_{-\infty}^{x_q} \int_0^{\infty} x \phi(x; \mu + w\lambda, w\sigma^2) f_{BS}(w; \alpha, 1)\, dw dx \\ &= \int_0^{\infty} \int_{-\infty}^{x_q} \frac{x - \mu - w\lambda}{\sqrt{w}\sigma} \phi\left(\frac{x - \mu - w\lambda}{\sqrt{w}\sigma}\right) f_{BS}(w; \alpha, 1)\, dx dw \\ &\quad + \int_0^{\infty} \int_{-\infty}^{x_q} \frac{\mu + w\lambda}{\sqrt{w}\sigma} \phi\left(\frac{x - \mu - w\lambda}{\sqrt{w}\sigma}\right) f_{BS}(w; \alpha, 1)\, dx dw \\ &= \int_0^{\infty} \Big(f_1(x_q) + f_2(x_q)\Big) f_{BS}(w; \alpha, 1)\, dw, \end{aligned}$$

where

$$f_1(x_q) = \int_{-\infty}^{x_q} \frac{x-\mu-w\lambda}{\sigma\sqrt{w}}\,\phi\left(\frac{x-\mu-w\lambda}{\sigma\sqrt{w}}\right)dx = -\sqrt{w}\sigma\phi(z_q; w\beta, w),$$

and

$$f_2(x_q) = \int_{-\infty}^{x_q} \frac{\mu+w\lambda}{\sqrt{w}\sigma}\,\phi\left(\frac{x-\mu-w\lambda}{\sqrt{w}\sigma}\right)dx = \big(\mu+w\lambda\big)\Phi(z_q; w\beta, w).$$

Therefore, we have

$$\begin{aligned}&\int_{-\infty}^{x_q} x f_X(x;\mu,\lambda,\sigma^2,\alpha)\,dx\\ &= E_W\big[(\mu+W\lambda)\Phi(z_q; W\beta, W)\big] - \int_0^{\infty}\sqrt{w}\sigma\phi(z_q; w\beta, w) f_{BS}(w;\alpha,1)dw.\end{aligned}$$

Finally, we complete the proof by noting that

$$\begin{aligned}&\int_0^{\infty}\sqrt{w}\sigma\phi(z_q; w\beta, w) f_{BS}(w;\alpha,1)dw\\ &= \frac{1}{2}\int_0^{\infty} w\sigma\phi(z_q; w\beta, w)\left\{f_{GIG}\Big(w;\frac{1}{2},\frac{1}{\alpha^2},\frac{1}{\alpha^2}\Big)+f_{GIG}\Big(w;\frac{-1}{2},\frac{1}{\alpha^2},\frac{1}{\alpha^2}\Big)\right\}dw,\\ &= \frac{1}{2}\sigma\Big(\frac{\alpha^{-2}+z_q}{\alpha^{-2}+\beta^2}\Big) f_{GH}\big(z_q;\beta,-0.5,\alpha^{-2},\alpha^{-2}\big) + \frac{1}{2}\sigma f_{GH}\big(z_q;\beta,0.5,\alpha^{-2},\alpha^{-2}\big).\end{aligned}$$

□

The VaR is a widely employed measure of downside risk in capital markets. Given a confidence level $q \in (0,1)$, the VaR is defined as the smallest $x_0 \in \mathbb{R}$ satisfying

$$VaR_q(X) = -\inf\{x \mid F_X(x) \geq 1-q\}. \tag{5}$$

Hence, VaR can be interpreted as the maximum loss of a portfolio $X = \boldsymbol{\pi}^{\mathrm{T}}\boldsymbol{Y}$, which should not be exceeded at a given confidence level, where $\boldsymbol{\pi} \in \mathbb{R}^d$ denotes the asset weights with the constraint $\sum_{i=1}^{d}\pi_i = 1$, and $\boldsymbol{Y}$ denotes the returns. However, VaR is often criticized for lack of coherence properties because it is sensitive to the shape of the tail of the loss distribution. As an alternative, TVaR is a coherent risk measure that fulfills the properties of monotonicity, sub-additivity, homogeneity, and translational invariance and can be viewed as the expected worse. More precisely, TVaR gives the expected amount of extreme loss under a given risk. Given a confidence level $q \in (0,1)$, the TVaR is defined as $TVaR(X) = -E\big[X|X \leq -VaR_q(X)\big]$, where $VaR_q(X)$ is the possible loss obtained by the $(1-q)$th percentile of X as defined in (5).

We characterize the well-known tail conditional expectation, namely the TVaR measure, in Theorem 3.

Theorem 3 *The TVaR measure of* $X \sim NMVBS(\mu, \lambda, \sigma^2, \alpha)$ *is*

$$\begin{aligned} TVaR(X) = \frac{-1}{1-q} E_W\big[(\mu + W\lambda)\Phi(z_q; W\beta, W)\big] \\ + \frac{\sigma}{2(1-q)}\Big(f_{GH}\big(z_q; \beta, 0.5, \alpha^{-2}, \alpha^{-2}\big) + \Big(\frac{\alpha^{-2} + z_q}{\alpha^{-2} + \beta^2}\Big) \\ \times f_{GH}\big(z_q; \beta, -0.5, \alpha^{-2}, \alpha^{-2}\big)\Big), \end{aligned}$$

where $W \sim BS(\alpha, 1)$ *and* $z_q = -(\mu + VaR_q(X))/\sigma$.

Proof By definition of the TVaR, we have

$$\begin{aligned} TVaR(X) &= \frac{-1}{1-q}\int_{-\infty}^{-VaR_q(X)} x f_X(x; \mu, \lambda, \sigma^2, \alpha)\, dx \\ &= \frac{1}{1-q}\big(TS_X(-VaR_q(X), \mu, \lambda, \sigma^2, \alpha) \\ &\quad + VaR_q(X) PS(-VaR_q(X), \mu, \lambda, \sigma^2, \alpha)\big), \end{aligned}$$

□

which completes the proof.

Let $\boldsymbol{\pi} \in \mathbb{R}^d$ be a vector of asset weights satisfying $\sum_{i=1}^d \pi_i = 1$. Considering the returns on a portfolio $\boldsymbol{X} \sim NMVBS_d(\boldsymbol{\mu}, \boldsymbol{\lambda}, \boldsymbol{\Sigma}, \alpha)$, it can be verified that

$$\begin{aligned} TVaR(\boldsymbol{\pi}^\top \boldsymbol{X}) &= -E\big[\boldsymbol{\pi}^\top \boldsymbol{X} | \boldsymbol{\pi}^\top \boldsymbol{X} \le -VaR_q(\boldsymbol{\pi}^\top \boldsymbol{X})\big] \\ &= -\sum_{i=1}^d E\big[\pi_i X_i | \boldsymbol{\pi}^\top \boldsymbol{X} \le -VaR_q(\boldsymbol{\pi}^\top \boldsymbol{X})\big]. \end{aligned} \tag{6}$$

The decomposition in (6) indicates that the TVaR of a portfolio is the sum of individual risk contributions of each asset in case where the relative portfolio loss exceeds $VaR_q(\boldsymbol{\pi}^\top \boldsymbol{X})$. Subsequently, we have Theorem 4 which is useful in applications for evaluating portfolio risks. The following lemma is required to verify the result in Theorem 4.

Lemma 1 *Let* $\begin{bmatrix} Z_1 \\ Z_2 \end{bmatrix} \sim N_2\left(\begin{bmatrix} 0 \\ 0 \end{bmatrix}, \begin{bmatrix} 1 & \rho \\ \rho & 1 \end{bmatrix}\right)$. *Then* $E(Z_1 \mid Z_2 < a) = \dfrac{\phi(a)}{\Phi(a)}\rho$.

Theorem 4 *Let*

$$\begin{bmatrix} X_1 \\ X_2 \end{bmatrix} \sim NMVBS_2\left(\begin{bmatrix} \mu_1 \\ \mu_2 \end{bmatrix}, \begin{bmatrix} \lambda_1 \\ \lambda_2 \end{bmatrix}, \begin{bmatrix} \sigma_1^2 & \sigma_{12} \\ \sigma_{21} & \sigma_2^2 \end{bmatrix}, \alpha\right).$$

It follows that

$$E(X_1|X_2 < s) = \mu_1 + \lambda_1 A^* + \frac{\sigma_{12}}{\sigma_2} B^*,$$

where

$$A^* = \frac{1}{2F_X(s; \mu_2, \lambda_2, \sigma_2^2, \alpha)}\left(\frac{K_{1.5}(\alpha^{-2})}{K_{0.5}(\alpha^{-2})} F_{GH}(s; \mu_2, \lambda_2, \sigma_2^2, 1.5, \alpha^{-2}, \alpha^{-2}) \right.$$
$$\left. + F_{GH}(s; \mu_2, \lambda_2, \sigma_2^2, 0.5, \alpha^{-2}, \alpha^{-2})\right),$$

and

$$B^* = \frac{1}{2F_X(s; \mu_2, \lambda_2, \sigma_2^2, \alpha)}\left(\frac{K_1(\alpha^{-2})}{K_{0.5}(\alpha^{-2})} f_{GH}(s; \mu_2, \lambda_2, \sigma_2^2, 1, \alpha^{-2}, \alpha^{-2}) \right.$$
$$\left. + \frac{K_0(\alpha^{-2})}{K_{0.5}(\alpha^{-2})} f_{GH}(s; \mu_2, \lambda_2, \sigma_2^2, 0, \alpha^{-2}, \alpha^{-2})\right).$$

Proof Suppose that $W \sim BS(\alpha, 1)$ and $\begin{bmatrix} Z_1 \\ Z_2 \end{bmatrix} \sim N_2\left(\begin{bmatrix} 0 \\ 0 \end{bmatrix}, \begin{bmatrix} 1 & \rho \\ \rho & 1 \end{bmatrix}\right)$. We have

$$\begin{bmatrix} X_1 \\ X_2 \end{bmatrix} \overset{\mathrm{d}}{=} \begin{bmatrix} \mu_1 + \lambda_1 W + \sqrt{W}\sigma_1 Z_1 \\ \mu_2 + \lambda_2 W + \sqrt{W}\sigma_2 Z_2 \end{bmatrix}.$$

Let the random vector $\boldsymbol{U}$ be distributed as

$$\begin{bmatrix} U_1 \\ U_2 \end{bmatrix} \overset{\mathrm{d}}{=} \begin{bmatrix} \mu_1 + \lambda_1 W + \sqrt{W}\sigma_1 Z_1 \\ W \end{bmatrix} \Bigg| \; (\mu_2 + \lambda_2 W + \sqrt{W}\sigma_2 Z_2 < s).$$

It follows immediately that

$$U_1 \mid (U_2 = u_2) \overset{\mathrm{d}}{=} (\mu_1 + \lambda_1 u_2 + \sqrt{u_2}\sigma_1 Z_1) \mid (\mu_2 + \lambda_2 u_2 + \sqrt{u_2}\sigma_2 Z_2 < s)$$
$$\overset{\mathrm{d}}{=} \mu_1 + \lambda_1 u_2 + \sqrt{u_2}\sigma_1\left(Z_1 \mid Z_2 < \frac{s - \mu_2 - \lambda_2 u_2}{\sqrt{u_2}\sigma_2}\right).$$

By Lemma 1, we can obtain

$$E(U_1|U_2 = u_2) = \mu_1 + \lambda_1 u_2 + \sqrt{u_2}\frac{\sigma_{12}\phi\left(\frac{s-\mu_2-\lambda_2 u_2}{\sqrt{u_2}\sigma_2}\right)}{\sigma_2\Phi\left(\frac{s-\mu_2-\lambda_2 u_2}{\sqrt{u_2}\sigma_2}\right)}.$$

Besides, the pdf of U_2 can be calculated as

$$f_{U_2}(u_2) = f_{BS}(u_2; \alpha, 1)\Phi\left(\frac{s-\mu_2-\lambda_2 u_2}{\sqrt{u_2}\sigma_2}\right) \Big/ F_X(s; \mu_2, \lambda_2, \sigma_2^2, \alpha).$$

Using the law of iterative expectations leads to

$$E(U_1) = \mu_1 + \lambda_1 A^* + \frac{\sigma_{12}}{\sigma_2} B^*,$$

where

$$A^* = E(U_2) = \frac{1}{F_X(s; \mu_2, \lambda_2, \sigma_2^2, \alpha)}\int_0^\infty u_2 f_{BS}(u_2; \alpha, 1)\Phi\left(\frac{s-\mu_2-\lambda_2 u_2}{\sqrt{u_2}\sigma_2}\right) du_2,$$

and

$$\begin{aligned} B^* &= E\left[\sqrt{U_2}\frac{\phi\left(\frac{s-\mu_2-\lambda_2 U_2}{\sqrt{U_2}\sigma_2}\right)}{\Phi\left(\frac{s-\mu_2-\lambda_2 U_2}{\sqrt{U_2}\sigma_2}\right)}\right] \\ &= \frac{1}{F_X(s; \mu_2, \lambda_2, \sigma_2^2, \alpha)}\int_0^\infty \sqrt{u_2} f_{BS}(u_2; \alpha, 1)\phi\left(\frac{s-\mu_2-\lambda_2 u_2}{\sqrt{u_2}\sigma_2}\right) du_2. \end{aligned}$$

□

This completes the proof.

The Esscher premium principle (Bühlmann 1980), which is a widely used measure in actuarial sciences, minimizes the expected loss using the loss function $L(x, P) = e^{hx}(x - P)^2$, where the loading factor $h > 0$ is a parameter reflecting the measure of risk aversion. By the Bayesian decision theory, the Esscher premium principle of X can be calculated as

$$\pi_h(X) = \frac{E\left[Xe^{hX}\right]}{E\left[e^{hX}\right]} = \frac{\partial}{\partial h}\ln M_X(h), \quad h > 0. \tag{7}$$

Notice that (7) enjoys some desirable properties such as non-negative safety loading, namely $\pi_h(X) \geq E(X)$, meaning that an insurance premium requires to charge at

least the expected payout of the risk X. Meanwhile, $\pi_h(X)$ is an increasing function of h for any risk X and fulfills the absence of rip-off condition, that is, it never exceeds the maximum value of X. Other properties related to the Esscher premium principle can refer to Goovaerts et al. (1984).

As an alternative to the VaR and TVaR risk measures, we derive the entropic risk measure which depends on the risk aversion of the user through the exponential utility function. For a random variable X, the entropic risk measure with the risk aversion parameter $\upsilon > 0$ takes the form of

$$\rho^{ent}(X) = \frac{1}{\upsilon} \ln E(\exp\{-\upsilon X\}) = \frac{1}{\upsilon} \ln M_X(-\upsilon).$$

The entropic risk measure is difficult to use in practice due to the difficulty of quantifying the risk aversion for an individual, but it is still theoretically interesting. See Föllmer and Knispel (2011) for further technical details.

The follow theorem provides the formulae of Esscher premium principle and entropic risk measure for a portfolio of NMVBS risks.

Theorem 5 *Suppose that* $X \sim NMVBS(\mu, \lambda, \sigma^2, \alpha)$. *The Esscher premium principle and entropic risk measures of* X *are given by*

$$\pi_h(X) = \mu + \frac{1}{\delta(h,\theta)} \left(\lambda + h\sigma^2 + \frac{\alpha^2\lambda + h\alpha^2\sigma^2}{\delta^2(h,\theta)\left(1+\delta^{-1}(h,\theta)\right)} \right), \quad h \in (0, -\lambda/\sigma^2 + B),$$

$$\rho^{ent}(X) = -\mu + \frac{1}{\upsilon} \left(-\ln 2 + \ln\left(1 + \frac{1}{\delta(-\upsilon,\theta)}\right) + \alpha^{-2}\left(1 - \delta(-\upsilon,\theta)\right)\right),$$

$$\upsilon \in (0, \lambda/\sigma^2 + B),$$

respectively, where $\delta(h,\theta) = \sqrt{1 - 2h\lambda\alpha^2 - h^2\alpha^2\sigma^2}$ *and* $B = \sqrt{\alpha^2\lambda^2 + \sigma^2}/(\alpha\sigma^2)$.

Proof As a direct consequence of Theorem 1, we have

$$\ln M_X(h) = -\ln 2 + \ln\left(\delta^{-1}(h,\theta) + 1\right) + \alpha^{-2}(1 - \delta(h,\theta)) + h\mu. \tag{8}$$

The first partial derivative of $\ln M_X(h)$ given in (8) with respect to h yields the Esscher premium principle, obtained as

$$\pi_h(X) = \mu + \frac{1}{\delta(h,\theta)} \left\{ \lambda + h\sigma^2 + \frac{\alpha^2\lambda + h\alpha^2\sigma^2}{\delta^2(h,\theta)\left(1+\delta^{-1}(h,\theta)\right)} \right\}.$$

□

To avoid getting imaginary number for $\delta(h,\theta)$, the necessary condition is $1 - 2h\lambda\alpha^2 - h^2\alpha^2\sigma^2 \geq 0$ which implies $h \in (-\lambda/\sigma^2 \pm B)$. On the other hand, since $h > 0$ and $B > \lambda/\sigma^2$, we have $h \in (0, -\lambda/\sigma^2 + B)$ if $\lambda \geq 0$, and

$h \in (0, |\lambda|/\sigma^2 + B)$ if $\lambda < 0$. As a result, $\pi_h(X)$ is well defined whenever $h \in (0, -\lambda/\sigma^2 + B)$. Similarly, the entropic risk measure can be written in terms of (8) by replacing h with $-\upsilon$.

4 Application to Stock Market Returns

4.1 Data and Descriptive Statistics

We apply our methods to four series of daily returns from international stock markets, including S&P 500, DOW and NASDAQ 100 in the U.S. and CAC40 in France. These data were extracted from Yahoo Finance with the period starting from 1st January 2010 and ending 31 December 2016. We consider the daily log returns in percentage, i.e., $r_t = 100 \times \log(P_t/P_{t-1})$, where P_t is the adjusted closing price of an asset on day t.

Table 1 summarizes basic descriptive statistics of log-returns of the four indices, including the number of observations (n), mean, standard deviation (St.Dev), minimum (min), maximum (max), skewness (γ_X), kurtosis (κ_X), 99% VaR and 99% TVaR. To test for normality, the Jarque-Bera test statistic (Jarque and Bera 1987) and the corresponding P-value for each asset are also listed in Table 1.

The results depicted in Table 1 reveal that the considered indices exhibit relatively high risk, if we take the standard deviation as a measure of risk, and somewhat high empirical VaR and TVaR values. The values of γ_X and κ_X show that these indices are skewed to the left and have fat tails. According to Fig. 1, which presents histograms and Q–Q plots for each index, and the Jarque-Bera test statistic along with extremely low P-values, none of the indices are normally distributed. These characteristics motive us to consider the skewed distributions which can take both skewness and kurtosis of the data into account and are expected to gain more appropriate statistical inference.

4.2 Model Comparison

We fit the NMVBS distribution described in Sect. 2 as a benchmark model to these log-returns data. The EM algorithm (Dempster et al. 1977) for estimating the NMVBS parameters is sketched in Appendix. For the sake of comparison, we also consider the fitting of normal, SN, ST and NIG distributions. We perform the R package `sn` (Azzalini 2004) to estimate SN and ST distributions, and the R package `ghyp` (Breymann and Luthi 2009) for the NIG distribution.

To select the most adequate model, we adopt the Akaike information criterion (AIC; Akaike (1927)) and the Bayesian information criterion (BIC; Schwarz (1978)), defined as $-2\ell_{\max} + mC_n$, where $\ell_{\max}$ is the maximized log-likelihood

Table 1 Descriptive statistics of log-return series for four considered market price indices from January 1, 2010 to December 31, 2016

	Measures									
Index	n	Mean	St. Dev	Min	Max	γ_X	κ_X	VaR	TVaR	Jarque-Bera	P-value
S&P500	1761	0.039	0.980	−6.896	4.632	−0.438	7.194	2.870	3.758	1351.805	$<2.2 \times 10^{-16}$
CAC40	1789	0.012	1.358	−8.384	9.221	−0.160	6.459	3.701	4.808	903.055	$<2.2 \times 10^{-16}$
DOW	1762	0.042	0.878	−5.706	4.153	−0.394	6.813	2.402	3.317	1117.539	$<2.2 \times 10^{-16}$
NASDAQ 100	1762	0.055	1.095	−6.305	4.937	−0.340	5.794	3.135	3.936	609.798	$<2.2 \times 10^{-16}$

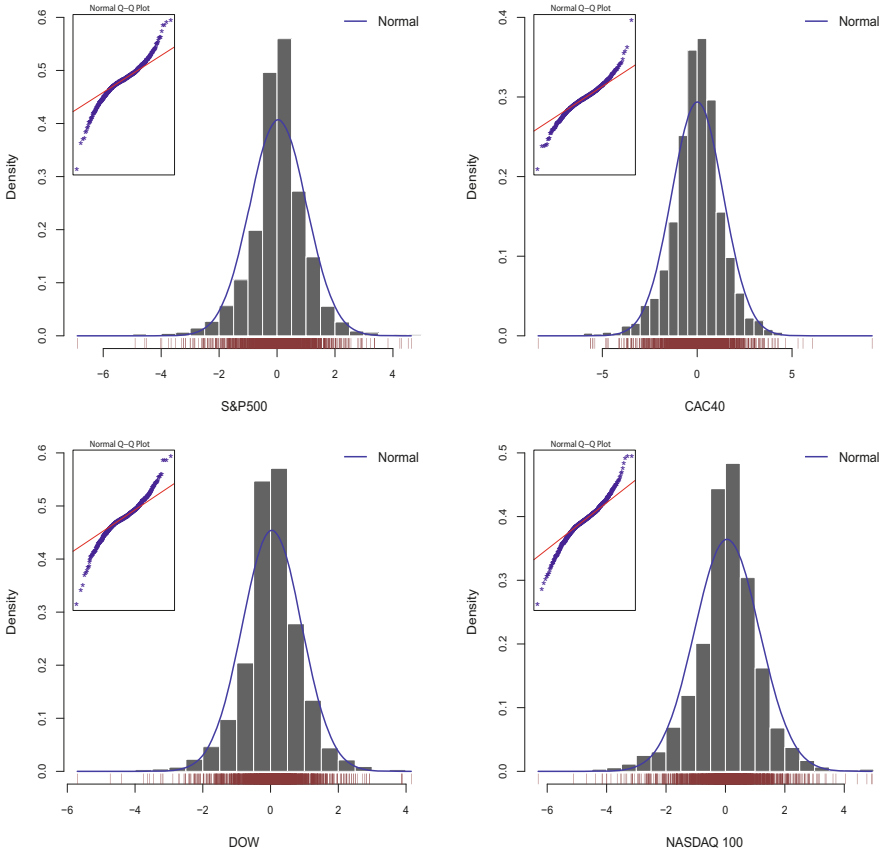

Fig. 1 Histogram overlaid with normal density and $Q - Q$ plots for four log-return market price indices

value and m represents the number of parameters. Note that the penalty term C_n is equal to 2 for AIC and $\log(n)$ for BIC. The model having the smallest AIC or BIC value is claimed to provide the best fit. Model comparison results displayed in Table 2 indicate that the NMVBS distribution provides the best fitting performance as it attains the lowest AIC and BIC scores. Meanwhile, the normal distribution has the worst performance, reinforcing the behavior of non-normality of these log-returns.

To assess the goodness-of-fit of these fitted distributions, we apply the Kolmogorov-Smirnov (K-S) test (Smirnov 1948) as a tool of discovering whether the theoretical distributions fit the empirical data well. Table 3 summarizes the K-S test statistics along with their corresponding P-values for the five fitted distributions. A smaller value of K-S statistic indicates a closer fit to the model with the underlying distributional assumption. With the K-S test, the null hypotheses of using the normal and SN distributions are rejected due to extremely small P-values. It is also shown

Table 2 Comparison of ML fitting results on four log-return market price indices

Data	Criteria	Model				
		Normal	SN	ST	NIG	NMVBS
S&P500	$\ell_{\max}$	−2462.761	−2447.080	−2315.566	−2307.350	−2305.505
	AIC	4929.522	4900.160	4639.132	4622.699	4619.010
	BIC	4940.469	4916.581	4661.027	4644.594	4640.905
CAC40	$\ell_{\max}$	−3086.225	−3079.929	−2989.059	−2986.098	−2986.025
	AIC	6176.450	6165.857	5986.118	5980.196	5980.051
	BIC	6187.429	6182.325	6008.075	6002.154	6002.008
DOW	$\ell_{\max}$	−2271.372	−2257.953	−2136.145	−2127.071	−2124.445
	AIC	4546.745	4521.907	4280.290	4262.141	4256.890
	BIC	4557.693	4538.329	4302.187	4284.038	4278.787
NASDAQ 100	$\ell_{\max}$	−2659.751	−2646.800	−2554.406	−2547.823	−2546.799
	AIC	5323.502	5299.600	5116.813	5103.645	5101.598
	BIC	5334.451	5316.023	5138.710	5125.542	5123.495

Table 3 Results of Kolmogorov-Smirnov test on four log-return market price indices

Model	S&P 500		CAC40		DOW		NASDAQ 100	
	KS	P-value	KS	P-value	KS	P-value	KS	P-value
Normal	0.084	0.000	0.059	0.000	0.088	0.000	0.076	0.000
SN	0.076	0.000	0.053	0.000	0.078	0.000	0.066	0.000
ST	0.021	0.429	0.013	0.907	0.028	0.111	0.022	0.359
NIG	0.016	0.746	0.008	0.999	0.023	0.311	0.016	0.733
NMVBS	0.015	0.814	0.011	0.985	0.020	0.463	0.015	0.835

that the NMVBS distribution tends to give the closest fit to all indices except that the NIG distribution outperforms slightly for CAC40. Again, this recommends that the NMVBS distribution can be a more promising tool for modeling asset returns than using other existing ones.

4.3 Performance on the VaR and TVaR Assessment

We now turn our attention to compare the accuracy of predicted VaR and TVaR values based on the fitted normal, SN, ST, NIG and NMVBS models. Because not all of the risk measures for some of the skew distributions have closed-form formulae, we generate Monte Carlo samples of size one million to evaluate VaR and TVaR. Recall that the VaR is the $1 - q$ quantile of the simulated loss samples, whereas TVaR is the mean loss and thus is greater than VaR.

Table 4 presents the predicted VaR and TVaR under 95 and 99% confidence levels for the log-returns of four indices based on the five fitted models. It is evidently seen that the NMVBS distribution provides a closer prediction of the empirical

Table 4 Comparison of estimated 99 and 95% VaR and TVaR of log-return market price indices based on various models

Data		q	Model					
			Empirical	Normal	SN	ST	NIG	NMVBS
S&P500	VaR	99%	2.8695	2.3378	2.3860	2.9765	2.9538	2.8643
		95%	1.6005	1.5722	1.6265	1.4948	1.5472	1.5539
	TVaR	99%	3.7581	2.5692	2.7735	4.6325	3.9736	3.7305
		95%	2.3917	1.9810	2.0924	2.5225	2.4330	2.3706
CAC40	VaR	99%	3.7010	3.1473	3.2892	3.8571	3.8726	3.8302
		95%	2.2784	2.2218	2.2743	2.1513	2.2035	2.2037
	TVaR	99%	4.8077	3.6062	3.8057	5.4128	5.0237	4.8968
		95%	3.2243	2.7887	2.8976	3.2819	3.2515	3.2194
DOW	VaR	99%	2.4021	2.0018	2.1168	2.5808	2.5714	2.5323
		95%	1.4396	1.4029	1.4440	1.3139	1.3644	1.3808
	TVaR	99%	3.3172	2.2991	2.4627	3.9710	3.4499	3.2915
		95%	2.1101	1.7700	1.8568	2.1894	2.1266	2.0991
NASDAQ 100	VaR	99%	3.1353	2.4921	2.6518	3.2416	3.2246	3.1622
		95%	1.7319	1.7460	1.8040	1.7050	1.7497	1.7446
	TVaR	99%	3.9356	2.8628	3.0870	4.7597	4.2695	4.0938
		95%	2.6278	2.2035	2.3244	2.7398	2.6776	2.6289

VaR and TVaR values in most cases. Figure 2 shows the empirical VaR and TVaR along with their predicted values obtained from each fitted model with confidence levels ranging between 90 and 99.5%. Looking at the figure, both NMVBS and NIG models predict the VaR and TVaR much better than normal, SN and ST models. To further assess the accuracy of prediction, we calculate the mean absolute relative error (MARE), defined as

$$\text{MARE} = \frac{1}{n_q} \sum_{i=1}^{n_q} \left| \frac{M - \hat{M}}{M} \right|,$$

where n_q represents the number of chosen confidence levels, and M and $\hat{M}$ are the empirical and predicted risk measures, respectively. It can be observed from Table 5 that the NMVBS model has less amount of MARE, indicating that the proposed model outperforms the other approaches in empirical estimation of VaR and TVaR.

To evaluate the in-sample performance of VaR models, we consider the exceeding ratio (ER) introduced by Choi and Min (2011). Let n be the sample size and υ the number of violations of VaR in the actual data. The ER is defined as the ratio of the estimated number of violations divided by the expected number of violations, namely $ER = \upsilon/(qn)$. The ER ratio examines how well the model estimates the VaR. If ER is greater than one, then it indicates the underlying model under-forecasts the VaR. Conversely, an ER value less than one implies an over-forecasting of the VaR. Table 6 shows the ER values estimated under three considered confidence

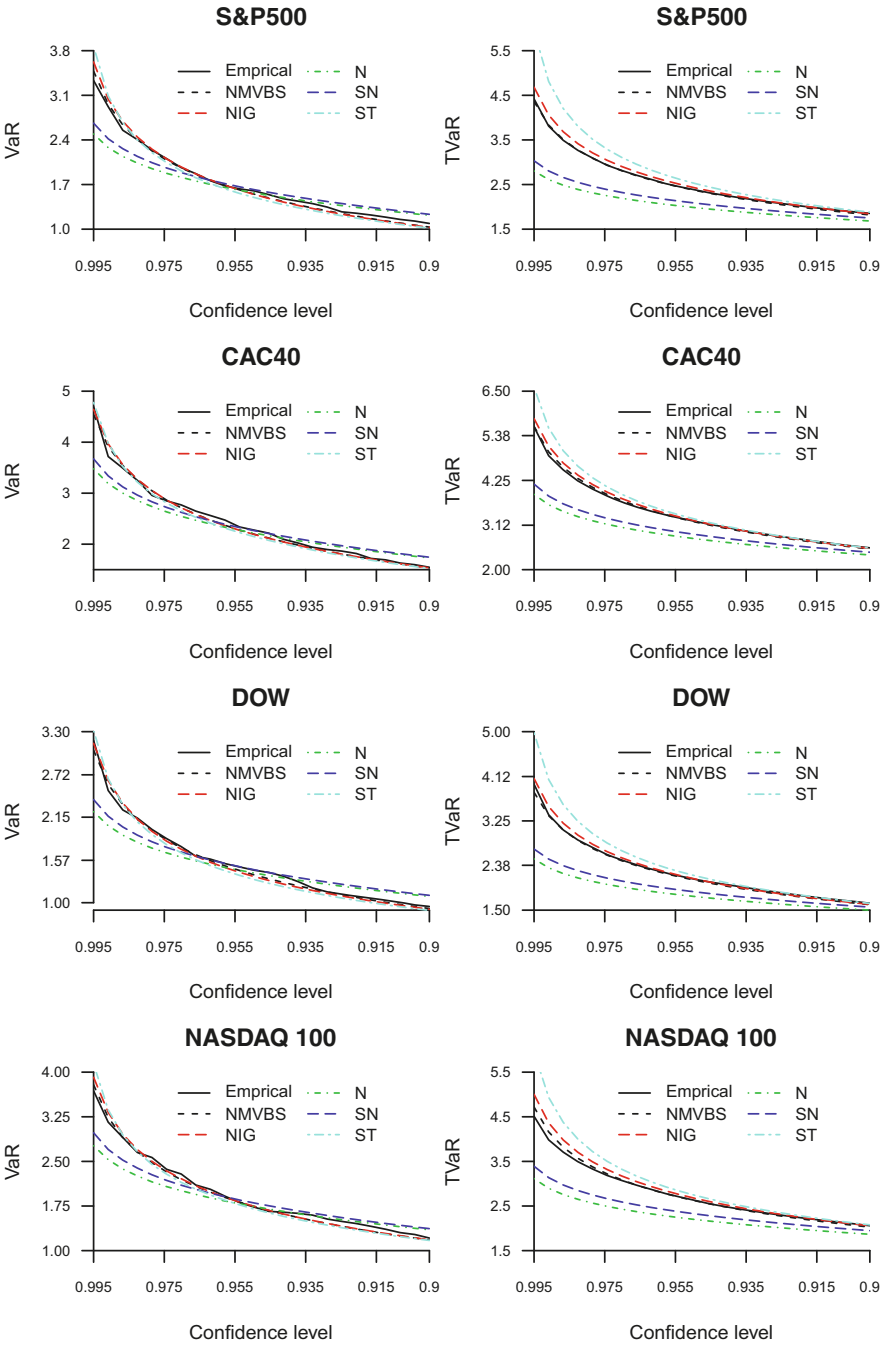

Fig. 2 Plots of VaR (left panel) and TVaR (right panel) as a function of confidence levels (q) for four log-return market price indices

Table 5 Comparison of estimation accuracy of VaR and TVaR in terms of MARE (%)

	Normal		SN		ST		NIG		NMVBS	
Data	VaR	TVaR	VaR	TVaR	VaR	TVaR	VaR	TVaR	VaR	TVaR
S&P500	8.300	18.349	7.790	13.792	6.039	8.176	3.616	2.245	2.682	0.927
CAC40	7.711	14.386	6.851	11.045	3.665	3.690	2.286	1.398	2.347	0.920
DOW	9.610	17.597	8.358	13.452	5.748	5.924	3.234	1.529	2.459	1.529
NASDAQ 100	7.694	17.072	7.092	12.343	4.944	6.787	3.191	2.750	3.153	1.335

Table 6 Exceeding ratio of various models on estimating VaR of four market price indices

Data	q	Normal	SN	ST	NIG	NMVBS
S&P500	99%	2.158	1.874	0.852	0.909	1.022
	97.5%	1.363	1.181	1.113	0.977	1.045
	95%	1.045	0.977	1.158	1.068	1.056
CAC40	99%	1.901	1.733	0.838	0.838	0.838
	97.5%	1.364	1.229	1.051	0.939	0.939
	95%	1.090	1.017	1.140	1.107	1.107
DOW	99%	2.100	1.873	0.738	0.738	0.795
	97.5%	1.226	1.203	1.112	1.044	1.044
	95%	1.101	1.000	1.215	1.169	1.158
NASDAQ 100	99%	2.497	1.703	0.851	0.851	0.908
	97.5%	1.385	1.271	1.180	1.067	1.089
	95%	0.999	0.931	1.056	0.999	0.999

levels. The results suggest that both normal and SN models tend to under-forecast the VaR in most cases. Further, it is evident that the NMVBS distribution can provide competitive or even much more accurate prediction of VaR as compared with the other four distributions.

5 Conclusion

We have proposed a novel tool using the NMVBS distribution for describing financial data and derived some important risk measures in general forms based on its tractable properties. We have also shown that liner combinations of multivariate NMVBS distribution is a univariate NMVBS distribution. This tractable property is useful especially when dealing with portfolio returns formed from weighted sum of different risky assets. In addition, a computational feasible EM algorithm is developed to estimate unknown parameters of the NMVBS distributions. Numerical results reveal that the NMVBS distribution is preferable over other competing distributions for modeling asset returns and a portfolio of risks.

The investigation of risk measures under finite mixtures of skew distributions has received increasing attention, see, for example, Vernic (2006); Bernardi (2013)

and Shushi (2017). However, there is relatively few studies to testify the practical facilities of these approaches with financial data up-to now. Therefore, it is of interest to study risk measures under a finite mixture formulation of NMVBS distributions and compare its performance theoretically and empirically to some existing competitors.

Acknowledgements Naderi's work is based upon research supported by the National Research Foundation, South Africa (Reference: SRUG190308422768 Grant Number: 120839 and STATOMET). Wan-Lun Wang and Tsung-I Lin acknowledge the support from the Ministry of Science and Technology of Taiwan under Grant nos. MOST 107-2628-M-035-001-MY3 and MOST 107-2118-M-005-002-MY2, respectively.

Appendix: ML Estimation for the NMVBS Distribution via the EM Algorithm

Let $\boldsymbol{X} = (\boldsymbol{X}_1, \ldots, \boldsymbol{X}_n)$ be a random sample from a population having the NMVBS distribution with parameters $\boldsymbol{\theta} = (\boldsymbol{\mu}, \boldsymbol{\Sigma}, \boldsymbol{\lambda}, \alpha)$. From (1), the NMVBS distribution admits a convenient hierarchical representation:

$$\boldsymbol{X}_i \mid (W = w_i) \sim N(\boldsymbol{\mu} + \boldsymbol{\lambda} w_i, \boldsymbol{\Sigma} w_i), \qquad W_i \sim BS(\alpha, 1). \tag{A.1}$$

By Bayes' Theorem, it suffices to show that

$$f(w_i \mid \boldsymbol{x}_i) = p(\boldsymbol{x}_i) f_{GIG}\left(w_i; 0, \chi(\boldsymbol{x}_i; \boldsymbol{\theta}), \psi(\boldsymbol{\theta})\right) + (1 - p(\boldsymbol{x}_i)) f_{GIG}$$
$$\left(w; -1, \chi(\boldsymbol{x}_i; \boldsymbol{\theta}), \psi(\boldsymbol{\theta})\right),$$

where

$$p(\boldsymbol{x}_i) = \frac{f_{GH}\left(\boldsymbol{x}_i; \boldsymbol{\mu}, \boldsymbol{\lambda}, \boldsymbol{\Sigma}, 0.5, \alpha^{-2}, \alpha^{-2}\right)}{f_{GH}\left(\boldsymbol{x}_i; \boldsymbol{\mu}, \boldsymbol{\lambda}, \boldsymbol{\Sigma}, 0.5, \alpha^{-2}, \alpha^{-2}\right) + f_{GH}\left(\boldsymbol{x}_i; \boldsymbol{\mu}, \boldsymbol{\lambda}, \boldsymbol{\Sigma}, -0.5, \alpha^{-2}, \alpha^{-2}\right)},$$

$\chi(\boldsymbol{x}_i; \boldsymbol{\theta}) = (\boldsymbol{x}_i - \boldsymbol{\mu})^\top \boldsymbol{\Sigma} (\boldsymbol{x}_i - \boldsymbol{\mu}) + \alpha^{-2}$, $\psi(\boldsymbol{\theta}) = \boldsymbol{\lambda}^\top \boldsymbol{\Sigma} \boldsymbol{\lambda} + \alpha^{-2}$, and $f_{GIG}(\cdot; \kappa, \chi, \psi)$ is the pdf of $GIG(\kappa, \chi, \psi)$. Consequently, we have

$$E\left[W_i^r \middle| \boldsymbol{X}_i = \boldsymbol{x}_i\right] = \left(\frac{\chi(\boldsymbol{x}_i; \boldsymbol{\theta})}{\psi(\boldsymbol{\theta})}\right)^{r/2} \left\{ p(\boldsymbol{x}_i) R_{(0,r)}\left(\sqrt{\psi(\boldsymbol{\theta}) \chi(\boldsymbol{x}_i; \boldsymbol{\theta})}\right) \right.$$
$$\left. + (1 - p(\boldsymbol{x}_i)) R_{(-1,r)}\left(\sqrt{\psi(\boldsymbol{\theta}) \chi(\boldsymbol{x}_i, \boldsymbol{\theta})}\right) \right\}, \tag{A.2}$$

where r can be any positive or negative integers.

Using (A.1), the log-likelihood function of $\boldsymbol{\theta}$ for the complete data $\boldsymbol{x} = (\boldsymbol{x}_1, \ldots, \boldsymbol{x}_n)$ and $\boldsymbol{W} = (W_1, \ldots, W_n)$, omitting additive constants, is

$$\ell_c(\boldsymbol{\theta} \mid \boldsymbol{x}, \boldsymbol{W}) = -n\log\alpha - \frac{n}{2}\log|\boldsymbol{\Sigma}| - \sum_{i=1}^{n}\left\{\frac{(W_i-1)^2}{2\alpha^2 W_i} + \frac{(\boldsymbol{x}_i-\boldsymbol{\mu})^\top\boldsymbol{\Sigma}^{-1}(\boldsymbol{x}_i-\boldsymbol{\mu})}{2W_i}\right.$$
$$\left. + \frac{W_i}{2}\boldsymbol{\lambda}^\top\boldsymbol{\Sigma}^{-1}\boldsymbol{\lambda} - (\boldsymbol{x}_i-\boldsymbol{\mu})^\top\boldsymbol{\Sigma}^{-1}\boldsymbol{\lambda}\right\}. \tag{A.3}$$

On the kth iteration of the E-step, we compute the expected value of (A.3) conditioning on the current parameter estimates $\hat{\boldsymbol{\theta}}^{(k)} = (\hat{\boldsymbol{\mu}}^{(k)}, \hat{\boldsymbol{\Sigma}}^{(k)}, \hat{\boldsymbol{\lambda}}^{(k)}, \hat{\alpha}^{(k)})$ and the observed data $\boldsymbol{x}$, called the Q-function:

$$Q(\boldsymbol{\theta} \mid \hat{\boldsymbol{\theta}}^{(k)}) = E[\ell_c(\boldsymbol{\theta} \mid \boldsymbol{x}, \boldsymbol{W}) \mid \boldsymbol{x}, \hat{\boldsymbol{\theta}}^{(k)}]. \tag{A.4}$$

Evaluation of (A.4) needs to calculate the following two conditional expectations

$$\hat{w}_i^{(k)} = E(W_i \mid \boldsymbol{x}_i, \hat{\boldsymbol{\theta}}^{(k)}) \text{ and } \hat{t}_i^{(k)} = E(W_i^{-1} \mid \boldsymbol{x}_i, \hat{\boldsymbol{\theta}}^{(k)})$$

whose solution are obtained by using (A.2). The resulting Q-function is

$$Q(\boldsymbol{\theta} \mid \hat{\boldsymbol{\theta}}^{(k)}) = -n\log\alpha - \frac{n}{2}\log\boldsymbol{\Sigma} - \frac{1}{2}\sum_{i=1}^{n}\left\{\frac{\hat{s}_i^{(k)}}{\alpha^2} + (\boldsymbol{x}_i-\boldsymbol{\mu})^\top\boldsymbol{\Sigma}^{-1}(\boldsymbol{x}_i-\boldsymbol{\mu})\hat{t}_i^{(k)}\right.$$
$$\left. + \hat{w}_i^{(k)}\boldsymbol{\lambda}^\top\boldsymbol{\Sigma}^{-1}\boldsymbol{\lambda} - 2(\boldsymbol{x}_i-\boldsymbol{\mu})^\top\boldsymbol{\Sigma}^{-1}\boldsymbol{\lambda}\right\}, \tag{A.5}$$

where $\hat{s}_i^{(k)} = \hat{w}_i^{(k)} + \hat{t}_i^{(k)} - 2$.

In the M-step, we maximize (A.5) with respect to each entry of $\boldsymbol{\theta}$, leading to the following closed-form estimators:

$$\hat{\boldsymbol{\mu}}^{(k+1)} = \frac{\sum_{i=1}^n \boldsymbol{x}_i\hat{t}_i^{(k)} - n\hat{\boldsymbol{\lambda}}^{(k+1)}}{\sum_{i=1}^n \hat{t}_i^{(k)}}, \quad \hat{\alpha}^{(k+1)} = \sqrt{\frac{\sum_{i=1}^n \hat{s}_i^{(k)}}{n}},$$
$$\hat{\boldsymbol{\lambda}}^{(k+1)} = \frac{\sum_{i=1}^n \hat{t}_i^{(k)}\sum_{i=1}^n \boldsymbol{x}_i - n\sum_{i=1}^n \boldsymbol{x}_i\hat{t}_i^{(k)}}{\sum_{i=1}^n \hat{t}_i^{(k)}\sum_{i=1}^n \hat{w}_i^{(k)} - n^2},$$

and

$$\hat{\boldsymbol{\Sigma}}^{(k+1)} = \frac{1}{n}\left[\sum_{j=1}^{n}\hat{t}_i^{(k)}(\boldsymbol{x}_i-\boldsymbol{\mu}^{(k+1)})(\boldsymbol{x}_i-\boldsymbol{\mu}^{(k+1)})^\top + \hat{\boldsymbol{\lambda}}^{(k+1)}\hat{\boldsymbol{\lambda}}^{\top(k+1)}\sum_{i=1}^{n}\hat{w}_i^{(k)}\right]$$
$$-\hat{\boldsymbol{\lambda}}^{(k+1)}(\bar{\boldsymbol{x}}-\boldsymbol{\mu}^{(k+1)})^\top - (\bar{\boldsymbol{x}}-\boldsymbol{\mu}^{(k+1)})\hat{\boldsymbol{\lambda}}^{\top(k+1)}$$

$$= \frac{1}{n}\left[\sum_{j=1}^{n} \hat{t}_i^{(k)} (\boldsymbol{x}_i - \boldsymbol{\mu}^{(k+1)})(\boldsymbol{x}_i - \boldsymbol{\mu}^{(k+1)})^\top - \hat{\boldsymbol{\lambda}}^{(k+1)} \hat{\boldsymbol{\lambda}}^{\top(k+1)} \sum_{i=1}^{n} \hat{w}_i^{(k)}\right],$$

where the last equality in $\hat{\boldsymbol{\Sigma}}^{(k+1)}$ is obtained by utilizing $n(\bar{\boldsymbol{x}} - \boldsymbol{\mu}^{(k+1)}) = \hat{\boldsymbol{\lambda}}^{(k+1)} \sum_{i=1}^{n} \hat{w}_i^{(k)}$.

References

Aas, K., & Haff, I. H. (2006). The generalized hyperbolic skew student's t-distribution. *Journal of Financial Econometrics, 4*, 275–309.

Adcock, C., Eling, M., & Loperfido, N. (2015). Skewed distributions in finance and actuarial science: A review. *The European Journal of Finance, 21*, 1253–1281.

Akaike, H. (1973). Information theory and an extension of the maximum likelihood principle. *Second International Symposium on Information Theory, Akaémiai Kiadó, Budapest* (pp. 267–281).

Artzner, P., Delbaen, F., Eber, J. M., & Heath, D. (1999). Coherent measures of risk. *Mathematical Finance, 9*, 203–228.

Azzalini, A. (1985). A class of distributions which includes the normal ones. *Scandinavian Journal of Statistics, 12*, 171–178.

Azzalini, A. (2004). The sn Package; R Reference Guide available from www.r-project.org.

Azzalini, A., & Capitaino, A. (2003). Distributions generated by perturbation of symmetry with emphasis on a multivariate skew t distribution. *Journal of the Royal Statistical Society, Series B, 65*, 367–389.

Barndorff-Nielsen, O. (1977). Exponentially decreasing distributions for the logarithm of particle size. *In Proceedings of the Royal Society of London A: Mathematical, Physical and Engineering Sciences, 1674*, 401–419.

Bernardi, M. (2013). Risk measures for skew normal mixtures. *Statistics and Probability Letters, 83*, 1819–1824.

Birnbaum, Z. W., & Saunders, S. C. (1969). A new family of life distributions. *Journal of Applied Probability, 6*, 319–327.

Breymann, W., & Luthi, D. (2009). *ghyp: A package on generalized hyperbolic distribution*. New York: Institute of data analysis and process design.

Brogan, A. J., & Stidham, S. (2008). Non-separation in the mean-lower-partial-moment portfolio optimization problem. *European Journal of Operational Research, 184*, 701–710.

Bühlmann, H. (1980). An economic premium principle. *ASTIN Bulletin: The Journal of the IAA, 11*, 52–60.

Choi, P., & Min, I. (2011). A comparison of conditional and unconditional approaches in value–at–risk estimation. *Japanese Economic Review, 62*, 99–115.

Dempster, A. P., Laird, N. M., & Rubin, D. B. (1977). Maximum likelihood from incomplete data via the EM algorithm. *Journal of the Royal Statistical Society. Series B, 39*, 1–38.

Desmond, A. F. (1986). On the relationship between two fatigue-life models. *IEEE Transactions on Reliability, 35*, 167–169.

Eling, M. (2012). Fitting insurance claims to skewed distributions: Are the skew-normal and skew-student good models? *Insurance: Mathematics and Economics, 51*, 239–248.

Eling, M. (2014). Fitting asset returns to skewed distributions: Are the skew-normal and skew-student good models? *Insurance: Mathematics and Economics, 59*, 45–56.

Föllmer, H., & Knispel, T. (2011). Entropic risk measures: Coherence vs. convexity, model ambiguity and robust large deviations. *Stochastics and Dynamics, 11*, 333–351.

Good, I. J. (1953). The population frequencies of species and the estimation of population parameters. *Biometrika, 40*, 237–260.

Goovaerts, M. J., de Vylder, F., & Haezendonck, J. (1984). *Insurance premiums: theory and applications*. Amsterdam: North-Holland.

Ho, H. J., Pyne, S., & Lin, T. I. (2012). Maximum likelihood inference for mixtures of skew Student-t-normal distributions through practical EM-type algorithms. *Statistics and Computing, 22*, 287–299.

Hu, W., & Kercheval, A. (2007). Risk management with generalized hyperbolic distributions. In *Proceedings of the Fourth IASTED International Conference on Financial Engineering and Applications* (pp. 19–24).

Jarque, C. M., & Bera, A. K. (1987). A test for normality of observations and regression residuals. *International Statistical Review/Revue Internationale de Statistique, 55*, 163–172.

Konlack Socgnia, V., & Wilcox, D. (2014). A comparison of generalized hyperbolic distribution models for equity returns. *Journal of Applied Mathematics, 2014*, 263465.

Lee, S. X., & McLachlan, G. J. (2013). Model-based clustering and classification with non-normal mixture distributions. *Statistical Methods and Applications, 22*, 427–454.

Lin, T. I., Ho, H. J., & Lee, C. R. (2014). Flexible mixture modelling using the multivariate skew-t-normal distribution. *Statistics and Computing, 24*, 531–546.

McNeil, A., Frey, R., & Embrechts, P. (2005). *Quantitative risk management: concepts, techniques and tools*. Princeton, NJ: Princeton University Press.

Naderi, M., Arabpour, A., Lin, T. I., & Jamalizadeh, A. (2017). Nonlinear regression models based on the normal mean-variance mixture of Birnbaum-Saunders distributions. *Journal of the Korean Statistical Society, 46*, 476–485.

Pourmousa, R., Jamalizadeh, A., & Rezapour, M. (2015). Multivariate normal mean-variance mixture distribution based on Birnbaum-Saunders distribution. *Journal of Statistical Computation and Simulation, 85*(13), 2736–2749.

Schwarz, G. (1978). Estimating the dimension of a model. *The Annals of Statistics, 6*, 461–464.

Shushi, T. (2017). Skew-elliptical distributions with applications in risk theory. *European Actuarial Journal, 7*, 277–296.

Smirnov, N. V. (1948). Tables for estimating the goodness of fit of empirical distributions. *The Annals of Mathematical Statistics, 19*, 279–281.

Vernic, R. (2006). Multivariate skew-normal distributions with applications in insurance. *Insurance: Mathematics and Economics, 38*, 413–426.

On the Distribution of Linear Combinations of Chi-Square Random Variables

Carlos A. Coelho

Abstract The distribution of linear combinations of independent chi-square random variables is intimately related with the distribution of quadratic forms in normal random variables. As such, this distribution has been studied by many authors. However, there is still some room left for improvement, since while some simpler approximations do not yield sufficiently good results, other approximations which show a better performance are sometimes too complicated to be implemented in practical terms. In this paper the exact distribution of linear combinations of independent chi-square random variables is obtained, for some particular cases, in closed finite highly manageable forms, while for more general cases near-exact approximations are obtained, which are able to yield very manageable and well-performing approximations. Numerical studies compare the performance of these near-exact distributions with other existing approximations and distributions and show how sharp are the approximations provided by these near-exact distributions. A useful subproduct that is obtained is closed form expressions for the distribution of quadratic forms and for some instances of ratios of quadratic forms, useful in ANOVA and other linear or mixed-linear models where heterocedasticity is present or assumed. Solutions for the problem of the distribution of the statistic associated with the Behrens–Fisher problem are then in turn obtained as a much useful subproduct of the distribution of ratios of quadratic forms. Modules programmed in Mathematica®, MAXIMA and R for the implementation of the distributions developed are made available at the site https://sites.google.com/site/lincombchisquares.

C. A. Coelho (✉)
Mathematics Department (DM) and Centro de Matemática e Aplicações (CMA), Faculdade de Ciências e Tecnologia, NOVA University of Lisbon, Caparica, Portugal
e-mail: cmac@fct.unl.pt

A. Bekker et al. (eds.), *Computational and Methodological Statistics and Biostatistics*, Emerging Topics in Statistics and Biostatistics,
https://doi.org/10.1007/978-3-030-42196-0_9

1 Introduction

The distribution of linear combinations of independent chi-square r.v.'s (random variables) has been addressed by a large number of authors and it has been obtained under a number of different forms.

This distribution is of interest not only given its relation with the distribution of quadratic forms in normal r.v.'s but also because it appears associated with the distribution of a number of statistics. Indeed in many cases it appears associated with the distribution of quadratic forms in normal r.v.'s, as it is for example the case of the works by Robbins (1948), Robbins and Pitman (1949), Box (1954), Ruben (1960, Sect. 7), Imhof (1961), Ruben (1962), Baldesari (1967), Kotz et al. (1967a,b), Johnson and Kotz (1968), Shah (1970), Solomon and Stephens (1977), Bock (1984), Bock and Solomon (1987), Morin-Wahhab (1988), Mathai and Provost (1992), Baksalary et al. (1994), Provost and Rudiuk (1996), and Lu (2006), to mention only a few, namely some of the former and some recent authors. In what concerns its relation with the distribution of statistics of interest, Chernoff and Lehmann (1954) show that the distribution of the common chi-square goodness-of-fit statistic, when maximum likelihood estimates based on the original data are used, is better approximated by the distribution of a linear combination of independent chi-square r.v.'s, all of them but one with one degree-of-freedom, and Durbin et al. (1975) show that the distribution of the Cramer-von Mises goodness-of-fit statistic may be written as that of an infinite linear combination of independent chi-square r.v.'s also all with one degree-of-freedom (d.f.). Ruben (1960, Sect. 7) refers cases where statistics of interest may have the distribution of linear combinations of independent chi-square r.v.'s with an even number of d.f.'s, and Alvo et al. (1982) show that the asymptotic distribution of the Kendall tau is the same as the distribution of a linear combination of two independent chi-square r.v.'s.

Robbins (1948) obtains the distribution of a linear combination of independent chi-square r.v.'s, all with one d.f., under the form of an infinite power series with a rate parameter that is equal to the geometric mean of the coefficients associated with the chi-square r.v.'s. Embedded in this series are some multinomial coefficients, which as the order of the terms increase get more and more complicated to be computed, but the author develops a recurrence relation which allows for a simpler computation. However, a power series will always need many more terms to converge than a series involving exponentials, as the ones that involve chi-square or Gamma densities. As such, the author also obtains the same distribution in the form of an infinite mixture of chi-square distributions. But one other problem that may arise is when some of the coefficients in the linear combination are equal, leading to chi-square r.v.'s with more than just one d.f., in which situation the author calls for the use of limits on the expressions used to define the weights in the mixture distribution. However, this may be a not completely straightforward and easy job, mainly when several of the coefficients in the linear combination are equal to other coefficients, leading to the existence of several chi-square r.v.'s with more than one d.f.. Robbins and Pitman (1949) obtain a somewhat similar representation where

the geometric mean of the coefficients is now replaced just by their minimum and where the weights in the mixture are to be obtained through the solution of a product identity, which solution may be not so simple for terms of larger order in the mixture. Ruben (1962) suggests the use of a similar mixture of Gamma distributions but with an arbitrary scale parameter, without giving explicit formulation for the weights.

Box (1954, Sect. 2, Thm. 2.4) obtains an interesting expression for the distribution of the linear combination of independent chi-square r.v.'s for the case when all these have an even number of d.f.'s. This distribution has close relations with the GIG (Generalized Integer Gamma) distribution (Coelho 1998) proposed in Sect. 2 for the same situation, but opposite to the GIG distribution, which has all the involved coefficients specified by their algebraic expressions, Box leaves some of the coefficients in the distribution to be obtained from derivatives of a function which involves the coefficients in the linear combination and the d.f.'s of the chi-square r.v.'s. It happens that for larger values of the d.f.'s these derivatives may be not completely so easy to obtain, and a general expression for them is not easy to spot, although they are indeed intimately related with the $c_{j,k}$ coefficients in the probability density function (p.d.f.) and in the cumulative distribution function (c.d.f.) of the GIG distribution (see e.g. Appendix 1).

Imhof (1961) refers in Sect. 2 of his paper this same case and also presents a finite closed form solution but he remarks not being able to establish a complete identity between his result and the one presented by Box (1954), although there is a clear similitude between the two solutions. While Box used the partial fraction technique, Imhof bases his result on the inversion of the characteristic function (c.f.). However, once again, the weights in the final mixture are to be obtained from successive derivatives of a function that involves the coefficients in the linear combination and the d.f.'s of the chi-square r.v.'s and which present the same problem as the ones in the mixture obtained by Box (1954), since, as remarked by the author "with increasing v_k's [the number of d.f.'s], the labour of computing the corresponding derivatives ... rapidly becomes considerable. The numerical method of the next section is then often easier to apply". Indeed then in Sect. 3 Imhof resorts to the numerical inversion of the c.f., based on Gil-Pelaez (1951) inversion formula. This is indeed a framework which we do not intend to engage into the present paper but which was pursued further by several authors, among which we may point out Davies (1980) and Lu (2006) who also use Gil-Pelaez (1951) inversion formula.

Kotz et al. (1967a), address, as other authors do, the case where all chi-square r.v.'s in the linear combination have just one only d.f., this because of the relation of this distribution with that of quadratic forms, and obtain in Sect. 3 expansions of the distribution of linear combinations of independent chi-square r.v.'s in terms of power series and series based on Laguerre polynomials which end up being infinite mixtures of chi-square distributions. These latter ones are indeed quite close to the series representation later obtained by Moschopoulos (1985) for the distribution of a linear combination of Gamma r.v.'s. Actually we will use Moschopoulos (1985) mixture distribution as a benchmark for comparison with the near-exact approximations developed in Sect. 4 of our paper, given its accuracy, the good convergence properties of the series and also its ease of implementation, given the

fact that the weights in the mixture and all other coefficients involved are explicitly given by algebraic expressions. While Kotz et al. (1967a) address the central case, Kotz et al. (1967b) address the non-central case, being the case that we will restrict our attention in the present paper to the case of linear combinations of central chi-square r.v.'s, which will allow for the obtention of simpler expressions, with closed forms for some particular cases.

Shah (1970) centers his attention on the distribution of matrix quadratic forms and obtains their distributions in the form of infinite series of zonal polynomials. Solomon and Stephens (1977) approximate the distribution of quadratic forms and that of a linear combination of independent chi-squares by a Pearson curve that matches the first four moments and by the distribution of a single chi-square multiplied by a constant, matching the first three exact moments of the quadratic form or linear combination of chi-squares, but these may indeed give only quite rough approximations. Bock (1984) expresses the distribution of quadratic forms in terms of the distributions of linear combinations of other quadratic forms and linear combinations of independent chi-square r.v.'s, but in Sect. 3 she deals with the distribution of a linear combination of only two independent chi-square r.v.'s, for which she proposes an expression involving the Kummer confluent hypergeometric function, and finds a finite sum representation when at least one of the two chi-square r.v.'s has an even number of d.f.'s, but this representation involves Dawson's integral. In Sect. 4 she addresses the distribution of a linear combination of chi-squares where all but one of the chi-squares have just 1 d.f.

Bock and Solomon (1987) obtain the distribution of a linear combination of only two independent chi-square r.v.'s in several forms, most of them involving modified Bessel functions and the distribution function of a linear combination of two independent chi-square r.v.'s, both with 1 d.f., which has then to be dealt with. Mathai and Provost (1992) provide several forms for the distribution of quadratic forms and as such also for the distribution of linear combinations of independent chi-square r.v.'s, in Chap. 4 of their book, in terms of power series and Laguerre polynomial series expansions, as well as in terms of chi-square distributions. For this latter case, although the authors refer that their result is similar to the one obtained by Ruben (1962), all coefficients in the expansion and the weights in the final mixture representation are given explicit expressions. It happens that since a chi-square r.v. multiplied by any constant is indeed a Gamma r.v., there is an intimate relation between the result obtained by Mathai and Provost and the result obtained by Moschopoulos (1985) for the linear combination of Gamma r.v.'s, which given our approach followed in Sect. 4, gives us, as already remarked, a more adequate and express benchmark for our work.

Provost and Rudiuk (1996) address the general case of the distribution of the difference of two linear combinations of independent chi-square r.v.'s, and express it in terms of a series of Whittaker functions. This distribution may indeed appear as a particular case of the distribution of linear combinations of independent chi-square r.v.'s when the coefficients in the linear combination have different signs, and it is addressed in Sect. 3 of the present paper, where a finite closed form is given for this

distribution for the case where all chi-square r.v.'s involved have an even number of d.f.'s.

In fact, besides the literature that addresses the distribution of linear combinations of independent chi-square r.v.'s in the domain of the distribution of quadratic forms, there is also a host of other authors who along the years have addressed the distribution of linear combinations of independent chi-square r.v.'s just by itself, as it is the case for example of Fleiss (1971) who obtained the distribution of a linear combination of chi-square r.v.'s in the form of a number of nested integrals. However, this form is not too adequate for implementation, since all the integrals, in equal number to the chi-square r.v.'s in the linear combination, have to be numerically solved. Davis (1977) uses a differential equation approach that gives a power series distribution which matches that of Robbins (1948) when all coefficients in the linear combination are positive. Moschopoulos and Canada (1984) obtained an infinite Gamma series, with intimate relations with the more embracing result in Moschopoulos (1985) on the distribution of a linear combination of independent Gamma r.v.'s. To address the non-central case, Castaño-Martínez and López-Blázquez (2005) use series expansions involving Laguerre polynomials, while more recently Ha and Provost (2013) use a linear combination of Laguerre polynomials together with a moment matching technique.

Gabler and Wolff (1987) approximate the distribution of a linear combination of chi-squares by a combination of a distribution function of a unique scaled chi-square and that of a finite mixture of scaled Gamma distributions. Other simple approximations for the distribution of a linear combination of independent chi-square r.v.'s by a single chi-square distribution, eventually with a non-integer number of d.f.'s, that is, actually by a Gamma distribution, are the ones by Satterthwaite (1941) and Welch (1947).

Other references to works on the distribution of linear combinations of independent chi-square r.v.'s, previous to 1994, may be found in Sect. 18.8 of Johnson et al. (1994).

Since indeed all linear combinations of independent chi-square r.v.'s are either sums or linear combinations of independent Gamma r.v.'s, also all the vast literature on the distribution of linear combinations or sums of independent Gamma r.v.'s is of interest. To mention only a few of those we feel as more important references, Mathai (1982) obtains this distribution as a finite sum but involving zonal polynomials or hypergeometric functions, while Moschopoulos (1985), as already mentioned, obtains it as an infinite mixture of Gamma distributions with rate parameters equal to the sum of the original rate parameters plus the index of the mixture, running from zero to infinity, and with a scale parameter that is the minimum of the scale parameters of the original Gamma r.v.'s in the linear combination. Also, as already mentioned, due to its good convergence properties (that is, the need for much lesser terms to obtain a good approximation to the exact distribution, then other series representations) and ease of implementation, since all parameters, coefficients and weights in the mixture are fully specified, this distribution will be used as a benchmark in Sect. 4 to be compared with the performance of the near-exact approximations there developed. Provost (1988)

obtains the distribution of a linear combination of independent Gamma r.v.'s in terms of integrals and Whittaker functions, while the same author in a 1989 paper (Provost 1989) obtains the distribution of the sum of independent Gamma r.v.'s as an infinite series, with some relations with the series obtained by Moschopoulos (1985), but with the common scale parameter of the Gamma distributions in the mixture as the geometric or harmonic means of the original scale parameters, instead of its minimum (see Sect. 4 of the present paper).

It is the aim of the present contribution to lend some new results and to sharpen some existing ones giving them a more workable form, which will surely be useful in applications and that may also be used to establish new results concerning the distribution of ratios of linear combinations of chi-squares and the distribution of the Behrens–Fisher statistic. Finite closed forms are provided for both the probability density and cumulative distribution functions of some cases of linear combinations of chi-square r.v.'s, being provided sharp approximations for the other cases. As a by-product we also obtain a form to build near-exact distributions for sums or linear combinations of independent Gamma r.v.'s.

Intentionally, only the central case is addressed, in order to be able to provide simpler results, including some simple finite closed form results, and to keep the contribution within an acceptable length.

In precise terms, we will address the problem of obtaining explicit manageable expressions for both the p.d.f. and the c.d.f. of the distribution of a r.v.

$$Z = \sum_{j=1}^{p} w_j \, Y_j \tag{1}$$

where $Y_j \sim \chi^2_{k_j}$ $(j = 1, \ldots, p)$, form a set of p independent r.v.'s and where w_j $(j = 1, \ldots, p)$ are real weights. We will consider a number of cases of interest where punctually some restrictions may be placed on the weights w_j or on the d.f.'s k_j in order to be able to obtain simpler results.

In Sect. 2 we will consider the case where all w_j are positive and all or all but one of the k_j are even. In Sect. 3 we will consider the case where all k_j are even and the w_j are real, and in Sect. 4 we will address the case where all w_j are positive and the d.f.'s k_j are left to be either even or odd. Then in Sect. 5 the distribution of ratios of linear combinations of chi-squares is addressed, which is intimately related with the distribution of statistics used in ANOVA and other models when heterocedasticity is present and in Sect. 6 is addressed the distribution of the statistic associated with the Behrens–Fisher problem, obtained as a by-product of the results in Sect. 5. In Sect. 7 are presented some examples of situations where the distributions developed in Sects. 2–5 arise and in Sect. 8 some conclusions are drawn.

2 The Case of Positive w_j with at Most One Odd k_j

Let us first address the case where all w_j are positive and all Y_j have an even number of d.f.'s, and let us denote by $X \sim \Gamma(r, \lambda)$ the fact that the r.v. X has a Gamma distribution with shape parameter r and rate parameter λ, that is, a r.v. with p.d.f.

$$f_X(x) = \frac{\lambda^r}{\Gamma(r)} e^{-\lambda x} x^{r-1} \quad (r, \lambda > 0; x > 0) .$$

Then we have, for $j = 1, \ldots, p$,

$$Y_j \sim \Gamma\left(\frac{k_j}{2}, \frac{1}{2}\right) \implies Z_j = w_j Y_j \sim \Gamma\left(\frac{k_j}{2}, \frac{1}{2w_j}\right) \tag{2}$$

where all $k_j/2$ are integers. In this case Z in (1) is thus a sum of p independent Gamma r.v.'s, all with integer shape parameters, and as such its distribution is a GIG distribution, with shape parameters $k_1/2, \ldots, k_p/2$, rate parameters $1/(2w_1), \ldots, 1/(2w_p)$ and depth p, this in case all $1/(2w_j)$ are different (see Appendix 1 and Coelho (1998) for details on the GIG distribution, its p.d.f. and c.d.f.).

In case some of the w_j's are equal, without any loss of generality, since the order of the r.v.'s Y_j in the sum in (1) is irrelevant, let us assume these are the ones indexed $1, \ldots, g(\leq p)$ and let us call w the common value of these g w_j's. Then all we have to do is to first add these g Gamma r.v.'s to obtain a $\Gamma\left(\sum_{j=1}^{g} \frac{k_j}{2}, \frac{1}{2w}\right)$, then yielding for Z a GIG distribution of depth $p - g + 1$, with rate parameters $\sum_{j=1}^{g} \frac{k_j}{2}, \frac{k_{g+1}}{2}, \ldots, \frac{k_p}{2}$ and shape parameters $\frac{1}{2w}, \frac{1}{2w_{g+1}}, \ldots, \frac{1}{2w_p}$. Of course, rate parameters may also be equal by 'sectors'. Then the above reasoning should be adequately adapted.

Assuming the case where all w_j are different and using the notation in Appendix 1 for the GIG p.d.f and c.d.f., the p.d.f. and c.d.f. of Z are written as

$$f_Z(z) = f^{GIG}\Big(z \,\Big|\, \{k_j/2\}_{j=1:p}; \{1/(2w_j)\}_{j=1:p}; p\Big), \quad (z > 0)$$

and

$$F_Z(z) = F^{GIG}\Big(z \,\Big|\, \{k_j/2\}_{j=1:p}; \{1/(2w_j)\}_{j=1:p}; p\Big), \quad (z > 0) .$$

In case among the p r.v.'s Y_j only one of them has an odd number of d.f.'s, then only one of the Z_j r.v.'s in (2) has a Gamma distribution with a non-integer shape parameter, and the distribution of Z will be what we call a GNIG (Generalized Near-Integer Gamma) distribution (see Appendix 1 and Coelho (2004) for details on this distribution, its p.d.f. and c.d.f.). In case all w_j are different, without any loss of generality, since as already stated, the ordering of the r.v.'s Y_j in (1) is irrelevant, let

the r.v. Y_j with an odd number of d.f.'s be indexed as Y_p. Then Z will have a GNIG distribution of depth p, with p.d.f. and c.d.f. which, using the notation in Appendix 1, may be respectively written as

$$f^{GNIG}\left(z \,\middle|\, \frac{k_1}{2}, \ldots, \frac{k_{p-1}}{2}; \frac{k_p}{2}; \frac{1}{2w_1}, \ldots, \frac{1}{2w_{p-1}}; \frac{1}{2w_p}; p\right)$$

and

$$F^{GNIG}\left(z \,\middle|\, \frac{k_1}{2}, \ldots, \frac{k_{p-1}}{2}; \frac{k_p}{2}; \frac{1}{2w_1}, \ldots, \frac{1}{2w_{p-1}}; \frac{1}{2w_p}; p\right).$$

In case some of the w_j are equal, say g of them, then the depth of the GNIG distribution will be equal to $p - g + 1$, being the case that the adjustment will be done in a similar way to that described above for the case of all even k_j.

The Mathematica® modules to implement the GIG and the GNIG distributions are available at https://sites.google.com/site/nearexactdistributions, with the modules for the GIG distribution also available in Sect. 2.7 of Coelho and Mexia (2010) and in Appendix 4.A of Coelho and Arnold (2019). The MAXIMA and R modules for the GIG distribution are also available at this book supplementary material site, at https://sites.google.com/site/meijerfoxfiniteforms.

3 The Case Where All k_j Are Even But the w_j May be Both Positive and Negative

Let us suppose that all chi-square r.v.'s Y_j in (1) have an even number of d.f.'s but some of the w_j are positive and some are negative. Without any loss of generality, since, as already mentioned, the order of the Y_j r.v.'s in (1) is irrelevant, let us consider that the w_j that are positive are the ones for $j = 1, \ldots, p_1 (< p)$, the others being negative. Let also $p_2 = p - p_1$. Then let us consider the r.v.'s

$$Z_1^* = \sum_{j=1}^{p_1} w_j Y_j \quad \text{and} \quad Z_2^* = \sum_{j=p_1+1}^{p} -w_j Y_j \,.$$

Since all k_j $(j = 1, \ldots, p)$ are even, both Z_1^* and Z_2^* have GIG distributions, which assuming that all w_j are different will have respectively depths p_1 and p_2. Then we have $Z = Z_1^* - Z_2^*$, where Z_1^* and Z_2^* are two independent GIG r.v.'s. Thus, the r.v. Z will have in this case what Coelho and Mexia (2010) call a DGIG (Difference of two GIG) distribution, with p.d.f. (see Appendix 2 for details on the DGIG distribution and the expressions for its p.d.f. and c.d.f.)

$$f_Z(z) = f^{\,DGIG}\left(z \middle| \left\{\frac{k_j}{2}\right\}_{j=1:p_1}; \left\{\frac{k_j}{2}\right\}_{j=p_1+1:p}; \left\{\frac{1}{2w_j}\right\}_{j=1:p_1}; \left\{\frac{1}{2w_j}\right\}_{j=p_1+1:p}; p_1, p_2\right),$$

and c.d.f.

$$F_Z(z) = F^{\,DGIG}\left(z \middle| \left\{\frac{k_j}{2}\right\}_{j=1:p_1}; \left\{\frac{k_j}{2}\right\}_{j=p_1+1:p}; \left\{\frac{1}{2w_j}\right\}_{j=1:p_1}; \left\{\frac{1}{2w_j}\right\}_{j=p_1+1:p}; p_1, p_2\right),$$

with $z \in \mathbb{R}$.

A caution note is here in place: as mentioned in Coelho and Mexia (2010), it is in this reference where the correct expressions for the p.d.f. and c.d.f. of the DGIG distribution are to be found, since the ones in Coelho and Mexia (2007) suffer from some typos in their writings.

In case some of the w_j for $j = 1, \ldots, p_1$, or some of the w_j for $j = p_1 + 1, \ldots, p$ are equal, then adjustments similar to the ones indicated in Sect. 2 should be made.

Mathematica® modules to implement the DGIG distribution are available in Sect. 2.7 of Coelho and Mexia (2010). MAXIMA and R modules are also available from the author or at https://sites.google.com/site/lincombchisquares.

4 The Case Where All w_j Are Positive and the k_j Are Both Even and Odd or All Odd

Let us take

$$\ell_j = \left\lfloor \frac{k_j}{2} \right\rfloor \quad \text{and} \quad \ell_j^* = \frac{k_j}{2} - \ell_j \quad (j = 1, \ldots, p) \tag{3}$$

respectively as the integer and non-integer parts of $k_j/2$ $(j = 1, \ldots, p)$, and let

$$Z_j^* \sim \Gamma\left(\ell_j, \frac{1}{2w_j}\right) \quad \text{and} \quad Z_j^{**} \sim \Gamma\left(\ell_j^*, \frac{1}{2w_j}\right), \quad j = 1, \ldots, p$$

be, for a given j, two independent r.v.'s, where Z_j^{**} vanishes if $\ell_j^* = 0$ and Z_j^* vanishes if $k_j = 1$. Then we have

$$Z_j = Z_j^* + Z_j^{**}.$$

Furthermore, let

$$Z^* = \sum_{j=1}^{p} Z_j^* \quad \text{and} \quad Z^{**} = \sum_{j=1}^{p} Z_j^{**} . \tag{4}$$

Then we have

$$Z = Z^* + Z^{**} ,$$

where Z^* and Z^{**} are two independent r.v.'s, and where, in case all w_j ($j = 1, \ldots, p$) are different, Z^* has a GIG distribution of depth p, with shape parameters ℓ_j and rate parameters $1/(2w_j)$, or a smaller depth, in case some of the w_j are equal, in which case a similar approach to the one described in Sect. 2 has to be taken.

In order to obtain a near-exact distribution for Z we will leave Z^* untouched and we will approximate the distribution of Z^{**} by a finite mixture of say $m^* + 1$ Gamma distributions, all with the same rate parameter λ, which may be obtained in a number of different ways, which will be discussed next. The shape parameters in this mixture will be equal to the sum of the shape parameters of the p r.v.'s Z_j^{**}, to which we add $0, 1, \ldots, m^*$.

We will be able to explain better and more precisely which will be the shape parameters of the distributions in this mixture and how the weights in this mixture will be determined if we consider the characteristic function (c.f.) of Z^{**}, which is

$$\Phi_{Z^{**}}(t) = \prod_{j=1}^{p} \left(\frac{1}{2w_j} \right)^{\ell_j^*} \left(\frac{1}{2w_j} - \mathrm{i}t \right)^{-\ell_j^*} , \tag{5}$$

where it is clear that if some ℓ_j^* is zero, then the corresponding r.v. vanishes, being its contribution for the product in (5) equal to 1.

Since the c.f. in (5) is the c.f. of a sum of independent $\Gamma(\ell_j^*, 1/(2w_j))$ r.v.'s and since from the results in Moschopoulos (1985) it is possible to show that this distribution is also the distribution of an infinite mixture of Gamma distributions with shape parameters $r + k$ ($k = 0, 1, \ldots$), where

$$r = \sum_{j=1}^{p} \ell_j^* , \tag{6}$$

we will approximate the c.f. in (5) by the c.f.

$$\Phi^*(t) = \sum_{k=0}^{m^*} \pi_k \lambda^{r+k} (\lambda - \mathrm{i}t)^{-(r+k)} , \tag{7}$$

which is the c.f. of a mixture with $m^* + 1$ components which are $\Gamma(r + k, \lambda)$ distributions, for $k = 0, 1, \ldots, m^*$, where r is given by (6) and where, as already mentioned, λ may be determined in a few different ways, which will be addressed

and discussed next. The weights π_k $(k = 0, \ldots, m^*)$ in (6) will be determined in such a way that the first m^* non-central moments of the distributions corresponding to $\Phi_{Z^{**}}(t)$ and $\Phi^*(t)$ are the same, that is, π_k for $k = 0, \ldots, m^* - 1$ will be determined as the solutions of the system of m^* equations

$$\left.\frac{\partial^h}{\partial t^h}\Phi_{Z^{**}}(t)\right|_{t=0} = \left.\frac{\partial^h}{\partial t^h}\Phi^*(t)\right|_{t=0}, \quad h = 1, \ldots, m^*, \tag{8}$$

taking then $\pi_{m^*} = 1 - \sum_{k=0}^{m^*-1} \pi_k$.

This approach will give as near-exact c.f. for Z the c.f.

$$\begin{aligned}\Phi_Z^*(t) &= \Phi_{Z^*}(t)\,\Phi^*(t) \\ &= \underbrace{\left\{\prod_{j=1}^{p}\left(\frac{1}{2w_j}\right)^{\ell_j}\left(\frac{1}{2w_j} - \mathrm{i}t\right)^{-\ell_j}\right\}}_{\Phi_{Z^*}(t)} \underbrace{\sum_{k=0}^{m^*}\pi_k\lambda^{r+k}\,(\lambda - \mathrm{i}t)^{-(r+k)}}_{\Phi^*(t)} \\ &= \sum_{k=0}^{m^*}\pi_k\left\{\prod_{j=1}^{p}\left(\frac{1}{2w_j}\right)^{\ell_j}\left(\frac{1}{2w_j} - \mathrm{i}t\right)^{-\ell_j}\right\}\lambda^{r+k}\,(\lambda - \mathrm{i}t)^{-(r+k)}\end{aligned} \tag{9}$$

which yields as near-exact distributions for Z mixtures with $m^* + 1$ components, each of which is either a GIG or a GNIG distribution of depth $p + 1$, according to the case of r being integer or not (we may note that it may happen quite often r to be an integer since ℓ_j^* is either zero, if k_j is even, or 1/2, if k_j is odd), with shape parameters $\ell_1, \ldots, \ell_p, r + k$ $(k = 0, \ldots, m^*)$ and rate parameters $1/(2w_1), \ldots, 1/(2w_p), \lambda$, and weights π_k $(k = 0, \ldots, m^* + 1)$. That is, from (9), the near-exact p.d.f.'s and c.d.f.'s of Z will be respectively written as

$$f_Z^*(z) = \sum_{k=0}^{m^*}\pi_k\, f^{GNIG}\left(z\,\middle|\,\ell_1, \ldots, \ell_p; r + k; \frac{1}{2w_1}, \ldots, \frac{1}{2w_p}; \lambda; p + 1\right)$$

and

$$F_Z^*(z) = \sum_{k=0}^{m^*}\pi_k\, F^{GNIG}\left(z\,\middle|\,\ell_1, \ldots, \ell_p; r + k; \frac{1}{2w_1}, \ldots, \frac{1}{2w_p}; \lambda; p + 1\right),$$

using the notation in Appendix 1 for the GNIG p.d.f. and c.d.f., and where the GNIG p.d.f. and c.d.f. are to be replaced by the GIG p.d.f. and c.d.f. in case r in (6) is an integer.

In implementing this near-exact approximation, the c.f. of Z^*, $\Phi_{Z^*}(t)$, which will be kept unchanged, is a 'major' part of the whole c.f. of Z, $\Phi_Z(t)$, in case all k_j are larger than 1, while the c.f. of Z^{**}, $\Phi_{Z^{**}}(t)$, is a 'smaller' part, since in this

case we have

$$\int_{-\infty}^{+\infty} |\Phi_Z(t) - \Phi_{Z^*}(t)|\, dt < \int_{-\infty}^{+\infty} |\Phi_Z(t) - \Phi_{Z^{**}}(t)|\, dt\,.$$

The distribution of Z^{**} is that of a sum of independent Gamma r.v.'s with possibly different rate parameters and non-integer, that is, half-integer, shape parameters. Such a distribution was obtained by several authors as an infinite mixture of Gamma distributions, as it is the case of Moschopoulos (1985), who obtained it in the form of an infinite mixture of Gamma distributions all with the same rate parameter, which is the maximum of the rate parameters of the Gamma distributions involved in the sum, and shape parameters $r + k$ ($k = 0, 1, \ldots$) for r in (6).

As such, the approach followed in approximating $\Phi_{Z^{**}}(t)$ by $\Phi^*(t)$ follows similar lines, to which was added what may be seen as a somewhat heuristic approach, by turning the infinite mixture into a finite mixture, which is then rendered extremely close to the exact distribution through the way its weights are determined.

Concerning the determination of the rate parameter λ in (7), several strategies may be taken, among which we will address the following ones:

(i) $\max_{j\in\{1,\ldots,p\}} \frac{1}{2w_j}$

(ii) $\min_{j\in\{1,\ldots,p\}} \frac{1}{2w_j}$

(iii) arithmetic mean of the $\frac{1}{2w_j}$ $(j = 1, \ldots, p)$

(iv) harmonic mean of the $\frac{1}{2w_j}$ $(j = 1, \ldots, p)$

(v) geometric mean of the $\frac{1}{2w_j}$ $(j = 1, \ldots, p)$

(vi) the rate parameter λ in $\widetilde{\Phi}(t) = \lambda^r(\lambda - \mathrm{i}t)^{-r}$, where

$$\frac{\partial^h}{\partial t^h}\Phi_{Z^{**}}(t)\bigg|_{t=0} = \frac{\partial^h}{\partial t^h}\widetilde{\Phi}(t)\bigg|_{t=0}\,, \quad h = 1, 2 \tag{10}$$

(vii) the rate parameter λ in $\widetilde{\Phi}(t) = \theta\lambda^{r_1}(\lambda - \mathrm{i}t)^{-r_1} + (1-\theta)\lambda^{r_2}(\lambda - \mathrm{i}t)^{-r_2}$, where

$$\frac{\partial^h}{\partial t^h}\Phi_{Z^{**}}(t)\bigg|_{t=0} = \frac{\partial^h}{\partial t^h}\widetilde{\Phi}(t)\bigg|_{t=0}\,, \quad h = 1, \ldots, 4\,.$$

These choices for λ will be denoted respectively by (i) 'Max', (ii) 'Min', (iii) 'A', (iv) 'H', (v) 'G', (vi) '2m' and (vii) '4m' in the Tables that appear in Sect. 4.1.

The choice in (i) is based on the paper by Moschopoulos (1985), where we should note that the author uses in the notation of the p.d.f. of the Gamma distribution a scale parameter instead of a rate parameter, so that his β_j are the reciprocals of our rate parameters $1/(2w_j)$. The choice in (ii) is made to show that in some cases this choice works better than the choice in (i). The choice in (iii), which as we will see shortly ahead works quite often better than the two previous ones, is inspired in the well-known fact that if all w_j are equal, say to a common value w, then

the distribution of Z^{**} (and actually the distribution of Z^{*} and of Z) will be just a Gamma distribution with a rate parameter equal to $1/(2w)$. So, we may think about taking the arithmetic average of the rate parameters $1/(2w_j)$ in case they are different. However, the choice in (iv) may be a better one, given the fact that the c.f. of Z^{**}, as shown in (5) is indeed a product, and it is in this product that we are kind of 'replacing' the set of p rate parameters $1/(2w_j)$ by just a single parameter, making then most sense to take the harmonic mean of the original parameters, instead of the arithmetic mean. The choice in (v) is made to see how the choice of the geometric mean compares with the harmonic mean and also say to 'complete' the set of the most common means. The choice in (vi) is a simplification of the choice in (vii), which is known to the author to provide generally very good results.

As we will see, options (iv), (v), (vi) and (vii) give the best results, in many situations just with slight differences among them. In these cases, options (iv) or (v) will be the preferred ones given their computational simplicity, compared with options (vi) and (vii). However, also option (i) may give very good results in some particular situations.

We may note that in case all k_j are equal to 1, then all ℓ_j will be equal to zero and in this case Z^{*} vanishes and the procedure developed will then provide a quite sharp asymptotic distribution for Z, rather than a near-exact one.

Modules programmed in Mathematica® to implement these near-exact distributions are available at https://sites.google.com/site/lincombchisquares.

4.1 On the Behavior of the Near-Exact Distributions for the Several Different Choices of λ in (10)

To assess the quality of the approximation provided by different near-exact distributions we use the measure

$$\Delta = \frac{1}{2\pi} \int_{-\infty}^{+\infty} \left| \frac{\Phi_Z(t) - \Phi_Z^*(t)}{t} \right| dt \tag{11}$$

where

$$\Phi_Z(t) = \prod_{j=1}^{p} \left(\frac{1}{2w_j} \right)^{k_j/2} \left(\frac{1}{2w_j} - \mathrm{i}t \right)^{-k_j/2} = \Phi_{Z^*}(t)\, \Phi_{Z^{**}}(t)$$

is the exact c.f. of Z and $\Phi_Z^*(t)$ is the near-exact c.f. of Z in (9).

The measure Δ, as defined in (11), is a sharp upper-bound on the difference between the exact and the near-exact c.d.f.'s, since we may write

$$\Delta \geq \max_{z>0} \left| F_Z(z) - F_Z^*(z) \right|, \tag{12}$$

where $F_Z(z)$ and $F_Z^*(z)$ represent respectively the exact and the near-exact c.d.f.'s of Z. Actually, both in (11) as well as in (12) one may use respectively $\Phi_Z^*(t)$ and

$F_Z^*(z)$ as the c.f. and the c.d.f. for any approximate distribution of Z as for example an asymptotic or a truncated distribution. This is exactly what we will do next when comparing the performance of the near-exact distributions with truncations of the infinite mixture obtained by Moschopoulos (1985).

To illustrate the behavior of the seven possible different choices for λ suggested in (10) we have chosen to use ten different scenarios, the first eight of which all deal with a set of $p = 5$ independent chi-square r.v.'s Y_j. In the first four scenarios the chi-square r.v's have $k_j = \{2, 7, 16, 17, 19\}$ d.f.'s, and then we study four different choices for the coefficients w_j $(j = 1, \ldots, 5)$. These four scenarios illustrate the following situations:

I scenario with values of $w_j = \{2.3, 3.4, 5.6, 7.8, 8.9\}$, that is, *larger* than 1 and which *increase* with increasing values for the d.f.'s

II scenario with values of $w_j = \{0.11, 0.13, 0.18, 0.29, 0.43\}$ *smaller* than 1 and which *increase* with increasing values for the d.f.'s

III scenario with values of $w_j = \{8.9, 7.8, 5.6, 3.4, 2.3\}$ *larger* than 1 and which *decrease* with increasing values for the d.f.'s

IV scenario with values of $w_j = \{0.43, 0.29, 0.18, 0.13, 0.11\}$ *smaller* than 1 and which *decrease* with increasing values for the d.f.'s.

For scenarios V–VIII we use respectively exactly the same w_j that are used for scenarios I–IV, with the difference that now the $p = 5$ independent chi-square r.v.'s Y_j have $k_j = \{12, 17, 26, 27, 29\}$ d.f.'s, that is, each one of them has ten more d.f.'s than in scenarios I–IV.

Then for scenarios IX and X we use four chi-square r.v.'s, respectively with $k_j = \{3, 1, 2, 2\}$ and $k_j = \{9, 3, 6, 6\}$ d.f.'s, in both cases with $w_j = \{2/5, 1/2, 1, 9\}$, in order to not only consider situations where the w_j take a wide range of values but also where they take values both smaller and larger than 1.

For each of the ten above scenarios the measure Δ in (11) was computed for the Moschopoulos (1985) distribution with truncations at 100, 150 and 200 terms and for the near-exact distributions with the seven different choices for λ in (10) (denoted by the descriptors listed right after (10)), for values of $m^* = 10$, $m^* = 15$ and $m^* = 20$, that is, for near-exact distributions that match $m^* = 10, 15$ or 20 of the exact moments of Z. The values for the measure Δ in (11) are shown in Tables 1, 2, and 3 and we will analyze the results for each scenario individually.

Our intent is to compare the near-exact distributions that match 10, 15 and 20 exact moments respectively with the Moschopoulos (1985) series distribution truncated to 100, 150 and 200 terms.

From Table 1 we may see that for Scenario I the Moschopoulos (1985) series truncated at 100 terms does have a very poor performance, with a quite large value of Δ, and that the Moschopoulos series distribution truncated at 150 terms is overpowered by all the near-exact distributions that match 15 exact moments, while the truncated series with 200 terms only beats the near-exact distribution that uses λ as the maximum of the rate parameters $1/(2w_j)$, with the near-exact distribution that uses λ defined as in (vii) in (10) showing the best performance among all near-

Table 1 Values of the measure Δ in (11) for scenarios I–IV, for truncations of the Moschopoulos (1985) series distribution with 100, 150 and 200 terms (respectively the columns marked with $m^* = 10$, $m^* = 15$ and $m^* = 20$), denoted by 'Mosc', and for the near-exact distributions with λ defined by the seven choices in (10), denoted by the descriptors indicated right after (10) in Sect. 4, for linear combinations of $p = 5$ independent chi-square r.v.'s with $k_j = \{2, 7, 16, 17, 19\}$ d.f.'s and with coefficients $w_j = \{2.3, 3.4, 5.6, 7.8, 8.9\}$ for Scenario I, $w_j = \{0.11, 0.13, 0.18, 0.29, 0.43\}$ for Scenario II, $w_j = \{8.9, 7.8, 5.6, 3.4, 2.3\}$ for Scenario III and $w_j = \{0.43, 0.29, 0.18, 0.13, 0.11\}$ for Scenario IV

	Scenario I		
	$m^* = 10$	$m^* = 15$	$m^* = 20$
Mosc	2.61×10^{-1}	4.43×10^{-5}	1.02×10^{-9}
Max	2.04×10^{-6}	4.39×10^{-7}	3.58×10^{-7}
Min	7.67×10^{-9}	4.65×10^{-11}	4.77×10^{-13}
A	1.04×10^{-8}	1.34×10^{-10}	4.30×10^{-12}
H	1.25×10^{-10}	1.92×10^{-13}	6.31×10^{-16}
G	1.36×10^{-9}	6.45×10^{-12}	7.06×10^{-14}
2m	4.62×10^{-10}	1.11×10^{-12}	4.85×10^{-15}
4m	2.48×10^{-11}	2.37×10^{-14}	4.05×10^{-17}

	Scenario II		
	$m^* = 10$	$m^* = 15$	$m^* = 20$
Mosc	1.19×10^{-2}	3.71×10^{-7}	2.81×10^{-12}
Max	5.52×10^{-6}	2.60×10^{-6}	4.35×10^{-6}
Min	1.05×10^{-7}	1.60×10^{-9}	3.93×10^{-11}
A	1.62×10^{-7}	1.05×10^{-8}	1.71×10^{-9}
H	6.60×10^{-9}	8.11×10^{-11}	2.16×10^{-12}
G	4.22×10^{-8}	1.34×10^{-9}	9.94×10^{-11}
2m	3.15×10^{-9}	1.63×10^{-11}	1.48×10^{-13}
4m	1.31×10^{-10}	4.49×10^{-13}	1.28×10^{-15}

	Scenario III		
	$m^* = 10$	$m^* = 15$	$m^* = 20$
Mosc	9.57×10^{-7}	4.96×10^{-13}	1.76×10^{-19}
Max	8.33×10^{-6}	4.44×10^{-6}	6.73×10^{-6}
Min	2.63×10^{-6}	8.38×10^{-8}	3.92×10^{-9}
A	7.19×10^{-9}	8.63×10^{-11}	2.00×10^{-12}
H	5.19×10^{-9}	2.55×10^{-11}	2.15×10^{-13}
G	3.17×10^{-10}	2.81×10^{-12}	3.95×10^{-15}
2m	8.12×10^{-9}	4.58×10^{-11}	4.42×10^{-13}
4m	2.17×10^{-9}	1.58×10^{-11}	2.00×10^{-13}

	Scenario IV		
	$m^* = 10$	$m^* = 15$	$m^* = 20$
Mosc	8.97×10^{-10}	3.44×10^{-16}	1.32×10^{-22}
Max	1.13×10^{-6}	1.80×10^{-7}	6.87×10^{-8}
Min	1.84×10^{-5}	8.80×10^{-7}	5.57×10^{-8}
A	1.06×10^{-9}	4.90×10^{-12}	4.13×10^{-14}
H	3.34×10^{-9}	9.63×10^{-12}	4.60×10^{-14}
G	1.70×10^{-10}	2.91×10^{-13}	3.88×10^{-16}
2m	8.79×10^{-10}	1.62×10^{-12}	5.07×10^{-15}
4m	1.17×10^{-9}	5.59×10^{-12}	4.93×10^{-14}

exact distributions, and the one that uses λ as the harmonic mean of the $1/(2w_j)$ coming second.

For Scenario II the distributions have a somewhat similar behavior as it happens for Scenario I, with all near-exact distributions that match 10 exact moments outperforming Moschopoulos series truncated at 100 terms and all but the one with λ defined as the maximum of the $1/(2w_j)$ showing better performances than the Moschopoulos series truncated at 150 terms. However, only the near-exact distributions that use λ defined as in (vii), (vi) and (iv) in (10) are able to outperform the Moschopoulos series truncated at 200 terms. In all cases it is the near-exact distribution λ given by (vii) in (10) that has the best performance followed by the one with λ given by (vi) in (10) and by the one that uses λ as the harmonic mean of the $1/(2w_j)$, with the one that uses λ as the geometric mean of the $1/(2w_j)$ coming in fourth place for the near-exact distributions that match 10 or 15 exact moments, but being beatten by the one that uses λ as the minimum of the $1/(2w_j)$ when we consider the near-exact distributions that match 20 exact moments.

In Scenario III while all near-exact distributions that match 10 exact moments, except the ones that use λ as the maximum or the minimum of the $1/(2w_j)$, beat the Moschopoulos series truncated at 100 terms, which already exhibits a much good performance, none of the near-exact distributions that match 15 exact moments is able to beat the Moschopoulos series truncated at 150 terms, neither none of the near-exact distributions that match 20 exact moments is able to outperform the Moschopoulos series truncated at 200 terms, although the near-exact distributions that match 20 exact moments and use λ given by (v), (vii), (iv) and (vi) in (10) beat the Moschopoulos series distribution truncated at 150 terms, with performances in that order, with the near-exact distribution with λ given by the geometric mean of the rate parameters $1/(2w_j)$ displaying the best behavior.

In Scenario IV, among the near-exact distributions that match 10 exact moments, only the one that uses λ as the geometric mean of the $1/(2w_j)$ is able to outperform the Moschopoulos series truncated at 100 terms. Indeed for this scenario the Moschopoulos series distribution displays an extraordinary good performance, with none of the near-exact distributions that match 15 or even 20 exact moments being able to beat the Moschopoulos series distribution truncated to 150 terms. Anyway, among the near-exact distributions it is the one that uses λ as the geometric mean of the rate parameters $1/(2w_j)$, that shows the best performance, followed by the one that uses λ given by (vi) in (10), leaving the one that uses λ given by (vii) in (10) with the third place among those that match 10 or 15 exact moments or the fourth place among those that match 20 exact moments, where the third place is taken by the near-exact distribution that uses λ given by the harmonic mean of the $1/(2w_j)$, which takes fourth place among the near-exact distributions that match 10 or 15 exact moments.

In the overall, for Scenarios I–IV, we may see that the Moschopoulos distribution shows very good performances for cases where the products $w_j k_j$ $(j = 1, \ldots, p)$ show a more balanced sequence of values, preferably with smaller values, that is, for Scenarios III and IV, where the w_j are inversely proportional to the k_j, while the near-exact distributions show clear advantages in the opposite situations, that is, in situations where the values of $w_j k_j$ $(j = 1, \ldots, p)$ are more unbalanced, which are the situations in Scenarios I and II, where the w_j have values proportional to the k_j.

Of course that since the numerical computation of the exact moments of Z is rather simple and the numerical solution of the system of equations in (8) is quite simple and quick, since it is a linear system of equations, we may always easily extend the value of m^* in (7) and (8), that is, the number of exact moments that the near-exact distributions match, in order to obtain a better fitting distribution. In this way we may always be able to beat the performance of any Moschopoulos series distribution truncation. For example if in Scenario IV we take the near-exact distribution with λ defined as the geometric mean of the $1/(2w_j)$ that matches 35 exact moments, we would obtain for this distribution a value of the measure Δ equal to $2,51 \times 10^{-23}$, this way beating the performance of the Moschopoulos series distribution truncated to 200 terms.

For Scenarios V–VIII, where the only change from Scenarios I–IV is in the d.f.'s of the chi-square r.v.'s involved, which now have ten more d.f.'s each, we may see,

Table 2 Values of the measure Δ in (11) for scenarios V–VIII, for truncations of the Moschopoulos (1985) series distribution with 100, 150 and 200 terms (respectively the columns marked with $m^* = 10$, $m^* = 15$ and $m^* = 20$), denoted by 'Mosc', and for the near-exact distributions with λ defined by the seven choices in (10), denoted by the descriptors indicated right after (10) in Sect. 4, for linear combinations of $p = 5$ independent chi-square r.v.'s with $k_j = \{12, 17, 26, 27, 29\}$ d.f.'s and with coefficients $w_j = \{2.3, 3.4, 5.6, 7.8, 8.9\}$ for Scenario V, $w_j = \{0.11, 0.13, 0.18, 0.29, 0.43\}$ for Scenario VI, $w_j = \{8.9, 7.8, 5.6, 3.4, 2.3\}$ for Scenario VII and $w_j = \{0.43, 0.29, 0.18, 0.13, 0.11\}$ for Scenario VIII

	Scenario V		
	$m^* = 10$	$m^* = 15$	$m^* = 20$
Mosc	1.39×10^{1}	1.35×10^{-1}	6.90×10^{-5}
Max	8.92×10^{-8}	3.42×10^{-9}	4.23×10^{-10}
Min	8.56×10^{-10}	2.39×10^{-12}	1.22×10^{-14}
A	6.35×10^{-10}	2.26×10^{-12}	2.08×10^{-14}
H	9.35×10^{-12}	4.81×10^{-15}	5.67×10^{-18}
G	9.21×10^{-11}	1.34×10^{-13}	4.72×10^{-16}
2m	4.32×10^{-11}	4.27×10^{-14}	8.33×10^{-17}
4m	2.00×10^{-12}	7.10×10^{-16}	4.87×10^{-19}

	Scenario VI		
	$m^* = 10$	$m^* = 15$	$m^* = 20$
Mosc	1.93×10^{0}	1.35×10^{-3}	8.96×10^{-8}
Max	2.41×10^{-7}	2.09×10^{-8}	5.87×10^{-9}
Min	1.35×10^{-8}	1.03×10^{-10}	1.39×10^{-12}
A	9.50×10^{-9}	1.62×10^{-10}	7.34×10^{-12}
H	4.74×10^{-10}	1.89×10^{-12}	1.76×10^{-14}
G	2.71×10^{-9}	2.50×10^{-11}	5.78×10^{-13}
2m	3.08×10^{-10}	6.78×10^{-13}	2.89×10^{-15}
4m	1.02×10^{-11}	1.42×10^{-14}	1.62×10^{-17}

	Scenario VII		
	$m^* = 10$	$m^* = 15$	$m^* = 20$
Mosc	2.72×10^{-1}	2.89×10^{-5}	3.63×10^{-10}
Max	4.86×10^{-8}	2.35×10^{-9}	3.56×10^{-10}
Min	1.03×10^{-7}	1.24×10^{-9}	2.55×10^{-11}
A	9.20×10^{-11}	2.09×10^{-13}	1.11×10^{-15}
H	8.72×10^{-11}	1.04×10^{-13}	2.60×10^{-16}
G	3.40×10^{-12}	8.99×10^{-15}	3.22×10^{-18}
2m	1.43×10^{-10}	2.03×10^{-13}	5.92×10^{-16}
4m	3.06×10^{-11}	4.48×10^{-14}	1.38×10^{-16}

	Scenario VIII		
	$m^* = 10$	$m^* = 15$	$m^* = 20$
Mosc	1.27×10^{-3}	1.02×10^{-8}	2.72×10^{-14}
Max	5.26×10^{-9}	9.16×10^{-11}	4.65×10^{-12}
Min	8.01×10^{-7}	1.63×10^{-8}	5.05×10^{-10}
A	9.90×10^{-12}	8.62×10^{-15}	1.72×10^{-17}
H	4.25×10^{-11}	2.99×10^{-14}	4.30×10^{-17}
G	1.62×10^{-12}	6.35×10^{-16}	2.09×10^{-19}
2m	9.88×10^{-12}	4.15×10^{-15}	3.66×10^{-18}
4m	1.08×10^{-11}	9.73×10^{-15}	2.02×10^{-17}

from Table 2, that the performance of the truncations of the Moschopoulos series distribution has worsened quite much, with the truncations with 100 terms even displaying for Scenarios V and VI values of the measure Δ which do not make sense, since these values are supposed to lie between zero and 1. Going in the opposite direction, all near-exact distributions show sharp improvements in the Δ values, when compared with the corresponding distributions in Scenarios I–IV.

We may see that now for Scenario V all near-exact distributions that match 10 exact moments even show a better performance than the Moschopoulos series truncated at 200 terms, a situation that is almost repeated for Scenario VI, with the only exception being the near-exact distribution with λ given by the maximum of the $1/(2w_j)$ and that matches 10 exact moments, which shows a less good performance than the Moschopoulos series truncated at 200 terms, but still showing a better performance than the Moschopoulos series truncated at 150 terms.

For Scenario VII only the near-exact distributions with λ given either by the maximum or the minimum of the $1/(2w_j)$, which match 10 or 15 exact moments are not able to beat the Moschopoulos series truncated at 200 terms, but with all near-exact distributions that match 10, 15 or 20 exact moments outperforming respectively the Moschopoulos series expansions with 100, 150 or 200 terms.

Even for Scenario VIII, which among the four Scenarios V–VIII is the most favorable one for the Moschopoulos series expansion, all near-exact distributions that match 10 exact moments are able to outperform the Moschopoulos series expansions with 100 terms, and among those that match 15 exact moments, only the near-exact distribution with λ defined as the minimum of the $1/(2w_j)$ is not able to outperform the Moschopoulos series truncated at 150 terms. Also, among the near-exact distributions that match 20 exact moments, only those with λ defined by either the maximum or the minimum of the $1/(2w_j)$ are not able to outperform the Moschopoulos series distribution truncated at 200 terms.

For Scenarios V–VIII the behavior of the near-exact distributions for the different choices of λ in (10) is similar in their interrelations to the ones described for Scenarios I–IV. For Scenarios I and V, the near-exact distributions ranking 1–4 in their performance are, in this order, the ones with λ given by (vii), (iv), (vi) and (v) in (10), while for Scenarios II and VI the near-exact distributions ranking 1–3 are the ones with λ given by (vii), (vi) and (iv) in (10), with a swap between the ones with λ given by (ii) and (v) for fourth and fifth place. Also for Scenarios III and VII the near-exact distributions ranking 1–5 in their performance are the same, being, in this order, the ones with λ given by (v), (vii), (iv), (vi) and (iii) in (10). Only for Scenarios IV and VIII there is a swap between the near-exact distributions with λ given by (iii) and (iv) in (10), for third and fifth performance places, but with the ones with λ given by (v), (vi) and (vii) in (10) keeping the first, second and fourth performance places. For these two scenarios there is a somewhat strange inversion in the performance of the near-exact distributions with λ given by (vii) and (vi) in (10), with this last one showing a better performance.

From the values in Table 3 we may see how truncations of the Moschopoulos distribution, actually as most other approximations and series distributions, have severe trouble handling the situations in scenarios IX and X and also how when the numbers of d.f.'s increase the situation becomes even worse.

By contrast, the near-exact distributions, namely those with λ defined as the maximum or the average of the $1/(2w_j)$ or those which use λ defined by (vi) or (vii) in (10) give extremely sharp approximations, and, as expected, even increase their performance when the k_j, that is, the number of d.f.'s, increase.

For these situations depicted in scenarios IX and X we would certainly choose to use λ defined as the maximum of the $1/(2w_j)$ or given by (vi) in (10).

Table 3 Values of the measure Δ in (11) for scenarios IX–X, for truncations of the Moschopoulos (1985) series distribution with 100, 150 and 200 terms (respectively the columns marked with $m^* = 10$, $m^* = 15$ and $m^* = 20$), denoted by 'Mosc', and for the near-exact distributions with λ defined by the seven choices in (10), denoted by the descriptors indicated right after (10) in Sect. 4, for linear combinations of $p = 4$ independent chi-square r.v.'s respectively with $k_j = \{3, 1, 2, 2\}$ and $k_j = \{9, 3, 6, 6\}$ d.f.'s and with coefficients $w_j = \{2/5, 1/2, 1, 9\}$ for both scenarios

	Scenario IX		
	$m^* = 10$	$m^* = 15$	$m^* = 20$
Mosc	3.92×10^{-1}	4.04×10^{-2}	4.16×10^{-3}
Max	3.76×10^{-12}	1.35×10^{-15}	6.43×10^{-19}
Min	4.92×10^{-2}	2.92×10^{-2}	1.85×10^{-2}
A	2.39×10^{-8}	1.61×10^{-10}	1.38×10^{-12}
H	2.00×10^{-3}	5.45×10^{-4}	1.66×10^{-4}
G	1.18×10^{-5}	6.60×10^{-7}	4.45×10^{-8}
2m	1.72×10^{-15}	1.95×10^{-20}	2.58×10^{-25}
4m	1.24×10^{-15}	1.58×10^{-20}	1.94×10^{-25}

	Scenario X		
	$m^* = 10$	$m^* = 15$	$m^* = 20$
Mosc	6.58×10^{0}	1.35×10^{0}	2.31×10^{-1}
Max	1.94×10^{-16}	1.36×10^{-20}	2.04×10^{-24}
Min	4.91×10^{-3}	2.08×10^{-3}	1.02×10^{-3}
A	9.33×10^{-12}	1.98×10^{-14}	7.30×10^{-17}
H	2.60×10^{-5}	4.00×10^{-6}	8.01×10^{-7}
G	1.99×10^{-8}	4.64×10^{-10}	1.63×10^{-11}
2m	1.36×10^{-19}	3.48×10^{-25}	1.56×10^{-30}
4m	9.89×10^{-20}	2.70×10^{-25}	1.11×10^{-30}

4.2 *A Note on Computation Times and the Use of the GNIG p.d.f. and c.d.f.*

We may note that although the general expressions for the p.d.f. and the c.d.f. of the GNIG distribution involve the Kummer confluent hypergeometric function

$$ {}_1F_1(a, b; z) = \sum_{i=0}^{\infty} \frac{\Gamma(a+i)}{\Gamma(a)} \frac{\Gamma(b)}{\Gamma(b+i)} \frac{1}{z^i} , $$

which is nowadays possible to compute precisely and efficiently with most symbolic softwares as it is for example the case of Mathematica® and also MAXIMA, in our case it is possible to use an even more efficient and convenient representation for these functions since their arguments a and b will always be half-integers. As such we may use the fact that for any odd integer k we may write

$$ {}_1F_1\left(\frac{k}{2}, \frac{k}{2}+1, z\right) = \frac{k\, e^z}{2^{(k+1)/2}\,(-z)^{k/2}} \left(\left\{ \prod_{j=1}^{\frac{k-1}{2}} (2j-1) \right\} e^{-z} \sqrt{\pi}\, \mathrm{Erf}\left(\sqrt{-z}\right) - \sum_{j=1}^{\frac{k-1}{2}} (-z)^{\frac{2j-1}{2}}\, 2^j \left\{ \prod_{\ell=0}^{\frac{k-3}{2}-j} 2\left(\frac{k-1}{2} - \ell\right) - 1 \right\} \right) \tag{13} $$

where

$$\text{Erf}(z) = \frac{2}{\sqrt{\pi}} \int_0^z e^{-t^2}\, dt$$

is the error function. This expression is computationally very convenient since most softwares can nowadays compute this error function very efficiently and then we may use the fact that

$${}_1F_1(a, a, -z) = e^{-z}$$

together with expression 13.4.2 in Slater (1972), which, for $j = 1, 2, \ldots$, in our case may be written as

$$\begin{aligned} {}_1F_1\left(\tfrac{k}{2}, \tfrac{k}{2} + j + 1, z\right) = -\tfrac{1}{z}\left(\tfrac{k}{2j} + 1\right) \Big\{ & \left(\tfrac{k}{2} + j - 1\right) {}_1F_1\left(\tfrac{k}{2}, \tfrac{k}{2} + j - 1, z\right) \\ & + \left(1 - \tfrac{k}{2} - j - z\right) {}_1F_1\left(\tfrac{k}{2}, \tfrac{k}{2} + j, z\right) \Big\}, \end{aligned}$$

to compute iteratively all Kummer confluent hypergeometric functions that appear in the expressions for the p.d.f. and the c.d.f. of the GNIG distributions used.

5 The Distribution of Some Instances of Ratios of Two Independent Linear Combinations of Independent Chi-Squares

The distribution of ratios of two independent linear combinations of independent chi-squares appears mostly as the distribution of ratios of independent quadratic forms in multivariate normal variates, each one of which has the distribution of a linear combination of independent chi-squares. In turn these ratios have since long been associated with tests in Analysis of Variance models where different variances are assumed for the populations associated with the different levels of the factor or factors (Box 1954; Welch 1947; Satterthwaite 1941). Based on the results obtained in Sects. 2 and 4 it is possible to obtain the exact distribution of a ratio of two independent linear combinations of independent chi-squares in one situation and an asymptotic distribution for another situation.

First of all we need to recognize that actually the GIG distribution may be seen as a mixture of Gamma distributions, all with integer shape parameters, since we may write the p.d.f. of the GIG distribution in (28) as

$$f_Z(z) = K \sum_{j=1}^{p} \sum_{k=1}^{r_j} c_{j,k}\, e^{-\lambda_j z}\, z^{k-1}$$
$$= \sum_{j=1}^{p} \sum_{k=1}^{r_j} \underbrace{\frac{K c_{j,k} \Gamma(k)}{\lambda_j^k}}_{p_{j,k}} \underbrace{\frac{\lambda_j^k}{\Gamma(k)} e^{-\lambda_j z} z^{k-1}}_{\text{p.d.f. of a } \Gamma(k,\lambda_j) \text{ dist.}} = \sum_{j=1}^{p} \sum_{k=1}^{r_j} p_{j,k}\, \frac{\lambda_j^k}{\Gamma(k)} e^{-\lambda_j z} z^{k-1} \tag{14}$$

which is the p.d.f. of a mixture of $\sum_{j=1}^{p} r_j$ distributions $\Gamma(k, \lambda_j)$, with weights $p_{j,k} = K c_{j,k} \Gamma(k)/\lambda_j^k$ $(j = 1, \ldots, p; k = 1, \ldots, r_j)$.

Second of all, we may note that if $X \sim \Gamma(r_1, \lambda_1)$ and $Y \sim \Gamma(r_2, \lambda_2)$ are two independent r.v.'s, then the r.v. $W = X/Y$ has p.d.f.

$$f_W(w) = \frac{k^{r_1}}{B(r_1, r_2)} (1 + kw)^{-r_1 - r_2} w^{r_1 - 1} \quad (w > 0) \tag{15}$$

and c.d.f.

$$\begin{aligned} F_W(w) &= \frac{k^{r_1}}{B(r_1, r_2)} \frac{w^{r_1}}{r_1} {}_2F_1(r_1 + r_2, r_1; r_1 + 1; -kw) \\ &= BR\left(r_1, r_2; \frac{kw}{kw + 1}\right) \quad (w > 0)\,, \end{aligned} \tag{16}$$

where $k = \lambda_1/\lambda_2$, $B(\cdot, \cdot)$ is the common Beta function, ${}_2F_1(\cdot, \cdot; \cdot)$ is the Gauss hypergeometric function and $BR(\cdot, \cdot; z)$ is the regularized incomplete Beta function, with

$$BR(r_1, r_2; z) = \frac{1}{B(r_1, r_2)} \int_0^z x^{r_1 - 1} (1 - x)^{r_2 - 1}\, dx\,.$$

Then, we have two important cases where it is possible to obtain closed form expressions for the p.d.f. and c.d.f. of the ratio of two independent linear combinations of independent chi-squares.

Let us suppose that

$$Z_1 = \sum_{j=1}^{p_1} w_j Y_j \quad \text{and} \quad Z_2 = \sum_{\ell=1}^{p_2} w_\ell^* Y_\ell^* \tag{17}$$

are two independent linear combinations of independent chi-squares, where

$$Y_j \sim \chi^2_{k_j} \quad \text{and} \quad Y_\ell^* \sim \chi^2_{k_\ell^*} \quad j = 1, \ldots, p_1; \ell = 1, \ldots, p_2$$

where all of k_j $(j = 1, \ldots, p_1)$ and k_ℓ^* $(\ell = 1, \ldots, p_2)$ are even integers.

Then the exact distribution of both Z_1 and Z_2 are GIG distributions, which in case all w_j ($j = 1, \ldots, p_1$) and also all w_ℓ^* ($\ell = 1, \ldots, p_2$) are different, will have respectively depths p_1 and p_2. But then, from the mixture representation of the GIG distribution we may see that in this case the exact distribution of

$$V = Z_1/Z_2$$

will be a double mixture of ratios of independent Gamma distributed r.v.'s, which, from (15), will have, for $v > 0$, p.d.f.

$$f_V(v) = \sum_{j=1}^{p_1} \sum_{\ell=1}^{p_2} \sum_{h=1}^{k_j/2} \sum_{i=1}^{k_\ell^*/2} p_{j,h}\, p_{\ell,i}^* \, \frac{\left(\frac{w_\ell^*}{w_j}\right)^h}{B(h,i)} \left(1 + \frac{w_\ell^*}{w_j} v\right)^{-h-i} v^{\,h-1} \tag{18}$$

and from (16), c.d.f.

$$F_V(v) = \sum_{j=1}^{p_1} \sum_{\ell=1}^{p_2} \sum_{h=1}^{k_j/2} \sum_{i=1}^{k_\ell^*/2} p_{j,h}\, p_{\ell,i}^* \; BR\left(h, i, \frac{\frac{w_\ell^*}{w_j} v}{\frac{w_\ell^*}{w_j} v + 1}\right) \tag{19}$$

where, from (14) and from (29),

$$p_{j,h} = \left\{ \prod_{j=1}^{p_1} \left(\frac{1}{2w_j}\right)^{k_j/2} \right\} \frac{c_{j,h}\, \Gamma(h)}{\left(\frac{1}{2w_j}\right)^h}, \quad j = 1, \ldots, p_1; h = 1, \ldots, k_j/2$$

and

$$p_{\ell,i}^* = \left\{ \prod_{\ell=1}^{p_2} \left(\frac{1}{2w_\ell^*}\right)^{k_\ell^*/2} \right\} \frac{c_{\ell,i}\, \Gamma(i)}{\left(\frac{1}{2w_\ell^*}\right)^i}, \quad \ell = 1, \ldots, p_2; i = 1, \ldots, k_\ell^*/2, \tag{20}$$

for $c_{j,h}$ and $c_{\ell,i}$ defined according to (30)–(32) in Appendix 1.

One other situation of interest, as we will see in Sect. 6, is when Z_1 in (17) is a linear combination of independent chi-squares, all with one d.f. In this case, if we take the approach described in Sect. 4, all the parameters ℓ_j in (3) will be equal to zero and the r.v. Z^* in (4) vanishes, while $\Phi_{Z^{**}}(\cdot)$, the c.f. to be asymptotically approximated, will be the whole c.f. of Z_1. Thus, in this case we will obtain for Z_1 not a near-exact distribution but simply an asymptotic distribution, as noted in Sect. 4. This asymptotic distribution, which will correspond to the c.f. $\Phi^*(\cdot)$ in (7) will then be a mixture of $m^* + 1$ independent $\Gamma(r + k, \lambda)$ distributions ($k = 0, \ldots, m^*$), where $r = p_1/2$ and λ is to be computed according to one of the strategies in (10).

Then, if the exact distribution of Z_2 remains being the one in (17), with all k_ℓ^* even, based on this asymptotic distribution for Z_1, the asymptotic distribution of $V = Z_1/Z_2$ will have p.d.f.

$$f_V(v) = \sum_{j=0}^{m^*} \sum_{\ell=1}^{p_2} \sum_{i=1}^{k_\ell^*/2} \pi_j \, p_{\ell,i}^* \, \frac{(2\lambda w_\ell^*)^{r+j}}{B(r+j,i)} \left(1 + 2\lambda w_\ell^* v\right)^{-r-j-i} v^{r+j-1} \tag{21}$$

and c.d.f.

$$F_V(v) = \sum_{j=0}^{m^*} \sum_{\ell=1}^{p_2} \sum_{i=1}^{k_\ell^*/2} \pi_j \, p_{\ell,i}^* \, BR\left(r+j, i; \frac{2\lambda w_\ell^* v}{1 + 2\lambda w_\ell^* v}\right), \tag{22}$$

for $v > 0$.

We may note that the part of the incomplete Beta function in both regularized incomplete Beta functions in (19) and (22), given the fact that the second argument is an integer, may be written as a finite sum, that is, in both cases we may write, for any $a > 0$ and any $z > 0$,

$$BR(a, i; z) = \frac{1}{B(a,i)} \sum_{j=0}^{i-1} \frac{(-1)^j}{a+j} \binom{i-1}{j} z^{a+j}.$$

6 The Distribution of the Behrens–Fisher Statistic

In this section we will address the distribution of the statistic used to test the equality of the expected values of two Normal r.v.'s, when their variances are assumed to be different. This testing problem is commonly known as the Behrens–Fisher problem (Behrens 1929; Fisher 1939), and we will call "Behrens–Fisher statistic" the associated test statistic.

We will consider this statistic to be the statistic $V = Q_B/(Q_W/(n_1 + n_2 - 2))$ where n_1 and n_2 are the sample sizes respectively for the samples of the first and second populations, that is, of $X_1 \sim N(\mu_1, \sigma_1^2)$ and $X_2 \sim N(\mu_2, \sigma_2^2)$, and where Q_B and Q_W are respectively the between and within sums of squares in Sect. 7 of Box (1954), for the case $k = 2$.

This statistic V may be seen as the square of the T statistic for the Behrens–Fisher problem. From Sect. 7 of Box (1954), Q_B is distributed as $w_1 \chi_1^2$, with

$$w_1 = (n_2\sigma_1^2 + n_1\sigma_2^2)/(n_1 + n_2), \tag{23}$$

which is the non-null eigenvalue of the matrix VM on page 298 of Box (1954), where

$$V = \begin{bmatrix} \sigma_1^2/n_1 & 0 \\ 0 & \sigma_2^2/n_2 \end{bmatrix} \quad \text{and} \quad M = \begin{bmatrix} n_1 - \frac{n_1^2}{n_1+n_2} & -\frac{n_1 n_2}{n_1+n_2} \\ -\frac{n_1 n_2}{n_1+n_2} & n_2 - \frac{n_2^2}{n_1+n_2} \end{bmatrix},$$

that is, $Q_B \sim \Gamma(1/2, \lambda)$, with $\lambda = 1/(2w_1)$, while Q_W is distributed as $\sigma_1^2 Y_1 + \sigma_2^2 Y_2$ where Y_1 and Y_2 are two independent r.v.'s, with $Y_1 \sim \chi^2_{n_1-1}$ and $Y_2 \sim \chi^2_{n_2-1}$.

The population variances, σ_1^2 and σ_2^2, in case they are not known, will appear as nuisance parameters in the distribution of V. In this case they may be replaced by their estimates (preferably the maximum likelihood or the common centered ones).

If one uses the statistic V to carry out the test, one will basically be testing the null hypothesis $H_0 : \mu_1 = \mu_2$ versus the alternative hypothesis $H_1 : \mu \neq \mu_2$, rejecting H_0 if the computed value of V exceeds the α-quantile of V. However, one may take the square root of the computed value of V affected by the sign of $\overline{X}_1 - \overline{X}_2$ (where $\overline{X}_1$ and $\overline{X}_2$ represent the sample means of the samples from X_1 and X_2) to carry out a one-sided test, where then the quantile to be used in order to carry out an α level test will be the square root of the 1-α quantile of V affected by the same sign. Alternatively, if one wants to take a p-value approach, this means that, taking $F_V(\cdot)$ as the c.d.f. of V and v as the computed value of V, while one would use $1 - F_V(v)$ as the p-value for the two-sided test, one would have to use $(1 - F_V(v))/2$ as the p-value for the one-sided test.

6.1 The Case of Both n_1 and n_2 Odd

In case n_1 and n_2 are both odd, the exact p.d.f. and c.d.f. of V may be obtained respectively either from (18) and (19) or from (21) and (22), since in this case the exact distribution of Q_W is a GIG distribution of depth 2, with $r_1 = (n_1 - 1)/2$, $r_2 = (n_2 - 1)/2$, $\lambda_1 = (n_1 + n_2 - 2)/(2\sigma_1^2)$ and $\lambda_2 = (n_1 + n_2 - 2)/(2\sigma_2^2)$. Let us then take (21) and (22) as the basis for the expressions of the p.d.f. and c.d.f. of V. Then, the exact p.d.f. of $V = Q_B/(Q_W/(n_1 + n_2 - 2))$ is given by (21) with $m^* = 0$, $\pi_0 = 1$, $p_2 = 2$, $k_1^* = n_1 - 1$, $k_2^* = n_2 - 1$, $r = 1/2$, $\lambda = 1/(2w_1)$, $w_1^* = \sigma_1^2/(n_1 + n_2 - 2)$ and $w_2^* = \sigma_2^2/(n_1 + n_2 - 2)$, that is, it will be given by

$$f_V(v) = \sum_{\ell=1}^{2} \sum_{i=1}^{(n_\ell-1)/2} p^*_{\ell,i} \, \frac{\sigma_\ell^2 \, \frac{n_1+n_2}{n_2\sigma_1^2+n_1\sigma_2^2}}{B\left(\frac{1}{2}, i\right)} \left(1 + \sigma_\ell^2 \frac{(n_1+n_2)\, v}{n_2\sigma_1^2 + n_1\sigma_2^2}\right)^{-\frac{1}{2}-i} v^{-1/2}$$

and the exact c.d.f. by

$$F_V(v) = \sum_{\ell=1}^{2} \sum_{i=1}^{(n_\ell-1)/2} p^*_{\ell,i} \; BR\left(\frac{1}{2}, i; \frac{\sigma_\ell^2 \, v \, (n_1+n_2)}{n_2\sigma_1^2 + n_1\sigma_2^2 + \sigma_\ell^2 v(n_1+n_2)}\right),$$

where the $p^*_{\ell,i}$ ($\ell = 1, 2$; $i = 1, \ldots, (n_\ell - 1)/2$) are given by (20).

6.2 The Case of Either n_1 or n_2 Odd and the Other One Even

In this case the distribution of Q_W is a GNIG distribution of depth 2 with parameters, which if, without any loss of generality, we assume n_1 to be odd and n_2 even, will be $r_1 = (n_1 - 1)/2$, $r_2 = (n_2 - 1)/2$, $\lambda_1 = (n_1 + n_2 - 2)/(2\sigma_1^2)$ and $\lambda_2 = (n_1 + n_2 - 2)/(2\sigma_2^2)$.

It happens that in this case, where the GIG part of the GNIG distribution has only depth 1, that is, is formed only by a single integer Gamma r.v., the coefficients $c_{j,k}$, which would only be $c_{1,k}$, are all null except c_{1,r_1}, a fact that is easily verified from (30)–(32) in Appendix 1. Furthermore, in this case we have $c_{1,r_1} = 1/(r_1 - 1)!$, which simplifies the expression for the p.d.f. of Q_W to (see (33) in Appendix 1)

$$f_{Q_W}(q) = K e^{-\lambda_1 q} \frac{1}{\Gamma(r_1 + r_2)} q^{r_1+r_2-1} \, {}_1F_1(r_2, r_2 + r_1, -(\lambda_2 - \lambda_1)q), \qquad (24)$$

for $K = \lambda_1^{r_1} \lambda_2^{r_2}$, with r_1, r_2, λ_1 and λ_2 as defined above.

Using then the series expansion of the Kummer confluent hypergeometric function, we are able to write the distribution of Q_W as an infinite mixture of Gamma distributions, since we may write

$$\begin{aligned} f_{Q_W}(q) &= \sum_{i=0}^{\infty} K \frac{\Gamma(r_2 + i)}{\Gamma(r_2)\,\Gamma(r_2 + r_1 + i)} \frac{(\lambda_1 - \lambda_2)^i}{i!} q^{r_1+r_2+i-1} e^{-\lambda_1 q} \\ &= \sum_{i=0}^{\infty} \underbrace{K \frac{\Gamma(r_2 + i)}{\Gamma(r_2)\,\lambda_1^{r_1+r_2+i}} \frac{(\lambda_1 - \lambda_2)^i}{i!}}_{p_i} \underbrace{\frac{\lambda_1^{r_1+r_2+i}}{\Gamma(r_1 + r_2 + i)} e^{-\lambda_1 q} q^{r_1+r_2+i-1}}_{\text{p.d.f. of } \Gamma(r_1+r_2+i,\lambda_1)}, \end{aligned}$$

which is the p.d.f. of an infinite mixture of $\Gamma(r_1 + r_2 + i, \lambda_1)$ distributions, with weights p_i $(i = 0, 1, \ldots)$.

Thus, since $Q_B \sim \Gamma(1/2, \lambda)$ with $\lambda = 1/(2w_1)$, for w_1 given by (23), the exact distribution of V is that of an infinite mixture of ratios of $\Gamma(1/2, \lambda)$ and $\Gamma(r_1 + r_2 + i, \lambda_1)$ distributions, with weights p_i $(i = 0, 1, \ldots)$, with p.d.f.

$$\begin{aligned} f_V(v) &= \sum_{i=0}^{\infty} K \frac{\Gamma(r_2+i)}{\Gamma(r_2)} \frac{\lambda^{1/2}}{B\left(\frac{1}{2}, r_1+r_2+i\right)} \frac{(\lambda_1-\lambda_2)^i}{i!} \left(\frac{1}{\lambda_1+\lambda v}\right)^{r_1+r_2+1/2+i} v^{-1/2} \\ &= K \left(\frac{\lambda}{v}\right)^{1/2} \left(\frac{1}{\lambda_1 + \lambda v}\right)^{r_1+r_2+1/2} \frac{1}{B\left(\frac{1}{2}, r_1 + r_2\right)} \\ &\quad \times \sum_{i=0}^{\infty} \frac{\Gamma(r_2 + i)}{\Gamma(r_2)} \frac{\Gamma(r_1 + r_2)}{\Gamma(r_1 + r_2 + i)} \frac{\Gamma(r_1 + r_2 + 1/2 + i)}{\Gamma(r_1 + r_2 + 1/2)} \left(\frac{\lambda_1 - \lambda 2}{\lambda_1 + \lambda v}\right)^i \frac{1}{i!} \end{aligned}$$

$$= K\left(\frac{\lambda}{v}\right)^{1/2}\left(\frac{1}{\lambda_1+\lambda v}\right)^{r_1+r_2+1/2}\frac{1}{B\left(\frac{1}{2},r_1+r_2\right)} \times {}_2F_1\left(r_2, r_1+r_2+\frac{1}{2}; r_1+r_2; \frac{\lambda_1-\lambda_2}{\lambda_1+\lambda v}\right)$$

and c.d.f.

$$F_V(v) = K\sum_{i=0}^{\infty}\frac{\Gamma(r_2+i)}{\Gamma(r_2)\,\lambda_1^{r_1+r_2+i}}\frac{(\lambda_1-\lambda_2)^i}{i!}\,BR\left(\frac{1}{2}, r_1+r_2+i; \frac{\lambda v}{\lambda_1+\lambda v}\right)$$

where the infinite summation for the c.d.f. may usually be cut short to just a few dozen terms and is nowadays easy to compute in a precise manner using any available symbolic software.

6.3 *The Case of Both n_1 and n_2 Even*

In this case there are indeed two strategies we may follow. We may use the near-exact approach in Sect. 4 to obtain a near-exact distribution for Q_W, which would then be a mixture of m^*+1 GIG distributions of depth 3, with shape parameters $(n_1-2)/2$, $(n_2-2)/2$ and $1+k$ $(k=0,\ldots,m^*)$ and rate parameters $\lambda_1 = (n_1+n_2-2)/(2\sigma_1^2)$, $\lambda_2 = (n_1+n_2-2)/(2\sigma_2^2)$ and λ given by one of the strategies in (10). Since each of these GIG distributions may then be seen as a finite mixture of Gamma distributions, a near-exact type of distribution for V would then be obtained as a double finite mixture of ratios of Gamma r.v.'s. But, we may take a different approach, in order to obtain the exact p.d.f. and c.d.f. of V in this case. Indeed, if we pay heed to the expression for the p.d.f. of Q_W in (24), we may see that it remains valid even if r_1 is not an integer. As such even when both n_1 and n_2 are even, the p.d.f. of Q_W remains given by (24). As such, all the results about the distribution of V obtained in the previous subsection remain valid for the case where n_1 and n_2 are both even.

7 Some Examples for the Distributions Mentioned in Sects. 2–5

In this section we will use a number of times the result in the following Theorem on the distribution of quadratic forms on Normal r.v.'s from Box (1954).

Theorem (Box, 1954, Thm. 2.1) *If* $\underline{X} \sim N_p(\underline{0}, \Sigma)$ *and* $Q = \underline{X}' M \underline{X}$, *where* M *is a* $p \times p$ *symmetric matrix with* $rank(M) = r \leq p$, *then*

$$Q \stackrel{d}{\equiv} \sum_{j=1}^{r} \mu_j Y_j$$

where $Y_j \sim \chi^2_1$ *are independent r.v.'s and* μ_j $(j = 1, \ldots, r)$ *are the non-null eigenvalues of* ΣM.

7.1 An Example of a Linear Combination of Chi-Squares with a GIG Distribution

Let us take Example 1 from Ha and Provost (2013). In this example the authors consider an approximation to the distribution of a quadratic form $Q = \underline{X}' M \underline{X}$ where $\underline{X} \sim N_6(\underline{0}, I_6)$ and M is a 6×6 positive-definite matrix with eigenvalues $\mu_1^* = \mu_2^* = 1$, $\mu_3^* = \mu_4^* = 2.5$ and $\mu_5^* = \mu_6^* = 9$. Since in this case we have only three different eigenvalues, each one with a multiplicity of 2, the distribution of the quadratic form Q is that of

$$\sum_{j=1}^{3} \mu_j Y_j$$

where $\mu_1 = 1$, $\mu_2 = 2.5$ and $\mu_3 = 9$ and $Y_j \sim \chi^2_2$ $(j = 1, 2, 3)$.

As such, the exact distribution of Q is obtained right away from the result in Sect. 2 as a GIG distribution of depth 3, with $p = 3$, $r_1 = r_2 = r_3 = 1$, $\lambda_1 = 1/2$, $\lambda_2 = 1/(2\times\frac{5}{2}) = 1/5$ and $\lambda_3 = 1/(2\times 9) = 1/18$. The coefficients $c_{j,k}$ are in this case very easy to compute, even by hand, and they are

$$c_{1,1} = \tfrac{15}{2}\,, \qquad c_{2,1} = -\tfrac{300}{13}\,, \qquad c_{3,1} = \tfrac{405}{26}\,,$$

so that the exact p.d.f. of Q is

$$f_Q(z) = \left(\frac{1}{2}\times\frac{1}{2}\times\frac{1}{18}\right)\left[\frac{15}{2}\,e^{-z/2} - \frac{300}{13}\,e^{-z/5} + \frac{405}{26}\,e^{-z/18}\right]$$

and its c.d.f.

$$F_Q(z) = 1 - \left(\frac{1}{2}\times\frac{1}{2}\times\frac{1}{18}\right)\left[\frac{15}{2}\times 2\times e^{-z/2} - \frac{300}{13}\times 5\times e^{-z/5} + \frac{405}{26}\times 18\times e^{-z/18}\right].$$

Quantiles for any GIG distribution may be readily and very quickly obtained using the Mathematica® module at https://sites.google.com/site/lincombchisquares.

This module uses some faster modules for the implementation of the p.d.f. and c.d.f. of the GIG distribution which are available in Appendix 4.A of Chapter 4 of Coelho and Arnold (2019). The exact quantiles computed from this distribution confirm the exact quantiles in Table 1 of Ha and Provost (2013).

7.2 An Example of a Linear Combination of Chi-Squares with a GNIG Distribution

Let us consider a simple case where $\underline{X} \sim N_7(\underline{0}, \Sigma)$ with

$$\Sigma = \frac{1}{12}\begin{bmatrix} 44 & -16 & -16 & 0 & 0 & 0 & 0 \\ -16 & 44 & -16 & 0 & 0 & 0 & 0 \\ -16 & -16 & 44 & 0 & 0 & 0 & 0 \\ 0 & 0 & 0 & 45 & -9 & -3 & -21 \\ 0 & 0 & 0 & -9 & 45 & -21 & -3 \\ 0 & 0 & 0 & -3 & -21 & 45 & -9 \\ 0 & 0 & 0 & -21 & -3 & -9 & 45 \end{bmatrix}$$

and where we are interested in the distribution of the quadratic form $Q = \underline{X}' M \underline{X}$, with

$$M = \frac{1}{12}\begin{bmatrix} 8 & 2 & 2 & 0 & 0 & 0 & 0 \\ 2 & 8 & 2 & 0 & 0 & 0 & 0 \\ 2 & 2 & 8 & 0 & 0 & 0 & 0 \\ 0 & 0 & 0 & 18 & -9 & -3 & 6 \\ 0 & 0 & 0 & -9 & 18 & 6 & -3 \\ 0 & 0 & 0 & -3 & 6 & 18 & -9 \\ 0 & 0 & 0 & 6 & -3 & -9 & 18 \end{bmatrix}.$$

Since the eigenvalues of ΣM are $\mu_1^* = \mu_2^* = 1$, $\mu_3^* = \mu_4^* = \mu_5^* = 5/2$ and $\mu_6^* = \mu_7^* = 9$, the exact distribution of Q is the same as that of

$$\sum_{j=1}^{3} \mu_j Y_j$$

where $\mu_1 = 1$, $\mu_2 = 9$, $\mu_3 = 5/2$ and $Y_1 \sim \chi_2^2$, $Y_2 \sim \chi_2^2$ and $Y_3 \sim \chi_3^2$. As such, from Sect. 2, the exact distribution of Q is a GNIG distribution of depth 3, with, using the notation in Appendix 1, $r_1 = r_2 = 1$ and $r_3 = 3/2$ and $\lambda_1 = 1/2$, $\lambda_2 = 1/18$ and $\lambda_3 = 1/5$, which makes the $c_{j,k}$ $(j = 1, 2; k = 1)$ parameters to be very easy to compute, with

$$c_{1,1} = -\frac{9}{4}\,, \qquad c_{2,1} = \frac{9}{4}\,.$$

Thus, the quadratic form Q has p.d.f.

$$f_Q(z) = \frac{1}{2\times 18}\left(\frac{1}{5}\right)^{3/2}\frac{z^{3/2}}{\Gamma(5/2)}\left[-e^{-\frac{1}{2}z}\frac{9}{4}\,{}_1F_1\left(\frac{3}{2},\frac{5}{2},\frac{3}{10}z\right)\right.$$
$$\left.+e^{-\frac{1}{18}z}\,\frac{9}{4}\,{}_1F_1\left(\frac{3}{2},\frac{5}{2},-\frac{13}{90}z\right)\right],$$

which using (13), that for our case may assume the form,

$${}_1F_1\left(\tfrac{3}{2},\tfrac{5}{2},z\right) = \tfrac{3}{4}\left((-z)^{-3/2}\sqrt{\pi}\,\mathrm{Erf}\left(\sqrt{-z}\right) + 2\,e^z\,\tfrac{1}{z}\right), \tag{25}$$

may be written as

$$f_Q(z) = \frac{1}{80}\left(\frac{1}{5}\right)^{1/2}\left[-e^{-\frac{1}{2}z}\left(-\frac{3}{10}\right)^{-3/2}\mathrm{Erf}\left(\sqrt{-\frac{3}{10}z}\right)\right.$$
$$\left.+e^{-\frac{1}{18}z}\left(\frac{13}{90}\right)^{-3/2}\mathrm{Erf}\left(\sqrt{\frac{13}{90}z}\right) - \frac{800}{39\sqrt{\pi}}\,e^{-\frac{1}{5}z}\,z^{1/2}\right]$$

and c.d.f.

$$F_Q(z) = \frac{\left(\frac{1}{5}\right)^{3/2}z^{3/2}}{\Gamma(5/2)}\left\{{}_1F_1\left(\frac{3}{2},\frac{5}{2},-\frac{1}{5}z\right) - \frac{1}{2}\frac{1}{18}\frac{9}{4}\left[-2\,e^{-\frac{1}{2}z}\,{}_1F_1\left(\frac{3}{2},\frac{5}{2},\frac{3}{10}z\right)\right.\right.$$
$$\left.\left.+18\,e^{-\frac{1}{18}z}\,{}_1F_1\left(\frac{3}{2},\frac{5}{2},-\frac{13}{90}z\right)\right]\right\},$$

which, using (25), may be written as

$$F_Q(z) = \mathrm{Erf}\left(\sqrt{\frac{z}{5}}\right) - \frac{1}{8}\left[-e^{-\frac{1}{2}z}\left(-\frac{3}{2}\right)^{-3/2}\mathrm{Erf}\left(\sqrt{-\frac{3z}{10}}\right)\right.$$
$$\left.+e^{-\frac{1}{18}z}\left(\frac{13}{18}\right)^{-3/2}\mathrm{Erf}\left(\sqrt{\frac{13z}{90}}\right)\right] + \frac{60\sqrt{5}}{234\sqrt{\pi}}e^{-\frac{1}{5}z}z^{1/2}\,.$$

7.3 An Example of a Linear Combination of Chi-Squares with a DGIG Distribution

To build a simple example where a quadratic form in Normal variables has a DGIG distribution we consider $\underline{X} \sim N_6(\underline{0}, \Sigma)$ and the quadratic form $Q = \underline{X}' M \underline{X}$ where

$$\Sigma = \frac{1}{2}\begin{bmatrix} 7 & -1 & -3 & -1 & 0 & 0 \\ -1 & 7 & -1 & -3 & 0 & 0 \\ -3 & -1 & 7 & -1 & 0 & 0 \\ -1 & -3 & -1 & 7 & 0 & 0 \\ 0 & 0 & 0 & 0 & 4 & -2 \\ 0 & 0 & 0 & 0 & -2 & 4 \end{bmatrix} \quad \text{and} \quad M = \frac{1}{4}\begin{bmatrix} -1 & 4 & -3 & 4 & 0 & 0 \\ 4 & -1 & 4 & -3 & 0 & 0 \\ -3 & 4 & -1 & 4 & 0 & 0 \\ 4 & -3 & 4 & -1 & 0 & 0 \\ 0 & 0 & 0 & 0 & -4 & 8 \\ 0 & 0 & 0 & 0 & 8 & -4 \end{bmatrix}.$$

Then the eigenvalues of ΣM are $\mu_1^* = \mu_2^* = 1$, $\mu_3^* = \mu_4^* = 5/2$ and $\mu_5^* = \mu_6^* = -9$. As such, in this case, from Theorem 2.1 in Box (1954), restated at the beginning of the present section, the quadratic form Q has the same distribution as $Z_1 - Z_2$, where Z_1 and Z_2 are independent, with

$$Z_1 = Y_1 + \frac{5}{2}Y_2 \quad \text{and} \quad Z_2 = 9Y_3$$

where Y_1, Y_2 and Y_3 are all chi-squares with 2 d.f.'s, so that the exact distribution of Q is a DGIG distribution with $p_1 = 2$ and $p_2 = 1$, and with $r_1 = r_2 = 1$, $s_1 = 1$, $\lambda_1 = 1/2$, $\lambda_2 = 1/5$ and $\nu_1 = 1/18$. It is then easy to compute

$$c_{1,1} = -\frac{10}{3}, \quad c_{2,1} = \frac{10}{3}, \quad d_{1,1} = 1$$

and obtain the p.d.f. of Q given by

$$f_Q(z) = \begin{cases} \frac{1}{180}\left(-\frac{10}{3}\,\frac{1}{\frac{1}{2}+\frac{1}{18}}\,e^{-\frac{1}{2}z} + \frac{10}{3}\,\frac{1}{\frac{1}{5}+\frac{1}{18}}\,e^{-\frac{1}{5}z}\right) \\ \frac{1}{180}\left(-\frac{10}{3}\,\frac{1}{\frac{1}{2}+\frac{1}{18}}\,e^{\frac{1}{18}z} + \frac{10}{3}\,\frac{1}{\frac{1}{5}+\frac{1}{18}}\,e^{\frac{1}{18}z}\right) \end{cases} = \begin{cases} \frac{1}{180}\left(-6\,e^{-\frac{1}{2}z} + \frac{300}{23}\,e^{-\frac{1}{5}z}\right), & z \geq 0 \\ \frac{9}{230}\,e^{\frac{1}{18}z}, & z \leq 0 \end{cases}$$

and c.d.f.

$$\begin{aligned} F_Q(z) &= \begin{cases} 1 - \frac{1}{180}\left(-\frac{10}{3}\,\frac{1}{\frac{1}{2}+\frac{1}{18}}\,\frac{e^{-\frac{1}{2}z}}{1/2} + \frac{10}{3}\,\frac{1}{\frac{1}{5}+\frac{1}{18}}\,\frac{e^{-\frac{1}{5}z}}{1/5}\right), & z \geq 0 \\ \frac{18}{180}\,e^{\frac{1}{18}z}\left(-\frac{10}{3}\,\frac{1}{\frac{1}{2}+\frac{1}{18}} + \frac{10}{3}\,\frac{1}{\frac{1}{5}+\frac{1}{18}}\right), & z \leq 0 \end{cases} \\ &= \begin{cases} 1 - \frac{1}{180}\left(-12\,e^{-\frac{1}{2}z} + \frac{1500}{23}\,e^{-\frac{1}{5}z}\right), & z \geq 0 \\ \frac{81}{115}\,e^{\frac{1}{18}z}, & z \leq 0\,. \end{cases} \end{aligned}$$

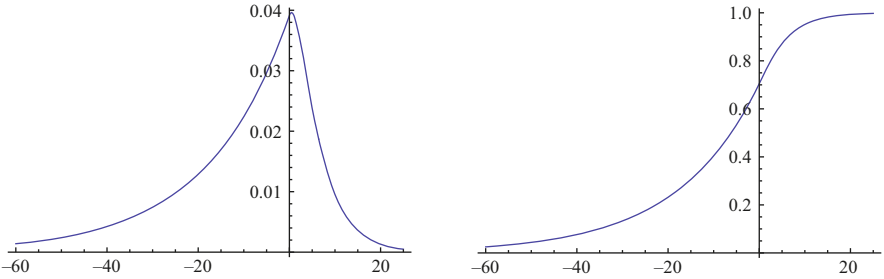

Fig. 1 Plots of the p.d.f. and c.d.f. of the DGIG distribution of Q

The plots of the above p.d.f. and c.d.f. are displayed in Fig. 1.

7.4 An Example of a Linear Combination of Chi-Squares with a Near-Exact Distribution Which Is a Mixture of GIG Distributions

Let now $\underline{X} \sim N_8(\underline{0}, \Sigma)$ and $Q = \underline{X}' M \underline{X}$ where

$$\Sigma = \frac{1}{10}\begin{bmatrix} 11 & -5 & -5 & 9 & 0 & 0 & 0 & 0 \\ -5 & 11 & 9 & -5 & 0 & 0 & 0 & 0 \\ -5 & 9 & 11 & -5 & 0 & 0 & 0 & 0 \\ 9 & -5 & -5 & 11 & 0 & 0 & 0 & 0 \\ 0 & 0 & 0 & 0 & 16 & 9 & -4 & -1 \\ 0 & 0 & 0 & 0 & 9 & 16 & -1 & -4 \\ 0 & 0 & 0 & 0 & -4 & -1 & 16 & 9 \\ 0 & 0 & 0 & 0 & -1 & -4 & 9 & 16 \end{bmatrix}, \quad M = \frac{1}{24}\begin{bmatrix} 8 & -2 & -2 & 0 & 0 & 0 & 0 & 0 \\ -2 & 8 & 0 & -2 & 0 & 0 & 0 & 0 \\ -2 & 0 & 8 & -2 & 0 & 0 & 0 & 0 \\ 0 & -2 & -2 & 8 & 0 & 0 & 0 & 0 \\ 0 & 0 & 0 & 0 & 5 & 2 & -2 & -3 \\ 0 & 0 & 0 & 0 & 2 & 5 & -3 & -2 \\ 0 & 0 & 0 & 0 & -2 & -3 & 5 & 2 \\ 0 & 0 & 0 & 0 & -3 & -2 & 2 & 5 \end{bmatrix}.$$

Then, the eigenvalues of ΣM are $\mu_1^* = \mu_2^* = \mu_3^* = 2/5$, $\mu_4^* = 1/2$, $\mu_5^* = \mu_6^* = 1$, $\mu_7^* = \mu_8^* = 9$, so that the distribution of Q is that of

$$\sum_{j=1}^{4} \mu_j Y_j$$

where $\mu_1 = 2/5$, $\mu_2 = 1/2$, $\mu_3 = 1$, $\mu_4 = 9$ and

$$Y_1 \sim \chi_3^2, \quad Y_2 \sim \chi_1^2, \quad Y_3 \sim \chi_2^2, \quad Y_4 \sim \chi_2^2$$

are four independent r.v.'s.

As such, we will have, from Sect. 4, the distribution of Q as that of

$$Z^* + Z^{**}$$

where

$$Z^* = Y_1^* + \mu_3 Y_3^* + \mu_4 Y_4^* \quad \text{and} \quad Z^{**} = \mu_1 Y_1^{**} + \mu_2 Y_2^{**}$$

where Y_1^*, Y_3^* and Y_4^* are all χ_2^2 r.v.'s and Y_1^{**} and Y_2^{**} are both χ_1^2 r.v.'s, and where the r.v.'s Y_2^*, Y_3^{**} and Y_4^{**} vanished.

As such, the exact distribution of Z^* is a GIG distribution of depth 3 with shape parameters $\ell_1 = \ell_2 = \ell_3 = 1$ and rate parameters $\lambda_1 = 5/4$, $\lambda_2 = 1/2$ and $\lambda_3 = 1/18$, and we will approximate the distribution of Z^{**} by a finite mixture of $m^* + 1$ $\Gamma(r + k, \lambda)$ distributions, for $k = 0, \ldots, m^*$, $r = \sum_{j=1}^{2} \ell_j^* = \frac{1}{2} + \frac{1}{2} = 1$ and λ given by one of the choices in (10). Since the case we are dealing with is exactly the one in scenario IX in Sect. 4.1, we know that good choices for λ are the maximum of λ_1, λ_2 and λ_3, that is, $\lambda = 5/4$, or the value obtained from (vi) in (10), which rounded to 6 decimal places is 1.097561.

Hence, the near-exact distribution obtained for Q is a mixture of $m^* + 1$ GIG distributions, which, if our choice is to use the value 1.097561 for λ, will have depth 4, with shape parameters $r_1 = r_2 = r_3 = 1$ and $r_4 = 1 + k$ ($k = 0, \ldots, m^*$) and rate parameters $\lambda_1 = 5/4$, $\lambda_2 = 1/2$, $\lambda_3 = 1/18$ and $\lambda_4 = 1.097561$, yielding for Z a p.d.f. which may be written as

$$f_Q(z) = \sum_{k=0}^{m^*} \pi_k \, f^{GIG}\left(z \,\middle|\, \{1, 1, 1, 1 + k\}; \{5/4, 1/2, 1/18, 1.097561\}; 4\right).$$

If our choice is to use $\lambda = 5/4$, the mixture components will be GIG distributions of depth 3, with shape parameters $r_1 = 2 + k$, $r_2 = r_3 = 1$ and rate parameters $\lambda_1 = 5/4$, $\lambda_2 = 1/2$, $\lambda_3 = 1/18$, yielding for Z a p.d.f. which may be written as

$$f_Q(z) = \sum_{k=0}^{m^*} \pi_k \, f^{GIG}\left(z \,\middle|\, \{2 + k, 1, 1\}; \{5/4, 1/2, 1/18\}; 3\right).$$

The weights π_k ($k = 0, \ldots, m^* - 1$) are then computed through the solution of the system of equations in (8), taking then $\pi_{m^*} = 1 - \sum_{k=0}^{m^*-1} \pi_k$.

7.5 An Example for the Distribution of Ratios of Linear Combinations of Chi-Squares

We take here the example in Sect. 7 of Box (1954) of a one-way ANOVA model "in which the observations are normally distributed but the variances differ from group to group" and we will show how using the results obtained we will be able to obtain near-exact distributions for the test statistic (which is the ratio of the between and the within sums of squares, each of which is both a quadratic form in Normal r.v.'s and a linear combination of independent chi-squares), and how these near-exact distributions will exactly reproduce the exact probabilities presented by Box (1954) in his paper.

Box (1954) states that the between groups sum of squares, Q_B, has, under the null hypothesis of equality of the k group means, the same distribution as that of

$$\sum_{\ell=1}^{k-1} \mu_\ell Y_\ell$$

where $Y_\ell \sim \chi_1^2$ are $k-1$ independent r.v.'s and μ_ℓ are the non-null eigenvalues of the matrix ΣM, where

$$\Sigma = diag\left(\sigma_\ell^2/n_\ell, \ell = 1, \ldots, k\right)$$

is the variance-covariance matrix of the observations, where σ_ℓ^2 is the variance in the ℓ-th group and n_ℓ the sample size in that group ($\ell = 1, \ldots, k$), and

$$M = diag\,(n_\ell, \ell = 1, \ldots, k) - \frac{1}{N}\,[n_1, n_2, \ldots, n_k]\,[n_1, n_2, \ldots, n_k]'$$

where $N = \sum_{\ell=1}^k n_\ell$, so that

$$\Sigma M = diag(\sigma_\ell^2) - \frac{1}{N} M^*$$

where M^* has its ℓj-th element equal to $\sigma_\ell^2 n_j$ ($\ell = 1, \ldots, k$; $j = 1, \ldots, k$).

Box (1954) also states that the within groups sum of squares, Q_W is distributed as

$$\sum_{\ell=1}^{k} \sigma_\ell^2 Y_\ell^*$$

where Y_ℓ^* are k independent $\chi_{n_\ell - 1}^2$ r.v.'s.

We will use example (4) in Table 4 of Box (1954), where $k = 3$, $\sigma_1^2 = 1$, $\sigma_2^2 = 2$, $\sigma_3^2 = 3$ and $n_1 = 7$, $n_2 = 5$, $n_3 = 3$, to illustrate how using a near-exact type of distribution we will be able to obtain the exact probabilities reported in that Table.

The exact distribution of Q_W is in this case a GIG distribution of depth 3, with shape parameters $r_1 = (n_1-1)/2 = 3$, $r_2 = (n_2-1)/2 = 2$, $r_3 = (n_3-1)/2 = 1$ and rate parameters $\lambda_1 = 1/(2\sigma_1^2) = 1/2$, $\lambda_2 = 1/(2\sigma_2^2) = 1/4$ and $\lambda_3 = 1/(2\sigma_3^2) = 1/6$, from which it is quite simple to compute

$$c_{1,1} = -3888\,,\quad c_{1,2} = -528\,,\quad c_{1,3} = -24\,,\quad c_{2,1} = 0\,,\quad c_{2,2} = -768\,,\quad c_{3,1} = 3888\,, \tag{26}$$

which may also be easily computed using module `Makec`, available in the references and web-pages referenced at the end of Sect. 2.

For Q_B, since the two chi-square r.v.'s involved have only 1 d.f., we obtain from Sect. 4, for $m^* = 4$ (an arbitrary choice, which we are sure to be good enough to assure the computation of tail probabilities with great accuracy), an asymptotic distribution as a mixture of five $\Gamma(1+k,\lambda)$ distributions, for $k = 0,\ldots,4$ and $\lambda = 15/64$, taken as the harmonic mean of $\lambda_1 = 1/(2\mu_1) = \frac{15}{2}\big/(32+\sqrt{79})$ and $\lambda_2 = 1/(2\mu_1) = \frac{15}{2}\big/(32-\sqrt{79})$, where $\mu_1 = \frac{1}{15}(32+\sqrt{79})$ and $\mu_2 = \frac{1}{15}(32-\sqrt{79})$ are the eigenvalues of the matrix ΣM. The weights π_k ($k = 0,\ldots,4$), rounded to 4 decimal places are

$$\begin{aligned} &\pi_0 = 1.0408\,,\quad \pi_1 = -0.0861\,,\quad \pi_2 = 0.0520\,,\quad \pi_3 = -0.0089 \\ &\text{and}\quad \pi_4 = 1-(\pi_0+\pi_1+\pi_2+\pi_3) = 0.0022\,. \end{aligned} \tag{27}$$

The asymptotic p.d.f. and c.d.f. of Q_B/Q_W are thus given respectively by (21) and (22) with $\lambda = 15/64$, $m^* = 4$, π_j ($j = 0,\ldots,4$) given by (27), $k_1^* = 6$, $k_2^* = 4$, $k_3^* = 2$, $w_1^* = 1$, $w_2^* = 2$ and $w_3^* = 3$, with $p_{\ell,i}^*$ given by (20) with the $c_{\ell,i}$ given by (26), for $\ell = 1, 2, 3$ and $i = 1,\ldots,k_\ell^*/2$.

The plots of this p.d.f. and c.d.f. are displayed in Fig. 2.

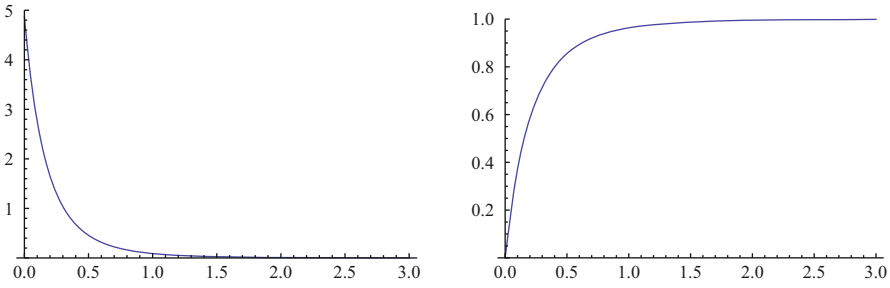

Fig. 2 Plots of the asymptotic p.d.f. and c.d.f. of Q_B/Q_W for example (4) in Table 4 of Box (1954)

Then, since d.f.$(Q_B)= k - 1 = 2$ and d.f.$(Q_W)= N - k = 12$ and the 0.95 quantile of an $F_{2,12}$ distribution, rounded to 6 decimal places is equal to 3.885294, the probability that the ratio of quadratic forms $V = Q_B/Q_W$ exceeds the 0.95 quantile of the $F_{2,12}$ distribution is (rounded to 6 decimal places)

$$1 - F_V\left(\frac{1}{6}\times 3.885296\right) = 0.092514$$

which exactly matches the exact probability reported by Box (1954) of 0.0925, thus showing the usefulness of this approach in obtaining distributions which have quite simple forms and that lie very close to the exact distribution. We should note that we need to multiply the quantile of the $F_{2,12}$ distribution by $1/6$ because the relation that may be established with the F distribution is indeed that of the distribution of the statistic $\frac{Q_B}{d.f.(Q_B)} \Big/ \frac{Q_W}{d.f.(Q_W)}$, where as stated above, $d.f.(Q_B) = 2$ and $d.f.(Q_W) = 12$ so that we have to multiply Q_B/Q_W by $12/2 = 6$, or divide the quantile of the $F_{2,12}$ distribution by 6 in order that the relation may be established.

In Fig. 3 is shown the Mathematica® implementation of this c.d.f., together with the result obtained.

Using a similar procedure, all exact probabilities in Table 4 of Box (1954) may be easily computed and confirmed, with the only remark that the exact probability for example (5) in that Table should rather be 3.25 and not 4.03.

```
k={6,4,2};
w={1,2,3};
c=Makec[k/2,1/(2*w),3];
pi={1.0408,-.0861,.0520,-.0089,.0022};
lambda=15/64;
r=1;
CDFV[z_]:=Sum[Sum[Sum[pi[[j+1]]*
  (Product[(1/(2*w[[ell]]))^(k[[ell]]/2),{ell,1,3}]*
              c[[ell]][[i]]*Gamma[i]/(1/(2*w[[ell]]))^i)*
  BetaRegularized[2*lambda*w[[ell]]*z/(2*lambda*w[[ell]]*z+1),
               r+j,i],{i,1,k[[ell]]/2}],{ell,1,3}],{j,0,4}]

1 - CDFV[1/6*3.885294]
0.0925144
```

Fig. 3 Mathematica® commands used to implement the c.d.f. of the ratio of quadratic forms Q_B/Q_W and to compute the probability reported in Table 4 of Box (1954)

8 Conclusions

Closed form expressions, with all parameters in the distributions with express algebraic expressions, and as such easy to implement with any symbolic software, are provided for the distribution of the linear combination of independent chi-square r.v.'s for the cases where all the chi-square r.v.'s involved have an even number of d.f.'s, both in the case that all coefficients in the linear combination are positive as well as in the case that some are positive and some negative.

Also for the case where all but one of the chi-square r.v.'s have an even number of d.f.'s and all the coefficients in the linear combination are positive, closed form representations are given for both the p.d.f. and the c.d.f. of the distribution of linear combinations of independent chi-square r.v.'s.

For the cases where the d.f.'s of the chi-square r.v.'s in the linear combination may be either even or odd, sharp near-exact approximations, based on mixtures of sums of independent Gamma r.v.'s, all or all but one of them, with integer shape parameters, and thus with closed form expressions for the distribution of their sums. In these cases one may have a choice to make in terms of the common rate parameter to be used for those Gamma r.v.'s. Numerical studies show that in general the best choices are: (i) for cases where the values $w_j k_j$ (where the w_j are the coefficients in the linear combination of the chi-square r.v.'s and the k_j their d.f.'s—see (1)) display an unbalanced set of values, the harmonic mean of the $1/(2w_j)$ or the definition of λ as in (vii) in (10), while (ii) for cases where the $w_j k_j$ display a quite balanced set of values, the geometric mean of the $1/(2w_j)$ is the best choice and (iii) for cases where the w_j exhibit values both above and below 1, the choices of λ as the maximum of the $1/(2w_j)$ or given by (vi) or (vii) in (10). In any case the choice of defining λ as in (vii) of (10) always leads to quite good behaviors, which in cases it is not the best choice, will anyway give very good results.

The exact and near-exact distributions obtained may then be used to obtain exact or asymptotic distributions for ratios of linear combinations of chi-squares and thus also for ratios of quadratic forms, some of which are important statistics in many ANOVA and other statistical models under heterocedasticity. Moreover, these distributions also allowed us to obtain the exact distribution of the Behrens–Fisher statistic.

Acknowledgements The author wants to thank the National Research Foundation from South-Africa for its support through Grant number 71199 and also two anonymous referees whose comments and remarks much contributed to a better paper.

Appendix 1: Notation and Expressions for the p.d.f. and c.d.f. of the GIG and GNIG Distributions

Let $Z_j \sim \Gamma(r_j, \lambda_j)$ $(j = 1, \ldots, p)$ be a set of p independent r.v.'s and consider the r.v.

$$Z = \sum_{j=1}^{p} Z_j \,.$$

In case all the $r_j \in \mathbb{N}$, the distribution of Z is what we call a GIG (Generalized Integer Gamma) distribution (Coelho 1998). If all the λ_j are different, Z has a GIG distribution of depth p, with shape parameters r_j and rate parameters λ_j, with p.d.f.

$$f_Z(z) = f^{GIG}\Big(z \,\Big|\, \{r_j\}_{j=1:p}; \{\lambda_j\}_{j=1:p}; p\Big) = K \sum_{j=1}^{p} P_j(z)\, e^{-\lambda_j z}\,, \quad (z > 0) \tag{28}$$

and c.d.f.

$$F_Z(z) = F^{GIG}\Big(z \,\Big|\, \{r_j\}_{j=1:p}; \{\lambda_j\}_{j=1:p}; p\Big) = 1 - K \sum_{j=1}^{p} P_j^*(z)\, e^{-\lambda_j z}\,, \quad (z > 0)$$

where

$$K = \prod_{j=1}^{p} \lambda_j^{r_j}\,, \qquad P_j(z) = \sum_{k=1}^{r_j} c_{j,k}\, z^{k-1} \tag{29}$$

and

$$P_j^*(z) = \sum_{k=1}^{r_j} c_{j,k}(k-1)! \sum_{i=0}^{k-1} \frac{z^i}{i!\,\lambda_j^{k-i}}\,,$$

with

$$c_{j,r_j} = \frac{1}{(r_j - 1)!} \prod_{\substack{i=1 \\ i \neq j}}^{p} (\lambda_i - \lambda_j)^{-r_i}\,, \quad j = 1, \ldots, p\,, \tag{30}$$

and, for $k = 1, \ldots, r_j - 1$ and $j = 1, \ldots, p$,

$$c_{j,r_j-k} = \frac{1}{k}\sum_{i=1}^{k} \frac{(r_j-k+i-1)!}{(r_j-k-1)!}\, R(i,j,p)c_{j,r_j-(k-i)}\,, \tag{31}$$

where

$$R(i,j,p) = \sum_{\substack{k=1\\k\neq j}}^{p} r_k(\lambda_j-\lambda_k)^{-i} \quad (i=1,\ldots,r_j-1)\,. \tag{32}$$

In case some of the λ_j assume the same value as other λ_j's, the distribution of Z still is a GIG distribution, but in this case with a reduced depth. In this more general case, let $\{\lambda_\ell;\, \ell=1,\ldots,g(\leq p)\}$ be the set of different λ_j's and let $\{r_\ell;\, \ell=1,\ldots,g(\leq p)\}$ be the set of the corresponding shape parameters, with r_ℓ being the sum of all r_j $(j\in\{1,\ldots,p\})$ which correspond to the λ_j assuming the value λ_ℓ. In this case Z will have a GIG distribution of depth g, with shape parameters r_ℓ and rate parameters λ_ℓ $(\ell=1,\ldots,g)$.

If all r.v.'s have Gamma distributions with different rate parameters λ_j and Z_p has a Gamma distribution with a non-integer shape parameter r_p, then we will say that the r.v. Z has a GNIG (Generalized Near-Integer Gamma) distribution of depth p. The probability density and cumulative distribution functions of Z are, for $z>0$, respectively given by Coelho (2004)

$$f^{GNIG}(z\,|\,r_1,\ldots,r_{p-1};r_p;\,\lambda_1,\ldots,\lambda_{p-1};\lambda_p;\,p)$$

$$= K\sum_{j=1}^{p-1} e^{-\lambda_j z}\sum_{k=1}^{r_j}\left\{c_{j,k}\frac{\Gamma(k)}{\Gamma(k+r_p)}z^{k+r_p-1}\,{}_1F_1(r_p,k+r_p,-(\lambda_p-\lambda_j)z)\right\}, \tag{33}$$

and

$$F^{GNIG}(z\,|\,r_1,\ldots,r_{p-1};r_p;\,\lambda_1,\ldots,\lambda_{p-1};\lambda_p;\,p) = \frac{\lambda_p^{r_p}z^{r_p}}{\Gamma(r_p+1)}\,{}_1F_1(r_p,r_p+1,-\lambda_p z)$$

$$-K\sum_{j=1}^{p-1} e^{-\lambda_j z}\sum_{k=1}^{r_j} c^*_{j,k}\sum_{i=0}^{k-1}\frac{z^{r_p+i}\lambda_j^i}{\Gamma(r_p+1+i)}\,{}_1F_1(r_p,r_p+1+i,-(\lambda_p-\lambda_j)z)\,,$$

with $K=\prod_{j=1}^{p}\lambda_j^{r_j}$ and $c^*_{j,k} = \frac{c_{j,k}\Gamma(k)}{\lambda_j^k}$ and where ${}_1F_1(a,b,z)$ represents the Kummer confluent hypergeometric function.

Appendix 2: Notation and Expressions for the p.d.f. and c.d.f. of the DGIG Distribution

Let,

$$Z_1^* \sim GIG(r_j, \lambda_j;\ j = 1, \ldots, p_1)\,, \quad \text{and} \quad Z_2^* \sim GIG(s_\ell, \nu_\ell;\ \ell = 1, \ldots, p_2)\,,$$

be two independent r.v.'s and let

$$Z = Z_1^* - Z_2^*\,.$$

Then Z has what we call a DGIG (Difference of two GIG) distribution, whose p.d.f. and c.d.f are given by Coelho and Mexia (2010, Sect. 2.5, Thm. 2.1).

Taking

$$K_1 = \prod_{j=1}^{p_1} \lambda_j^{r_j} \quad \text{and} \quad K_2 = \prod_{\ell=1}^{p_2} \nu_\ell^{s_\ell}\,,$$

and taking $c_{j,k}$ defined in a similar manner to $c_{j,k}$ in (30)–(32), with p replaced by p_1 and $d_{\ell,h}$ defined in a corresponding manner, with p replaced by p_2, λ_j $(j = 1, \ldots, p)$ replaced by ν_ℓ $(\ell = 1, \ldots, p_2)$ and r_j $(j = 1, \ldots, p)$ replaced by s_ℓ $(\ell = 1, \ldots, p_2)$, the p.d.f. of Z is given by

$$f_Z(z) = \begin{cases} K_1 K_2 \sum_{j=1}^{p_1} P_{1j}^{**}(z)\, e^{-\lambda_j z} & z \geq 0 \\ K_1 K_2 \sum_{\ell=1}^{p_2} P_{2\ell}^{**}(z)\, e^{\nu_\ell z} & z \leq 0 \end{cases}$$

where

$$P_{1j}^{**}(z) = \sum_{k=1}^{r_{1j}} c_{j,k} \sum_{\ell=1}^{p_2} \sum_{h=1}^{r_{2\ell}} d_{\ell,h} \sum_{i=0}^{k-1} \binom{k-1}{i} z^{k-1-i} \frac{(h+i-1)!}{(\lambda_j + \nu_\ell)^{h+i}}$$

and

$$P_{2\ell}^{**}(z) = \sum_{h=1}^{r_{2\ell}} d_{\ell,h} \sum_{j=1}^{p_1} \sum_{k=1}^{r_{1j}} c_{j,k} \sum_{i=0}^{h-1} \binom{h-1}{i} (-z)^{h-1-i} \frac{(k+i-1)!}{(\lambda_j + \nu_\ell)^{k+i}}$$

and the c.d.f. by

$$F_Z(z) = \begin{cases} 1 - K_1 K_2 \sum_{j=1}^{p_1} P_{1j}^{***}(z)\, e^{-\lambda_j z} & z \geq 0 \\ K_1 K_2 \sum_{\ell=1}^{p_2} P_{2\ell}^{***}(z)\, e^{\nu_\ell z} & z \leq 0 \end{cases}$$

with

$$P_{1j}^{***}(z) = \sum_{k=1}^{r_{1j}} c_{j,k} \sum_{\ell=1}^{p_2} \sum_{h=1}^{r_{2l}} d_{\ell,h} \sum_{i=0}^{k-1} \binom{k-1}{i} \frac{(h+i-1)!}{(\lambda_j + \nu_\ell)^{h+i}} \sum_{t=0}^{k-1-i} \frac{(k-1-i)!}{t!} \frac{z^t}{\lambda_j^{k-i-t}}$$

and

$$P_{2\ell}^{***}(z) = \sum_{h=1}^{r_{2\ell}} d_{\ell,h} \sum_{j=1}^{p_1} \sum_{k=1}^{r_{1j}} c_{j,k} \sum_{i=0}^{h-1} \binom{h-1}{i} \frac{(k+i-1)!}{(\lambda_j + \nu_\ell)^{k+i}} \sum_{t=0}^{h-1-i} \frac{(h-1-i)!}{t!} \frac{(-z)^t}{\nu_\ell^{h-i-t}}.$$

As a short notation for the p.d.f. and c.d.f. of the r.v. Z we will use

$$f_Z(z) = f^{DGIG}\Big(z \big| \{r_j\}_{j=1:p_1}; \{s_\ell\}_{\ell=1:p_2}; \{\lambda_j\}_{j=1:p_1}; \{\nu_\ell\}_{\ell=1:p_2}; p_1, p_2\Big), \quad (z \in \mathbb{R})$$

and

$$F_Z(z) = F^{DGIG}\Big(z \,\big|\, \{r_j\}_{j=1:p_1}; \{s_\ell\}_{\ell=1:p_2}; \{\lambda_j\}_{j=1:p_1}; \{\nu_\ell\}_{\ell=1:p_2}; p_1, p_2\Big), \quad (z \in \mathbb{R}).$$

References

Alvo, M., Cabilio, P., & Feigin, P. D. (1982). Asymptotic theory for measures of concordance with special reference to average Kendall Tau. *The Annals of Statistics, 10*, 1269–1276.

Baksalary, J. K., Hauke, J., & Styan, G. P. H. (1994). On some distributional properties of quadratic forms in normal variables and on some associated matrix partial orderings. In T. W. Anderson, K. T. Fang & I. Olkin (Eds.), *Multivariate analysis and its applications*. *IMS lecture notes-monograph series* (vol. 24, pp. 111–121). Hayward, CA: Institute of Mathematical Statistics.

Baldesari, B. (1967). The distribution of a quadratic form of normal random variables. *Annals of Mathematical Statistics, 38*, 1700–1704.

Behrens, W. H. V. (1929). Ein Beitrang zur Fehlerberchnung bei wenigen Beobachtungen. *Landwirtsch Jahrbucher, 68*, 807–837.

Bock, M. E. (1984). *Distribution Results for Positive Definite Quadratic Forms with Repeated Roots*. Tech. Rep. No. 347. Stanford University, CA: Department of Statistics.

Bock, M. E., & Solomon, H. (1987). *Distributions of Quadratic Forms*. Tech. Rep. No. 398. Stanford University, CA: Department of Statistics.

Box, G. E. P. (1954). Some theorems on quadratic forms applied in the study of analysis of variance problems, I. effect of inequality of variance in the one-way classification. *Annals of Mathematical Statistics, 25*, 290–302.

Castaño-Martínez, A., & López-Blázquez, F. (2005). Distribution of a sum of weighted noncentral chi-square variables. *Test, 14*, 397–415.

Chernoff, H., & Lehmann, E. L. (1954). The use of maximum likelihood estimates in χ^2 tests for goodness of fit. *Annals of Mathematical Statistics, 25*, 579–586.

Coelho, C. A. (1998). The generalized integer gamma distribution – a basis for distributions in multivariate statistics. *Journal of Multivariate Analysis, 64*, 86–102.

Coelho, C. A. (2004). The generalized near-integer Gamma distribution: a basis for 'near-exact' approximations to the distribution of statistics which are the product of an odd number of independent Beta random variables. *Journal of Multivariate Analysis, 89*, 191–218.

Coelho, C. A., & Arnold, B. C. (2019). *Finite forms representations for Meijer G and Fox H functions – applied to multivariate likelihood ratio tests using mathematica®*, MAXIMA *and R. Lecture notes in statistics*. Berlin: Springer.

Coelho, C. A., & Mexia, J. T. (2007). On the distribution of the product and ratio of independent generalized gamma-ratio random variables. *Sankhyā, 69*, 221–255.

Coelho, C. A., & Mexia, J. T. (2010). *Product and ratio of generalized gamma-ratio random variables: Exact and near-exact distributions - applications* (145+v pp.). Saarbrücken, Germany: Lambert Academic Publishing AG & Co. KG. (isbn: 978-3-8383-5846-8).

Davies, R. B. (1980). Algorithm AS 155. The distribution of a linear combination of χ^2 random variables. *Journal of the Royal Statistical Society. Series C, 29*, 323–333.

Davis, A. W. (1977). A differential equation approach to linear combinations of independent chi-squares. *Journal of the American Statistical Association, 72*, 212–214.

Durbin, J., Knott, M., & Taylor, C. C. (1975). Components of Cramer-von Mises statistics. II. *Journal of the Royal Statistical Society. Series B, 37*, 216–237.

Fisher, R. A. (1939). The comparison of samples with possibly unequal variances. *Annals of Eugenics, 9*, 174–180.

Fleiss, J. L. (1971). On the distribution of a linear combination of independent chi-squares. *Journal of the American Statistical Association, 66*, 142–144.

Gabler, S., & Wolff, C. (1987). A quick and easy approximation to the distribution of a sum of weighted chi-square variables. *Statistical Papers, 28*, 317–325.

Gil-Pelaez, J. (1951). Note on the inversion theorem. *Biometrika, 38*, 481–482.

Ha, H.-T., & Provost, S. B. (2013). An accurate approximation to the distribution of a linear combination of non-central chi-square random variables. *REVSTAT – Statistical Journal, 11*, 231–254.

Imhof, J. P. (1961). Computing the distribution of quadratic forms in normal variables. *Biometrika, 48*, 419–426.

Johnson, N. L., & Kotz, S. (1968). Tables of distributions of positive definite quadratic forms in central normal variables. *Sankhyā, Ser. B, 30*, 303–314.

Johnson, L., Kotz, S., & Balakrishnan, N. (1994). *Continuous univariate distributions*. *Wiley series in probability and statistics* (vol.1, 2nd edn.). New York: Wiley.

Kotz, S., Johnson, N. L., & Boyd, D. W. (1967a). Series representations of distributions of quadratic forms in normal variables. I. Central case. *Annals of Mathematical Statistics, 38*, 823–837.

Kotz, S., Johnson, N. L., & Boyd, D. W. (1967b). Series representations of distributions of quadratic forms in normal variables. II. Non-central case. *Annals of Mathematical Statistics, 38*, 838–848.

Lu, Z.-H. (2006). The numerical evaluation of the probability density function of a quadratic form in normal variables. *Computational Statistics and Data Analysis, 51*, 1986–1996.

Mathai, A. M. (1982). Storage capacity of a dam with gamma type inputs. *Annals of the Institute of Statistical Mathematics, 34*, 591–597.

Mathai, A. M., & Provost, S. B. (1992). *Quadratic forms in random variables*. New York: Marcel Dekker.

Morin-Wahhab, D. (1988). *On some functions of quadratic forms and related topics*. Ph. D. Thesis, Department of Mathematics and Statistics, McGill University, Montréal, Québec.

Moschopoulos, P. G. (1985). The distribution of the sum of independent Gamma random variables. *Annals of the Institute of Statistical Mathematics, 37*, 541–544.

Moschopoulos, P. G., & Canada, W. B. (1984). The distribution function of a linear combination of chi-squares. *Computers & Mathematcs with Applications, 10*, 383–386.

Provost, S. B. (1988). The exact density of a general linear combination of gamma variates. *Metron, 46*, 61–69.

Provost, S. B. (1989). On sums of independent gamma random variables. *Statistics, 20*, 583–591.

Provost, S. B., & Rudiuk, E. M. (1996). The exact distribution of indefinite quadratic forms in noncentral normal vectors. *Annals of the Institute of Statistical Mathematics, 48*, 381–394.

Robbins, H. (1948). The distribution of a definite quadratic form. *Annals of Mathematical Statistics, 19*, 266–270.

Robbins, H., & Pitman, E. J. G. (1949). Application of the method of mixtures to quadratic forms in normal variates. *Annals of Mathematical Statistics, 20*, 552–560.

Ruben, H. (1960). Probability content of regions under spherical normal distributions, I. *Annals of Mathematical Statistics, 31*, 598–618.

Ruben, H. (1962). Probability content of regions under spherical normal distributions, IV: The distribution of homogeneous and non-homogeneous quadratic functions of normal variables. *Annals of Mathematical Statistics, 33*, 542–570.

Satterthwaite, F. E. (1941). Synthesis of variance. *Psychometrika, 6*, 309–316.

Shah, B. K. (1970). Distribution theory of a positive definite quadratic form with matrix argument. *Annals of Mathematical Statistics, 41*, 692–697.

Slater, L. J. (1972). Confluent hypergeometric functions. In Abramowitz, M. & Stegun, I. A. (Eds.) *Handbook of mathematical functions with formulas, graphs, and mathematical tables*. *National bureau of standards applied mathematics series, # 55*, 10th Printing. Washington, D.C.: U.S. Government Printing Office.

Solomon, H., & Stephens, M. A. (1977). Distribution of a sum of weighted chi-square variables. *Journal of the American Statistical Association, 72*, 881–885.

Welch, B. L. (1947). The generalization of 'Student's' problem when several different population variances are involved. *Biometrika, 34*, 28–35.

Part II
Recent Developments in Supervised and Unsupervised Modelling

Conjugate Bayesian Regression Models for Massive Geostatistical Data Sets

Sudipto Banerjee

Abstract Geographic Information Systems and related technologies are routinely used to construct massive amounts of spatially oriented data. This, in turn, has generated substantial interest among statisticians for modelling and analysing large spatial datasets. Scalable spatial process models have been found especially attractive due to their richness and flexibility and, particularly so in the Bayesian paradigm, due to their presence in hierarchical model settings. A substantial amount of research articles focus upon innovative theory and more complex model development, but limited attention has been accorded to approaches for easily implementable scalable hierarchical models for the practising scientist or spatial analyst. This article outlines how point-referenced spatial process models can be cast within the framework of conjugate Bayesian linear regression that can rapidly deliver inference on spatial processes. The approach directly samples from the exact joint posterior distribution of regression parameters, the latent process and the predictive random variables, and can be easily implemented on statistical programming environments such as `R`.

1 Introduction

The modelling and analysis for spatial and spatial-temporal data have witnessed an explosion of interest stemming from computerized Geographic Information Systems (GIS) and accompanying technologies. Bayesian hierarchical spatiotemporal process models have become widely deployed statistical tools for researchers to better understand the complex nature of spatial and temporal variability; see, for example, the books by Schabenberger and Gotway (2004), Gelfand et al. (2010), Cressie and Wikle (2011), and Banerjee et al. (2014) for a variety of methods and applications. Technological advances in diverse scientific disciplines have produced massive spatially and temporally indexed databases on a variety of health outcomes

S. Banerjee (✉)
UCLA Department of Biostatistics, University of California, Los Angeles, CA, USA
e-mail: sudipto@ucla.edu

A. Bekker et al. (eds.), *Computational and Methodological Statistics and Biostatistics*, Emerging Topics in Statistics and Biostatistics,
https://doi.org/10.1007/978-3-030-42196-0_10

and risk factors that are accessible to public health researchers, administrators, and policy-makers. This "data deluge" poses new challenges and critical barriers in data analysis for the next generation of biostatisticians and spatial data analysts.

Several methods and approaches, both classical and Bayesian, have been developed and evaluated to address the needs of spatial analysts encountering massive spatial datasets and increasingly complex scientific questions. There is already a substantial literature on modelling and analysing massive spatial datasets and a comprehensive review is beyond the scope of this article; see, e.g., Banerjee (2017) for a focused review on a couple of popular Bayesian approaches and Heaton et al. (2019) for a comparative evaluation for contemporary statistical methods for large spatial data. Here, I will provide develop how elementary conjugate Bayesian linear regression models can be exploited to provide a quick Bayesian analysis of massive spatial datasets. These approaches can be described as model-based solutions for very large spatial datasets that can be executed on modest computing environments.

2 Bayesian Modelling for Point-Referenced Data

Point-referenced spatial data are referenced by locations with coordinates (latitude-longitude, Easting-Northing etc.) and are customarily modelled using a random field. This random field is an uncountable set of random spatial surfaces, say $\{w(\ell) : \ell \in \mathcal{L}\}$, defined over a domain of interest $\mathcal{L}$. This uncountable set is modelled using a stochastic process which ensures the existence of a well-defined probability law for any finite collection of random variables from the underlying random field. Furthermore, the process models the spatial association among the random variables as a function of the locations, typically of the distance between pairs of locations.

For example, in spatial modelling $\mathcal{L}$ is often assumed to be a subset of points in the Euclidean space $\Re^d$ (usually $d = 2$ or 3) or, perhaps, a set of geographic coordinates over a sphere or ellipsoid. Such processes are specified with a *covariance function* $K_\theta(\ell, \ell')$ that gives the covariance between $w(\ell)$ and $w(\ell')$ for any two points ℓ and ℓ' in $\mathcal{L}$. For any finite collection $\mathcal{U} = \{\ell_1, \ell_2, \ldots, \ell_n\}$ in $\mathcal{L}$, the covariance matrix for $w(\ell_i)$'s over $\mathcal{U}$ is the $n \times n$ matrix K_θ whose (i, j)-th entry is the covariance $K_\theta(\ell_i, \ell_j)$. Covariance functions cannot be any function and need to ensure positive-definiteness of the resulting covariance matrix for any finite sample of locations in the domain. A rich literature exists on characterizations for covariance functions, their different properties and their impact on subsequent inference; see, e.g., any of the aforementioned books on spatial statistics. For any two finite subsets $\mathcal{A}$ and $\mathcal{B}$ of $\mathcal{L}$, we will let $K_\theta(\mathcal{A}, \mathcal{B})$ be the matrix whose (i, j)-th entry is the covariance function $K_\theta(\cdot, \cdot)$ evaluated between the i-th location in $\mathcal{A}$ and the j-th location in $\mathcal{B}$. In particular, we denote the $n \times n$ spatial covariance matrix $K_\theta(\mathcal{L}, \mathcal{L})$ simply by K_θ.

A geostatistical setting customarily assumes a response or dependent variable $y(\ell)$ observed at a generic point ℓ along with a $p \times 1$ vector of spatially referenced

predictors $x(\ell)$. Model-based geostatistical data analysis customarily envisions a spatial regression model,

$$y(\ell) = x^{\top}(\ell)\beta + w(\ell) + \epsilon(\ell) \ , \tag{1}$$

where β is the $p \times 1$ vector of slopes, and the residual from the regression is the sum of a spatial process, $w(\ell) \sim GP(0, K_\theta(\cdot, \cdot))$ capturing spatial dependence, and an independent process, $\epsilon(\ell)$, modelling measurement error or fine scale variation attributed to disturbances at distances smaller than the minimum observed inter-site distance. A Bayesian spatial model can now be constructed from (1) as

$$p(\theta, w, \beta, \tau \mid y) \propto p(\theta, \beta, \tau) \times N(w \mid 0, K_\theta) \times N(y \mid X\beta + w, D_\tau) \ , \tag{2}$$

where $y = (y(\ell_1), y(\ell_2), \ldots, y(\ell_n))^{\top}$ is the $n \times 1$ vector of observed outcomes, X is the $n \times p$ matrix (we assume $p < n$) of regressors with i-th row $x^{\top}(\ell_i)$ and the noise covariance matrix $D(\tau)$ represents measurement error or micro-scale variation and depends upon a set of variance parameters τ. A common specification is $D_\tau = \tau^2 I_n$, where τ^2 is called the "nugget." The hierarchy is completed by assigning prior distributions to β, θ and τ.

The primary computational bottleneck emerges from the size of K_θ in computing (2). Since θ is unknown, each iteration of the model fitting algorithm will involve decomposing or factorising K_θ, which typically requires $\sim n^3$ floating point operations (flops). Memory requirements are of the order $\sim n^2$. These become prohibitive for large values of n when K_θ has no exploitable structure. For Gaussian likelihoods, one can integrate out the random effects w from (2) and work with the posterior

$$p(\theta, \beta, \tau \mid y) \propto p(\theta, \beta, \tau) \times N(y \mid X\beta, K_\theta + D_\tau) \ , \tag{3}$$

This reduces the parameter space to $\{\tau^2, \theta, \beta\}$, but one still needs to work with $K_\theta + D_\tau$, which is still $n \times n$. These settings are referred to as "big-n" or "high-dimensional" problems in geostatistics and are widely encountered in environmental sciences today.

3 Conjugate Bayesian Linear Geostatistical Model

A conjugate Bayesian linear regression model is written as

$$y \mid \beta, \sigma^2 \sim N(X\beta, \sigma^2 V_y) \ ; \quad \beta \mid \sigma^2 \sim N(\beta \mid \mu_\beta, \sigma^2 V_\beta) \ ; \quad \sigma^2 \sim IG(a_\sigma, b_\sigma) \ , \tag{4}$$

where y is an $n \times 1$ vector of observations of the dependent variable, X is an $n \times p$ matrix (assumed to be of rank p) of independent variables (covariates or predictors)

and its first column is usually taken to be the intercept, V_y is a fixed (i.e., known) $n \times n$ positive definite matrix, μ_β, V_β, a_σ and b_σ are assumed to be fixed hyper-parameters specifying the prior distributions on the regression slopes β and the scale σ^2. This model is easily tractable and the posterior distribution is

$$p(\beta, \sigma^2 \mid y) = \underbrace{IG(\sigma^2 \mid a_\sigma^*, b_\sigma^*)}_{p(\sigma^2 \mid y)} \times \underbrace{N(\beta \mid Mm, \sigma^2 M)}_{p(\beta \mid \sigma^2, y)}, \tag{5}$$

where $a_\sigma^* = a_\sigma + n/2$, $b_\sigma^* = b_\sigma + (1/2)\left\{\mu_\beta^\top V_\beta^{-1}\mu_\beta + y^\top V_y^{-1} y - m^\top M m\right\}$, $M^{-1} = V_\beta^{-1} + X^\top V_y^{-1} X$ and $m = V_\beta^{-1}\mu_\beta + X^\top V_y^{-1} y$. Sampling from the joint posterior distribution of $\{\beta, \sigma^2\}$ is achieved by first sampling $\sigma^2 \sim IG(a_\sigma^*, b_\sigma^*)$ and then sampling $\beta \sim N(Mm, \sigma^2 M)$ for each sampled σ^2. This yields marginal posterior samples from $p(\beta \mid y)$, which is a non-central multivariate t distribution but we do not need to work with its complicated density function. See Gelman et al. (2013) for further details on the conjugate Bayesian linear regression model and sampling from its posterior.

We will adapt (4) to accommodate (2) or (3). Let us first consider (3) with the customary specification $D_\tau = \tau^2 I$ and let $K_\theta = \sigma^2 R(\phi)$, where $R(\phi)$ is a correlation matrix whose entries are given by a correlation function $\rho(\phi;\ \ell_i, \ell_j)$. Thus, $\theta = \{\sigma^2, \phi\}$, where σ^2 is the spatial variance component and ϕ is a spatial decay parameter controlling the rate at which the spatial correlation decays with separation between points. A simple example is $\rho(\phi;\ \ell_i, \ell_j) = \exp(-\phi\|\ell_i - \ell_j\|)$, although much richer choices are available (Banerjee et al. 2014, see, e.g., Ch 3 in). Therefore, we can write $K_\theta = \sigma^2 V_y$, where $V_y = R(\phi) + \delta^2 I$ and $\delta^2 = \tau^2/\sigma^2$ is the ratio between the "noise" variance and "spatial" variance. If we assume that ϕ and δ^2 are fixed and that the prior on $\{\beta, \sigma^2\}$ are as in (4), then we have reduced (3) to (4) and direct sampling from its posterior is easily achieved as described below (5). We will return to the issue of fixing $\{\phi, \delta^2\}$ shortly.

Let us turn to accommodating (2) within (4), which would include directly sampling the spatial random effects w from their marginal posterior $p(w \mid y)$. Here, it is instructive to write the joint distribution of y and w in (2) as a linear model,

$$\underbrace{\begin{bmatrix} y \\ \mu_\beta \\ 0 \end{bmatrix}}_{y_*} = \underbrace{\begin{bmatrix} X & I_n \\ I_p & O \\ O & I_n \end{bmatrix}}_{X_*} \underbrace{\begin{bmatrix} \beta \\ w \end{bmatrix}}_{\gamma} + \underbrace{\begin{bmatrix} \eta_1 \\ \eta_2 \\ \eta_3 \end{bmatrix}}_{\eta}, \tag{6}$$

where $\eta \sim N(0, \sigma^2 V_{y_*})$ and $V_{y_*} = \begin{bmatrix} \delta^2 I_n & O & O \\ O & V_\beta & O \\ O & O & R(\phi) \end{bmatrix}$. If we assume that δ^2 and ϕ are fixed at known values, then V_{y_*} is fixed. Under this parametrisation, we have a conjugate Bayesian linear regression model $y_* = X_*\gamma + \eta$, where γ has a flat prior

and $\sigma^2 \sim IG(a_\sigma, b_\sigma)$. Thus,

$$p(\gamma, \sigma^2 \mid y) = \underbrace{IG(\sigma^2 \mid a_\sigma^*, b_\sigma^*)}_{p(\sigma^2 \mid y)} \times \underbrace{N(\beta \mid M_* m_*, \sigma^2 M_*)}_{p(\gamma \mid \sigma^2, y)}, \tag{7}$$

where $a_\sigma^* = a_\sigma + (2n + p)/2$, $b_\sigma^* = b_\sigma + (1/2)\left\{y_*^\top V_{y_*}^{-1} y_* - m_*^\top M_* m_*\right\}$, $M_*^{-1} = X_*^\top V_{y_*}^{-1} X_*$ and $m_* = X_*^\top V_{y_*}^{-1} y_*$. Note that the posterior mean of γ is given by $\hat{\gamma} = Mm = \left(X_*^\top V_{y_*}^{-1} X_*\right)^{-1} X_*^\top V_{y_*}^{-1} y_*$, which is the generalized least squares estimate obtained from the augmented linear system in (6). Sampling from the posterior proceeds analogous to that described below (5).

From the preceding account we see that fixing the spatial range decay parameter ϕ and the noise-to-spatial variance ratio δ^2 casts the Bayesian geostatistical model into a conjugate framework that will allow inference on $\{\beta, w, \sigma^2\}$. Note that multiplying the posterior samples of σ^2 by the fixed quantity δ^2 fetches us the posterior samples of τ^2. Therefore, the uncertainty quantification is entirely lost only for the spatial range parameter ϕ and partially for one of the variance components due to fixing their ratio. This, however, provides the computational advantage that inference can be carried out without resorting to expensive iterative algorithms such as Markov chain Monte Carlo that require several iterations before sampling from the posterior distribution. This computational benefit becomes especially relevant when handling massive spatial data. Furthermore, fixing the values of δ^2 and ϕ is not entirely unreasonable given that the identifiability of these parameters from the data are known to be problematic and thwarts posterior learning in any case. Nevertheless, the inference will depend upon these fixed parameters so we discuss a practical approach to fix ϕ and δ^2 at reasonable values.

One simple approach to setting values for ϕ and δ^2 is by conducting some simple spatial exploratory data analysis using the "variogram". The variogram for a zero-centred spatial process $w(\ell)$ is defined as

$$\mathrm{E}[w(\ell + h) - w(\ell)]^2 = \mathrm{var}\{w(\ell + h) - w(\ell)\} = 2\gamma(h), \tag{8}$$

which is meaningful only if the above expression depends solely on h and, whereupon, $\gamma(h)$ is called the "semivariogram". If the process $w(\ell)$ is weakly stationary in the sense that the covariance between $w(\ell)$ and $w(\ell')$ is a function only of the separation $h = \ell' - \ell$, then a simple calculation reveals that $\gamma(h) = K_\theta(0) - K_\theta(h)$, where $K_\theta(\ell, \ell') = K_\theta(\ell' - \ell) = K(h)$. The variogram is usually computed for the observations $y(\ell)$ or for the residuals from a linear model to ascertain the presence of spatial structure underlying the data after adjusting for explanatory variables.

Several practical algorithms exist for empirically calculating the variogram (or semivariogram) from observations by approximating (8) using finite sample moments. Many of these methods for variograms are now offered in user-friendly `R` packages hosted by the Comprehensive R Archive Network (CRAN) (https://cran.

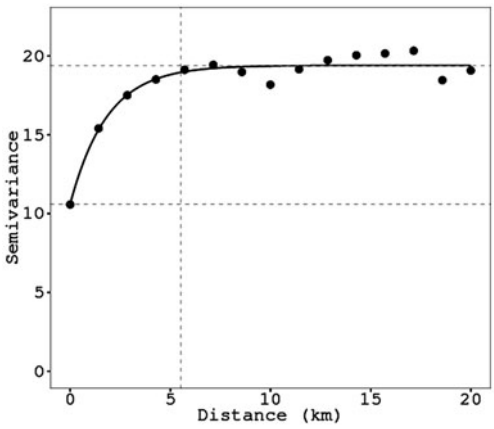

Fig. 1 Variogram of the residuals from non-spatial regression indicates strong spatial pattern

r-project.org). As one example, Finley et al. (2019) investigate the impact of tree cover and occurrence of forest fires on forest height. They first fit an ordinary linear regression of the form $y_{FH} = \beta_0 + \beta_1 x_{\text{tree}} + \beta_2 x_{\text{fire}} + \epsilon$ and then compute a variogram for the residuals from the ordinary linear regression.

Figure 1 depicts the variogram, which helps glean from three process parameters. The lower horizontal line represents the "nugget" or the micro-scale variation captured by the measurement error variance component τ^2. The top horizontal line represents the "sill" (or ceiling) which is the total variation captured by $\sigma^2 + \tau^2$. Therefore, the difference between the two horizontal lines is called the "partial sill" and is captured by σ^2. Finally, the vertical line represents the distance beyond which the variogram flattens or the covariance tends to zero. One can provide "eye-ball" estimates for these quantities and, in particular, fix the values of ϕ and $\delta^2 = \tau^2/\sigma^2$. Fixing these values from the variogram yields the desired highly accessible conjugate framework and the models can be estimated without resorting to Markov chain Monte Carlo (MCMC) as described earlier.

4 Bayesian Modelling for Massive Spatial Data

Conjugate models can be estimated by sampling directly from their joint posterior density and, therefore, completely obviates problems associated with MCMC convergence. This is a major computational benefit. However, the challenges in analysing massive spatial data do not quite end here. When the number of spatial locations providing measurements are in the order of millions as in Finley et al. (2019), then the matrices K_θ, V_y or V_{y_*} that we encountered earlier in different model parametrisations will be too massive to be efficiently loaded on to the machine's CPU, let alone be computed with. This precludes efficient likelihood computations and has led several researchers to propose models specifically adapted

for spatial analysis. We briefly present adaptations of (6) using two different classes of models for massive spatial data: (1) low-rank process models and (2) nearest-neighbour Gaussian process models.

In low rank models, the spatial process is approximated as $w(\ell) \approx b_\theta^\top(\ell)z$, where $b_\theta(\ell)$ is an $r \times 1$ vector of r basis functions, each evaluated at ℓ, and z is an $r \times 1$ vector of coefficients. This means that the $n \times 1$ spatial effect w in (2) is replaced by $B_\theta z$, where B_θ is the $n \times r$ matrix whose i-th row is $b_\theta^\top(\ell_i)$. Dimension reduction is achieved by fixing r to be much smaller than n so that we only deal with r random effects instead of n. The framework in (6) can be easily adapted to this situation as below:

$$\underbrace{\begin{bmatrix} y \\ \mu_\beta \\ 0 \end{bmatrix}}_{y_*} = \underbrace{\begin{bmatrix} X & B_\theta \\ I_p & O \\ O & I_r \end{bmatrix}}_{X_*} \underbrace{\begin{bmatrix} \beta \\ z \end{bmatrix}}_{\gamma} + \underbrace{\begin{bmatrix} \eta_1 \\ \eta_2 \\ \eta_3 \end{bmatrix}}_{\eta}, \quad (9)$$

where $\eta \sim N(0, \sigma^2 V_{y_*})$ and $V_{y_*} = \begin{bmatrix} \delta^2 I_n & O & O \\ O & V_\beta & O \\ O & O & V_z \end{bmatrix}$ is $(n+p+r) \times (n+p+r)$ and fixed, and V_z is now $r \times r$ instead of the $n \times n$ matrix $R(\phi)$ in (6). Benefits accrue in terms of storage and the number of floating point operations (flops) when conducting the exact conjugate Bayesian analysis for this model. Note that the marginal density $p(y_* \mid \gamma, \theta, \tau)$ corresponds to the linear model $y_* = X_*\hat{\gamma} + \eta$, where $\hat{\gamma}$ is the generalized least square estimate of γ obtained by solving the linear system $X_*^\top V_{y_*}^{-1} X_* \gamma = X_*^\top V_{y_*}^{-1} y_*$. Computational benefits accrue from the block diagonal structure of V_{y_*}. To be precise, let $V_z^{1/2}$ and $V_\beta^{1/2}$ be matrix square roots of V_z and V_β, respectively. For example, $V_\beta^{1/2}$ and $V_z^{1/2}$ can be the triangular (upper or lower) Cholesky factor of the $r \times r$ matrices V_β and V_z, respectively. Then, the corresponding Cholesky factor of V_{y_*} is given by the block diagonal matrix $V_{y_*}^{1/2} = \begin{bmatrix} \delta I_n & O & O \\ O & V_\beta^{1/2} & O \\ O & O & V_z^{1/2} \end{bmatrix}$. Once we obtain the square root $V_{y_*}^{1/2}$, we can make the transformations $\tilde{y}_* = V_{y_*}^{-1/2} y_*$ and $\tilde{X}_* = V_{y_*}^{-1/2} X_*$, where $V_{y_*}^{-1/2}$ is cheaply obtained from $V_{y_*}^{1/2}$ because it inverts only a triangular matrix. Now the posterior mean $\hat{\gamma}$ can be obtained using ordinary least squares from the model $\tilde{y}_* = \tilde{X}_*\hat{\gamma} + e_*$, where $e_* \sim N(0, I_{n+p+r})$. Banerjee (2017) provides a more detailed discussion on hierarchical low-rank models, biases they induce and how bias-adjustments and improvements can be made.

Low-rank models continue to be popular choices for analysing spatial data. The cost for fitting low-rank models typically decrease from $O(n^3)$ to $O(nr^2 + r^3) \approx O(nr^2)$ flops since $n >> r$. However, when n is large, empirical investigations suggest that r must be fairly large to adequately approximate the original process and

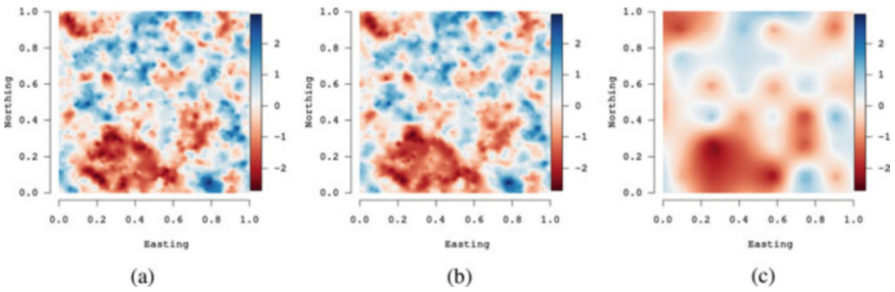

Fig. 2 Comparing estimates of a simulated random field using a full-rank Gaussian Process (Full GP) and a Gaussian Predictive process (PPGP) with 64 knots. The oversmoothing by the low-rank model is evident. (**a**) True w. (**b**) Full GP. (**c**) PPGP 64 knots

the nr^2 flops become exorbitant. Furthermore, low-rank models can perform poorly depending upon the smoothness of the underlying process or when neighbouring observations are strongly correlated and the spatial signal dominates the noise.

As an example, consider part of the simulation experiment presented in Datta et al. (2016a), where a spatial random field was generated over a unit square using a Gaussian process with fixed spatial process parameters over a set of 2500 locations. We then fit a full Gaussian process model and a particular low-rank model called the predictive process model (Banerjee et al. 2008) with 64 knots. Figure 2 presents the results. While the estimated random field from the full Gaussian process is almost indistinguishable from the true random field, the surface obtained from the predictive process with 64 locations substantially oversmooths. This oversmoothing can be mitigated by using a larger number of knots, but this adds to the computational burden.

Figure 2 serves to reinforce findings that low-rank models may be limited in their ability to produce accurate representation of the underlying process at massive scales. They will need a considerably larger number of basis functions to capture the features of the process and will require substantial computational resources for emulating results from a full GP. As the demands for analysing large spatial datasets increase from the order of $\sim 10^4$ to $\sim 10^6$ locations, low-rank models may struggle to deliver acceptable inference. In this regard, enhancements such as the multi-resolution predictive process approximations (Katzfuss 2017) are highly promising.

An alternative to low-rank models is to develop full rank models that can exploit sparsity. Here, too, there are different options. One approach draws on the concept of sparse precision matrices. There are numerous specifications but the one that is effective, scalable and easy to compute is based upon modelling the Cholesky decomposition of the precision matrix of w in a sparse manner.

Writing $N(w \mid 0, \sigma^2 R_\phi)$ as $p(w_1) \prod_{i=2}^{n} p(w_i \mid w_1, w_2, \ldots, w_{i-1})$ is equivalent to the following set of linear models,

$$w_1 = 0 + \eta_1 \quad \text{and} \quad w_i = a_{i1} w_1 + a_{i2} w_2 + \cdots + a_{i,i-1} w_{i-1} + \eta_i \text{ for } i = 2, \ldots, n,$$

or, more compactly, simply $w = Aw + \eta$, where A is $n \times n$ strictly lower-triangular with elements $a_{ij} = 0$ whenever $j \geq i$ and $\eta \sim N(0, D)$ and D is diagonal with diagonal entries $d_{11} = \text{var}\{w_1\}$ and $d_{ii} = \text{var}\{w_i \mid w_j : j < i\}$ for $i = 2, \ldots, n$. From the structure of A it is evident that $I - A$ is unit lower-triangular, hence nonsingular, and $R_\phi = (I - A)^{-1} D (I - A)^{-\top}$.

We now introduce sparsity in $R_\phi^{-1} = (I - A)^\top D (I - A)$ by letting $a_{ij} = 0$ whenever $j \geq i$ (since A is strictly lower-triangular) and also whenever ℓ_j is not among the m nearest neighbours of ℓ_i, where m is fixed by the user to be a small number. It turns out that a very effective approximation emerges by recognising that the lower-triangular elements of A are precisely the coefficients of a linear combination of $w(\ell_j)$'s equating to the conditional expectation $\text{E}[w(\ell_i) \mid \{w(\ell_j) : j < i\}]$. Thus, the $m \times 1$ vector $\tilde{a}_i$ of non-zero entries in the i-th row of A are obtained by solving the $m \times m$ linear system $\tilde{R}_{\phi, N_i, N_i} \tilde{a}_i = R_{\phi, N_i, i}$, where $\tilde{R}_{\phi, N_i, N_i}$ is the $m \times m$ principal submatrix extracted from R_ϕ corresponding to the m neighbours of i (indexed by elements of a neighbour set N_i) and $R_{\phi, N_i, i}$ is the $m \times 1$ vector extracted by choosing the m indices in N_i from the i-th column of R_ϕ. Once $\tilde{a}_i$ is obtained, the i-th diagonal entry of D is obtained as $d_{ii} = R_\phi[i, i] - \tilde{a}_i^\top R_{\phi, N_i, i}$. These computations need to be carried out for each $i = 2, \ldots, n$ (note that for $i = 1$, $d_{11} = \sigma^2$ and $a_{11} = 0$), but m can be kept very small (say 5 or 10 even if n 10^7) so that the expense is $O(nm^3)$ and still feasible. The details can be found in Banerjee (2017). This notion is familiar in Gaussian Graphical models and have been used by Vecchia (1988) and, more recently, by Datta et al. (2016a) and Finley et al. (2019) to tackle massive amounts of spatial locations.

The framework in (6) now assumes the form

$$\underbrace{\begin{bmatrix} y \\ \mu_\beta \\ 0 \end{bmatrix}}_{y_*} = \underbrace{\begin{bmatrix} X & I_n \\ I_p & O \\ O & D^{-1/2}(I - A) \end{bmatrix}}_{X_*} \underbrace{\begin{bmatrix} \beta \\ w \end{bmatrix}}_{\gamma} + \underbrace{\begin{bmatrix} \eta_1 \\ \eta_2 \\ \eta_3 \end{bmatrix}}_{\eta}, \quad (10)$$

where $\eta \sim N(0, \sigma^2 V_{y_*})$ and $V_{y_*} = \begin{bmatrix} \delta^2 I_n & O & O \\ O & V_\beta & O \\ O & O & I_n \end{bmatrix}$ is $(2n + p) \times (2n + p)$ and fixed with much greater sparsity. While this approach can also be subsumed into the framework of (6), its efficient implementation on standard computing architectures needs careful consideration and involves solving a large linear system with $(n + p) \times (n + p)$ coefficient matrix $X_*^\top X_*$. This matrix is large, but is sparse because of sparsity in $(I - A)^\top D^{-1} (I - A)$. Since $(I - A)$ has at most $m + 1$ nonzero entries in each row, an upper bound of nonzero entries in $(I - A)$ is $n(m + 1)$ and, therefore, the upper bound in $(I - A)^\top D^{-1} (I - A)$ is $n(m + 1)^2$. This sparsity can be exploited by sparse linear solvers such as conjugate gradient methods that can be implemented on modest computing environments.

Sampling from the joint posterior distribution $p(\gamma, \sigma^2 \mid y_*)$ is achieved in the following manner. First, the least-squares estimate $\hat{\gamma}$ is obtained using a sparse least-square solver using a preconditioned conjugate gradient algorithm. Subsequently, σ^2 is sampled from its marginal posterior density $IG(a_*, b_*)$, where $a_* = a_\sigma + n/2$ and $b_* = b_\sigma + (1/2)(y_* - X_* \hat{gamma})^\top (y_* - X_* \hat{\gamma})$, and then for each sampled σ^2, γ is sampled from $N\left(\hat{\gamma}, \sigma^2 \left(X_*^\top V_{y_*}^{-1} X_*\right)^{-1}\right)$. Details on such implementations can be found in a recent article by.

5 Spatial Prediction

Let $\tilde{\mathcal{L}} = \{\tilde{\ell_1}, \tilde{\ell_2}, \ldots, \tilde{\ell_{\tilde{n}}}\}$ be a set of $\tilde{n}$ locations where we wish to predict the outcome $y(\ell)$. Let $\tilde{Y}$ be an $\tilde{n} \times 1$ vector with i-th element $\tilde{Y}(\tilde{\ell_i})$ and let $\tilde{w}$ be the $\tilde{n} \times 1$ vector with elements $w(\tilde{\ell_i})$. The predictive model augments $p(\theta, w, \beta, \tau, y)$ to

$$p(\theta, \tau, \beta, w, y, \tilde{w}, \tilde{Y}) = p(\theta, \tau, \beta) \times p(w \mid \theta) \times p(y \mid \beta, w, \tau) \times p(\tilde{w} \mid w, \theta) \times p(\tilde{Y} \mid \beta, \tilde{w}, \tau) \,. \tag{11}$$

The factorisation in (11) implies that $\tilde{Y}$ and w are conditionally independent of each other given $\tilde{w}$ and β. Predictive inference for spatial data evaluates the posterior predictive distribution $p(\tilde{Y}, \tilde{w} \mid y)$. This is the joint posterior distribution for the outcomes and the spatial effects at locations in $\tilde{\mathcal{L}}$. This distribution is easily derived from (11) as

$$p(\tilde{Y}, \tilde{w}, \beta, w, \theta, \tau \mid y) \propto p(\beta, w, \theta, \tau \mid y) \times p(\tilde{w} \mid w, \theta) \times p(\tilde{Y} \mid \beta, \tilde{w}, \tau) \,. \tag{12}$$

Sampling from (12) is achieved by first sampling $\{\beta, w, \theta, \tau\}$ from the posterior distribution $p(\beta, w, \theta\tau \mid y)$. For each drawn sample, we make one draw of the $\tilde{n} \times 1$ vector $\tilde{w}$ from $p(\tilde{w} \mid w, \theta)$ and then, using this sampled $\tilde{w}$, we make one draw of $\tilde{Y}$ from $p(\tilde{Y} \mid \beta, \tilde{w}, \tau)$. The resulting samples of $\tilde{w}$ and $\tilde{Y}$ will be draws from the desired posterior predictive distribution $p(\tilde{w}, \tilde{Y} \mid y)$. This delivers inference on both the latent spatial random effect $\tilde{w}$ and the outcome $\tilde{Y}$ at arbitrary locations since $\mathcal{L}$ can be any finite collection of samples. Summarizing these distributions by computing their sample means, standard errors, and the 2.5-th and 97.5-th quantiles (to produce a 95% credible interval) yields point estimates with associated uncertainty quantification.

It is instructive to see how the entire inference for Gaussian outcomes can be cast into an augmented linear regression model. The predictive model for $\tilde{Y}$ can be written as a spatial regression

$$\tilde{Y} = \tilde{X}\beta + \tilde{w} + \tilde{\epsilon}\,; \quad \tilde{w} = Cw + \omega\,, \tag{13}$$

where $\tilde{X}$ is the $\tilde{n} \times p$ matrix of predictors observed at locations in $\tilde{\mathcal{L}}$ and $\tilde{\epsilon} \sim N(0, \tilde{D}_\tau)$, where $\tilde{\epsilon}$ is the $\tilde{n} \times 1$ vector with elements $\epsilon(\tilde{\ell}_i)$. The second equation in (13) expresses the relationship between the spatial effects $\tilde{w}$ across the unobserved locations in $\tilde{\mathcal{L}}$ and the spatial effects across the observed locations in $\mathcal{L}$. Since there is one underlying random field over the entire domain, the covariance function for the random field specifies the $\tilde{n} \times n$ coefficient matrix C. In particular, if $w \sim N(0, K_\theta)$, then $C = K_\theta(\tilde{\mathcal{L}}, \mathcal{L})K_\theta^{-1}$ and $\omega \sim N(0, F_\theta)$, where $F_\theta = K_\theta(\tilde{\mathcal{L}}, \tilde{\mathcal{L}}) - K_\theta(\tilde{\mathcal{L}}, \mathcal{L})K_\theta^{-1}K_\theta(\mathcal{L}, \tilde{\mathcal{L}})$. The model for the data and the predictions is combined into

$$\underbrace{\begin{bmatrix} y \\ \mu_\beta \\ 0 \\ 0 \\ 0 \end{bmatrix}}_{y_*} = \underbrace{\begin{bmatrix} X & I_n & O & O \\ I_p & O & O & O \\ O & C & -I_{\tilde{n}} & O \\ \tilde{X} & O & I_{\tilde{n}} & -I_{\tilde{n}} \end{bmatrix}}_{X_*} \underbrace{\begin{bmatrix} \beta \\ w \\ \tilde{w} \\ \tilde{Y} \end{bmatrix}}_{\gamma} + \underbrace{\begin{bmatrix} \eta_1 \\ \eta_2 \\ \eta_3 \\ \eta_4 \\ \eta_5 \end{bmatrix}}_{\eta}, \quad \text{where}$$

$$\eta \sim N\left(0, \begin{bmatrix} D_\tau & O & O & O & O \\ O & V_\beta & O & O & O \\ O & O & K_\theta & O & O \\ O & O & O & F_\theta & O \\ O & O & O & O & \tilde{D}_\tau \end{bmatrix}\right) \tag{14}$$

If locations where predictions are sought are fixed by study design, then fitting (14) using the Bayesian conjugate framework can be beneficial. On the other hand, one can first estimate $\{\beta, w, \sigma^2\}$ and store samples from their posterior distribution. Then, for any arbitrary set of points in $\tilde{\mathcal{L}}$, for each stored sample of the parameters we draw one sample of $\tilde{w} \sim N(Cw, F_\theta)$ followed by one draw of $\tilde{Y} \sim N(\tilde{X}\beta + \tilde{w}, \tilde{D}_\tau)$. The resulting $\{\tilde{w}, \tilde{Y}\}$ will be the desired posterior predictive samples for the latent spatial process and the unobserved outcomes.

6 An Example

We present a synopsis of the analysis by Zhang et al. (2019) of a spatial dataset from NASA comprising sea surface temperature observations over 2,827,252 spatial locations of which approximately 90% (2,544,527) were used for model fitting and the rest were withheld for cross-validatory predictive assessment. Details of the dataset can be found in http://modis-atmos.gsfc.nasa.gov/index.html and details on the analysis can be found in Zhang et al. (2019). The salient feature of the analysis

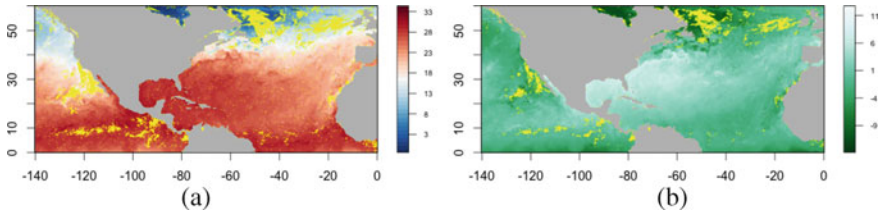

Fig. 3 Posterior predictive maps of sea-surface temperature and latent spatial effects. The land is colored by gray, locations in the ocean without observations are colored by yellow. (**a**) Posterior predictive map of sea-surface temperature. (**b**) Posterior predictive map of latent spatial effects

is that a conjugate Bayesian framework for the NNGP model as in (10) was able to deliver full inference including the estimation of the spatial latent effects in about 2387 s. Sampling from the posterior distribution was achieved using direct sampling as described below (10). Since this algorithm is fast and exact, it was run over a grid of values of $\{\delta^2, \phi\}$. For each such value, a posterior predictive assessment over the cross-validatory hold-out set was carried out and the value of $\{\delta^2, \phi\}$ producing the least root mean square prediction error (RMSPE) was selected as optimal inputs. Figure 3 presents the posterior predictive maps of (a) the response and (b) the latent spatial effects from the conjugate model.

7 Concluding Remarks

This short article has demonstrated how the familiar theory of conjugate Bayesian linear regression models can be adapted to spatial models and used effectively to analyse massive spatial datasets without requiring MCMC algorithms. The article has attempted to provide some insight into constructing highly scalable Bayesian hierarchical models for very large spatial datasets using low-rank and sparsity-inducing processes. Such models are increasingly being employed to answer complex scientific questions and analyse massive spatiotemporal datasets in the natural and environmental sciences. Exploratory data analysis tools such as the variogram can be used to fix the spatial decay parameter and the ratio between the spatial and non-spatial variance components. An alternative is a cross-validatory approach, where a grid of values of the process parameters is used and a fast and exact conjugate Bayesian analysis is performed for each of the values on the grid. The inference from the optimal value of the process parameters based upon RMSPE over hold-out locations is then presented. While these approaches may produce slightly shrunk credible and prediction intervals due to the effect of fixing a parameter, the effect is seen to be moderate in practical spatial analysis and the approach could form a useful tool for quick spatial analysis within the Bayesian paradigm for massive spatial datasets.

References

Banerjee, S. (2017). High-dimensional Bayesian geostatistics. *Bayesian Analysis, 12*, 583–614.

Banerjee, S., Carlin, B. P., & Gelfand, A. E. (2014). *Hierarchical modeling and analysis for spatial data*. Boca Raton, FL: CRC Press.

Banerjee, S., Gelfand, A.E., Finley, A.O., & Sang, H. (2008). Gaussian predictive process models for large spatial datasets. *Journal of the Royal Statistical Society, Series B, 70*, 825–848.

Cressie, N., & Wikle, C. K. (2011). *Statistics for spatio-temporal data*. Hoboken, NJ: Wiley.

Datta, A., Banerjee, S., Finley, A. O., & Gelfand, A. E. (2016a). Hierarchical nearest-neighbor gaussian process models for large geostatistical datasets. *Journal of the American Statistical Association, 111*, 800–812. http://dx.doi.org/10.1080/01621459.2015.1044091

Finley, A. O., Datta, A., Cook, B. C., Morton, D. C., Andersen, H. E., & Banerjee, S. (2019). Efficient algorithms for Bayesian nearest neighbor gaussian processes. *Journal of Computational and Graphical Statistics, 28*(2), 401–414.

Gelfand, A. E., Diggle, P., Guttorp, P., & Fuentes, M. (2010). *Handbook of spatial statistics*. Boca Raton, FL: CRC Press.

Gelman, A., Carlin, J. B., Stern, H. S., Dunson, D. B., Vehtari, A., & Rubin, D. B. (2013). *Bayesian data analysis*. *Chapman & Hall/CRC Texts in Statistical Science* (3rd edn.). Boca Raton, FL: Chapman & Hall/CRC.

Heaton, M., Datta, A., Finley, A., Furrer, R., Guinness, J., Guhaniyogi, R., et al. (2019). Methods for analyzing large spatial data: A review and comparison. *Journal of Agricultural, Biological and Environmental Statistics, 24*(3), 398–425. https://doi.org/10.1007/s13253-018-00348-w

Katzfuss, M. (2017). A multi-resolution approximation for massive spatial datasets. *Journal of the American Statistical Association, 112*, 201–214. http://dx.doi.org/10.1080/01621459.2015.1123632

Schabenberger, O., & Gotway, C. A. (2004). *Statistical methods for spatial data analysis* (1st edn.). Boca Raton, FL: Chapman and Hall/CRC Press.

Vecchia, A. V. (1988). Estimation and model identification for continuous spatial processes. *Journal of the Royal Statistical society, Series B, 50*, 297–312.

Zhang, L., Datta, A., & Banerjee, S. (2019). Practical Bayesian modeling and inference for massive spatial datasets on modest computing environments. *Statistical Analysis and Data Mining: The ASA Data Science Journal, 12*(3), 197–209. https://doi.org/10.1002/sam.11413

Using Improved Robust Estimators to Semiparametric Model with High Dimensional Data

Mahdi Roozbeh, Nor Aishah Hamzah, and Nur Anisah Mohamed

Abstract In classical regression analysis, the ordinary least-squares estimation is the best estimation if the essential assumptions are satisfied. However, if the data does not satisfy some of these assumptions, then results can be misleading. Especially, outliers violate the assumption of normally distributed residuals in the least-squares regression. Robust regression is a modern technique for analyzing data that are contaminated with outliers. The standard setup is to assume that the given samples are derived from a nice distribution, but that an adversary as the power to arbitrary corrupt a constant fraction of the observed data. With advances in technologies, most data problems carry structures such as the number of covariates (p) may exceed the sample size (n), as in the case with high dimensional dataset. Due to some limitations in high dimensional problems, the classical approaches may no longer be useful. One of the alternative approaches commonly used in the ridge estimator introduced by Hoerl and Kennard (Technometrics 12:55–67, 1970). The robust ridge regression provides a solution for the high dimensional dataset with outliers. To be more specific, when prior information (in the form of non-sample information) is available about the vector parameter, the estimation can be improved. This information, known as uncertain prior information or restriction, is useful in the estimation procedure, especially, when the information based on the sample data may be limited. The information may be due to (a) a fact known from theoretical or experimental considerations, (b) a hypothesis that need to be tested or, (c) an artificially imposed condition to reduce or eliminate redundancy in the description of the model. On the other hand, in some experimental cases, it is not certain whether this prior information hold. The consequence of incorporating

M. Roozbeh (✉)
Department of Statistics, Faculty of Mathematics, Statistics and Computer Sciences, Semnan University, Semnan, Iran
e-mail: mahdi.roozbeh@semnan.ac.ir

N. A. Hamzah · N. A. Mohamed
UM Centre for Data Analytics, Institute of Mathematical Sciences, Faculty of Science, University of Malaya, Kuala Lumpur, Malaysia

A. Bekker et al. (eds.), *Computational and Methodological Statistics and Biostatistics*, Emerging Topics in Statistics and Biostatistics,
https://doi.org/10.1007/978-3-030-42196-0_11

non-sample information depends on the quality or reliability of the information introduced in the estimation process. This uncertain prior information, in the form of hypotheses, can be used in two different ways: (a) a preliminary test estimation procedure, and (b) the Stein-type shrinkage estimation. We consider robust ridge estimation in semiparametric high dimensional data and propose a preliminary test, Stein-type and positive-rule Stein-type robust estimators. For these estimators, a real data example is considered to illustrate the efficiency of the estimators.

1 Introduction

Many data problems that we have today carry structures where the number of covariates, p, exceed the sample size n, i.e., $p > n$. In such a setting, a huge amount of work has been pursued in addressing prediction of a new response variable, estimation of an underlying parameter vector and variable selection (see Hastie et al. 2009 and Bühlmann and van de Geer 2011). In a nutshell, we consider ridge regression estimation in sparse semiparametric models in which the condition $p > n$, that is, when classical analysis is no longer valid.

Let $(y_1, \boldsymbol{x}_1, t_1), \cdots, (y_n, \boldsymbol{x}_n, t_n)$ be observations that follow the semiparametric regression model (SRM)

$$y_i = \boldsymbol{x}_i^\top \boldsymbol{\beta} + f(t_i) + \epsilon_i, \quad i = 1, \ldots, n \tag{1.1}$$

where $\boldsymbol{x}_i^\top = (x_{i1}, x_{i2}, \ldots, x_{ip})$ is p-dimensional vector of observed covariates or explanatory variables, $\boldsymbol{\beta} = (\beta_1, \beta_2, \ldots, \beta_p)^\top$ is a p-dimensional vector of unknown parameters, the t_i's are known and non-random in some bounded domain $D \subset \mathbb{R}$, $f(t_i)$ is an unknown smooth function and ϵ_i's are independent and identically distributed random errors with zero mean and variance σ^2, which are independent of $(\boldsymbol{x}_i, t_i)$. Semiparametric regression models are more flexible than standard linear models since they have a parametric and a nonparametric component. They can be a suitable choice when one suspects that the response y linearly depends on x, but nonlinearly related to t.

Estimations and applications of the model (1.1) can be found in the monograph of Härdle et al. (2000).

The theory of linear models is well established for traditional setting $p < n$. With modern technologies, however, especially in many biological, medical, social, and economic studies, p is equal or greater than n, thus making valid statistical inference a great challenge. In the case of $p < n$, there is a rich literature on model estimation. However, classical statistical methods cannot be used for estimating parameters of the model (1.1) when $p > n$, because they would overfit the data, besides severe identifiability issues. A way out of the ill-posedness of estimation in model (1.1) is given by assuming a sparse structure where only a few of the components of $\boldsymbol{\beta}$ are "important" or "non-zero". Estimation of a full parametric regression model in the case of $p > n$ and statistical inference has started about a decade ago. See,

for example, Zhang and Huang (2008), Fan and Lv (2010), Shao and Deng (2012), Bühlmann (2013), Bühlmann et al. (2014) for some references.

Now, consider a semiparametric regression model in the presence of multicollinearity. The existence of multicollinearity may lead to wider confidence intervals for the individual parameters or linear combination of the parameters and may produce estimates with wrong signs. For our purpose we only employ the ridge regression concept due to Hoerl and Kennard (1970), to combat multicollinearity. There are many related research works adopting ridge regression methodology to overcome the multicollinearity problem. For a few recent researches in full-parametric and semiparametric regression models, see Saleh (2006), Akdenïz and Tabakan (2009), Akdenïz Duran et al. (2012), Roozbeh and Arashi (2013), Amini and Roozbeh (2015), Arashi and Valizadeh (2015), Roozbeh (2015), Ghapani et al. (2018), and Wu and Yang (2016). In this article, it can be shown that high-dimensional semiparametric regression models can be analyzed under some levels of sparsity with the aid of ridge regression estimation. The other alternative methods to combat multicollinearity problem can be found in Amini and Roozbeh (2016), Roozbeh and Arashi (2016), Babaie-Kafaki and Roozbeh (2017), Roozbeh (2018), Akdeniz and Roozbeh (2019) and Roozbeh et al. (2020).

The restricted models are widely applicable to the problem of general hypothesis testing, especially the generalized likelihood ratio (GLR) tests in regression models. Defined a restricted LASSO estimator and configured three classes of LASSO type estimators to fulfill both variable selection and restricted estimation in regression model. Akdenïz and Tabakan (2009) and Akdeniz et al. (2015) developed the restricted ridge and Liu estimators in semiparametric regression models. The problem of restricted ridge partial residual estimation in a semiparametric regression model with correlated errors is studied by Amini and Roozbeh (2015) who used generalized cross-validation (GCV) criteria for optimal bandwidth and ridge parameter selection in model (1.1) simultaneously.

Besides multicollinearity, outliers (data points that deviate from the major bulk of the data) are another common problem in regression analysis. Robust regression methods are used to overcome the effects of outliers (such as inflated sum of squares, bias or distortion of estimation, distortion of p-values, etc.). In this article, we only consider the least trimmed squares semiparametric regression estimators for semiparametric regression model. It is well-known that the ordinary least-squares estimator is sensitive to outliers. Examples of recent researches in full-parametric regression include the studies made by Nguyen and Welsch (2010), Roozbeh and Babaie-Kafaki (2016), Roozbeh (2016), and Roozbeh and Arashi (2017).

The basic measure of the robustness of an estimator is its breakdown point, that is, the fraction (up to 50%) of outlying data points that can corrupt the estimator arbitrarily. The study of efficient algorithms for robust statistical estimators has been an active area of research in computational geometry. Many researchers cited the work of Rousseeuws on least median of squares (LMS) estimator which is defined to be the hyperplane that minimizes the median squared residual (for example, see Rousseeuw 1984). Although the vast majority of works on robust linear estimation in the field of computational geometry has been devoted to the study of the least

median squares (LMS) estimator, it has been observed by Rousseeuw and Leroy (1987) that LMS is not the estimator of choice from the perspective of statistical properties. They argued that a better choice is the least trimmed squares (LTS). The breakdown point of LTS and LMS are the same. Like the LMS, the LTS estimator is a robust estimator with a 50%-breakdown point which means that the estimator is insensitive to the contamination made by outliers, provided that the outliers constitute less than 50% of the data set. However, the LTS has a number of advantages in contrast to LMS. The LTS objective function is smoother than that of LMS. LTS has better statistical efficiency because it is asymptotically normal (see Rousseeuw 1984) and converges faster than LMS. Rousseeuw and van Driessen (2006) recommended that, for these reasons, LTS is more suitable as a starting point for two-step robust estimators such as the MM-estimator (see Yohai 1987) and generalized M-estimators (see Simpson et al. 1992).

This chapter is organized as follows: Sect. 2 contains the classical estimators of restricted semiparametric regression model based on kernel approach for low-dimensional case $p < n$. The sparse multicollinear semiparametric regression model and its estimation together with asymptotic distributions under some regularity conditions are considered in Sect. 3. In Sect. 4, we propose some improved shrinkage estimators in a sparse multicollinear restricted semiparametric regression model, while their asymptotic biases and risks are derived in Sect. 5. We review the least trimmed squares estimators in restricted semiparametric regression model in Sect. 6 and then, propose a new robust estimator in restricted semiparametric regression model for high-dimensional data set in Sect. 7. Performances of proposed robust shrinkage estimators are evaluated through a real data example in Sect. 8.

2 The Classical Estimators

Consider the following semiparametric regression model

$$\boldsymbol{y} = \boldsymbol{X}\boldsymbol{\beta} + \boldsymbol{f}(t) + \boldsymbol{\epsilon}, \tag{2.1}$$

where $\boldsymbol{y} = (y_1, \ldots, y_n)^\top$, $\boldsymbol{X} = (\boldsymbol{x}_1, \ldots, \boldsymbol{x}_n)^\top$ is an $n \times p$ matrix, $\boldsymbol{f}(t) = (f(t_1), \ldots, f(t_n))^\top$ and $\boldsymbol{\epsilon} = (\epsilon_1, \ldots, \epsilon_n)^\top$.

We assume that in general, $\boldsymbol{\epsilon}$ is a vector of disturbances, with a multivariate normal distribution, $N_n(\boldsymbol{0}, \sigma^2 \boldsymbol{V})$, where $\boldsymbol{V}$ is a symmetric, positive definite known matrix and σ^2 is an unknown parameter.

To estimate the parameters of model (2.1), we begin with the removal of the the non-parametric effect. Assuming $\boldsymbol{\beta}$ to be known, a natural nonparametric estimator of $f(.)$ is $\hat{f}(t) = \boldsymbol{k}(t)(\boldsymbol{y} - \boldsymbol{X}\boldsymbol{\beta})$, with $\boldsymbol{k}(t) = (K_{\omega_n}(t, t_1), \ldots, K_{\omega_n}(t, t_n))$, where $K_{\omega_n}(.)$ is a kernel function of order m with bandwidth parameter ω_n. For the existence of $\hat{f}(t, \boldsymbol{\beta})$ at the optimal convergence rate $n^{-4/5}$, in semiparametric regression models with probability one, we need some conditions on kernel function. See

Müller (2000) for more details. Replacing $f(t)$ by $\hat{f}(t)$ in (2.1), the model can be written as

$$\widetilde{\boldsymbol{y}} = \widetilde{\boldsymbol{X}}\boldsymbol{\beta} + \boldsymbol{\epsilon}, \tag{2.2}$$

where $\widetilde{\boldsymbol{y}} = \big(\boldsymbol{I}_n - \boldsymbol{K}\big)\boldsymbol{y}$, $\widetilde{\boldsymbol{X}} = \big(\boldsymbol{I}_n - \boldsymbol{K}\big)\boldsymbol{X}$ and $\boldsymbol{K}$ is the smoother matrix with i, jth component $K_{\omega_n}(t_i, t_j)$.

We can estimate the linear parameter $\boldsymbol{\beta}$ in (2.1) under the assumption $\mathrm{cov}(\boldsymbol{\epsilon}) = \sigma^2\boldsymbol{V}$, by minimizing the generalized sum of squared errors

$$SS(\omega_n, \boldsymbol{\beta}) = (\widetilde{\boldsymbol{y}} - \widetilde{\boldsymbol{X}}\boldsymbol{\beta})^\top \boldsymbol{V}^{-1}(\widetilde{\boldsymbol{y}} - \widetilde{\boldsymbol{X}}\boldsymbol{\beta}). \tag{2.3}$$

The unique minimizer of (2.3) is the partially generalized least squares estimator (PGLSE) given by

$$\hat{\boldsymbol{\beta}}_{PG}(\omega_n) = \mathrm{argmin}_{\boldsymbol{\beta}}\ SS(\omega_n, \boldsymbol{\beta}) = \boldsymbol{C}^{-1}(\omega_n)\widetilde{\boldsymbol{X}}^\top \boldsymbol{V}^{-1}\widetilde{\boldsymbol{y}}^{-1}, \quad \boldsymbol{C}(\omega_n) = \widetilde{\boldsymbol{X}}^\top \boldsymbol{V}^{-1}\widetilde{\boldsymbol{X}}. \tag{2.4}$$

Motivated by Fallahpour et al. (2012), we partition the regression parameter $\boldsymbol{\beta}$ as $\boldsymbol{\beta} = (\boldsymbol{\beta}_1^\top, \boldsymbol{\beta}_2^\top)^\top$, where the subvector $\boldsymbol{\beta}_i$ has dimension p_i, $i = 1, 2$ and $p_1 + p_2 = p$. Thus the underlying model has form

$$\widetilde{\boldsymbol{y}} = \widetilde{\boldsymbol{X}}_1\boldsymbol{\beta}_1 + \widetilde{\boldsymbol{X}}_2\boldsymbol{\beta}_2 + \boldsymbol{\epsilon}, \tag{2.5}$$

where $\widetilde{\boldsymbol{X}}$ is partitioned according to $(\widetilde{\boldsymbol{X}}_1, \widetilde{\boldsymbol{X}}_2)$ in such a way that $\widetilde{\boldsymbol{X}}_i$ is a $n \times p_i$ submatrix, $i = 1, 2$. With respect to this partitioning, the PGLSEs of $\boldsymbol{\beta}_1$ and $\boldsymbol{\beta}_2$ are respectively given by

$$\begin{aligned}
\hat{\boldsymbol{\beta}}_{PG1}(\omega_n) &= \boldsymbol{S}_1^{-1}(\omega_n)\widetilde{\boldsymbol{X}}_1^\top \boldsymbol{\Sigma}_2^{-1}(\omega_n)\widetilde{\boldsymbol{y}}, \quad \boldsymbol{S}_1(\omega_n) = \widetilde{\boldsymbol{X}}_1^\top \boldsymbol{\Sigma}_2^{-1}(\omega_n)\widetilde{\boldsymbol{X}}_1 \\
\hat{\boldsymbol{\beta}}_{PG2}(\omega_n) &= \boldsymbol{S}_2^{-1}(\omega_n)\widetilde{\boldsymbol{X}}_2^\top \boldsymbol{\Sigma}_1^{-1}(\omega_n)\widetilde{\boldsymbol{y}}, \quad \boldsymbol{S}_2(\omega_n) = \widetilde{\boldsymbol{X}}_2^\top \boldsymbol{\Sigma}_1^{-1}(\omega_n)\widetilde{\boldsymbol{X}}_2
\end{aligned} \tag{2.6}$$

where

$$\boldsymbol{\Sigma}_i^{-1}(\omega_n) = \boldsymbol{V}^{-1} - \boldsymbol{V}^{-1}\widetilde{\boldsymbol{X}}_i(\widetilde{\boldsymbol{X}}_i^\top \boldsymbol{V}^{-1}\widetilde{\boldsymbol{X}}_i)^{-1}\widetilde{\boldsymbol{X}}_i^\top \boldsymbol{V}^{-1}, \quad i = 1, 2. \tag{2.7}$$

The sparse model is defined when $\mathcal{H}_o : \boldsymbol{\beta}_2 = 0$ is true. In this paper, we refer the restricted semiparametric regression model (RSRM) to the sparse model.

For the RSRM, the partially generalized restricted least squares estimator (PGRLSE) takes the form of

$$\hat{\boldsymbol{\beta}}_{PGR1}(\omega_n) = \boldsymbol{C}_1^{-1}(\omega_n)\widetilde{\boldsymbol{X}}_1^\top \boldsymbol{V}^{-1}\widetilde{\boldsymbol{y}}, \quad \boldsymbol{C}_1(\omega_n) = \widetilde{\boldsymbol{X}}_1^\top \boldsymbol{V}^{-1}\widetilde{\boldsymbol{X}}_1. \tag{2.8}$$

According to Saleh (2006), the PGRLSE performs better than PGLSE when model is sparse. However, the former estimator performs poorly as $\boldsymbol{\beta}_2$ deviates from the origin. The following result provides the relation between the submodel and fullmodel estimators of $\boldsymbol{\beta}_1$.

Proposition 2.1 *Under the assumptions in Eqs.* (2.6) *and* (7.2)*, we have*

$$\hat{\boldsymbol{\beta}}_{PG1}(\omega_n) = \hat{\boldsymbol{\beta}}_{PGR1}(\omega_n) - \boldsymbol{C}_1^{-1}(\omega_n)\widetilde{\boldsymbol{X}}_1^{\top}\boldsymbol{V}^{-1}\widetilde{\boldsymbol{X}}_2\hat{\boldsymbol{\beta}}_{PG2}(\omega_n).$$

3 Sparse Semiparametric Regression Model

Under situations in which the matrix $\boldsymbol{C}(\omega_n)$ is ill-conditioned due to linear relationship among the covariates of $\widetilde{\boldsymbol{X}}$ matrix (as in multicollinearity) or the number of independent variables (p) is larger than the sample size (n), the proposed estimators in the previous section are not applicable, because, we always find a linear combination of the columns in $\widetilde{\boldsymbol{X}}$ which is exactly equal to one other column. Mathematically, the design matrix is not full rank, $rank(\widetilde{\boldsymbol{X}}) \leq \min(n, p) < p$ for $p > n$, and one may write $\widetilde{\boldsymbol{X}}\boldsymbol{\beta} = \widetilde{\boldsymbol{X}}(\boldsymbol{\beta} + \boldsymbol{\zeta})$ for every $\boldsymbol{\zeta}$ in the null space of $\widetilde{\boldsymbol{X}}$. Therefore, without further assumptions, it is impossible to infer or estimate $\boldsymbol{\beta}$ from data. We note that this issue is closely related to the classical setting with $p < n$ but with $rank(\widetilde{\boldsymbol{X}}) < p$ (due to linear dependence among covariables) or ill-conditioned design leading to difficulties with respect to identifiability. We note, however, that for prediction or estimation of $\widetilde{\boldsymbol{X}}\boldsymbol{\beta}$ (that is the underlying semiparametric regression surface), identifiability of the parameters is not necessarily needed. From a practical point of view, high empirical correlations among two or a few other covariables lead to unstable results for estimating $\boldsymbol{\beta}$ or for pursuing variable selection. To overcome this problem, we follow Roozbeh (2015) and obtain the restricted ridge estimator by minimizing the sum of squared partial residuals with a spherical restriction and a linear restriction $\boldsymbol{\beta}_2 = 0$, i.e., the RSRM is transformed into an optimal problem with two restrictions:

$$\min_{\boldsymbol{\beta}} \ (\widetilde{\boldsymbol{y}} - \widetilde{\boldsymbol{X}}\boldsymbol{\beta})^{\top}\boldsymbol{V}^{-1}(\widetilde{\boldsymbol{y}} - \widetilde{\boldsymbol{X}}\boldsymbol{\beta}) \quad \text{subject to} \quad \boldsymbol{\beta}^{\top}\boldsymbol{\beta} \leq \phi^2 \ \text{ and } \ \boldsymbol{\beta}_2 = \boldsymbol{0}.$$

The resulting estimator is partially generalized restricted ridge estimator (PGRRE), given by

$$\begin{aligned}
\hat{\boldsymbol{\beta}}_{PGR1}(\omega_n, k_n) &= \boldsymbol{C}_1^{-1}(\omega_n, k_n)\widetilde{\boldsymbol{X}}_1^{\top}\boldsymbol{V}^{-1}\widetilde{\boldsymbol{y}} \\
&= \left(\boldsymbol{I}_{p_1} + k_n(\widetilde{\boldsymbol{X}}_1^{\top}\boldsymbol{V}^{-1}\widetilde{\boldsymbol{X}}_1)^{-1}\right)^{-1}\hat{\boldsymbol{\beta}}_{PGR1}(\omega_n) \\
&= \boldsymbol{T}_1(\omega_n, k_n)\hat{\boldsymbol{\beta}}_{PGR1}(\omega_n), \\
&\qquad \boldsymbol{T}_1(\omega_n, k_n) = \left(\boldsymbol{I}_{p_1} + k_n(\widetilde{\boldsymbol{X}}_1^{\top}\boldsymbol{V}^{-1}\widetilde{\boldsymbol{X}}_1)^{-1}\right)^{-1}, \qquad (3.1)
\end{aligned}$$

where $k_n \geq 0$ is the ridge parameter as a function of sample size n and $\boldsymbol{C}_1(\omega_n, k_n) = \widetilde{\boldsymbol{X}}_1^{\top}\boldsymbol{V}^{-1}\widetilde{\boldsymbol{X}}_1 + k_n\boldsymbol{I}_{p_1}$.

In a similar manner shown previously, the partially generalized unrestricted ridge estimators (PGUREs) of $\boldsymbol{\beta}_1$ and $\boldsymbol{\beta}_2$ respectively have forms

$$\begin{aligned}\hat{\boldsymbol{\beta}}_{PG1}(\omega_n, k_n) &= \boldsymbol{S}_1^{-1}(\omega_n, k_n)\widetilde{\boldsymbol{X}}_1^{\top}\boldsymbol{\Sigma}_2^{-1}(\omega_n, k_n)\widetilde{\boldsymbol{y}} \\ &= \left(\boldsymbol{I}_{p_1} + k_n(\widetilde{\boldsymbol{X}}_1^{\top}\boldsymbol{\Sigma}_2^{-1}(\omega_n, k_n)\widetilde{\boldsymbol{X}}_1)^{-1}\right)^{-1}\hat{\boldsymbol{\beta}}_{PG1}(\omega_n) \\ &= \boldsymbol{R}_1(\omega_n, k_n)\hat{\boldsymbol{\beta}}_{PG1}(\omega_n), \\ \boldsymbol{R}_1(\omega_n, k_n) &= \left(\boldsymbol{I}_{p_1} + k_n(\widetilde{\boldsymbol{X}}_1^{\top}\boldsymbol{\Sigma}_2^{-1}(\omega_n, k_n)\widetilde{\boldsymbol{X}}_1)^{-1}\right)^{-1}, \end{aligned} \tag{3.2}$$

$$\begin{aligned}\hat{\boldsymbol{\beta}}_{PG2}(\omega_n,k_n) &= \boldsymbol{S}_2^{-1}(\omega_n, k_n)\widetilde{\boldsymbol{X}}_2^{\top}\boldsymbol{\Sigma}_1^{-1}(\omega_n, k_n)\widetilde{\boldsymbol{y}} \\ &= \left(\boldsymbol{I}_{p_2} + k_n(\widetilde{\boldsymbol{X}}_2^{\top}\boldsymbol{\Sigma}_1^{-1}(\omega_n, k_n)\widetilde{\boldsymbol{X}}_2)^{-1}\right)^{-1}\hat{\boldsymbol{\beta}}_{PG2}(\omega_n) \\ &= \boldsymbol{R}_2(\omega_n, k_n)\hat{\boldsymbol{\beta}}_{PG2}(\omega_n), \\ \boldsymbol{R}_2(\omega_n, k_n) &= \left(\boldsymbol{I}_{p_2} + k_n(\widetilde{\boldsymbol{X}}_2^{\top}\boldsymbol{\Sigma}_1^{-1}(\omega_n, k_n)\widetilde{\boldsymbol{X}}_2)^{-1}\right)^{-1}, \end{aligned} \tag{3.3}$$

where $\boldsymbol{S}_1(\omega_n, k_n) = \widetilde{\boldsymbol{X}}_1^{\top}\boldsymbol{\Sigma}_2^{-1}(\omega_n, k_n)\widetilde{\boldsymbol{X}}_1 + k_n\boldsymbol{I}_{p_1}$, $\boldsymbol{S}_2(\omega_n, k_n) = \widetilde{\boldsymbol{X}}_2^{\top}\boldsymbol{\Sigma}_1^{-1}(\omega_n, k_n)\widetilde{\boldsymbol{X}}_2 + k_n\boldsymbol{I}_{p_2}$ and

$$\boldsymbol{\Sigma}_i^{-1}(\omega_n, k_n) = \boldsymbol{V}^{-1} - \boldsymbol{V}^{-1}\widetilde{\boldsymbol{X}}_i(\widetilde{\boldsymbol{X}}_i^{\top}\boldsymbol{V}^{-1}\widetilde{\boldsymbol{X}}_i + k_n\boldsymbol{I}_{p_i})^{-1}\widetilde{\boldsymbol{X}}_i^{\top}\boldsymbol{V}^{-1}, \quad i = 1, 2. \tag{3.4}$$

Similar to Proposition 2.1, we have the following result without proof.

Proposition 3.1 *The partially generalized restricted and unrestricted ridge estimators of* $\boldsymbol{\beta}_1$ *have the following relation*

$$\hat{\boldsymbol{\beta}}_{PG1}(\omega_n, k_n) = \hat{\boldsymbol{\beta}}_{PGR1}(\omega_n, k_n) - \boldsymbol{C}_1^{-1}(\omega_n, k_n)\widetilde{\boldsymbol{X}}_1^{\top}\boldsymbol{V}^{-1}\widetilde{\boldsymbol{X}}_2\hat{\boldsymbol{\beta}}_{PG2}(\omega_n, k_n).$$

Up to this point, we supposed that the null hypothesis $\mathcal{H}_o : \boldsymbol{\beta}_2 = 0$ is true; however, it must be tested that one can incorporate the PGURE in practice. For this purpose, following Saleh (2006) and Yuzbashi and Ahmed (2015), we use the following test statistic for testing the sparsity hypothesis $\mathcal{H}_o$

$$\pounds_n(\omega_n, k_n) = \frac{\hat{\boldsymbol{\beta}}_{PG2}^{\top}(\omega_n, k_n)\boldsymbol{S}_2(\omega_n, k_n)\hat{\boldsymbol{\beta}}_{PG2}(\omega_n, k_n)}{(n - p_1)s^2(\omega_n, k_n)}, \tag{3.5}$$

where,

$$s^2(\omega_n, k_n) = \frac{1}{n - p_1}\left(\widetilde{\boldsymbol{y}} - \widetilde{\boldsymbol{X}}_1\hat{\boldsymbol{\beta}}_{PG1}(\omega_n, k_n)\right)^{\top}\boldsymbol{V}^{-1}\left(\widetilde{\boldsymbol{y}} - \widetilde{\boldsymbol{X}}_1\hat{\boldsymbol{\beta}}_{PG1}(\omega_n, k_n)\right). \tag{3.6}$$

Later, it will be shown that the test statistic $\pounds_n(\omega_n, k_n)$ has an asymptotic chi-square distribution with p_2 degrees of freedom. To this end, we need to take the following assumptions as regularity conditions:

(A1) $\max_{1\leq i\leq n} \widetilde{\boldsymbol{x}}_i^\top \left(\widetilde{\boldsymbol{X}}^\top \boldsymbol{V}^{-1}\widetilde{\boldsymbol{X}} + k_n \boldsymbol{I}_p\right)^{-1} \widetilde{\boldsymbol{x}}_i = o(n)$, where $\widetilde{\boldsymbol{x}}_i^\top$ is the ith row of $\widetilde{\boldsymbol{X}}$.

(A2) $\frac{k_n}{n} \to k_o$ as $n \to \infty$,

(A3) Let

$$\begin{aligned}\boldsymbol{A}_n &= \widetilde{\boldsymbol{X}}^\top \boldsymbol{V}^{-1}\widetilde{\boldsymbol{X}} + k_n \boldsymbol{I}_p \\ &= \begin{pmatrix} \widetilde{\boldsymbol{X}}_1^\top \\ \widetilde{\boldsymbol{X}}_2^\top \end{pmatrix} \boldsymbol{V}^{-1}(\widetilde{\boldsymbol{X}}_1\ \widetilde{\boldsymbol{X}}_2) + k_n \boldsymbol{I}_p \\ &= \begin{pmatrix} \widetilde{\boldsymbol{X}}_1^\top \boldsymbol{V}^{-1}\widetilde{\boldsymbol{X}}_1 & \widetilde{\boldsymbol{X}}_1^\top \boldsymbol{V}^{-1}\widetilde{\boldsymbol{X}}_2 \\ \widetilde{\boldsymbol{X}}_2^\top \boldsymbol{V}^{-1}\widetilde{\boldsymbol{X}}_1 & \widetilde{\boldsymbol{X}}_2^\top \boldsymbol{V}^{-1}\widetilde{\boldsymbol{X}}_2 \end{pmatrix} + k_n \begin{pmatrix} \boldsymbol{I}_{p_1} & \boldsymbol{0}_{p_1\times p_2} \\ \boldsymbol{0}_{p_2\times p_1} & \boldsymbol{I}_{p_2} \end{pmatrix} \\ &= \begin{pmatrix} \boldsymbol{A}_{n11} & \boldsymbol{A}_{n12} \\ \boldsymbol{A}_{n21} & \boldsymbol{A}_{n22} \end{pmatrix}.\end{aligned}$$

Then, there exists a positive definite matrix $\boldsymbol{A}$ such that

$$\frac{1}{n}\boldsymbol{A}_n \to \boldsymbol{A} = \begin{pmatrix} \boldsymbol{A}_{11} & \boldsymbol{A}_{12} \\ \boldsymbol{A}_{21} & \boldsymbol{A}_{22} \end{pmatrix}, \quad \text{as} \quad n \to \infty.$$

(A4) $\widetilde{\boldsymbol{X}}_2^\top \boldsymbol{V}^{-1}\widetilde{\boldsymbol{X}}_2 + k_n \boldsymbol{I}_{p_2} = o(\sqrt{n})$.

(A5) $\widetilde{\boldsymbol{x}}_i^\top \widetilde{\boldsymbol{x}}_j = o(\sqrt{n}), i, j = 1, \ldots, n$.

Note that by (A2), (A4) and (A5), one can directly conclude that $\boldsymbol{\Sigma}_2^{-1}(\omega_n, k_n) \to \boldsymbol{V}^{-1}$ as $n \to \infty$.

The following result is a direct conclusion of Theorem 2 of Knight and Fu (2000).

Proposition 3.2 *Let* $\hat{\boldsymbol{\beta}}_{PG}(\omega_n, k_n) = (\widetilde{\boldsymbol{X}}^\top \boldsymbol{V}^{-1}\widetilde{\boldsymbol{X}} + k_n \boldsymbol{I}_p)^{-1}\widetilde{\boldsymbol{X}}^\top \boldsymbol{V}^{-1}\widetilde{\boldsymbol{y}}$. *Then, under the regularity conditions (A1)–(A3),* $\sqrt{n}\left(\hat{\boldsymbol{\beta}}_{PG}(\omega_n, k_n) - \boldsymbol{\beta}\right) \xrightarrow{\mathcal{D}} N_p\left(-k_o \boldsymbol{A}^{-1}\boldsymbol{\beta}, \sigma^2 \boldsymbol{A}^{-1}\right)$.

According to Saleh (2006), the test statistic diverges as $n \to \infty$, under any fixed alternatives $A_{\boldsymbol{\xi}} : \boldsymbol{\beta}_2 = \boldsymbol{\xi}$. To overcome this difficulty, we consider the local alternatives

$$K_{(n)} : \boldsymbol{\beta}_2 = \boldsymbol{\beta}_{2(n)} = n^{-\frac{1}{2}}\boldsymbol{\xi}, \tag{3.7}$$

where $\boldsymbol{\xi} = (\xi_1, \ldots, \xi_{p_2})^T \in \mathbb{R}^{p_2}$ is a fixed vector.

For notational convenience, let

$$\begin{aligned} -k_o \boldsymbol{A}^{-1}\boldsymbol{\beta} = \boldsymbol{\mu} &= (\boldsymbol{\mu}_1^\top, \boldsymbol{\mu}_2^\top)^\top, \\ \boldsymbol{\delta} &= \boldsymbol{A}_{11}^{-1}\boldsymbol{A}_{12}\boldsymbol{\xi}, \\ \boldsymbol{\mu}_{11.2} &= \boldsymbol{\mu}_1 - \boldsymbol{A}_{12}\boldsymbol{A}_{22}^{-1}\left((\boldsymbol{\beta}_2 - \boldsymbol{\xi}) - \boldsymbol{\mu}_2\right), \\ \boldsymbol{\gamma} &= \boldsymbol{\mu}_{11.2} + \boldsymbol{\delta}, \\ \boldsymbol{A}_{22.1} &= \boldsymbol{A}_{22} - \boldsymbol{A}_{21}\boldsymbol{A}_{11}^{-1}\boldsymbol{A}_{12}, \\ \boldsymbol{B} &= \boldsymbol{A}_{21}\boldsymbol{A}_{11}^{-2}\boldsymbol{A}_{12}\boldsymbol{A}_{22.1}^{-1}. \end{aligned} \tag{3.8}$$

In the following, similar to approaches by Saleh (2006) and Yuzbashi and Ahmed (2015), some asymptotic distributional results involving the proposed estimators are given.

Lemma 3.1 *Under the regularity conditions (A1)–(A3) and local alternatives* $\{K_{(n)}\}$

(i) $\boldsymbol{V}_{(n)}^{(1)} = \sqrt{n}\left(\hat{\boldsymbol{\beta}}_{PG1}(\omega_n, k_n) - \boldsymbol{\beta}_1\right) \xrightarrow{\mathcal{D}} N_{p_1}(-\boldsymbol{\mu}_{11.2}, \sigma^2\boldsymbol{A}_{11.2}^{-1})$

(ii) $\boldsymbol{V}_{(n)}^{(2)} = \sqrt{n}\left(\hat{\boldsymbol{\beta}}_{PGR1}(\omega_n, k_n) - \boldsymbol{\beta}_1\right) \xrightarrow{\mathcal{D}} N_{p_1}(-\boldsymbol{\gamma}, \sigma^2\boldsymbol{A}_{11}^{-1})$

(iii) $\boldsymbol{V}_{(n)}^{(3)} = \sqrt{n}\left(\hat{\boldsymbol{\beta}}_{PGR1}(\omega_n, k_n) - \hat{\boldsymbol{\beta}}_{PG1}(\omega_n, k_n)\right) \xrightarrow{\mathcal{D}} N_{p_1}(-\boldsymbol{\gamma}+\boldsymbol{\mu}_{11.2}, \sigma^2(\boldsymbol{A}_{11}^{-1} - \boldsymbol{A}_{11.2}^{-1}))$

where $\boldsymbol{A}_{11.2} = \boldsymbol{A}_{11} - \boldsymbol{A}_{12}\boldsymbol{A}_{22}^{-1}\boldsymbol{A}_{21}$.

The following result is a direct conclusion of Proposition 3.2 and Lemma 3.1.

Theorem 3.1 *Under the regularity conditions (A1)–(A3) and local alternatives* $\{K_{(n)}\}$, $\pounds_n$ *is asymptotically distributed according to a non-central chi-square distribution with* p_2 *degrees of freedom and non-centrality parameter* $\frac{1}{2}\Delta^*$, *where*

$$\Delta^* = \frac{1}{\sigma^2}\boldsymbol{\xi}^\top \boldsymbol{A}_{22.1}\boldsymbol{\xi}, \quad \boldsymbol{A}_{22.1} = \boldsymbol{A}_{22} - \boldsymbol{A}_{21}\boldsymbol{A}_{11}^{-1}\boldsymbol{A}_{12}.$$

4 Shrinkage Estimation Methodologies

In many practical situations, along with the model one may suspect that $\boldsymbol{\beta}$ belongs to the sub-space defined by $\boldsymbol{\beta}_2 = \boldsymbol{0}$. In such situation one combines the estimate of $\boldsymbol{\beta}$ and the test-statistic to obtain improved estimators of $\boldsymbol{\beta}$. First, we consider the preliminary test partially generalized restricted ridge estimator (PTPGRRE) defined by

$$\begin{aligned}\hat{\boldsymbol{\beta}}^{PT}_{PGR1}(\omega_n, k_n) &= \hat{\boldsymbol{\beta}}_{PGR1}(\omega_n, k_n) + \left[1 - I(\pounds_n(\omega_n, k_n) \leq \chi^2_{p_2}(\alpha))\right] \\ &\qquad \left(\hat{\boldsymbol{\beta}}_{PG1}(\omega_n, k_n) - \hat{\boldsymbol{\beta}}_{PGR1}(\omega_n, k_n)\right) \\ &= \boldsymbol{T}_1(\omega_n, k_n)\hat{\boldsymbol{\beta}}_{GR1}(\omega_n) + \left[1 - I(\pounds_n(\omega_n, k_n) \leq \chi^2_{p_2}(\alpha))\right] \\ &\quad \times\left(\boldsymbol{R}_1(\omega_n, k_n)\hat{\boldsymbol{\beta}}_{PG1}(\omega_n) - \boldsymbol{T}_1(\omega_n, k_n)\hat{\boldsymbol{\beta}}_{PGR1}(\omega_n)\right) \qquad (4.1)\end{aligned}$$

where $\chi^2_{p_2}(\alpha)$ is the upper α-level critical value ($0 < \alpha < 1$) from the central chi-square distribution and $I(A)$ is the indicator function of the set A.

The PTPGRRE has the disadvantage that it depends on α, the level of significance, and also it yields the extreme results, namely $\hat{\boldsymbol{\beta}}_{GR1}(k)$ and $\hat{\boldsymbol{\beta}}_{G1}(k)$ depending on the outcome of the test. Later, we will discuss in detail of the Stein-type partially generalized restricted ridge estimator (SPGRRE) defined by

$$\begin{aligned}\hat{\boldsymbol{\beta}}^{S}_{PGR1}(\omega_n, k_n) &= \hat{\boldsymbol{\beta}}_{PGR1}(\omega_n, k_n) + (1 - d\pounds_n^{-1}(\omega_n, k_n)) \\ &\qquad \left(\hat{\boldsymbol{\beta}}_{PG1}(\omega_n, k_n) - \hat{\boldsymbol{\beta}}_{PGR1}(\omega_n, k_n)\right) \\ &= \boldsymbol{T}_1(\omega_n, k_n)\hat{\boldsymbol{\beta}}_{PGR1}(\omega_n) + (1 - d\pounds_n^{-1}(\omega_n, k_n)) \\ &\quad \times\left(\boldsymbol{R}_1(\omega_n, k_n)\hat{\boldsymbol{\beta}}_{PG1}(\omega_n) - \boldsymbol{T}_1(\omega_n, k_n)\hat{\boldsymbol{\beta}}_{PGR1}(\omega_n)\right) \qquad (4.2)\end{aligned}$$

where $d = p_2 - 2 > 0$. The SPGRRE has the disadvantage that it has strange behavior for small values of $\pounds_n$. Also, the shrinkage factor $(1 - d\pounds_n^{-1})$ becomes negative for $\pounds_n < d$. Hence, we consider the positive-rule Stein-type partially generalized restricted ridge estimator (PRSPGRRE) defined by

$$\begin{aligned}\hat{\boldsymbol{\beta}}^{S+}_{PGR1}(\omega_n, k_n) &= \hat{\boldsymbol{\beta}}^{S}_{PGR1}(\omega_n, k_n) - (1 - d\pounds_n^{-1}(\omega_n, k_n))I(\pounds_n(\omega_n, k_n) \leq d) \\ &\quad \times\left(\hat{\boldsymbol{\beta}}_{PG1}(\omega_n, k_n) - \hat{\boldsymbol{\beta}}_{PGR1}(\omega_n, k_n)\right). \qquad (4.3)\end{aligned}$$

Shrinkage estimators has been considered by Arashi and Tabatabaey (2009), Arashi et al. (2010), Arashi (2012), Arashi et al. (2012), Arashi et al. (2014) and extended to semiparametric partially linear regression models by Arashi and Roozbeh (2019).

5 Asymptotic Properties of Shrinkage Estimators

In this section, we provide the expressions for the asymptotic distributional bias (ADB) and quadratic risk (ADQR) of the estimators. Suppose for any estimator $\boldsymbol{\beta}^*$ of $\boldsymbol{\beta}$, the asymptotic cumulative distribution function (c.d.f) under $K_{(n)}$, exists and has form

$$G_p(x) = \lim_{n\to\infty} P_{K_{(n)}}\left(\sqrt{n}(\boldsymbol{\beta}^* - \boldsymbol{\beta}) \le \boldsymbol{x}\right).$$

Then, the ADB of $\boldsymbol{\beta}^*$ is evaluated by

$$ADB(\boldsymbol{\beta}^*) = \lim_{n\to\infty} E\left(\sqrt{n}(\boldsymbol{\beta}^* - \boldsymbol{\beta})\right) = \int \boldsymbol{x} dG_p(\boldsymbol{x}),$$

Let

$$M(\boldsymbol{\beta}^*) = \int \boldsymbol{x}\boldsymbol{x}^T dG_p(\boldsymbol{x}) = \lim_{n\to\infty} E\left(n(\boldsymbol{\beta}^* - \boldsymbol{\beta})(\boldsymbol{\beta}^* - \boldsymbol{\beta})^\top\right).$$

Then, the ADQR of $\boldsymbol{\beta}^*$ is defined as

$$ADQR(\boldsymbol{\beta}^*) = \mathrm{tr}\left(M(\boldsymbol{\beta}^*)\right) = \lim_{n\to\infty} E\left(n(\boldsymbol{\beta}^* - \boldsymbol{\beta})^\top(\boldsymbol{\beta}^* - \boldsymbol{\beta})\right).$$

The proofs of the following theorems can be derived parallel to that of Roozbeh (2015) with utilities in Saleh (2006) and the fact that $\boldsymbol{R}_1(\omega_n, k_n) \to \boldsymbol{T}_1(\omega_n, k_n)$ as $n \to \infty$.

Theorem 5.1 *Under the foregoing regularity conditions and local alternatives* $\{K_{(n)}\}$*, the ADB of the estimators are given by*

$$\begin{aligned}
ADB\left(\hat{\boldsymbol{\beta}}_{PG1}(\omega_n, k_n)\right) &= -\boldsymbol{\mu}_{11.2}\\
ADB\left(\hat{\boldsymbol{\beta}}_{PGR1}(\omega_n, k_n)\right) &= ADB\left(\hat{\boldsymbol{\beta}}_{PG1}(\omega_n, k_n)\right) - \boldsymbol{T}_1(\omega_n, k_n)\boldsymbol{\delta}\\
ADB\left(\hat{\boldsymbol{\beta}}^{PT}_{PGR1}(\omega_n, k_n)\right) &= ADB\left(\hat{\boldsymbol{\beta}}_{PG1}(\omega_n, k_n)\right) - \boldsymbol{T}_1(\omega_n, k_n)\boldsymbol{\delta} H_{p_2+2}(d, \Delta^*)\\
ADB\left(\hat{\boldsymbol{\beta}}^{S}_{PGR1}(\omega_n, k_n)\right) &= ADB\left(\hat{\boldsymbol{\beta}}_{PG1}(\omega_n, k_n)\right) - d\boldsymbol{T}_1(\omega_n, k_n)\boldsymbol{\delta} E\left(\chi^{-2}_{p_2+2}(\Delta^*)\right)\\
ADB\left(\hat{\boldsymbol{\beta}}^{S+}_{PGR1}(\omega_n, k_n)\right) &= ADB\left(\hat{\boldsymbol{\beta}}^{S}_{PGR1}(\omega_n, k_n)\right) - \boldsymbol{T}_1(\omega_n, k_n)\boldsymbol{\delta}\\
&\quad \times\Big[H_{p_2+2}(d, \Delta^*) - dE\left(\chi^{-2}_{p_2+2}(\Delta^*) I\left(\chi^2_{p_2+2}(\Delta^*) \le d\right)\right)\Big],
\end{aligned}$$

where $H_\nu(\cdot; \Delta^2)$ *denotes the c.d.f. of the* χ^2*-distribution with* ν *degree of freedom (d.f.) and non centrality parameter* $\Delta^2/2$*.*

Theorem 5.2 *Under the foregoing regularity conditions and local alternatives* $\{K_{(n)}\}$*, the ADQR of the estimators are given by*

$$\begin{aligned}
ADQR\left(\hat{\boldsymbol{\beta}}_{PG1}(\omega_n, k_n)\right) &= \sigma^2\,\mathrm{tr}\left(\boldsymbol{T}_1(\omega_n, k_n)\boldsymbol{A}^{-1}_{11.2}\boldsymbol{T}_1(\omega_n, k_n)\right) + \boldsymbol{\mu}^\top_{11.2}\boldsymbol{\mu}_{11.2}\\
ADQR\left(\hat{\boldsymbol{\beta}}_{PGR1}(\omega_n, k_n)\right) &= ADQR\left(\hat{\boldsymbol{\beta}}_{PG1}(\omega_n, k_n)\right) + \boldsymbol{\delta}^\top\boldsymbol{T}^2_1(\omega_n, k_n)\boldsymbol{\delta}\\
&\quad + 2\boldsymbol{\delta}^\top\boldsymbol{T}_1(\omega_n, k_n)\boldsymbol{\mu}_{11.2} - \sigma^2\,\mathrm{tr}\left(\boldsymbol{T}_1(\omega_n, k_n)\boldsymbol{B}\boldsymbol{T}_1(\omega_n, k_n)\right)
\end{aligned}$$

$$
\begin{aligned}
ADQR\Big(\hat{\boldsymbol{\beta}}^{PT}_{PGR1}(\omega_n, k_n)\Big) &= ADQR\big(\hat{\boldsymbol{\beta}}_{PG1}(\omega_n, k_n)\big) + \boldsymbol{\delta}^{\top}\boldsymbol{T}_1^2(\omega_n, k_n) \\
&\quad \boldsymbol{\delta}\big(2H_{p_2+2}(d, \Delta^*) - H_{p_2+4}(d, \Delta^*)\big) \\
&\quad +2\boldsymbol{\delta}^{\top}\boldsymbol{T}_1(\omega_n, k_n)\boldsymbol{\mu}_{11.2}H_{p_2+2}(d, \Delta^*) \\
&\quad -\sigma^2 \operatorname{tr}\big(\boldsymbol{T}_1(\omega_n, k_n)\boldsymbol{B}\boldsymbol{T}_1(\omega_n, k_n)\big)H_{p_2+2}(d, \Delta^*) \\
ADQR\Big(\hat{\boldsymbol{\beta}}^{S}_{PGR1}(\omega_n, k_n)\Big) &= ADQR\big(\hat{\boldsymbol{\beta}}_{PG1}(\omega_n, k_n)\big) + 2\boldsymbol{\delta}^{\top}\boldsymbol{T}_1(\omega_n, k_n)\boldsymbol{\mu}_{11.2} \\
&\quad E\big(\chi^{-2}_{q+2}(\Delta^*)\big) \\
&\quad -d\sigma^2 \operatorname{tr}\big(\boldsymbol{T}_1(\omega_n, k_n)\boldsymbol{B}\boldsymbol{T}_1(\omega_n, k_n)\big)\Bigg\{E\big(\chi^{-4}_{q+2}(\Delta^*)\big) \\
&\quad +\left[1 - \frac{\boldsymbol{\delta}^{\top}\boldsymbol{T}_1^2(\omega_n, k_n)\boldsymbol{\delta}}{2\sigma^2\Delta^* \operatorname{tr}(\boldsymbol{T}_1(\omega_n, k_n)\boldsymbol{B}\boldsymbol{T}_1(\omega_n, k_n))}\right] \\
&\quad (2\Delta^*)E\big(\chi^{-4}_{q+4}(\Delta^*)\big)\Bigg\},
\end{aligned}
$$

$$
\begin{aligned}
&ADQR\Big(\hat{\boldsymbol{\beta}}^{S+}_{PGR1}(\omega_n, k_n)\Big) \\
&\quad = ADQR\Big(\hat{\boldsymbol{\beta}}^{S}_{PGR1}(k_n)\Big) - \sigma^2 \operatorname{tr}(\boldsymbol{T}_1(\omega_n, k_n)\boldsymbol{B}\boldsymbol{T}_1(\omega_n, k_n)) \\
&\quad \times E\left[\left(1 - d\chi^{-2}_{p_2+2}(\Delta^*)\right)^2 I\left(\chi^2_{p_2+2}(\Delta^*) \le d\right)\right] \\
&\quad +\boldsymbol{\delta}^{\top}\boldsymbol{T}_1^2(\omega_n, k_n)\boldsymbol{\delta}E\left[\left(1 - d\chi^{-2}_{p_2+4}(\Delta^*)\right)^2 I\left(\chi^2_{p_2+4}(\Delta^*) \le d\right)\right] \\
&\quad -2\boldsymbol{\delta}^{\top}\boldsymbol{T}_1^2(\omega_n, k_n)\boldsymbol{\delta}E\left[\left(d\chi^{-2}_{p_2+2}(\Delta^*) - 1\right)I\left(\chi^2_{p_2+2}(\Delta^*) \le d\right)\right] \\
&\quad -2\boldsymbol{\delta}^{\top}\boldsymbol{T}_1(\omega_n, k_n)\boldsymbol{\mu}_{11.2}E\left[\left(\chi^{-2}_{p_2+2}(\Delta^*) - 1\right)I\left(\chi^2_{p_2+2}(\Delta^*) \le d\right)\right].
\end{aligned}
$$

6 Robust Approach

We have mentioned that outliers can strongly corrupt the least-squares fit due to their dominant effect on the objective function. The LTS approach attempts to solve this problem by minimizing the sum of the smallest h squared residuals rather than the complete sum of squares. Here, h is a threshold such that the ratio $\alpha = (n-h)/n$ represents the percentage of the outlying observations.

Let z_i be the indicator whether observation i is a good observation or not. Consider the LTS problem in RSRM as follows:

$$\begin{aligned} \min_{\boldsymbol{\beta},z} \quad & \psi(\boldsymbol{\beta},z) = (\widetilde{\boldsymbol{y}} - \widetilde{\boldsymbol{X}}\boldsymbol{\beta})^{\top}\boldsymbol{V}^{-1/2}\boldsymbol{Z}\boldsymbol{V}^{-1/2}(\widetilde{\boldsymbol{y}} - \widetilde{\boldsymbol{X}}\boldsymbol{\beta}) \\ s.t. \quad & \boldsymbol{\beta}_2 = \mathbf{0}, \\ & \boldsymbol{e}^{\top}\boldsymbol{z} = h, \\ & z_i \in \{0,1\},\ i = 1,\ldots,n, \end{aligned} \tag{6.1}$$

where $\boldsymbol{Z}$ is the diagonal matrix with diagonal elements $\boldsymbol{z} = (z_1,\ldots,z_n)^{\top}$ and $\boldsymbol{e} = (1,\ldots,1)^{\top}_{n\times 1}$. The resulting estimator is the robust partially generalized restricted least squares estimator (RPGRLSE), which is given by

$$\hat{\boldsymbol{\beta}}^{LTS}_{PGR1}(\omega_n,z) = C_1(\omega_n,z)^{-1}\widetilde{\boldsymbol{X}}^{\top}\boldsymbol{V}^{-1/2}\boldsymbol{Z}\boldsymbol{V}^{-1/2}\widetilde{\boldsymbol{y}}, \tag{6.2}$$

where $\boldsymbol{C}_1(\omega_n,z) = \widetilde{\boldsymbol{X}}^{\top}\boldsymbol{V}^{-1/2}\boldsymbol{Z}\boldsymbol{V}^{-1/2}\widetilde{\boldsymbol{X}}$. With respect to the partitioning (2.5), the RPGLSEs of $\boldsymbol{\beta}_1$ and $\boldsymbol{\beta}_2$ are respectively given by

$$\begin{aligned} \hat{\boldsymbol{\beta}}^{LTS}_{PG1}(\omega_n,z) &= \boldsymbol{S}_1^{-1}(\omega_n,z)\widetilde{\boldsymbol{X}}_1^{\top}\boldsymbol{\Sigma}_2^{-1}(\omega_n,z)\widetilde{\boldsymbol{y}}, \quad \boldsymbol{S}_1(\omega_n,z) = \widetilde{\boldsymbol{X}}_1^{\top}\boldsymbol{\Sigma}_2^{-1}(\omega_n,z)\widetilde{\boldsymbol{X}}_1 \\ \hat{\boldsymbol{\beta}}^{LTS}_{PG2}(\omega_n) &= \boldsymbol{S}_2^{-1}(\omega_n,z)\widetilde{\boldsymbol{X}}_2^{\top}\boldsymbol{\Sigma}_1^{-1}(\omega_n,z)\widetilde{\boldsymbol{y}}, \quad \boldsymbol{S}_2(\omega_n,z) = \widetilde{\boldsymbol{X}}_2^{\top}\boldsymbol{\Sigma}_1^{-1}(\omega_n,z)\widetilde{\boldsymbol{X}}_2 \end{aligned} \tag{6.3}$$

where

$$\begin{aligned} \boldsymbol{\Sigma}_i^{-1}(\omega_n,z) = {} & \boldsymbol{V}^{-1/2}\boldsymbol{Z}\boldsymbol{V}^{-1/2} \\ & -\boldsymbol{V}^{-1/2}\boldsymbol{Z}\boldsymbol{V}^{-1/2}\widetilde{\boldsymbol{X}}_i(\widetilde{\boldsymbol{X}}_i^{\top}\boldsymbol{V}^{-1/2}\boldsymbol{Z}\boldsymbol{V}^{-1/2}\widetilde{\boldsymbol{X}}_i)^{-1}\widetilde{\boldsymbol{X}}_i^{\top}\boldsymbol{V}^{-1/2}\boldsymbol{Z}\boldsymbol{V}^{-1/2}, \\ & i = 1,2. \end{aligned} \tag{6.4}$$

7 Robust Shrinkage Estimator for High-Dimensional Data with Outliers

As stated earlier, under situations in which the matrix $\boldsymbol{C}(\omega_n,z)$ is ill-conditioned or the number of independent variables (p) is larger than sample size (n), the proposed estimators in previous sections are no longer applicable and it is impossible to infer or estimate $\boldsymbol{\beta}$ from data. In these situations, we will use robust shrinkage estimators based on the LTS approach. Following Arashi and Roozbeh (2019), the optimization problem is:

$$\begin{aligned}
&\min_{\boldsymbol{\beta},z} \ \psi(\boldsymbol{\beta},z)=(\widetilde{\boldsymbol{y}}-\widetilde{\boldsymbol{X}}\boldsymbol{\beta})^{\top}\boldsymbol{V}^{-1/2}\boldsymbol{Z}\boldsymbol{V}^{-1/2}(\widetilde{\boldsymbol{y}}-\widetilde{\boldsymbol{X}}\boldsymbol{\beta})+k(\boldsymbol{\beta}^{\top}\boldsymbol{\beta}-\phi^2)\\
&s.t. \ \ \boldsymbol{\beta}_2=\boldsymbol{0},\\
&\qquad \boldsymbol{e}^{\top}\boldsymbol{z}=h,\\
&\qquad z_i\in\{0,1\},\ i=1,\ldots,n. \qquad (7.1)
\end{aligned}$$

The resulting estimator is a robust partially generalized restricted ridge estimator (RPGRRE), given by

$$\hat{\boldsymbol{\beta}}^{LTS}_{PGR1}(\omega_n,z,k_n)=C(\omega_n,k_n,z)^{-1}\widetilde{\boldsymbol{X}}^{\top}\boldsymbol{V}^{-1/2}\boldsymbol{Z}\boldsymbol{V}^{-1/2}\widetilde{\boldsymbol{y}}, \qquad (7.2)$$

where $\boldsymbol{C}(\omega_n,k_n,z)=\boldsymbol{C}(\omega_n,z)+k_n\boldsymbol{I}_{p_1}$.

By direct computations, the robust partially generalized unrestricted ridge estimators (RPGUREs) of $\boldsymbol{\beta}_1$ and $\boldsymbol{\beta}_2$ respectively have forms

$$\begin{aligned}
\hat{\boldsymbol{\beta}}^{LTS}_{PG1}(\omega_n,k_n,z)&=(\widetilde{\boldsymbol{X}}_1^{\top}\boldsymbol{\Sigma}_2^{-1}(\omega_n,k_n,z)\widetilde{\boldsymbol{X}}_1+k_n\boldsymbol{I}_{p_1})^{-1}\widetilde{\boldsymbol{X}}_1^{\top}\boldsymbol{\Sigma}_2^{-1}(\omega_n,k_n,z)\widetilde{\boldsymbol{y}}\\
&=\Big(\boldsymbol{I}_{p_1}+k_n(\widetilde{\boldsymbol{X}}_1^{\top}\boldsymbol{\Sigma}_2^{-1}(\omega_n,k_n,z)\widetilde{\boldsymbol{X}}_1)^{-1}\Big)^{-1}\hat{\boldsymbol{\beta}}_{PG1}(\omega_n,z) \qquad (7.3)
\end{aligned}$$

$$\begin{aligned}
\hat{\boldsymbol{\beta}}^{LTS}_{PG2}(\omega_n,k_n,z)&=(\widetilde{\boldsymbol{X}}_2^{\top}\boldsymbol{\Sigma}_1^{-1}(\omega_n,k_n,z)\widetilde{\boldsymbol{X}}_2+k_n\boldsymbol{I}_{p_2})^{-1}\widetilde{\boldsymbol{X}}_2^{\top}\boldsymbol{\Sigma}_1^{-1}(\omega_n,k_n,z)\widetilde{\boldsymbol{y}}\\
&=\Big(\boldsymbol{I}_{p_2}+k_n(\widetilde{\boldsymbol{X}}_2^{\top}\boldsymbol{\Sigma}_1^{-1}(\omega_n,z,k_n)\widetilde{\boldsymbol{X}}_2)^{-1}\Big)^{-1}\hat{\boldsymbol{\beta}}_{PG2}(\omega_n,z), \qquad (7.4)
\end{aligned}$$

where

$$\begin{aligned}
\boldsymbol{\Sigma}_i^{-1}(\omega_n,k_n,z)=\boldsymbol{V}^{-1/2}\boldsymbol{Z}\boldsymbol{V}^{-1/2}-\boldsymbol{V}^{-1/2}\boldsymbol{Z}\boldsymbol{V}^{-1/2}\widetilde{\boldsymbol{X}}_i(\widetilde{\boldsymbol{X}}_i^{\top}\boldsymbol{V}^{-1/2}\boldsymbol{Z}\boldsymbol{V}^{-1/2}\\
\widetilde{\boldsymbol{X}}_i+k_n\boldsymbol{I}_{p_i})^{-1}\\
\times\widetilde{\boldsymbol{X}}_i^{\top}\boldsymbol{V}^{-1/2}\boldsymbol{Z}\boldsymbol{V}^{-1/2},\ i=1,2. \qquad (7.5)
\end{aligned}$$

Now, suppose $s^2(\omega_n,k_n,z)$ denotes the estimated value of σ^2 based on $\hat{\boldsymbol{\beta}}^{LTS}_{PG1}(\omega_n,k_n,z)$. Let $g(.)$ and $G(.)$ be the density function and cumulative distribution function of $(\sigma^2\boldsymbol{V})^{-1/2}\boldsymbol{\epsilon}$, respectively. According to Roozbeh and Arashi (2017), it can be verified that

$$\begin{aligned}
s^2(\omega_n,k_n,z)&=\frac{1}{h}\big(\widetilde{\boldsymbol{y}}-\widetilde{\boldsymbol{X}}\hat{\boldsymbol{\beta}}^{LTS}_{PG1}(\omega_n,k_n,z)\big)^{\top}\boldsymbol{V}^{-1/2}\boldsymbol{Z}\boldsymbol{V}^{-1/2}\big(\widetilde{\boldsymbol{y}}-\widetilde{\boldsymbol{X}}\hat{\boldsymbol{\beta}}^{LTS}_{PG1}(\omega_n,k_n,z)\big)\\
&\xrightarrow{\mathcal{P}}\sigma^2\frac{\kappa_u}{1-\alpha},
\end{aligned}$$

where $u_\alpha=G^{-1}(1-\alpha/2)$ be the $(1-\alpha/2)$ upper quantile of $g(.)$ and

$$\kappa_u = \int_{-u_\alpha}^{u_\alpha} z^2 \mathrm{d}G(z).$$

Following Roozbeh and Arashi (2017) and Arashi and Roozbeh (2019), the robust test statistic for testing the null-hypothesis $\mathcal{H}_o : \boldsymbol{\beta}_2 = 0$ is given by

$$\pounds_n(\omega_n, k_n, z) = \frac{l_\alpha}{s^2(\omega_n, k_n, z)} \Big(\hat{\boldsymbol{\beta}}_{PG2}^{LTS^\top}(\omega_n, k_n, z) \boldsymbol{S}_2(\omega_n, k_n, z) \hat{\boldsymbol{\beta}}_{PG2}^{LTS}(\omega_n, k_n, z) \Big), \tag{7.6}$$

where $\boldsymbol{S}_2(\omega_n, k_n, z) = \widetilde{\boldsymbol{X}}_2^\top \boldsymbol{\Sigma}_1^{-1}(\omega_n, k_n, z) \widetilde{\boldsymbol{X}}_2 + k_n \boldsymbol{I}_{p_2}, l_\alpha = (1 - \alpha - 2u_\alpha g(u_\alpha))^2 / (1 - \alpha)$ and $\pounds_n(\omega_n, k_n, z)$ has an asymptotic chi-square distribution with p_2 degree of freedom under the null-hypothesis.

In continuation, we introduce the robust preliminary test partially generalized restricted ridge estimator (RPTPGRRE) defined by

$$\begin{aligned} \hat{\boldsymbol{\beta}}_{PGR1}^{LTS-PT}(\omega_n, k_n, z) = \hat{\boldsymbol{\beta}}_{PGR1}^{LTS}(\omega_n, k_n, z) + \big[1 - I(\pounds_n(\omega_n, k_n, z) \le \chi^2_{p_2}(\alpha))\big] \\ \times \big(\hat{\boldsymbol{\beta}}_{PG1}^{LTS}(\omega_n, k_n, z) - \hat{\boldsymbol{\beta}}_{PGR1}^{LTS}(\omega_n, k_n, z) \big). \end{aligned} \tag{7.7}$$

We next consider the robust Stein-type partially generalized restricted ridge estimator (RSPGRRE) defined by

$$\begin{aligned} \hat{\boldsymbol{\beta}}_{PGR1}^{LTS-S}(\omega_n, k_n, z) = \hat{\boldsymbol{\beta}}_{PGR1}^{LTS}(\omega_n, k_n, z) + (1 - d\pounds_n^{-1}(\omega_n, k_n, z)) \\ \times \big(\hat{\boldsymbol{\beta}}_{PG1}^{LTS}(\omega_n, k_n, z) - \hat{\boldsymbol{\beta}}_{PGR1}^{LTS}(\omega_n, k_n, z) \big). \end{aligned} \tag{7.8}$$

Finally, due to some drawbacks of RSPGRRE as stated earlier, we introduce the robust positive-rule Stein-type partially generalized restricted ridge estimator (RPRSPGRRE) defined by

$$\begin{aligned} \hat{\boldsymbol{\beta}}_{PGR1}^{LTS-S+}(\omega_n, k_n, z) = \hat{\boldsymbol{\beta}}_{PGR1}^{LTS-S}(\omega_n, k_n, z) - (1 - d\pounds_n^{-1}(\omega_n, k_n, z)) I(\pounds_n(\omega_n, k_n, z) \le d) \\ \times \big(\hat{\boldsymbol{\beta}}_{PG1}^{LTS}(\omega_n, k_n, z) - \hat{\boldsymbol{\beta}}_{PGR1}^{LTS-S}(\omega_n, k_n, z) \big). \end{aligned} \tag{7.9}$$

8 Application

In this section, we demonstrate the application of the proposed method to the riboflavin production data set (see e.g., Bühlmann et al. 2014).

To illustrate the usefulness of the suggested strategies for high-dimensional data in the semiparametric regression model, we consider the data set on riboflavin (vitamin B2) production in Bacillus subtilis, which can be found in R package

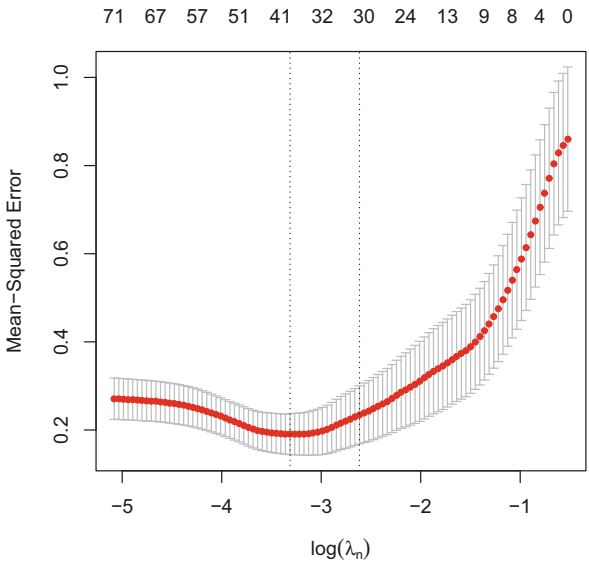

Fig. 1 The diagram of cross–validation curve (the red dotted line), and upper and lower standard deviation curves along the sequence $\{\lambda_n\}$

"hdi". This data consist of a logarithm of the riboflavin production rate as the response variable along with $p = 4088$ covariates measuring the logarithm of the expression level of 4088 genes for $n = 71$ patients. We use the least absolute shrinkage and selection operator (LASSO) approach for extracting the effective genes in riboflavin production rate. Based on 100-fold cross validation, the LASSO shrinks 4047 parameters to zero with remaining $p_1 = 41$ significant explanatory variables. As shown in Fig. 1, the best value of the LASSO parameter (λ_n) which minimizes the cross–validation criterion is achieved at 0.0364.

Since the primary aim of this study is to improve the prediction accuracy in genome regression model, we further focus on the visualization of the data. Apart from the high-dimensional nature of this data, we detected outliers. As a first step to data visualization, we employ diagnostic plots to identify data that are 'inconsistent' with the main bulk of the data sets. We label an observations as 'outlier' if the absolute standardized residual for the point is larger than 2; observations 27, 31, 33, and 71 are outliers as shown in Fig. 2. The presence of these outliers will inevitably affect the parameter estimation in the model. Thus, the need to develop an efficient robust estimation strategy is necessary.

The bivariate boxplot may be useful in indicating the distributional properties of the data and in identifying possible outliers. The bivariate boxplot, as displayed in Fig. 3, is a two-dimensional analogue of the boxplot for univariate data proposed by Goldberg and Iglewicz (1992). This boxplot is based on calculating the robust measures of location, scale, and correlation; it consists essentially a pair of concentric ellipses, the inner ellipse includes 50% of the data and other (called the fence) of which delineates potentially influential outliers. In addition, resistant regression lines of both response (y) on predictor (X) and vice versa are shown; the

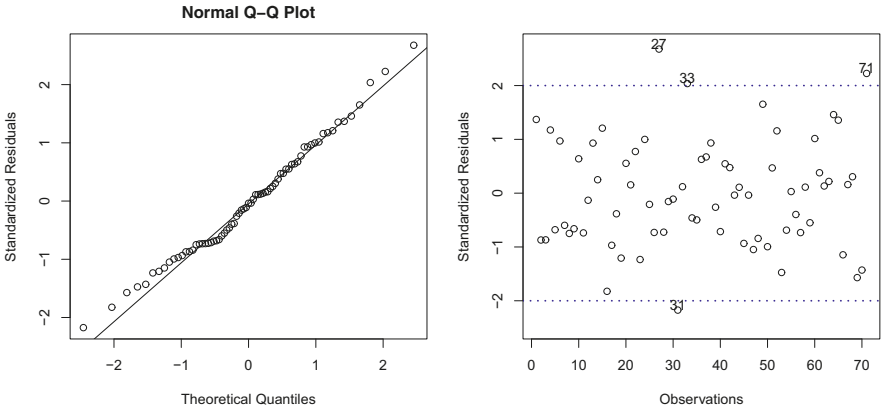

Fig. 2 Diagnostic plots for the riboflavin production data set

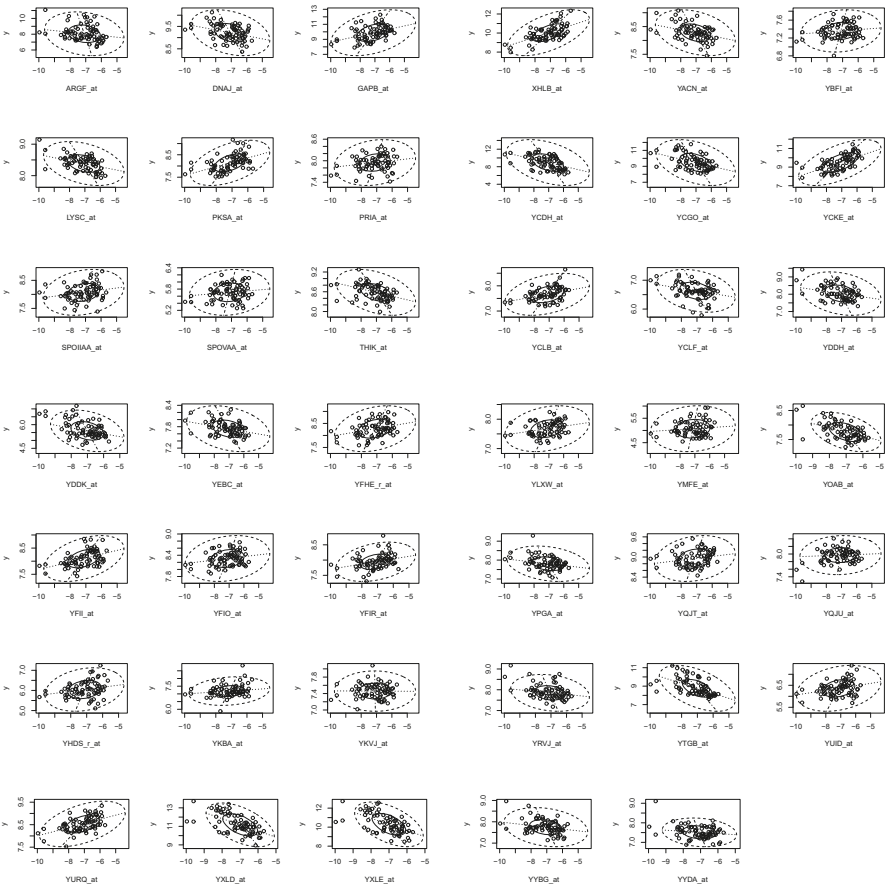

Fig. 3 Bivariate boxplot of the riboflavin production data set for effective genes

intersection provides the bivariate location estimator and the acute angle between the regression lines gives a measure of correlation where small angle indicates a large absolute value of correlations. Figure 3 showed that the data contains some outliers.

To detect the nonparametric part of the model, we calculate

$$s_i^2(\omega_n, z) = \frac{1}{h}\big(\widetilde{y} - X_1[,-i]\hat{\boldsymbol{\beta}}_{PG1}^{LTS}(\omega_n, z)\big)^{\top} \boldsymbol{V}^{-1/2}\boldsymbol{Z}\boldsymbol{V}^{-1/2}$$
$$\big(\widetilde{y} - X_1[,-i]\hat{\boldsymbol{\beta}}_{PG1}^{LTS}(\omega_n, k_n, z)\big),\ i = 1, \ldots, 41,$$

where $\boldsymbol{X}_1[,-i]$ is obtained by deleting the ith column of matrix $\boldsymbol{X}_1$. Among all 41 remained genes, "$DNAJ\_at$" had minimum $s_i^2(\omega_n, z)$ value and so this can be considered as a nonparametric part. We also use the added-variable plots to identify the parametric and nonparametric components of the model. Added-variable plots enable us to visually assess the effect of each predictor, having adjusted for the effects of the other predictors. By looking at added-variable plot (Fig. 4), we consider "$DNAJ\_at$" as a nonparametric part. As it can be seen from this figure, the nonlinear relation between "$DNAJ\_at$" and the response variable seems to have a better fit than linear relation after removing the effects of other predictors, and so, the specification of the sparse semiparametric regression model can be written as

$$\boldsymbol{y} = \boldsymbol{X}_1\boldsymbol{\beta}_1 + \boldsymbol{X}_2\boldsymbol{\beta}_2 + \boldsymbol{f}(t) + \boldsymbol{\epsilon}, \quad t = DNAJ\_at \tag{8.1}$$

where $p_1 = 40$ and $p_2 = 4047$.

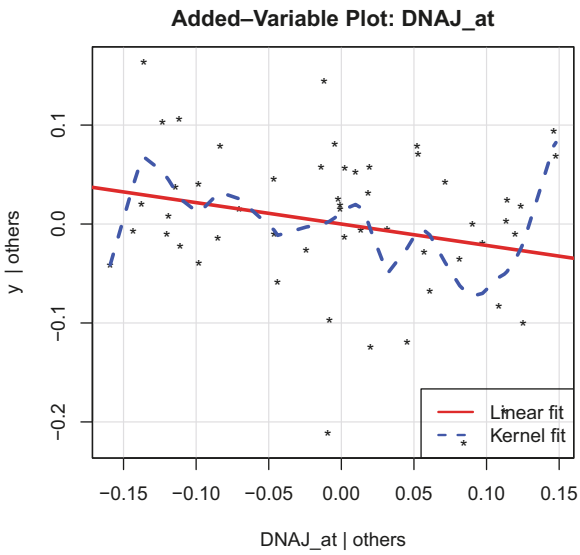

Fig. 4 Added-variable plot of explanatory variables $DNAJ\_at$ vs. dependent variable, linear fit (red solid line) and kernel fit (blue dashed line)

For estimating the nonparametric part of the model, $f(t)$, we use

$$W_{\omega_n}(t_j) = \frac{1}{n\omega_n} K\Big(\frac{t-tj}{\omega_n}\Big) = \frac{1}{n\omega_n}.\frac{1}{\sqrt{2\pi}} \exp\Big\{-\frac{(t_i-t_j)^2}{2\omega_n^2}\Big\},$$

which is Priestley and Chao's weight with the Gaussian kernel. We apply the robust cross-validation (R.C.V.) method to select the optimal bandwidth ω_n and k_n, which minimizes the following R.C.V. function

$$R.C.V.(\omega_n, k_n) = \frac{1}{h}\Big(\widetilde{\boldsymbol{y}}^{(-i)} - \widetilde{\boldsymbol{X}}^{(-i)}\hat{\boldsymbol{\beta}}^{(-i)}(\omega_n, k_n)\Big)^{\top} \boldsymbol{Z}\Big(\widetilde{\boldsymbol{y}}^{(-i)} - \widetilde{\boldsymbol{X}}^{(-i)}\hat{\boldsymbol{\beta}}^{(-i)}(\omega_n, k_n)\Big),$$

where $\hat{\boldsymbol{\beta}}^{(-i)}$ obtain by replacing $\widetilde{\boldsymbol{X}}$ and $\widetilde{\boldsymbol{y}}$ with $\widetilde{\boldsymbol{X}}^{(-i)} = \Big(\tilde{x}_{jk}^{(-i)}\Big)$, $1 \le k \le n$, $1 \le j \le p$, $\widetilde{\boldsymbol{y}}^{(-i)} = \Big(\tilde{y}_1^{(-i)}, \ldots, \tilde{y}_n^{(-i)}\Big)$, $\tilde{x}_{sk}^{(-i)} = x_{sk} - \sum_{j\neq i}^{n} W_{nj}(t_i)x_{sj}$, $\tilde{y}_k^{(-i)} = y_k - \sum_{j\neq i}^{n} W_{nj}(t_i)y_j$.

All computations were conducted using the statistical package R. Table 1 shows a summary of the results. In this table, the SSE and R^2 respectively are the residual sum of squares and coefficient of determination of the model, i.e., $SSE = \sum_{i=1}^{n} z_i(y_i - \hat{y}_i)^2$, $\hat{y}_i = \boldsymbol{x}_i^{\top}\hat{\boldsymbol{\beta}} + \hat{f}(t_i)$, and $R^2 = 1 - SSE/S_{yy}$. The RPGRRE and RPRSPGRRE are the best estimators with the relatively smallest SSE and largest R^2 values. For estimation of nonparametric effect, at first we estimated the parametric effects by one of the proposed methods and then, a local polynomial approach was applied to fit $y_i - \boldsymbol{x}_i^{\top}\hat{\boldsymbol{\beta}}$ on t_i, $i = 1, \ldots, n$ (Fig. 5). As displayed in

Table 1 Evaluation of proposed robust estimators for the riboflavin production data

Method	RPGURE	RPGRRE	RSPGRRE	RPRSPGRRE
SSE	11.8548	1.1783	2.4741	1.1755
R^2	0.5215	0.9524	0.9001	0.9526

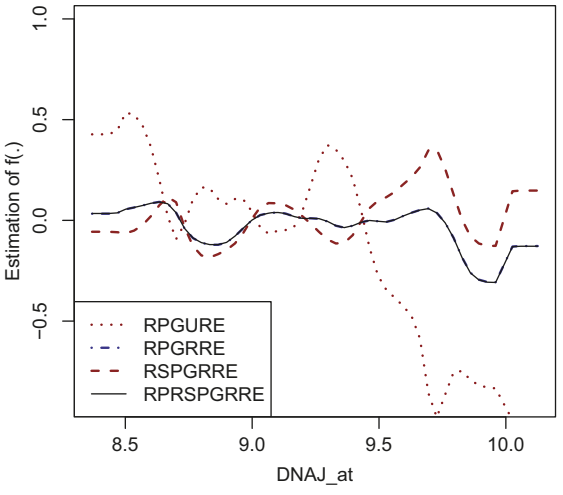

Fig. 5 Fitted curves of nonparametric part of model (8.1)

Fig. 5, because of sparsity of the model, RPGURE has been completely corrupted and led to bad fit. The RPGRRE and RPRSPGRRE resulted in the same fits. The results of Table 1 also confirm this findings.

9 Summary and Conclusions

In this paper, under sparsity assumption on some elements of $\boldsymbol{\beta}$, we proposed a robust partially generalized restricted ridge estimator in a semiparametric regression model when the errors were dependent. We introduced the robust Stein-type partially generalized restricted ridge estimator and its positive-rule after deriving the robust test statistic for testing the sparsity of the model and its asymptotic distribution for application in the high-dimensional data set. Finally, a real data example analyzed to compare the performance of the proposed estimators numerically. In the real example study, as it can be seen from Fig. 4, the nonlinear relation between the dependent variable and DNAJ_at can be detected and so, the pure parametric model does not fit to the data and semiparametric regression model fits more significantly. Further, from Table 1 and Fig. 5, it can be deduced that RPGRRE and RPRSPGRRE are quite efficient in the sense that they have significant values of goodness of fit. Moreover, because of the sparsity of the data, RPGURE was the worst estimator for the parametric part in this examples.

Acknowledgements We would like to thank two anonymous reviewers for their valuable comments and suggestions on the earlier version which significantly improved the presentation. The first and second authors gratefully acknowledge the research grant support RP009B–13AFR from the University of Malaya.

References

Akdeniz, F., & Roozbeh, M. (2019). Generalized difference-based weighted mixed almost unbiased ridge estimator in partially linear models. *Statistical Papers, 60*, 1717–1739.

Akdenïz, F., & Tabakan, G. (2009). Restricted ridge estimators of the parameters in semiparametric regression model. *Communications in Statistics—Theory and Methods, 38*, 1852–1869.

Akdeniz, F., Akdeniz Duran, E., Roozbeh, M., & Arashi, M. (2015). Efficiency of the generalized difference-based Liu estimators in semiparametric regression models with correlated errors. *Journal of Statistical Computation & Simulation, 85*, 147–165.

Amini, M., & Roozbeh, M. (2015). Optimal partial ridge estimation in restricted semiparametric regression models. *Journal of Multivariate Analysis, 136*, 26–40.

Amini, M., & Roozbeh, M. (2016). Least trimmed squares ridge estimation in partially linear regression models. *Journal of Statistical Computation & Simulation, 86*, 2766–2780.

Arashi, M. (2012). Preliminary test and Stein estimators in simultaneous linear equations. *Linear Algebra and Its Applications, 436*(5), 1195–1211.

Arashi, M., Kibria, B. M. G., Norouzirad, M., & Nadarajah, S. (2014). Improved preliminary test and Stein-rule Liu estimators for the ill-conditioned elliptical linear regression model. *Journal of Multivariate Analysis, 124*, 53–74.

Arashi, M., & Roozbeh, M. (2019). Some improved estimation strategies in high-dimensional semiparametric regression models with application to riboflavin production data. *Statistical Papers, 60*, 317–336.

Arashi, M., Saleh, A. K. M. E., & Tabatabaey, S. M. M. (2010). Estimation of parameters of parallelism model with elliptically distributed errors. *Metrika, 71*, 79–100.

Arashi, M., & Tabatabaey, S. M. M. (2009). Improved variance estimation under sub-space restriction. *Journal of Multivariate Analysis, 100*, 1752–1760.

Arashi, M., Tabatabaey, S. M. M., & Soleimani, H. (2012). Simple regression in view of elliptical models. *Linear Algebra and Its Applications, 437*, 1675–1691.

Arashi, M., & Valizadeh, T. (2015). Performance of Kibria's methods in partial linear ridge regression model. *Statistical Papers, 56*, 231–246.

Babaie-Kafaki, S., & Roozbeh, M. (2017). A revised Cholesky decomposition to combat multicollinearity in multiple regression models. *Journal of Statistical Computation & Simulation, 87*, 2298–2308.

Bühlmann, P. (2013). Statistical significance in high-dimensional linear models. *Bernoulli, 19*, 1212–1242.

Bühlmann, P., Kalisch, M., & Meier, L. (2014). High-dimensional statistics with a view towards applications in biology. *Annual Review of Statistics and Its Application, 1*, 255–278.

Bühlmann, P., & van de Geer, S. (2011). *Statistics for high-dimensional data: Methods, theory and applications*. Heidelberg: Springer.

Duran, A. E., Härdle, W. K., & Osipenko, M. (2012). Difference based ridge and Liu type estimators in semiparametric regression models. *Journal of Multivariate Analysis, 105*, 164–175.

Fallahpour, S., Ahmed, S. E., & Doksum, K. A. (2012). L1 penalty and shrinkage estimation in partially linear models with random coefficient autoregressive errors. *Applied Stochastic Models in Business and Industry, 28*, 236–250.

Fan, J., & Lv, J. (2010). A selective overview of variable selection in high dimensional feature space. *Statistica Sinica, 20*, 101–148.

Ghapani, F., Rasekh, A. R., & Babadi, B. (2018). The weighted ridge estimator in stochastic restricted linear measurement error models. *Statistical Papers, 59*, 709–723.

Goldberg, K., & Iglewicz, B. (1992). Bivariate extensions of the boxplot. *Technometrics, 34*, 307–320.

Härdle, W., Liang, H., & Gao, J. (2000). *Partially linear models*. Heidelberg: Physika Verlag.

Hastie, T., Tibshirani, R., & Friedman, J. (2009). *The elements of statistical learning: Data mining, inference, and prediction* (2nd ed.). New York: Springer.

Hoerl, A. E., & Kennard, R. W. (1970). Ridge regression: Biased estimation for non-orthogonal problems. *Technometrics, 12*, 55–67.

Knight, K., & Fu, W. (2000). Asymptotic for lasso-type estimators. *Annals of Statistics, 28*, 1356–1378.

Müller, M. (2000). *Semiparametric extensions to generalized linear models*. Habilitationsschrift.

Nguyen, T. D., & Welsch, R. (2010). Outlier detection and least trimmed squares approximation using semi-definite programming. *Computational Statistics & Data Analysis, 54*, 3212–3226.

Roozbeh, M. (2015). Shrinkage ridge estimators in semiparametric regression models. *Journal of Multivariate Analysis, 136*, 56–74.

Roozbeh, M. (2016). Robust ridge estimator in restricted semiparametric regression models. *Journal of Multivariate Analysis, 147*, 127–144.

Roozbeh, M. (2018). Optimal QR-based estimation in partially linear regression models with correlated errors using GCV criterion. *Computational Statistics & Data Analysis, 117*, 45–61.

Roozbeh, M., & Arashi, M. (2013). Feasible ridge estimator in partially linear models. *Journal of Multivariate Analysis, 116*, 35–44.

Roozbeh, M., & Arashi, M. (2016). Shrinkage ridge regression in partial linear models. *Communications in Statistics – Theory & Methods, 45*, 6022–6044.

Roozbeh, M., & Arashi, M. (2017). Least-trimmed squares: Asymptotic normality of robust estimator in semiparametric regression models. *Journal of Statistical Computation and Simulation, 87*, 1130–1147.

Roozbeh, M., & Babaie-Kafaki, S. (2016). Extended least trimmed squares estimator in semiparametric regression models with correlated errors. *Journal of Statistical Computation and Simulation, 86*, 357–372.

Roozbeh, M., Arashi, M., & Hamzah, N. A. (2020). Generalized cross-validation for simultaneous optimization of tuning parameters in ridge regression. *Iranian Journal of Science and Technology, Transactions A: Science*. https://doi.org/10.1007/s40995-020-00851-1.

Rousseeuw, P. J. (1984). Least median of squares regression. *Journal of American. Statistical Association, 79*, 871–880.

Rousseeuw, P. J., & Leroy, A. M. (1987). *Robust regression and outlier detection*. New York: Wiley.

Rousseeuw, P. J., & van Driessen, K. (2006). Computing LTS regression for large data sets. *Data Mining and Knowledge Discovery, 12*, 29–45.

Saleh, A. K. M. E. (2006). *Theory of preliminary test and stein-type estimation with applications*. New York: Wiley.

Shao, J., & Deng, X. (2012). Estimation in high-dimensional linear models with deterministic design matrices. *Annals of Statistics, 40*, 812–831.

Simpson, D. G., Ruppert, D., & Carroll, R. J. (1992). On one-step GM estimates and stability of influences in linear regression. *Journal of American. Statistical Association, 87*, 439–450.

Wu, J., & Yang, H. (2016). More on the unbiased ridge regression estimation. *Statistical Papers, 57*, 31–42.

Yohai, V. J. (1987). High breakdown-point and high efficiency robust estimates for regression. *Annals of Statistics, 15*, 642–656.

Yuzbashi, B., & Ahmed, S. E. (2015). Shrinkage ridge regression estimators in high-dimensional linear models. In *Proceedings of the 19th International Conference on Management Science and Engineering Management*. Berlin: Springer. https://doi.org/10.1007/978-3-662-47241-5_67.

Zhang, C. H., & Huang, J. (2008). The sparsity and bias of the LASSO selection in high-dimensional linear regression. *Annals of Statistics, 36*, 1567–1594.

Optimal Allocation for Extreme Value Regression Under Time Censoring

Ping Shing Chan, Hon Yiu So, Hon Keung Tony Ng, and Wei Gao

Abstract In this paper, we discuss the optimal allocation problem in a multi-level accelerated life testing experiment under time (Type-I) censoring when an extreme-value regression model is used for statistical analysis. We derive the expected Fisher information and the asymptotic variance-covariance matrix of the maximum likelihood estimators. Three optimality criteria are considered and the corresponding optimal allocations are determined. Under Type-I censoring, because the optimal allocations are depending on the model parameters, the sensitivity of the optimal allocations due to mis-specification of the model parameters is studied. A numerical example is used to illustrate the methodologies developed in this paper.

1 Introduction

Optimal design of regression experiments has long been studied in the literature, for example, Elfving (1952), Gaylor and Sweeny (1965), Fedorov (1972), Silvey (1980). It is one of the important problems in statistical and engineering sciences because a well designed experiment not only reduces the cost of the experiment but also improves the efficiency of the statistical inference. For results in optimal design of linear regression models with complete data and extensive developments

P. S. Chan
Department of Statistics, The Chinese University of Hong Kong, Shatin, N. T., Hong Kong SAR
e-mail: benchan@cuhk.edu.hk

H. Y. So
Department of Statistics and Actuarial Science, University of Waterloo, Waterloo, ON, Canada

H. K. T. Ng (✉)
Department of Statistical Science, Southern Methodist University, Dallas, TX, USA
e-mail: ngh@mail.smu.edu

W. Gao
School of Mathematics and Statistics, Northeast Normal University, Changchun, Jilin, China
e-mail: gaow@nenu.edu.cn

A. Bekker et al. (eds.), *Computational and Methodological Statistics and Biostatistics*, Emerging Topics in Statistics and Biostatistics,
https://doi.org/10.1007/978-3-030-42196-0_12

in this area, one may refer to Silvey (1980), Box and Draper (1987), Seber and Wild (1989), Atkinson and Donev (1992), Liski et al. (2002) and a concise introduction by O'Brien and Funk (2003). For multi-stress levels extreme value regression model, Nelson and Kielpinski (1976) and Nelson and Meeker (1978) noted that the optimal allocation in the complete sample situation uses only the highest and the lowest stress levels for their optimality criteria using intuitive arguments. Ng et al. (2007) established this result in a formal manner by providing a mathematical proof of the results. Besides the multi-stress levels regression models, optimal designs of accelerated life tests under different statistical models have also been studied, see, for example, Bai and Chung (1991, 1992), Bai and Kim (1993) and Monroe et al. (2010). For a comprehensive review and bibliography on accelerated test plans, one may refer to Nelson (2005a,b).

In industrial and clinical experiments, there are many situations in which units (or subjects) are lost or removed from the experiment before failure. The experimenter may not always obtain complete information on failure times for all experimental units. Data obtained from such experiments is called *censored data*. Censoring can be unintentional due to accidental breakage or an individual under study drops out, or it can be intentional in which the removal of units or subjects is pre-planned. Common reasons for pre-planned censoring are saving the total time on test and saving the cost associated with failure of the units. Nevertheless, this kind of incomplete data will reduce the efficiency of statistical inference compared to complete data.

Two types of censoring, namely Type-I censoring and Type-II censoring, are commonly used in industrial experiments. For Type-I censoring, the life-testing experiment is planned to be terminated at a pre-fixed time T. Then, only the failures until time T will be observed. The incomplete data obtained from such an experiment will be referred to as a *Type-I censored sample* or *time-censored sample*. Note that the number of failures observed in a Type-I censored experiment is random but the total experimental time is fixed. For Type-II censoring, the life-testing experiment is planned to be terminated as soon as the r-th (where r is pre-fixed) failure is observed. Then, only the first r failures out of n units under test will be observed. The incomplete data obtained from such a restrained experiment will be referred to as a *Type-II censored sample*. Note that in this case, in contrast to Type-I censoring, the number of failures observed is fixed (viz., r) while the duration of the experiment is random. For a concise review of censoring methodology, one may refer to Ng (2010). In the context of optimal design of regression experiments, Ka et al. (2011) further discussed the optimal allocation problem in the multi-level stress testing with extreme-value regression model under Type-II censored experiments. Due to the complexity of the Fisher information matrix in presence of censoring, the optimal allocations are determined numerically and asymptotic optimal allocations are also studied in Ka et al. (2011). However, the optimal allocation problem in the multi-level stress testing with extreme-value regression model under Type-I censored experiments has not been formally studied. Although similar approaches used in Ka et al. (2011) for Type-II censored experiments can be adopted to solve the optimal allocation problem under Type-I censoring with

suitable modification, the problem is more complicated and the modifications are not straightforward because the numbers of observed failures at different stress levels are random variables with distributions depending on the model parameters. Therefore, it is important to develop methodology to obtain optimal allocation and to investigate the sensitivity of the allocations due to the mis-specification of the parameters.

In this paper, we discuss the optimal allocation problem in a multi-level accelerated life testing experiment under Type-I censoring when an extreme-value regression model is used for statistical analysis. In Sect. 2, we introduce the statistical model and the set-up of the optimal allocation problem. The Fisher information and asymptotic variance-covariance matrices of the maximum likelihood estimators (MLEs) are then derived in Sect. 3. Three optimal criteria considered in this paper are also presented in this section. Then, in Sect. 4, the sensitivity of the optimal allocations due to mis-specification of the model parameters is studied. A numerical example given by McCool (1980) is used to illustrate the sensitivity analysis in Sect. 5. Finally, some concluding remarks are given in Sect. 6.

2 Model and Maximum Likelihood Estimation

Consider the following life-testing experiment: suppose we have N items available for the test at k ordered stress level, say $x_1 < x_2 < \cdots < x_k$, we assign n_i items for testing at stress level x_i $(i = 1, 2, \ldots, k)$ with $\sum_{i=1}^{k} n_i = N$. We further fix the duration of experiment to be t_c, i.e., only failures occur before time t_c are observed and items which not yet failed at t_c will be treated as right-censored at t_c. As discussed in the previous section, this experimental scheme is known as *Type-I censoring* or *time-censoring* scheme.

We further assume that the lifetimes of items under testing are Weibull distributed with a scale parameter depending on the stress level x_i. That is, the lifetime of item, T, under stress level x_i have probability density function (p.d.f.)

$$f_T(t; \alpha(x_i), \delta) = \frac{\delta}{\alpha(x_i)} \left(\frac{t}{\alpha(x_i)}\right)^{\delta-1} \exp\left[-\left(\frac{t}{\alpha(x_i)}\right)^{\delta}\right], \; t > 0,$$

where $\alpha(x_i) > 0$ is the scale parameter and $\delta > 0$ is the shape parameter. Upon making a logarithmic transformation on T, $Y = \ln T$ follows the extreme-value (Gumbel Type-I) distribution with p.d.f.

$$f_Y(y; \mu(x_i), \sigma) = \frac{1}{\sigma} \exp\left[\left(\frac{y-\mu(x_i)}{\sigma}\right) - \exp\left(\frac{y-\mu(x_i)}{\sigma}\right)\right], \quad -\infty < y < \infty, \quad (1)$$

where $\mu(x_i) = \ln \alpha(x_i)$ and $\sigma = 1/\delta$. We can then write Y in a location-scale form as

$$Y = \mu(x_i) + \sigma Z, \tag{2}$$

where Z has a standard extreme-value distribution with p.d.f.

$$f_Z(z) = \exp(z - \exp(z)), \qquad -\infty < z < \infty. \tag{3}$$

A simple functional form for $\mu(x)$ in (2) is the linear form given by

$$\mu(x_i) = \nu_0 + \nu_1 x_i,$$

where ν_0 and ν_1 are the regression parameters.

Since the duration of experiment is fixed to be t_c, the number of observed failures at each stress level is a random variable. We denote the number of observed failures at stress level x_i by R_i and the ordered log-lifetimes by $Y_{1:n_i} < Y_{2:n_i} < \cdots < Y_{R_i:n_i}$, $i = 1, 2, \ldots, k$. The corresponding observed values of R_i and $Y_{j:n_i}$ are denoted by r_i and $y_{j:n_i}$, $j = 1, 2, \ldots, r_i$, respectively. Note that R_i is a binomial random variable with sample size n_i and probability of successes $F_Y(t_c^*; \mu(x_i), \sigma)$, where $t_c^* = \log(t_c)$ and F_Y is the cumulative distribution function (c.d.f.) of Y. Then, given the observed values of r_i and $y_{j:n_i}$, $i = 1, 2, \ldots, k$, $j = 1, 2, \ldots, n_i$, the likelihood function is given by

$$\begin{aligned} L(\nu_0, \nu_1, \sigma) = & \prod_{i=1}^{k} \frac{n_i!}{(n_i - r_i)!} \\ & \times \left\{ \prod_{j=1}^{r_i} \frac{1}{\sigma} \exp\left[\frac{y_{j:n_i} - \nu_0 - \nu_1 x_i}{\sigma} - \exp\left(\frac{y_{j:n_i} - \nu_0 - \nu_1 x_i}{\sigma} \right) \right] \right. \\ & \left. \times \left\{ \exp\left[-\exp\left(\frac{t_c^* - \nu_0 - \nu_1 x_i}{\sigma} \right) \right] \right\}^{n_i - r_i} \right\} \end{aligned} \tag{4}$$

and the log-likelihood function is given by

$$\begin{aligned} \log L(\nu_0, \nu_1, \sigma) = & \text{ constant} - \sum_{i=1}^{k} r_i \log\sigma \\ & + \sum_{i=1}^{k} \sum_{j=1}^{r_i} \left[\frac{y_{j:n_i} - \nu_0 - \nu_1 x_i}{\sigma} - \exp\left(\frac{y_{j:n_i} - \nu_0 - \nu_1 x_i}{\sigma} \right) \right] \\ & - \sum_{i=1}^{k} (n_i - r_i) \exp\left(\frac{t_c^* - \nu_0 - \nu_1 x_i}{\sigma} \right). \end{aligned} \tag{5}$$

With $z_{j:n_i} = (y_{j:n_i} - \nu_0 - \nu_1 x_i)/\sigma$ and $t_i^* = (t_c^* - \nu_0 - \nu_1 x_i)/\sigma$, the score functions can be written as

$$\frac{\partial \log L}{\partial \nu_0} = -\frac{1}{\sigma}\sum_{i=1}^{k}\left\{\sum_{j=1}^{r_i}\left[1-\exp\left(z_{j:n_i}\right)\right] - (n_i - r_i)\exp\left(t_i^*\right)\right\}, \tag{6}$$

$$\frac{\partial \log L}{\partial \nu_1} = -\frac{1}{\sigma}\sum_{i=1}^{k}\left\{x_i\left[\sum_{j=1}^{r_i}[1-\exp\left(z_{j:n_i}\right)] - (n_i - r_i)\exp\left(t_i^*\right)\right]\right\}, \tag{7}$$

$$\frac{\partial \log L}{\partial \sigma} = -\frac{1}{\sigma}\sum_{i=1}^{k}\left\{r_i - (n_i - r_i)t_i^*\exp\left(t_i^*\right) + \sum_{j=1}^{r_i} z_{j:n_i}\left[1-\exp\left(z_{j:n_i}\right)\right]\right\}. \tag{8}$$

The MLEs $\hat{\nu}_0$, $\hat{\nu}_1$ and $\hat{\sigma}$ of ν_0, ν_1 and σ can be obtained by solving simultaneously the equations $\partial \log L/\partial \nu_0 = 0$, $\partial \log L/\partial \nu_1 = 0$ and $\partial \log L/\partial \sigma = 0$. Since these equations cannot be solved analytically, numerical methods such as Newton-Raphson or some other iterative procedures must be employed. There are computational algorithms available in some commonly used statistical packages such as R (R Core Team 2019) and SAS (SAS Institute Inc. 2008) to obtain the MLEs.

3 Expected Fisher Information

The asymptotic variances and covariances of the MLE $\hat{\nu}_0$, $\hat{\nu}_1$ and $\hat{\sigma}$ can be obtained by inverting the expected Fisher information matrix

$$\mathbf{I}(\nu_0, \nu_1, \sigma) = -E\begin{bmatrix} \frac{\partial^2 \log L}{\partial \nu_0^2} & \frac{\partial^2 \log L}{\partial \nu_0 \partial \nu_1} & \frac{\partial^2 \log L}{\partial \nu_0 \partial \sigma} \\ \frac{\partial^2 \log L}{\partial \nu_0 \partial \nu_1} & \frac{\partial^2 \log L}{\partial \nu_1^2} & \frac{\partial^2 \log L}{\partial \nu_1 \partial \sigma} \\ \frac{\partial^2 \log L}{\partial \nu_0 \partial \sigma} & \frac{\partial^2 \log L}{\partial \nu_1 \partial \sigma} & \frac{\partial^2 \log L}{\partial \sigma^2} \end{bmatrix}, \tag{9}$$

where

$$-\frac{\partial^2 \log L}{\partial \nu_0^2} = \frac{1}{\sigma^2}\sum_{i=1}^{k}\left\{\sum_{j=1}^{r_i}\exp\left(z_{j:n_i}\right) + (n_i - r_i)\exp(t_i^*)\right\},$$

$$-\frac{\partial^2 \log L}{\partial \nu_1^2} = \frac{1}{\sigma^2}\sum_{i=1}^{k}\left\{x_i^2\left[\sum_{j=1}^{r_i}\exp\left(z_{j:n_i}\right) + (n_i - r_i)\exp(t_i^*)\right]\right\},$$

$$-\frac{\partial^2 \log L}{\partial \sigma^2} = \frac{1}{\sigma^2}\sum_{i=1}^{k}\left\{\sum_{j=1}^{r_i}\left[z_{j:n_i}^2 \exp(z_{j:n_i}) + z_{j:n_i}\exp(z_{j:n_i}) - z_{j:n_i}\right]\right.$$
$$\left.+(n_i - r_i)\left[T_i^* \exp\left(t_i^*\right) + t_i^{*2}\exp\left(t_i^*\right)\right]\right\},$$

$$-\frac{\partial^2 \log L}{\partial \nu_0 \partial \nu_1} = \frac{1}{\sigma^2}\sum_{i=1}^{k}\left\{x_i\left[\sum_{j=1}^{n_i}\exp(z_{j:n_i}) + (n_i - r_i)\exp(t_i^*)\right]\right\},$$

$$-\frac{\partial^2 \log L}{\partial \nu_0 \partial \sigma} = \frac{1}{\sigma^2}\sum_{i=1}^{k}\left\{\sum_{j=1}^{r_i} z_{j:n_i}\exp(z_{j:n_i}) + (n_i - r_i)T_i^*\exp(t_i^*)\right\},$$

$$-\frac{\partial^2 \log L}{\partial \nu_1 \partial \sigma} = \frac{1}{\sigma^2}\sum_{i=1}^{k}\left\{x_i\left[\sum_{j=1}^{r_i} z_{j:n_i}\exp(z_{j:n_i}) + (n_i - r_i)t_i^*\exp(t_i^*)\right]\right\}.$$

Note that Paul and Thiagarajah (1996) also derived asymptotic variances and covariances of the MLEs of the parameters in a extreme value regression model with type-I censoring. Here, in order to compute the expected Fisher information in (9), we apply the double expectations formula

$$E[g(R_i, Z_{j:n_i})] = E_{R_i}\left\{E_{Z_{j:n_i}}[g(R_i, Z_{j:n_i})|R_i]\right\},$$

where g is a function and E_{R_i} and $E_{Z_{j:n_i}}$ are the expectations taken with respect to R_i and $Z_{j:n_i}$, respectively. To compute the expectation $E_Z(Z_{j:n_i})$, we apply a modification of the theorem given by Arnold et al. (1992) as follows.

Theorem 1 *Suppose that $X_1, X_2, \ldots, X_n$ is a random sample from an absolute continuous population with c.d.f. $F(\cdot)$ and p.d.f. $f(\cdot)$ and let $X_{1:n} < X_{2:n} < \cdots < X_{n:n}$ denote the order statistics obtained from this sample. Then, the conditional distribution of $X_{i:n}$ given that $X_{r:n} \le t < X_{r+1:n}$ for $0 \le i \le r$, is same as the distribution of the i-th order statistic in a sample of size r from a population with density function $f(\cdot)/F(t)$ which is the left-truncated distribution of $f(\cdot)$ at t.*

Proof See Appendix.

Using the result presented in Theorem 1, we have

$$E_Z\left(\sum_{j=1}^{r_i} Z_{j:n_i}\right) = r_i E_Z(Z|Z < t_i^*) = r_i\frac{G_1(t_i^*)}{F_1(t_i^*)},$$

$$E_Z\left(\sum_{j=1}^{r_i}\exp(Z_{j:n_i})\right) = r_i E_Z(e^Z|Z<t_i^*) = r_i\frac{F_2(t_i^*)}{F_1(t_i^*)},$$

$$E_Z\left(\sum_{j=1}^{r_i}Z_{j:n_i}\exp(Z_{j:n_i})\right) = r_i E_Z(Ze^Z|Z<t_i^*) = r_i\frac{G_2(t_i^*)}{F_1(t_i^*)},$$

$$E_Z\left(\sum_{j=1}^{r_i}Z_{j:n_i}^2\exp(Z_{j:n_i})\right) = r_i E_Z(Z^2e^Z|Z<t_i^*) = r_i\frac{H_2(t_i^*)}{F_1(t_i^*)},$$

where

$$F_\kappa(t) = \int_{-\infty}^{t}\frac{e^{\kappa x-e^x}}{\Gamma(\kappa)}dx,\quad G_\kappa(t) = \int_{-\infty}^{t}\frac{xe^{\kappa x-e^x}}{\Gamma(\kappa)}dx,\quad H_\kappa(t) = \int_{-\infty}^{t}\frac{x^2e^{\kappa x-e^x}}{\Gamma(\kappa)}dx.$$

Furthermore, the expected value of the number of failures at stress level x_i, R_i, is

$$E_{R_i}(R_i) = n_i F_1(t_i^*). \tag{10}$$

Therefore, the entries of expected Fisher information matrix can be expressed as

$$E\left(-\frac{\partial^2\log L}{\partial\nu_0^2}\right) = \frac{N}{\sigma^2}\sum_{i=1}^{k}q_i p_i,\quad E\left(-\frac{\partial^2\log L}{\partial\nu_1^2}\right) = \frac{N}{\sigma^2}\sum_{i=1}^{k}x_i^2 q_i p_i,$$

$$E\left(-\frac{\partial^2\log L}{\partial\sigma^2}\right) = \frac{N}{\sigma^2}\sum_{i=1}^{k}e_i p_i,\quad E\left(-\frac{\partial^2\log L}{\partial\nu_0\partial\nu_1}\right) = \frac{N}{\sigma^2}\sum_{i=1}^{k}x_i q_i p_i,$$

$$E\left(-\frac{\partial^2\log L}{\partial\nu_0\partial\sigma}\right) = \frac{N}{\sigma^2}\sum_{i=1}^{k}d_i p_i,\quad E\left(-\frac{\partial^2\log L}{\partial\nu_1\partial\sigma}\right) = \frac{N}{\sigma^2}\sum_{i=1}^{k}x_i d_i p_i,$$

where

$$p_i = \frac{n_i}{N},\ q_i = F_1(t_i^*),\ d_i = G_1(t_i^*)+F_1(t_i^*),\text{ and } e_i = H_1(t_i^*)+2G_1(t_i^*)+F_1(t_i^*).$$

For given values of N, t_c and $(x_1, x_2, \ldots, x_k)$, the problem of finding the optimal allocation $(n_1, n_2, \ldots, n_k)$ can be expressed as finding the optimal values of $(p_1, p_2, \ldots, p_k)$ with $\sum_{i=1}^{k}p_i = 1$. Since there is no close form solution for the optimization problem involving the above expected Fisher information matrix, the optimal allocation under different optimality criteria related to the expected Fisher information matrix can be determined numerically by direct search method. Computer program written in R (R Core Team 2019) is used to compute the

expected Fisher information and variance-covariance matrices as well as obtaining the optimal allocations. The program is available from the authors upon request.

Suppose that we are interested in the estimation of the model parameters (ν_0, ν_1, σ), the following three different optimality criteria can be considered:

[C1] Maximization of the determinant of the Fisher information matrix:
This is known as D-optimality, wherein the determinant of the Fisher information matrix is maximized, which results in minimum volume for the Wald-type joint confidence region for the model parameter (ν_0, ν_1, σ).

[C2] Minimization the asymptotic variance of $\hat{\nu}_1$:
In many situations, the slope parameter ν_1 is more important since it links the mean lifetimes and the stress levels. Therefore, the precision of the estimator of ν_1 is desired. This is known as V-optimality.

[C3] Minimization of the trace of the asymptotic variance-covariance matrix $(\mathbf{I}^{-1})$ of the MLEs:
This criterion is known as A-optimality, which minimizes the sum of the variances of the parameter estimates and provides an overall measures of variability from the marginal variabilities.

4 Sensitivity Analysis

Since the expected Fisher information matrix depends on the model parameters ν_0, ν_1 and σ, the optimal allocation also depends on these parameter values. In other words, one has to specify the values of parameters ν_0, ν_1 and σ in order to obtain an optimal allocation. In practice, these values are usually provided based on prior knowledge of the parameters or opinions from experts. Mis-specification of these parameter values may lead to a different optimal allocation which affect the efficiency of statistical inference from the experiment. Therefore, it is important to ensure that the optimal allocation obtained from the proposed method is robust to the uncertainty of parameters. Sensitivity analysis is used here to study the influence of mis-specification of the model parameters to the effectiveness of the statistical inference based on the optimal allocation. This provides important information to the practitioners to ensure small to modest mis-specifications in model parameters will not result in unacceptable changes in the precision of estimation.

In order to study the sensitivity of the optimal allocation, we define the relative efficiency of a set of parameter values $\boldsymbol{\theta}^*$ compared to the set of true parameter values $\boldsymbol{\theta}_0$ based on the optimal criteria **[C1]**, **[C2]** and **[C3]**, respectively, as

$$\mathrm{RE_D}(\boldsymbol{\theta}^*) = \frac{\det[\mathbf{I}(\boldsymbol{\theta}_0)] \text{ corresponding to the optimal allocation based on } \boldsymbol{\theta}^*}{\det[\mathbf{I}(\boldsymbol{\theta}_0)] \text{ corresponding to the optimal allocation based on } \boldsymbol{\theta}_0},$$

$$\mathrm{RE_V}(\boldsymbol{\theta}^*) = \frac{\mathrm{var}(\hat{\nu}_1) \text{ corresponding to the optimal allocation based on } \boldsymbol{\theta}_0}{\mathrm{var}(\hat{\nu}_1) \text{ corresponding to the optimal allocation based on } \boldsymbol{\theta}^*},$$

$$\text{and } \mathrm{RE_A}(\boldsymbol{\theta}^*) = \frac{\mathrm{tr}([\mathbf{I}^{-1}(\boldsymbol{\theta}_0)]) \text{ corresponding to the optimal allocation based on } \boldsymbol{\theta}_0}{\mathrm{tr}([\mathbf{I}^{-1}(\boldsymbol{\theta}_0)]) \text{ corresponding to the optimal allocation based on } \boldsymbol{\theta}^*}.$$

Here, the experimental duration t_c is assumed to be fixed. The closer the values of $\mathrm{RE_D}(\boldsymbol{\theta}^*)$, $\mathrm{RE_V}(\boldsymbol{\theta}^*)$, $\mathrm{RE_A}(\boldsymbol{\theta}^*)$ to 1, the less sensitive the optimal allocation to the mis-specification of the model parameters.

Beside studying the effect of the mis-specification of the model parameters to the objective functions, we also consider the effect of the experimental duration t_c to the objective functions. This provides valuable insights on the effect of experiential durations and hence the cost of the experiment induced by the time spent on the experiment to the effectiveness of statistical inference. We define the relative efficiency of the experiment with duration t_c compared to experiments with complete sample (i.e., $t_c \to +\infty$) based on the optimal criteria [**C1**], [**C2**] and [**C3**], respectively, as

$$\mathrm{RE}^*_{\mathrm{D}}(t_c) = \frac{\det[\mathbf{I}(\boldsymbol{\theta}_0)] \text{ when the experiment stopped at } t_c}{\det[\mathbf{I}(\boldsymbol{\theta}_0)] \text{ based on complete sample}},$$

$$\mathrm{RE}^*_{\mathrm{V}}(t_c) = \frac{\mathrm{var}(\hat{\nu}_1) \text{ based on complete sample}}{\mathrm{var}(\hat{\nu}_1) \text{ when the experiment stopped at } t_c},$$

$$\text{and } \mathrm{RE}^*_{\mathrm{A}}(t_c) = \frac{\mathrm{tr}([\mathbf{I}^{-1}(\boldsymbol{\theta}_0)]) \text{ based on complete sample}}{\mathrm{tr}([\mathbf{I}^{-1}(\boldsymbol{\theta}_0)]) \text{ when the experiment stopped at } t_c}.$$

Note that the values of the objective functions for complete sample in the above definitions can be obtained by using the formulae provided in Ng et al. (2007). Once again, the closer the values of $\mathrm{RE}^*_{\mathrm{D}}(t_c)$, $\mathrm{RE}^*_{\mathrm{V}}(t_c)$ and $\mathrm{RE}^*_{\mathrm{A}}(t_c)$ to 1, the less sensitive the optimal allocation to the experimental time.

Since the results of sensitivity analysis are depending on many factors such as the number of stress levels k, the stress levels $(x_1, x_2, \ldots, x_k)$ and the true parameter values of ν_0, ν_1 and σ, therefore, we choose to use an numerical example in the following section to illustrate the idea of the sensitivity analysis and provide recommendations.

5 Numerical Illustrations

McCool (1980) presented the failure times for hardened steel specimens in a rolling contact fatigue test; 10 independent observations were taken at each of four values of contact stress. He assumed that at stress level s, failure times follow a Weibull distribution with a scale parameter α related to s by a power law relationship $\alpha = cs^q$, where c and q are constants, and with a shape parameter δ independent of s. For our purpose, suppose that the experiment was terminated at time $t_c = 4$. The observations are presented in Table 1.

Table 1 The data of McCool (1980) if censored at $t_c = 4.0$

Stress (10^6 psi)	Ordered failure times
0.87	1.67, 2.20, 2.51, 3.00, 3.90, 4.00+, 4.00+, 4.00+, 4.00+, 4.00+
0.99	0.80, 1.00, 1.37, 2.25, 2.95, 3.70, 4.00+, 4.00+, 4.00+, 4.00+
1.09	0.012, 0.18, 0.20, 0.24, 0.26, 0.32, 0.32, 0.42, 0.44, 0.88
1.18	0.073, 0.098, 0.117, 0.135, 0.175, 0.262, 0.270, 0.350, 0.386, 0.456

+ right-censored

Table 2 Model parameter values considered in the sensitivity analysis

Model coefficient	Low −	Mid-point 0	High +
ν_0	0.531	0.664	0.800
ν_1	−10.322	−12.903	−15.484
σ	0.654	0.818	0.982

Table 3 Optimal allocations based on $\boldsymbol{\theta}^*$ and its relative efficiency compared to $\boldsymbol{\theta}_0$, where the values of ν_0, ν_1 and σ (−, 0 and +) are presented in Table 2

Setting	υ_0	υ_1	σ	[**C1**]	$\text{RE}_\text{D}(\boldsymbol{\theta})$	[**C2**]	$\text{RE}_\text{V}(\boldsymbol{\theta})$	[**C3**]	$\text{RE}_\text{A}(\boldsymbol{\theta})$
0	0	0	0	(0,19,0,21)	1.0000	(12,11,0,17)	1.0000	(12,11,0,17)	1.0000
1	−	−	−	((1,18,0,21)	0.9864	(19,4,0,17)	0.9620	(19,4,0,17)	0.9585
2	−	−	+	(12,5,0,23)	0.7321	(23,0,0,17)	0.8962	(23,0,0,17)	0.8907
3	−	+	−	(0,19,0,21)	1.0000	(0,20,0,20)	0.9335	(0,20,0,20)	0.9361
4	−	+	+	(0,19,0,21)	1.0000	(12,11,0,17)	1.0000	(11,12,0,17)	0.9999
5	+	−	−	(0,19,0,21)	1.0000	(12,11,0,17)	1.0000	(12,11,0,17)	1.0000
6	+	−	+	(9,8,0,23)	0.8129	(23,0,0,17)	0.8962	(23,0,0,17)	0.8907
7	+	+	−	(0,18,0,22)	0.9994	(0,21,0,19)	0.9342	(0,21,0,19)	0.9375
8	+	+	+	(0,18,0,22)	0.9994	(5,17,0,18)	0.9760	(4,18,0,18)	0.9713

Based on the Type-I censored sample presented in Table 1, the MLEs of the parameters ν_0, ν_1 and σ are $\hat{\nu}_0 = 0.664$, $\hat{\nu}_1 = -12.903$ and $\hat{\sigma} = 0.818$. To plan a future experiment with the same stress levels $(x_1, x_2, x_3, x_4) = (\ln 0.87, \ln 0.99, \ln 1.09, \ln 1.18)$, $N = 40$ and $t_c = 4$, suppose these MLEs are used as hypothesized values. Following Monroe et al. (2010) wherein they suggested the true values of the model parameters deviate no more than 20% from the hypothesized values, the minimum and maximum values for each parameter estimate are computed as 20% deviations from these estimates and they are presented in Table 2. Specifically, in Table 2, the "Low −" value is the estimate multiply by 0.8 and the "High +" value is the estimate multiply by 1.2.

The relative efficiency of a set of parameter values $\boldsymbol{\theta}^*$ compared to the set of true parameter values $\boldsymbol{\theta}_0 = (0.664, -12.903, 0.818)$ based on the optimal criteria [**C1**], [**C2**] and [**C3**] are presented in Table 3.

From Table 3, we observe that the optimal allocation based on V-optimality and A-optimality are relatively insensitive to the deviations in the parameter values because all the relative efficiencies are greater than 89%. However, the optimal

allocation based on D-optimality is relatively sensitive to the deviations of the parameter values, especially on the parameter σ. For instance, in Table 3, Settings 2 and 6 give relative efficiencies $\mathrm{RE_D}(\boldsymbol{\theta}) = 73.21\%$ and 81.29%, respectively. This suggests that if one wants to avoid substantial loss in the efficiency of estimation when D-optimality is considered, extra effort is required to increase the accuracy in specifying the parameter σ during the design stage.

To study the effect of the duration t_c in this numerical example, the plots of the $\mathrm{RE^*_D}(t_c)$, $\mathrm{RE^*_V}(t_c)$ and $\mathrm{RE^*_A}(t_c)$ versus t_c are presented in Fig. 1. It is not a surprise to see that the relative efficiencies increase towards 1 as the duration t_c increases. The rate of change of the relative efficiencies among these three optimal criteria are similar.

To further study the sensitivity of the optimal allocations against different parameter settings, we use the same parameter values as before but changing the stress levels (x_1, x_2, x_3, x_4). Three different sets of log stress levels are considered:

1. $(x_1, x_2, x_3, x_4) = (-0.200, \ -0.100, \ -0.046, \ 0.083)$;
2. $(x_1, x_2, x_3, x_4) = (-0.081, \ -0.052, \ -0.021, \ 0.083)$;
3. $(x_1, x_2, x_3, x_4) = (-0.005, \ 0.006, \ 0.020, \ 0.083)$.

These three settings of stress levels are selected to make the expected proportions of observed failures to be 0.1, 0.5 and 0.9, respectively, which can reflect different levels of censoring (heavy, moderate and light). To compute the relative efficiencies $\mathrm{RE_D}(\boldsymbol{\theta}^*)$, $\mathrm{RE_V}(\boldsymbol{\theta}^*)$ and $\mathrm{RE_A}(\boldsymbol{\theta}^*)$, we keep two of the three parameters fixed at the hypothetical true values and change the remaining one. Plots of the relatively efficiencies versus the parameter being varies are presented in Figs. 2, 3, and 4.

To observe the effect of the intercept parameter ν_0, we can focus on the plots in the first column of Figs. 2, 3, and 4. From Fig. 2, we can observe that the optimal allocations are not sensitive to the intercept parameter for the D-optimality regardless to the proportions of censoring. Similar conclusions can be drawn for the other two optimal criteria by looking at the plots in the first column of Figs. 3 and 4. To study the effect of the slope parameter ν_1, we can focus on the plots in the second column of Figs. 2, 3, and 4. We observe that the optimal allocations are quite sensitive to the slope parameter. The sensitivity of the optimal allocations also depends on the proportion of censoring whereas the smaller the censoring proportions, the less sensitive are the optimal allocations. The effect of σ is similar to the slope parameter. It can be explained as follows. Both slope parameter and σ determine the relationship between the stress levels x_i and the proportions of observing failure and these proportions play major role on the determination of optimal allocations.

6 Concluding Remarks

In this paper, we provide a framework on obtaining the optimal allocations in a multi-level accelerated life testing experiment under time censoring when an

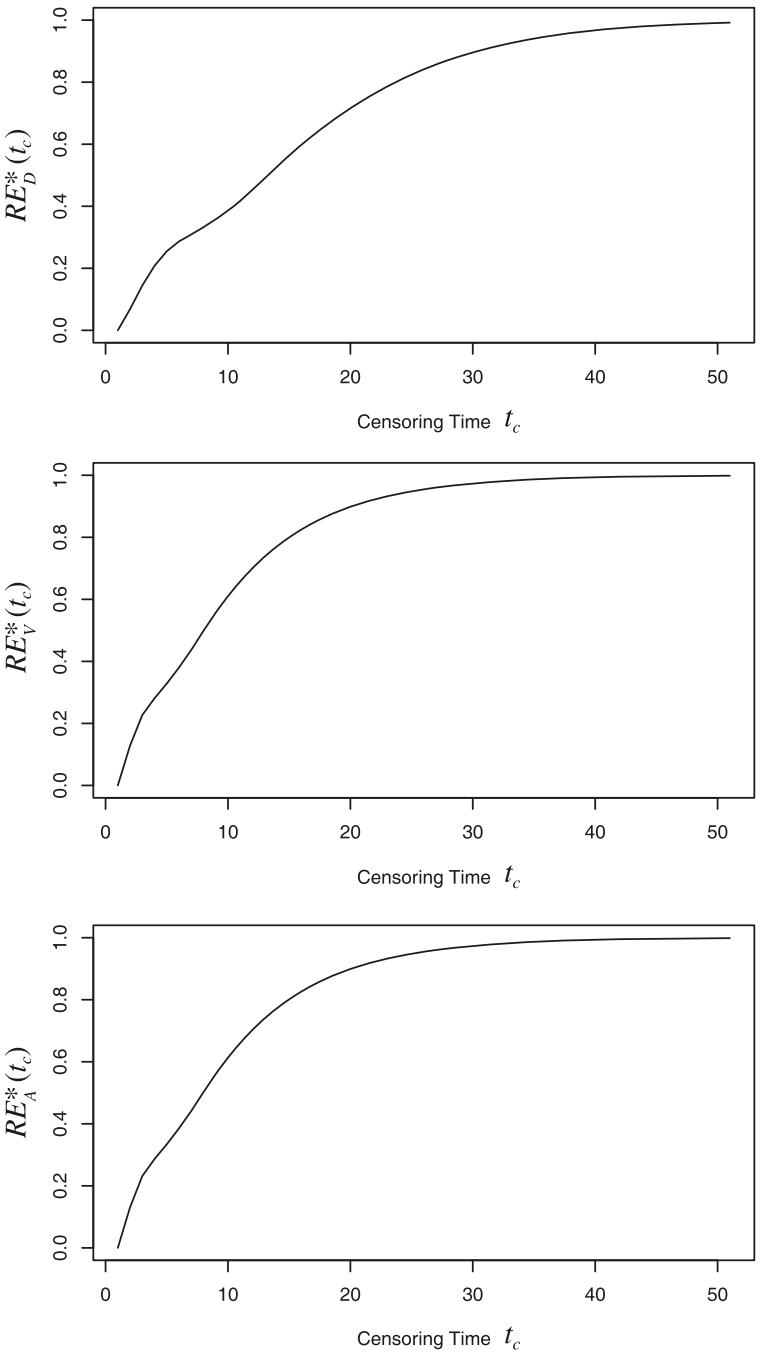

Fig. 1 Relative efficiencies $RE_D^*(t_c)$, $RE_V^*(t_c)$ and $RE_A^*(t_c)$ versus censoring time t_c

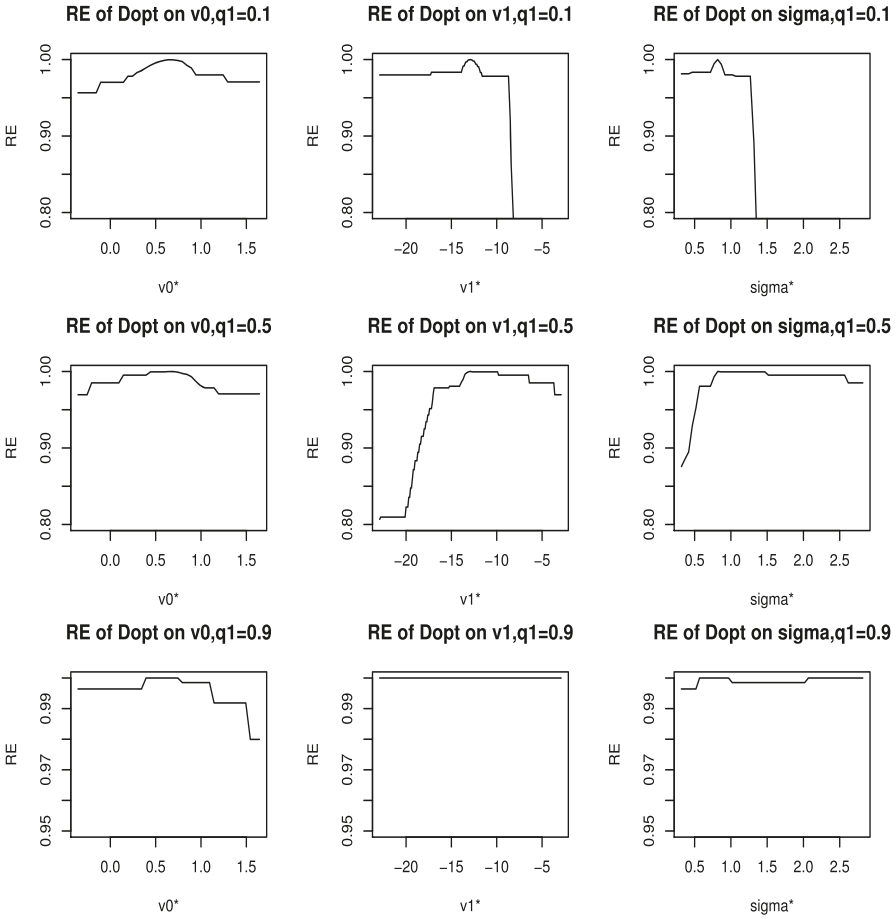

Fig. 2 Relative efficiencies $\mathrm{RE}_{\mathrm{D}}(\boldsymbol{\theta}^*)$ for the three different settings

extreme-value regression model is used for statistical analysis. The expected Fisher information and asymptotic variance-covariance matrices for the MLEs are derived. Three different commonly used optimal criteria are considered and computer programs to obtain the optimal allocation for each criterion are developed and made available. Due to the optimal allocations are inevitably depending on the model parameters, we study the sensitivity of optimal allocation on the model parameters as well as the censoring proportions. These sensitivity analyses provide important information and guidelines to practitioners on how much resources are needed to obtain crucial preliminary information on the parameter values. These results will be useful in avoiding serious lost in precision due to mis-specification of parameter values in practice.

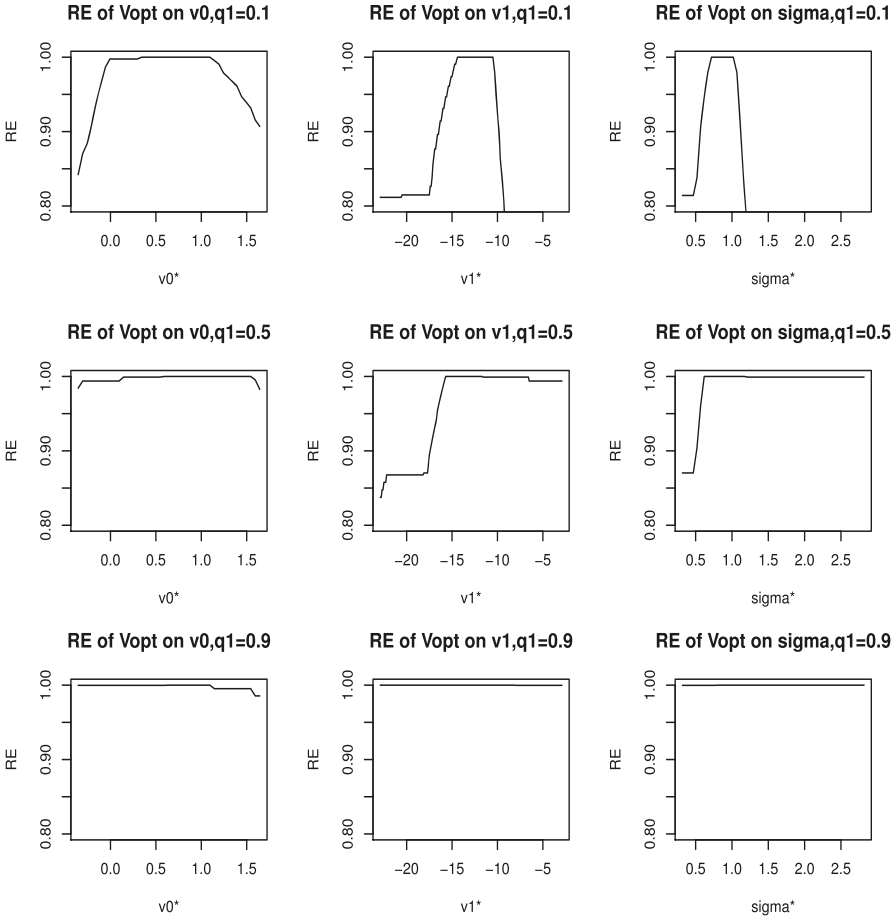

Fig. 3 Relative efficiencies $\mathrm{RE}_{\mathrm{V}}(\boldsymbol{\theta}^*)$ for the three different settings

Appendix: Proof of Theorem 1

Suppose that $X_1, X_2, \ldots, X_n$ is a random sample from an absolute continuous population with c.d.f. $F(\cdot)$ and p.d.f. $f(\cdot)$ and let $X_{1:n} < X_{2:n} < \cdots < X_{n:n}$ denote the order statistics obtained from this sample. The joint probability density function of $X_{i:n}$, $X_{r:n}$ and $X_{r+1:n}$ is

$$f_{i,r,r+1:n}(x_i, x_r, x_{r+1}) = \frac{n!}{(i-1)!(r-i-1)!(n-r-1)!} f(x_i) f(x_r) f(x_{r+1}) \times [F(x_i)]^{i-1} [F(x_r) - F(x_i)]^{r-i-1} [1 - F(x_i)]^{n-r-1}, \quad x_i < x_r < x_{r+1}.$$

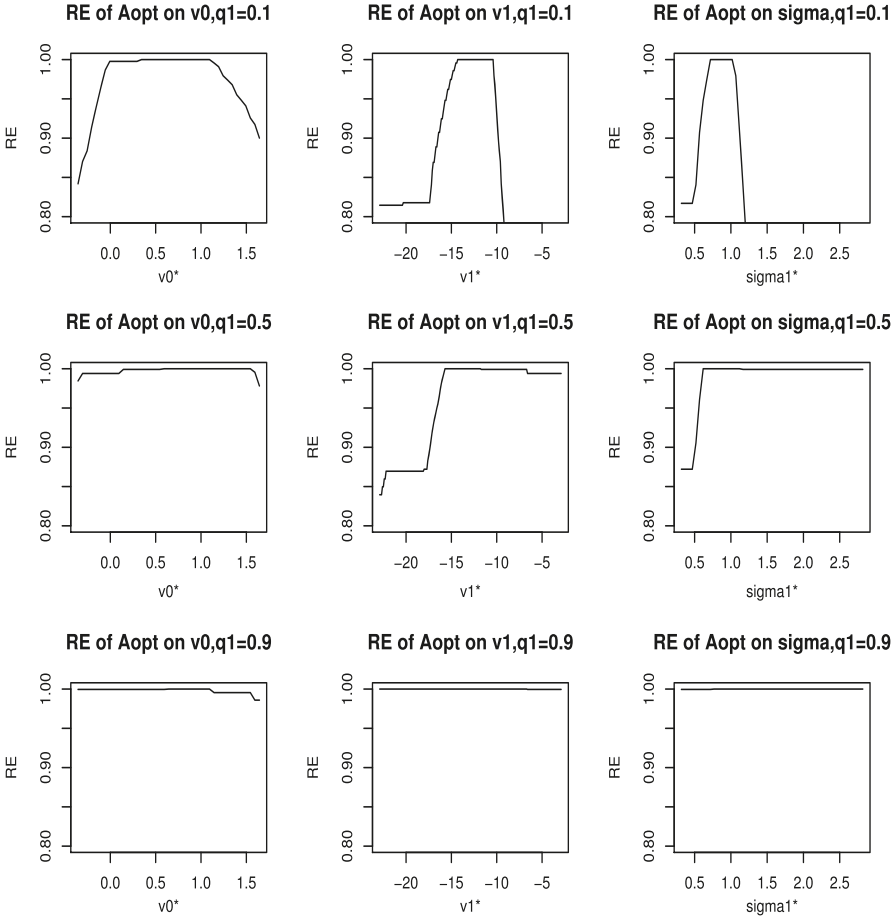

Fig. 4 Relative efficiencies $\mathrm{RE}_{\mathrm{A}}(\boldsymbol{\theta}^*)$ for the three different settings

Note that the probability that $X_{r:n} < t < X_{r+1:n}$ is equivalent to the probability that exactly r out of n observations are less than t, i.e.,

$$\Pr(X_{r:n} < t < X_{r+1:n}) = \frac{n!}{r!(n-r)!}[F(t)]^r[1-F(t)]^{n-r}.$$

Hence, given $X_{r:n} < t < X_{r+1:n}$, the probability density function of $X_{i:n}$ can be obtained as

$$f_{i:n}(x_i|x_{r:n} < t < x_{r+1:n}) = \frac{\int_t^\infty \int_{x_i}^t f_{i,r,r+1:n}(x_i, x_r, x_{r+1})dx_r dx_{r+1}}{\Pr(X_{r:n} < t < X_{r+1:n})}.$$

Since we have

$$\int_t^\infty f(x_{r+1})[1-F(x_{r+1})]^{n-r-1}dx_{r+1} = \int_0^{1-F(t)} u^{n-r-1}du = \frac{[1-F(t)]^{n-r}}{(n-r)}$$

$$\text{and } \int_{x_i}^t f(x_{r+1})[F(x_r)-F(x_i)]^{r-i-1}dx_r = \int_0^{F(t)-F(x_i)} u^{r-i-1}du = \frac{[F(t)-F(x_i)]^{r-i}}{(r-i)},$$

then we can write

$$\int_t^\infty \int_{x_i}^t f_{i,r,r+1:n}(x_i, x_r, x_{r+1})dx_r dx_{r+1}$$
$$= \frac{n!}{(i-1)!(r-i)!(n-r)!} f(x_i)[F(x_i)]^{i-1}[F(t)-F(x_i)]^{r-i}.$$

Therefore, the conditional distribution of $X_{i:n}$ given that $X_{r:n} \le t < X_{r+1:n}$ for $0 \le i \le r$, is

$$f_{i:n}(x_i | x_{r:n} < t < x_{r+1:n})$$
$$= \frac{r!}{(r-i)!(i-1)!} \frac{f(x_i)[F(x_i)]^{i-1}[F(t)-F(x_i)]^{n-i}}{[F(t)]^r}$$
$$= \frac{r!}{(r-i)!(i-1)!} \left[\frac{f(x_i)}{F(t)}\right] \left[\frac{F(x_i)}{F(t)}\right]^{i-1} \left[1-\frac{F(x_i)}{F(t)}\right]^{n-i},$$

for $x_i < t$, which is the distribution of the i-th order statistic in a sample of size r from a population with left-truncated distribution $f(\cdot)/F(t)$.

Acknowledgements Our sincere thanks go to the reviewer for the valuable comments and suggestions. The authors would also like to thank the editors of this book volume for an invitation which provided an impetus for preparing this article.

References

Arnold, B. C., Balakrishnan, N., & Nagaraja, H. N. (1992). *A first course in order statistics*. New York: Wiley.

Atkinson, A. C., & Donev, A. N. (1992). *Optimum experimental designs*. Oxford: Oxford University Press.

Bai, D. S., & Chung, S. W. (1991). An optimal design of accelerated life test for exponential distribution. *Reliability Engineering and System Safety, 31*, 57–64.
Bai, D. S., & Chung, S. W. (1992). Optimal design of partially accelerated life tests for the exponential distribution under type-I censoring. *IEEE Transactions on Reliability, 41*, 400–406.
Bai, D. S., & Kim, M. S. (1993). Optimum simple step-stress accelerated life tests for the Weibull distribution and type I censoring. *Naval Research Logistics, 40*, 193–210.
Box, G. E. P., & Draper, N. R. (1987). *Empirical model building and response surfaces*. New York: Wiley.
Elfving, G. (1952). Optimum allocation in linear regression theory. *Annual of Mathematical Statistics, 23*, 255–262.
Fedorov, V. V. (1972). *Theory of optimal experiments*. New York: Academic.
Gaylor, D. W., & Sweeny, H. C. (1965). Design for optimal prediction in simple linear regression. *Journal of the American Statistical Association, 60*, 205–216.
Ka, C. Y., Chan, P. S., Ng, H. K. T., & Balakrishnan, N. (2011). Optimal sample size allocation for multi-level stress testing with Weibull regression under type-II censoring. *Statistics, 45*, 257–279.
Liski, E. P., Mandal, N. K., Shah, K. R., & Sinha, B. K. (2002). *Topics in optimal design*. New York: Springer.
McCool, J. I. (1980). Confidence limits for Weibull regression with censored data. *IEEE Transactions on Reliability, 29*, 145–150.
Monroe, E. C., Pan, R., Anderson-Cook, C. M., Montgomery, D. G., & Borror, C. M. (2010). Sensitivity analysis of optimal designs for accelerated life testing. *Journal of Quality Technology, 42*, 121–135.
Nelson, W. (2005a). A bibliography of accelerated test plans, part I: Overview. *IEEE Transactions on Reliability, 54*, 194–197.
Nelson, W. (2005b). A bibliography of accelerated test plans, part II: References. *IEEE Transactions on Reliability, 54*, 370–373.
Nelson, W., & Kielpinski, T. J. (1976). Theory for optimum censored accelerated life tests for normal and lognormal life distributions. *Technometrics, 18*, 105–114.
Nelson, W., & Meeker, W. Q. (1978). Theory for optimum accelerated censored life tests for Weibull and extreme value distributions. *Technometrics, 20*, 171–177.
Ng, H. K. T. (2010). Censoring methodology. In M. Lovric (Ed.), *International encyclopedia of statistical science*. New York: Springer.
Ng, H. K. T., Balakrishnan, N., & Chan, P. S. (2007). Optimal sample size allocation for tests with multiple levels of stress with extreme value regression. *Naval Research Logistics, 54*, 237–249.
O'Brien, T. E., & Funk, G. M. (2003). A gentle introduction to optimal design for regression models. *The American Statistician, 57*, 265–267.
Paul, S. R., & Thiagarajah, K. (1996). Approximate variance covariance of maximum likelihood estimators for the parameters of extreme value regression models for censored data. *Sankhya B, 58*, 28–37.
R Core Team (2019). *R: A language and environment for statistical computing*. R Foundation for Statistical Computing, Vienna, Austria. http://www.R-project.org.
SAS Institute Inc. (2008). *SAS/STAT® 9.2 user's guide*. Cary, NC: SAS Institute Inc.
Seber, G. A. F., & Wild, C. J. (1989). *Nonlinear regression*. New York: Wiley.
Silvey, S. D. (1980). *Optimal design*. New York: Chapman and Hall.

Spatial Interpolation of Extreme PM_1 Values Using Copulas

Alfred Stein, Fakhereh Alidoost, and Vera van Zoest

Abstract Air quality is a common cause for respiratory health problems. It shows high temporal and spatial variability within urban areas and currently sensors are installed to monitor air quality. The objective of this paper is to investigate its spatial variability during peak hours. Spatial statistical methods are based upon copula theory, integrating distributions from different pollutants and at different locations. In this paper attention focused on PM_1 as one of the neglected components of air quality so far. Using observations from the Netherlands, we compared two hours: the first hour of the New Year, and an hour with a high traffic congestion. We investigated the size of the sensor network by analyzing observations from a city with 35 sensors with a city with four sensors and a city with one sensor. In the absence of an environmental standard for PM_1, the paper defined a threshold related to existing thresholds of $PM_{2.5}$ and PM_{10}. Results showed the adequacy of the large network, generating a varying pattern during the high peak hour, whereas in cities with less sensors both the spatial spread and possibly large values are missed. In particular the first hour of the New Year showed large concentrations and high probabilities that a threshold was exceeded, whereas the second peak hour showed values well below the threshold. We conclude that the mapping of PM_1 concentrations can well be done by copula interpolation. Using one or three sensors may save expenses, but this is at the cost of missing extreme values as well as spatial patterns. Both are potentially important for public health measures.

A. Stein (✉)
Faculty of Geo-Information Science and Earth Observation (ITC), University of Twente, Enschede, The Netherlands
e-mail: a.stein@utwente.nl

F. Alidoost
Netherlands E-Science Centre, Amsterdam, The Netherlands

V. van Zoest
Department of Information Technology, Uppsala University, Uppsala, Sweden

A. Bekker et al. (eds.), *Computational and Methodological Statistics and Biostatistics*, Emerging Topics in Statistics and Biostatistics,
https://doi.org/10.1007/978-3-030-42196-0_13

1 Introduction

There is an increasing concern about air quality. It is affected by heavy traffic, industrial activities, wood burning in hearths and incidental activities like firework, to name a few. Also, concerns exist on the effects of air quality on—in particular—respiratory health. In order to obtain a better quantitative understanding, extensive monitoring networks have been set up that measure the air quality at a high frequency. The idea behind such networks is that they not only help to measure local air quality, but also that they can cover the city as a whole. Moreover, with repeated observations, it becomes possible as well to monitor air quality during the day, between days in the weeks and over longer periods of times. Despite the sometimes large number of sensors, however, measurements are essentially point data and spatial interpolation is required to make a complete spatial coverage. In this paper we focus on assessing the air quality in situations of a low air quality.

Air quality has been studied extensively (Arslan et al. 2010; Khodarahmi et al. 2015; Zwozdziak et al. 2016; Van Zoest et al. 2018, 2019). Typical constituents that are monitored are particulate matters ($PM_{2.5}$ and PM_{10}), NO2 and ozone, whereas in the network that we use in our study also attention is given on PM_1 and ultrafine particles. In our recent work, attention has been given to the occurrence of outliers, to calibration and validation of the sensors and to spatial interpolation. For interpolation, increasing attention is given on copulas. They allow one to combine observations of a relatively low quality with related observations that are more abundant. They are essentially based upon distribution functions. The theory around copulas has been developed by Sklar (1973), and subsequent studies were done by Gräler and Bárdossy and Li (2008). Recently, several studies focusing on weather data have been carried out as well (Alidoost et al. 2018). In this paper we aim to pay attention to a few issues that were somewhat less represented so far. We will consider the number of sensors within a city, making a comparison between three cities: one city with an extensive network of 35 sensors, one city with four sensors and one city with one sensor. Short term economic considerations often aim to take as low a number of sensors as possible for financial reasons, whereas the amount of information thus obtained is limited. We will further consider two rather extreme situations in this paper: $\boldsymbol{d_1}$, the one single hour between 12 am and 1 am on New Year's morning when the use of fireworks is abundant in the three studied cities and $\boldsymbol{d_2}$, the one single hour between 7:30 and 8:30 am, in the early morning rush hour with intense traffic. We will consider the issue of time, where we use the 10 min values and compare them with aggregate values over a full hour. Finally, we consider the probabilities of exceeding threshold values set as national standards.

The objective of this paper is to predict high air quality values. We focus on PM_1 as one of the least known constituents in air quality. Research questions to address are: is the number of sensors adequate to obtain good insight into the high concentrations during peak hour; can we make probability maps of pollution levels exceeding an environmental threshold; and can registered covariates be used successfully for mapping PM_1 concentrations.

2 Methodology

2.1 Copulas

In this study we consider copulas as an interpolator. A copula is a joint distribution function, developed in the nineteen seventies, when it was shown that a copula assigns each pair of variables to their joint probability (Sklar 1973). The definition of copulas is without indication about the underlying process, and hence any joint distribution can be written in terms of a copula. The family distribution of copula can be different from the family of distributions of the pair of variables. For example, the two variables can each follow a Gaussian distribution, but their joint distribution (the copula) can be a non-Gaussian function. From the copula families reported in the literature (Joe 1993; Nelsen 2003; Demarta and McNeil 2005; Manner 2007), we selected the Gaussian, Student's t, Clayton, Gumbel and Frank families because other families lead to computational limitations (Gräler 2014). The definition of copula can also be extended to higher dimensions including several random variables in space. They allow us to include related variables and observations at nearby locations efficiently. To describe it, we focus on data that are collected at k locations $s_1, \ldots, s_k$, where s_i is expressed in terms of the x and y coordinates. We ignore the z coordinate as in this study the sensors are collected at approximately the same height, as well as the time coordinate as the sensors were not moved. We consider a location s_0 where a prediction is to be made, for example the node of a fine-mazed grid. The data in this study concern particulate matter concentrations, denoted by $PM_1(s)$. As a basic assumption to apply copulas, we take that the marginal cumulative distribution function F_1 of $PM_1(.)$ is identical at the locations $\{s_i\}_{i=1,\ldots,k}$.

We consider a copula that relates the distribution at s_0 with its distributions at the k nearest neighbors. The conditional expectation of this multivariate distribution is used as the optimal predictor, minimizing mean squared prediction error (Cressie 1993). The prediction value at location s_0 equals:

$$\hat{PM}_{1,mean}(s_0) = \int_0^1 F_1^{-1}(u) \cdot c_{k+1}(u|u_1, \ldots, u_k)\, du \tag{1}$$

where c_{k+1} is the conditional density.

$$c_{k+1}(u_0|u_1, \ldots, u_k) = \frac{c_{k+1}(u_0, u_1, \ldots, u_k)}{c_k(u_1, \ldots, u_k)} u_i, i \in [0, k]. \tag{2}$$

The expression u denotes rank of the variable $PM_1(.)$ evaluated in the observation points, e.g. $u_i = j$ if $PM_1(s_i)$ is the jth largest among the k observations. As in Alidoost et al. (2018), we will use the empirical marginal probability u_i at location s_i defined using the rank-order-transformation $u_i = \frac{\text{rank}(PM_1(s_i))}{N+1}$, where N denotes

the total number of observations. Such an empirical marginal distribution avoids using any theoretical marginal distributions that might affect the estimation of copula parameter. Kernel density estimation then allows us to obtain a continuous approximation of the marginal distribution F under the assumption of stationarity. Note that the empirical probabilities are limited to observations and therefore, the interpolation methods are unable to predict extreme values outside the range of the observations.

We will now turn to the use of covariates where we condition the distribution of PM_1 on related variables Y and Z. To do so, we need the conditional copula C of the predictand on the two covariates. The conditional copula is obtained as:

$$p_i = C\Big(U \leq u_i | \, V = v_i, \mathrm{W} = w_i\Big). \tag{3}$$

The conditional probability p_i is used as the probability of nearest neighbour i for copula in (1) and the final form of the predictor equals:

$$\hat{PM}_{1,mean} = \int_0^1 F_1^{-1}(u) \cdot c\,(U|U = p_1, \ldots, U = p_n, V = v_0, W = w_0)\, du. \tag{4}$$

In this way, the collocated covariates at the nearest neighbour i.e. v_i and w_i are incorporated into the predictor. This predictor is called mixed copula interpolator. A similar ranking transformation as is also applied to y_i and z_i.

In our study, the spatial copula interpolator including covariates addresses one variable $PM_1(s_0)$ and one or two covariates $PM_{2.5}(s_0)$ and $PM_{10}(s_0)$. The aim is to predict $\hat{PM}_1\,(s_0)$ with a finite sample of PM. Samples of $PM_{2.5}$ and PM_{10} are available at neighboring locations and are more abundant than those on X. The conditional copula density function in this specific setting then equals.

$$\begin{aligned} &c\,(U|U = u_1, \ldots, U = u_n, V = v_0, W = w_0)\,, \\ &\text{where } v_0 = F_{2.5}\,(PM_x\,(s_0))\,,\ w_0 = F_{10}\,(PM_x\,(s_0))\,, \end{aligned} \tag{5}$$

with the subscript 0 denoting an unvisited location, and $F_{2.5}$ and F_{10} are the marginal distribution functions of the covariates. By conditioning on $PM_{2.5}$ and PM_{10}, the collocated covariates at s_0, i.e. v_0 and w_0 are incorporated into the predictor. The conditional distribution can be extended to higher dimensions for including more than two covariates.

We evaluated the results using the mean absolute error (MAE), the mean absolute relative error (MARE), and the root mean squared error (RMSE). A leave-2-out cross validation is carried out using 50 runs.

2.2 Risk Maps

Of a specific concern for health and management aspects is the exceedance of environmental thresholds. A high probability of exceeding such a threshold value may indicate that health standards are not met and that for example windows have to be closed or traffic has to be reduced in intensity and speed. At present there are no official limit values for PM_1, and this leads to a vicious circle: there are no regular monitoring networks for PM_1 because there are no threshold values, hence no thresholds can be made because the limit values for health effects are unknown and hence the limit values for health effects are unknown because there are no regular monitoring networks. Our sensor networks can be helpful to assess these health effects. We propose to set a threshold value as the ratio between concentrations of PM_1 and $PM_{2.5}$ in Eindhoven, and then base a threshold on this ratio with the threshold of $PM_{2.5}$. The World Health Organization (WHO 2006) reported a guideline threshold of 25 $\mu g\ m^{-3}$ for $PM_{2.5}$ (daily mean). In addition, a threshold can be set on European law, we use the ratio with PM_{10}, for which the daily threshold value is 50 $\mu g\ m^{-3}$ (European Parliament and Council of the European Union 2008).

2.3 Data Description

The data were collected from the monitoring network in Eindhoven including the nearby village of Waalre, containing 35 air boxes that measure air quality at a 10 min interval. We considered two time stamps with reportedly high observations: $\boldsymbol{d_1}$: 0:00–01:00 on 01 Jan. 2017, i.e. New Year's eve, $\boldsymbol{d_2}$: 7:30–8:30 on 20 Nov. 2017, a day with very high traffic density. On $\boldsymbol{d_1}$, data from only 26 stations were received, whereas on $\boldsymbol{d_2}$ data from 31 stations were received. These 10-min data are point measurements within a 10 min interval. The air quality sensor network in Eindhoven (Fig. 1) was established by the AiREAS civil initiative in November 2013 and has continuously been operated since (Close 2016). The airboxes contain an array of sensors measuring particulate matter (PM), temperature and relative humidity (RH). Some airboxes also measure ozone (O_3), nitrogen dioxide (NO_2) or both. The focus of this study is on PM_1, which is measured in all airboxes. The airboxes are attached to lighting poles for power supply. The airboxes send data to a server every 10 min using a GPRS connection.

In addition to the sensors in the city of Eindhoven, the network has also been extended towards two cities in the same province: four sensors in the city of Breda and one sensor in the city of Helmond. On both $\boldsymbol{d_1}$ and $\boldsymbol{d_2}$ only three sensors in Breda provided data, albeit these were different sets of three. One of the aims of the paper is to consider the spatial representation of the information. The results included below will largely follow our analysis for $\boldsymbol{d_1}$, whereas that for $\boldsymbol{d_2}$ is included in the Appendix.

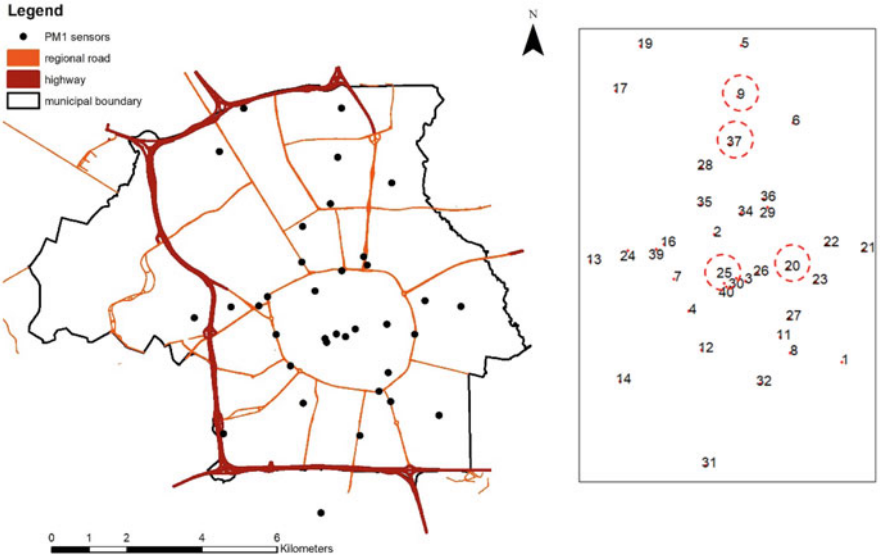

Fig. 1 Locations of the airboxes and conventional monitors in the city of Eindhoven (left) and position of the four boxes with relatively large values (right)

3 Results

3.1 Distribution of the Data

Considering the data in Table 1, we notice that the 10-min observations are around 20 $\mu g\ m^{-3}$. Peak values up to 33 $\mu g\ m^{-3}$ occur, throughout the hour. One hour observations of variables are obtained by the average of the observations at each location. The mean (standard deviation) of PM_1 are equal to 19.61 (4.97) for $\boldsymbol{d_1}$ and 5.04 (0.87) for $\boldsymbol{d_2}$. The marginal distribution of PM_1 is obtained by kernel density estimation, assumed to be the same throughout the city. Figure 2 shows the probability distributions of the PM_1 data. We note that the PM_1 values for the whole city display a smooth curve, ranging from 10 to slightly above 30 $\mu g\ m^{-3}$. We notice that in the city of Breda where only three spatial observations it is still possible to make a probability density curve. They showed different values, with the maximum at about 2/3 of the 26 sensors in Eindhoven. Although this situation could happen, the cities are within the same province and there is little reason to assume that the population is behaving differently and that hence different values are justifiable. The potential presence of any high, threatening value is absent in the curve. For the city of Helmond, with only one observation even the fitting of a distribution curve is impossible. We conclude from the density curves, that with 26 sensors a proper distribution can be fitted, but that using only three observations is likely to underestimate the risk.

Table 1 Descriptive statistics, predictions using the mixed copula interpolator and prediction evaluations on the observed locations

		Observation	Prediction			Observation	Prediction
t10	MAE	–	3.27	t50	MAE	–	3.00
	MARE	–	19.67		MARE	–	15.59
	RMSE	–	4.10		RMSE	–	3.59
	Corr	1.00	0.64		Corr	1.00	0.80
	Min	9.00	5.98		Min	12.00	14.06
	Mean	18.04	18.05		Mean	20.58	22.09
	Max	25.00	26.07		Max	33.00	36.41
t20	MAE	–	2.92	t60	MAE	–	4.43
	MARE	–	18.09		MARE	–	24.76
	RMSE	–	4.34		RMSE	–	5.59
	Corr	1.00	0.76		Corr	1.00	0.40
	Min	7.00	10.46		Min	13.00	13.57
	Mean	19.31	20.73		Mean	20.04	21.09
	Max	29.00	30.22		Max	32.00	35.68
t30	MAE	–	2.22	Hour average	MAE	–	2.53
	MARE	–	10.94		MARE	–	13.05
	RMSE	–	3.27		RMSE	–	3.42
	Corr	1.00	0.80		Corr	1.00	0.77
	Min	10.00	11.13		Min	10.50	12.25
	Mean	20.19	19.62		Mean	19.69	20.13
	Max	31.00	29.72		Max	30.00	30.08
t40	MAE	–	2.59				
	MARE	–	14.49				
	RMSE	–	3.40				
	Corr	1.00	0.82				
	Min	12.00	11.51				
	Mean	21.27	20.35				
	Max	32.00	30.90				

All data are expressed in $\mu g\ m^{-3}$. Time intervals are denoted as t10: 0:00–0:10, t20: 0:10–0:20, t30: 0:20–0:30, t40: 0:30–0:40, t50: 0:40–0:50 and t60: 0:50–1:00, on the 1st of January 2017

As a small related study, we considered four locations with relatively high observations. When considering those, we note that obviously low values are underrepresented, but that the extreme values on the upper side are present. Clearly, they show a different pattern as compared to the three stations in Breda. For the single observation in the city of Helmond we only observe that the value 26 $\mu g\ m^{-3}$ occurs five times and 21 $\mu g\ m^{-3}$ once. These values are on the low side, as compared to the Eindhoven data, but that may be due to the specific position of the sensor, and therefore they can not lead to any representative spatial conclusion.

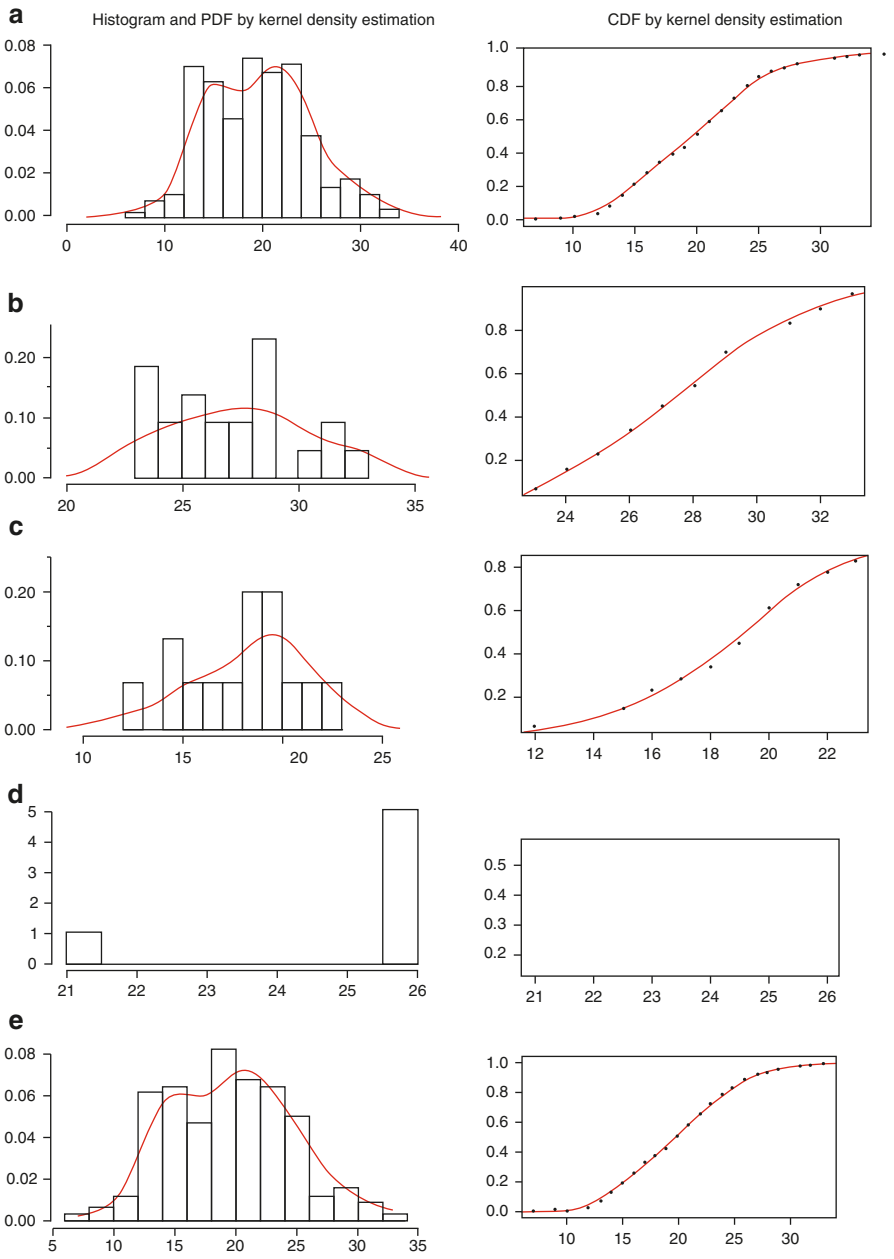

Fig. 2 Probability distribution function (PDF) and cumulative distribution function (CDF) for PM_1 on 2017 01 01. (**a**) for all the Eindhoven locations, (**b**) for four locations within the city with relatively high values, (**c**) for the three Breda locations, (**d**) for the single Helmond location and (**e**) for all the data

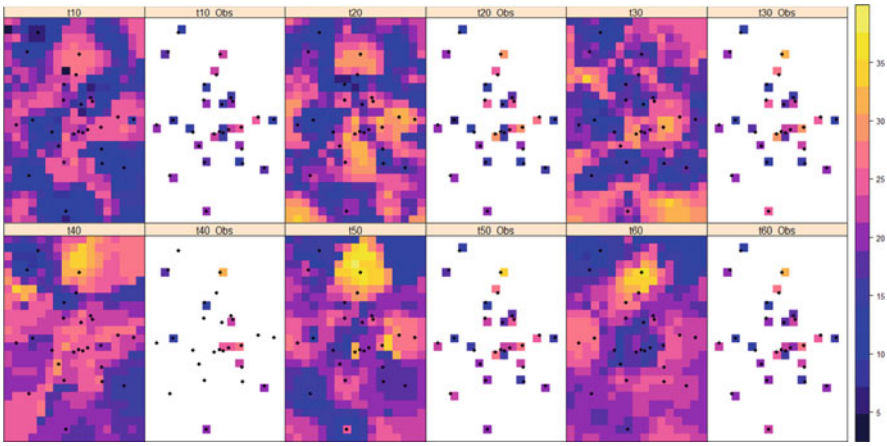

Fig. 3 PM_1 concentrations and their maps at intervals of 10 min after midnight, 1st January, 2018. Right are the concentrations, left are the maps

3.2 Spatial Patterns and Maps

Next, we interpolated the PM_1 data for Eindhoven for each of the six time intervals. Spatial correlations for three (946 m, 2157 m, 3465 m) and five spatial lags (561 m, 1352 m, 2110 m, 3028 m, 3855 m) are very weak (not shown). Figure 3 shows the observations (right) and the interpolated maps (left). The interpolated maps were the result of applying the mixed copula interpolation method including two covariates $PM_{2.5}$ and PM_{10}. Correlations of PM_1 with $PM_{2.5}$ and PM_{10} are equal to 0.53 and 0.01 on $\boldsymbol{d_1}$ and to 0.94 and 0.65 on $\boldsymbol{d_2}$, respectively. The PM_{10} and $PM_{2.5}$ maps (not shown) were thus used as covariates. The grid size of the maps is 500 m.

The maps show a clear pattern of high and low concentrations. These concentrations reach their peak in the southern part of the city earlier than in the northern part of the city. This could be caused by the prevailing wind direction. We notice that the high observations in the south are not really supported by observations as they occur as an extrapolation both at t20 and at t30. The high observations in the north are supported by a single observation point. At the earlier moments this is largely smoothed by the neighboring values with lower observations, but at t40 till t60 there clearly is a spatial peak in the concentrations. It may very well be that this subarea within the city has a much larger firework activity than the other parts of the city.

3.3 Towards Health Effects

We next considered the full hour data, taken as the average of the 10 min data, resulting in Fig. 4. Similar as for the 10 min data, the interpolated PM_1 data for $\boldsymbol{d_1}$ was supported by the two covariates $PM_{2.5}$ and PM_{10} using the mixed copula interpolation method. The $PM_{2.5}$ and PM_{10} maps are the results of copula

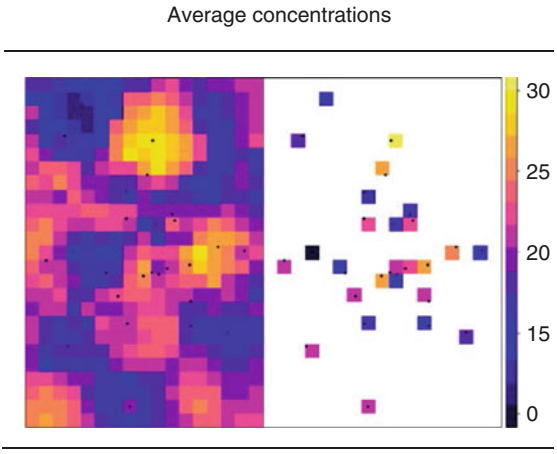

Fig. 4 Map of the average concentration between midnight and 1 am, on January 1stm 2018. Right are the concentrations, left is the map

interpolation method (not shown). The spatial resolution of the map is 500 m. The high values on the western side of the city are supported by less data and should be interpreted with care.

The three evaluation criteria are listed in Table 1. Because of the weak spatial correlations, non-spatial dependencies dominate spatial dependencies and methods including covariates performed better. The RMSE value is largest at t60, which indicates that at that moment of the night the predictive quality of the interpolator becomes less reliable. This may be caused by prevailing weather conditions that result in a more scattered type of concentrations. It may, for instance, be very well the case that the single peak value in the northern part of the city is the cause.

3.4 Risk Maps

We finally produced risk maps, where in the absence of European or World Health Organization (WHO) standards we proceeded as follows taking both the WHO guideline threshold of 25 μg m^{-3} for $PM_{2.5}$ and the threshold based on European law, equal to 50 μg m^{-3} for PM_{10}. We found the average $\overline{PM}_1$ of the PM_1 data in Eindhoven equal 6.08, the average $\overline{PM}_{2.5}$ of $PM_{2.5}$ equal to 8.56 μg m^{-3} and the average $\overline{PM}_{10}$ of PM_{10} equal to 15.12 μg m^{-3}, taken as daily values for all the data in 2015. The WHO $PM_{2.5}$-based threshold value then equals $6.08/8.56 \times 25 = 17.8$ μg m^{-3}, whereas the EU PM_{10}-based threshold equals $6.08/15.12 \times 50 = 20$ μg m^{-3}. Both thresholds are an approximation only, where the first one seems to be more reliable because it takes more account of the smaller particles in $PM_{2.5}$ that have greater health effects than PM_{10}. For PM_1, the health

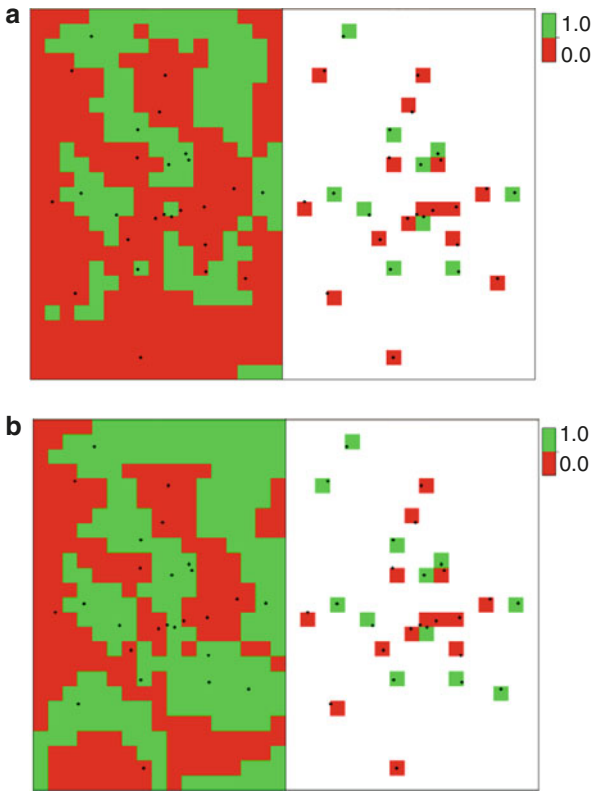

Fig. 5 Risk maps for Eindhoven on $\boldsymbol{d_1}$, in (**a**) for the WHO based threshold of 17.8, and in (**b**) for the EU based threshold equal to 20. The risk maps are produced using: hourly averages of interpolated maps (the left images), hourly averages of observed values (the right images)

effects are even greater than $PM_{2.5}$, and more of those small particles fit into 1 μg m^{-3}. The risk maps are shown in Fig. 5.

We notice from these maps that the area for exceeding the threshold WHO-based is larger than that of exceeding the EU based threshold, as the latter has a higher value and hence will less likely be exceeded. These maps have to be treated with care, as both thresholds consider daily averages, whereas we have hourly data. In that sense, it is difficult to base any policy measures on these maps.

3.5 A Comparison Between the Two Different Dates

Tables 2 and 3 show the results for the two different dates. Table 2 that displays leave-2-out cross validation shows substantially lower values at $\boldsymbol{d_2}$ than at $\boldsymbol{d_1}$. We interpret this that the firework related high PM_1 concentrations shows higher values

Table 2 The average of the three evaluation criteria obtained by 50 runs of the leave-2-out cross validation using observations in Eindhoven only, excluding Waalre, Breda and Helmond. Predictions are the results of applying the spatial copula interpolator including covariates

d_1	MAE	MARE (%)	RMSE	d_2	MAE	MARE (%)	RMSE
1: no covariate	4.37	22.31	5.11		0.47	10.07	0.51
2: with PM_{10}	4.42	22.85	5.10		0.46	9.53	0.52
3: with $PM_{2.5}$	4.26	22.13	4.65		0.26	5.36	0.29
4: with PM_{10} and $PM_{2.5}$	3.68	18.95	4.02		0.26	5.24	0.28

Table 3 The three evaluation criteria, the minimum, maximum, mean and correlations of observations and predictions using observations in Eindhoven only, excluding Waalre, Breda and Helmond. Predictions are the results of applying the spatial copula interpolator including covariates

Interpolators on d_1	MAE	MARE (%)	RMSE	Correlation	Minimum	Mean	Maximum
1: no covariate	3.36	18.30	4.10	0.72	16.99	19.40	21.42
2: with PM_{10}	3.47	18.94	4.21	0.63	16.96	19.41	21.71
3: with $PM_{2.5}$	3.00	16.62	3.88	0.62	14.83	19.86	27.40
4: with PM_{10} and $PM_{2.5}$	1.64	8.65	2.18	0.90	13.67	20.15	28.89
Observations	–	–	–	–	10.50	19.61	30.00
Interpolators on d_2							
1: no covariate	0.71	13.88	0.93	0.11	3.99	5.06	6.33
2: with PM_{10}	0.53	10.23	0.74	0.51	4.25	5.02	6.70
3: with $PM_{2.5}$	0.29	5.36	0.39	0.90	3.83	5.00	6.86
4: with PM_{10} and $PM_{2.5}$	0.24	4.51	0.35	0.92	3.79	5.01	7.08
Observations	–	–	–	–	4.00	5.04	8.00

and more spatial variation than traffic induced PM_1 concentrations. We further note that for d_1 inclusion of $PM_{2.5}$ as a covariate results in reduction of the RMSE values, whereas inclusion of both the covariates PM_{10} and $PM_{2.5}$ results in a further reduction. This is not surprising, as PM_1 covers a larger fraction of $PM_{2.5}$ than of PM_{10} and hence has a higher correlation. Therefore the PM_1 map has a higher similarity with the $PM_{2.5}$ map than with the PM_{10} map leading to a larger reduction in the RMSE values.

Table 3 shows the similarities and dissimilarities between the observations and predictions. Of interest is that at d_2 the values are more difficult to predict, resulting in lower correlations than at d_1. However, including $PM_{2.5}$ as covariate results in a large improvement, with the correlation increasing to 0.90 (with only $PM_{2.5}$ as a covariate) and 0.92 (with $PM_{2.5}$ and PM_{10} as covariates). As argued earlier, inclusion of PM_{10} is not very effective to increase the interpolation precision.

A further spatial analysis showed that the fireworks d_1 created some local hotspots with peaking PM_{10} concentrations. PM_1, although elevated throughout the whole city, did not show these local peaks. The extremes in PM_{10} led to the low correlation with PM_1 and also influence the usability of PM_{10} as a covariate. The predictions are the results of applying the spatial copula interpolator including covariates (Fig. 6).

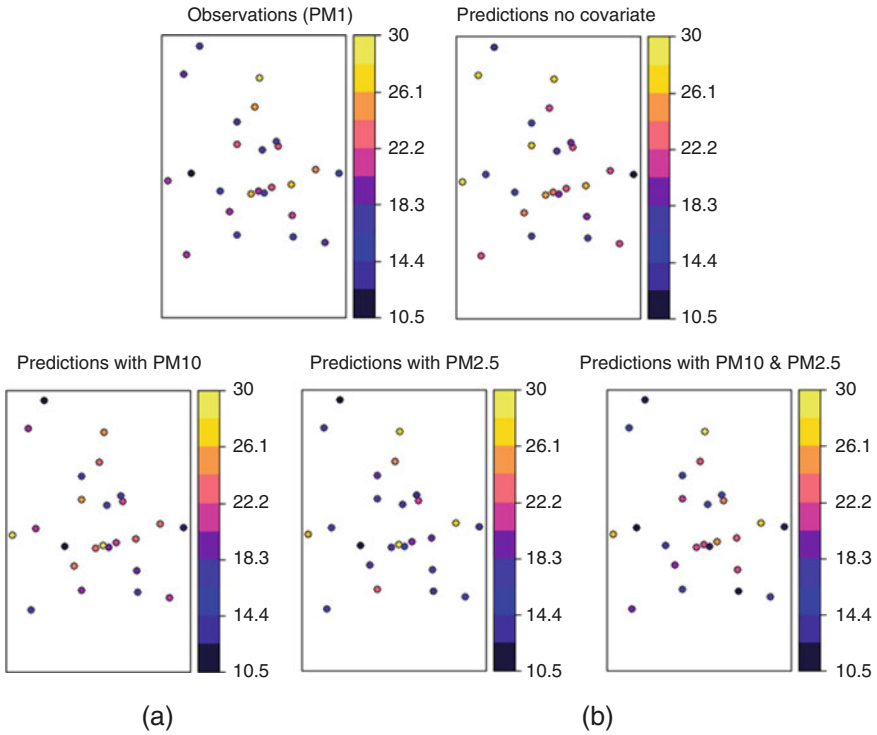

Fig. 6 Observations and predictions of PM_1 with copulas using different covariates

4 Discussion

We note that firework related air quality has a much higher PM_1 value than a day with a heavy traffic density. Apparently, the particulate matter generated by constituents of the firework resulted in higher PM_1 values. This is based on one day only, and weather conditions at that particular moment may have a large influence. It would be fair to make a comparison with another new year's early morning to see whether this effect is incidental or structural. Also important is that the concentrations are still relatively low at a day with a high traffic density. This applies for the city of Eindhoven, with its very specific traffic conditions, geographical position and population size.

Assessing health effects from the above study is still a challenge. We obtained 10 min data, and we analyzed air quality with the 10 min data and the average one hour data. One may question whether the average is the correct value, or that in fact we should sum the observations to obtain a total burden. In epidemiological studies the average is generally used, and it is so far still unclear how exactly particulate matter behaves within the respiratory system of the human body. We know that smaller particles penetrate deeper into the human lungs and cardiovascular system, but quantifications of exposure-response functions for PM_1 are limited. Related is

the lack of a definition of an environmental threshold for PM_1. Here we approached a value as described before. We realize though that in terms of health effects, the $PM_1/PM_{2.5}$ ratio might be a little on the high side, but that seems to be a point for discussion. PM_1 monitoring networks are needed to assess health effects and set more appropriate thresholds.

The study paid some attention to the dataset that should be collected for being able to make spatially explicit statements. We note that with one observation as in the city of Helmand not much can be done: there is an observation, even every 10 min, but its spatial representativeness is highly erroneous. The observation is not likely to be representative for any other location in the city. For instance, in the Eindhoven area a distinction is already made between urban background sensors and urban traffic sensors. Even that simple distinction cannot be made with a single sensor. A similar conclusion should be drawn from the four stations in Breda. Of some interest here is the comparison with the four sensors in Eindhoven with high values: those values cannot be reproduced by observations of the four stations in Breda. The chance of obtaining with more than 3 observations is higher, but it still does not give certainty. More research is needed to optimize the number and the allocation of air quality sensors within a medium sized city.

5 Conclusions

This study focusing on PM_1 air quality within a city in the Netherlands leads to the following conclusions. It displays several steps to relate air quality with its spatio-temporal variability towards health issues. A standard has been defined and its exceedance probabilities have been obtained on two peak hours. This gives a clear direction to relate health with geographical variability.

Copula-based interpolators can adequately be used to spatially predict PM_1. The case study shows that inclusion of $PM_{2.5}$ as a covariate was most successful, being highest correlated with PM_1. Replacing $PM_{2.5}$ by PM_{10}, or adding PM_{10} as a covariate did not lead to better results. In terms of the number of sensors, it is inadequate to try and measure air quality with a low number of sensors. Although it is difficult to say what the optimal number should be, it appears that with the network in the city of Eindhoven equaling 26 sensors a pattern of PM_1 air quality can be observed that potentially could be used for urban management. Finally, we conclude that there is a strong need to also have standardized threshold values for PM_1. In this study we successfully established two thresholds that corresponded well with each other. Those thresholds were exceeded in a large part of the city on the first hour of the New Year, but not during an hour of heavy traffic density. However, a single widely accepted standard is to be preferred.

Data and Software

The data that were used for this research are available at the site http://data.aireas.com/csv/. Software is available upon request from the second author: f.alidoost@utwente.nl.

An Analysis of the Data on November 20th, 2017, Between 7:30 and 8:30 am. This Time Step Is Reportedly a Moment with a High Traffic Density (Figs. 7, 8, 9, 10, 11, 12 and Table 4)

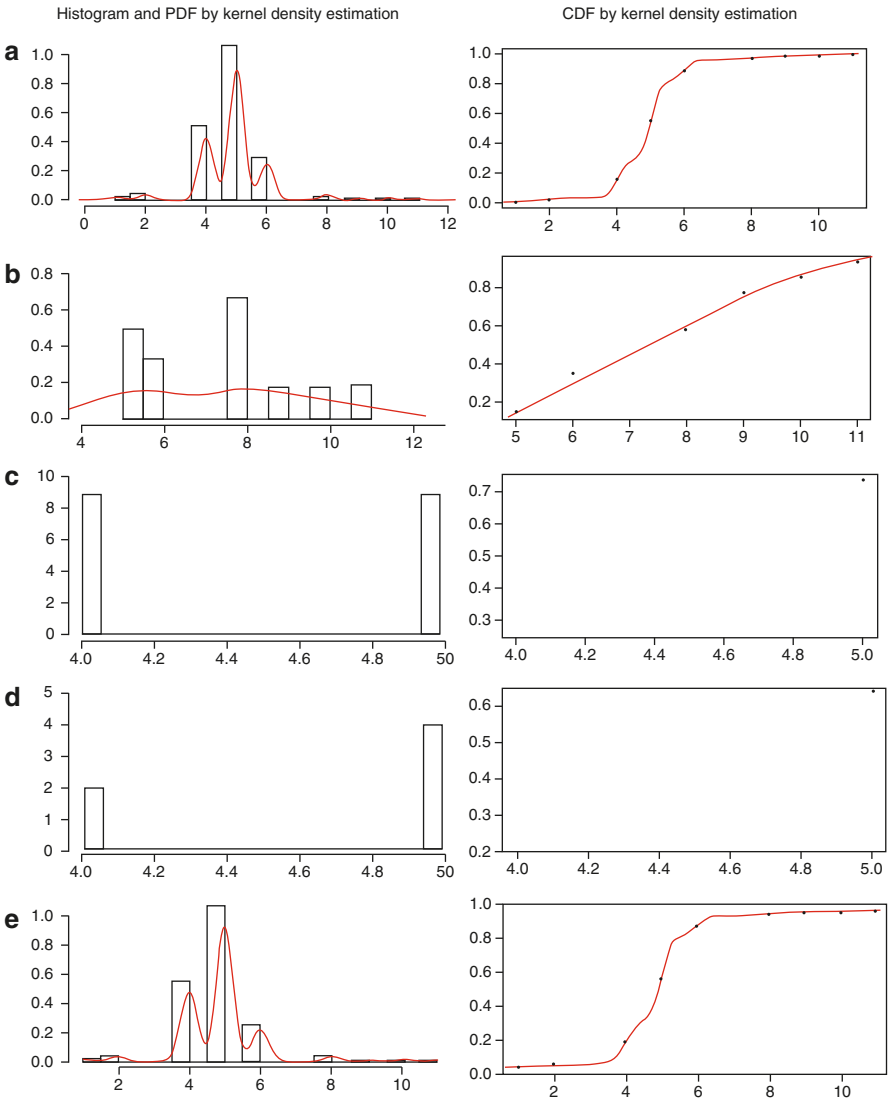

Fig. 7 Probability distribution function (PDF) and cumulative distribution function (CDF) on 2017 11 20. (**a**) the Eindhoven data, (**b**) four locations with relatively large values, (**c**) the city of Breda (three observations), (**d**) the city of Helmond (one observation) and (**e**) all data

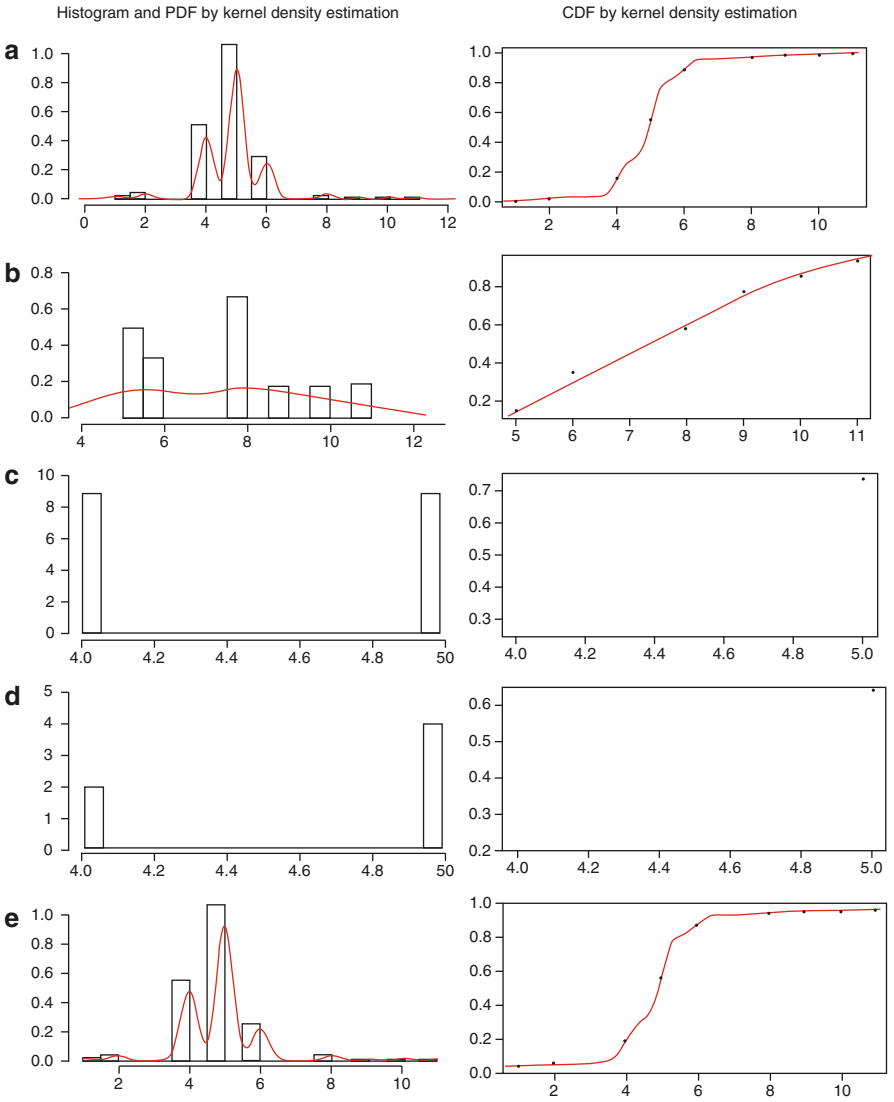

Fig. 8 Probability distribution function (PDF) and cumulative distribution function (CDF). (**a**) the Eindhoven data, (**b**) four locations with relatively large values, (**c**) the city of Breda (three observations), (**d**) the city of Helmond (one observation) and (**e**) all data

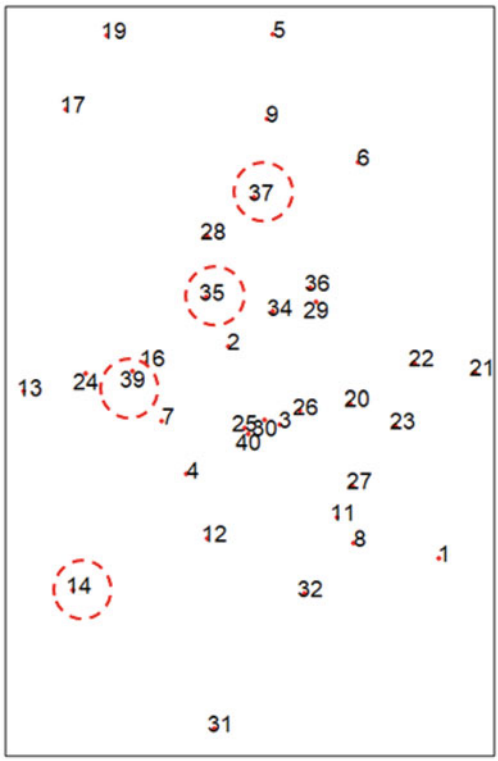

Fig. 9 Four locations in the city with relatively high values. Note that these lcations are different from the ones at January 1st.

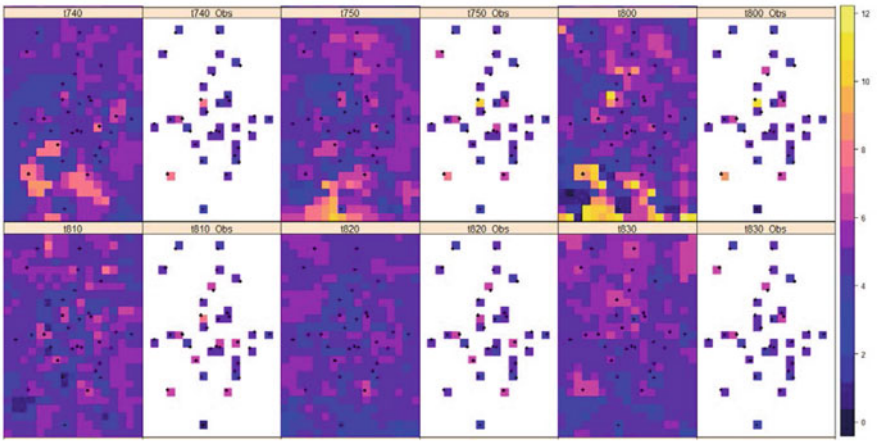

Fig. 10 Interpolated PM_1 data for the six time steps: 7:40, 7:50, 8:00, 8:10, 8:20 and 8:30 am. The predictions are the results of applying the mixed copula interpolator

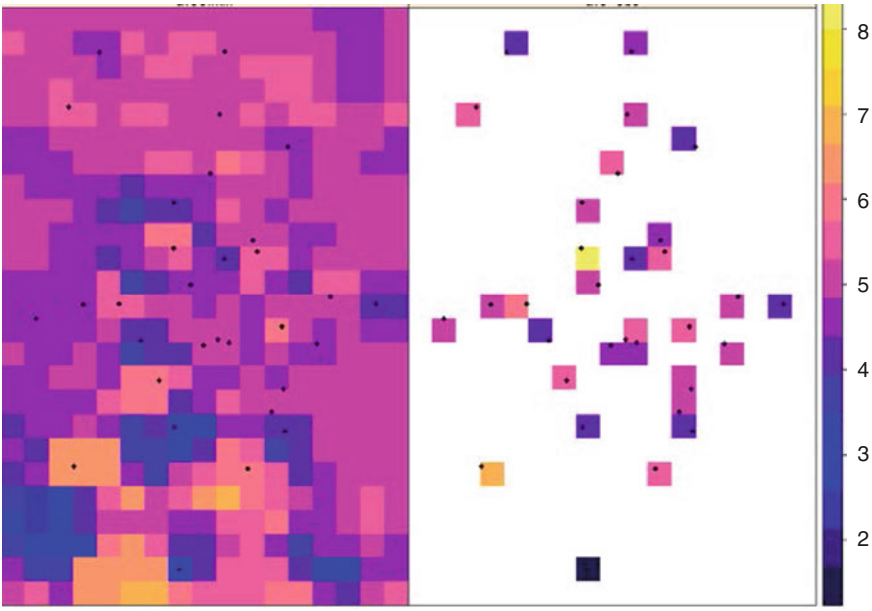

Fig. 11 Interpolated hourly PM_1 data taken as the average concentrations over the six time steps

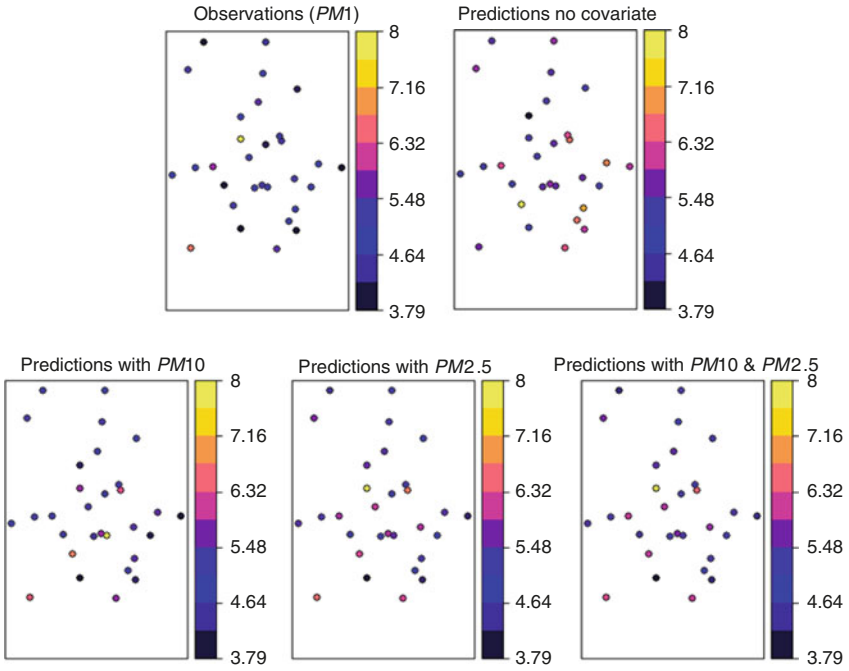

Fig. 12 Predictions with copulas using the spatial copula interpolator including different covariates

Table. 4 Descriptive statistics for the six different time steps and for the hourly data

		Observation	Prediction			Observation	Prediction
1	MAE	0.00	0.70	5	MAE	0.00	0.39
	MARE	0.00	15.60		MARE	0.00	8.28
	RMSE	0.00	1.08		RMSE	0.00	0.58
	Corr	1.00	0.56		Corr	1.00	0.77
	Min	2.00	3.76		Min	2.00	1.62
	Mean	4.84	4.99		Mean	4.84	4.68
	Max	8.00	8.25		Max	6.00	6.20
2	MAE	0.00	0.84	6	MAE	0.00	0.42
	MARE	0.00	17.50		MARE	0.00	9.95
	RMSE	0.00	1.18		RMSE	0.00	0.57
	Corr	1.00	0.49		Corr	1.00	0.75
	Min	2.00	3.53		Min	2.00	3.36
	Mean	5.06	4.94		Mean	4.77	4.91
	Max	10.00	6.32		Max	6.00	6.58
3	MAE	0.00	0.52	Hourly data	MAE	0.00	0.42
	MARE	0.00	8.99		MARE	0.00	9.79
	RMSE	0.00	1.03		RMSE	0.00	0.62
	Corr	1.00	0.77		Corr	1.00	0.80
	Min	1.00	1.01		Min	1.67	2.97
	Mean	5.06	4.95		Mean	4.93	4.87
	Max	11.00	8.94		Max	8.00	6.62
4	MAE	0.00	0.71				
	MARE	0.00	21.25				
	RMSE	0.00	1.06				
	Corr	1.00	0.55				
	Min	1.00	0.75				
	Mean	5.00	4.72				
	Max	8.00	6.10				

References

Alidoost, F., Stein, A., & Su, Z. (2018). Copula-based interpolation methods for air temperature data using collocated covariates. *Spatial Statistics, 28*, 128–140.

Arslan, S., Aybek, A., & Ekerbđçer, H. C. (2010). Measurement of personal PM_{10}, $PM_{2.5}$ and PM_1 exposures in tractor and combine operations and evaluation of health disturbances of operators. *Journal of Agricultural Sciences, 16*, 104–115.

Bárdossy, A., & Li, J. (2008). Geostatistical interpolation using copulas. *Water Resour Res., 44*, 15.

Close, J. P. (2016). AiREAS: Sustainocracy for a healthy city. In *The invisible made visible phase 1*. Cham: Springer. https://doi.org/10.1007/978-3-319-26940-5.

Cressie, N. (1993). *Statistics for spatial data* (pp. 105–110). New York: John Wiley.

Demarta, S., & McNeil, A. J. (2005). The *t* copula and related copulas. *International Statistical Review/Revue Internationale de Statistique, 73*(1), 111–129.

European Parliament and Council of the European Union. (2008). Directive 2008/50/EC of the European Parliament and of the Council of 21 May 2008 on ambient air quality and cleaner air for Europe. *Official Journal of the European Union, L152*(51), 1–44.

Gräler, B. (2014). Modelling skewed spatial random fields through the spatial vine copula. *Spatial Statistics, 10*(2014), 87–102.

Khodarahmi, F., Soleimani, Z., Yousefzadeh, S., Alavi, N., Babaei, A., Mohammadi, M. J., et al. (2015). Levels of PM_{10}, $PM_{2.5}$ and PM_1 and impacts of meteorological factors on particle matter concentrations in dust events and non-dusty days. *International Journal of Health Studies, 1*(3), 7–12.

Joe, H. (1993). Parametric families of multivariate distributions with given margins. *Journal of Multivariate Analysis, 46*(2), 262–282.

Manner, H. (2007). *Estimation and model selection of copulas with an application to exchange rates*. Maastricht: Maastricht Research School of Economics of TEchnology and ORganizations.

Nelsen, R. (2003). Properties and applications of copulas: A brief survey. In J. Dhaene, N. Kolev, & P. Morettin (Eds.), *Proceedings of the First Brazilian Conference on Statistical Modeling in Insurance and Finance*. Sao Paulo: University Press USP.

Sklar, A. (1973). Random variables, joint distribution functions, and copulas. *Kybernetika, 9*(6), 449–460.

Van Zoest, V., Osei, F. B., Stein, A., & Hoek, G. (2019). Calibration of low-cost NO2 sensors in an urban air quality network. *Atmospheric Environment, 210*, 66–75. https://doi.org/10.1016/j.atmosenv.2019.04.048.

Van Zoest, V. M., Stein, A., & Hoek, G. (2018). Outlier detection in urban air quality sensor networks. *Water, Air, and Soil Pollution, 229*, 111.

WHO. (2006). *WHO air quality guidelines for particulate matter, ozone, nitrogen dioxide and sulfur dioxide: Global update 2005—Summary of risk assessment*. Geneva: WHO.

Zwozdziak, A., Sówka, I., Willak-Janc, E., Zwozdziak, J., Kwiecińska, K., & Balińska-Miśkiewicz, W. (2016). Influence of PM_1 and $PM_{2.5}$ on lung function parameters in healthy schoolchildren-a panel study. *Environmental Science and Pollution Research International, 23*(23), 23892–23901. https://doi.org/10.1007/s11356-016-7605-1.

A Scale Mixture Approach to *t*-Distributed Mixture Regression

Frans Kanfer and Sollie Millard

Abstract Mixture of linear regressions frequently assume Gaussian distributions for the mixture components. Data from many applications follows leptokurtic and platykurtic shapes. The use of scale mixtures of distributions from the exponential family (SME) of distributions is considered due to its ability to provide more flexibility in the tail behaviour of a distribution. The *t*-distribution is identified as a member of the SME. This chapter considers robust mixture of regressions with errors from SME distributions, specifically the *t*-distribution. The technique is illustrated using generated data and an application on managed health care data is given. In the application, different behavioural claim segments are identified using the estimated mixture regression model facilitating better claims differentiation strategies.

1 Introduction

Mixture of linear regressions are frequently assumed to have components from Gaussian distributions (Yao et al. 2014). There is, however, evidence that in many applications the Gaussian assumption is not appropriate. Data typically show leptokurtic and platykurtic shapes. An alternative choice to the Gaussian distribution is to use scale mixtures of distributions in the exponential family (EF) due to its ability to provide more flexibility in tail behaviour in modelling real world phenomena (Choy and Chan 2008). The Pearson Type VII distribution, Johnson et al. (2005), is a more general class of distributions of which *t*-distribution is a special case. It was proposed by Seneta (2004) to use the variance gamma distribution in modelling financial and insurance data. This distribution has similar tail behaviour to that of the *t*-distribution. Scale mixtures have been studied extensively and are used widely in many statistical applications. These include Zeller et al. (2016) who

F. Kanfer · S. Millard (✉)
Department of Statistics, University of Pretoria, Pretoria, South Africa
e-mail: frans.kanfer@up.ac.za; sollie.millard@up.ac.za

A. Bekker et al. (eds.), *Computational and Methodological Statistics and Biostatistics*, Emerging Topics in Statistics and Biostatistics,
https://doi.org/10.1007/978-3-030-42196-0_14

developed an EM type algorithm to model mixture of scale mixtures of skewed normal distributions and the paper by Choy and Chan (2008) on the use of scale mixtures in statistical modelling. Mixture of linear mixed models is considered by Bai et al. (2016) where the random effects follow a multivariate t-distribution.

This chapter specifically considers the concept of robust mixture of regressions with errors from scale mixtures exponential family distributions (SME). This is done by first describing typical business problems in Sect. 2, followed by the theoretical framework of SME distributions, in Sect. 3 and mixture of scale mixtures of Gaussian distributions in Sect. 4. A special case of a mixture of a scale mixture of a Gaussian and gamma distribution, resulting in a mixture of t-distributed regressions is derived in Sect. 6. In Sect. 7, the suggested approach is illustrated on generated data and in Sect. 8 an application on managed health care data is given.

2 The Business Problem

Regression modelling and clustering frequently form part of data analytics in business to address contemporary problems. In insurance there is almost without exception the need to understand the behaviour of customers in different market segments (Jiang and Tanner 1999). This is frequently done by first clustering the data and then to estimate appropriate regression models for each of the identified clusters. Mixture of regression models give the researcher the ability to simultaneously identify different market segments or clusters based on the specific phenomena relating the response and explanatory variables in each cluster. It is also common to find outliers in the response variable, therefore the necessity to also consider robust mixture of regressions, Yao et al. (2014).

3 SME Distributions

Often mixture models are based on Gaussian distributions and are therefore sensitive to heavy-tailed errors (Bai et al. 2012). As noted in Sect. 1, scale mixtures play an important role in statistical modelling. In such cases, developing robust mixture models based on distributions different to the Gaussian are of interest.

In this chapter mixture models based on scale mixtures in the EF are considered. It is shown that the t-distribution is a special case of the SME. Mixture of regressions with t-distributed errors are considered due to its robustness properties.

Definition 1 Scale mixture of exponential family distributions (SME).
The variable Y has a SME if its PDF can be expressed as

$$\begin{aligned} f(y|\eta,\phi,\nu) &= \int_0^\infty h(y,k(u)\phi)exp\left(\frac{\eta^T T(y)-A(\eta)}{k(u)\phi}\right)q(u|\boldsymbol{\nu})du \\ &= SME(y|\eta,\phi,\nu) \end{aligned}$$

where $k(u)$ is a positive function of u and $q(.|\nu)$ is a PDF defined on R^+ with parameter ν. We refer to $k(u)$ as the mixing parameter and $q(.|\nu)$ as the mixing density of the SME, respectively.

The family of SME distributions includes many distributions. The t-distribution is a member since it is a scale mixture of a Gaussian distribution and a gamma distribution.

Proposition 1 *The class of scale mixtures of Gaussian distributions (SMG) is a subset of the SME family.*

Proof From Definition 1, setting $\eta = \mu$, $T(y) = y$, $\phi = \sigma^2$, and $h(y, k(u)\phi) = \frac{exp(\frac{y^2}{k(u)\sigma^2})}{\sqrt{2\pi\, k(u)}\sigma}$, we then have

$$\begin{aligned} f(y|\mu, \sigma^2, \nu) &= \int_0^\infty \frac{1}{\sqrt{2\pi}\sqrt{k(u)}\,\sigma} exp\left(-\frac{1}{2}\left(\frac{y-\mu}{\sqrt{k(u)}\sigma}\right)^2\right) q(u|\nu)du \\ &= \int_0^\infty N(y|\mu, k(u)\sigma^2) q(u|\nu)du \\ &= SMG(y|\mu, \sigma^2, \nu) \end{aligned}$$

which is the PDF of SMG distributions according to Andrews and Mallows (1974). □

Proposition 2 *The Student t-distribution is a member of the SME.*

Proof From Definition 1 using Proposition 1, taking $k(u) = \frac{1}{u}$ and $q(u|\nu)$ to be the PDF of a $GAMMA(\frac{\nu}{2}, \frac{\nu}{2})$ distribution, it follows from the SMG that

$$\begin{aligned} f(y|\mu, \sigma^2, \nu) &= \int_0^\infty N\left(y|\mu, \frac{\sigma^2}{u}\right) \Gamma\left(u|\frac{\nu}{2}, \frac{\nu}{2}\right) du \\ &= t(y|\mu, \sigma^2, \nu) \end{aligned} \tag{1}$$

which is the PDF of a t-distribution with ν degrees of freedom, location parameter μ and scale parameter σ, see Choy and Chan (2008) for more detail. □

Remark 1 Let $Z \sim N(0, 1)$ and the PDF of U be $q(u|\nu)$. Then

$$X = \mu + Z\sigma\sqrt{k(U)}$$

follows a $N(\mu, \sigma^2 k(U))$ distribution. The variable X is the constant μ contaminated with a zero mean Gaussian with random variance $\sigma^2 k(U)$. The joint PDF of X and U therefore is

$$f_{XU}(x, u|\mu, \sigma^2, \nu) = N(x|\mu, \sigma^2 k(u))q(u|\nu).$$

4 Mixture of SMG

The PDF of a random variable Y, from a mixture distribution with component density function $SMG(\mu_k, \sigma_k^2, \nu_k)$ for $k = 1, \ldots, K$, is

$$f(y|\boldsymbol{\theta}) = \Sigma_{k=1}^{K} \pi_k SMG(y|\mu_k, \sigma_k^2, \nu_k),$$

where $\boldsymbol{\theta} = (\boldsymbol{\pi}, \boldsymbol{\mu}, \boldsymbol{\sigma}^2) = (\pi_1, \ldots, \pi_K, \mu_1, \ldots, \mu_K, \sigma_1^2, \ldots, \sigma_K^2)$ and $\boldsymbol{\nu} = (\nu_1, \ldots, \nu_K)$.

The log-likelihood function for a random sample $y_1, \ldots, y_n$ of Y is

$$l(\boldsymbol{\theta}|\boldsymbol{y}) = \sum_{i=1}^{n} log \left(\sum_{k=1}^{K} \pi_k SMG(y_i|\mu_k, \sigma_k^2, \nu_k) \right).$$

Let $\boldsymbol{Z} = (z_{ik})$ with

$$z_{ik} = \begin{cases} 0 \text{ if observation } i \text{ is not from component } k \\ 1 \text{ if observation } i \text{ is from component } k \end{cases}$$

for $i = 1, \ldots, n$ and $k = 1, \ldots, K$. Including these unobserved observations into the likelihood function, the complete data log-likelihood is

$$l_z(\boldsymbol{\theta}|\boldsymbol{y}) = \sum_{i=1}^{n} \sum_{k=1}^{K} z_{ik} \, log \left(\pi_k SMG(y_i|\mu_k, \sigma_k^2, \nu_k) \right).$$

Introducing additional missing data, $\boldsymbol{u} = (u_i, \ldots, u_n)$ with PDF of $u_i|z_{ik} \sim q_k(u_i|\nu_k)$, the complete data log-likelihood is

$$l_c(\boldsymbol{\theta}|\boldsymbol{y}) = \sum_{i=1}^{n} \sum_{k=1}^{K} z_{ik} \, log \left(\pi_k N(y_i|\mu_k, k(u_i)\, \sigma_k^2) q_k(u_i|\nu_k) \right) \tag{2}$$

using Remark 1. The expression $l_c(\boldsymbol{\theta}|\boldsymbol{y})$ in (2), can be partitioned as follows

$$\begin{aligned} l_c(\boldsymbol{\theta}|\boldsymbol{y}) &= \sum_{i=1}^{n}\sum_{k=1}^{K} z_{ik} log\pi_k \\ &\quad + \sum_{i=1}^{n}\sum_{k=1}^{K} z_{ik} log q_k(u_i|\nu_k) \\ &\quad + \sum_{i=1}^{n}\sum_{k=1}^{K} z_{ik} log N(y_i|\mu_k, k(u_i)\sigma_k^2) \\ &= \sum_{i=1}^{n}\sum_{k=1}^{K} z_{ik} log\pi_k \\ &\quad + \sum_{i=1}^{n}\sum_{k=1}^{K} z_{ik} log q_k(u_i|\nu_k) \\ &\quad + \sum_{i=1}^{n}\sum_{k=1}^{K} z_{ik} \left[-\frac{1}{2} log(2\pi) - \frac{1}{2} log\, \sigma_k^2 - \frac{1}{2} log(k(u_i)) - \frac{1}{2}\frac{(y_i-\mu_k)^2}{k(u_i)\sigma_k^2} \right], \end{aligned} \tag{3}$$

where $\boldsymbol{\theta} = (\pi_1, \ldots, \pi_K, \mu_1, \ldots, \mu_K, \sigma_1^2, \ldots, \sigma_K^2, \nu_1, \ldots, \nu_K)$.

The t-distribution plays an important role in robust analysis. Since the t-distribution is a special case of the SMG, we present a mixture of t-distributions in Sect. 5 and mixture of regression models using t-distributions in Sect. 6.

5 Mixture of t-Distributions

The t-distribution is a member of SMG, see Proposition 2, hence a member of SME. A random variable Y follows a mixture of t-distributions if

$$\begin{aligned} f_Y(y|\boldsymbol{\theta}) &= \sum_{k=1}^{K} \pi_k t(y|\mu_k, \sigma_k^2, \nu_k) \\ &= \sum_{k=1}^{K} \int_0^{\infty} N\left(y|\mu_k, \frac{\sigma_k^2}{u}\right) \Gamma\left(u|\frac{\nu_k}{2}, \frac{\nu_k}{2}\right), \end{aligned}$$

with component mixing density a $GAMMA(\frac{\nu_k}{2}, \frac{\nu_k}{2})$ and mixing parameter $k(u) = \frac{1}{u}$. The complete data log-likelihood function, following (3), is

$$
\begin{aligned}
l_c(\boldsymbol{\theta}|\boldsymbol{y}, \boldsymbol{Z}) = & \sum_{i=1}^{n}\sum_{k=1}^{K} z_{ik} log \pi_k \\
& + \sum_{i=1}^{n}\sum_{k=1}^{K} z_{ik}\left[-log\,\Gamma(\frac{\nu_k}{2}) + \frac{\nu_k}{2} log(\frac{\nu_k}{2}) + (\frac{\nu_k}{2} - 1)\, log\,(u_i) - \frac{\nu_k}{2} u_i\right] \\
& + \sum_{i=1}^{n}\sum_{k=1}^{K} z_{ik}\left[-\frac{1}{2} log(2\pi) - \frac{1}{2} log\,\sigma_k^2 + \frac{1}{2} log(u_i) - \frac{u_i}{2}\left(\frac{y_i - \mu_k}{\sigma_k}\right)^2\right].
\end{aligned}
\tag{4}
$$

Proposition 3 *If R has a $GAMMA(\alpha, \beta)$ distribution then*

$$E(log\ R) = \psi(\alpha) - log\beta,$$

where $\psi(.)$ is the digamma function given by

$$\psi(\alpha) = \frac{\Gamma'(\alpha)}{\Gamma(\alpha)}.$$

Proof *For the proof see Peel and McLachlan (2000).* □

Using the EM algorithm to calculate the ML estimates requires taking the expectation over the latent variables in the E-Step and performing maximisation for the M-Step.

E-Step
Taking conditional expectations over the latent variables in (4) requires the calculation of

$$E_{\boldsymbol{\theta}}\,(Z_{ik}|y_i) = \gamma_{ik},$$

$$E_{\boldsymbol{\theta}}\,(U_i|y_i, z_{ik}) = u_{ik}, \text{ and}$$

$$E_{\boldsymbol{\theta}}\, log(U_i|y_i, z_{ik}) = l_{ik}.$$

It follows that

$$\gamma_{ik} = \frac{\pi_k t(y_i|\mu_k, \sigma^2{}_k, \nu_k)}{\sum_{j=1}^{K} \pi_j t(y_i|\mu_j, \sigma^2{}_j, \nu_j)}, \tag{5}$$

$$u_{ik} = \frac{\nu_k + 1}{\nu_k + \left(\frac{y_i - \mu_k}{\sigma_k}\right)^2} \tag{6}$$

since $U_i|y_i, z_{ik} \sim GAMMA\left(\frac{1}{2}(\nu_k + 1), \frac{1}{2}\left[\nu_k + \left(\frac{y_i - \mu_k}{\sigma_k}\right)^2\right]\right)$.

Using the distribution of $U_i|y_i, z_{ik}$ and Proposition 3, we get

$$l_{ik} = \psi\left(\frac{\nu_k + 1}{2}\right) - log\left[\frac{1}{2}\left(\nu_k + \left(\frac{y_i - \mu_k}{\sigma_k}\right)^2\right)\right].$$

Substituting the conditional expectations into (4) yields

$$Q(\boldsymbol{\theta}) = Q_{\boldsymbol{\pi}}(\boldsymbol{\theta}) + Q_{\boldsymbol{\nu}}(\boldsymbol{\theta}) + Q_{\boldsymbol{\mu},\boldsymbol{\sigma}^2}(\boldsymbol{\theta}), \tag{7}$$

where

$$Q_{\boldsymbol{\pi}}(\boldsymbol{\theta}) = \sum_{i=1}^{n}\sum_{k=1}^{K}\gamma_{ik}\, log(\pi_k),$$

$$Q_{\boldsymbol{\nu}}(\boldsymbol{\theta}) = \sum_{i=1}^{n}\sum_{k=1}^{K}\gamma_{ik}\left[-log\left(\Gamma\left(\frac{\nu_k}{2}\right)\right) + \frac{\nu_k}{2}\, log\left(\frac{\nu_k}{2}\right) + \left(\frac{\nu_k}{2} - 1\right) l_{ik} - \frac{\nu_k}{2}\, u_{ik}\right]$$

and

$$Q_{\boldsymbol{\mu},\boldsymbol{\sigma}^2}(\boldsymbol{\theta}) = \sum_{i=1}^{n}\sum_{k=1}^{K}\gamma_{ik}\left[-\frac{1}{2}\log\, 2\pi - \frac{1}{2}\, log\, \sigma_k^2 + \frac{1}{2} l_{ik} + \frac{u_{ik}}{2}\left(\frac{y_i - \mu_k}{\sigma_k}\right)^2\right]. \tag{8}$$

M-Step

Obtaining updates for the parameters $\boldsymbol{\pi}$, $\boldsymbol{\nu}$, $\boldsymbol{\mu}$ and $\boldsymbol{\sigma}^2$ for the next iteration step requires maximisation of (7), which is equivalent to the maximisation of the three terms separately.

Maximising $Q_{\boldsymbol{\pi}}(\boldsymbol{\theta})$ under the current parameter estimate, $\boldsymbol{\theta}$, and the constraint $\sum_{k=1}^{K}\pi_k = 1$, results in the closed form solution

$$\pi_k = \frac{\sum_{i=1}^{n}\gamma_{ik}}{n}$$

for the update of π_k.

Differentiating (8) with respect to μ_k and setting equal to 0 yields

$$\frac{\partial}{\partial \mu_k} Q_{\boldsymbol{\mu},\boldsymbol{\sigma}^2}(\boldsymbol{\theta}) = \sum_{i=1}^{n}\gamma_{ik} u_{ik}(y_i - \mu_k) = 0.$$

Hence, we obtain

$$\mu_k = \frac{\sum_{i=1}^{n} \gamma_{ik} u_{ik} y_i}{\sum_{i=1}^{n} \gamma_{ik} u_{ik}}.$$

The updated μ_k therefore is the weighted sample mean.

Similarly, the update rule for σ_k^2 is obtained by differentiating (8) with respect to σ_k^2 and setting equal to 0, yielding

$$\sum_{i=1}^{n} \gamma_{ik} \frac{1}{\sigma_k^2} - \sum_{i=1}^{n} \gamma_{ik} u_{ik} \left(\frac{(y_i - \mu_k)}{\sigma_k^2} \right)^2 = 0.$$

After some algebra we have

$$\sigma_k^2 = \sum_{i=1}^{n} \frac{\gamma_{ik} u_{ik} (y_i - \mu_k)^2}{n_k} \tag{9}$$

with $n_k = \sum_{i=1}^{n} \gamma_{ik}$, the effective number of observations in component k.

Replacing the denominator in (9) with $\sum_{i=1}^{n} \gamma_{ik} u_{ik}$ can lead to faster convergence, see Kent et al. (1994).

Two approaches can be followed in determining the updated value of ν_k:

1. Estimating ν_k outside the EM algorithm, using a profile likelihood, which has the effect that $Q_{\boldsymbol{\nu}}(.)$ will not play a role in optimising $Q(\boldsymbol{\theta})$, (7). The EM algorithm for mixture of t-distributions with a common and fixed ν are given in Algorithm 1. This algorithm can be applied to a grid of values of ν to assist in making an optimal selection for ν.
2. Alternatively $Q_{\boldsymbol{\nu}}(.)$ can be maximised, taking the partial derivative with respect to ν_k, as in Peel and McLachlan (2000), iteratively solving for ν_k in the M step to obtain an update rule. Algorithm 2 gives the EM algorithm for this case.

6 Mixture of Regressions with t-Distributed Errors

Consider the mixture of K, with $k = 1, \ldots, K$, regressions model:

$$Y = \begin{cases} \boldsymbol{x}^T \boldsymbol{\beta}_1 + \epsilon_1, & \text{with probability } \pi_1 \\ \boldsymbol{x}^T \boldsymbol{\beta}_2 + \epsilon_2, & \text{with probability } \pi_2 \\ \vdots & \\ \boldsymbol{x}^T \boldsymbol{\beta}_K + \epsilon_K, & \text{with probability } \pi_K \end{cases} \tag{10}$$

Algorithm 1 EM algorithm for a mixture of t-distributions with common and fixed degrees of freedom

1. Choose initial values $\boldsymbol{\theta}^{old} = (\boldsymbol{\pi}, \boldsymbol{\mu}, \boldsymbol{\sigma}^2)$ for a given value of ν.
2. E-Step: Calculate the responsibilities and additional weights

$$\gamma_{ik}^{new} = \frac{\pi_k t(y_i|\mu_k^{old}, \sigma^{2\,old}_k, \nu)}{\Sigma_{j=1}^{K} \pi_j^{old} t(y_i|\mu_j^{old}, \sigma^{2\,old}_j, \nu)}, \text{ and}$$

$$u_{ik}^{new} = \frac{\nu + 1}{\nu + \left(\frac{y_i - \mu_k^{old}}{\sigma_k^{old}}\right)^2}.$$

3. M-Step: Calculate the updated parameter values

$$\pi_k^{new} = \frac{\sum_{i=1}^{n} \gamma_{ik}^{new}}{n},$$

$$\mu_k^{new} = \frac{\sum_{i=1}^{n} \gamma_{ik}^{new} u_{ik}^{new} y_i}{\sum_{i=1}^{n} \gamma_{ik}^{new} u_{ik}^{new}}, \text{ and}$$

$$\sigma_k^{2\,new} = \sum_{i=1}^{n} \frac{\gamma_{ik}^{new} u_{ik}^{new} (y_i - \mu_k^{new})^2}{n_k^{new}}$$

   for $n_k^{new} = \sum_{i=1}^{n} \gamma_{ik}^{new}$.
4. Set $\boldsymbol{\theta}^{old} = \boldsymbol{\theta}^{new}$.
5. Repeat (2) to (4) until convergence.

where Y is the response variable, $\boldsymbol{x}$ is a p-dimensional vector of explanatory variables including the intercept term, $\boldsymbol{\beta}_k$ a p-dimensional vector of regression coefficients of the kth component, π_k the mixing probabilities $0 < \pi_k < 1$, $\sum_{k=1}^{K} \pi_k = 1$ and ϵ_k random errors.

Select a t-distribution with ν degrees of freedom and scale parameter σ for ϵ_k. The PDF of component k, using (1), is

$$\begin{aligned} f_k(y - \boldsymbol{x}^T \boldsymbol{\beta}_k | \boldsymbol{x}, \boldsymbol{\beta}_k, \nu, \sigma) &= t_k(\epsilon_k | \boldsymbol{x}, \boldsymbol{\beta}_k, \nu, \sigma) \\ &= \frac{\Gamma(\frac{\nu+1}{2}) \sigma^{-1}}{(\pi\nu)^{1/2} \Gamma(\frac{\nu}{2}) \left\{1 + \frac{\epsilon^2}{\sigma^2 \nu}\right\}^{\frac{1}{2}(\nu+1)}}. \end{aligned} \tag{11}$$

Algorithm 2 EM algorithm for a mixture of t-distributions with ν_k degrees of freedom

1. Choose initial values $\boldsymbol{\theta}^{old} = (\boldsymbol{\pi}, \boldsymbol{\mu}, \boldsymbol{\sigma}^2, \boldsymbol{\nu})$.
2. E-Step
   a. Calculate the responsibilities, γ_{ik}, and additional weights, u_{ik} as in Algorithm 1.
   b. Calculate

$$l_{ik} = \psi(\frac{\nu_k + 1}{2}) - log\left[\frac{1}{2}\left(\nu_k + \left(\frac{y_i - \mu_k}{\sigma_k}\right)^2\right)\right].$$

3. M-Step
   a. Calculate the updated mixing probabilities, component location parameters and variances using the M-Step in Algorithm 1, and
   b. the update of ν_k is obtained by solving

$$\left\{-\psi\left(\frac{1}{2}\nu_k\right) + 1 + log\left(\frac{1}{2}\nu_k\right) + \frac{1}{n_k^{new}}\sum_{i=1}^{n}\gamma_{ik}^{new}\left(l_{ik}^{new} - u_{ik}^{new}\right) + \psi\left(\frac{\nu_k^{old} + 1}{2}\right) - log\left(\frac{\nu_k^{old} + 1}{2}\right)\right\} = 0.$$

4. Set $\boldsymbol{\theta}^{old} = \boldsymbol{\theta}^{new}$.
5. Repeat (2) and (4) until convergence.

Assuming ν to be known, the log-likelihood is

$$l(\boldsymbol{\theta}|\boldsymbol{X}, \boldsymbol{y}) = \sum_{i=1}^{n} log\left\{\sum_{k=1}^{K}\pi_k t_k(y_i - \boldsymbol{x}_i^T\boldsymbol{\beta}_k)|\boldsymbol{x}_i, \boldsymbol{\beta}_k, \nu, \sigma\right\}$$

with $\boldsymbol{\theta} = (\pi_1, \ldots, \pi_K, \boldsymbol{\beta}_1, \ldots, \boldsymbol{\beta}_K, \sigma)$.

Let $\boldsymbol{Z} = (z_{ik})$ with

$$z_{ik} = \begin{cases} 0 \text{ if observation } i \text{ is not from component } k \\ 1 \text{ if observation } i \text{ is from component } k \end{cases}$$

for $i = 1, \ldots, n$ and $k = 1, \ldots, K$. The complete data log-likelihood is

$$
\begin{aligned}
l_c(\boldsymbol{\theta}|\boldsymbol{X}, \boldsymbol{y}, \boldsymbol{Z}) &= \sum_{i=1}^{n}\sum_{k=1}^{K} z_{ik} log\pi_k \left\{ t_k(y_i - \boldsymbol{x}_i^T \boldsymbol{\beta}_k | z_{ik}, \boldsymbol{x}_i, \boldsymbol{\beta}_k, \nu, \sigma) \right\} \\
&= \sum_{i=1}^{n}\sum_{k=1}^{K} z_{ik} log\pi_k \\
&\quad + \sum_{i=1}^{n}\sum_{k=1}^{K} z_{ik} \left[-log\,\Gamma(\frac{\nu}{2}) + \frac{\nu}{2} log(\frac{\nu}{2}) + (\frac{\nu}{2} - 1)\, log\,(u_i) - \frac{\nu}{2} u_i \right] \\
&\quad + \sum_{i=1}^{n}\sum_{k=1}^{K} z_{ik} \left[-\frac{1}{2} log(2\pi) - \frac{1}{2} log\,\sigma_k^2 + \frac{1}{2} log(u_i) - \frac{u_i}{2} \left(\frac{y_i - \boldsymbol{x}_i^T \boldsymbol{\beta}_k}{\sigma_k} \right)^2 \right]
\end{aligned}
\tag{12}
$$

which is maximised using the EM algorithm.

The EM algorithm for mixture of t-distributed regressions is similar to Algorithm 1.

E-Step

Determining the responsibilities from expression (5) and the additional weights from (6), setting $\nu_k = \nu$ with ν known,

$$
\gamma_{ik} = \frac{\pi_k t(y_i - \boldsymbol{x}_i^T \boldsymbol{\beta}_k | \boldsymbol{x}_i, \boldsymbol{\beta}_k, \sigma^2{}_k, \nu)}{\sum_{j=1}^{K} \pi_j t(y_i - \boldsymbol{x}_i^T \boldsymbol{\beta}_k | \boldsymbol{x}_i, \boldsymbol{\beta}_j \sigma^2{}_j, \nu)}, \text{ and}
$$

$$
u_{ik} = \frac{\nu + 1}{\nu + \left(\frac{y_i - \boldsymbol{x}_i^T \boldsymbol{\beta}_k}{\sigma_k} \right)^2}.
$$

Replacing the missing data with these expected values in the complete data log-likelihood (12), discarding terms not involving parameters, yields

$$
Q(\boldsymbol{\theta}) = Q_{\boldsymbol{\pi}}(\boldsymbol{\theta}) + Q_{\boldsymbol{\mu}, \boldsymbol{\sigma}^2}(\boldsymbol{\theta}),
$$

where

$$Q_{\boldsymbol{\pi}}(\boldsymbol{\theta}) = \sum_{i=1}^{n}\sum_{k=1}^{K}\gamma_{ik}\, log(\pi_k) \text{and}$$

$$Q_{\boldsymbol{\beta},\boldsymbol{\sigma}^2}(\boldsymbol{\theta}) = \sum_{i=1}^{n}\sum_{k=1}^{K}\gamma_{ik}\left[-\frac{1}{2}log\,\sigma_k^2 + \frac{u_{ik}}{2}\left(\frac{y_i - \boldsymbol{x}_i^T\boldsymbol{\beta}_k}{\sigma_k}\right)^2\right].$$

M-Step
Updates for the parameter, $\boldsymbol{\theta}$, is obtained by partial differentiation of $Q_{\boldsymbol{\beta},\boldsymbol{\sigma}^2}(\boldsymbol{\theta})$ and $Q_{\boldsymbol{\pi}}(\boldsymbol{\theta})$ with respect to π_k, $\boldsymbol{\beta}_k$ and $\boldsymbol{\sigma}_k$ respectively, setting the resultant equal to zero, yields the following update rules. For π_k the update rule is

$$\pi_k = \sum_{i=1}^{n}\gamma_{ik}/n,$$

and the update rule for $\boldsymbol{\beta}_k$ is

$$\begin{aligned}\boldsymbol{\beta}_k &= \left(\sum_{i=1}^{n}\boldsymbol{x}_i\boldsymbol{x}_i^T\gamma_{ik}\times u_{ik}\right)^{-1}\left(\sum_{i=1}^{n}\boldsymbol{x}_i y_i\gamma_{ik}\times u_{ik}\right)\\ &= (\boldsymbol{X}^T\boldsymbol{W}_k\boldsymbol{X})^{-1}(\boldsymbol{X}^T\boldsymbol{W}_k\boldsymbol{y})\end{aligned}$$

where $\boldsymbol{W_k}$ is a diagonal matrix with diagonal elements $(\gamma_{ik}\times u_{ik})$ and updates for σ_k are obtained using

$$\sigma_k = \left(\frac{\sum_{i=1}^{n}\gamma_{ik}\times u_{ik}(y_i - \boldsymbol{x}_i^T\beta_k)^2}{n_k}\right)^{1/2}$$

with $n_k = \sum_{i=1}^{n}\gamma_{ik}$.

The EM algorithm for a mixture of regressions using t-distributed errors is summarised in Algorithm 3.

6.1 Choice of the Degrees of Freedom for the Component t-Distribution

In the previous section the degrees of freedom, ν, was assumed to be known. The degrees of freedom, ν, can be chosen using an adaptive process based on maximising the profile likelihood for ν. The profile log-likelihood for ν is defined as

Algorithm 3 EM estimation for a mixture of regressions with t-distributed errors

1. Choose initial values $\boldsymbol{\theta}^{old} = (\pi_1, \ldots, \pi_K, \boldsymbol{\beta}_1^{old}, \ldots \boldsymbol{\beta}_K^{old}, \sigma_1^{old}, \ldots, \sigma_K^{old})$.
2. E-Step: Calculate the responsibilities and additional weights

$$\gamma_{ik}^{new} = E(z_{ik}|\boldsymbol{X}, \boldsymbol{y}, \boldsymbol{\theta}^{old}), = \frac{\pi_k^{old} f(y_i - \boldsymbol{x}_i^T \beta_k^{old}; \sigma^{old}, \nu_k)}{\sum_{l=1}^K \pi_l^{old} f(y_i - \boldsymbol{x}_i^T \beta_l^{old}; \sigma^{old}, \nu_l)}$$

   where $f(\epsilon; \sigma, \nu)$ is as defined in (11), and

$$u_{ik}^{new} = E(u_i|\boldsymbol{X}, \boldsymbol{y}, \boldsymbol{\theta}^{old}, z_{ik} = 1) = \frac{\nu + 1}{\nu + \left\{(y_i - \boldsymbol{x}_i^T \boldsymbol{\beta}_k)/\sigma^{old}\right\}^2}.$$

3. M-Step: update the parameter values

$$\pi_k^{new} = \sum_{i=1}^n \gamma_{ik}^{new}/n,$$

$$\boldsymbol{\beta}_k^{new} = (\boldsymbol{X}^T \boldsymbol{W}_k \boldsymbol{X})^{-1} (\boldsymbol{X}^T \boldsymbol{W}_k \boldsymbol{y})$$

   where $\boldsymbol{W}_k$ is a diagonal matrix with diagonal elements $\left(\gamma_{ik}^{new} \times u_{ik}^{new}\right)$.

$$\sigma_k^{new} = \left\{ \frac{\sum_{i=1}^n \gamma_{ik}^{new} \times u_{ik}^{new} (y_i - \boldsymbol{x}_i^T \beta_k^{new})^2}{n_k} \right\}^{1/2}.$$

4. Set $\boldsymbol{\theta}^{old} = \boldsymbol{\theta}^{new}$.
5. Repeat the (2) and (4) until convergence.

$$l(\nu) = \max_{\boldsymbol{\theta}} \sum_{i=1}^n log \sum_{k=1}^K \left\{ \pi_k f(y_i - \boldsymbol{x}_i^T \beta_k)|\sigma \nu \right\}. \tag{13}$$

The profile log-likelihood, $l(\nu)$, is evaluated using a grid of appropriate values of ν and the value of ν maximising (13) is chosen.

7 Example of a Mixture of t-Distributed Regressions

Consider the mixture regression model

$$y_i = \begin{cases} \boldsymbol{x}_i^T \boldsymbol{\beta}_1 + \epsilon_{i1} \text{ with probability } \pi_1 \\ \boldsymbol{x}_i^T \boldsymbol{\beta}_2 + \epsilon_{i2} \text{ with probability } \pi_2 \end{cases} \tag{14}$$

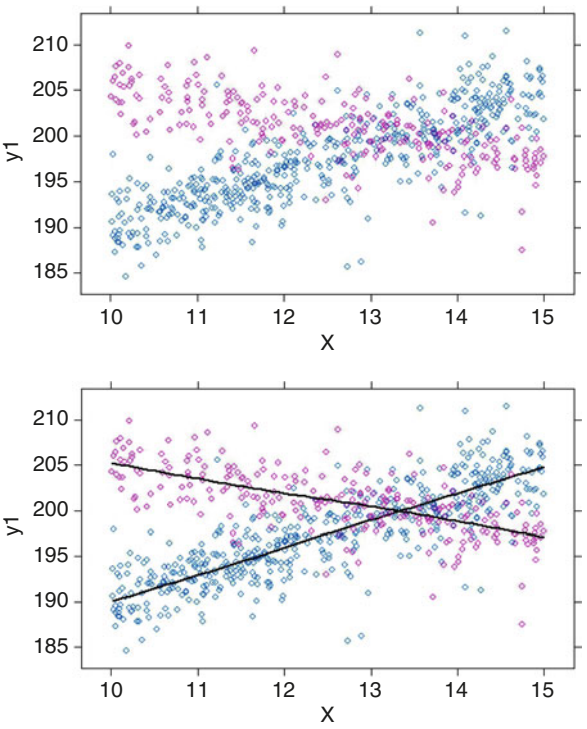

Fig. 1 Mixture of t-distributed regressions model, observed data in the upper pane and the estimated mixture of regressions model in the bottom pane

Table 1 MLEs for the 2 component mixture of t-distributed regressions model

	Component 1	Component 2
Parameter	$k = 1$	$k = 2$
β_{1k}	159.940	221.350
β_{2k}	3.000	-1.613
π_k	0.684	0.316
σ_k	2.461	2.784
ν	5	
BIC	4097.100	

with random errors ϵ_{ik} each from a t-distribution with $\nu = 5$ degrees of freedom, scale parameter $\sigma = 3$, $\boldsymbol{\beta}_1 = \begin{pmatrix} 160 \\ 3 \end{pmatrix}$, $\boldsymbol{\beta}_2 = \begin{pmatrix} 220 \\ -1.5 \end{pmatrix}$, $\boldsymbol{\pi} = \begin{pmatrix} 0.67 \\ 0.33 \end{pmatrix}$ and $\epsilon_{ik} \sim t(5)$.

A random sample of $n = 750$ from this mixture regression model (14) is presented in the top pane of Fig. 1.

The MLEs, using Algorithm 3, are given in Table 1.

The fitted model, shown in the bottom panel of Fig. 1, which represents the generative model well. Comparing the BIC of models with $\nu = 3, 4, 5$ and 6 respectively confirms the choice of $\nu = 5$.

8 Health Care Claims Modelling

Predictive modelling is increasingly used in modelling and forecasting of health care costs in the managed health care sector (Powers et al. 2005). In a recent survey (Tomar and Agarwal 2013), the popularity of machine and statistical learning techniques, in health care, is highlighted. These models are utilised, among other, to identify and manage high risk participants and health care service providers.

Total claims cost is modelled as a function of the other variables in Table 2. A mixture regression model approach is used to determine the impact of these explanatory variables on the total cost and also to determine if there are groups of medical insurance companies in which the impacts differ, hence profiling the companies. Differences between the impacts identified through the component models are usually very insightful and are used for managerial and governance purposes.

In this application, also considered by Millard (2018), we use a mixture of regressions model with t-distributed errors for the modelling of medical insurance data. The data consists of aggregated claims from 375 medical insurance companies, for a specific year.

8.1 Observed Data

Table 2 gives a description of the variables used.

Figure 2 gives a scatter plot matrix for the standardised variables in Table 2 indicating substantial correlation between the response variable claims and the explanatory variables *female_ratio, age, pens_ratio and depen_ratio*.

Table 2 Variables considered in modelling claims data

Variable	Description
Claims	Total claims cost (response variable)
Beneficiaries	Number of beneficiaries
Age	Average age of members
Pens_Ratio	Ratio of pensioners to the total number of members
Female_Ratio	Ratio of female beneficiaries to the total number of members
Depen_Ratio	Average dependency ratio per policy

All variables are measured on the continuous scale

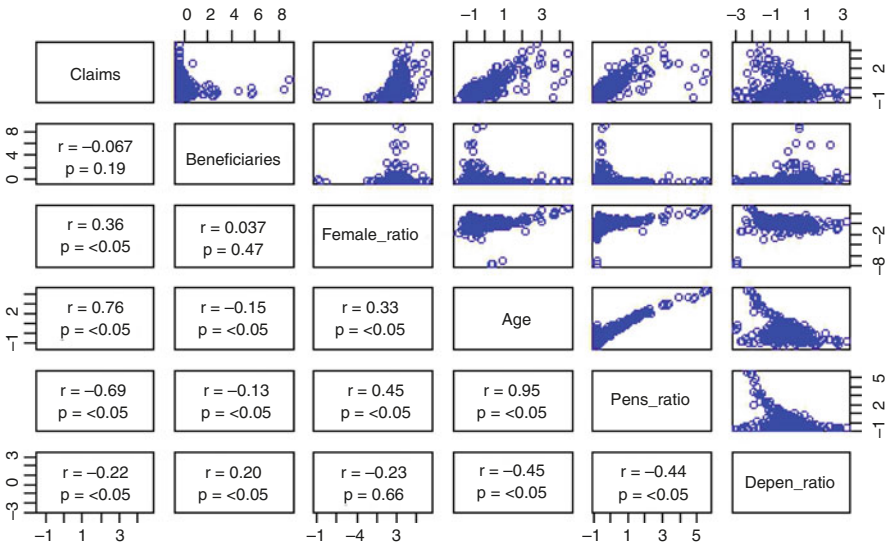

Fig. 2 Association between all variable pairs are visualised in the upper triangle with the corresponding correlations in the lower triangle. Variable names are given on the diagonal

8.2 Modelling

The mixture of t-distributions regression model, (10), is fitted for $K = 1, 2, 3, 4$ with different choices of $\nu = 2, 3, \ldots, 7$, with results in Table 3. This table also includes a mixture of Gaussian regressions model. Model selection is based on BIC also used as a measure of relative goodness of fit.

From Table 3 it can be seen that the mixture regression model with t-distributed errors with 4 degrees of freedom, $t(4)$, yields a better fit than the model based on Gaussian error terms, with a $BIC = 616.2$. Various t-distributed mixture regression models were fitted, with the three component model with 4 degrees of freedom resulting in the lowest value of BIC. It is also apparent that there are clearly different structures in the component regression models, Fig. 3. The figure shows different components in the observed data with respect to the relationship with the explanatory variables. The top panes show the relationship between the response, claims and the explanatory variables age and pens_ratio with an overlay of the estimated component regression models. From this different behaviour of medical insurance providers, with respect to these explanatory variables, is observed. The bottom panes show a similar, but less clear, situation with respect to the variables depen_ratio, female_ratio and beneficiaries.

The estimated mixture regression model enables the researcher to better understand the phenomena and to identify possible drivers of behaviour. The model can also be used to manage the claims process originating from different insurance companies as well as the detection of fraudulent claims.

Table 3 Estimated three component mixture regression results, mixture of t-distributions regression compared to mixture of Gaussian distributions regression

		$t(4)$	Gaussian
Component	Variable/Effect	Parameter estimate	Parameter estimate
1	Intercept	−0.576	−0.523
1	Beneficiaries	0.016	0.034
1	Age	0.322	0.370
1	Pens_ratio	−0.109	−0.197
1	Female_Ratio	0.204	0.238
1	Depen_ratio	0.015	0.045
2	Intercept	−0.085	0.039
2	Beneficiaries	0.107	0.011
2	Age	0.717	0.940
2	Pens_ratio	0.099	−0.145
2	Female_Ratio	0.096	0.137
2	Depen_ratio	0.119	0.174
3	Intercept	0.396	0.378
3	Beneficiaries	−0.011	0.042
3	Age	1.012	1.295
3	Pens_ratio	0.213	−0.058
3	Female_Ratio	0.108	0.164
3	Depen_ratio	0.112	0.047
1	Scale/Var	0.041	0.096
2	Scale/Var	0.039	0.165
3	Scale/Var	0.079	0.093
1	Mixing probability	0.254	0.293
2	Mixing probability	0.331	0.402
3	Mixing probability	0.415	0.305
	BIC	616.2	632.0

9 Discussion

In this chapter SME's are introduced and the t-distribution is identified as a special case. Mixture of regressions with errors from a scale mixture of exponential family distributions were considered, focused on mixture of t-distributed regression models. The mixture regression model addresses the component impact of explanatory variables. Latent behavioural segments are also identified, differentiating between subgroups therefore enhancing the understanding of the underlying phenomena. The t-distribution mixture of regressions model also allows for heavier tails, hence addressing the impact of outliers.

It is of interest to also consider the identifiability of the mixture of scale mixtures approach. This should be addressed in more depth in future work.

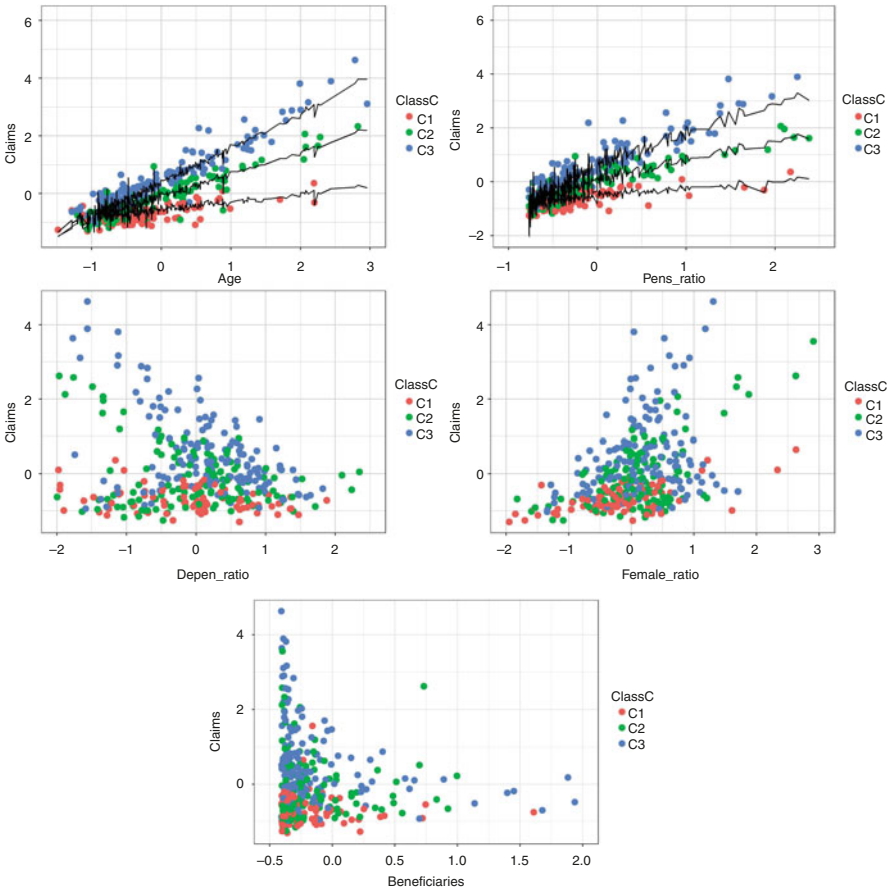

Fig. 3 Components from the estimated mixture of t-distributions regression model. The top panes give the observed data and predicted values against age and pens_ratio respectively. The lower panes give the observed data against depen_ratio, female_ratio and beneficiaries. Colours of the observed data give the component to which an observation belongs. The roughness in the component predictions is due to the marginal views presented

Acknowledgement This research was supported by STATOMET, the Bureau for Statistical and Survey Methodology at the University of Pretoria.

References

Andrews, D. F., & Mallows, C. L. (1974). Scale mixtures of normal distributions. *Journal of the Royal Statistical Society. Series B (Methodological), 36*(1), 99–102.

Bai, X., Chen, K., & Yao, W. (2016). Mixture of linear mixed models using multivariate t distribution. *Journal of Statistical Computation and Simulation, 86*(4), 771–787.

Bai, X., Yao, W., & Boyer, J. E. (2012). Robust fitting of mixture regression models. *Computational Statistics & Data Analysis, 56*(7), 2347–2359.

Boris Choy, S. T., & Chan, J. S. K. (2008). Scale mixtures distributions in statistical modelling. *Australian & New Zealand Journal of Statistics, 50*(2), 135–146.

Jiang, W., & Tanner, M. A. (1999). Hierarchical mixtures-of-experts for exponential family regression models: Approximation and maximum likelihood estimation. *The Annals of Statistics, 27*(3), 987–1011.

Johnson, N. L., Kemp, A. W., & Kotz, S. (2005). *Univariate discrete distributions* (Vol. 3). New Jersey: Wiley.

Kent, J. T., Tyler, D. E., & Vard, Y. (1994). A curious likelihood identity for the multivariate t-distribution. *Communications in Statistics-Simulation and Computation, 23*(2), 441–453.

Millard, S. M. (2018). *Contributions to mixture regression modelling with applications in industry*. PhD Thesis, University of Pretoria, South Africa, 2018.

Peel, D., & McLachlan, G. J. (2000). Robust mixture modelling using the t distribution. *Statistics and Computing, 10*(4), 339–348.

Powers, C. A., Meyer, C. M., Roebuck, M. C., & Vaziri, B. (2005). Predictive modeling of total healthcare costs using pharmacy claims data: A comparison of alternative econometric cost modeling techniques. *Medical Care, 43*(11), 1065–1072.

Seneta, E. (2004). Fitting the variance-gamma model to financial data. *Journal of Applied Probability, 41*(A), 177–187.

Tomar, D., & Agarwal, S. (2013). A survey on data mining approaches for healthcare. *International Journal of Bio-Science and Bio-Technology, 5*(5), 241–266.

Yao, W., Wei, Y., & Yu, C. (2014). Robust mixture regression using the t-distribution. *Computational Statistics & Data Analysis, 71*, 116–127.

Zeller, C. B., Cabral, C. R. B., & Lachos, V. H. (2016). Robust mixture regression modeling based on scale mixtures of skew-normal distributions. *Test, 25*(2), 375–396.

On Improving the Performance of Logistic Regression Analysis Via Extreme Ranking

Hani M. Samawi

Abstract Logistic regression models for dichotomous or ordinal dependent variables is one of the generalized linear models. They have been frequently applied in several fields. In this chapter, we present more efficient and powerful performance of the logistic regression models analysis when a modified extreme ranked set sampling (modified ERSS) or moving extreme ranked set sampling (MERSS) are used and further improving the performance when a modified Double extreme ranked set sampling (modified DERSS) is used. We propose that ranking could be performed based on an available and easy to rank auxiliary variable which is associated with the response variable. Analytically and through simulations, we showed the superiority performance of the logistics regression analysis when modified ERSS, MERSS, and DERSS are used compared with using the simple random sample (SRS). For illustration purposes of the procedures developed, we use a real dataset from 2011/12 National Survey of Children's Health (NSCH).

1 Introduction

The logistic regression model is one of the important statistical approaches for analyzing categorical response variables. Logistic regression models have less restricted assumptions than that for ordinary regression models. In particular, the analysis of logistic regression model does not require the normally distributed assumption of the dependent variable or the assumption of the homogeneity of the errors term variance. On the other hand, there are some restrictions on the logistic regression implementation in practice. For example, some of the restrictions are the specification error, multicollinearity, and zero cells and complete separation (Menard 1995). Logistic models are practical in various areas and can be easily

H. M. Samawi (✉)
Department of Biostatistics, Epidemiology and Environmental Health Sciences, Jiann-Ping Hsu College of Public Health, Georgia Southern University, Statesboro, GA, USA
e-mail: hsamawi@georgiasouthern.edu

A. Bekker et al. (eds.), *Computational and Methodological Statistics and Biostatistics*, Emerging Topics in Statistics and Biostatistics,
https://doi.org/10.1007/978-3-030-42196-0_15

interpreted in terms of odds ratio or conditional odds ratio for certain risk factor. One of logistic regression model features is, it can be used to find the risk factors among various potential predictors of disease in medical and epidemiological research (Steinmann et al. 2007).

When the response variable is dichotomous, it could follow an extremely unbalanced distribution, when one category is scarce as compared to the other. Consequently, the logistic regression model could suffer from serious limitations when a population has such an imbalance in the probability of outcomes. In this case, logistic regression will be severely underpowered with the presence of rare and potentially underestimated events (see, King and Zeng 2001). Thus it is difficult to predict rare events with the standard application of logistic regression. In the literature, there are some attempts to address this issue by using some alternative sampling strategies. For example, over-sampling (i.e., increasing the number of units in the minority class) and under-sampling (i.e., decreasing the number of units in the majority class were commonly used procedure (Maalouf and Trafalis 2011). However, these two methods result in biased estimates of the model parameters. Therefore, to address the shortcoming, it is necessary to seek sampling strategies that are cost-effective, powerful and efficient for the inference of the logistic models without using the sampling methods as mentioned above or use large sample size.

Data collection is an essential process for all statistical procedures. There are many sampling schemes in the literature. The most assumed common sampling scheme is the simple random sampling (SRS). In some situations, SRS provides a non-representative sample to the target population. A possible solution to address the issue mentioned above is to use a cost-effective and more structural approach. Ranked set sampling (RSS) and its variations are important candidates to draw a more cost-effective and structural sample. RSS was proposed by McIntyre (1952).

For balanced RSS, first, randomly draw m sets each contains m subjects from a specific population. Within each set, of size m, rank subjects visually or by non-costly means. The subject ranked lowest is chosen for actual quantification from the first set. The subject ranked second lowest is measured from the second. Repeated the process until the subject with the maximum rank is measured from the mth set. It was first proposed by Lynne Stokes (1977) that RSS may be used to collect data in some vital field. She proposed to use easy to rank auxiliary variable which is correlated with the variable of interest. However, the amount of improvement in the precision of using RSS estimator depends on the strength of the correlation between the available auxiliary variable and the variable of interest see Chen et al. (2005).

RSS considered for regression models in the attempt to improve their performance (see Samawi and Ababneh 2001; Samawi and Abu-Dayyeh 2002; Samawi and Al-Saleh 2002; Samawi and Al-Saleh 2004; Twidwell 2000; Murff and Sager 2006; Chen and Wang 2004; Özdemir and Esin 2007). Our recent investigation revealed no improvement in the model parameters' estimation, odds ratios and the power of testing some hypotheses for the logistic regression models. There is still a need for more efficient sampling schemes to improve the performance of the logistic regression analysis. Samawi et al. (1996) introduced a variety of the extreme ranked set sample (ERSS) for the population mean estimation. Al-Odat and

Al-Saleh (2001) introduced a modification to ERSS and called it moving extreme ranked set sampling (MERSS). Samawi et al. (2017) utilized MERSS to improve the performance of logistic regression analysis and showed a significant improvement in the performance of the model inference. In addition, double extreme ranked set sampling (DERSS) is introduced by Samawi (2002). The purpose of this chapter is to propose using a modify vision of DERSS and ERSS as well as MERSS which proposed Samawi et al. (2017) to improve the performance of the logistic regression. The modifications of ERSS and DERSS is as follows:

A modification of ERSS procedure:

1. From the target population, draw randomly m sets each contains m subjects.
2. Rank subjects within each set with respect to the characteristic, such as an available concomitant (auxiliary) variable;
3. Measure the maximum (minimum) from each set.

This complete one cycle. If a larger sample size is needed, the entire cycle can be repeated (Step 1–3), r times to obtain a sample of larger size, $n = rm$. This modified ERSS is denoted by $\text{ERSS}_{\max}$ ($\text{ERSS}_{\min}$).

As an extension to the modified ERSS, the modified DERSS is as follows:

1. Draw randomly m $\text{ERSS}_{\max}$ ($\text{ERSS}_{\min}$) samples of size m each as described above without quantification to the sampling units.
2. Repeat steps 2 and 3 above.

This complete one cycle. If a larger sample size is needed, the entire cycle can be repeated (Step 1–3), r times to obtain a sample of larger size, $n = rm$. This modified DERSS is denoted by DERSSmax (DERSSmin).

Another modification of RSS, namely Moving Extreme Ranked Set Sampling (MERSS), was introduced by Al-Odat and Al-Saleh (2001). The MERSS procedure can be implemented as follows:

1. Select m simple random samples of size 1, 2, 3,..., m, respectively;
2. Order the elements in each sample with respect to the characteristic of interest simply by visual inspection or some other means not requiring the actual measurement;
3. Accurately measure the maximum (or minimum) ordered observation from each set.

The entire cycle can be repeated (Steps 1–3), if necessary, r times to obtain a sample of larger size, $n = rm$. This sampling scheme is known as $\text{MERSS}_{\max}$ (or $\text{MERSS}_{\min}$). Samawi and Al-Saleh (2013) implemented these two types of MERSS to provide valid and more efficient estimates of the odds ratio. Moreover, Samawi et al. (2018a), Samawi et al. (2018b), Samawi et al. (2017) and Linder et al. (2018) implemented ERSS and/or MERSS to improve the performance of Cox model, AFT model, logistic model, and Poisson regression model respectively.

This chapter presents the implementation of $\text{ERSS}_{\max}$ ($\text{ERSS}_{\min}$), $\text{MERSS}_{\max}$ ($\text{MERSS}_{\max}$) and $\text{DERSS}_{\max}$ ($\text{DERSS}_{\min}$) to improve the performance of the logistic regression models analysis compared to SRS. We are interesting in using

the modified, MERSS, ERSS and DERSS when ranking is performed based on one of the available auxiliary variables (Z) which are correlated with the variable of interest. Modified, DERSS, MERSS, and ERSS procedures only identified the maximum (or minimum) from each set for quantification. Thus these schemes can be easily implemented for large m.

We suggest to use $\text{ERSS}_{\min}$, $\text{MERSS}_{\min}$, and $\text{DERSS}_{\min}$ when Z is positively correlated with the response variable. In case of negative correlation, we recommend to use $\text{ERSS}_{\max}$, $\text{MERSS}_{\max}$, and $\text{DERSS}_{\max}$. In this chapter, we are presenting the cases for $\text{ERSS}_{\min}$, $\text{MERSS}_{\min}$, and $\text{DERSS}_{\min}$. The other cases are similar, so we discuss in the simulation study. Therefore, in Sect. 2 we discussed the logistic regression analysis and the resulting properties when $\text{DERSS}_{\min}$ is used. The other sampling schemes are similar and will be discussed in the simulation studies. The simulation study is provided in Sect. 3 in order to compare the performance of logistic regression models analysis based on $\text{DERSS}_{\min}$, $\text{MERSS}_{\min}$, $\text{ERSS}_{\min}$, and SRS schemes. The proposed methods are illustrated using children health behavior from (NSCH 2011) data in Sect. 4. In Sect. 5, we provide the final remarks.

1.1 Sample Notation and Some Basic Results

For the k-th cycle, let $Z^1_{11k}, Z^1_{12k}, \ldots, Z^1_{1mk}, Z^1_{21k}, Z^1_{22k}, \ldots, Z^1_{2mk}; \ldots; Z^1_{m1k}, Z^1_{m2k}, \ldots, Z^1_{mmk}; Z^m_{11k}, Z^m_{12k}, \ldots, Z^m_{1mk}, Z^m_{21k}, Z^m_{22k}, \ldots, Z^m_{2mk}; \ldots; Z^m_{m1k}, Z^m_{m2k}, \ldots, Z^m_{mmk}$; $k = 1, 2, \ldots, r$, be the m independent sets each with sample size m^2. Note that Z^l_{ijk} is the j-th sample unit in the i-th row (sample) of the k-th set. Assume that each element Z^l_{ijk} in the sample has a p.d.f. $f_Z(z)$ and a distribution function $F_Z(z)$ (absolutely continuous). For selecting $\text{ERSS}_{\min}$ and $\text{DERSS}_{\min}$, after ranking the sample units within each sample in each set (visually or by any not costly way), we obtain:

$$\begin{bmatrix} Z^1_{1(1)k}, & Z^1_{1(2)k}, & \cdots, & Z^1_{1(m)k} \\ Z^1_{2(1)k}, & Z^1_{2(2)k}, & \cdots, & Z^1_{2(m)k} \\ \cdots & \cdots & \cdots & \cdots \\ Z^1_{m(1)k}, & Z^1_{m(2)k}, & \cdots, & Z^1_{m(m)k} \end{bmatrix}, \ldots, \begin{bmatrix} Z^m_{1(1)k}, & Z^m_{1(2)k}, & \cdots, & Z^m_{1(m)k} \\ Z^m_{2(1)k}, & Z^m_{2(2)k}, & \cdots, & Z^m_{2(m)k} \\ \cdots & \cdots & \cdots & \cdots \\ Z^m_{m(1)k}, & Z^m_{m(2)k}, & \cdots, & Z^m_{m(m)k} \end{bmatrix},$$

$k = 1, 2, \ldots, r$. Thus the first stage will yield m $\text{ERSS}_{\min}$ samples:

$$A_{1k} = \left\{ Z^1_{1(1)k}, Z^1_{2(1)k}, \ldots, Z^1_{m(1)k} \right\} \ldots,$$

$$A_{2k} = \left\{ Z^2_{1(1)k}, Z^2_{2(1)k}, \ldots, Z^2_{m(1)k} \right\}.$$

$A_{mk} = \left\{ Z^m_{1(1)k}, Z^m_{2(1)k}, \ldots, Z^m_{m(1)k} \right\}$Now let $V_{1(1)k} = \min(A_{1k})$, $V_{2(1)k} = \min(A_{2k})$, ..., $V_{m(1)k} = \min(A_{mk})$ Then $V_{1(1)k}, V_{2(1)k}, \ldots, V_{m(1)k}$ $k = 1, 2, ..., r$, denotes $\text{DERSS}_{\min}$. For $\text{DERSS}_{\max}$ is similar but selecting the maximum instead of the minimum. It is easy to show that the p.d.f of the smallest and the largest order statistics are i.i.d. sample of size m with p.d.f $f_Z(z)$ are respectively given by: $f_{Z(1)}(z) = m(1 - F_Z(z))^{m-1} f_Z(z)$ and$f_{Z(m)}(z) = m(F_Z(z))^{m-1} f_Z(z)$Also, let $V_{i(1)k}$have p.d.f $g_{(1)}(z)$and c.d.f $G_{(1)}(z)$ and$V_{i(m)k}$have p.d.f $g_{(\mathrm{m})}(z)$and c.d.f $G_{(\mathrm{m})}(z)$where $i = 1,2,\ldots,m$ *and* $k = 1, 2, ..., r$. Clearly, $V_{1(1)k}, V_{2(1)k}, \ldots, V_{m(1)k}, k = 1, 2, ..., r$, are independent and identically distributed. Using the above description of $\text{DERSS}_{\min}$ (DERSSmax), we have the following results:

1. $G_{V_{(1)}}(z) = 1 - \left[1 - F_{Z_{(1)}}(z)\right]^m = 1 - [1 - F_Z(z)]^{m^2}$
2. $g_{V_{(1)}}(z) = m f_{Z_{(1)}}(z)\left[1 - F_{Z_{(1)}}(z)\right]^{m-1} = m^2 f_Z(z)\,[1 - F_Z(z)]^{m^2-1}$
3. $G_{V_{(m)}}(z) = [F_Z(z)]^{m^2}$
4. $g_{V_{(\mathrm{m})}}(z) = \mathrm{m}^2 f_Z(z)\,[F_Z(z)]^{m^2-1}$

Next, we will present the derivation of the logistic regression when $\text{DERSS}_{\min}$ is used. The derivation for the other sampling schemes $\text{ERSS}_{\min}$ and $\text{MERSS}_{\min}$ are similar and will be discussed in the simulation.

2 Logistic Regression Analysis for $\text{DERSS}_{\min}$

Using similar notation and definition of the logistic regression model as in Samawi et al. (2017) we have

$$\pi(\mathbf{x}; z) = P(Y = 1|\mathbf{x}; z) = \frac{\exp\left(\beta_0 + \beta_1 x_1 + \cdots + \beta_p x_p + \delta z\right)}{1 + \exp\left(\beta_0 + \beta_1 x_1 + \cdots + \beta_p x_p + \delta z\right)}, \tag{1}$$

where Y is a binary response variable with two distinct outcomes as 1 (success) and 0 (failure), which can be viewed as a Bernoulli random variable with the probability of success π and$\delta$is the slope of Z. For some explanatory variables,$X_1, X_2, \ldots, X_p$, which have a certain association with the response variable Y. Assume the auxiliary variable, denoted by Z, having a strong association with Y to be used in selecting the modified ERSS and DERSS. We assume Z to be an easy-to-rank visually or with little cost. Using the logit link, we can write (1) as

$$Log\left(\frac{\pi(\mathbf{x}; z)}{1 - \pi(\mathbf{x}; z)}\right) = \beta_0 + \beta_1 x_1 + \cdots + \beta_p x_p + \delta z, \tag{2}$$

where the n binary responses are treated as independent Bernoulli random variables.

We denote$\mathbf{w}_i = (x_{i0}x_{i1}, \ldots, x_{ip}, z_i)'$as the vector containing the measurements on p explanatory variables and one auxiliary variable for the ith setting, where $i = 1, 2, \ldots, L$. For the model properties and fitting process see Agresti (2002).

Here, we investigate the improvement of the logistic regression model analyses under $\text{DERSS}_{\min}$ sampling scheme. The ranking of selecting a $\text{DERSS}_{\min}$ is assumed to be performed based on an easy-to-rank auxiliary variable Z associated with the response variable. We denote$V_{1(1)k}, V_{2(1)k}, \ldots, V_{m(1)k}, k = 1, 2, ..., r$ as the measurements acquired from a $\text{DERSS}_{\min}$ of size$n = r.m$. Therefore, we can assume that the judgment on the ranking is perfect ranking. However, if there was some ranking error our method still valid and perform at least as good as SRS. Let $V_{i(1)k}$ denotes as the minimum order statistic for an $\text{ERSS}_{\min}$ of size m from $F_Z(.)$. Then we select the subjects based on these double minimum ranked auxiliary variable Z.

Meanwhile, the vector $\mathbf{w}_{i[1]k} = (x_{ik0}x_{i[1]k1}, \ldots, x_{i[1]p}, z_{i(1)k})'$, $i = 1, 2, \ldots, m$; $k = 1, 2, \ldots, r$ represents the observations on the p explanatory variables and one auxiliary variable obtained from the sampled unit in the kth cycle of the ith set. Furthermore, assume $x_{ik0}$to be 1. Therefore, under $\text{DERSS}_{\min}$ we have

$$\pi\left(\mathbf{w}_{\mathbf{i}[1]k}\right) = \frac{\exp\left(\sum_{h=0}^{p} \beta_h x_{i[1]kh} + \delta v_{i(1)k}\right)}{1 + \exp\left(\sum_{h=0}^{p} \beta_h x_{i[1]kh} + \delta v_{i(1)k}\right)}. \tag{3}$$

Clearly, $Y_{i[1]k}$ is a binary response with the probability of success denoted by $\pi(\mathbf{w}_{\mathbf{i}[1]k})$. Now,$\{Y_{i[1]k}, i = 1, 2, \ldots, m; k = 1, 2, .., r\}$ can be viewed as independent Bernoulli random variables with$E(Y_{i[1]k}) = \pi(\mathbf{w}_{\mathbf{i}[1]k})$. Therefore, as in Samawi et al. (2017), the likelihood function is given by

$$\begin{aligned} l(\boldsymbol{\beta}) &= \prod_{i=1}^{m}\prod_{k=1}^{r} \pi\left(\mathbf{w}_{\mathbf{i}[1]k}\right)^{y_{i[1]k}}\left[1 - \pi\left(\mathbf{w}_{\mathbf{i}[1]k}\right)\right]^{1-y_{i[1]k}} \\ &= \left[\prod_{i=1}^{m}\prod_{k=1}^{r}\left[1 - \pi\left(\mathbf{w}_{\mathbf{i}[1]k}\right)\right]\right]\left[\exp\left\{\sum_{i=1}^{r}\sum_{j=1}^{m} y_{i[1]k}\log\left(\frac{\pi\left(\mathbf{w}_{\mathbf{i}[1]k}\right)}{1-\pi\left(\mathbf{w}_{\mathbf{i}[1]k}\right)}\right)\right\}\right]. \end{aligned} \tag{4}$$

Taking the natural logarithm of the log likelihood in (4) we get

$$\frac{dL}{d\beta_c} = \left(\sum_{i=1}^{m}\sum_{k=1}^{r} y_{i[1]k}x_{i[1]kc}\right) - \sum_{i=1}^{m}\sum_{k=1}^{r} x_{i[1]kc}\left(\frac{\exp\left(\sum_{h=0}^{p}\beta_h x_{i[1]kh} + \delta v_{i(1)k}\right)}{1 + \exp\left(\sum_{h=0}^{p}\beta_h x_{i[1]kh} + \delta v_{i(1)k}\right)}\right). \tag{5}$$

Then the MLE can be obtained by solving the following normal equation,

$$\left(\sum_{i=1}^{m}\sum_{k=1}^{r} y_{i[1]k}x_{i[1]kc}\right) - \sum_{i=1}^{m}\sum_{k=1}^{r} \hat{\pi}_{i[1]k}x_{i[1]kc} = 0. \tag{7}$$

These equations could be solved iteratively using the Newton-Raphson method (See, Agresti 2002). For a detailed discussion about the existent and uniqueness of MLE see Agresti (2002), Lehmann and Casella (1998), Albert and Anderson 1984 and Rashid and Shifa (2009). They also showed that MLE ofβs are consistent estimators and have an asymptotic normal distribution.

Let $\mathbf{W}_{[R]}$ denote the $n \times (p+2)$ matrix of $\{w_{i[1]kh}\}$ values for matrix notations. As in Samawi et al. (2017), we can write (7) as

$$\mathbf{W}'_{[R]}\mathbf{y}_{[R]} = \mathbf{W}'_{[R]}\hat{\mathbf{E}}_{[R]},$$

and $\hat{E}_{i[1]k} = \hat{\pi}_{i[1]k}$. Then the variance-covariance matrix can be estimated as the inverse of the information matrix. The Fisher's information matrix can be obtained as

$$\begin{aligned}\frac{d^2L}{d\beta_c d\beta_d} &= -\sum_{i=1}^{m}\sum_{k=1}^{r}\left(\frac{x_{i[1]kc}x_{i[1]kd}\exp\left(\sum_{h=0}^{p}\beta_h x_{i[1]kh} + \delta v_{i(1)k}\right)}{\left[1+\exp\left(\sum_{h=0}^{p}\beta_h x_{i[1]kh} + \delta v_{i(1)k}\right)\right]^2}\right) \\ &= -\sum_{i=1}^{m}\sum_{k=1}^{r} x_{i[1]kc}x_{i[1]kd}\pi_{i[1]k}\left(1-\pi_{i[1]k}\right).\end{aligned} \tag{8}$$

Note that (8) is free of $\{y_{i[1]k}\}$. This implies that the observed and the expected second derivatives are the same in term of$y_{i[1]k}$. Then the variance-covariance matrix can be calculated as:

$$\hat{C}ov\left(\hat{\boldsymbol{\beta}}_{[R]}\right) = \left\{\mathbf{W}'_{[R]}Diag\left[\hat{\pi}_{i[1]k}\left(1-\hat{\pi}_{i[1]k}\right)\right]\mathbf{W}_{[R]}\right\}^{-1}. \tag{9}$$

Additionally, $I(\boldsymbol{\beta})_{DERSS_{\min}} = -E_{Z_{i[1]}}\left(\frac{\partial^2 L(\boldsymbol{\beta})}{\partial\boldsymbol{\beta}'\partial\boldsymbol{\beta}}\right)_{(p+2)x(p+2)}$,represents the Fisher's information matrix.

Consequently, to make an inference aboutβ_j, we need to calculate the Fisher's information with respect toβ_j in order to study the performance of our proposed procedure. Note that, Fisher's information can be used as a measure of the parameter estimator precision as well. Now assume that the auxiliary variable Z is random. To show that the Fisher's information of estimating βusing DERSS is larger than using ERSS and SRS, thus we need to show that $I(\beta_j)_{DERSS_{\min}} \geq I(\beta_j)_{ERSS_{\min}} \geq I(\beta_j)_{SRS}$. Similarly, we can show that$I(\beta_j)_{MERSS_{\min}} \geq I(\beta_j)_{SRS}$. For the j^{th} covariate, we can derive $I_{DERSS_{\min}}(\beta_j)$as

$$I_{DERSS_{\min}}(\beta_j) = -E_{V_{(1)}}\left(\frac{\partial^2 L(\boldsymbol{\beta})}{\partial \beta_j^2}\right) = E_{V_{(1)}}\left[\sum_{i=1}^{m}\sum_{k=1}^{r}\left(\frac{x_{i[1]kj}^2 \exp\left(\sum_{h=0}^{p}\beta_h x_{i[1]kh}+\delta V_{i(1)k}\right)}{\left[1+\exp\left(\sum_{h=0}^{p}\beta_h x_{i[1]kh}+\delta V_{i(1)k}\right)\right]^2}\right)\right]$$
$$= E_{V_{(1)}}\left[\sum_{i=1}^{m}\sum_{k=1}^{r} x_{i[1]kj}^2\left(\pi\left(x_{i[1]kj}, V_{i(1)k}\right)\left(1-\pi\left(x_{i[1]kj}, V_{i(1)k}\right)\right)\right)\right]. \tag{10}$$

Let the ranking variable Z follows a continuous distribution$F_Z(z)$, with a density function$f_Z(z)$.For$\delta > 0$, we have taken the minimum judgment ranking, from each set of size m. However, from the above derivation in Sect. 1.1, the density function of $V_{[1]}$is given by $f_{V_{(1)}}(v) = m f_{Z_{(1)}}(v)\left(1 - F_{Z_{(1)}}(v)\right)^{m-1}$. Then from (10),

$$I(\beta_j)_{DERSS_{\min}} = -E_{V_{[1]}}\left(\frac{\partial^2 L(\boldsymbol{\beta})}{\partial \beta_j^2}\right)$$
$$= \sum_{i=1}^{m}\sum_{k=1}^{r} x_{i[1]kj}^2 \int_v \left(\pi\left(x_{1[1]kj}, v_{i[1]k}\right)\left(1-\pi\left(x_{1[1]kj}, v_{i[1]k}\right)\right)\right.$$
$$\left. m f_{Z_{(1)}}(v)\left(1 - F_{Z_{(1)}}(v)\right)^{m-1} dv.\right. \tag{11}$$

Since we assume that$\delta > 0$, then $(\pi(x_{1[1]kj}, v_{i(1)k})(1 - \pi(x_{1[1]kj}, v_{i(1)k}))$ is a decreasing function of v for fixed$x_{ik0}x_{i[1]k1}\ldots x_{i[1]kp}$, and$v_{i[1]k} > 0$ (this restriction can be achieved by shifting v to be positive). In addition, $m\left(1 - F_{Z_{(1)}}(z)\right)^{m-1}$is a decreasing function of z. Therefore, by See and Chen (2008), we have

$$\text{Since } \int_v m f_{Z_{(1)}}(v)\left(1 - F_{Z_{(1)}}(v)\right)^{m-1} dv = 1,$$

$$\text{then } I(\beta_j)_{DERSS_{\min}} \geq \sum_{i=1}^{m}\sum_{k=1}^{r} x_{i[1]kj}^2 \int_v \left(\left(\pi\left(x_{1[1]kj}, v_{i[1]k}\right)\left(1-\pi\left(x_{1[1]kj}, v_{i[1]k}\right)\right)\right)\right)$$

$$f_{Z_{(1)}}(v)dv = I_{ERSS_{\min}}(\beta_j) \geq I_{SRS}(\beta_j). \tag{12}$$

We can achieve the last inequality in a similar way as in Samawi et al. (2017). Likewise, we can demonstrate that the inequality in (12) holds when the association between Y and Z is negative.

3 Simulation Studies and Results

To assess the performance of the logistic regression analyses based on using $DERSS_{min}$ compared with $ERSS_{min}$, $MERSS_{min,}$ and SRS, we conducted simulation studies to get some insight. The simulation studies are designed to estimate the power of testing the hypothesis of no association between the response variable and a predictor. We have separate simulation studies one for continuous predictors and one for a dichotomous predictor. Also, for both continuous and dichotomous predictors, using the simulation studies, we estimated the MSE, the confidence intervals and the coverage probabilities of the conditional odds ratio. In the simulation, we consider some association levels between the risk factors and the auxiliary covariate (i.e.,β_1=0.0, 0.2, 0.5, 1.0). In this study we provide only simulation results for (m = 30, r = 20) and (m = 50, r = 10).The simulation results were based on 5000 replication for each combination of set sizes parameters setting.

The results of the simulation for continuous predictors are provided in Tables 1, 2, and 3, while the simulation results for dichotomous predictors are provided in Tables 4, 5, and 6. In Tables 1 and 4, we estimate the empirical powers, while in Tables 2 and 5, we report the conditional odds ratio estimates, their MSEs, and the relative efficiencies

$$\left\{RE_1 = \frac{MSE(ERSS)}{MSE(DERSS)}, RE_2 = \frac{MSE(SRS)}{MSE(DERSS)}, RE_3 = \frac{MSE(SRS)}{MSE(ERSS)}\right\}.$$

Table 1 Estimation of the power of testing $H_o : \beta_2 = 0$ vs $H_a : \beta_2 \neq 0$ adjusting for the auxiliary variable (Z) in the model (continuous risk factor)

		$m = 30$ and $r = 20$			$m = 50$ and $r = 10$		
β_1	β_2	Power of the test using $DERSS_{min}$	Power of the test using $ERSS_{min}$	Power of the test using SRS	Power of the test using $DERSS_{min}$	Power of the test using $ERSS_{min}$	Power of the test using SRS
0.2	0.0	0.0434	0.0492	0.0512	0.0480	0.0460	0.0530
0.2	0.1	0.1110	0.0982	0.0804	0.0964	0.0846	0.0788
0.2	0.3	0.5782	0.4908	0.3614	0.5236	0.4312	0.3002
0.2	0.5	0.9552	0.9066	0.7584	0.9372	0.8686	0.6918
0.5	0.0	0.0510	0.0414	0.0488	0.0462	0.0518	0.0520
0.5	0.1	0.1634	0.1250	0.0812	0.1506	0.1172	0.0744
0.5	0.3	0.8498	0.6834	0.3614	0.8098	0.6456	0.3154
0.5	0.5	0.9986	0.9862	0.8038	0.9968	0.9756	0.7138
1.0	0.0	0.0468	0.0430	0.0532	0.0466	0.0506	0.0474
1.0	0.1	0.2216	0.1900	0.0962	0.1844	0.1720	0.0846
1.0	0.3	0.9372	0.8922	0.4394	0.8790	0.8638	0.3680
1.0	0.5	1.0000	0.9998	0.8598	0.9992	0.9992	0.7882

Table 2 Odds ratio (OR) estimation and their MSE (continuous risk factor)

		$m = 30$ and $r = 20$						Relative efficiency		
		$DERSS_{min}$		$ERSS_{min}$		SRS				
β_1	OR	Estimate	MSE	Estimate	MSE	Estimate	MSE	RE_1	RE_2	RE_3
0.0	1.000	1.009	0.023	1.013	0.028	1.021	0.042	1.223	1.837	1.502
0.0	1.105	1.118	0.028	1.122	0.035	1.127	0.051	1.240	1.786	1.440
0.0	1.350	1.368	0.038	1.372	0.048	1.385	0.079	1.260	2.060	1.635
0.0	1.649	1.672	0.059	1.678	0.073	1.689	0.112	1.223	1.879	1.536
0.5	1.000	1.006	0.011	1.008	0.016	1.014	0.039	1.408	3.385	2.404
0.5	1.105	1.112	0.014	1.115	0.021	1.127	0.047	1.508	3.451	2.289
0.5	1.350	1.358	0.020	1.360	0.029	1.371	0.070	1.472	3.552	2.413
0.5	1.649	1.670	0.031	1.671	0.045	1.689	0.097	1.432	3.087	2.155
1.0	1.000	1.002	0.007	1.006	0.009	1.012	0.033	1.268	4.657	3.673
1.0	1.105	1.111	0.009	1.112	0.011	1.129	0.041	1.295	4.743	3.662
1.0	1.350	1.358	0.015	1.359	0.017	1.383	0.060	1.177	4.094	3.479
1.0	1.649	1.666	0.025	1.664	0.027	1.697	0.093	1.107	3.747	3.386
$m = 50$ and $r = 10$										
0.0	1.000	1.012	0.026	1.015	0.033	1.028	0.054	1.256	2.054	1.635
0.0	1.105	1.120	0.032	1.121	0.039	1.133	0.066	1.217	2.045	1.680
0.0	1.350	1.372	0.044	1.374	0.058	1.386	0.094	1.307	2.109	1.614
0.0	1.649	1.683	0.067	1.686	0.088	1.704	0.142	1.306	2.116	1.620
0.5	1.000	1.004	0.012	1.009	0.019	1.016	0.047	1.564	3.876	2.479
0.5	1.105	1.111	0.015	1.114	0.024	1.127	0.057	1.557	3.762	2.416
0.5	1.350	1.364	0.023	1.368	0.034	1.386	0.090	1.484	3.971	2.675
0.5	1.649	1.668	0.035	1.681	0.052	1.696	0.130	1.479	3.732	2.523
1.0	1.000	1.005	0.009	1.006	0.010	1.022	0.038	1.137	4.245	3.734
1.0	1.105	1.112	0.011	1.111	0.013	1.130	0.049	1.111	4.367	3.932
1.0	1.350	1.361	0.018	1.360	0.019	1.378	0.071	1.047	3.878	3.703
1.0	1.649	1.666	0.031	1.671	0.031	1.696	0.111	1.000	3.575	3.577

Finally, the estimation of the 95% confidence intervals of the odds ratios and their coverage probabilities are provided in Tables 3 and 6.

From our simulation studies, it is clear that the modified DERSS outperform the ERSS and SRS in terms of empirical power, MSEs, and confidence interval coverage probabilities in case of continuous or dichotomous predictors (see Tables 1, 2, 3, 4, 5, 6, respectively.) We notice that the power of the test and the efficiency of estimating the odds ratio increases as the set size (m) increase in all presented cases.

From Samawi et al. (2017) we extracted the following tables for comparison purposes with DERSS and ERSS.

From Tables 7, 8, and 9, we can observe that DERSS outperform ERSS and MERSS for a given set size and cycle size. However, all proposed sampling

Table 3 95% confidence interval of the odds ratio (OR) (continuous risk factor)

		$m = 30$ and $r = 20$								
		$DERSS_{min}$			$ERSS_{min}$			SRS		
β_1	OR	Lower	Upper	Coverage %	Lower	Upper	Coverage %	Lower	Upper	Coverage %
0.0	1.000	0.755	1.348	0.957	0.736	1.396	0.951	0.696	1.498	0.949
0.0	1.105	0.840	1.488	0.951	0.817	1.541	0.946	0.769	1.653	0.953
0.0	1.350	1.035	1.809	0.953	1.006	1.872	0.951	0.948	2.028	0.949
0.0	1.649	1.273	2.198	0.948	1.238	2.277	0.948	1.161	2.461	0.948
0.5	1.000	0.821	1.233	0.949	0.787	1.292	0.959	0.701	1.468	0.951
0.5	1.105	0.909	1.361	0.947	0.872	1.426	0.946	0.780	1.632	0.953
0.5	1.350	1.111	1.661	0.952	1.066	1.736	0.952	0.952	1.978	0.955
0.5	1.649	1.361	2.050	0.955	1.309	2.132	0.948	1.176	2.429	0.954
1.0	1.000	0.850	1.182	0.953	0.837	1.209	0.957	0.724	1.417	0.947
1.0	1.105	0.941	1.312	0.955	0.926	1.337	0.950	0.808	1.581	0.944
1.0	1.350	1.144	1.612	0.948	1.127	1.637	0.946	0.989	1.934	0.951
1.0	1.649	1.390	1.997	0.949	1.372	2.019	0.952	1.213	2.374	0.950
$m = 50$ and $r = 10$										
0.0	1.000	0.742	1.381	0.952	0.719	1.435	0.954	0.675	1.568	0.947
0.0	1.105	0.825	1.522	0.950	0.796	1.579	0.947	0.744	1.727	0.945
0.0	1.350	1.019	1.850	0.955	0.984	1.921	0.955	0.914	2.106	0.949
0.0	1.649	1.257	2.256	0.950	1.214	2.343	0.949	1.128	2.577	0.949
0.5	1.000	0.810	1.244	0.954	0.776	1.311	0.948	0.677	1.527	0.948
0.5	1.105	0.898	1.374	0.949	0.859	1.445	0.947	0.751	1.695	0.950
0.5	1.350	1.103	1.688	0.949	1.057	1.771	0.951	0.926	2.076	0.950
0.5	1.649	1.342	2.073	0.951	1.298	2.179	0.950	1.137	2.534	0.956
1.0	1.000	0.835	1.209	0.953	0.829	1.221	0.949	0.707	1.478	0.953
1.0	1.105	0.923	1.340	0.948	0.915	1.349	0.950	0.782	1.635	0.944
1.0	1.350	1.122	1.652	0.953	1.116	1.657	0.950	0.954	1.992	0.953
1.0	1.649	1.359	2.044	0.951	1.360	2.053	0.956	1.172	2.458	0.951

schemes, ERSS, DERSS and MERSS outperform SRS for estimation and testing hypotheses.

4 Application Using NSCH 2011 Data

To illustrate the proposed method we used the data obtained from 2011 the National Survey of Children's Health (NSCH) conducted every two years by the Center for Disease Control's (CDC) Division of Adolescent and School Health (Statistics, 11/29/2011, 10/30/2013, http://www.cdc.gov/nchs/slaits/nsch.htm). To demonstrate the methodology, we focused on children aged between 11 and 17 with a total sample size of 41,323 children. We treated the survey data as a population and randomly selected three samples, namely $DERSS_{min}$ (with m = 20, r = 30, and

Table 4 Estimation of the power of testing $H_o : \beta_2 = 0$ vs $H_a : \beta_2 \neq 0$ adjusting for the auxiliary variable (Z) in the model (dichotomous risk factor)

		$m = 30$ and $r = 20$			$m = 50$ and $r = 10$		
β_1	β_2	Power of the test using $DERSS_{min}$	Power of the test using $ERSS_{min}$	Power of the test using SRS	Power of the test using $DERSS_{min}$	Power of the test using $ERSS_{min}$	Power of the test using SRS
0.2	0.0	0.0436	0.0510	0.0416	0.0464	0.0510	0.0392
0.2	0.1	0.0624	0.0652	0.0524	0.0600	0.0546	0.0490
0.2	0.3	0.1486	0.1344	0.1028	0.1344	0.1212	0.0982
0.2	0.5	0.3266	0.2806	0.2028	0.2726	0.2242	0.1816
0.5	0.0	0.0488	0.0442	0.0430	0.0486	0.0462	0.0410
0.5	0.1	0.0704	0.0656	0.0576	0.0718	0.0658	0.0470
0.5	0.3	0.2930	0.1950	0.1140	0.2566	0.1808	0.1098
0.5	0.5	0.6102	0.4366	0.2288	0.5708	0.4128	0.1924
1.0	0.0	0.0516	0.0510	0.0418	0.0500	0.0466	0.0442
1.0	0.1	0.0880	0.0836	0.0598	0.0854	0.0772	0.0638
1.0	0.3	0.4390	0.3394	0.1388	0.3780	0.3170	0.1142
1.0	0.5	0.8528	0.7198	0.2558	0.7780	0.6862	0.2314

Table 5 Odds ratio (OR) estimation and their MSE (dichotomous risk factor)

		$m = 30$ and $r = 20$						Relative efficiency		
		$DERSS_{min}$		$ERSS_{min}$		SRS				
β_1	OR	Estimate	MSE	Estimate	MSE	Estimate	MSE	RE_1	RE_2	RE_3
0.0	1.000	1.051	0.107	1.068	0.144	1.073	0.212	1.346	1.985	1.475
0.0	1.105	1.164	0.144	1.188	0.187	1.195	0.289	1.299	2.010	1.547
0.0	1.350	1.436	0.243	1.459	0.330	1.482	0.503	1.360	2.074	1.526
0.0	1.649	1.781	0.494	1.808	0.622	1.862	0.952	1.261	1.929	1.530
0.5	1.000	1.020	0.046	1.035	0.069	1.057	0.183	1.490	3.968	2.663
0.5	1.105	1.131	0.057	1.146	0.092	1.183	0.259	1.599	4.501	2.815
0.5	1.350	1.395	0.100	1.407	0.157	1.485	0.475	1.576	4.758	3.020
0.5	1.649	1.707	0.164	1.727	0.268	1.853	0.868	1.636	5.305	3.243
1.0	1.000	1.012	0.030	1.019	0.038	1.057	0.136	1.240	4.485	3.618
1.0	1.105	1.117	0.036	1.127	0.046	1.177	0.194	1.302	5.427	4.168
1.0	1.350	1.375	0.055	1.373	0.075	1.453	0.329	1.370	5.994	4.375
1.0	1.649	1.682	0.083	1.691	0.122	1.773	0.524	1.470	6.313	4.293
$m = 50$ and $r = 10$										
0.0	1.000	1.053	0.128	1.073	0.168	1.089	0.286	1.316	2.234	1.698
0.0	1.105	1.184	0.187	1.181	0.210	1.229	0.438	1.124	2.342	2.085
0.0	1.350	1.450	0.308	1.480	0.389	1.517	0.737	1.263	2.390	1.892
0.0	1.649	1.788	0.571	1.819	0.812	1.939	1.698	1.422	2.972	2.091
0.5	1.000	1.024	0.053	1.037	0.082	1.073	0.233	1.562	4.421	2.830
0.5	1.105	1.138	0.069	1.156	0.107	1.218	0.333	1.569	4.867	3.102
0.5	1.350	1.389	0.108	1.406	0.179	1.531	0.760	1.666	7.061	4.239
0.5	1.649	1.710	0.180	1.755	0.315	1.886	1.193	1.752	6.639	3.790
1.0	1.000	1.015	0.037	1.023	0.042	1.081	0.195	1.112	5.223	4.695
1.0	1.105	1.124	0.046	1.123	0.050	1.194	0.258	1.091	5.612	5.144
1.0	1.350	1.381	0.069	1.378	0.077	1.472	0.409	1.126	5.957	5.291
1.0	1.649	1.682	0.103	1.694	0.124	1.836	0.951	1.207	9.255	7.665

Table 6 95% confidence interval of the odds ratio (OR) (dichotomous risk factor)

		$m = 30$ and $r = 20$								
		$DERSS_{min}$			$ERSS_{min}$			SRS		
β_1	OR	Lower	Upper	Coverage %	Lower	Upper	Coverage %	Lower	Upper	Coverage %
0.0	1.000	0.588	1.881	0.956	0.562	2.033	0.949	0.493	2.353	0.958
0.0	1.105	0.641	2.120	0.948	0.615	2.299	0.950	0.539	2.672	0.955
0.0	1.350	0.764	2.705	0.955	0.727	2.942	0.953	0.639	3.464	0.958
0.0	1.649	0.908	3.509	0.953	0.859	3.835	0.959	0.759	4.637	0.963
0.5	1.000	0.680	1.530	0.951	0.632	1.696	0.956	0.500	2.245	0.957
0.5	1.105	0.748	1.708	0.958	0.693	1.899	0.953	0.550	2.557	0.957
0.5	1.350	0.908	2.142	0.951	0.830	2.387	0.951	0.663	3.353	0.952
0.5	1.649	1.091	2.672	0.947	0.992	3.011	0.950	0.788	4.407	0.957
1.0	1.000	0.729	1.405	0.948	0.707	1.468	0.949	0.539	2.076	0.958
1.0	1.105	0.805	1.551	0.950	0.779	1.630	0.951	0.592	2.347	0.954
1.0	1.350	0.991	1.909	0.950	0.940	2.006	0.945	0.708	2.994	0.955
1.0	1.649	1.209	2.339	0.946	1.145	2.499	0.952	0.834	3.787	0.958
$m = 50$ and $r = 10$										
0.0	1.000	0.562	1.976	0.954	0.536	2.156	0.949	0.462	2.594	0.961
0.0	1.105	0.622	2.263	0.950	0.580	2.413	0.954	0.509	3.016	0.957
0.0	1.350	0.734	2.879	0.954	0.696	3.167	0.960	0.598	3.919	0.951
0.0	1.649	0.863	3.734	0.956	0.813	4.115	0.955	0.713	5.465	0.958
0.5	1.000	0.668	1.571	0.951	0.615	1.748	0.954	0.471	2.462	0.959
0.5	1.105	0.736	1.759	0.945	0.678	1.970	0.948	0.524	2.854	0.960
0.5	1.350	0.885	2.181	0.953	0.805	2.458	0.950	0.626	3.807	0.950
0.5	1.649	1.068	2.740	0.953	0.975	3.162	0.955	0.730	4.985	0.956
1.0	1.000	0.702	1.466	0.950	0.696	1.504	0.953	0.515	2.277	0.956
1.0	1.105	0.779	1.621	0.951	0.761	1.657	0.953	0.560	2.556	0.950
1.0	1.350	0.960	1.987	0.948	0.927	2.049	0.954	0.667	3.265	0.957
1.0	1.649	1.170	2.419	0.948	1.127	2.548	0.953	0.795	4.298	0.954

n = 600), $ERSS_{min}$ (with $m = 20$, $r = 30$, and $n = 600$) and SRS ($n = 600$). As birth weight is a good indicator for teenage obesity, we used standardized birthweight as our ranking variable. In addition to this,we tested for association of obesity (BMI > 30) as a binary response variable with age and gender as covariates. We repeated this process of 1000 times to evaluate the bias and MSEs in estimating coefficients for age and gender.

Based on full data ($N = 41{,}323$), the coefficients for age and sex are reported in Table 10. These estimates can be treated as a true parameter for comparison purpose. Table 10 represents the bias and MSEs for parameter estimation for age and sex on children's obesity status. From Table 10, we can conclude that $DERSS_{min}$, $ERSS_{min}$ and SRS provide a close approximation to the population parameters; however, MSEs for $DERSS_{min}$ is smaller than both $ERSS_{min}$ and SRS.

Table 7 Estimation of the power of testing $H_o : \beta_2 = 0$ vs $H_a : \beta_2 \neq 0$ adjusting for the auxiliary variable (Z) in the model (continuous risk factor)

		$m = 5$ and $r = 100$		$m = 30$ and $r = 20$		$m = 50$ and $r = 10$	
ρ	β_2	Power of the test using $\text{MERSS}_{\text{min}}$	Power of the test using SRS	Power of the test using $\text{MERSS}_{\text{min}}$	Power of the test using SRS	Power of the test using $\text{MERSS}_{\text{min}}$	Power of the test using SRS
0.0	0.0	0.0482	0.0478	0.0570	0.0446	0.0520	0.0504
0.0	0.1	0.1726	0.1610	0.2270	0.1914	0.1986	0.1604
0.0	0.3	0.8730	0.8400	0.9428	0.8892	0.9006	0.8290
0.0	0.5	0.9994	0.9990	0.9998	0.9992	0.9998	0.9974
0.3	0.0	0.0474	0.0494	0.0516	0.0488	0.0494	0.0462
0.3	0.1	0.1624	0.1452	0.2086	0.1702	0.1838	0.1556
0.3	0.3	0.8478	0.7884	0.9160	0.8620	0.8694	0.7918
0.3	0.5	0.9964	0.9964	1.0000	0.9992	0.9988	0.9946
0.5	0.0	0.0526	0.0496	0.0496	0.0496	0.0432	0.0532
0.5	0.1	0.1476	0.1238	0.1772	0.1648	0.1576	0.1338
0.5	0.3	0.7662	0.7122	0.8622	0.7936	0.8038	0.7028
0.5	0.5	0.9926	0.9842	0.9994	0.9952	0.9956	0.9870
0.8	0.0	0.0540	0.0488	0.0552	0.0414	0.0512	0.0502
0.8	0.1	0.1002	0.0928	0.1044	0.0968	0.0860	0.0900
0.8	0.3	0.4670	0.4062	0.5550	0.4674	0.4802	0.3998
0.8	0.5	0.8660	0.8188	0.9228	0.8706	0.8664	0.8088

From Samawi et al. (2017)

Table 8 Odds ratio (OR) estimation and their MSE (continuous risk factor)

		$m = 30$ and $r = 20$				$m = 50$ and $r = 10$			
		$\text{MERSS}_{\text{min}}$		SRS		$\text{MERSS}_{\text{min}}$		SRS	
ρ	OR	Estimate	MSE	Estimate	MSE	Estimate	MSE	Estimate	MSE
0.0	1.0000	1.0040	0.0074	1.0070	0.0089	1.0030	0.0089	1.0030	0.0112
0.0	1.1050	1.1130	0.0088	1.1130	0.0115	1.1120	0.0107	1.1110	0.0138
0.0	1.3500	1.3570	0.0143	1.3600	0.0179	1.3610	0.0174	1.3660	0.0220
0.0	1.6490	1.6660	0.0242	1.6650	0.0274	1.6640	0.0284	1.6600	0.0339
0.3	1.0000	1.0050	0.0081	1.0080	0.0100	1.0040	0.0095	1.0050	0.0118
0.3	1.1050	1.1110	0.0102	1.1110	0.0120	1.1120	0.0116	1.1160	0.0151
0.3	1.3500	1.3560	0.0156	1.3620	0.0195	1.3630	0.0195	1.3630	0.0236
0.3	1.6490	1.6620	0.0253	1.6700	0.0317	1.6670	0.0312	1.6680	0.0384
0.5	1.0000	1.0050	0.0099	1.0090	0.0120	1.0070	0.0113	1.0060	0.0147
0.5	1.1050	1.1120	0.0123	1.1190	0.0158	1.1140	0.0141	1.1140	0.0185
0.5	1.3500	1.3580	0.0188	1.3650	0.0236	1.3670	0.0234	1.3630	0.0281
0.5	1.6490	1.6660	0.0317	1.6700	0.0388	1.6700	0.0397	1.6740	0.0450
0.8	1.0000	1.0090	0.0211	1.0090	0.0242	1.0140	0.0300	1.0150	0.0312
0.8	1.1050	1.1140	0.0255	1.1190	0.0327	1.1170	0.0300	1.1280	0.0401
0.8	1.3500	1.3630	0.0405	1.3700	0.0501	1.3710	0.0491	1.3760	0.0626
0.8	1.6490	1.6800	0.0678	1.6810	0.0803	1.6850	0.0844	1.6850	0.0942

From Samawi et al. (2017)

Table 9 95% confidence interval of the odds ratio (OR) (continuous risk factor)

		$m = 30$ and $r = 20$				$m = 50$ and $r = 10$			
		$\text{MERSS}_{\min}$		SRS		$\text{MERSS}_{\min}$		SRS	
ρ	OR	Lower	Upper	Lower	Upper	Lower	Upper	Lower	Upper
0.0	1.0000	0.8516	1.1834	0.8369	1.2093	0.8383	1.2004	0.8196	1.2280
0.0	1.1050	0.9430	1.3124	0.9252	1.3386	0.9286	1.3322	0.9071	1.3608
0.0	1.3500	1.1449	1.6083	1.1265	1.6429	1.1302	1.6388	1.1100	1.6797
0.0	1.6490	1.3930	1.9923	1.3682	2.0255	1.3687	2.0232	1.3389	2.0586
0.3	1.0000	0.8458	1.1942	0.8301	1.2226	0.8320	1.2124	0.8134	1.2424
0.3	1.1050	0.9344	1.3210	0.9154	1.3483	0.9207	1.3441	0.9020	1.3803
0.3	1.3500	1.1352	1.6204	1.1168	1.6608	1.1211	1.6562	1.0967	1.6952
0.3	1.6490	1.3787	2.0040	1.3589	2.0532	1.3570	2.0471	1.3301	2.0922
0.5	1.0000	0.8314	1.2157	0.7968	1.2474	0.8183	1.2389	0.7968	1.2702
0.5	1.1050	0.9189	1.3454	0.9036	1.3863	0.9042	1.3719	0.8813	1.4091
0.5	1.3500	1.1168	1.6519	1.0968	1.6986	1.1024	1.6961	1.0723	1.7330
0.5	1.6490	2.0467	0.9498	1.3311	2.0949	1.3307	2.0971	1.3052	2.1482
0.8	1.0000	0.7675	1.3279	0.7426	1.3714	0.7519	1.3681	0.7246	1.4213
0.8	1.1050	0.8460	1.4663	0.8218	1.5237	0.8265	1.5094	0.8041	1.5837
0.8	1.3500	1.0279	1.8081	1.0001	1.8759	1.0037	1.8733	0.9737	1.9438
0.8	1.6490	1.2477	2.2570	1.2164	2.3258	1.2106	2.3473	1.1806	2.4049

From Samawi et al. (2017)

Table 10 Parameters estimation for covariates age and gender on children's obesity status ($N = 41{,}323$)

Covariates	True parameter	$\text{DERSS}_{\min}$		$\text{ERSS}_{\min}$		SRS	
		Bias	MSEs	Bias	MSEs	Bias	MSEs
Intercept	1.4643	−0.0118	0.2877	−0.0198	0.3879	−0.0221	0.4524
Age	−0.1289	−0.0025	0.0010	0.0011	0.0017	0.00171	0.0019
Gender	−0.4197	0.0022	0.0234	0.0065	0.0318	−0.0022	0.0350

5 Final Remarks

Whenever it is possible, in many statistical studies for different areas of applications, it essential to obtain a cost-effective and more structural samples. In the literature, we found that RSS and its variations are promising sampling schemes which provide more powerful and more efficient performance in statistical procedures. Through our investigations, we found that the modified ERSS, MERSS and DERSS, presented in this chapter, provide a more efficient performance of the logistic regression analyses compared with SRS. We suggested that the ranking process for selecting the study subjects could be based on an easy-to-rank and available auxiliary variable known to be associated with the variable of the response variable. We showed theoretically and through our simulation studies that using the modified ERSS, MERSS and DERSS, provide more efficient MLEs of the logistic models'

parameters with larger Fisher's information compared with SRS. Our simulation results showed that, for continuous risk factors, the power of the test increases as the set size *m* increase. Besides, for the logistic regression analyses, the modified DERSS outperform using the modified MERSS, ERSS and SRS.

References

Agresti, A. (2002). *An introduction to categorical data analysis* (Vol. 135). New York: Wiley.

Albert, A., & Anderson, J. (1984). On the existence of maximum likelihood estimates in logistic regression models. *Biometrika, 71*(1), 1–10.

Al-Odat, M., & Al-Saleh, M. F. (2001). A variation of ranked set sampling. *Journal of Applied Statistical Science, 10*(2), 137–146.

Chen, H., Stasny, E. A., & Wolfe, D. A. (2005). Ranked set sampling for efficient estimation of a population proportion. *Statistics in Medicine, 24*(21), 3319–3329.

Chen, Z., & Wang, Y. G. (2004). Efficient regression analysis with ranked-set sampling. *Biometrics, 60*(4), 997–1004.

King, G., & Zeng, L. (2001). Logistic regression in rare events data. *Political Analysis, 9*(2), 137–163.

Lehmann, E. L., & Casella, G. (1998). *Theory of point estimation* (2nd ed.). New York: Springer.

Linder, D., Yin, J., Rochani, H., Samawi, H., & Sethi, S. (2018). Increased Fisher's information for parameters of association in count regression via extreme ranks. *Communication of Statistics: Theory and Methods, 47*(5), 1181–1203.

Lynne Stokes, S. (1977). Ranked set sampling with concomitant variables. *Communications in Statistics: Theory and Methods, 6*(12), 1207–1211.

Maalouf, M., & Trafalis, T. B. (2011). Robust weighted kernel logistic regression in imbalanced and rare events data. *Computational Statistics & Data Analysis, 55*(1), 168–183.

McIntyre, G. (1952). A method for unbiased selective sampling, using ranked sets. *Crop and Pasture Science, 3*(4), 385–390.

Menard, S. (1995). *Applied logistic regression analysis: Sage university series on quantitative applications in the social sciences*. Thousand Oaks, CA: Sage.

Murff, E. J. T., & Sager, T. W. (2006). The relative efficiency of ranked set sampling in ordinary least squares regression. *Environmental and Ecological Statistics, 13*(1), 41–51.

National Survey of Children's Health. (2011). Statistics, N. C. f. H. (11/29/2011, 10/30/2013). Retrieved February 24, 2015, from http://www.cdc.gov/nchs/slaits/nsch.htm.

Özdemir, Y. A., & Esin, A. A. (2007). Parameter estimation in multiple linear regression models using ranked set sampling. *Communications Series A1 Mathematics & Statistics, 56*, 1.

Rashid, M., & Shifa, N. (2009). Consistency of the maximum likelihood estimator in logistic regression model: A different approach. *Journal of Statistics, 16*, 1–11.

Samawi, H., & Ababneh, F. (2001). On regression analysis using ranked set sample. *Journal of Statistical Research (JSR), 35*(2), 93–105.

Samawi, H., Rochani, H., Linder, D., & Chatterjee, A. (2017). More efficient logistic analysis using moving extreme ranked set sampling. *Journal of Applied Statistics, 44*(4), 753–766.

Samawi, H., Yu, L., Rochani, H., & Vogel, R. (2018b). Reducing sample size needed for cox- proportional hazards model analysis using more efficient sampling method. *Online Communication of Statistics: Theory and Methods, 49*, 1281–1298. https://doi.org/10.1080/03610926.2018.1554141.

Samawi, H. M. (2002). On double extreme ranked set sample with application to regression estimator. *Metron, LX*(1–2), 53–66.

Samawi, H. M., & Abu-Dayyeh, W. (2002). On regression analysis with random regressors using ranked samples. *International Journal of Information and Management Sciences, 13*(3), 19–36.

Samawi, H. M., Ahmed, M. S., & Abu-Dayyeh, W. (1996). Estimating the population mean using extreme ranked set sampling. *Biometrical Journal, 38*(5), 577–586.

Samawi, H. M., & Al-Saleh, M. F. (2002). On regression analysis using bivariate ranked set samples. *Metron, 60*(3), 29–48.

Samawi, H. M., & Al-Saleh, M. F. (2004). On bivariate ranked set sampling for distribution and quantile estimation and quantile interval estimation using ratio estimator. *Communications in Statistics-Theory and Methods, 33*(8), 1801–1819.

Samawi, H. M., & Al-Saleh, M. F. (2013). Valid estimation of odds ratio using two types of moving extreme ranked set sampling. *Journal of the Korean Statistical Society, 42*(1), 17–24.

Samawi, H. M., Helu, A., Rochani, H., Yin, J., Yu, L., & Vogel, R. (2018a). Reducing sample size needed for accelerated failure time model using more efficient sampling methods. *Statistical Theory and Practice, 12*(3), 530–541. https://doi.org/10.1080/15598608.2018.1431574.

See, C., & Chen, J. (2008). Inequalities on the variance of convex functions of random variables. *Journal of Inequalities in Pure and Applied Mathematics, 9*(3), 1–5.

Steinmann, P., Zhou, X.-N., Li, Y.-L., Li, H.-J., Chen, S.-R., Yang, Z., et al. (2007). Helminth infections and risk factor analysis among residents in Eryuan county, Yunnan province, China. *Acta Tropica, 104*(1), 38–51.

Twidwell, S. (2000). Bioaccumulation of mercury in selected east Texas water bodies. Texas Natural Resource Conservation Commission.

Applications of Spatial Statistics in Poverty Alleviation in China

Yong Ge, Shan Hu, and Mengxiao Liu

Abstract China is the most populous country in the world, especially a large number of impoverished people concentrated in rural area. The uneven distribution of impoverished people in China has made it necessary to investigate its spatial patterns and driving forces. In this chapter, several methods of spatial statistics that have been employed to poverty issues analysis were reviewed. These methods were mainly used to investigate the driving forces, spatial patterns, and spatial temporal changes of poverty. Three case studies of China were then conducted to provide the detail illustrations of the application of the methods.

1 Background

Poverty is a common challenge that accompanies the progress of human society. The first goal of the sustainable development goals (SDGs) proposed by the United Nations is to end poverty in all its forms everywhere by 2030 (United Nations 2015a). China, a developing country with a large rural poor population, has made great efforts to improve development in poor areas over the past decades and has seen tremendous improvements (Information Office of the State Council 2011). Despite this great achievement, there are some issues such as poverty-returning phenomenon, developmental contradiction between economy and ecology, and regional development disparities that also need to be addressed (Wang et al. 2014). In addition, the distribution of the impoverished people in China is uneven, which makes it necessary to investigate spatial patterns and driving forces to better support effective poverty reduction measures.

Y. Ge (✉) · S. Hu · M. Liu
State Key Laboratory of Resources and Environmental Information System, Institute of Geographical Sciences and Natural Resources Research, Chinese Academy of Sciences, Beijing, China
e-mail: gey@lreis.ac.cn

A. Bekker et al. (eds.), *Computational and Methodological Statistics and Biostatistics*, Emerging Topics in Statistics and Biostatistics,
https://doi.org/10.1007/978-3-030-42196-0_16

1.1 Poverty in China: Responses, Achievements, and Problems

China has made great efforts to reduce the rural poor population over the past decades. Various policies and measures have been implemented with positive results. Despite this, China still faces several challenges in poverty alleviation.

Since the reform and opening up in 1978, China has entered a critical period of urbanization and industrialization, leading to fast economic development, a considerable increase in living standards, and an unprecedented decline in poverty (Wang et al. 2014). China has made numerous efforts to accelerate development in poverty-stricken areas. Specifically, it has implemented the Seven-Year Priority Poverty Reduction Program (1994–2000), Outline for Poverty Reduction and Development of China's Rural Areas (2001–2010), Outline for Development-Oriented Poverty Reduction for China's Rural Areas (2011–2020), and Targeted Poverty Reduction Strategy (2013) (Zuo 2016; The State Council 2011). These policies and programs have significantly promoted development in poverty-stricken areas and helped thousands of people out of poverty.

Benefitting from various measures, China became the first developing country in the world to achieve the poverty reduction target set by the Millennium Development Goals of halving the proportion of people whose income is less than $1.25 per day. Owing to China's progress, the extreme poverty rate in eastern Asia has dropped from 61% in 1990 to only 4% in 2015 (United Nations 2015b). Based on the current national poverty line, CNY 2300 per capita annual net income, the poverty headcount ratio in China has fallen from 97.5% in 1978 to 1.7% in 2018 (Department of Household Surveys, National Bureau of Statistics of China 2018; National Bureau of Statistics 2019). On top of that, housing, education, transportation, and medical care have all seen significant improvements. In particular, the implementation of the Entire-Village Advancement, which covers basic farmland, drinking water, roads, social undertakings, and other aspects that affect impoverished villages, has significantly improved the living standard in rural areas (Li et al. 2016; Zhou et al. 2018; Liu et al. 2018).

Owing to a poor economic foundation and restriction of natural environment conditions, central and western China are still developing slowly, and regional disparities, especially rural–urban disparities, are increasing (Dollar 2007). At the end of 2018, there were 16.60 million people living below the national poverty line (Li et al. 2016). Moreover, a number of people who returned to poverty started to appear, owing to such factors as disasters, illness, disability, and school costs (Zhou et al. 2018). Meanwhile, a strong connection between poverty-stricken areas and ecologically protected areas has led to a contradiction between a balanced development of socioeconomic and ecological conditions (Ouyang et al. 2016; Xu et al. 2017). Regional development disparities and inequality has also put pressure on China's poverty reduction efforts.

1.2 Spatial Characteristics of Poverty in China

China's poverty-stricken areas are mainly concentrated in central and western China, most of which are hilly and mountain areas.

The distribution of poverty-stricken areas in China has an obvious spatial agglomeration feature. Liu et al. (2017) found that impoverished people mainly concentrate in the remote deep mountain areas, border areas, and minority areas of central and western China, and they gradually gather towards the southwestern region. After the promulgation of the Outline for Development-Oriented Poverty Reduction for China's Rural Area (2011–2020) in 2011, the Chinese government identified 14 poverty-stricken areas as the main battleground for the new round of poverty reduction and development efforts. Figure 1 shows that poverty-stricken areas are mainly located in Western and Central China. The 14 poverty-stricken areas contain 680 counties and cover approximately one third of China, with mountainous and hilly areas accounting for 86.8% of the land (Zuo 2016).

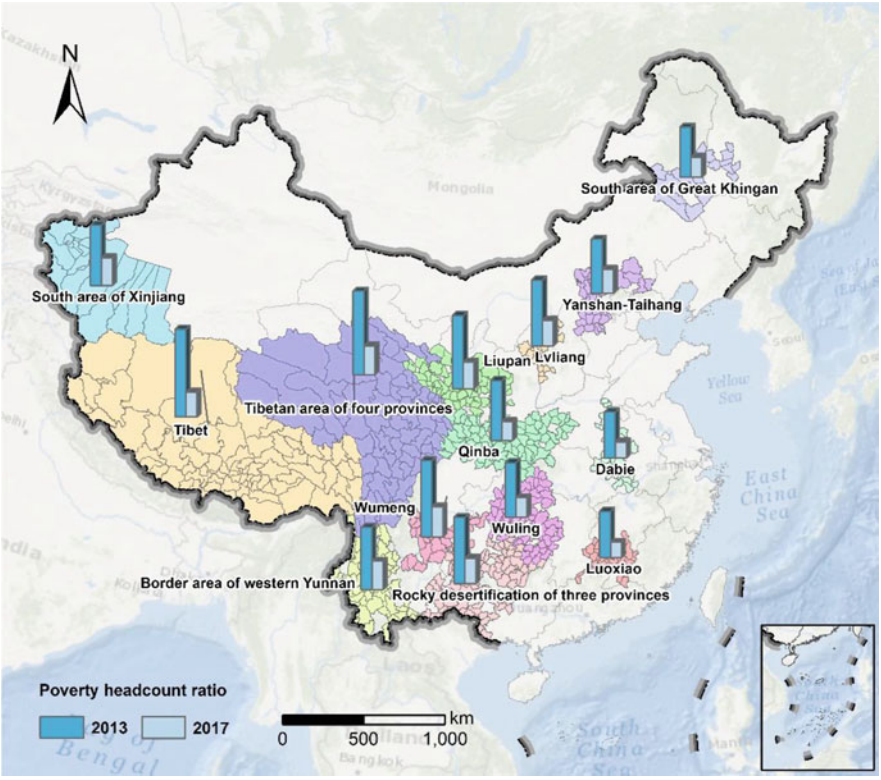

Fig. 1 Fourteen continuously poverty-stricken areas and their poverty headcount ratio in 2013 and 2017, respectively

The uneven distribution of China's rural poor population has made it necessary to explore the spatial pattern and their main causes. The geography of poverty has been developing rapidly in China since the vigorous carrying out of poverty reduction actions. A large number of spatial statistical methods were employed to explore geographical distribution patterns (Liu et al. 2017; Chen and Ge 2015), causes of poverty (Ren et al. 2017), geographical identification of poverty (Liu and Xu 2016), spatial-temporal changes of poverty (Li et al. 2015), poverty alleviation effectiveness assessment (Ge et al. 2017), and relationships between poverty and geographical elements (Okwia et al. 2007). The spatial temporal patterns and driving forces of poverty are revealed by spatial analysis and poverty mapping, which can support effective policies for poverty reduction and sustainable development in poverty-stricken areas.

2 Applications of Spatial Statistical Methods on Poverty

Evidences from various theoreticasl analysis of poverty have shown that poverty has spatial attributes (Bird 2019; Jalan and Ravallion 1997). Spatial statistical methods provide diverse tools for geographical poverty identification, spatial disparities analysis, and spatial-temporal analysis.

2.1 Datasets

Poverty headcount ratio is the percentage of people living below the poverty line. The poverty headcount ratio is usually used as a response variable in poverty related spatial statistical analysis. The potential explanatory variables were selected from the aspects of income, education, healthcare, housing, and infrastructure for a region. Meanwhile, the spatially referenced environmental indicators such as topography, land cover and land use, access to public services were also selected as potential explanatory variables.

Poverty was initially treated as an economic phenomenon and was usually measured by the amount of money a person had to meet certain basic needs (Sen 1976; Atkinson 1987). Amartya Sen put forward the concept of capability poverty in his book Development as Freedom (Sen 2001). This revolutionary leap helped many researchers understand poverty from different perspectives. Now, poverty is identified as a multidimensional phenomenon that includes various elements, such as economic shortage, social exclusion, and vulnerability (Alkire and Foster 2011; Satya and Chakravarty 2006). Based on these varying perspectives of understanding poverty, there are also multiple ways to measure poverty. From measuring just income to including other factors such as health, education, and social services, the measurement of poverty has gradually extended to appraise the sustainable livelihoods of the poor population (Alkire and Fang 2018). Income poverty, the

Table 1 Part of the county level socioeconomic data this chapter used

County name	Poverty headcount ratio (%)	Teachers per 10,000 persons (persons/10,000)	Number of beds utilized in health care institutions per 10,000 persons (persons/10,000)	Disposable income of rural household (CNY)
Kangding	12.10	111.27	91.88	6554.17
Luding	16.30	107.21	30.76	5772.54
Danba	15.44	114.32	36.79	6356.66
Jiulong	14.84	93.56	29.84	7004.28
Yajiang	18.65	86.96	27.00	5374.37
Daofu	19.89	76.59	30.35	5047.35
Luhuo	19.86	97.92	41.36	4989.93
Ganzi	20.85	86.60	41.50	5161.84
Xinlong	19.70	88.28	23.05	5022.94
Dege	23.52	72.57	15.00	4884.12

human development index (HDI), and the multidimensional poverty index (MPI) are all widely used to measure global poverty (Wang 2012).

Income poverty is the most widely used tool to measure poverty. The World Bank built bridges to global poverty measurement. The $1.90 per day is the new international poverty line determined by the World Bank in 2015 (The World Bank 2018). The current national poverty line in China is CNY 2300 per capita annual net income (Department of Household Surveys, National Bureau of Statistics of China 2018). The population living below the poverty line are identified as impoverished people. The poverty headcount ratio is the proportion of the impoverished people to the total population. In this chapter, the poverty headcount ratio is used as a response variable. Table 1 provides part of the poverty headcount ratio at the county level of China in 2013.

The HDI and MPI are looks beyond the income to measure poverty. HDI is a summary measure of average achievement in three dimensions of human development for a country: a long and healthy life, being knowledgeable, and have a decent standard of living (UNDP 2010). While MPI emphasizes multiple deprivations at the household and individual level in health, education and standard of living. The specific indicators of MPI include nutrition, child mortality, years of schooling, school attendance, cooking fuel, sanitation, drinking water, electricity, housing, and assets (Alkire and Foster 2011). These widely recognized literatures provide the basis for indicators selection. In this chapter, we selected county-level indicators from the aspects of regional economic, infrastructure, housing, healthcare, education, and medical care, as shown in Table 2.

Evidences from poverty mapping of China shows that the distribution of poverty is not homogenous (Zhang et al. 2014). From the perspective of geography, the heterogeneities are largely caused by the disparities in geographical conditions such as resource endowment, ecological environment, access to public services, and regional culture and polices (Zhou and Liu 2019). Existing researches have shown

Table 2 Lists of the socioeconomic indicators

Contents	Indicators
Education	Teachers per 10,000 persons (persons/10,000)
	Ratio of expenditure on science and education to GDP (%)
Health care	Medical technical personnel in health care institutions per 10,000 persons (persons/10,000)
	Number of beds utilized in health care institutions per 10,000 persons (persons/10,000)
Living standard	Engel's coefficient (%)
Infrastructure	Popularization rate of tap water (%)
	Ratio of administrative villages that can be reached by road (%)
Housing	Per-capita living space (m^2 per capita)
Medical care	New Rural Co-operative Medical System participants as a proportion of total population (%)
Income	Disposable income of rural household (CNY)

Table 3 Lists of the environmental indicators

contents	Indicators
Environmental	Mean elevation
	Standard deviation of elevation
	Mean slope
	Standard deviation of slope
	Proportion of cropland
	Proportion of forest
	Proportion of grassland
	Proportion of built-up land
	Road density (km/km^2)

that topography, elevation, slope, land use types are all closely related to poverty (Zhou and Liu 2019; Cheng et al. 2018; Watmough et al. 2019). This chapter has also selected few Geographical Information System-based indicators as explanatory variables to investigate the relationship between environmental factors and poverty, as shown in Table 3.

The sources of socioeconomic data mainly included: (1) the socioeconomic data from 2010 to 2016 in Ganzi collected from the statistical yearbook of Ganzi Tibetan Autonomous Prefecture (2011–2017) and the statistical bulletins of the national economic and social development from 2010 to 2016 in Ganzi Tibetan Autonomous Prefecture; (2) The impoverished population data in 2013 were provided by the State Council Leading Group Office of Poverty Alleviation and Development.

The sources of Geographical Information System-based data mainly included: (1) Elevation data was obtained from ASTER GDEM (Advanced Spaceborne Thermal Emission and Reflection Radiometer Global Digital Elevation Model) with resolution of 30 × 30 m., which was downloaded from Geospatial Data Cloud Web (http://www.gscloud.cn/). (2) Slope data were extracted from the DEM. (3) The land

cover and land use was collected from China's Land-Use/cover Datasets (CLUDs), which are provided by Resources and Environmental Data CloudPlatform(resdc.cn) with the spatial resolution of 1 × 1 km. (4) Road data was obtained from National Catalogue Service For Geographic Information with the scale of 1:250000.

2.2 Causes of Poverty

Identifying the determinants of poverty is crucial for making effective poverty reduction policies in a region. This part introduces three widely employed spatial statistic methods for causes of poverty analysis: Geographical detector, Spatial regression, and Geographically Weighted Regression.

The geographical detector was developed by Wang et al. (2010), and was first applied in public health risk assessment. The core concept of the geographic detector is based on the assumption that if an explanatory variable has an important effect on the response variable, then the spatial distribution of the explanatory variable and response variable will be similar (Wang et al. 2010, 2016). All the results are based on the geographical detector q-statistic, which is defined as:

$$\mathrm{q} = 1 - \frac{SSW}{SST} \tag{2-1}$$

$$\mathrm{SSW} = \sum\nolimits_{h=1}^{L} N_h \sigma_h^2 \ \mathrm{SST} = \mathrm{N}\sigma^2 \tag{2-2}$$

$h(1, 2 \ldots \mathrm{L})$ is the strata of the explanatory variable (X) or response variable (Y). N and σ^2 are the number of units and the variance of Y in the study area, respectively. N_h and σ_h^2 are the number of units and the variance of Y in stratum h, respectively. SSW and SST are the within sum of squares and total sum of squares, respectively. The value of the q-statistic is within [0,1]. When response variable Y is stratified by Y itself, then the larger the q value, the more obvious the spatial stratified heterogeneity of Y. When Y is stratified by X, a larger q value indicates that X could explain more of Y, especially when $\mathrm{q} = 1$ indicates that Y is completely determined by X (Wang et al. 2016). Based on the geographical detector, Liu and Li (2017) investigated the spatial heterogeneity mechanism of poverty in Fuping County, China. They denoted the poverty headcount ratio at village level as the response variable, and chose slope, elevation, per capita cropland, and distance to the town as the explanatory variables.

Classic ordinary least squares (OLS) regression assumes that the observations of explanatory variables are independent from each other and always in a normal distribution, as well as the error term (Anselin 2002; Anselin and Rey 1991). Therefore, if there is spatial autocorrelation in the data, the assumptions are violated. The regression models that take spatial autocorrelation into consideration are called

spatial regression models. Spatial autocorrelation can be detected by the global and local autocorrelation model, including Geary's C, G statistic, Moran's I index, and the local indicator of spatial association (LISA) (Anselin 1995; Getis 1994). The spatial regression model includes two main variations: the spatial lag model and the spatial error model. Spatial-lag model applies to a situation in which the response variable in one region is affected by the response variable in nearby regions; Spatial error model applies to a situation in which the error for the model in one region is correlated with the error terms in its neighboring regions (Anselin 2001; Paul Elhorst 2014). Paul O. Okwia et al. (2007) employed the spatial regression model to investigate how and which spatial factors are related to poverty and how much of the variation in poverty incidence can be explained by environmental factors in rural Kenya.

$$\text{Spatial lag model}: y_i = \lambda \sum_{j \neq i} w_{ij} y_j + \boldsymbol{\beta} X_j + \varepsilon_j \tag{2-3}$$

$$\text{Spatial error model}: y_i = \boldsymbol{\beta} X_j + \lambda \sum_{j \neq i} w_{ij} y_j \varepsilon_j + \varepsilon_j \tag{2-4}$$

y_i is the response variable for region i; λ is the spatial autoregressive coefficient; w_{ij} is the spatial weight reflecting the proximity of i and j; y_j is the response variable for region j; β is a vector of coefficients; X_j is a matrix of explanatory variables; ε_j is the error term (Paul Elhorst 2014).

Geographically weighted regression (GWR) was proposed by Fotheringham et al., which allowed the relationships to vary over space (Fotheringham et al. 2002). GWR is a local version of spatial regression that runs a regression for each location instead of a single regression model for the whole study area (Zhang et al. 2011; Tu and Xia 2008). GWR is also popular in the spatial modeling of poverty for providing a method to assess the degree to which the relationship between the potential determinants and the poverty rate varies across space. Steven Deller employed GWR to analyze the spatial variation in the role of tourism and recreation in changing poverty rates (Deller 2010).

$$y_i = \beta_0 (u_i, v_i) + \beta_1 (u_i, v_i) x_{1i} \cdots + \beta_n (u_i, v_i) x_{ni} + \varepsilon_i \tag{2-5}$$

y_i is the response variable for location i; β_i are to be estimated at location i whose coordinates are given by the vector (u_i, v_i). The regression model is calibrated for a location by combing all other available data points to which weights are applied according to a continuous distance–decay function. The decay function could be fixed (commonly the Gaussian function is adopted) or adaptive. The shape of the function, defined by the adaptive bandwidth, may vary depending on the density of data points in the immediate neighborhood of the regression point (Fotheringham et al. 2015).

2.3 Spatial Pattern of Poverty

The spatial patterns can be recognized as cluster, randomness, dispersed, and uniformity. Understanding the spatial patterns of poverty areas and poverty populations can help uncover the causes of poverty and effectively implement poverty reduction measurements.

The multi-distance spatial cluster based on Ripley's K is a method that can analyze spatial patterns of point data (Ripley 1977). It summarizes the objects clustering or objects dispersion over a range of distances, which can be used to investigate how the clustering or dispersion of objects changes from distances. Therefore, the starting distance and distance increment are needed for a multi-distance spatial cluster analysis. It calculates the average number of neighboring objects associated with each object in a given distance.

$$\hat{K}(d) = \frac{A}{n^2} \sum_{i=1}^{n} \sum_{j \neq i}^{n} w_{ij} I\left(d_{ij} < d\right). \tag{2-6}$$

$$\hat{L}(d) = \sqrt{K(d)/\pi} - d \tag{2-7}$$

A is the area of observed points; n is the number of points; w_{ij} is an edge-correction term to remove the bias; $I(d_{ij} < d)$ is an indicator function that takes the value 1 when distance d_{ij} between point i and j is less than d. $\hat{L}_0(d)$ is compared with expected value $\hat{L}_e(d)$ for a random sample of points from a complete spatial randomness pattern. If $\hat{L}_0(d) - \hat{L}_e(d) > 0$, the pattern of observed points at a distance scale d is cluster. If$\hat{L}_0(d) - \hat{L}_e(d) < 0$, the pattern is dispersed. If $\hat{L}_0(d) - \hat{L}_e(d) = 0$, the pattern is randomness.

The average nearest neighbor (ANN) ratio measures the distance between each object's centroid and its nearest neighbor's centroid location first, and then it averages all the nearest neighbor distances (Ebdon 1985). If the average nearest neighbor distance is less than the average for a hypothetical random distribution, the distribution of the objects is recognized as clustering. Conversely, if the average nearest distance is greater than the average for a hypothetical random distribution, the distribution of the objects is recognized as dispersed. Then, the average nearest neighbor ratio is calculated by the observed average distance and divided by the expected average distance. If the value of the average nearest neighbor ratio is less than 1, then it indicates a clustering pattern, while greater than 1 indicates a dispersed pattern.

$$ANN = \frac{\overline{D_0}}{\overline{D_e}} \tag{2-8}$$

$$\overline{D_0} = n^{-1} \sum_{i=1}^{n} d_i \tag{2-9}$$

$$\overline{D_e} = 0.5(n/A)^{-0.5} \tag{2-10}$$

$\overline{D_0}$ is the mean distance between each observed point and its nearest neighbor; $\overline{D_e}$ is the expected mean distance from the points given in complete spatial randomness pattern; d_i is the distance between point i and its nearest neighbor; A is the area of observed points; n is the number of points.

Chen and Ge (2015) employed the multi-distance spatial cluster method to analyze the spatial pattern variation characteristics of 191,537 administrative villages in the 14 poverty-stricken areas of China. Meanwhile, they estimated the spatial pattern of villages in each county by using the average nearest neighbor ratio. The spatial pattern of the villages within each county is shown in Fig. 2. They found that village-clustered counties are the Tibet area and Tibetan ethnic areas in Sichuan, Yunnan, Gansu, and Qinghai provinces. Meanwhile, with the increase of distance, different

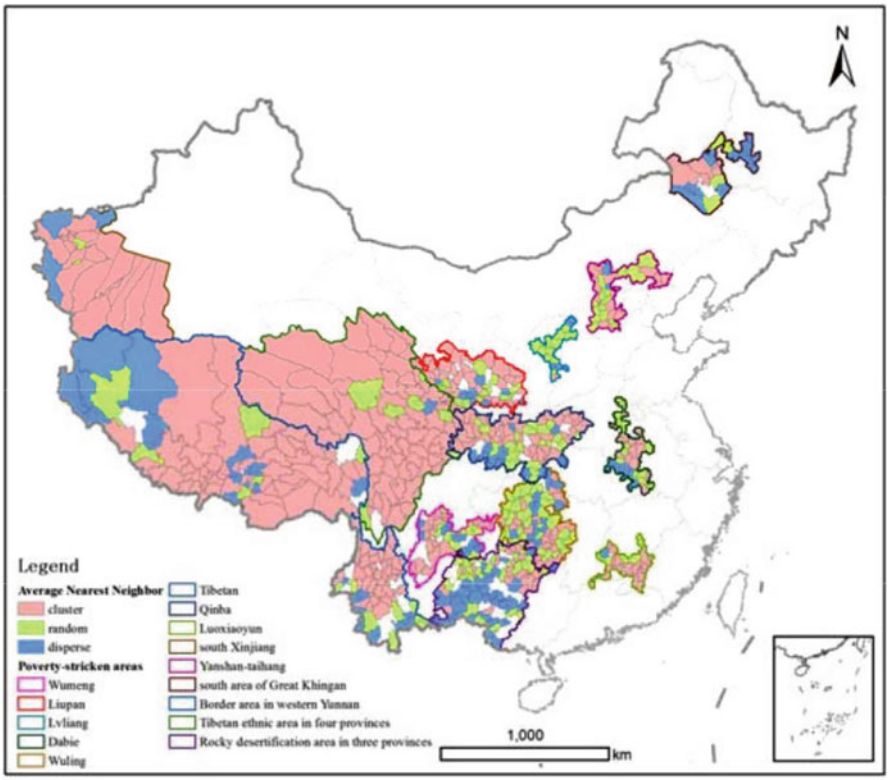

Fig. 2 Point pattern of villages within each county in the 14 poverty-stricken areas of China (Source: Yuehong Chen, Yong Ge. Spatial point pattern analysis on the villages in China's poverty-stricken areas. Procedia Environment Sciences 27(2015) 98–105)

poverty-stricken areas presented different distribution characteristics. Some areas showed spatial aggregation with distance, while others showed a pattern from aggregation to dispersion.

LISA is also used to investigate the spatial pattern of poverty areas or poor populations. The local Moran's I was used to obtain cluster maps of local indicators of spatial association that included statistically significant clusters of high values (high–high), clusters of low values (low–low), outliers in which a high value is surrounded primarily by low values (high–low), and outliers in which a low value is surrounded by high values (low–high) (Anselin 1995). Various researches use LISA to obtain the spatial pattern of the poverty rate, MPI index, and other comprehensive assessment indices at a county or village level.

$$I_i = \frac{\sum_{i=1}^{n} \sum_{j=1}^{n} W_{ij} \times (x_i - \overline{x}) \left(x_j - \overline{x}\right)}{\frac{1}{n}(x_i - \overline{x})^2} \tag{2-11}$$

I_i is the local Moran's I for region i, x_i is the attribute of region i,$\overline{x}$ is the mean of the corresponding attribute, w_{ij} is the spatial weight between counties i and j, and n is the total number of regions.

2.4 Spatial-Temporal Analysis of Poverty

Poverty is changing in number and region. The proportion of people living on less than $1.25 per day globally fell from 36% in 1990 to 12% in 2015. While this achievement has been experienced in south Asia and Latin America, the sub-Saharan Africa region still lags behind (United Nations 2015b). Under the background of an unprecedented execution of poverty reduction policies, China's poverty-stricken areas are experiencing great changes. It is necessary to analyze the spatial-temporal change of the distribution of poor populations, causes of poverty, and economic-social-ecological conditions in China's poverty-stricken areas.

The most widely used and easiest way to explore the spatial-temporal change of poverty is to map the evaluation value of different times and compare them. However, if the observed time period is long and we want to investigate the continuous time series change pattern, then it will be time consuming and missing some information. Therefore, methods that can capture the change trajectories and spatial pattern is needed. The Bayesian hierarchical model (BHM) is used in the space-time analysis of burglary risk and incidence of poverty (Li et al. 2014; Sparks and Campbell 2013). Bayesian inferences combine the data with additional prior information to obtain more stable results. BHM considers the spatial and temporal correlation through prior information. BHM can quantitatively estimate the overall spatial distribution pattern, overall change trend, and local change trend in the spatial-temporal process (Haining 1990). It can also be employed to analyze the

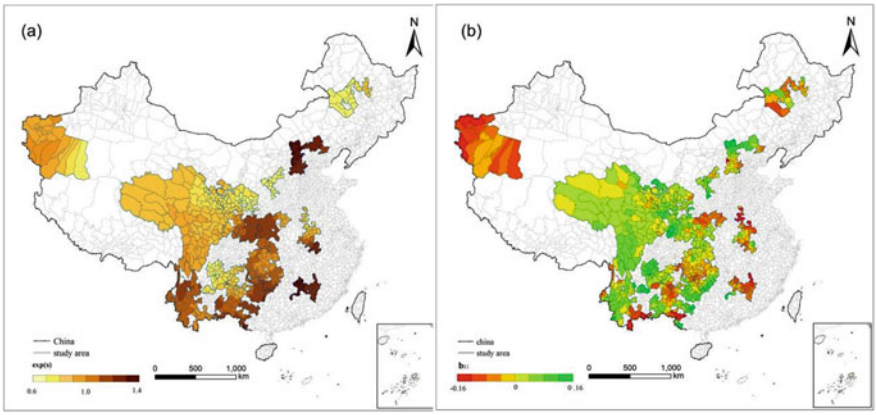

Fig. 3 (**a**) Estimates from model: common spatial component (posterior medians of $\exp(S_i)$); (**b**) Estimate from model: local trends' departure from overall trend (Source: Yong Ge, Yue Yuan, Shan Hu, Zhoupeng Ren, Yijin Wu. Space–time variability analysis of poverty alleviation performance in China's poverty-stricken areas. Spatial Statistic 21(2017) 460–474)

spatial-temporal change of poverty. Corey Sparks and Joey (2014) employed BHM to model and estimate the poverty rate in the United States at the county level. Ge et al. (2017) used BHM to assess the poverty reduction performance of China's poverty-stricken areas; they found a stable spatial pattern of higher effectiveness of poverty reduction in eastern China and lower in the western region, as shown in Fig. 3a. Meanwhile, for capturing spatial-temporal changes, the increasing trend of poverty reduction effectiveness presents a pattern of "high in the center, low in the east-west," Fig. 3b, and the most poverty-stricken counties' development of poverty reduction effectiveness are consistent with the overall trend.

3 Case Studies for China

Based on the spatial statistical methods described in Sect.2, this part conducted three case studies in China. In the first case, we analysis the spatial pattern of poverty headcount ratio of China's poverty-stricken areas by using LISA. The second case employed the GWR to explore the spatial nonstationary of the effect of geographic factors over the space in Hubei province of China. The third case first evaluate the living standard in Ganzi Tibetan Autonomous Prefecture from the aspects of housing, infrastructure, medical care, social security, and education based on the entropy weighting method and gray rational analysis. Then, the Bayesian hierarchical model wad used to investigate the spatial-temporal changes of evaluated living standard index of each county in Ganzi from 2010 to 2016.

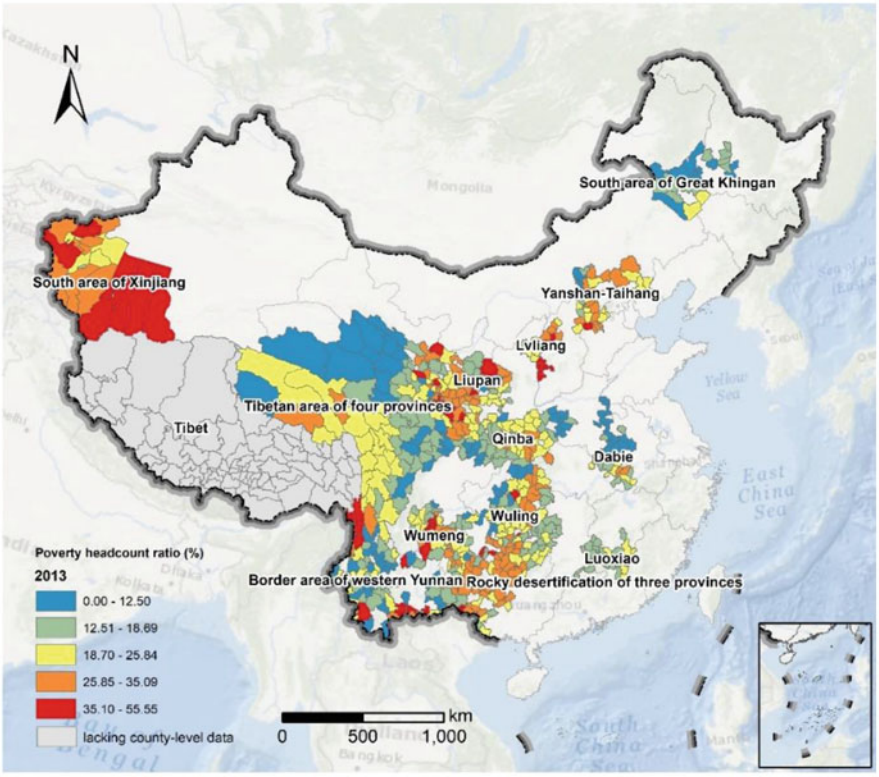

Fig. 4 The poverty headcount ratio of poverty-stricken counties in 2013

3.1 Spatial Pattern of Poverty Headcount Ratio

As it shows that in Fig. 1, China has identified 14 poverty-stricken areas as the new battleground of poverty reduction and development. Here we chose 13 of them, except Tibet area as it lacks county-level data, 601 counties in total to investigate the spatial pattern of poverty headcount ration in 2013. Figure 4 mapped the poverty headcount ration of poverty-stricken counties in 2013.

Local indicators of spatial association (LISA) was calculated by using the GeoDa software. Figure 5 shows the cluster maps of poverty headcount ratio for poverty-stricken areas. The counties that have high poverty rate mainly concentrated in South area of Xinjiang, most area of which is desert and Gobi. While the counties that have low poverty rate mainly located in Dabie area and South area of Great Khingan Great, both of which are national major grain producing areas.

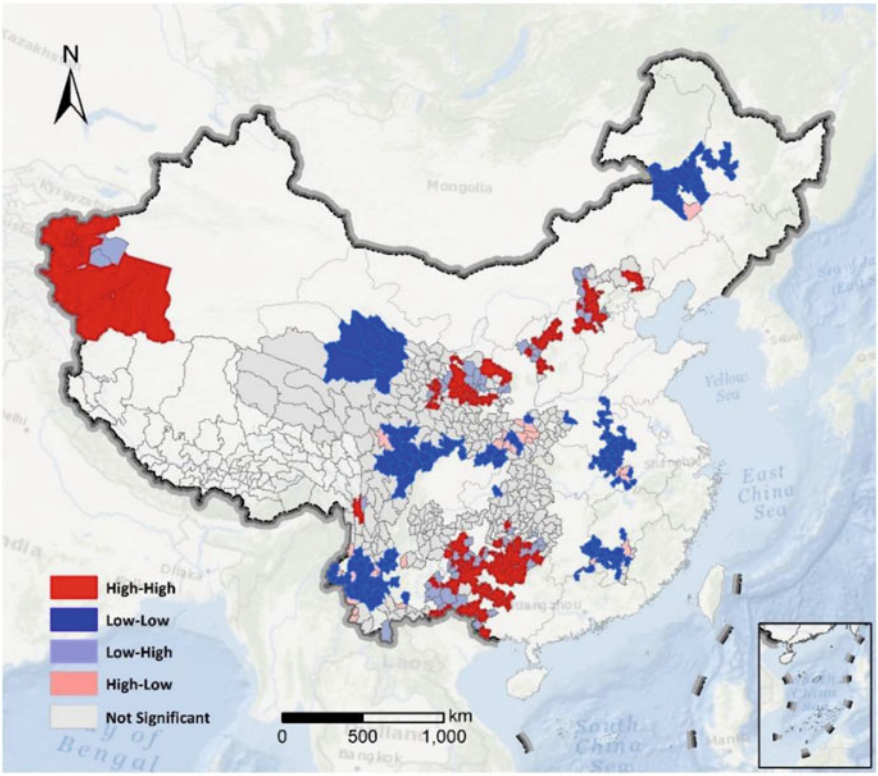

Fig. 5 Cluster maps for poverty headcount ratio in poverty-stricken areas

3.2 Spatial Correlation Analysis: Case Study of Hubei Province in China

Hubei province located in central China. The central and southern Hubei mainly belongs to Jianghan Plain while the western and the peripheries are mountain areas. G_i^* was adopted to investigate the local spatial autocorrelation in Hubei province. The results shown in Fig. 6 suggested that a high-high cluster of Hubei province appeared in the west of Hubei province while a low-low cluster appeared in the surrounding areas of the capital city Wuhan. Poverty headcount ratio in Hubei province showed an obvious spatial pattern.

Some potential geographic factors contributing to poverty having available data and a narrow relevance were proposed as explanatory variables in this case. A total of 11 indicators were selected as the explanatory variables for the spatial regression analysis. The detailed description of the explanatory variables is presented in Table 3. The environment dimension includes topography and land resources. The

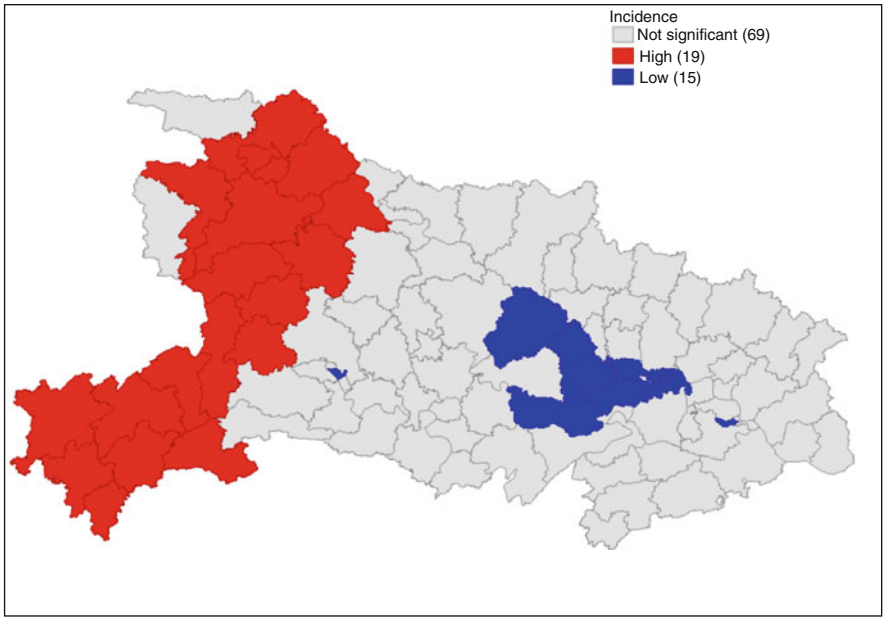

Fig. 6 Cluster map of poverty headcount ratio of Hubei province in 2013

elevation and slope are the most commonly used factors to describe the local terrain. The mean value and standard deviation of elevation and slope were adopted to describe the average level and dispersion degree of altitude and slope. Road density was chosen to indicate the overall transportation convenience and capacity in the region. Cropland is vital to the rural households for agriculture is the main mode of production in rural China. Furthermore, GDP per capita was selected to reflect the economic development and economic activity from statistic year book of Hubei province.

The correlation matrix of the correlation analysis suggests multicollinearity between variables with larger correlation coefficients. The step regression model was further employed to wipe out the collinearity problem between variables. Based on the results of step regression model, the variables mean elevation, GDP per capita and proportion of cropland were recognized for they made the most significant contribution to the regression model and are independent of each other. These three variables were entered into GWR model. The estimated results in the GWR models showed that the adjusted R^2 of the model with the three variables is 0.71, which is higher than the value of 0.68 determined by the OLS model. The local R^2 and explanatory variable coefficient of the variables in the GWR model were shown in Fig. 7.

The distribution of local R^2 values presented great spatial variation, which implies the explanatory ability of the GWR model varies with county. Meanwhile,

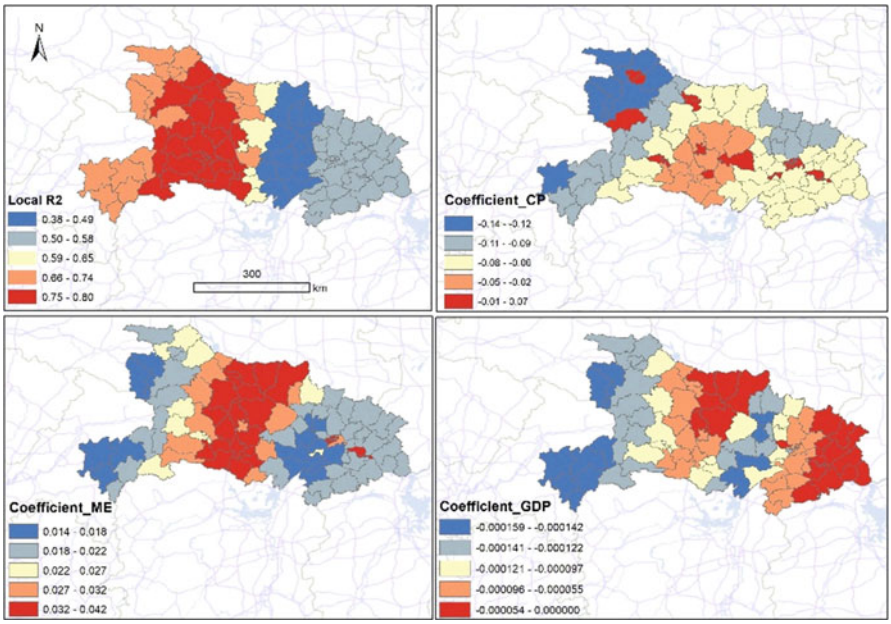

Fig. 7 Local R^2 and the three explanatory variable coefficients in GWR (CP means proportion of cropland in the total area of a region; ME means mean elevation)

the spatial distribution of each explanatory variable coefficients is similar but present different influence over space. Specifically, the mean elevation has a positive impact on the regional poverty, while GDP per capita and crop proportion have a negative impact, although the extent of this positive effect varies spatially. In addition, the spatial distribution of local R^2 values and the coefficients of explanatory variables followed a similar characteristic of stratification that generally increased from east to west, implying the strength of the explanatory ability of the GWR model increases gradually from east to west.

3.3 Spatial-Temporal Analysis: Case Study of an Alpine Area in China

Ganzi Tibetan Autonomous Prefecture is a high poverty, alpine, ethnic, and ecologically protected area. This area plays an important role both in national ecological security and national harmony. Here we want to evaluate the living standard in Ganzi from the aspects of housing, infrastructure, medical care, social security, and education. Ten indicators were chosen to measure the living standard of Ganzi. Based on the collected socioeconomic data from Ganzi during the period of 2010–

2016, combined with the entropy weighting method and gray rational analysis, we evaluated the living standard in Ganzi from 2010 to 2016. Then, the spatial-temporal changes of evaluated living standard index of each county in Ganzi were investigated by using the Bayesian hierarchical model.

3.3.1 Study Area

Ganzi Tibetan Autonomous Prefecture, located in the plateau region of western Sichuan Province, which belongs to the Tibetan ethnic areas of Sichuan, Yunnan, Gansu, and Qinghai (Fig. 1). Ganzi, with 18 counties, is the largest Tibetan area in Sichuan Province and covers approximately 153 thousand km^2. The highest altitude is 7556 m and the lowest is 1000 m. According to its geographical location, Ganzi was officially divided into three regions, northern, southern, and eastern Ganzi. Northern Ganzi has a higher altitude and harsher natural environment than the other two regions. Consequently, the socioeconomic conditions in northern Ganzi is quite lower than in eastern and southern Ganzi.

The high altitude leads to backward transportation and communication conditions in Ganzi. Furthermore, Ganzi is an ethnic minority area where Tibetan is dominant, accounting for 78.46% of the total population. Factors such as ideology, language barrier, and education level restrict poverty reduction and development. Moreover, Ganzi is located near the upper Yangtze river, which is also a water conservation area and plateau ecological barrier. Ganzi plays an important role both in national ecological security and national harmony. As an alpine area, ethnic area, and ecologically protected area, Ganzi faces serious challenges in poverty reduction and development. At the end of 2017, the poverty rate of Ganzi was 8.65%, the location of Ganzi is shown in Fig. 8.

3.3.2 Evaluation of Living Standard in Ganzi

The living standard evaluation includes ten indicators, as shown in Table 2. The chosen indicator categories were housing situation, infrastructure of rural village, medical care, social security, and education. Per capita living space was selected to reflect the housing situation. The population rate of tap water usage and the number of administrative villages that could be reached by road were used to measure the infrastructure. Medical technical personnel in health care institutions per 10,000 persons and the number of beds utilized in health care institutions per 10,000 persons were chosen to illustrate the medical care. New Rural Co-operative Medical System participants as a proportion of the total population was selected to represent the level of social security. The number of teachers per 10,000 persons and the ratio of expenditure on science and education to GDP indicated the education situation. The disposable income of rural households was chosen to reflect the income standard. Engel's coefficient was used to reflect the overall living condition

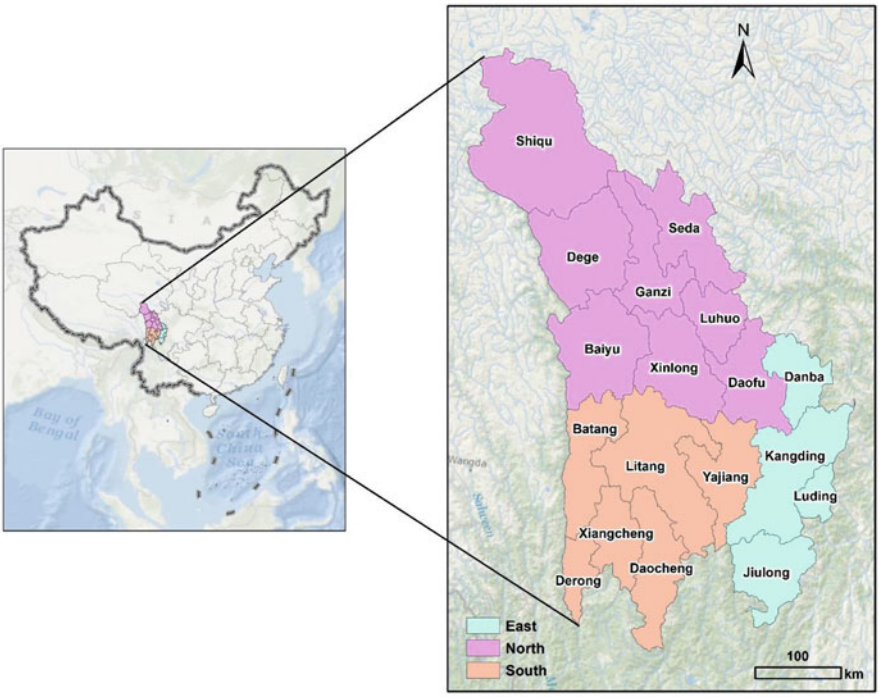

Fig. 8 Location of Ganzi Tibetan autonomous prefecture

in poor areas. Moreover, Engel's coefficient is a negative indicator in our evaluation index system, because the greater the value of Engel's coefficient means the poorer the living standard of people.

The entropy weighting method was employed to define the weights for each evaluation indicator. After that, the Grey relational analysis was used to integrate various indicators into a comprehensive evaluation value to better assess the living standard in Ganzi from 2010 to 2016. Shannon's entropy is widely used to determine weights, which is an objective method and determines weights only by data (Shannon 1984; Lotfi and Fallahnejad 2010). Here we used the entropy weighting method to determine the weights of each index. Gray system theory is proposed by Deng (1989). Grey relational analysis uses the order of Grey relational degrees to judge the strength or order of correlation between indicators and is widely applied for various evaluations (Tan and Deng 1995).

Supposing that there are m(m = 18) counties with n(n = 10) evaluated indicators, then the index system can be defined as:

$$X = \begin{bmatrix} x_{11} & \cdots & x_{1n} \\ \vdots & \ddots & \vdots \\ x_{m1} & \cdots & x_{mn} \end{bmatrix} \tag{3-1}$$

A standardization method was adopted to transform different value scales of indicator j into common measurable units by using:

$$\boldsymbol{y}_{.j} = \frac{\boldsymbol{x}_{.j} - \min\left(\boldsymbol{x}_{.j}\right)}{\max\left(x_{,j}\right) - \min\left(\boldsymbol{x}_{.j}\right)} \tag{3-2}$$

The information entropy of indicator j can be obtained by:

$$E_j = -\ln(n)^{-1} \sum_{i=1}^{n} \rho_{ij} \ln \rho_{ij} \tag{3-3}$$

$$\rho_{ij} = y_{ij} / \sum_{i=1}^{n} y_{ij} \tag{3-4}$$

Let $\lim_{\rho_{ij} \to 0} \rho_{ij} \ln \rho_{ij} = 0$, the weight of j can be obtained by:

$$w_j = \frac{1 - E_j}{n - \sum E_j} \, (j = 1, 2, \ldots, n) \tag{3-5}$$

Then, gray rational analysis was employed to obtain the evaluation index of living standard. First, we needed to normalize each indicator. For positive indicator j:

$$c_{ij} = \begin{cases} 1, x_{ij} > S_j \\ \frac{x_{ij}}{S_j}, x_{ij} \le S_j \end{cases} \tag{3-6}$$

For positive indicator j:

$$c_{ij} = \begin{cases} 1, x_{ij} \le S_j \\ \frac{x_{ij}}{S_j}, x_{ij} > S_j \end{cases} \tag{3-7}$$

where S_j is the reference value for indicator j,as shown in Table 4. The normalized indicator matrixC $= [\boldsymbol{c}_{i1}, \boldsymbol{c}_{i2} \cdots \boldsymbol{c}_{in}]$. Based on gray system theory, a standardization process is implemented on the normalized matrix to get the referential vector of indicators as$c^* = \left[c_1^*, c_2^* \cdots c_n^*\right]$. Then, the relational coefficient of indicator j for county i can be calculated by:

Table 4 Evaluation index framework of living standard in Ganzi

Project	Indicators	Reference value
Assessment of living standard in Ganzi Tibetan autonomous prefecture	Teachers per 10,000 persons[a]	100
	Medical technical personnel in health care institutions per 10,000 persons[a]	60
	Number of beds utilized in health care institutions per 10,000 persons[a]	50
	Engel's coefficient (%)[a]	40
	Popularization rate of tap water (%)[a]	100
	Ratio of administrative villages that can be reached by road (%)[a]	100
	Per-capita living space (m^2 per capita)[a]	30
	New Rural Co-operative Medical System participants as a proportion of total population (%)	100
	Ratio of expenditure on science and education to GDP (%)[a]	6
	Disposable income of rural household (yuan)[b]	8000

[a]National standard
[b]Local standard

$$\xi_{ij} = \frac{\min\limits_{i}\max\limits_{j}\left|c_j^* - c_{ij}\right| + \partial\max\limits_{i}\min\limits_{j}\left|c_j^* - c_{ij}\right|}{\left|c_j^* - c_{ij}\right| + \partial\max\limits_{i}\max\limits_{j}\left|c_j^* - c_{ij}\right|} \tag{3-8}$$

where $\partial\epsilon(0, \infty)$ is a predefined coefficient, set to 0.5. Finally, the evaluated living standard values can be calculated by:

$$R_i = \sum_{j=1}^{n} w_j * \xi_{ij} \tag{3-9}$$

Then the evaluation values were divided into five levels and labeled I to V to indicate the living standard in Ganzi from low to high, for each year.

The living standard in Ganzi improved remarkably, with an average growth rate of 24.72% from 2010 to 2016. As seen in Fig. 9, all the living standard evaluation indicators increased from 2010 to 2016. The disposable income of rural households was the major contributor to social condition growth, which was about 2.5 times higher in 2016 than it was in 2010. The housing, medical care, and educational conditions in Ganzi all saw significant improvement. The continuous improvement of social conditions from 2010 to 2016 in Ganzi can also be observed in Fig. 10.

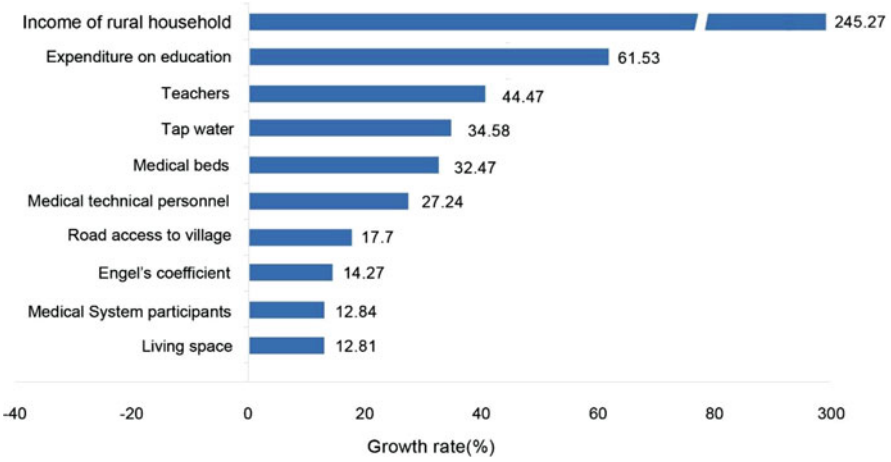

Fig. 9 Growth rate of evaluation indicators from 2010 to 2016 in Ganzi

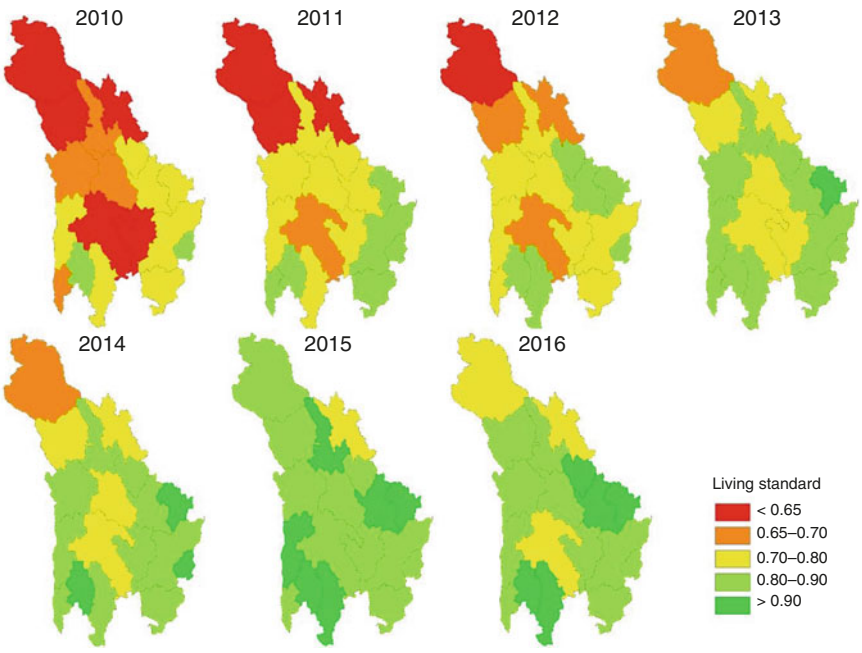

Fig. 10 Living standard evaluation index, categorized in five levels from 2010 to 2016 for Ganzi

The living standard also presented a regional difference, with higher living standard in eastern and southern Ganzi, and lower living standard in the northern region.

3.3.3 Spatial-Temporal Changes of Living Standard in Ganzi

The Bayesian hierarchical model was employed to explore the spatial-temporal pattern of the living standard in Ganzi from 2010 to 2016.The Bayesian hierarchical model was implemented using a statistical software named Open BUGS (Bayesian Inference Using Gibbs Sampling).

Based on the obtained living standard evaluation values, we investigated the spatial-temporal change pattern of the living standard in Ganzi. We denoted that y_{it} represents the evaluation value of ith (i $= 1, 2 \ldots 18$) county at tth(t $= -3, -2, -1, 0, 1, 2, 3$) year.

$$\mathrm{y}_{it} \sim Normal\left(\mu_{it}, \sigma^2\right) \tag{3-10}$$

Thus, the μ_{it} can be modeled as:

$$\log\left(\mu_{it}\right) = \alpha + S_i + b_0 t + v_t + b_{1i} t + \varepsilon_{it} \tag{3-11}$$

where α is the intercept term and assigned to follow a prior distribution of uniform distribution. S_i is the spatial term that describes the stable spatial pattern across the whole study area during the study period. $b_0 t + v_t$ describe the overall time trend pattern of the whole study area. $b_{1i} t$ allows each county to have its own change trend. ε_{it} captures the additional variability in the data not explained by other model components. Prior distributions are needed to assigned for model parameters. The prior distributions of S_i and $b_{1i} t$ are determined by the Besag York Mollie (BYM) model (Besag et al. 1991). In order to enhance the random effect of spatial structure in BYM, the conditional autoregressive (CAR) prior with a spatial adjacency matrix were employed at the same time (Li et al. 2014). The uniform distribution is assigned to b_0 and α. In addition, v_t is modeled as $v_t \tilde{}\mathrm{N}\ (0, \sigma_v^2)$, and ε_{it} is modeled as $\varepsilon_{it} \tilde{}\mathrm{N}\ (\sigma_\varepsilon^2)$. Both models were implemented using statistical software named OpenBUGS, which is specially designed for Bayesian analysis. Through Gibbs sampling and Metropolis algorithm, it could sample from complete conditional probability distribution and form MCMC chains, and finally estimating the parameters of the model through iteration (Lunn et al. 2000).

The obtained posterior median exp(S_i) indicates the stable spatial component of the living standard from 2010 to 2016. The posterior of exp(S_i) measured the living standard in ith county relative to the overall mean condition of the whole study area over the study period. The posterior median of exp(S_i) more than 1 indicated a higher level than the overall condition, while less than 1 indicated a lower level than the overall condition. Figure 11a maps the posterior median of exp(S_i). There were 10 counties that had a higher level of living standard than the overall living standard in Ganzi, while 8 counties had a lower level of living standard. Luding County obtained the highest value of the posterior median of exp(S_i) and Shiqu County obtained the lowest value. Furthermore, the distribution of the posterior median of

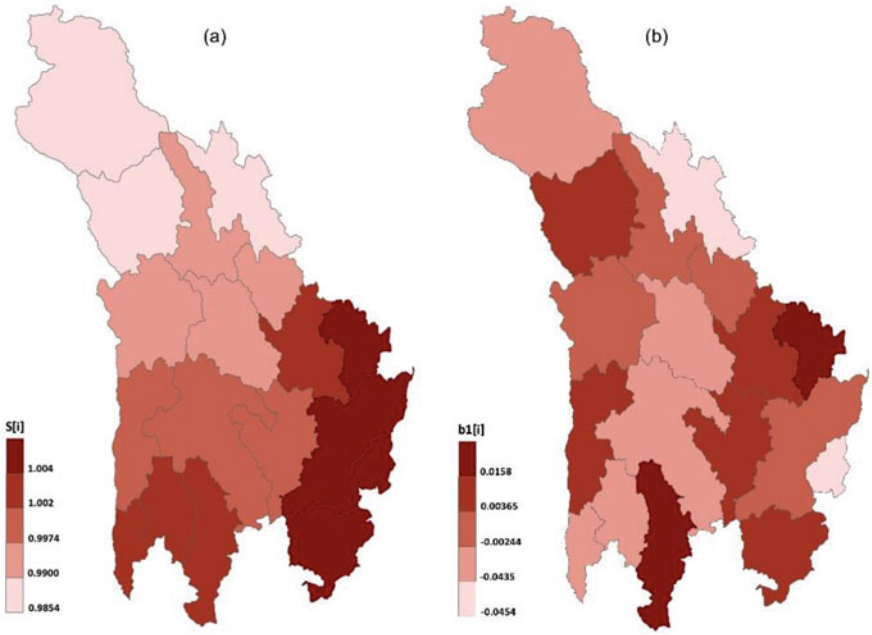

Fig. 11 (**a**) The obtained posterior medians of (exp(S_i)) for living standard in each county of Ganzi (**b**) The deviations of the local trend to the overall trend (b_{1i}) of living standard in each county of Ganzi

exp(S_i) presents an obvious regional disparity, with a high value concentrated in the eastern and southern regions and a low value concentrated in the northern region.

The obtained posterior median of b_{1i} measures the deviations of the local trend to the overall trend. A negative value of the posterior median of b_{1i} indicates that the speed of change of the evaluation index of *i*th county is slower than the overall change in Ganzi from 2010 to 2016. Conversely, a positive value of the posterior median of b_{1i} indicates that the speed of change of the evaluation index of *i*th county is more rapid than the overall change. Figure 11b maps the values of the posterior median of b_{1i}. Although the evaluation value of the living standard is quite low in northern Ganzi, such as Dege County and Ganzi County, they had more rapidly increased speed than the overall increase. Likewise, Luding County and Kangding County, located in eastern Ganzi, had the highest levels of living standard, but had a slower increase speed than the overall increase.

The obtained posterior median of exp($b_0 + v_t$) measures the overall temporal change trend of living standard in Ganzi from 2010 to 2016. Figure 12 plots the posterior median of exp($b_0 + v_t$) from 2010 to 2016. In Fig. 12, the living standard was continuously increasing from 2010 to 2016.

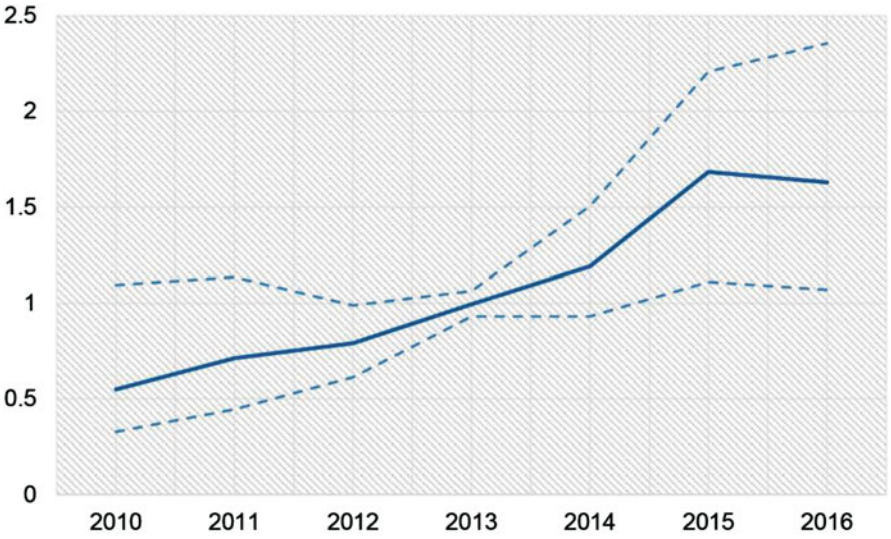

Fig. 12 The temporal overall changing trend ($\exp(b_0 t + v)$) of living standard in Ganzi from 2010 to 2016

References

Alkire, S., & Fang, Y. (2018). Dynamics of multidimensional poverty and uni-dimensional income poverty: An evidence of stability analysis from China. *Social Indicators Research, 142*(1), 25–64.

Alkire, S., & Foster, J. (2011). Counting and multidimensional poverty measurement. *Journal of Public Economics, 95*(7–8), 476–487.

Anselin, L. (1995). Local indicators of spatial association-LISA. *Geographical Analysis, 1*(1), 1–24.

Anselin, L. (2001). Spatial econometrics. In *A companion to theoretical econometrics* (pp. 311–330). Malden: Blackwell.

Anselin, L. (2002). Under the hood Issues in the specification and interpretation of spatial regression models. *Agricultural Economics, 27*(2002), 247–267.

Anselin, L., & Rey, S. (1991). Properties of tests for spatial dependence in linear regression models. *Geographical Analysis, 23*, 112–131.

Atkinson, A. B. (1987). On the measurement of poverty. *Econometrica, 55*, 749–764.

Besag, J., York, J., & Mollié, A. (1991). Bayesian image restoration, with two applications in spatial statistics. *Annals of the Institute of Statistical Mathematics, 43*(1), 1–20.

Bird, K. (2019). *Addressing spatial poverty traps*. New York: United Nations.

Chen, Y., & Ge, Y. (2015). Spatial point pattern analysis on the villages in China's poverty-stricken areas. *Procedia Environmental Sciences, 27*, 98–105.

Cheng, X., Shuai, C., Wang, J., Li, W., Shuai, J., & Liu, Y. (2018). Building a sustainable development model for China's poverty-stricken reservoir regions based on system dynamics. *Journal of Cleaner Production, 176*, 535–554.

Deller, S. (2010). Rural poverty, tourism and spatial heterogeneity. *Annals of Tourism Research, 37*(1), 180–205.

Deng, J. L. (1989). Introduction to grey system theory. *Journal of Grey System, 1*(1), 1–24.

Department of Household Surveys, National Bureau of Statistics of China. (2018). *Poverty monitoring report of China, 2018*. Beijing.

Dollar, D. (2007). *Poverty, inequality and social disparities during China's economic reform*. The World Bank Policy Research Working Paper No. 4253, Washington, DC, 1–28.

Ebdon, D. (1985). *Statistics in geography*. Oxford: Blackwell.

Fotheringham, S., Brunsdon, C., & Charlton, M. (2002). *Geographically weighted regression: the analysis of spatially varying relationships*. Chichester: Wiley.

Fotheringham, A. S., Crespo, R., & Yao, J. (2015). Geographical and temporal weighted regression (GTWR). *Geographical Analysis*, 1–22.

Ge, Y., Yuan, Y., Hu, S., Ren, Z., & Yijin, W. (2017). Space–time variability analysis of poverty alleviation performance in China's poverty-stricken areas. *Spatial Statistic, 21*, 460–474.

Getis, A. (1994). Spatial dependence and heterogeneity and proximal databases. In S. Fortheringham & P. Rogerson (Eds.), *Spatial analysis and GIS* (pp. 105–120). Oxford: Taylor and Francis.

Haining, R. (1990). *Spatial data analysis in the social and environmental sciences*. Cambridge: Cambridge University Press.

Information Office of the State Council. (2011). *New progress in development-oriented poverty reduction program for rural China*. Beijing.

Jalan, J., & Ravallion, M. (1997). *Spatial poverty traps? The World Bank* (Policy Research Working Paper No. 1862). Washington, DC.

Li, G., et al. (2014). Space–time variability in burglary risk: A Bayesian spatio-temporal modelling approach. *Spatial Statistics, 9*, 180–191.

Li, Y., Long, H., & Liu, Y. (2015). Spatio-temporal pattern of China's rural development: A rurality index perspective. *Journal of Rural Studies, 38*, 12–26.

Li, Y., Su, B., & Liu, Y. (2016). Realizing targeted poverty alleviation in China. *China Agricultural Economic Review, 8*(3), 443–454.

Liu, Y. S., & Li, J. (2017). Geographic detection and optimizing decision of the differentiation mechanism of rural poverty in China. *Acta Geographica Sinica, 72*(1), 161–173.

Liu, Y., & Xu, Y. (2016). A geographic identification of multidimensional poverty in rural China under the framework of sustainable livelihoods analysis. *Applied Geography, 73*, 62–76.

Liu, Y., Liu, J., & Zhou, Y. (2017). Spatio-temporal patterns of rural poverty in China and targeted poverty alleviation strategies. *Journal of Rural Studies, 52*, 66–75.

Liu, Y., Guo, Y., & Zhou, Y. (2018). Poverty alleviation in rural China: Policy changes, future challenges and policy implications. *China Agricultural Economic Review, 10*(2), 241–259.

Lotfi, F. H., & Fallahnejad, R. (2010). *Imprecise Shannon's entropy and multi attribute decision making*. *Entropy, 12*(1), 53–62.

Lunn, D. J., Thomas, A., Best, N., & Spiegelhalter, D. (2000). WinBUGS—A Bayesian modelling framework: Concepts, structure, and extensibility. *Statistics and Computing, 10*, 325–337.

National Bureau of Statistics. (2019). *Statistical bulletin of the People's Republic of China on national economic and social development in 2018*. Beijing.

Okwia, P. O., Ndeng'e, G., Kristjanson, P., Arunga, M., Notenbaert, A., Omolo, A., Henninger, N., Benson, T., Kariuki, P., & Owuor, J. (2007). Spatial determinants of poverty in rural Kenya. *PNAS, 104*(43), 16769–16774.

Ouyang, Z. Y., Zheng, H., Xiao, Y., Polasky, S., Liu, J., Xu, W., et al. (2016). *Improvements in ecosystem services from investments in natural capital*. *Science, 352*(6292), 229–251.

Paul Elhorst, J. (2014). *Spatial econometrics: From cross-sectional data to spatial panels*. Berlin Heidelberg: Springer.

Ren, Z., Ge, Y., Wang, J., Mao, J., Zhang, Q., et al. (2017). Understanding the inconsistent relationships between socioeconomic factors and poverty incidence across contiguous poverty-stricken regions in China: Multilevel modelling. *Spatial Statistics, 21*, 406–420.

Ripley, B. D. (1977). Modelling spatial patterns. *Journal of Royal Statistical Society, 39*, 172–212.

Satya, R., & Chakravarty, C. D. A. (2006). *The measurement of social exclusion*. *Review of Income and Wealth,**52***, 377–398.

Sen, A. K. (1976). Poverty: An ordinal approach tomeasurement. *Econometrica, 44*, 219–231.

Sen, A. K. (2001). *Development as freedom* (2nd ed.). Oxford New York: Oxford University Press.
Shannon, C. E. (1984). *A mathematical theory of communication* (Vol. 27, pp. 379–423). Urbana: University of Illinois Press.
Sparks, C., & Campbell, J. (2013). An application of Bayesian methods to small area poverty rate estimates. *Population Research and Policy Review, 33*(3), 455–477.
Sparks, C., & Campbell, J. (2014). An application of Bayesian methods to small area poverty rate estimates. *Population Research and Policy Review, 33*(3), 455–477.
Tan, X. R., & Deng, J. L. (1995). *Grey relational analysis: A new method of multi factors statistical*. *Statistical Research, 3*, 46–48.
The State Council. (2011). *The outline for development-oriented poverty reduction for China's rural area (2011–2020)*. Beijing: State Council.
The World Bank. (2018). *Poverty and shared prosperity 2018: Piecing together the poverty puzzle*. Washington, DC: World Bank.
Tu, J., & Xia, Z. G. (2008). Examining spatially varying relationships between land use and water quality using geographically weighted regression I: Model design and evaluation. *Science of the Total Environment, 407*(1), 358–378.
UNDP. (2010). *Human development report 2010: The real wealth of nations: Pathways to human development*. New York: Palgrave Macmillan.
United Nations. (2015a). *Transforming our world: the 2030 agenda for sustainable development*. New York: United Nations.
United Nations. (2015b). *The millennium development goals report*. New York: United Nations.
Wang, X. (2012). Poverty criteria and global poverty situation. *Review of Economic Research, 55*, 41–50.
Wang, J. F., et al. (2010). Geographical detectors-based health risk assessment and its application in the neural tube defects study of the Heshun Region, China. *International Journal of Geographical Information Science, 24*(1), 107–127.
Wang, X. L., Wang, L. M., & Wang, Y. (2014). *The quality of growth and poverty reduction in China*. Berlin: Springer.
Wang, J. F., Zhang, T. L., & Fu, B. J. (2016). A measure of spatial stratified heterogeneity. *Ecological Indicators, 67*, 250–256.
Watmough, G. R., et al. (2019). Socioecologically informed use of remote sensing data to predict rural household poverty. *Proceedings of the National Academy of Sciences of the United States of America, 116*(4), 1213–1218.
Xu, W., et al. (2017). Strengthening protected areas for biodiversity and ecosystem services in China. *Proceedings of the National Academy of Sciences of the United States of America, 114*(7), 1601–1606.
Zhang, C., Tang, Y., Xu, X., & Kiely, G. (2011). Towards spatial geochemical modelling: use of geographically weighted regression for mapping soil organic carbon contents in Ireland. *Applied Geochemistry, 26*(7), 1239–1248.
Zhang, C., et al. (2014). Are poverty rates underestimated in China? New evidence from four recent surveys. *China Economic Review, 31*, 410–425.
Zhou, Y., & Liu, Y. (2019). The geography of poverty: Review and research prospects. *Journal of Rural Studies*. https://doi.org/10.1016/j.jrurstud.2019.01.008.
Zhou, Y., Guo, Y., Liu, Y., Wu, W., & Li, Y. (2018). Targeted poverty alleviation and land policy innovation: Some practice and policy implications from China. *Land Use Policy, 74*, 53–65.
Zuo, C. S. (2016). *Evolution of China's poverty alleviation and development policy (2001–2015)* (pp. 16–18, 73). Beijing: Social Science Academic Press.

Part III
Recent Developments in Biostatistics

Novel Bayesian Adaptive Designs and Their Applications in Cancer Clinical Trials

Ruitao Lin and J. Jack Lee

Abstract Clinical trial is a prescribed learning process for identifying safe and effective treatments. In recent years, rapid advancements in cancer biology, immunology, genomics, and treatment development have demanded innovative methods to identify better therapies for the most appropriate population in a timely, efficient, accurate, and cost-effective way. In this chapter, we will first illustrate the concept of Bayesian update and Bayesian inference, which is a superior alternative to the traditional frequentist approach. Bayesian methods take the "learn as we go" approach, making them innately suitable for clinical trials. Then, we will give an overview of Bayesian adaptive designs in the areas of adaptive dose finding, posterior probability and predictive probability calculation, outcome adaptive randomization, multi-endpoint phase II design, multi-arm, multi-stage platform design, hierarchical modeling, etc. In particular, a new class of model-assisted designs will be introduced, which combine the transparency and simplicity of conventional algorithm-based designs with the superiority and rigorousness of model-based designs. These designs enjoy superior performance comparable to more complicated, model-based designs, though they are also capable of simplicity similar to conventional designs. Examples of the Bayesian optimal interval (BOIN), the keyboard, the time-to-event BOIN (TITE-BOIN), the BOIN combination, and the Bayesian Optimal Phase 2 (BOP2) designs will be discussed. Real applications, including BATTLE trial in lung cancer, I-SPY 2 trial in breast cancer, and GBM AGILE in glioblastoma, will be given. The chapter will also introduce software tools, including downloadable programs and online Shiny applications for the design and conduct of clinical trials. Bayesian adaptive clinical trial designs increase study efficiency, allow more flexible trial conduct, and treat a greater number of patients with more effective treatments in the trial. They also possess desirable

R. Lin · J. J. Lee (✉)
Department of Biostatistics, The University of Texas MD Anderson Cancer Center, Houston, TX, USA
e-mail: RLin@mdanderson.org; jjlee@mdanderson.org

A. Bekker et al. (eds.), *Computational and Methodological Statistics and Biostatistics*, Emerging Topics in Statistics and Biostatistics,
https://doi.org/10.1007/978-3-030-42196-0_17

frequentist properties. Useful software tools can be found at: https://biostatistics.mdanderson.org/SoftwareDownload/ and https://trialdesign.org/.

1 Introduction

Clinical trial is a prescribed learning process for identifying safe and effective treatments (Berry 2006; Friedman et al. 2010; Piantadosi 2017). Since the launch of the first randomized controlled trial in 1946 (the streptomycin trial for curing pulmonary tuberculosis), clinical trials have been the bedrock of medical advancement and the development of new drugs (Bhatt 2010). Carefully designed and implemented trials provide sound evidence of the toxicity and efficacy of the treatments evaluated. Through rigorous pre-clinical and clinical drug development processes, new treatments are evaluated and compared with the standard of care. Safe and efficacious drugs are approved eventually. The traditional drug development process, however, is time-consuming and extremely expensive. In a recent estimate, the total cost for successfully developing a new drug reaches $3 billion dollars (Avorn 2015). Furthermore, rapid advancements in biology, immunology, genomics, and treatment development demand innovative methods to identify better therapies for the most appropriate population in a timely, efficient, accurate, and cost-effective way. In this chapter, we propose to apply Bayesian adaptive designs to address these issues. We use cancer drug development as a platform. However, many of the methods discussed can be readily applied to other disease settings.

2 Statistical Inference: Frequentist Versus Bayesian Frameworks

Through clinical trials, we collect data to inform the parameter of interest, θ, such as the treatment effect or the side effect of a new therapy. In general, there are two major schools of statistical inference: frequentist and Bayesian. In the frequentist framework, the data collected through the trial are considered to be random and the parameter θ is assumed to be fixed, yet unknown. Thus, frequentist makes inferences on θ by evaluating the likelihood function $\Pr(Data \mid \theta)$. For example, if a parametric form is assumed for $\Pr(Data \mid \theta)$, the standard maximum likelihood estimation can be performed to estimate and infer the unknown parameter θ. On the other hand, the Bayesian paradigm assumes that data are fixed, because they have been observed and the unknown parameter θ is random. By modeling θ as a random variable with some prespecified probability distribution, Bayesian inference is made through the posterior probability function $\Pr(\theta \mid Data)$, which can be computed using the famous Bayes theorem: $\Pr(\theta \mid Data) \propto \Pr(\theta) \Pr(Data \mid \theta)$. Here, $\Pr(\theta)$ is the prior probability function of θ, which characterizes all available information before conducting the trial. Although being philosophically different, they provide

complementary perspectives and tools in clinical trials (Berger 2010; Lee and Chu 2012).

Bayesian inference universally follows three steps: (1) Elicit the prior distribution of the unknown parameter. The prior distribution generally can be determined based on historical or external trials, expert opinions, and plausible initial inference. In addition, the prior distribution can be either informative or non-informative, depending on the specific features of the trial. (2) Obtain the likelihood function based on the data collected during the study. (3) Synthesize the prior information and the observed data likelihood into a posterior distribution of the parameter of interest. When the posterior distribution is in the same probability distribution family as the prior distribution, the prior is called a conjugate prior. The conjugate prior gives a closed-form expression for the posterior, which makes the posterior computation more convenient. On the other hand, when the posterior distribution $\Pr(\theta \mid Data)$ does not have a standard distributional form, inference on θ can be made by drawing posterior samples of θ from $\Pr(\theta \mid Data)$ via Markov Chain Monte Carlo (MCMC) algorithms. MCMC algorithms, together with ever-increasing computation power, greatly assist the development of Bayesian statistics.

During a study, the Bayesian method updates the prior to form the posterior distribution coherently and continuously based on the accumulating data. In other words, the Bayesian inference has an adaptive "learn-as-we-go" nature, which provides an ideal framework for adaptive clinical trials. In addition, when there are subsequent studies, the posterior distribution obtained from the current study can be naturally transitioned to the prior distribution for future studies. This additionally demonstrates the adaptive learning feature of the Bayesian method.

Compared to the frequentist approach, some unique strengths of Bayesian methods in clinical trials are highlighted as follows (Lee and Chu 2012): (1) the Bayesian approach directly models the parameter of interest using a probability distribution, which leads to a more intuitive and easier-to-interpret answer to the scientific question at hand. (2) The Bayesian inference is a continuous learning process; as long as there are new data/information, they can be naturally synthesized in the posterior inference. This feature greatly facilitates more frequent monitoring and decision making in adaptive clinical trials, without compromising performance and implementation. (3) Prior or external information can be accounted for in Bayesian methods. This makes the inference more efficient, and would, in turn, save the required sample size, reduce trial cost, and accelerate drug development. (4) The distribution of future outcomes can be predicted based on the current data, which renders more flexibility in adaptively treating future patients. (5) The Bayesian inference naturally accommodates hierarchical modelling, which makes borrowing information across different treatments or disease subtypes possible. (6) The Bayesian approach can formally incorporate the "gain/loss" utility, assisting informed decision making in a complex setting of balancing efficacy/toxicity, cost/benefit, and pros/cons in general. Optimal decisions can be obtained by maximizing the gain or minimizing the loss.

3 Overview and Features of Bayesian Adaptive Designs

Traditional clinical trials are usually conducted in a static way, such that many elements (e.g., sample size, treatment assignment, enrolled population) are fixed in advance, and the interim data observed during a trial are rarely used to guide the subsequent course of the study. Static trials are simple, easy to implement, and result in statistically valid inference. However, the restriction of flexibility under static designs may be overly conservative, leading to efficiency loss. For example, clinical observations collected during the midcourse of a phase II cancer trial may indicate that the considered treatment is futile. Since static trials rarely terminate early based on interim data, they result in slow and unnecessarily costly drug development (Lee and Berry 2016).

Nowadays, adaptive designs are increasingly being adopted in cancer trials, due to the dynamic nature that allows for adaptations of the trial conduct according to the interim trial data. An adaptive design is formally defined as a trial design that enables pre-specified, well-defined modifications during trial conduct on the basis of observed data. The main purpose of the adaptive design is to provide the investigator the flexibility to identify the best clinical benefit of the treatment in real time and then use that information to guide further treatment of patients or treatment selection without undermining scientific validity, efficiency, and safety (Mahajan and Gupta 2010). In general, an adaptive design may allow for adaptive estimation of treatment effect, adaptive dose escalation/de-escalation, early stopping of the trial for toxicity/efficacy or futility, dropping or adding new treatment arms, using a seamless phase transition, adjusting an adaptive randomization scheme based on patient response or covariates, subgroup enrichment, sample size re-estimation, biomarker-guided treatment allocation, etc. (Chow and Chang 2008; Zang and Lee 2014).

While adaptive trial designs can be developed under either frequentist or Bayesian paradigms, the Bayesian method provides a naturally ideal framework due to the "learn-as-we-go" characteristics and a consistent probability-based inferential framework. In this section, we will describe several important features of Bayesian adaptive designs.

3.1 Bayesian Outcome Adaptive Randomization

Randomized clinical trials are the gold standard for comparing the differential effects of various treatments. To ensure an objective comparison, patient allocation should be random or unpredictable, balancing out both known and unknown prognostic factors and potential confounders. Based on study objectives, randomization takes various forms, such as equal randomization, random permuted block, covariate-adaptive randomization, Pocock-Simon dynamic allocation, response or

outcome adaptive randomization, and covariate-adjusted response adaptive randomization (Hu and Rosenberger 2006). Different schemes may also have different frequentist or Bayesian approaches to perform randomization. The focus of this section is outcome adaptive randomization (OAR), which allows alteration of allocation probabilities as the trial proceeds so that the probability for a patient to be assigned to a better performing treatment increases. There are many popular frequentist OAR procedures, such as the play-the-winner rule (Rosenberger 1999) and the optimal OAR (Rosenberger et al. 2001). Bayesian OAR procedures provide additional flexibility by incorporating prior information, as well as the estimation variability in determining randomization probabilities (Thall and Wathen 2007).

Consider a two-arm clinical trial with binary responses, and denote p_1 and p_2 as the response rates of the two treatments, respectively. Based on the interim data (D) that are accumulated in the trial, it is feasible to obtain the posterior probability that treatment 1 has a higher response rate than treatment 2, which is given by

$$\lambda = \Pr\left(p_1 > p_2 \mid D\right).$$

The simplest model for the above Bayesian inference is the Beta-Binomial model, which assigns independent Beta prior distributions for the binomial probabilities p_1 and p_2, respectively. Due to conjugacy, the posterior distribution of p_1 (or p_2) is still a Beta distribution, and the quantity λ can be easily computed.

Under the Bayesian framework, a new patient is assigned to treatment 1 with probability

$$\pi\left(\lambda, \gamma\right) = \frac{\lambda^{\gamma}}{\lambda^{\gamma} + (1-\lambda)^{\gamma}}.$$

Here, $\gamma \in [0, \infty]$ is a tuning parameter that controls the degree of randomization imbalance: when $\gamma = 0$, it reduces to an equal randomization procedure with the randomization probability being 0.5, regardless of the value of λ; when $\gamma = \infty$, it corresponds to the play-the-winner rule. The selection of γ depends on the needs, as well as the setting of the trial. Usually, a larger value of γ is preferred when the efficacy difference between treatments is large, such that individual ethics can be enhanced. More sophisticatedly, the tuning parameter can be a function of the sample size to reflect the inference uncertainty. Thall and Wathen (2007) suggested $\gamma = n/(2N)$, where n is the interim sample size and N is the total sample size planned for the trial. At the beginning of the trial, the uncertainty of the treatment effect is large due to the sparsity of the data, so γ is close to zero, which is nearly the equal randomization. As the trial proceeds with more data accumulated, the randomization skews more towards the better performing treatment. Note that, by comparing the posterior distributions p_1 and p_2, λ automatically accounts for both the point and variance estimates of the treatment response rates. Therefore, compared to the frequentist approach, the Bayesian randomization probability not only considers the prior information, but also takes into account the inference variability of the treatment effect. Due to its flexibility and satisfactory performance,

the Bayesian randomization procedure has been applied to many applications. For example, Yin et al. (2012) proposed a Bayesian phase II randomized clinical trial design using Bayesian adaptive randomization and predictive probability. Wathen and Thall (2017) applied Bayesian adaptive randomization to multi-armed trials. Ventz et al. (2017) developed a basket trial design based on Bayesian OAR.

3.2 Bayesian Posterior Probability

Interim analysis is essential in adaptive trials, such that the trial can be adaptively and timely modified based on the data gathered by the time of interim analysis. For example, in phase I dose-finding trials, interim analysis is performed to decide on dose escalation, de-escalation, or to stay at the same dose for the next cohort of patients (O'Quigley et al. 1990); in phase II two-stage trials, "go/no-go" decisions can be made in the middle of the trial (Simon 1989); in phase III confirmatory trials, interim analysis can effectively adjust the sample size of the trial (Proschan and Hunsberger 1995) or even can modify the patient inclusion criteria (Simon and Simon 2017). For Bayesian adaptive designs, it is natural to perform the interim analysis based on the Bayesian posterior probability.

For illustration, consider a single-arm phase II trial to assess the therapeutic effect of the new treatment. Let p_S and p_E denote the response rates of the standard and experimental drugs, respectively. During the trial, the data D are observed and the posterior probability that the experimental drug has a higher response rate than the standard drug, i.e., $\Pr(p_E > p_S + \delta | D)$, is updated continuously, where δ is the improvement margin of the response rate of the experimental drug over that of the standard drug. As the trial proceeds, "go/no-go" decisions can be made adaptively based on the posterior probability (Thall and Simon 1994): if $\Pr(p_E > p_S + \delta | D)$ is very large, say, greater than a prespecified upper probability cutoff θ_U, then the trial can be terminated early, as the experimental drug is likely to be promising; on the other hand, if the posterior probability is very small, say, smaller than a lower probability cutoff θ_L, then the trial can be terminated early for futility; otherwise, there is not adequate information to deliver any conclusion, so the trial continues to collect more data.

The "go/no-go" decision rules of the above monitoring procedure, based on Bayesian posterior probability, is easy to understand and implement. The entire procedure can be carefully calibrated by adjusting the probability cutoffs θ_U and θ_L to control the type I or type II error rates. In the case of binary endpoints, the Beta distribution can serve as a convenient prior distribution for the response rate. It is also easy to elicit the hyper-parameters of the Beta distribution based on the prior information. Generalization of this Bayesian monitoring procedure can be found in Thall et al. (1995), Heitjan (1997), Thall et al. (2003), and Zhou et al. (2017), among others.

3.3 Bayesian Predictive Probability

In phase II clinical trials, Bayesian predictive probability can serve as a good alternative tool to the posterior probability in interim decision making. Given the observed data D, the predictive distribution of the number of responses among the total sample size N can be obtained. In general, the Bayesian predictive probability procedure continuously calculates the probability of rejecting the null hypothesis (a positive conclusion), if the current trial continues to the maximum planned sample size given the interim data (Lee and Liu 2008).

Similarly to the posterior probability monitoring, the "go/no-go decisions based on the predictive probability monitoring also can be made by comparing the predictive probability with prespecified upper and lower probability cutoffs. However, unlike the posterior probability monitoring, which only considers the interim observed data, the predictive probability monitoring mimics the decision-making process of claiming the drug promising or non-promising by projecting the result to the end of the trial. Hence, not only the interim observed data, but also the future unobserved data make a difference in interim decision making. The predictive probability calculation is more elaborate, but still as easy to implement as posterior probability monitoring. Both approaches are more adaptable than traditional multistage designs. Predictive probability monitoring is conceptually appealing because it takes into account the uncertainty of future data, and it is based on a consistent inferential framework. It is also flexible in allowing for continuous monitoring and can be generated to more complex trial settings, such as randomized phase II trials (Yin et al. 2012), trials with time-to-event endpoints (Yin et al. 2018), and platform trials (Hobbs et al. 2018).

3.4 Bayesian Adaptive Trials at the University of Texas MD Anderson Cancer Center

Due to the appealing strengths of Bayesian adaptive designs in clinical trials, they are being increasingly used in real trials at The University of Texas MD Anderson Cancer Center. Biswas et al. (2009) identified 964 MD Anderson Cancer Center trials registered in the institutional protocol system between 2000 and early 2005. In an update to this data, Tidwell et al. (2019) recently reviewed 1020 trials that were submitted between January 2009 and December 2013. Table 1 presents the trial features and whether Bayesian methods were used. Of the 964 trials between 2000 and early 2005, approximately 20% (195/964) used Bayesian designs and analyses. This percentage increased to 28% (283/1020) for the period from 2009 to 2013. Among the trials conducted solely at MD Anderson Cancer Center, the percentage of Bayesian trials was much larger, approximately 30% (169/570) and 56% (189/335) for the two time periods, respectively. This also indicates an expansion of use of Bayesian trial methods within the institution, implying that statisticians and clinical investigators are favoring the Bayesian approach. Figure 1

Table 1 Protocol features by Bayesian status (two time periods: 2000 to early 2005 and January 2009 to December 2013)

	Bayesian		
	Yes	No	
Protocol feature	N (%)	N (%)	All N (%)
2000 to early 2005 (Biswas et al.2009)			
All	195 (20%)	769 (80%)	964 (100%)
Year			
<2001	20 (16%)	104 (84%)	124 (13%)
2001	22 (19%)	96 (81%)	118 (12%)
2002	34 (29%)	84 (71%)	118 (12%)
2003	62 (26%)	172 (74%)	234 (24%)
2004	50 (17%)	246 (83%)	296 (31%)
2005 (partial)	7 (7%)	65 (93%)	74 (8%)
Site			
MD Anderson only	169 (30%)	401 (70%)	570 (59%)
Multi center	26 (20%)	368 (80%)	394 (41%)
2009–2013 (Tidwell et al.2019)			
All	283 (28%)	737 (72%)	1020 (100%)
Year			
2009	57 (27%)	155 (73%)	212 (21%)
2010	57 (26%)	162 (74%)	219 (21%)
2011	57 (28%)	146 (72%)	203 (20%)
2012	52 (28%)	132 (72%)	184 (18%)
2013	60 (30%)	142 (70%)	202 (20%)
Site			
MD Anderson only	189 (56%)	146 (44%)	335 (33%)
Multi center	94 (14%)	582 (86%)	676 (66%)
Other sites only	0 (0%)	9 (100%)	9 (1%)

depicts the development phases of the trials for the two time periods. It shows that the Bayesian approach was frequently adopted in early phase trials, such as phase I, phase I-II, and phase II trials. This is because early phase trials have smaller sample sizes, yet multiple interim looks; the Bayesian approach usually is more flexible than the frequentist method in terms of borrowing prior information and making multiple sequential decisions. In addition, the regulatory considerations for early phase trials are less stringent than late phase III trials. Therefore, implementation of Bayesian trials is more acceptable. Early phase trials also do not require rigorous type I/II error controls.

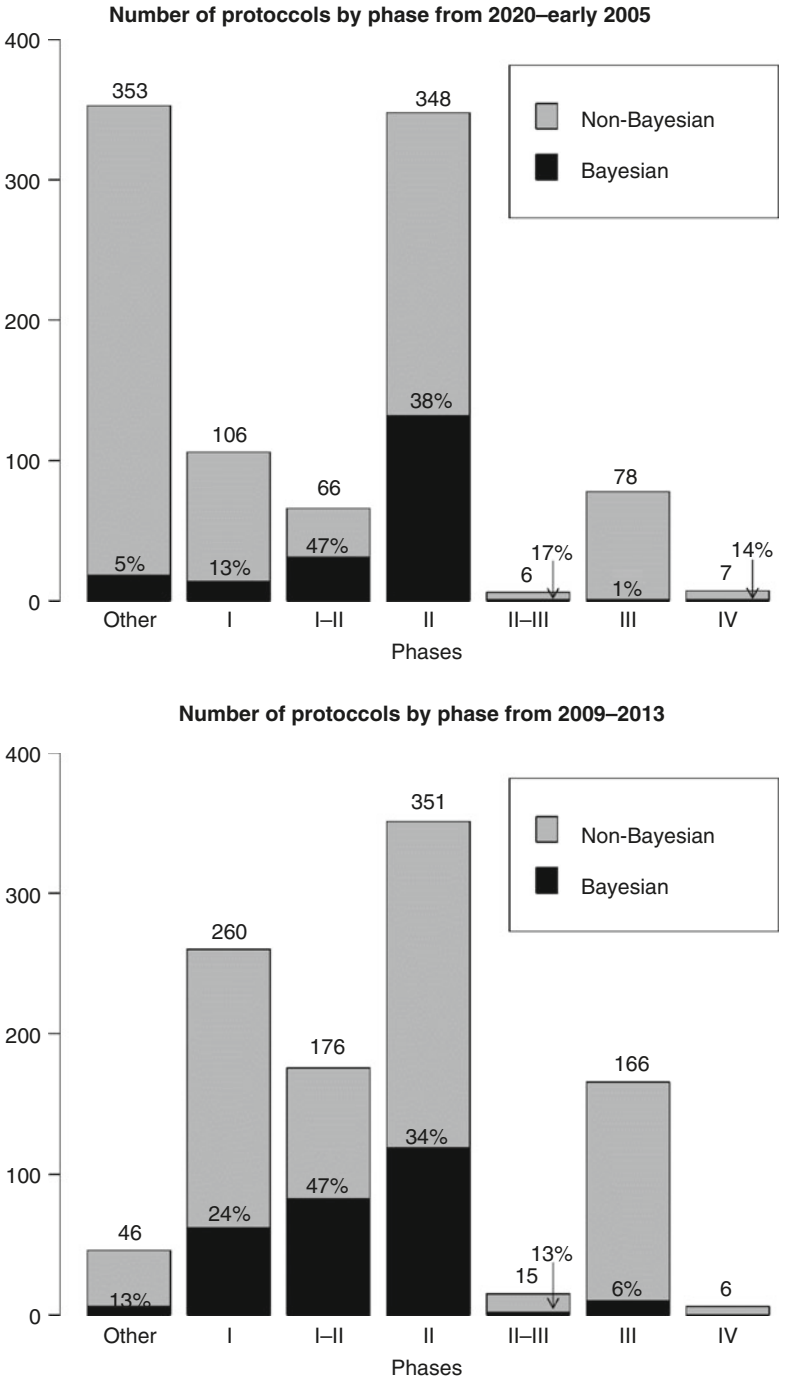

Fig. 1 Number of protocols by phase of development. The number above the bar indicates the total number of protocols, and the percentage number indicates the percentage of Bayesian trials

4 Adaptive Designs for Dose Finding

Phase I clinical trials are the first step of testing a new treatment in human beings to examine safety of the new agent and understand its tolerance. The primary objective of phase I clinical trials is to identify the maximum tolerated dose (MTD), which is defined as the dose level that has the dose-limiting toxicity (DLT) probability closest to the target toxicity rate. In general, phase I clinical trial designs can be classified into algorithm-based designs, model-based designs, and model-assisted designs (Zhou et al. 2018b). Algorithm-based designs, mostly the 3 + 3 design, conduct the phase I trial based on a predefined, yet simple dose-escalation/de-escalation rule. Due to its simplicity and transparency, the 3 + 3 design is dominant in practice, regardless of its poor characteristics. Model-based designs, such as the well-known continual reassessment method (CRM), adopt statistical models for informative decision making by using all available information (O'Quigley et al. 1990). The model-based designs usually improve the performance of MTD identification over the algorithm-based designs; however, the application of model-based designs has been limited in practice, due to computational complexity and a seemingly "black-box" decision-making style. In addition, the model-based designs may not be robust to model misspecification. Model-assisted designs have emerged as an attractive approach for phase I clinical trials, as they combine the simplicity of algorithm-based designs with the superior performance of model-based designs. The novel model-assisted designs use a model for efficient decision making like model-based designs, while their dose-finding rules can be pre-calculated and tabulated before a trial starts as with algorithm-based designs (Zhou et al. 2018a, b). Typical examples include the Bayesian optimal interval (BOIN) design (Liu and Yuan 2015), the keyboard design (Yan et al. 2017), and the modified probability interval (mTPI) design (Ji et al. 2010), among others (Lin and Yin 2018; Lin and Yuan 2019).

In this section, we will review some Bayesian adaptive dose-finding designs, including one model-based design (i.e., the CRM) and one model-assisted design (i.e., the BOIN design). We will also introduce some extensions of these designs in the situation of more complicated phase I dose-finding trials, such as drug-combination trials and trials with delayed toxicity.

4.1 Continual Reassessment Method

In phase I trials, several dose levels of the new drug are specified by the clinicians for investigation. Suppose that J dose levels are considered, and let p_j denote the probability of DLT at dose level $j = 1, \ldots, J$. A key assumption for phase I trials is that the dose—toxicity relationship is monotonically increasing (i.e., $p_1 < \cdots < p_J$). Given a target toxicity probability ϕ, the MTD j^* is the dose level that satisfies the following condition:

$$j^* = \underset{j=1,\ldots,J}{\text{argmin}} \mid p_j - \phi \mid .$$

To identify the MTD from J dose levels, the CRM assumes a working dose—toxicity model, such as the hyperbolic tangent, one-parameter logistic regression, or the power model (O'Quigley et al. 1990). For example, the power model is defined as:

$$p_j = \pi_j^{\exp(\alpha)},$$

where $\pi_1 < \cdots < \pi_J$ is the set of J prespecified toxicity probabilities (known as the skeleton of the power model), and α is the unknown parameter. Suppose that n_j patients have been treated at dose level j, and y_j patients have experienced the DLT. Then the likelihood function is a standard Binomial likelihood as follows,

$$L\left(D|\alpha\right) \propto \prod_{(j=1)}^{J} \left\{\pi_j^{\exp(\alpha)}\right\}^{y_j} \left\{1 - \pi_j^{\exp(\alpha)}\right\}^{n_j - y_j}.$$

Given a prior distribution $f(\alpha)$, the posterior distribution of α can be derived based on the Bayes theorem:

$$f\left(\alpha \mid D\right) \propto f\left(\alpha\right) L\left(D \mid \alpha\right).$$

Due to the flexibility of Bayesian approaches, various inferences can be made based on the posterior distribution. For example, in addition to $f(\alpha| D)$, it is also possible to obtain the posterior distribution of p_j, as well as the posterior mean $\hat{p}_j$. In particular, the CRM uses $\hat{p}_j$ to determine the dose escalation or de-escalation: if the current dose level is lower than the dose level that has the posterior mean $\hat{p}_j$ closest to ϕ, then the next dose is escalated to level $j + 1$; if the current dose level is higher than the dose level that has $\hat{p}_j$ closest to ϕ, then the next dose is de-escalated to level $j - 1$; otherwise, the next dose stays at the current dose level.

In the standard CRM, the one-parameter power model is adopted. This is because the sample size of phase I studies is typically small, and the one-parameter model is convenient to accommodate the dose-toxicity relationships. In some cases, one can also use more complicated models, such as the two-parameter logistic regression model. However, it has been shown that the one-parameter power model is sufficient to result in satisfactory performance in many settings, while increasing model dimensionality may lead to erratic behaviors (Iasonos et al. 2016). To improve the robustness of the CRM, Bayesian model averaging CRM has also been proposed (Yin and Yuan 2009b).

The decision-making process behind the CRM is a typical example of Bayesian adaptive designs. In other words, the observations made during the trial are used for decision making and affect the subsequent course of the trial. Since the CRM uses all available data in the trial for determining subsequent dose assignments, it performs uniformly better than the conventional 3 + 3 design in terms of MTD

identification. As such, more patients are treated at doses closer to the MTD. But caution is warranted when implementing the CRM. Due to its model-based nature, the CRM tends to be sensitive to model misspecification (e.g., the specification of the model skeleton or the prior distribution), and it sometimes risks patients to overdoses (Neuenschwander et al. 2008). To avoid overdose allocation and ensure robust performance, modification has been suggested, including starting at the lowest dose level and not skipping the untested doses in dose escalation, enrolling more than one patient at a dose, and having at least one patient completed one cycle before enrolling additional patients in a new dose, among others (Goodman et al. 1995). In addition, extensive preliminary simulation is warranted to calibrate the design parameters under various scenarios.

The CRM can be extended to dose finding in more complex settings. A key assumption behind the CRM is that the toxicity outcome can be quickly observed before dose escalation or de-escalation decisions can be made. However, the toxicity evaluation sometimes may take longer than the patient accrual, especially in radiation oncology and immunotherapy trials. As a result, the toxicity outcomes of some previously treated patients may be still pending by the arrival of the new patients. To avoid potential trial delay, Cheung and Chappell (2000) developed a time-to-event CRM by weighting each patient by his/her follow-up proportion. As a result, when the patient has finished toxicity evaluation, the weight equals to one; otherwise, the weight is a fraction of one to reflect the amount of information currently available for this patient.

Drug-combination therapy provides an effective way to obtain synergistic treatment effects and overcome resistance of monotherapy. Drug-combination trials are more complicated than single-agent trials, due to the higher dimensionality of the dose searching space and the incomplete order between the combined doses (Riviere et al. 2015). Most of the model-based drug-combination designs (Braun and Wang 2010; Thall et al. 2003; Yin and Yuan 2009a) adopt similar dose-finding strategies as the CRM in phase I trials with combined drugs. In general, a particular model is needed to quantify the dose—toxicity relationship, then the model estimate would be continuously updated for dose-assignment decisions based on the accumulating data. Since the model for the dose—toxicity relationship in drug-combination trials requires more parameters, the need to calibrate the model-based drug-combination designs is much greater than the standard CRM.

One limitation of the CRM is that it only considers the toxicity data, while neglecting the efficacy information in decision making. In some situations, however, the MTD may not be biologically optimal in terms of toxicity—efficacy tradeoffs, especially when the dose—efficacy curves may have plateaued or taken on an inverted-U shape. To obtain an optimal biological dose, it is more desirable to account for both toxicity and efficacy in the trial. This setting corresponds to a so-called seamless phase I/II trial (Thall and Cook 2004). Readers may refer to Zang et al. (2014), Zang and Lee (2017), and Yuan et al. (2017) for a comprehensive review of Bayesian adaptive designs for phase I/II clinical trials.

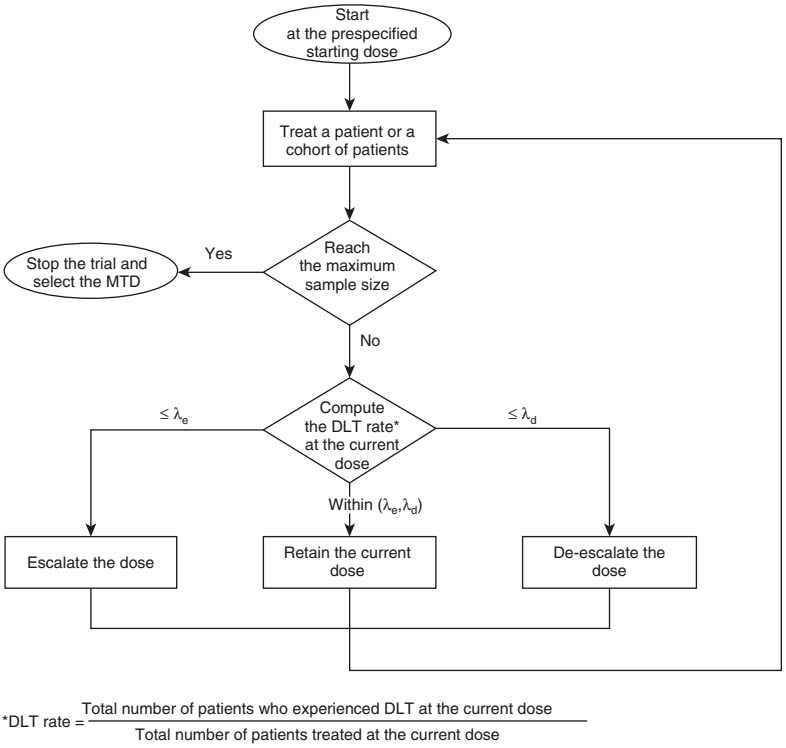

Fig. 2 The flowchart of the Bayesian optimal interval (BOIN) design

4.2 Bayesian Optimal Interval Design

Unlike the CRM, which uses a parametric model to quantify the dose-toxicity relationship and makes decisions based on data across all dose levels, the BOIN design models only "local" data observed at the current dose, typically using a binomial model, to guide dose assignments (Liu and Yuan 2015). In particular, the dose escalation/de-escalation decisions of BOIN are made by comparing the observed toxicity rate $\hat{p}_j = y_j/n_j$ at the current dose level j with respect to the dose escalation and de-escalation boundaries λ_e and λ_d, respectively. Suppose j is the current dose level, the dose-finding rule of BOIN can be described as follows (see also Fig. 2):

- If $\hat{p}_j \leq \lambda_e$, then the dose for the next cohort of patients is escalated to level $j+1$.
- If $\hat{p} \geq \lambda_d$, then the dose for the next cohort of patients is de-escalated to level $j-1$.
- Otherwise, if $\lambda_e < \hat{p}_j < \lambda_d$ or the next assignment is outside of the prespecified dose range, then the next cohort is treated at the same dose level j.

The BOIN design determines the pair of λ_e and λ_d by formulating the dose-finding problem in a Bayesian decision-making framework. Specifically, for each dose level j, the BOIN design considers the following hypotheses,

$$H_{0j} : p_j = \phi, H_{1j} : p_j = \phi_1, H_{2j} : p_j = \phi_2,$$

where $\phi_1 < \phi < \phi_2$ are design parameters that should be prespecified. Here, H_{0j} indicates that the current level j is a desirable dose; H_{1j} indicates that level j is sub-therapeutic, such that dose escalation is warranted; and H_{2j} indicates that level j is an overdose, such that dose de-escalation is needed. Suppose that the prior probabilities for the three hypotheses are π_0, π_1, and π_2, respectively. By minimizing the probability of incorrect decisions of dose escalation and de-escalation, the optimal values of λ_e and λ_d are given by

$$\lambda_e = \frac{\log\left(\frac{1-\phi_1}{1-\phi}\right) + n_j^{-1}\log\left(\frac{\pi_1}{\pi_0}\right)}{\log\left\{\frac{\phi(1-\phi_1)}{\phi_1(1-\phi)}\right\}}, \lambda_d = \frac{\log\left(\frac{1-\phi}{1-\phi_2}\right) + n_j^{-1}\log\left(\frac{\pi_0}{\pi_2}\right)}{\log\left\{\frac{\phi_2(1-\phi)}{\phi(1-\phi_2)}\right\}}.$$

In general, the prior information on the hypotheses is limited in most phase I trials. Therefore, we can use the non-informative prior $\pi_0 = \pi_1 = \pi_2 = 1/3$, which further simplifies the above optimal boundary formulae. Moreover, when the non-informative prior is used, the Bayes factors are equivalent to the likelihood ratio test, which is uniformly most powerful. In other words, BOIN also enjoys the optimality from the frequentist viewpoint. As a default, Liu and Yuan (2015) recommended $\phi_1 = 0.6\phi$ and $\phi_2 = 1.4\phi$ for general use. The design parameters ϕ_1 and ϕ_2 can also be prespeficied to reflect a particular requirement of the trial at hand.

The BOIN design enjoys many advantages similar to the $3 + 3$ design, as its dose-finding decisions can be tabulated before a trial starts. Table 2 shows the default dose escalation and de-escalation boundaries of the BOIN design. For example, given the target toxicity rate $\phi = 0.30$, the corresponding dose escalation boundary $\lambda_e = 0.236$ and the de-escalation boundary $\lambda_d = 0.358$. Suppose that the observed toxicity rate at the current dose level $\hat{p}_j = 0.40$, since $\hat{p}_j > \lambda_d$, dose de-escalation is needed; similarly, if $\hat{p}_j = 0.15$, then dose escalation is needed.

For illustration, we consider a trial with a target toxicity rate of 0.3. Six dose levels are considered, a total of 24 patients with three patients in a cohort are planned for the trial. Based on the target toxicity rate $\phi = 0.3$, the dose escalation and de-

Table 2 Dose escalation and de-escalation boundaries of the BOIN design based on the default setting $\phi_1 = 0.6\phi$ and $\phi_2 = 1.4\phi$

	Target toxicity rate ϕ					
Boundaries	0.15	0.20	0.25	0.30	0.35	0.40
λ_e (escalation)	0.118	0.157	0.197	0.236	0.276	0.316
λ_d (de-escalation)	0.179	0.238	0.298	0.358	0.419	0.479

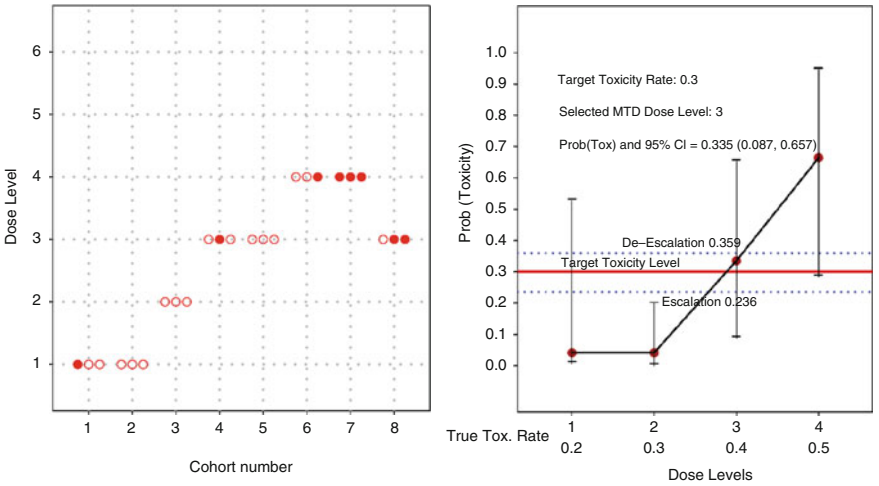

Fig. 3 A trial example based on the BOIN design with a target toxicity probability $\phi = 0.30$. The left panel shows the sequence of dose assignments, where a circle indicates one patient without DLT and a dot indicates one patient with DLT. The right panel presents the final estimate of the toxicity probabilities for the four dose levels. Dotted horizontal lines indicate the dose escalation and de-escalation boundaries of the BOIN design

escalation boundaries of the BOIN design are given in Table 2. The dose-assignment decisions through the trial are displayed in Fig. 3. According to the dose-finding rule, the trial starts by treating the first cohort of patients at the lowest dose level. Since the estimated toxicity rate at dose level 1 is 1/3, this leads to the dose retaining decision for cohort 2. None of the patients in cohort 2 has experienced the DLT, hence, dose escalation is made by treating cohort 3 at dose level 2. Figure 3 (left panel) shows the path of the dose assignments for the subsequent cohorts, from which we can see that the BOIN design can search the MTD adaptively and treat most of the patients at the right dose level. After the trial completes, the estimate of the toxicity rate for each dose level is given in the right panel of Fig. 3. Since dose level 3 has an observed rate of 1/3, which is closest to ϕ among all six dose levels, it is selected as the MTD.

Modelling the "local data" observed at the current dose level renders BOIN enumerating all possible decisions before the trial begins. The decision rules in Table 2 makes the BOIN design transparent and easy to implement. A potential concern for BOIN is whether using only "local data" at the current dose, while ignoring the data observed from other doses, causes efficiency loss in MTD identification and patient treatment. To answer this question, extensive simulation studies have been conducted by comparing the performance of BOIN with that of a design that uses more data in decision making (Lin and Yuan 2019; Zhou et al. 2018a). It has been shown that the BOIN design is as efficient as model-based designs in terms of finding MTD, while the implementation of BOIN is much easier (Zhou et al. 2018a). One explanation is that the dose escalation/de-escalation

determined by the observed data has the ordered relationship embedded. Although the data from other dose levels are not used directly, their contribution is made indirectly by incorporating the history leading to the current dose level.

Since the decision of BOIN solely depends on data from the current dose level, it avoids complicated modelling and model fitting. Upon completion of the trial, the dose—toxicity curve can be constructed by connecting the probability of toxicity estimates at each dose level by applying isotonic regression. The point estimate and the 95% credible interval estimation of the toxicity rate at each dose level are shown in the right panel of Fig. 3.

Note that the Keyboard design (Yan et al. 2017) is another model-assisted Phase I design that yields similar performance to BOIN. The original modified probability interval (mTPI) design has flaws and errors, which have been corrected in the mTPI-2 design (Guo et al. 2017). This updated design is essentially the same as the keyboard design.

Another advantage of BOIN is that its dose escalation and de-escalation rules can be directly used for drug-combination trials (hereafter referred to as Comb-BOIN). The only issue with this is that when a dose escalation (or de-escalation) decision is made in a drug-combination trial with drug A and drug B, there are more than one option to choose from: we can escalate (de-escalate) either the dose of drug A or the dose of drug B. Lin and Yin (2017a) proposed an adaptive rule to select the dose when dose escalation/de-escalation is needed. Specifically, suppose the current dose level is (u, v) which is the combined dose of uth level of drug A and vth level of drug B. Define an admissible dose escalation set $A_E = \{(u+1, v), (u, v+1)\}$ and an admissible dose de-escalation set $A_D = \{(u-1, v), (u, v-1)\}$. When dose escalation is needed, the dose combination that belongs to A_E and has the highest value of $\Pr(p_{uv} \in (\lambda_e, \lambda_d) \mid D_{uv})$ is selected; and when de-escalation is needed, the dose combination that belongs to A_D and has the highest value of $\Pr(p_{uv} \in (\lambda_e, \lambda_d) \mid D_{uv})$ is selected. Here, p_{uv} denotes the toxicity probability of dose combination (u, v), and D_{uv} is the observed data at that dose. Despite being simple, the BOIN combination design yields excellent performance comparable to and often superior to more complicated model-based designs (Lin and Yin 2017a).

The BOIN design can be also generated as a time-to-event BOIN (TITE- BOIN), which addresses the issue of late-onset toxicity (Yuan et al. 2018). TITE-BOIN works by predicting the unobserved, pending DLT outcome using the follow-up time of the patient whose toxicity profile is still unavailable. Then the toxicity rate at the current dose level can be estimated in real time by using the observed and the predicted DLT data. Therefore, the dose-finding rule of BOIN is still applicable in a seamless way when a new patient is accrued, avoiding potential trial delays. The TITE-BOIN design inherently possesses the features of BOIN, such that its decision rule can be completely pre-tabulated. Numerical study shows that TITE-BOIN yields superior performance comparable to that of model-based designs (e.g., TITE-CRM (Cheung and Chappell 2000)), and outperforms the rolling six design (Skolnik et al. 2008) with substantially higher accuracy to identify the MTD and allocate more patients to the MTD (Yuan et al. 2018).

Due to its attractive features and good performance, the extension of BOIN has been studied in various settings. Zhang and Yuan (2016) proposed a waterfall BOIN design to identify the maximum tolerated dose contour in phase I drug-combination trials. Lin and Yin (2017b) and Takeda et al. (2018) generalized BOIN by considering efficacy and toxicity simultaneously. Lin (2018) considered a multiple toxicity constraint for BOIN.

The software for the BOIN design is available in three forms, including a graphical user interface based Windows desktop program (including BOIN, TITE-BOIN, and Comb-BOIN), which is freely available from the MD Anderson Software Download Kiosk https://biostatistics.mdanderson.org/SoftwareDownload/SingleSoftware/Index/99, Shiny online apps (including BOIN, TITE-BOIN, and Comb-BOIN) freely available at http://trialdesign.org, and an R package "BOIN" (including BOIN, Comb-BOIN, and waterfall BOIN for drug combination studies) available from the CRAN website. For users who are not familiar with R, the Windows desktop program is a good option. It has an intuitive graphical user interface and the function to automatically generate the protocol template for the trial (see Fig. 4).

5 Adaptive Designs for Multiple Outcomes

Traditional phase II trial studies usually adopt a binary efficacy endpoint to screen out inefficacious treatments (Simon 1989). However, with the advent of novel molecular targeted agents and immunotherapy, using a single endpoint sometimes may be insufficient to characterize the treatment effect of a new drug. As a result, phase II trials have become much more complicated with multiple endpoints, such as the ordinal endpoint or co-primary efficacy and toxicity endpoints. The Bayesian Optimal Phase 2 (BOP2) design provides a simple, flexible, and efficient tool to allow for multiple interim looks and handle different endpoints under a unified framework (Zhou et al. 2017).

To illustrate the main idea of the BOP2 design, we consider a phase II trial with co-primary efficacy and toxicity endpoints. In this trial, the objective response (OR) rate is considered as the efficacy endpoint and the DLT rate is considered as the toxicity endpoint. The trial jointly monitors the efficacy and toxicity, such that the treatment will be deemed as futile if the ORR is too low, say, less than ϕ_{OR}, or the treatment is overly toxic if the DLT rate is unacceptably large, say, greater than ϕ_{DLT}.

Statistically speaking, different forms of clinical endpoints can be unified and represented using a single multinomial random variable Y with K distinct categories that represent all possible values (Zhou et al. 2017). In the aforementioned example, $Y = (Y_1, Y_2, Y_3, Y_4)$ has four categories with 1 = (OR, DLT), 2 = (OR, no DLT), 3 = (no OR, DLT), and 4 = (no OR, no DLT). Let (p_1, p_2, p_3, p_4) be the probability

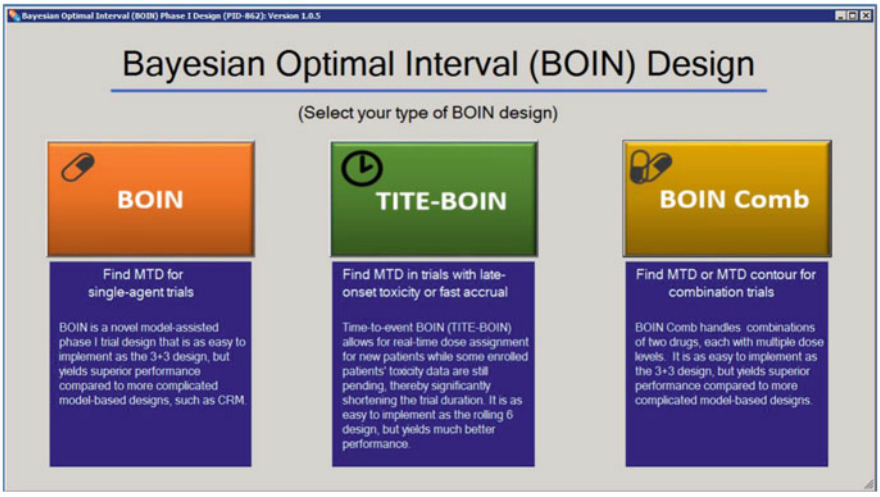

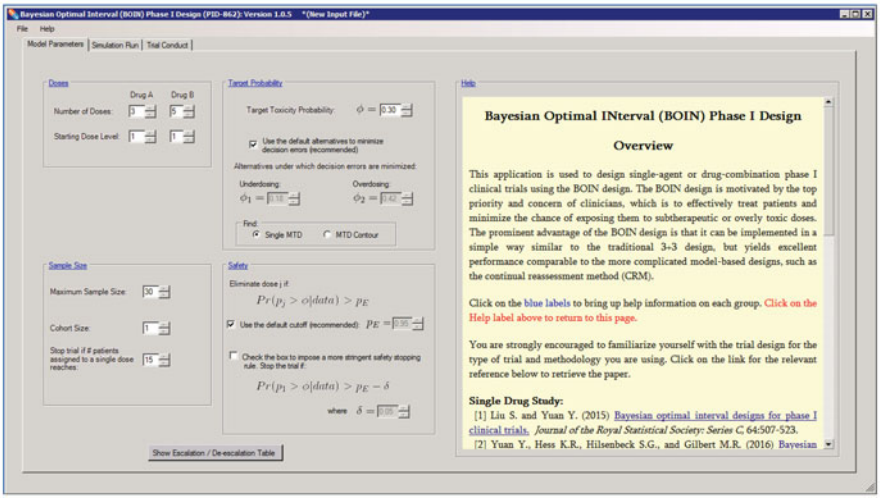

Fig. 4 The user interface of the BOIN software available from https://biostatistics.mdanderson.org/SoftwareDownload/SingleSoftware/Index/99

vector associated with the four categories of Y. By this way, the OR rate is $p_1 + p_2$, and the DLT rate is $p_1 + p_3$. For additional examples and the relationship between the multimodal variable Y and the original multiple endpoints, see Zhou et al. (2017).

The BOP2 design assumes that Y follows a Dirichlet-Multinomial model:

$$Y \mid p_1, p_2, p_3, p_4 \sim Multinomial\,(p_1, p_2, p_3, p_4)\,,$$

$$(p_1, p_2, p_3, p_4) \sim Dirichlet\,(\alpha_1, \alpha_2, \alpha_3, \alpha_4)\,,$$

where $(\alpha_1, \alpha_2, \alpha_3, \alpha_4)$ are prespecified hyperparameters. Compared to the approach of considering and modelling each OR or DLT independently, this approach naturally accounts for the correlation between different endpoints. Given the interim data D_n collected from n patients, the posterior distribution of $(p_1, p_2, p_3, p_4) \mid D_n$ follows a Dirichlet distribution. It also can be shown that the marginal posterior distribution of ORR or DLT is a standard Beta distribution.

At each interim, BOP2 uses the following Bayesian stopping criteria to make "go/no-go" decisions:

If $\Pr(OR\ rate < \phi_{OR} \mid D_n) > C_n$ or $\Pr(DLT\ rate > \phi_{DLT} \mid D_n) > C_n$, stop the trial; otherwise continue the trial.

Here, the posterior probability $\Pr(OR\ rate < \phi_{OR} \mid D_n)$ measures how likely it is that the true OR rate is futile, $\Pr(DLT\ rate > \phi_{DLT} \mid D_n)$ measures the likelihood that the true DLT rate is overly toxic, and C_n is an adaptive probability cutoff, depending on the interim sample size n, such that the stopping criteria are lenient with sparse data at the beginning of the trial and become increasingly stricter as the trial moves forward. This Bayesian rule says that if the interim data suggest that the treatment is unlikely to reach the minimal efficacy requirement or exceed the maximum toxicity threshold, then we stop the trial early for futility or toxicity.

Zhou et al. (2017) proposed a functional form for the probability cutoff C_n, such that C_n can be adaptively adjusted based on the amount of information observed thus far. In fact, C_n can be calibrated using simulation studies to ensure a desirable performance. This calibration procedure mimics the numerical searching in Simon's two-stage design (Simon 1989). First, a null hypothesis and an alternative hypothesis that define the joint response probabilities should be specified. Second, grid searching is performed to identify all possible values of C_n that lead to a desirable level of type I error rate. Last, an optimal C_n that maximizes the statistical power can be selected from the set collected in the previous step. This calibration procedure is commonly used for most Bayesian adaptive designs to evaluate the frequentist operating characteristics (Zhang et al. 2019).

The BOP2 design is particularly flexible in number of multiple endpoints and multiple interim looks. A potential challenge with Bayesian adaptive designs that deal with such trials with multiple endpoints and interim looks is the complexity of design implementation. If the implementation of the design is difficult, it may decrease use in practice. However, one prominent advantage of the BOP2 design is that, thanks to the simple Dirichlet-Multinomial model, one can enumerate the stopping boundaries of BOP2 prior to the start of the trial. This greatly simplifies the implementation and increases trial transparency.

The BOP2 design can be easily implemented using the online R shiny app, which is freely available at www.trialdesign.org. Users can use the shiny app to calculate the decision boundaries of BOP2 by inputting the design parameters, conduct simulation studies based on various scenarios, and obtain the trial protocol template. As an illustration, we consider a trial with co-primary efficacy and toxicity

endpoint. Suppose that $\phi_{OR} = 0.45$ and $\phi_{DLT} = 0.30$, and the maximum sample size is 40. We plan to make "go/no-go" decisions when the number of treated patients reaches 10, 15, 20, 25, 30, 35, and 40. Suppose that the type I error rate is 0.1, the null hypothesis is Pr(OR) = 0.45, Pr(DLT) = 0.3, Pr(OR & DLT) = 0.15, and the alternative hypothesis is H1: Pr(OR) = 0.60, Pr(DLT) = 0.2, Pr(OR & DLT) = 0.18. The decision boundaries of BOP2 calculated using the shiny app are provided in Fig. 5. We also provide two trial examples in Fig. 5, with the "go/no-go" regions highlighted in both panels (a) and (b). In panel (a), the "go/no-go" boundary has never been crossed; as a result, we conclude that the treatment is acceptable. On the other hand, in panel (b), the number of DLT exceeds the "go/no-go" boundary when 30 patients have been treated. As a result, we terminate the trial early and conclude that the treatment is overly toxic.

One limitation of the BOP2 design is that it can only deal with those outcomes that can be quickly available after the treatment of patients. Some agents, such as immunotherapy, may need a longer time (e.g., several months) to show treatment effects, compared to the accrual rate of new patients. Standard practice under such a situation may need to suspend the accrual to wait for the availability of the interim data, which may prolong the trial duration and delay the treatment of new patients. Built upon the basis of BOP2, the time-to-event Bayesian optimal phase (TOP) II design was proposed to make real-time "go/no-go" interim decisions in the presence of late-onset responses by using all available data, including the observed responses and patients' follow-up times (Lin et al. 2019). The TOP design inherits the transparency and the simplicity of BOP2, such that that its "go/no-go" decision rules can be tabulated and included in the protocol prior to the conduct of the trial. The software to implement the TOP design is also available at www.trialdesign.org.

6 Adaptive Designs for Multi-Arm, Multi-Stage Platform Trials

The drug development process is costly and time consuming. Nowadays, for complex diseases such as cancer, many new agents and many more combination therapies need to be evaluated as biological knowledge advances with lightning speed. Traditional clinical trials are straightforward and investigate the treatments one-at-a-time in a sequential manner; such an approach suffers from several deficiencies, especially in the era of precision medicine. In general, the success rate for such "one-treatment-at-a-time" drug development is particularly low (DiMasi et al. 2013). As shown in Fig. 6, traditional two-arm sequential designs have several discrete phases. In each discrete phase, an experimental treatment is compared with the standard-of-care control, leading to many patients being allocated to the control arm. This approach only considers a single, specific scientific question at each discrete phase, which can barely touch the complicated cancer system (Berry 2015). Furthermore, "white space" is formed in between each discrete phase, because

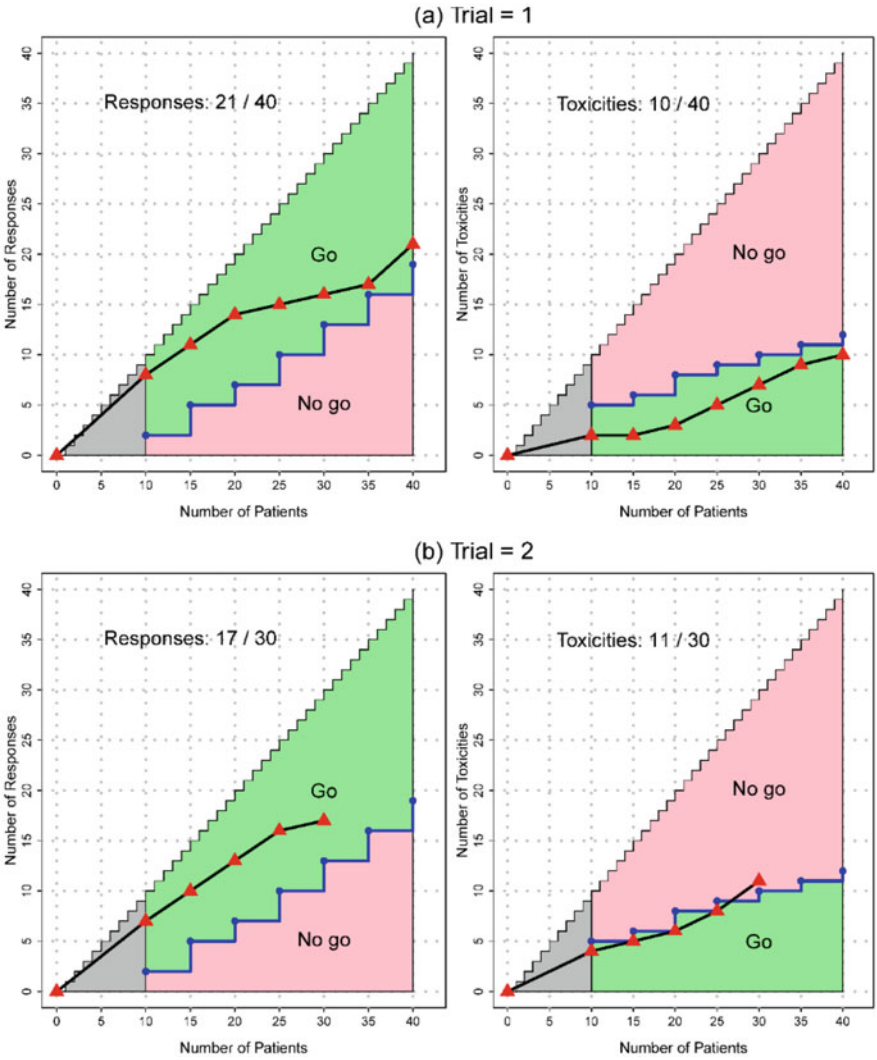

Fig. 5 Illustration of the BOP2 design based on two trial examples. Interim analyses are performed when the number of treated patients reaches 10, 15, 20, 25, 30, and 35, and a final analysis is performed when the maximum sample size of 40 is reached. If the number of responses crosses the "go/no-go" boundary, we stop the trial for futility or toxicity and conclude that the treatment is unacceptable. Otherwise, we continue the trial. If the null hypothesis is rejected at the final analysis, we conclude the treatment is acceptable. The null and alternative hypotheses are specified as H_0: Pr(OR) = 0.45, Pr(DLT) = 0.3, Pr(OR & DLT) = 0.15 vs. H_1: Pr(OR) = 0.60, Pr(DLT) = 0.2, Pr(OR & DLT) = 0.18. The line with triangle points corresponds to the number of observed responses

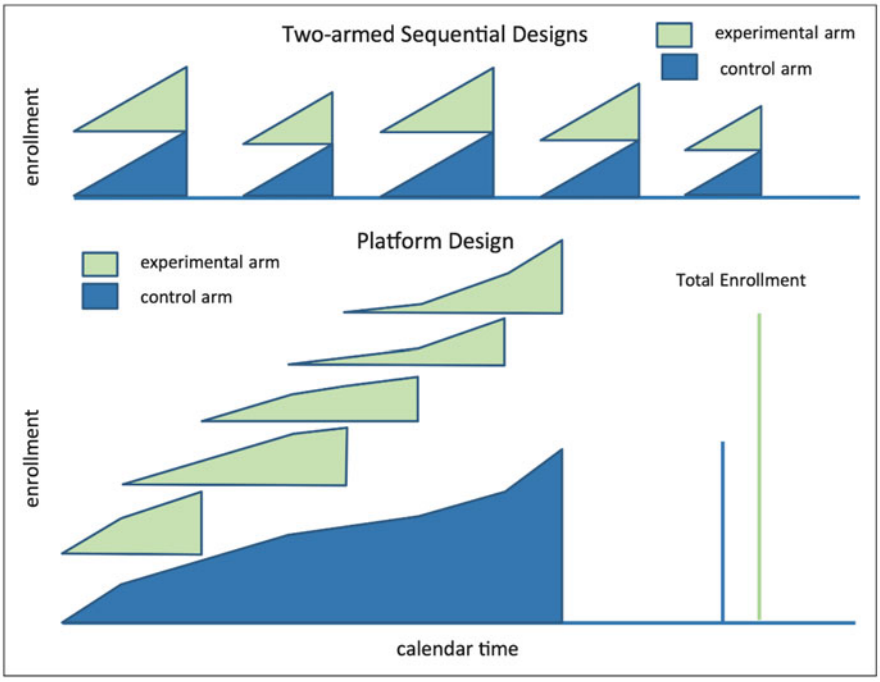

Fig. 6 Sequential two-arm design versus multi-arm platform design in randomized phase II trials. Each shape denotes a study arm. The sequential two-arm design has five independent randomized subtrials, with each subtrial including a control arm. The multi-arm platform design is a master protocol study with only one control arm included. The horizontal axis indicates the calendar time, and the vertical axis indicates the enrollment. The enrollment increases with the time for the active arms

each discrete phase needs to go through the review and approval process. This approach not only wastes time and resources between phases, it also adds the entire drug development process timeframe. The subsequent nature of discrete phases additionally hinders information borrowing across different phases, and thus can potentially result in efficiency loss (Hobbs et al. 2018).

Viewing the drug development process as a whole system, the multi-arm multi-stage (MAMS) platform trial design provides an effective way to efficiently evaluate modern treatments (Saville and Berry 2016). As shown in Fig. 6, the MAMS platform design is a broad class of randomized trials that includes a single control arm and screens multiple agents simultaneously. During the trial, the MAMS platform design can sequentially graduate a promising treatment for efficacy or drop the inefficacious agent for futility. Meanwhile, new treatments also can be adaptively added into the ongoing comparative study for investigation. The MAMS platform design has many other prominent features that differ from the traditional two-arm

sequential designs, such as controlling the family-wise type I error rate with multiple testing procedures to reduce false positives, using outcome adaptive randomization to assign more patients to a better treatment arm, etc. For overviews of the MAMS platform design, see Lee and Chu (2012), Wason and Jaki (2012), Wason et al. (2016), and Howard et al. (2018).

Although some frequentist MAMS platform designs have been proposed (Lee et al. 2019; Wason and Jaki 2012), the Bayesian paradigm provides a natural framework to accommodate the aforementioned adaptive features. Hobbs et al. (2018) proposed a MAMS platform design using Bayesian predictive probability (hereafter referred to as the PP-MAMS design). In particular, a simple Beta-Binomial model is adopted to derive the posterior distribution of the response probability. Denote π_j as the probability of response for arm j, $j = 0, 1, \ldots, J$ with $j = 0$ indicating the control arm and J as the total number of the experimental arms. Based on the beta prior distribution, $\pi_j \sim Beta(\alpha_j, \beta_j)$, $\alpha_j, \beta_j > 0$, the posterior for π_j after observing r_j responses from n_j patients is still a beta distribution, given by

$$\pi_j \mid r_j \sim Beta\left(\alpha_j + r_j, \beta_j + n_j - r_j\right).$$

Under the Bayesian paradigm, we declare the drug is efficacious, if the following decision criteria are satisfied:

$$\Pr\left(\pi_j > \pi_0 + \delta \mid r_0, r_j\right) > \theta,$$

where $\delta > 0$ determines the extent to which an improvement is deemed as clinically meaningful, and $\theta \in (0, 1)$ is the posterior probability cutoff that governs the amount of "evidence" required to conclude success.

The predictive probability monitoring under the PP-MAMS design bases the decisions not only on the currently observed data, but also on the future data for incoming patients. In particular, let R_j denote the unobserved number of responses from up to N_{max} patients, i.e., the maximum sample size for each arm. Given the current observations (r_0, r_j), the predictive probability that the trial ultimately demonstrates improvement for treatment j over the control is

$$\lambda\left(r_0, r_1\right) = E_{R_0, R_1}\left[I\left\{\Pr\left(\pi_j > \pi_0 + \delta \mid R_0, R_j\right) > \theta\right\} \mid r_0, r_j\right]$$

$$= \sum_{u=0}^{N_{max}-n_0} \sum_{v=0}^{N_{max}-n_j} I\left\{\Pr\left(\pi_j > \pi_0 + \delta \mid r_0 + u, r_j + v\right) > \theta\right\} \times$$

$$\Pr\left(R_0 = r_0 + u \mid r_0\right) \Pr\left(R_j = r_j + v \mid r_j\right).$$

Where $I\{\cdot\}$ represents the indicator function, and $\Pr(R_j = r_j + v \mid r_j)$ is the predictive probability distribution of R_j. The "go/no-go" decision for each treatment arm j can be expressed as follows:

- If $\lambda(r_0, r_1) < \phi$, then drop treatment arm j from the study for futility.
- If $\lambda(r_0, r_1) \geq \phi$, then continue to randomize patients to treatment arm j.

Here, ϕ is the prespecified probability cutoff, which can be calibrated to satisfy the type I/II error constraints. The sequential monitoring based on the predictive probability not only accounts for uncertainty amongst observed data, but also variability for outcomes yet to be observed in the trial. This enhances the robustness of the design, especially when the sample sizes between two arms are imbalanced.

Besides the key elements introduced above, the PP-MAMS design is very flexible and can be generated to accommodate various features, such as adding new treatment arms at random entry times—including adaptive randomization schemes to allocate more patients to a better treatment arm—among others. For further readings on the performance of the PP-MAMS design, which is better than two-arm sequential trials, see Hobbs et al. (2018).

7 Examples of Bayesian Adaptive Trials

In this section, we discuss three recently conducted prototypical examples that adopted Bayesian adaptive designs: the Biomarker-based approaches of targeted therapy for lung cancer elimination (BATTLE) trial, the investigation of serial studies to predict your therapeutic response with imaging and molecular analysis 2 (I-SPY 2) trial, and the adaptive global innovative learning environment for glioblastoma (GBM AGILE) trial. Each of these examples shows the feasibility of the Bayesian approach in recent cancer trials.

7.1 BATTLE Trials

The BATTLE project consists of one umbrella protocol and adaptive randomized phase II studies with four biomarker-based targeted therapies in patients with advanced non-small cell lung cancer (NSCLC) (Kim et al. 2011; Zhou et al. 2008). Four types of biomarker classes assessed in the trial were EGFR mutation/amplification, KRAS and BRAF mutation, VEGF and VEGFR expressions, and Cyclin D1/RXR expressions. In general, the four binary biomarkers can lead to $2^4 = 16$ different biomarker combinations, but the BATTLE trial used an alternative criteria to classify the patients into five marker groups (See Fig. 7). The four targeted therapies were erlotinib, sorafenib, vandetanib, and the combination of erlotinib and bexarotene, with each treatment being more efficacious in certain marker groups that match the agent's action mechanism. The primary endpoint was defined as the eight-week disease control rate, which was the percentage of patients who had no disease progression at 8 weeks after randomization. Figure 7 presents the schema of the BATTLE trial. The goal of the BATTLE design was to examine the efficacy of

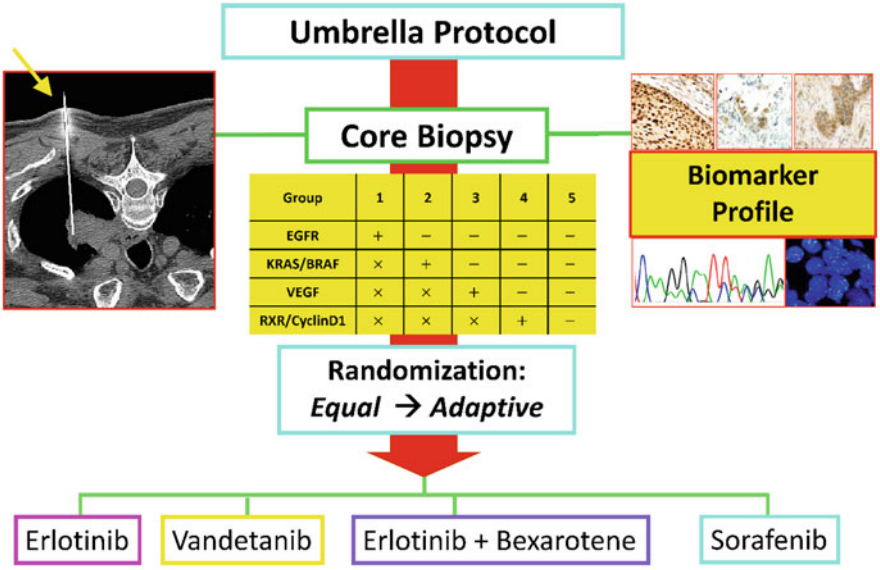

Fig. 7 The schema of the BATTLE trial

molecular targeted therapies in advanced NSCLC patients using the biomarker data, and to identify potential predictive biomarker profiles.

The Bayesian approach was applied to the BATTLE trial, where a hierarchical model was built to characterize the disease control rate for each targeted agent by marker subgroups. Such a hierarchical model facilitates use of data from prior studies, as well as allows for information borrowing across marker groups within and across treatments. Since patients with different biomarker profiles may respond differentially to different targeted therapies, a Bayesian OAR procedure was implemented, such that more patients in each marker group were more likely to be assigned to the better performing treatment. The BATTLE design used Bayesian posterior probability to continuously monitor the trial. In particular, if the posterior probability of obtaining a target disease control rate in a certain treatment by some marker subgroup was particularly small, then the treatment was suspended for that marker group. At the completion of the trial, Bayesian posterior probability was also used to identify the effective treatment for each subgroup.

In the BATTLE trial, a total of 341 patients were enrolled from November 2006 to October 2009. Among the 341 patients, 255 eligible patients were randomized under the proposed OAR scheme. The overall 8-week disease control rate was 46%, and the marginal disease control rates were 34%, 58%, 33%, and 50% for erlotinib, sorafenib, vandetanib, and the combination of erlotinib and bexarotene, respectively. In particular, the trial showed that sorafenib has a higher disease control rate in patients in the KRAS/BRAF marker group, and therefore most of the KRAS/BRAF patients were assigned to the sorafenib arm.

The BATTLE trial has demonstrated the success of the application of the Bayesian adaptive approach to real trials. Both clinicians and patients were enthusiastic to participate in the study (Liu and Lee 2015). The BATTLE design required that the biomarkers and marker groups be pre-determined before the trial. As a result, the ongoing trial data could not validate biomarker selection, possibly ignoring some important biomarkers during the pre-determination process. This poses a major limitation of the BATTLE design. To remedy this problem, the BATTLE-2 design was proposed as a two-stage adaptive randomized trial design (Gu et al. 2016; Papadimitrakopoulou et al. 2016). The first stage was treated as a training step, where several potential prognostic and predictive markers are selected and adaptive randomization was used to randomize patients to the treatment. At the end of the first stage, a variable selection procedure was performed to identify relevant biomarkers via adaptive LASSO. In the second stage, refined adaptive randomization based on the markers selected in the first stage was to be applied to treat patients. Therefore, treatment effects, marker effects, and their interactions were to be estimated and tested using data acquired from both stages in the BATTLE-2 design.

7.2 I-SPY 2 Trial

The ISPY-2 trial is an on-going phase II, multicenter, adaptively randomized, platform trial to evaluate multiple experimental agents in combination with standard neoadjuvant chemotherapy in patients with high-risk neoadjuvant breast cancer (Barker et al. 2009; Carey and Winer 2016; Park et al. 2016; Rugo et al. 2016). This is a multi-arm trial with a common control group with a standard neoadjuvant therapy. The trial is planned to screen 12 different experimental drugs, with the primary endpoint being the pathological complete response at the time of surgery. The primary goal of the ISPY-2 trial is to facilitate the rapid and efficient identification of promising agents and biomarker profiles that are likely to succeed in subsequent phase III trials.

In the ISPY-2 trial, patients are classified into eight prospectively defined disease subtypes based on three biomarkers (i.e., hormone receptor status, human epidermal growth factor receptor two status, and risk level as assessed with the 70-gene assay) assessed at baseline. In each subtype, 20% of the patients are assigned to the standard control therapy. Bayesian adaptive randomization is used to assign the remaining 80% to the available experimental regimens in proportion to each regimens' current posterior probability of being the most effective therapy for that subtype. Bayesian monitoring is used to evaluate the efficacy of the experimental regimens continuously. Specifically, a treatment graduates to a subsequent phase III trial when the Bayesian predictive probability of success in a traditional 300-patient randomized phase III trial against the standard treatment is high; say, greater than 0.85.

A prominent feature of the ISPY-2 trial is that it will graduate a successful regimen, drop an unsuccessful regimen, and add a newly available regimen during the trial, rather than having to initiate a new protocol. This will save a considerable amount of time and accelerate the whole process of drug development. To date, the ISPY-2 trial has successfully identified two treatment combinations with higher rates of pathological complete response than standard therapy alone, warranting further phase III trials (Park et al. 2016; Rugo et al. 2016)

7.3 GBM AGILE Trial

GBM AGILE is a novel, multi-arm, seamless Phase II/III response adaptive randomization platform trial designed to evaluate multiple therapies in newly diagnosed and recurrent glioblastoma (Alexander et al. 2018). The trial uses overall survival as the primary endpoint, with the goal to screen effective treatment and biomarker pairs for glioblastoma. GBM AGILE is composed of two stages under a single master protocol, allowing multiple drugs or drug combinations from different pharmaceutical companies to be evaluated simultaneously. In the first stage, Bayesian adaptive randomization is used to identify effective drugs within disease subtype. The randomization probabilities to the treatments within subtypes are proportional to the Bayesian posterior probabilities of prolonging overall survival longer than the control. Highly promising treatments will seamlessly graduate to the second stage, which is a phase III, equally randomized, confirmatory trial in the identified population. If some treatment cannot transit to the confirmatory stage, the relevant data collected in the first screening stage are still valuable to refine biomarker hypotheses and inform better decision making for trials outside of GBM AGILE (Alexander et al. 2018). Like the ISPY-2 trial, GBM AGILE also allows for adding therapeutic arms with biomarkers to the trial over time, which can substantially reduce cost and shorten the drug development process.

8 Discussions

Bayesian adaptive approaches hold great promise for improving the flexibility and efficiency of clinical trials. Successful implementations of Bayesian methods have already been demonstrated in a wide range of clinical trial applications. However, there are several challenges and practical concerns in using Bayesian adaptive trial designs.

Prior specification is critical to the performance of Bayesian inference. Especially in early-phase trials when the sample size is typically small, different prior distributions may lead to varied interim decisions or final conclusions (Yin and Lin 2015). In addition, the consequence of using a subjective prior is like a double-edged sword.

If the subjective prior is consistent with the current data, proper use would increase the trial efficiency and render earlier decision making. In contrast, improper use of the subjective prior may be subject to biased inference and incorrect conclusions. Hence, the choice of prior distribution should be carefully made according to the clinical setting, the question at hand, expert knowledge, and sufficient simulation studies.

Over recent decades, the robustness of Bayesian adaptive designs has been largely ignored. Most Bayesian methods use sophisticated parametric probability distributions to model the parameter of interest. For example, the logistic regression model is usually considered to quantify the relationship between the toxicity and dose levels in dose-finding designs (Neuenschwander et al. 2008), and exponential distribution is used to model the time-to-event data in phase II designs (Yin et al. 2018). Because of the parametric assumption, the Bayesian adaptive methods tend to be sensitive to model misspecifications. When the model is correctly specified, there is efficiency gain in decision making and inference. On the other hand, inefficient decisions or biased inferences are expected if the model is misspecified. When the sample size is small such as in early-phase trials, the performance of Bayesian adaptive designs to the model specifications can be particularly sensitive (Neuenschwander et al. 2008). Therefore, it is desirable to develop a design that yields robust performance across various underlying scenarios. Common approaches to robustify Bayesian adaptive designs include using nonparametric or flexible models (Liu and Johnson 2016; Liu and Yuan 2015), borrowing strength from ensemble approaches (Lin and Yin 2016; Yin and Yuan 2009b), or calibrating the model parameters based on extensive simulation studies (Yuan et al. 2017).

In practice, the adoption of novel Bayesian adaptive designs to improve the efficiency and success rate of trials is in urgent need (Biswas et al. 2009; Chevret 2012; Rogatko et al. 2007). Mainly due to their simplicity, poorly performing conventional designs are still dominantly used. A major barrier preventing translation in practice is that most Bayesian adaptive designs require complicated statistical modeling and intensive computation, making them difficult to understand and requiring expensive infrastructure to implement (Yuan et al. 2019). Efforts to increase the use of Bayesian adaptive designs among statisticians and clinicians should be made. Statisticians can develop well-performing, yet easy-to-implement approaches that can satisfactorily balance the simplicity-versus-performance trade-off (Yuan et al. 2019). To this end, model-assist designs show great promise in taking the best of two worlds: having the superior performance as with model-based designs, while preserving the simplicity in study conduct as with rule-based designs. When superiority meets simplicity, these model-assisted designs fit the new *KISS* principle: *K*eep *I*t *S*imple and *S*mart (Yuan et al. 2019). More collaborations and educational activities between statisticians and clinicians should be still stressed.

Software applications can help disseminate and transfer the knowledge of applying novel Bayesian designs in clinical trials. The software online sites at MD Anderson Cancer Center (https://biostatistics.mdanderson.org/softwareonline/ and https://trialdesign.org) provide more than 80 freely available software programs

for clinical trial design and analysis. This has led to more than 21,000 downloads between 2004 and 2019. Nonetheless, statisticians should be aware of the lack of available software packages for most existing Bayesian adaptive methods. Sustained efforts are always needed to develop and keep updated the user-friendly software and to educate clinical trialists on how to implement it.

Adaptive designs play an important role in clinical trials. To accelerate drug development, umbrella trials, basket trials, enrichment trials, and platform trials are more and more popular nowadays. In era of precision medicine, the new features of targeted agents and immunotherapies complicate the design and conduct of clinical trials, and the need for novel trial methods is ever increasing (Nass et al. 2018). Bayesian methods provide a flexible and coherent framework to address trial complexity, and an efficient learning process to study the treatments. Teamwork is required, such that statisticians work closely with clinicians, researchers, and personnel from pharmaceutical companies and regulatory agencies to develop better trials using more intelligent approaches, such as Bayesian methods, and implement them in the fight against cancer.

References

Alexander, B. M., Ba, S., Berger, M. S., Berry, D. A., Cavenee, W. K., Chang, S. M., et al. (2018). Adaptive global innovative learning environment for Glioblastoma: GBM AGILE. *Clinical Cancer Research, 24*(4), 737–743.

Avorn, J. (2015). The $2.6 billion pill - methodologic and policy considerations. *New England Journal of Medicine, 372*(20), 1877–1879.

Barker, A. D., Sigman, C. C., Kelloff, G. J., Hylton, N. M., Berry, D. A., & Esserman, L. J. (2009). I-SPY 2: An adaptive breast cancer trial design in the setting of neoadjuvant chemotherapy. *Clinical Pharmacology & Therapeutics, 86*(1), 97–100.

Berger, Z. (2010). Bayesian and frequentist models: Legitimate choices for different purposes of clinical research. *Journal of Evaluation in Clinical Practice, 16*(6), 1045–1047.

Berry, D. A. (2006). Bayesian clinical trials. *Nature Reviews Drug Discovery, 5*(1), 27–36.

Berry, D. A. (2015). The Brave New World of clinical cancer research: Adaptive biomarker-driven trials integrating clinical practice with clinical research. *Molecular Oncology, 9*(5), 951–959.

Bhatt, A. (2010). Evolution of clinical research: A history before and beyond james lind. *Perspectives in Clinical Research, 1*(1), 6–10.

Biswas, S., Liu, D. D., Lee, J. J., & Berry, D. A. (2009). Bayesian clinical trials at the University of Texas M. D. Anderson Cancer Center. *Clinical Trials, 6*(3), 205–216.

Braun, T. M., & Wang, S. (2010). A hierarchical Bayesian design for phase I trials of novel combinations of cancer therapeutic agents. *Biometrics, 66*(3), 805–812.

Carey, L. A., & Winer, E. P. (2016). I-SPY 2–toward more rapid progress in breast cancer treatment. *The New England Journal of Medicine, 375*(1), 83–84.

Cheung, Y. K., & Chappell, R. (2000). Sequential designs for phase I clinical trials with late-onset toxicities. *Biometrics, 56*(4), 1177–1182.

Chevret, S. (2012). Bayesian adaptive clinical trials: A dream for statisticians only? *Statistics in Medicine, 31*(11–12), 1002–1013.

Chow, S. C., & Chang, M. (2008). Adaptive design methods in clinical trials - a review. *Orphanet Journal of Rare Diseases, 3*, 11.

DiMasi, J. A., Reichert, J. M., Feldman, L., & Malins, A. (2013). Clinical approval success rates for investigational cancer drugs. *Clinical Pharmacology & Therapeutics, 94*(3), 329–335.

Friedman, L. M., Furberg, C., & DeMets, D. L. (2010). *Fundamentals of clinical trials* (4th ed.). New York: Springer.

Goodman, S. N., Zahurak, M. L., & Piantadosi, S. (1995). Some practical improvements in the continual reassessment method for phase-I studies. *Statistics in Medicine, 14*(11), 1149–1161.

Gu, X., Chen, N., Wei, C., Liu, S., Papadimitrakopoulou, V. A., Herbst, R. S., et al. (2016). Bayesian two-stage biomarker-based adaptive design for targeted therapy development. *Statistics in Biosciences, 8*(1), 99–128.

Guo, W., Wang, S.-J., Yang, S., Lynn, H., & Ji, Y. (2017). A Bayesian interval dose-finding design addressing Ockham's razor: mTPI-2. *Contemporary Clinical Trials, 58*, 23–33.

Heitjan, D. F. (1997). Bayesian interim analysis of phase II cancer clinical trials. *Statistics in Medicine, 16*(16), 1791–1802.

Hobbs, B. P., Chen, N., & Lee, J. J. (2018). Controlled multi-arm platform design using predictive probability. *Statistical Methods in Medical Research, 27*(1), 65–78.

Howard, D. R., Brown, J. M., Todd, S., & Gregory, W. M. (2018). Recommendations on multiple testing adjustment in multi-arm trials with a shared control group. *Statistical Methods in Medical Research, 27*(5), 1513–1530.

Hu, F., & Rosenberger, W. F. (2006). *The theory of response-adaptive randomization in clinical trials* (Vol. 525). Hoboken: John Wiley & Sons.

Iasonos, A., Wages, N. A., Conaway, M. R., Cheung, K., Yuan, Y., & O'Quigley, J. (2016). Dimension of model parameter space and operating characteristics in adaptive dose-finding studies. *Statistics in Medicine, 35*(21), 3760–3775.

Ji, Y., Liu, P., Li, Y., & Bekele, B. N. (2010). A modified toxicity probability interval method for dose-finding trials. *Clinical Trials, 7*(6), 653–663.

Kim, E. S., Herbst, R. S., Wistuba, I. I., Lee, J. J., Blumenschein, G. R., Tsao, A., et al. (2011). The BATTLE trial: Personalizing therapy for lung cancer. *Cancer Discovery, 1*(1), 44–53.

Lee, J. J., & Berry, D. A. (2016). Statistical innovations in cancer research. *Holland-Frei Cancer Medicine, 6*, 1–18.

Lee, J. J., & Chu, C. T. (2012). Bayesian clinical trials in action. *Statistics in Medicine, 31*(25), 2955–2972.

Lee, J. J., & Liu, D. D. (2008). A predictive probability design for phase II cancer clinical trials. *Clinical Trials, 5*(2), 93–106.

Lee, K. M., Wason, J., & Stallard, N. (2019). To add or not to add a new treatment arm to a multiarm study: A decision-theoretic framework. *Statistics in Medicine, 32*, 3305–3321.

Lin, R. (2018). Bayesian optimal interval design with multiple toxicity constraints. *Biometrics, 74*(4), 1320–1330.

Lin, R., Coleman, R. L., & Yuan, Y. (2019). Top: Time-to-event bayesian optimal phase ii trial design for cancer immunotherapy. *Journal of the National Cancer Institute, 112*(1), 38–45.

Lin, R., & Yin, G. (2016). Bootstrap aggregating continual reassessment method for dose finding in drug-combination trials. *Annals of Applied Statistics, 10*(4), 2349–2376.

Lin, R., & Yin, G. (2017a). Bayesian optimal interval design for dose finding in drug-combination trials. *Statistical Methods in Medical Research, 26*(5), 2155–2167.

Lin, R., & Yin, G. (2017b). STEIN: A simple toxicity and efficacy interval design for seamless phase I/II clinical trials. *Statistics in Medicine, 36*(26), 4106–4120.

Lin, R., & Yin, G. (2018). Uniformly most powerful Bayesian interval design for phase I dose-finding trials. *Pharmaceutical Statistics, 17*(6), 710–724.

Lin, R., & Yuan, Y. (2019). On the relative efficiency of model-assisted designs: A conditional approach. *Journal of Biopharmaceutical Statistics, 29*, 648–662.

Liu, S., & Lee, J. J. (2015). An overview of the design and conduct of the BATTLE trials. *Chinese Clinical Oncology, 4*(3), 33.

Liu, S. Y., & Johnson, V. E. (2016). A robust Bayesian dose-finding design for phase I/II clinical trials. *Biostatistics, 17*(2), 249–263.

Liu, S. Y., & Yuan, Y. (2015). Bayesian optimal interval designs for phase I clinical trials. *Journal of the Royal Statistical Society Series C-Applied Statistics, 64*(3), 507–523.

Mahajan, R., & Gupta, K. (2010). Adaptive design clinical trials: Methodology, challenges and prospect. *Indian Journal of Pharmacology, 42*(4), 201–207.

Nass, S. J., Rothenberg, M. L., Pentz, R., Hricak, H., Abernethy, A., Anderson, K., et al. (2018). Accelerating anticancer drug development - opportunities and trade-offs. *Nature Reviews Clinical Oncology, 15*(12), 777–786.

Neuenschwander, B., Branson, M., & Gsponer, T. (2008). Critical aspects of the Bayesian approach to phase I cancer trials. *Statistics in Medicine, 27*(13), 2420–2439.

O'Quigley, J., Pepe, M., & Fisher, L. (1990). Continual reassessment method: A practical design for phase 1 clinical trials in cancer. *Biometrics, 46*(1), 33–48.

Papadimitrakopoulou, V., Lee, J. J., Wistuba, I. I., Tsao, A. S., Fossella, F. V., Kalhor, N., et al. (2016). The BATTLE-2 study: A biomarker-integrated targeted therapy study in previously treated patients with advanced non-small-cell lung cancer. *Journal of Clinical Oncology, 34*(30), 3638–3647.

Park, J. W., Liu, M. C., Yee, D., Yau, C., van't Veer, L. J., Symmans, W. F., et al. (2016). Adaptive randomization of Neratinib in Early Breast Cancer. *The New England Journal of Medicine, 375*(1), 11–22.

Piantadosi, S. (2017). *Clinical trials: A methodologic perspective* (3rd ed.). Hoboken: Wiley.

Proschan, M. A., & Hunsberger, S. A. (1995). Designed extension of studies based on conditional power. *Biometrics, 51*(4), 1315–1324.

Riviere, M. K., Dubois, F., & Zohar, S. (2015). Competing designs for drug combination in phase I dose-finding clinical trials. *Statistics in Medicine, 34*(1), 1–12.

Rogatko, A., Schoeneck, D., Jonas, W., Tighiouart, M., Khuri, F. R., & Porter, A. (2007). Translation of innovative designs into phase I trials. *Journal of Clinical Oncology, 25*(31), 4982–4986.

Rosenberger, W. F. (1999). Randomized play-the-winner clinical trials: Review and recommendations. *Controlled Clinical Trials, 20*(4), 328–342.

Rosenberger, W. F., Stallard, N., Ivanova, A., Harper, C. N., & Ricks, M. L. (2001). Optimal adaptive designs for binary response trials. *Biometrics, 57*(3), 909–913.

Rugo, H. S., Olopade, O. I., DeMichele, A., Yau, C., van't Veer, L. J., Buxton, M. B., et al. (2016). Adaptive randomization of veliparib-carboplatin treatment in breast cancer. *The New England Journal of Medicine, 375*(1), 23–34.

Saville, B. R., & Berry, S. M. (2016). Efficiencies of platform clinical trials: A vision of the future. *Clinical Trials, 13*(3), 358–366.

Simon, N., & Simon, R. (2017). Using Bayesian modeling in frequentist adaptive enrichment designs. *Biostatistics, 19*(1), 27–41.

Simon, R. (1989). Optimal two-stage designs for phase II clinical trials. *Controlled Clinical Trials, 10*(1), 1–10.

Skolnik, J. M., Barrett, J. S., Jayaraman, B., Patel, D., & Adamson, P. C. (2008). Shortening the timeline of pediatric phase I trials: The rolling six design. *Journal of Clinical Oncology, 26*(2), 190–195.

Takeda, K., Taguri, M., & Morita, S. (2018). BOIN-ET: Bayesian optimal interval design for dose finding based on both efficacy and toxicity outcomes. *Pharmaceutical Statistics, 17*(4), 383–395.

Thall, P. F., & Cook, J. D. (2004). Dose-finding based on efficacy-toxicity trade-offs. *Biometrics, 60*(3), 684–693.

Thall, P. F., Millikan, R. E., Mueller, P., & Lee, S. J. (2003). Dose-finding with two agents in Phase I oncology trials. *Biometrics, 59*(3), 487–496.

Thall, P. F., & Simon, R. (1994). Practical Bayesian guidelines for phase IIB clinical trials. *Biometrics, 50*(2), 337–349.

Thall, P. F., Simon, R. M., & Estey, E. H. (1995). Bayesian sequential monitoring designs for single-arm clinical trials with multiple outcomes. *Statistics in Medicine, 14*(4), 357–379.

Thall, P. F., & Wathen, J. K. (2007). Practical Bayesian adaptive randomisation in clinical trials. *European Journal of Cancer, 43*(5), 859–866.

Thall, P. F., Wathen, J. K., Bekele, B. N., Champlin, R. E., Baker, L. H., & Benjamin, R. S. (2003). Hierarchical Bayesian approaches to phase II trials in diseases with multiple subtypes. *Statistics in Medicine, 22*(5), 763–780.

Tidwell, R. S. S., Peng, A., Chen, M., Liu, D., Yuan, Y., & Lee, J. J. (2019). Bayesian clinical trials at the University of Texas MD Anderson Cancer Center: An update. *Clinical Trials, 16*(6), 645–656.

Ventz, S., Barry, W. T., Parmigiani, G., & Trippa, L. (2017). Bayesian response-adaptive designs for basket trials. *Biometrics, 73*(3), 905–915.

Wason, J., Magirr, D., Law, M., & Jaki, T. (2016). Some recommendations for multi-arm multi-stage trials. *Statistical Methods in Medical Research, 25*(2), 716–727.

Wason, J. M., & Jaki, T. (2012). Optimal design of multi-arm multi-stage trials. *Statistics in Medicine, 31*(30), 4269–4279.

Wathen, J. K., & Thall, P. F. (2017). A simulation study of outcome adaptive randomization in multi-arm clinical trials. *Clinical Trials, 14*(5), 432–440.

Yan, F., Mandrekar, S. J., & Yuan, Y. (2017). Keyboard: a novel Bayesian toxicity probability interval design for phase i clinical trials. *Clinical Cancer Research, 23*(15), 3994–4003.

Yin, G., Chen, N., & Lee, J. J. (2012). Phase II trial design with Bayesian adaptive randomization and predictive probability. *Journal of the Royal Statistical Society. Series C, Applied Statistics, 61*(2), 219–235.

Yin, G., Chen, N., & Lee, J. J. (2018). Bayesian adaptive randomization and trial monitoring with predictive probability for time-to-event endpoint. *Statistics in Biosciences, 10*(2), 420–438.

Yin, G., & Lin, R. (2015). Comments on 'competing designs for drug combination in phase I dose-finding clinical trials' by M-K. Riviere, F. Dubois, and S. Zohar. *Statistics in Medicine, 34*(1), 13–17.

Yin, G. S., & Yuan, Y. (2009a). Bayesian dose finding in oncology for drug combinations by copula regression. *Journal of the Royal Statistical Society Series C-Applied Statistics, 58*, 211–224.

Yin, G. S., & Yuan, Y. (2009b). Bayesian model averaging continual reassessment method in Phase I clinical trials. *Journal of the American Statistical Association, 104*(487), 954–968.

Yuan, Y., Lee, J. J., & Hilsenbeck, S. G. (2019). Model-assisted designs for early phase clinical trials: Simplicity meets superiority. *JCO Precision Oncology, 3*, 1–12.

Yuan, Y., Lin, R., Li, D., Nie, L., & Warren, K. E. (2018). Time-to-event Bayesian optimal interval design to accelerate Phase I trials. *Clinical Cancer Research, 24*(20), 4921–4930.

Yuan, Y., Nguyen, H. Q., & Thall, P. F. (2017). *Bayesian designs for phase I-II clinical trials*. Boca Raton: Chapman and Hall/CRC.

Zang, Y., & Lee, J. J. (2014). Adaptive clinical trial designs in oncology. *Chinese Clinical Oncology, 3*(4), 49.

Zang, Y., & Lee, J. J. (2017). A robust two-stage design identifying the optimal biological dose for phase I/II clinical trials. *Statistics in Medicine, 36*(1), 27–42.

Zang, Y., Lee, J. J., & Yuan, Y. (2014). Adaptive designs for identifying optimal biological dose for molecularly targeted agents. *Clinical Trials, 11*(3), 319–327.

Zhang, L. C., & Yuan, Y. (2016). A practical Bayesian design to identify the maximum tolerated dose contour for drug combination trials. *Statistics in Medicine, 35*(27), 4924–4936.

Zhang, Y., Trippa, L., & Parmigiani, G. (2019). Frequentist operating characteristics of Bayesian optimal designs via simulation. *Statistics in Medicine, 38*(21), 4026–4039.

Zhou, H., Lee, J. J., & Yuan, Y. (2017). BOP2: Bayesian optimal design for phase II clinical trials with simple and complex endpoints. *Statistics in Medicine, 36*(21), 3302–3314.

Zhou, H., Murray, T. A., Pan, H., & Yuan, Y. (2018a). Comparative review of novel model-assisted designs for phase I clinical trials. *Statistics in Medicine, 37*(14), 2208–2222.

Zhou, H., Yuan, Y., & Nie, L. (2018b). Accuracy, safety, and reliability of novel Phase I trial designs. *Clinical Cancer Research, 24*(18), 4357–4364.

Zhou, X., Liu, S., Kim, E. S., Herbst, R. S., & Lee, J. J. (2008). Bayesian adaptive design for targeted therapy development in lung cancer - a step toward personalized medicine. *Clinical Trials, 5*(3), 181–193.

Topological Data Analysis of *Clostridioides difficile* Infection and Fecal Microbiota Transplantation

Pavel Petrov, Stephen T. Rush, Shaun Pinder, Christine H. Lee, Peter T. Kim, and Giseon Heo

Abstract Computational topologists recently developed a method, called persistent homology to analyze data presented in terms of similarity or dissimilarity. Indeed, persistent homology studies the evolution of topological features in terms of a single index, and is able to capture higher order features beyond the usual clustering techniques. There are three descriptive statistics of persistent homology, namely barcode, persistence diagram and more recently, persistence landscape. Persistence landscape is useful for statistical inference as it belongs to a space of $p-$integrable functions, a separable Banach space. We apply tools in both computational topology and statistics to DNA sequences taken from *Clostridioides difficile* infected patients treated with an experimental fecal microbiota transplantation. Our statistical and

P. Petrov
Data Scientist at Rocky Mountaineer, Vancouver, BC, Canada
e-mail: ppetrov@rockymountaineer.com

S. T. Rush
Senior Statistician at AstraZeneca, Mölndal, Sweden
e-mail: stephen.rush@astrazeneca.com

S. Pinder
Methodologist at Statistics Canada, Ottawa, ON, Canada
e-mail: spinder@alumni.uoguelph.ca

C. H. Lee
Clinical Professor at Department of Pathology and Laboratory Medicine, University of British Columbia, Vancouver, BC, Canada

Department of Microbiology, Royal Jubilee Hospital, Victoria, BC, Canada
e-mail: christine.lee@viha.ca

P. T. Kim (✉)
Department of Mathematics & Statistics, University of Guelph, Guelph, ON, Canada
e-mail: pkim@uoguelph.ca

G. Heo
School of Dentistry, Department of Mathematical and Statistical Sciences, University of Alberta, Edmonton, AB, Canada
e-mail: gheo@ualberta.ca

A. Bekker et al. (eds.), *Computational and Methodological Statistics and Biostatistics*, Emerging Topics in Statistics and Biostatistics,
https://doi.org/10.1007/978-3-030-42196-0_18

topological data analysis are able to detect interesting patterns among patients and donors. It also provides visualization of DNA sequences in the form of clusters and loops.

1 Introduction

Topological data analysis has become a formidable technique for analyzing high-dimensional data, especially when the purpose is for classification and discrimination. Methodological advancement has been rampant along with applications to medical or scientific data, see for example Nicolau et al. (2011), Heo et al. (2012) and more recently (Kovacev-Nikolic et al. 2016). In this paper we propose making use of computational topological techniques to analyze gut microbiome data at the basic DNA sequence level based on data collected from sequencing the 16S rRNA gene. We are particularly interested in seeing changes in patient gut microbiome for a certain hypervirulent infectious disease following a radical experimental procedure that is gaining widespread attention and usage in medicine.

Clostridioides (formerly *Clostridium*) *difficile* (*C. difficile*) infection (CDI) is the most frequent cause of healthcare-associated infections and its rates are growing in the community (Kelly and LaMont 2008; Loo et al. 2005). One of the major risk factors for developing CDI is through antibiotics. The healthy and diverse bacteria which reside within the colon are the major defense against the growth of *C. difficile*. Antibiotics kill these bacteria and allow *C. difficile* to multiply, produce toxins and cause disease. The current standard of care for this infection are the antibiotics: metronidazole, vancomycin and more recently, fidaxomicin. The efficacy of these antibiotics is limited as vancomycin and metronidazole also suppress the growth of anaerobic bacteria such as *Bacteriodes fragilis* group which protect against proliferation of *C. difficile*. The efficacy of the recent narrower spectrum fidaxomicin is still under investigation although the initial data shows promise, Louie et al. (2011). The persistent disruption of healthy colonic flora may in part explain the reason for recurrences following a course of treatment with these antibiotics.

An alternative to antibiotic therapy for CDI, in particular for recurrent and refractory diseases, is to infuse healthy gut bacteria directly into the colon of infected patients to combat *C. difficile* by a procedure known as fecal microbiota transplantation (FMT). FMT is a process in which a healthy donor's stool is infused into an affected patient. This can be performed using a colonoscope, nasogastric tube, enema, or more recently, in capsulized pill form, Khanna et al. (2016). FMT serves to reconstitute the altered colonic flora, in contrast to treatment with antibiotic(s), which can further disrupt the establishment of key microbes essential in preventing recurrent CDI. The literature reveals a cumulative clinical success rate of over 90% in confirmed recurrent CDI cases (Gough et al. 2011).

There has been a growing interest into the microbiome of CDI patients (Dethlefsen et al. 2008; Manges et al. 2010; Vincent et al. 2013; Petrof et al. 2013; Schubert et al. 2014) especially those involved with FMTs (Shahinas et al. 2012;

Van Nood et al. 2013; Hamilton et al. 2013; Song et al. 2013; Weingarden et al. 2014; Seekatz et al. 2014). In case of the latter, there are differences in: the route of administration with all forms covered; different donor selection criteria, some used family members, some used a pool of donors; different sample sizes; and different sequencing procedures and equipment. Despite these differences, there seems to be two fundamental points of agreement across all studies. The first is that CDI patients have low diversity in their microbiome, and that after receiving an FMT(s), their diversity was increased. The second fundamental agreement is that CDI patients who were treated with FMT undergo changes in their microbiome that at least initially have similarities to that of their donors. This paper provides further reinforcing evidence to support these two fundamental points in the framework of FMT delivered by enema, with a small exclusive donor pool. The novelty comes from using computational topological techniques to demonstrate this.

We now summarize the paper. In Sect. 2 we explain the details of the clinical data. In Sect. 3 we provide topological preliminaries where we go over the Vietoris-Rips complex, and three topological descriptors: barcodes, persistence diagrams, and persistence landscapes. In the following Sect. 4, we apply these techniques and demonstrate the added value of the topological approach at the basic DNA sequence level. We complete our article in Sect. 5 with a summary of the key findings.

2 CDI FMT and 16S rRNA Data

From Lee et al. (2014), 19 patients had stool samples available for sequencing their 16S rRNA gene prior to treatment, pre-FMT, followed by a post treatment, post-FMT. The full details are described in Pinder (2013).

The gender of the patients was 63% female. The average age (to the time of their first FMT) was 77.11 with a standard deviation of 9.54 years, range 49–92 years. In-hospital patients accounted for 53% while the total peripheral white blood count ($\times 10^9$/L) had a median of 14.63 with an inter-quartile range of 7.9–16.5. Three patients had temperature greater than 38 °C, and 11 patients experienced abdominal pain. Approximately half (53%) of the patients were on proton-pump inhibitors. Eight patients were refractory to treatment with metronidazole and four patients were refractory to vancomycin. These four patients were also refractory to metronidazole. No patients were on fidaxomicin as it had not been commercially available at that time, Lee et al. (2014). The patient characteristics are provided in Table 1.

Predisposing conditions that may have resulted in CDI were: cellulitis, extreme fatigue, respiratory tract infections, septicemia, surgery and open wounds, and urinary tract infections. Some conditions were unknown. The majority of patients received the following antibiotics prior to contracting CDI: amoxicillin, azithromycin, cefazolin, cefprozil, cephalexin, ciprofloxacin, clindamycin, clarithromycin, cloxacillin, levofloxacin, moxifloxacin and nitrofurantoin. Some

Table 1 Patient demographics and pre-FMT conditions

Covariate	
Age–years	
Mean ± Standard Deviation	77.11 ± 9.54
Range	49–92
White Blood Count–$\times 10^9$ per litre	
Median	14.63
Inter-quartile range	7.9–16.5
Female–count(%)	12 (63%)
In-hospital–count(%)	10 (53%)
Fever–count(%)	3 (16%)
Abdominal Pain–count(%)	11 (58%)
Proton pump inhibitor–count(%)	10 (53%)
Refractory to Metronidazole(%)	8 (42%)
Refractory to Vancomycin(%)	4 (21%)

Table 2 Pre-FMT treatment for CDI

Standard of care treatment	
Metronidazole(%)	17 (90%)
Metronidazole–days	
Mean ± Standard deviation	23.74± 16.51
Range	01–70
Vancomycin(%)	18 (95%)
Vancomycin–days	
Mean ± Standard deviation	32.58± 20.94
Range	7–86
Vancomycin taper(%)	6 (32%)
Vancomycin taper–days	
Mean ± Standard deviation	37.58± 93.86
Range	38–390
Metronidazole-Vancomycin(%)	3 (16%)
Metronidazole vancomycin–days	
Mean ± Standard deviation	5.21± 18.55
Range	2–80

patients claimed no prior antibiotics used. In an interesting paper, the affects of ciprofloxacin was studied Dethlefsen et al. (2008) using 16S rRNA deep sequencing.

The patients all had varying pre-FMT regimens to treat their CDI. All had undergone multiple rounds of traditional antibiotic therapy with metronidazole and/or vancomycin before being administered an FMT. Seventeen received at least one course of metronidazole monotherapy, 18 received vancomycin monotherapy, 6 received vancomycin taper, and 3 received concomitant metronidazole and vancomycin therapy. Patients generally received two courses of metronidazole followed by multiple courses of vancomycin before receiving FMT(s). The number of days every patient received each therapy are summarized by their means and standard deviations and reported below in Table 2.

Each patient had two stool samples sequenced, one representing a pre-FMT sequence, and one representing a post-FMT sequence. We attempted to sequence each patient prior to them receiving any FMT which for the most part occurred, except for one patient who failed their first FMT and their stool sample sequenced was taken right after that event but prior to their next FMT. This patient had multiple FMT failures, hence we took that stool sample as the pre-FMT sequence. We also took a stool sample following each patient's pre-FMT sample with at least one FMT in between. For the most part, the latter occurred following their last FMT which was the case if the patient resolved their CDI, but if they did not, then the post-FMT sequence was not necessarily their last. We would also like to make clear that 4+-FMT means that a patient had at least four treatments but could have had more. We indicate such as '4+' to be consistent with our clinical paper, Lee et al. (2014).

The breakdown of the data is presented in Table 3 with the above qualifications. All patients received a single treatment, 1-FMT and 9 of them clinically resolved their CDI. All who failed the first treatment went on to receive a second treatment. Of the remaining patients who received 2-FMT, 2 resolved, while the remaining went on to receive a third treatment. There were 2 successes, and 1 failure, meaning they did not go on to receive additional treatments. Of the remaining patients who went on to 4+-FMT, 1 resolved, 1 resolved with antibiotics used in between treatments, and there were 3 failures.

There were several patients who received antibiotics in between FMTs as described in our previous report (Lee et al. 2014). In addition four healthy volunteers served as donors and were screened for transmissible pathogens and this was outlined in an earlier report (Kassam et al. 2012). The donors took no antibiotics for 6 months prior to stool donation. Seven donor samples taken at various times were sequenced.

All *C. difficile* infections were confirmed by in-hospital real-time polymerase chain reaction (PCR) testing for the toxin B gene. This study sequenced the forward V3-V5 region of the 16S rRNA gene from 19 CDI patients who were treated with FMT(s). A pre-FMT, a corresponding post-FMT, and 7 samples from four donors, corresponding altogether to 45 fecal samples were sequenced. All sequencing was performed on the 454 Life Sciences, GS Junior Titanium Series. The Qiagen Stool Extraction Kit from (Omega BIO-TEK, Norcross, Georgia) was used to extract the DNA from the fecal samples following the 'stool DNA protocol for pathogen detection'. Subsequent DNA amplification was done using PCR forward

Table 3 Clinical resolution of CDI following FMT(s)

FMT	Resolution	Resolution*	Failures	Total
1	9	–	0	9
2	2	–	0	2
3	2	–	1	3
4+	1	1	3	5
–	14	1	4	19

Patients who received antibiotics in-between FMTs are marked with an asterisk

and reverse primers. One round of DNA amplicon purification was performed using the QIAquick PCR Purification Kit (Qiagen, Valencia, CA) followed by two rounds of purification using Agencourt AMPure XP beads (Beckman Coulter Inc., Mississauga, ON).

We examined 19 pairs of pre-FMT and post-FMT patients, as well as donors, selected from the 94 CDI patients treated by the fourth author over the period 2008–12, Lee et al. (2014). The selection was not random and was chosen based on availability of stool samples as well as costs. Furthermore, there were 4 FMT failures. It was perhaps through the failures that we learned the most. The failed FMT cases were ultimately resolved with antibiotics even though some patients were refractory to metronidazle and/or vancomycin beforehand. Indeed FMT acted as a 'gut primer' for antibiotics to fulfill it's role in clearing recurrent and refractory CDI. This phenomenon of failed FMT patients resolved with antibiotics afterwards has been observed in our work, Lee et al. (2014), as well as others, see for example Rubin et al. (2013). The data comes from the clinical work of the fourth author who is a practising physician. Some of this data was also examined in Rush et al. (2016).

Table 4 below, provides some descriptive statistics about the total and unique number of DNA sequences found in the 45 samples. Note that it is impossible to ensure that we have an approximately equal number of sequences in each sample (Li et al. 2008).

Consider DNA sequences λ and μ. Let x be the number of point dissimilarities between DNA bases in λ and μ, and let x_λ and x_μ be the number of DNA bases in λ and μ, respectively. Let x_O be the number of places where one sequence contains a DNA base and the other an O, a gap. Let y_λ and y_μ be the number of gaps in λ and μ, respectively. Let z be the length of the alignment sequences; we can assume they are equal otherwise we choose the smaller. The various dissimilarity metrics are the following.

The *one-gap* distance d_O is defined by

$$d_O(\lambda, \mu) = \frac{x + \min\{y_\lambda, y_\mu\}}{\min\{x_\lambda + y_\lambda, x_\mu + y_\mu\}}.$$

It treats a string of O's flanked by any DNA bases in one sequence and the corresponding region in the other as one mismatch.

The *no-gap* distance d_N is defined by

$$d_N(\lambda, \mu) = \frac{x}{\min\{x_\lambda, x_\mu\}}.$$

Table 4 Descriptive statistics for unique (total) number of DNA sequences of pre-FMT and post-FMT samples

	Min	Max	Mean	Median	S.D.
Pre-FMT	147 (3230)	879 (15,140)	428.89 (9534.9)	364 (9777)	217.26 (3545.9)
Post-FMT	185 (2294)	1114 (28,566)	486.42 (11,308.11)	460 (10,570)	230.57 (6642.6)

It ignores gaps in a sequence and the corresponding region in the other sequence.

The *each-gap* distance d_E is defined by

$$d_E(\lambda, \mu) = \frac{x + x_O}{z}.$$

It treats every DNA base-placeholder pair as a mismatch.

These measures produce distance matrices, which are symmetric and contain zeros on the diagonal. For this and most studies, the metric of interest is the one-gap metric, Rush et al. (2012). As an example, suppose there are two DNA sequences with the following base pair orientation: `ATGCATGCATGC` and `ACGC--CATCC`. Here there are two mismatches and one gap. The distance is calculated as the number of mismatches divided by length of the shorter sequence. The length of the shorter sequence is 10 base pairs, since the gap is considered a single position. Hence distance is 0.3, Rush et al. (2012). We can use the other definitions of distance, but the definition provided is the one most commonly used. In addition, the results do not vary significantly. Most of the DNA sequences found in the samples appear several times, and hence the distance between them will be zero as they are identical. For this reason, the unique DNA sequences are taken.

Table 4 shows the minimum number of unique sequences is 147. DNA sequencing does not provide exact results, hence as the number of sequences in a sample increases, some mutations inevitably occur and these are recorded as unique sequences (Rush et al. 2012). In other words, as the total number of sequences increase, the number of unique sequences is also inflated. For this reason, it is necessary to subsample from the number of unique sequences. The smallest number of unique sequences is 147, hence a weighted subsample of size 147 is taken from the number of unique sequences for our research. The pairwise distance between the 147 sequences is calculated in each of the 45 samples using the one-gap metric. Thus the data used for the primary analysis are the 147×147 distance matrices for each of the 45 patients and donors. The exact details are provided in Petrov (2014).

3 Some Topological Preliminaries

Persistent homology is a branch of computational topology that has been popularized by Edelsbrunner et al. (2002) and Zomorodian and Carlsson (2005). Several researchers have shown that persistent homology works well on detecting topological and geometrical features in high dimensional data, see Edelsbrunner and Harer (2008) and Nicolau et al. (2011), for example. Let us suppose that we have points on a manifold whose dimension is not necessarily known. Topology studies the connectivity of these points. Each point is replaced by a disk (ball) with radius ε centered at each point. If the disks overlap, connect those center points with edges. As the radius increases, more points will be connected and so the number of connected components will decrease. This is analogous to clustering

analysis in statistics. The connected components (clusters) are considered as 0-degree topological features. The number of connected components is denoted as the 0-th Betti number, β_0. Connecting the points with edges will also create simplices (convex hull of a geometrically independent set of points) and produce topological features in higher dimensions. The low dimensional simplices are well known; a vertex (0-degree simplex), an edge (1-degree simplex), a triangle (2-degree simplex), and a tetrahedron (3-degree simplex). A loop is also called a 1-degree topological feature and a void is a 2-degree topological feature. The $k-$th Betti number β_k counts the number of $k-$degree topological features ($k-$dimensional 'holes').

Persistent homology studies the history of topological features as the parameter ε increases. It records the time at which a topological feature appears and disappears. The birth, death, and survival time of features are recorded as a barcode (Collins et al. 2004). A true feature in the data lives over a long time while noise is short lived. We illustrate a fundamental idea of persistent homology in Fig. 1 with 40 randomly selected points from a double annulus. The loops in the middle of each annulus are prominent 1-degree features and their intervals in the barcode shows their persistence.

Clusters come in different shapes, see a few synthetic examples in Fig. 2. Clusters are homogeneous subgroups where the meaning of homogeneity is dependent on the types of similarity measure. In the double annulus, Fig. 1, if we consider geodesic

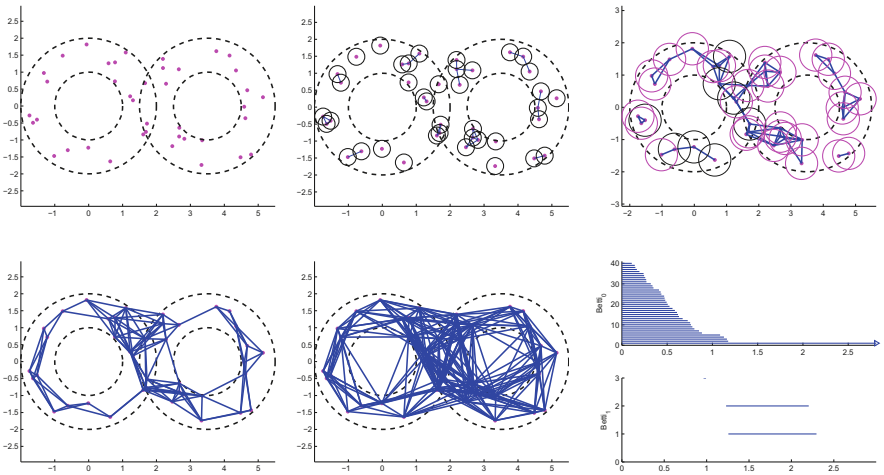

Fig. 1 Forty points are sampled randomly from a double annulus with inner circle radius 1 and outer circle radius 2. Forty components (top left) yield $\beta_0 = 40$ at $\varepsilon = 0$; nineteen (top middle) connected components, that is, $\beta_0 = 19$ at $\varepsilon = 0.5$; top right $\beta_0 = 5$ at $\varepsilon = 1.0$; the two most persistent loops (bottom left and middle) in the middle of the double annulus that are born at about $\varepsilon = 1.5$ die around $\varepsilon = 2.4$ showing two 'true' persistent loops. The long $(0, \infty)$ bar in β_0 (bottom right) barcode indicates the one persistent component while two longer bars in β_1 barcode indicate two loops

Fig. 2 Synthetic examples of clusters in different forms. From 'blobs'-intuitively familiar clusters, to curves, 'leaves', and Swiss roll

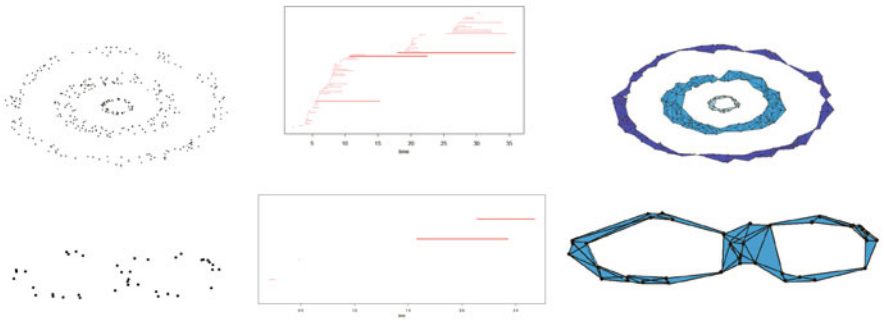

Fig. 3 Top: random points are generated to mimic concentric rings analysed in Ben-Hur et al. (2001). The three long intervals in the barcode shows three persistent loops. The three persistent loops are drawn which correspond to three clusters in Ben-Hur et al. (2001). Bottom: point clouds of numeric number 8 with noise. β_1-barcode indicates two persistent signals. Two possible clusters are detected as two loops, that is, 1-degree topological feature

distance between points, those points are connected to form simplices (edges and triangles). All the edges and triangles together form a band which is homotopy equivalent to a circle (1-degree topological feature). The authors in Ben-Hur et al. (2001) applied support vector clustering to concentric rings and were able to detect three rings as clusters. In Fig. 3, we generate similar concentric rings as in Ben-Hur et al. (2001). Persistent homology analysis shows three persistent loops which correspond to three clusters in Ben-Hur et al. (2001). Consider another example, where points are randomly sampled from the number 8 with noise, see Fig. 3. What are the clusters in this data? If one thinks of 'blobs' as clusters, there are several patches made up with a few points. However, each loop, 1-degree topological feature, is represented as the set of points which are close in the sense of the shortest path distance.

To study the connectivity of a space, the space need not be represented as a point cloud. All we need to know is how close the points are in a space where they live. Thus point clouds or matrices of (dis-)similarity measurements among other data forms are input data for analysis of persistent homology. A good reference for algebraic topology and persistent homology is Edelsbrunner and Harer (2010).

3.1 Vietoris-Rips Complex and Topological Descriptors

We will further explain Fig. 1 and then introduce three topological descriptors, barcode, persistence diagram (Edelsbrunner et al. 2002) and persistence landscape (Bubenik 2015). A collection of point cloud data in a metric space is converted to a combinatorial graph whose edges are determined by closeness between the points. While a graph captures connectivity and clustering of data, it ignores higher dimensional features. This idea of graph can be extended to a simplicial complex, which is a collection of simplices.

Suppose there is a finite set of points $\{v_i\}_1^n$ in $\mathbb{R}^{\mathrm{d}}$ and (dis-)similarity measure is denoted as $d(v_i, v_j)$. A $k-$simplex is a set of all points $x \in \mathbb{R}^{\mathrm{d}}$ such that $x = \sum_{i=1}^{k}, a_i v_i$, where $\sum a_i = 1, a_i \geq 0$. It is easy to picture low dimensional simplices; a 0-simplex a vertex, a 1-simplex an edge joining two vertices, a 2-simplex a triangle, a 3-simplex a tetrahedron. The *Vietoris-Rips* complex $\mathcal{V}_\varepsilon$ is a set of simplices whose vertices have pairwise distance within $d(v_i, v_j) \leq \varepsilon$. Algebraic topology adds group structure onto the complex, $H_k(\mathcal{V}_\varepsilon)$, called the $k-$th homology group. For coefficients in a field, $H_k(\mathcal{V}_\varepsilon)$ is a vector space, whose basis consist of linearly independent $k-$dimensional cycles that are not boundaries. The $k-$th Betti number β_k, is the rank of $H_k(\mathcal{V}_\varepsilon)$ and counts the number of $k-$dimensional holes of a simplicial complex.

At each fixed ε, the homology group $H_k(\mathcal{V}_\varepsilon)$ can be calculated, but computational topologists think of persistence. The simplicial complexes grow as ε increases, that is, $\mathcal{V}_\varepsilon \subseteq \mathcal{V}_{\varepsilon *}$, for $\varepsilon \leq \varepsilon^*$, this inclusion induces a linear map, $H_k(\mathcal{V}_\varepsilon) \rightarrow H_k(\mathcal{V}_{\varepsilon^*})$. This allows us to examine the filtration of homology. The evolution of the simplicial complexes over increasing values of ε can be completely tracked using barcodes or persistence diagrams. Barcode is the multiset of intervals $(\varepsilon', \varepsilon'')$, where ε' and ε'' indicate birth and death time of a topological feature. Alternatively, the birth and death times can be represented by a point $(\varepsilon', \varepsilon'')$ in $\mathbb{R}^2$. The collection of these points in $\mathbb{R}^2$ is a persistence diagram (see Fig. 5). The Vietoris-Rips complex and its evolution are demonstrated with random points selected from a double annulus, see Fig. 1.

In a simple summary, the point cloud data are transformed to barcodes or persistence diagrams in each dimension. Is it possible to calculate means and variances of barcodes or persistence diagrams? It is well known that the Fréchet mean of barcode (persistence diagram) is not unique. Many researchers have advanced this research area (Fasy et al. 2013; Mileyko et al. 2011). Bubenik (2015) introduced a third topological descriptor, persistence landscape. Given an interval (b, d), with $b \leq d$, define a function leading to an isosceles triangle, $f_{(b,d)} : \mathbb{R} \rightarrow \mathbb{R}$, $f_{(b,d)} = \min(t - b, d - t)_+$, where $u_+ = \max(u, 0)$. The persistence landscape corresponds to a multiset of intervals $\{(b_i, d_i) : b_i \leq d_i\}$ and to a set of functions, $\{\lambda(k, t) : \mathbb{N} \times \mathbb{R} \rightarrow \mathbb{R}\}$ where: $\lambda(k, t)$ is the $k-$th largest value of $\{f_{(b_i,d_i)}\}$. See an illustration in Fig. 4.

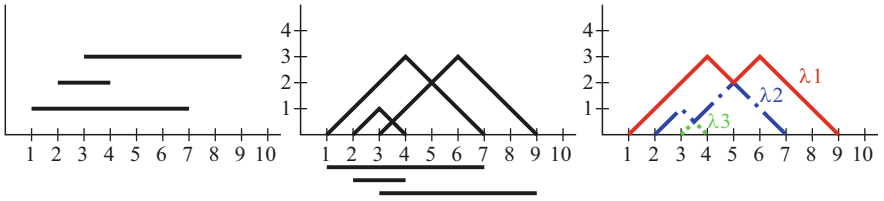

Fig. 4 (Left) Three intervals in a barcode. (Middle) Isosceles triangles of intervals. (Right) Persistence landscape

3.2 Statistical Inference with Persistence Landscape

On $\mathbb{N} \times \mathbb{R}$, the product of the counting measure on $\mathbb{N}$ and the Lebesgue measure on $\mathbb{R}$ are used. The persistence landscape, $\lambda(k,t) : \mathbb{N} \times \mathbb{R} \to \mathbb{R}$, is bounded and nonzero on a bounded domain. Hence persistence landscape belongs to $\mathrm{L}^p(\mathbb{N} \times \mathbb{R})$, with a metric induced by p-integrable functions and hence is a separable Banach space (Bubenik 2015). Bubenik also showed that when $p \geq 2$, with finite first and second moments, persistence landscape satisfies a Strong Law of Large Numbers (SLLN) and a Central Limit Theorem (CLT). Suppose $\Lambda_1, \ldots, \Lambda_n$ are the random variables corresponding to persistence landscapes. The vector space structure of $\mathrm{L}^p(\mathbb{N}\times\mathbb{R})$ induces the mean landscape as the pointwise mean, $\bar{\lambda}(k,t) = \frac{1}{n}\sum_{i=1}^{n} \lambda_i(k,t)$.

On p-integrable space, $\mathrm{L}^p(\mathbb{N} \times \mathbb{R})$, where $p \geq 2$ and under the assumption of finite first and second moments, for any continuous linear functional f, the random variable $f(\lambda(k,t))$ also satisfies SLLN and CLT (Ledoux and Talagrand 2002). There are many choices of f, but the integration of λ might be a natural choice, $f(\lambda(k,t)) = \sum_k \int_{\mathbb{R}} \lambda(k,t)\, dt$. It has a good interpretation; the values of f are an enclosed total area of all curves $\lambda(k,t)$. Choice of f might depend on data, see other choices in Bubenik (2015). With the integration as a functional choice, we are ready to set hypotheses. Let $Y_1 = f(\lambda_1(k,t))$ and $Y_2 = f(\lambda_2(k,t))$ be random variables for groups 1 and 2. We let μ_1 and μ_2 be corresponding population means. The hypothesis of interest is

$$H_0 : \mu_1 - \mu_2 = 0 \ \text{ vs. } \ H_a : \mu_1 - \mu_2 \neq 0. \tag{1}$$

We also consider the similarity measure between persistence landscapes as well as between persistence diagrams. The measure between persistence landscape is defined as the p-norm of difference. Suppose there are two samples that have landscapes denoted as $\lambda_1(k,t)$ and $\lambda_2(k,t)$. Then the L_p-norm is defined in (2). This compares pairwise the area under the contours between $\lambda_1(k,t)$ and $\lambda_2(k,t)$

$$||\lambda_1 - \lambda_2||_p = \left(\sum_k \int_{\mathbb{R}} |\lambda_1(k,t) - \lambda_2(k,t)|^p \right)^{1/p}. \quad (2)$$

For our data, we will calculate the persistence landscape distance using both L_1 and L_2 norm in (2). Wasserstein distance (see Edelsbrunner and Harer 2010, for example) is a popular measure of dissimilarity between persistence diagrams. All the results based on persistence landscape ($p = 1, 2$) and Wasserstein distance are similar and so all our statistics and presentations are based on L_2 norm in the following sections.

4 Topological Data Analysis

The computation of the Vietoris-Rips complex, which is computationally intensive, is carried out using the `phom` package in R (Tausz 2011). The scale of the computing required the resources of the *Westgrid* computer network. All 45 samples had barcodes in degrees zero and one. However in degree two, only 12 of the pre-FMT samples and 15 of the post-FMT samples have intervals in barcode. Persistence diagram makes visual pairwise comparisons easier than barcode. Figure 5 shows the corresponding persistence diagrams of patient 10 before and after the FMT treatment. Similar results were obtained from other patients and are reported in Petrov (2014). At first glance there does not appear to be anything interesting but there are some general trends. We observe that the degree 0 persistence diagram for the pre-FMT samples have components that die a lot sooner than those in the post-FMT samples. Similarly, the birth and death times of these loops are shorter for the pre-FMT samples than for the post-FMT samples. These observations may indicate that there could be a true difference in the topological structure in degrees zero and one between the two groups. On the other hand, many of the intervals in degree one are very short, thus what we observe may be noise rather than signal.

Unlike barcode or persistence diagrams, we can calculate means and variances of persistence landscapes. Figure 6, shows the average persistence landscapes of pre-FMT and post-FMT samples in degree 0 and 1. The trend in average persistence landscapes is the same as in persistence diagrams or barcodes, that is, the post-FMT samples have slightly longer intervals than the pre-FMT in degree 0 and 1. Similar type of results can be obtained using area under the curve (AUC) and is reported in Martinez et al. (2019).

Quadratic discriminant analysis (QDA) was performed on the β_0- and β_1-Isomap embedded coordinates, see Fig. 7. Three groups are well separated on the plane of both degree 0 and 1. It is interesting to see that the donors are grouped on one side and pre-FMT patients on the other side, and post-FMT patients between the two. This is in complete agreement with what clinicians believe is happening and it is frequently reported that patients gut microbiome take on the characteristics of the donor microbiome following an FMT, see Shahinas et al. (2012), Weingarden et al.

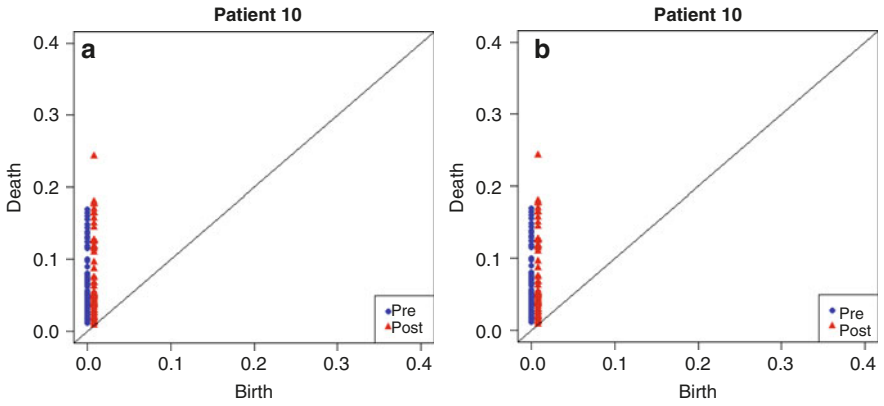

(a) Degree 0-patient 10 (b) Degree 1-patient 10

Fig. 5 Persistence diagrams for patient 10 before (in blue) and after (in red) FMT in (**a**) degrees zero and (**b**) one. Note that the triangles in (**a**) have birth at time zero but are moved slightly for visual purposes

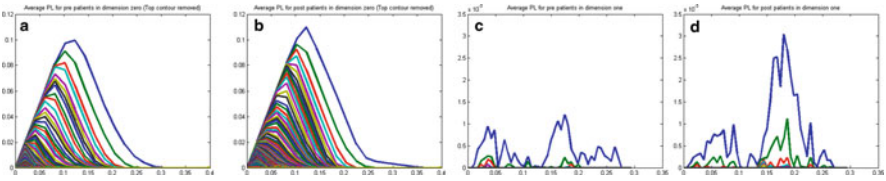

Fig. 6 Average persistence landscapes for pre-FMT and post-FMT patients in degrees zero and one. In degree zero, the post-FMT group has a denser grouping of contours, which means that there are more clusters than in the post-FMT samples. In degree one, the pre-FMT group has three persistent loops on average and the post-FMT sample has two. However, the post-FMT sample loops are more persistent than the pre-FMT samples. We note that the vertical scales in the plots in degree 0 and 1 are different. (**a**) Pre-FMT-degree 0. (**b**) Post-FMT-degree 0. (**c**) Pre-FMT-degree 1. (**d**) Post-FMT-degree 1

(2014) and Khanna et al. (2016). A description of QDA can be found in any standard multivariate analysis text, for example, Johnson and Wichern (2007).

It would have been very interesting to compare the matched donor and the patient after FMT, but this information was not recorded during this study, Lee et al. (2014). The classification in $\mathbb{R}^2$ of degree 0 in Fig. 7 show patients 7, 16 and 19 post-FMT, become much like the donors, particularly donors 2 and 3. Patients 9 and 15 post-FMT did not appear to change much from their pre-FMT. The classification in $\mathbb{R}^2$ of degree 1 in Fig. 7 show a few post-FMT patients (7, 10, 15) are close to the donors after FMT while most post-FMT patients remain similar to pre-FMT. Following Lee et al. (2014), a clinical trial comparing the efficacy of frozen *versus* fresh FMT has been completed, see Lee et al. (2016). Here stool samples were collected at pre-FMT, followed by day-10, week-5, week-13 following a patients last FMT along with the exact donor stool sample pairing. Sequencing of this data is currently underway.

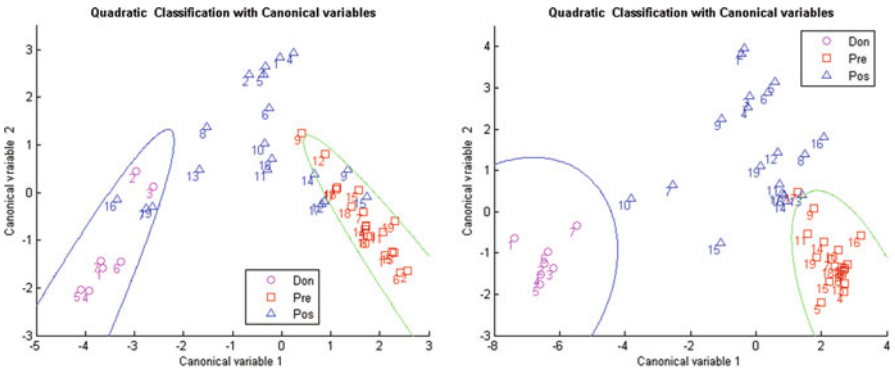

(a) Degree 0 (b) Degree 1

Fig. 7 Classification in two-dimensional space. Three groups are well separated in $\mathbb{R}^2$ for both degree 0 and 1. The canonical functions for both β_0- and β_1- Isomap discriminate pre-FMT patients and donors on each quadrant while post-FMT patients are located between the two. (Left) Patients 7, 16 and 19 post-FMT are classified as donors, possibly indicating their donors might be 2 and 3. Patients 9 and 15 do not appear 'improved' after FMT as they are classified as the group of patients before the treatment. Patients 7, 16 and 19 are not only similar to donors but also further away then their pre-FMT position. This may indicate they have improved the most after the treatment. (Right) In terms of loops in DNA sequences, a cluster of post-FMT patients are similar to the group of post-FMT treated patients. Donor 7 could be the donor for patient 10

We recall that our 'raw' data was the dissimilarity matrix between 147 unique DNA sequences *per* subject so that there is a total of forty five 147×147 matrices. For each matrix, we construct a Vietoris-Rips complex, then calculate persistence landscapes which enables us to perform statistical inference. Hypothesis test (1) was carried out to compare pre-FMT and post-FMT samples. The $p-$values of the paired $t-$tests are 0.0064, 0.0083 and 0.2591 in degree 0, 1, and 2, respectively. Since all of the analysis above is based on the 147 sequences randomly chosen from those patients whose number of DNA sequences are bigger than 147, we repeated this analysis 10 times with independent 147 DNA samples. The test statistics and $p-$values for 10 runs are similar showing consistency of the result regardless of which 147 DNA sequences were applied.

Hypothesis tests show significant difference of topological features in degree 0 and 1 between patients before and after FMT treatment. For degree 0, this implies that the number of clusters and their persistence on DNA sequences in pre-FMT samples are different from those in post-FMT samples. For degree 1, this implies that the number of loops (cycles) and their persistence in DNA sequences in pre-FMT samples are different from those post-FMT samples. We present DNA sequences as points cloud in $\mathbb{R}^3$ and observe patterns of clustering and loops in DNA sequences in the following section.

4.1 Clusters and Loops in DNA Sequences

Applying the dimension reduction methods, Isomap and multidimensional scaling (MDS), to the dissimilarity measure between DNA sequences, we project the DNA sequences to $\mathbb{R}^3$ and obtain embedded coordinates. Scree plots appear to indicate embedding dimension of the DNA sequences is 3. The residual variance in MDS was much higher than for Isomap, hence the figures based on Isomap are presented below.

Figure 8 shows the Isomap embedded coordinates for donor 3, post-FMT patient 7 and pre-FMT/post-FMT patient 19. From the Fig. 8, it can be seen that donor 3 and post-FMT patient 7 have a similar spread among the sequences and there are 2–3 distinct clusters. We have also noticed that donor 2 and post-FMT patient 18 also have similar structures. The donors generally have a wider spread, which would

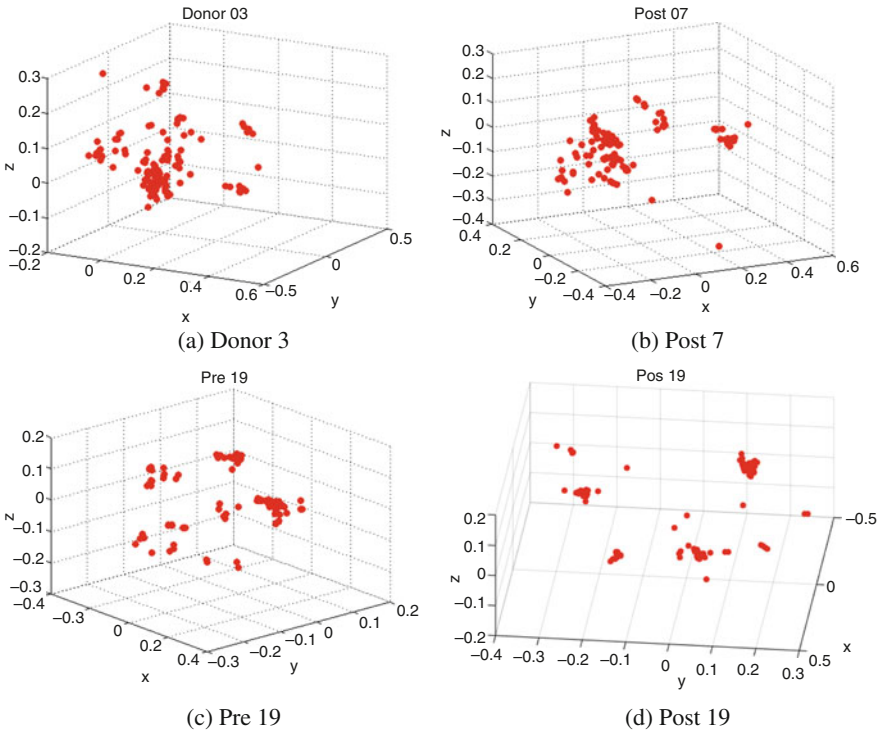

(a) Donor 3 (b) Post 7

(c) Pre 19 (d) Post 19

Fig. 8 Plots (**a**) and (**b**): 147 DNA sequences donor 3 and post-FMT patient 7 on Isomap embedded coordinates. Both samples have roughly the same number of clusters. In general, donors and patients that were close in $\mathbb{R}^2$ in Fig. 7 had similar number of clusters. Plots (**c**) and (**d**): 147 DNA sequences of pre-FMT and post-FMT of patient 19 on Isomap embedded coordinates. There are several clusters in both pre-FMT/post-FMT patient 19. The number of clusters in DNA sequences of post-FMT patient 19 is higher, but there are many clusters formed by a single DNA

indicate more diverse DNA sequences and hence a healthier gut microbiome. For the number of clusters, there are higher number of clusters in post-FMT samples, however some clusters contain only one DNA sequence and are more spread out. For example, there are about 5 groups in pre-FMT patient 19; many clusters with fewer number of DNA sequences in each cluster in post-FMT patient 19. Ignoring the clusters with singletons, we observe two large clusters in post-FMT patient 19. This information was shown in Fig. 8 as well as on the barcode and the persistence diagram. The two clusters in post-FMT patient 19 can be seen in the barcode diagram as the two points that have the highest 'death' time. The spread of clusters in pre-FMT patient 19 are shown as the bars that have the earlier birth and earlier death times (figures are not shown here). This trend is visible in other samples and may explain the small $p-$value for testing the difference in area under the persistence landscapes which was calculated in Sect. 4.

5 Conclusions

We illustrated how topological data analysis can be applied to similarity measures of DNA sequences. DNA sequence data was analyzed using three summary statistics of persistent homology; namely, barcodes, persistence diagrams and persistence landscapes. The main objective was to see if there are any differences in the topological feature of DNA sequences in the gut microbiome of CDI patients before and after FMT treatment.

From visual inspection of barcodes and persistence diagrams it was seen that the components in dimensions zero and one died sooner in the pre-FMT samples than in the post-FMT samples. Persistence landscapes were able to present this difference more formally, showing that there was a difference in the average area under the persistence landscapes for pre-FMT and post samples. Alternative interpretation of this was that there was a difference in the number and size of clusters in dimension zero, and the number and size of loops in dimension one. The post-FMT samples had more clusters than the pre-FMT samples, whereas there was no visually obvious difference in the size of the loops, but the loops were bigger for the post samples.

We performed discriminant analysis on β_0, β_1-Isomap embedded coordinates. The classification on two dimensional space for both degree 0 and 1 show good separation among three groups. For degree 0, the first two discriminant function separates pre-FMT patients and donors, and post-FMT patients sit between the two. For degree 1, the first two discriminant function separates pre-FMT and post-FMT patients and donors are between the two.

The major drawback of this analysis is that information about individual sequences is lost. This project looked at the topological structure created by the sequences but no details were provided about the individual sequences. As the microbiological technology and methods improve it may be interesting to incorporate this information. Also of interest would be meaningful identification of bacterial species. Studies of the 16S rRNA gene only measure presence of the

species, but do not say anything about their functionality. For the latter one has to turn to the metabolome which is currently under investigation with the patients in Lee et al. (2016).

Acknowledgements We are grateful to all of the donors, families and patients who took part in this study. We also appreciate the clinical and research staffs at St Joseph's Healthcare Hamilton where the clinical work had been performed. The corresponding author would also like to thank the participants of the SAMSI Working Group "Nonlinear Low-dimensional Structures in High-dimensions for Biological Data" which was part of the 2013–14 SAMSI LDHD Program. Much of the discussions were centred on the work presented.

We also thank Violeta Kovacev-Nikolic for her help with matlab code and Fig. 1; Professor Patrick Schloss for his help using `mothur`; and Yi Zhou for his help with Figs. 2 and 3. Computations in this research were largely enabled by resources provided by WestGrid and Compute Canada.

Funding support was provided by: CANSII CRT; CIHR 413548-2012; McIntyre Memorial Fund; Michael Smith Foundation Health Research Grant; NSERC DG 293180, 46204; NSF DMS-1127914; and, PSI Foundation Health Research Grant 2013, 2017. The study and permission protocol was approved by the Hamilton Integrated Research Ethics Board #12-3683, the University of Guelph Research Ethics Board 12AU013 and the University of Alberta, Health Ethics approval Pro00047221.

Appendix: Clinical and Microbiome Data

Description of the data:

sex	Female
age	Years to the first treatment
inst	hospitalized at the first treatment
fever	Above 38 °C
abd	Abdominal pain
wbc	White blood count
ppi	Proton pump inhibitor
res1	Resolution 1-FMT
res2	Resolution 2-FMT
d1	Days between 1-FMT and 2-FMT
res3	Resolution 3-FMT
d2	Days between 2-FMT and 3-FMT
res4	Resolution 4-FMT
d3	Days between 3-FMT and 4-FMT
nft	Number of FMTs
res	Resolution
pre-fmt	Number of days prior to first FMT sequenced
post-fmt	Number of days past last FMT sequenced
rmet	Refractory to metronidazle
met	Metronidazle
durm	Duration of metronidazle

rvan	Refractory to vancomycin
van	Vancomyin
durv	Duration of vancomycin
vata	Vancomycin taper
durvt	Duration of vancomycin taper
meva	Metronidazle vancomycin concomitantly
dmeva	Duration of metronidazle vancomycin concomitantly
abx	Antiobiotics in between FMTs

The phylum count data:

b's	The pre-FMT sample
a's	The post-FMT sample
1	Firmicutes
2	Proteobacteria
3	Bacteroidetes
4	Actinobacteria
5	Unclassified(92);unclassified(92);unclassified(92);unclassified(92);unclassified(92);
6	Synergistetes
7	Fusobacteria
8	Verrucomicrobia
9	Tenericutes
10	Acidobacteria
11	Spirochaetes
12	Deinococcus-Thermus

Data-1

CSV spreadsheets: 19_patients.csv; 7_donors.csv.

Data-2

Pavel thesis (contains codes and sequence data): https://drive.google.com/drive/folders/1ooBJYOpwW8OStPo3An-l-shkR62lzxXT

References

Ben-Hur, A., Horn, D., Siegelmann, H., & Vapnik, V. (2001). Support vector clustering. *Journal of Machine Learning Research, 2*, 125–137.

Bubenik, P. (2015). Statistical topological data analysis using persistence landscapes. *Journal of Machine Learning Research, 16*, 77–102.

Collins, A., Zomorodian, A., Carlsson, G., & Guibas, L. J. (2004). A barcode shape descriptor for curve point cloud data. *Computers and Graphics, 28*, 881–894.

Dethlefsen, L., Huse, S., Sogin, M., & Relman, D. (2008). The pervasive effects of an antibiotic on the human gut microbiota, as revealed by deep 16S rRNA sequencing. *PLoS Bio, 6*(11), e280.

Edelsbrunner, H., & Harer, J. (2008). Persistent Homology-a survey. *Contemporary Mathematics, 453*, 257–282.

Edelsbrunner, H., & Harer, J. (2010). *Computational topology, an introduction*. Providence: American Mathematical Society.

Edelsbrunner, H., Letscher, D., & Zomorodian, A. (2002). Topological persistence and simplification. *Discrete and Computational Geometry, 28*, 511–533.

Fasy, B., Lecci, F., Rinaldo, A., Wasserman, L., Balakrishnan, S., & Singh, A. (2013). *Statistical inference for persistent homology: Confidence sets for persistence diagrams*. arXiv:1303.7117.

Gough, E., Shaikh, H., & Manges, A. (2011). Systematic review of intestinal microbiota transplantation (fecal bacteriotherapy) for recurrent *Clostridium difficile* infection. *Clinical Infectous Diseases, 53*(10), 994–1002.

Hamilton, M., Weingarden, A., Unno, T., Khoruts, A., & Sadowsky, M. (2013). High-throughput DNA sequence analysis reveals stable engraftment of gut microbiota following transplantation of previously frozen fecal bacteria. *Gut Microbes, 4*(2), 125–133.

Heo, G., Gamble, J., & Kim, P. (2012). Topological analysis of variance and the maxillary complex. *Journal of the American Statistical Association, 107*, 477–492.

Johnson, R., & Wichern, D. (2007). *Applied multivariate statistical anaysis*. Upper Saddle River: Pearson Prentice Hall.

Kassam, Z., Hudal, R., Marshall, J., & Lee, C. (2012). Fecal transplantation via retention enema is effective for refractory or recurrent *Clostridium difficile* infection. *Archives of Internal Medicine, 172*, 191–3.

Kelly, C., & LaMont, J. (2008). *Clostridium difficile*-more difficult than ever. *New England Journal of Medicine, 359*(18), 1932–40.

Khanna, S., Pardi, D., Kelly, C., Kraft, C., Dhere, T., Henn, M., et al. (2016). A novel microbiome therapeutic increases gut microbial diversity and prevents recurrent *Clostridium difficile* infection. *Journal of Infectious Diseases, 214*(2), 173–81.

Kovacev-Nikolic, V., Bubenik, P., Nikolić, D., & Heo, G. (2016). Using cycles in high dimensional data to analyze protein binding. *Statistical Applications in Genetics and Molecular Biology, 15*(1), 19–38.

Ledoux, M., & Talagrand, M. (2002). *Probability in banach spaces: Isoperimetry and processes* (1st reprint 2002 edition). A Series of Modern Surveys in Mathematics Series. Berlin: Springer.

Lee, C., Bellanger, J., Kassam, Z., Smieja, M., Higgins, D., Broukhanski, G., et al. (2014). The outcome of long-term follow-up of patients with recurrent and refractory *Clostridium difficile* infection using multiple fecal microbiota transplants via retention enema: A case series of 94 patients. *European Journal of Clinical Microbiology and Infectious Diseases, 33*(8), 1425–1428.

Lee, C., Steiner, T., Petrof, E., Smieja, M., Roscoe, D., Nemataliah, A., et al. (2016). Frozen vs. fresh fecal microbiota transplantation and clinical resolution of diarrhea in patients with recurrent *Clostridium difficile* infection: A randomized clinical trial. *Journal of the American Medical Association, 315*(2), 142–149.

Li, H., Ruan, J., & Durbin, R. (2008). Mapping short DNA sequencing reads and calling variants using mapping quality scores. *Genome Research, 18*, 1851–1858.

Loo, V., Poirier, L., Miller, M., Oughton, M., Libman, M., Michaud, S., et al. (2005). A predominantly clonal multi-institutional outbreak of *Clostridium difficile*-associated diarrhea with high morbidity and mortality. *New England Journal of Medicine, 353*(20), 2442–9.

Louie, T., Miller, M., Mullane, K., Weiss, K., Lentnek, A., Golan, Y., et al. (2011). Fidaxomicin versus vancomycin for *Clostridium difficile* infection. *New England Journal of Medicine, 364*(5), 422–31.

Manges, A., Labbe, A., Loo, V., Atherton, J., Behr, M., Masson, L., et al. (2010). Comparative metagenomic study of alterations to the intestinal microbiota and risk of noscomial *Clostridium difficile*-associated disease. *Journal of Infectious Diseases, 202*(12), 1877–1884.

Martinez, D., Lee, C., Kim, P., & Mio, W. (2019). Probing the geometry of data with diffusion Fréchet functions. *Applied and Computational Harmonic Analysis, 47*(3), 935–947.

Mileyko, Y., Mukherjee, S., & Harer, J. (2011). Probability measures on the space of persistence diagrams. *Inverse Problems, 27*, 1–22.

Nicolau, M., Levine, A. J., & Carlsson, G. (2011). Topology based data analysis identifies a subgroup of breast cancers with a unique mutational profile and excellent survival. *Proceedings of the National Academy of Sciences, 108*, 7265–7270.

Petrof, E., Gloor, G., Vanner, S., Weese, S., Carter, D., Daigneault, M., et al. (2013). Stool substitute transplant therapy for the eradication of *Clostridium difficile* infection: 'RePOOPulating' the gut. *Microbiome, 1*(3), 1–12.

Petrov, P. (2014). *Topological data analysis of DNA sequence data in human gut microbiome*. Master's Thesis, University of Alberta, Department of Mathematical and Statistical Sciences.

Pinder, S. (2013). *Detecting changes in the gut microbiome following human biotherapy via pyrosequencing of the 16s rRNA gene*. Master's thesis, University of Guelph, Department of Mathematics and Statistics.

Rubin, T., Gessert, C., Aas, J., & Bakken, J. (2013). Fecal microbiome transplantation for recurrent *Clostridium difficile* infection: Report on a case series. *Anaerobe, 19*, 22–26.

Rush, S., Lee, C., Mio, W., & Kim, P. (2016). *The phylogenetic lasso and the microbiome*. arXiv:1607.08877.

Rush, S., Pinder, S., Costa, M., & Kim, P. (2012). A microbilogy primer for pyrosequencing. *Quantitative Bio-Science, 31*, 53–81.

Schubert, A., Rogers, M., Ring, C., Mogle, J., Petrosino, J., Young, V., et al. (2014). Microbiome data distinguish patients with *Clostridium difficile* infection and non-*Clostridium difficile*-associated diarrhea from healthy controls. *mBio, 5*(3), 1–9.

Seekatz, A., Aas, J., Gessert, C., Rubin, T., Saman, D., Bakken, J., et al. (2014). Recovery of the gut microbiome following Fecal Microbiota transplantation. *mBio, 5*(5), e00893–14.

Shahinas, D., Silverman, M., Sittler, T., Chiu, C., Kim, P., Allen-Vercoe, E., et al. (2012). Toward an understanding of changes in diversity associated with fecal microbiome transplantation based on 16S rRNA gene deep sequencing. *mBio, 3*(5), e00338–12.

Song, Y., Garg, S., Girotra, M., Maddox, C., von Rosenvinge, E., Dutta, A., et al. (2013). Microbiota dynamics in patients treated with fecal microbiota transplantation for recurrent *Clostridium difficile* infection. *Plos ONE, 8*(11), e81330.

Tausz, A. (2011). `phom`: *Persistent homology in R, version 1.0.3*. Available at CRAN http://cran.r-project.org

Van Nood, E., Vrieze, A., Nieuwdorp, M., Fuentes, S., Zoetendal, E., de Vos, W. M., et al. (2013). Duodenal infusion of donor feces for recurrent *Clostridium difficile*. *New England Journal of Medicine, 368*(5), 407–15.

Vincent, C., Stephens, D., Loo, V., Edens, T. J., BehrM. A., Dewar, K., et al. (2013). Reductions in intestinal Clostridiales precede the development of nosocomial *Clostridium difficile* infection. *Microbiome, 1*(18), 1–11.

Weingarden, A., Chen, C., Bobr, A., Yao, D., Lu, Y., Nelson, V., et al. (2014). Microbiota transplantation restores normal fecal bile acid composition in recurrent *Clostridium difficle* infection. *Gastronintestinal Liver Physiology, 306*(4), 310–319.

Zomorodian, A., & Carlsson, G. (2005). Computing persistent homology. *Discrete and Computational Geometry, 33*, 249–274.

Simultaneous Variable Selection and Estimation in Generalized Semiparametric Mixed Effects Modeling of Longitudinal Data

Mozghan Taavoni and Mohammad Arashi

Abstract Longitudinal data frequently arises in biological, medical and epidemiological studies, and the main characteristic of it is that repeated measurements from the same subjects are correlated over time. This chapter considers the problem of simultaneous variable selection and estimation in the generalized semiparametric mixed effects model (GSMM) for longitudinal data. The GSMM is a natural extension of the semiparametric mixed effects model where accommodates response variables that follow distributions other than the normal, presents an arbitrary nonparametric smooth function to model the complicated time trend and account for the within subject correlation using the random effects. When a large number of variables are available in the data, it is of critical importance to select the best subset of variables in order to develop an informative yet parsimonious model. The challenge in analyzing longitudinal data when responses are non-normal is the difficulty to specify the full likelihood function. A standard approach to deal with this is to use the generalized estimating equations (GEE). We propose a penalization type of GEE while using regression spline to approximation the nonparametric component. This approach apply the penalty functions such as SCAD to the estimating equation objective function in order to simultaneously estimate parameters and select the important variables. The proposed penalized estimation technique involves the specification of the posterior distribution of the random effects, which cannot be evaluated in closed form. However, it is possible to approximate this posterior distribution by producing random draws from the distribution using a Metropolis algorithm, which does not require the specification of the posterior distribution. Moreover, we discuss how to select the regularization parameters and the model selection procedure for assessing the fits of candidate models is also addressed. For practical implementation, we adopt an appropriate iterative algorithm to select the

M. Taavoni · M. Arashi (✉)
Department of Statistics, Faculty of Mathematical Sciences, Shahrood University of Technology, Shahrood, Iran

A. Bekker et al. (eds.), *Computational and Methodological Statistics and Biostatistics*, Emerging Topics in Statistics and Biostatistics,
https://doi.org/10.1007/978-3-030-42196-0_19

significant variables and estimate the nonzero coefficient functions. Performance of the proposed penalization technique is analyzed through a simulation study along with the analysis of HIV data.

1 Introduction

In biological, medical, and epidemiological studies, we frequently involve longitudinal data and the main characteristic of it is that repeated measurements from the same subjects are correlated over time. Linear mixed effects models (LMM) proposed by Laird and Ware (1982) is popularly applied, using random component which takes care the correlation among observations from the same subject. Motivated by beeing restrictive LMM to the linear relationship between the response and the covariates, especially when the variety of response over time is in a complicated manner and it is difficult to model its time trend using a simple parametric function, Zeger and Diggle (1994) introduced the partially linear mixed models (PLMM) which have received increasing attention in recent years to analyze longitudinal data, because of most flexibility by including nonparametric function and also conserning within subject correlation. Earlier developments of PLMM can be found in Zhang (2004), Li and Zhu (2010) and Sinha and Sattar (2015).

In many research areas, longitudinal data are commonly encountered from repeated categorical or non-normal data, such as binomial or poisson type responses. An approach that can be applied in such situations is to use the generalized linear model (GLM, McCullagh and Nelder (1989)). The challenge in analyzing longitudinal data when responses are non-normal is that it is difficult to specify the full likelihood function. This motivated (Liang and Zeger 1986) to develop an approach called generalized estimating equation (GEE) which is a multivariate analogue of the quasi-likelihood. Generalized linear mixed effects model (GLMM) was proposed by Fitzmaurice et al. (2004), which accommodates response variables that follow distributions other than the normal one and contains random effects in the linear predictor, is a useful extension of the GLM and has also become a very popular method to analyze longitudinal data. To eliminate the limitation of the GLMM for modeling non linear time trend, a generalized partially linear mixed model (GPLMM), a natural extension of the GLMM, is widely used to analyze longitudinal data by incorporating the within subject correlation using random effects and an arbitrary smooth function to model the time effect. Further developments along this line in the framework of the GPLMM can be found in Fan et al. (2007), Qin and Zhu (2007), Qin and Zhu (2009), Liang (2009) and Kurum et al. (2016) to mention afew.

When a large number of variables are available in the data, it is of critical importance to select the best subset of variables in order to develop an informative yet parsimonious model. There is a large body of variable selection methods for cross-sectional data. For example, Frank and Friedman (1993) considered the L_q

penalty, which yields the bridge Regression. Tibshirani (1996) proposed the least absolute shrinkage and selection operator (LASSO), which can be viewed as a solution to the penalized least squares with the L_1 penalty. Zou (2006) further developed the adaptive Lasso to fulfill oracle properties. Through combining both ridge (L_2) and lasso (L_1) penalty together, Zou and Hastie (2005) proposed the Elastic-net, which also has the sparsity property, to solve the collinearity problems. Fan and Li (2001) proposed the smoothly clipped absolute diviation (SCAD) penalty method and proved the SCAD estimators enjoy the oracle properties. All these variable selection procedures are based on penalized estimation using penalty functions, which have a singularity at zero. Consequently, these estimation procedures require convex optimization, which incurs a computational burden. To overcome this problem, Ueki (2009) developed a new variable selection procedure called the smooth-threshold estimating equations that can automatically eliminate irrelevant parameters by setting them as zero. In addition, the resulting estimator enjoys the oracle property in the sense (Fan and Li 2001) suggested. Bondell et al. (2010) proposed simultaneous selection of the fixed and random factors using a penalized joint log likelihood for the LMM. Ni et al. (2010) proposed a double-penalized likelihood approach for simultaneous model selection and estimation for PLMM. Ma et al. (2013) applied proper penalty functions in additive partially linear models.

In contrast to extensive attention on model selection for Gaussian longitudinal data, research on model selection for non-Gaussian longitudinal data in the framework of GLM remains largely unexplored. To do variable selection, Pan (2001) developed a quasi-likelihood information criterion (QIC) which is analogous to AIC; Cantoni et al. (2005) generalized Mallow's C_p criterion; and Wang and Qu (2009) proposed a BIC criterion based on the quadratic inference function. These are best subset type model selection procedures which become computationally intensive when number of parameters is moderately large. Regarding regularization methods for longitudinal data, Fu (2003) proposed a generalization of the bridge and Lasso penalties to GEE models. Xu et al. (2012) proposed a weighted least-squares (WLS) type function to study the longitudinal GLMs with a diverging number of parameters. Dziak (2006) generalized the Lasso and SCAD methods to the longitudinal GLMs and studied the pn consistency, the asymptotic normality, and the oracle property of the penalized GEE estimator in the chapter "Multivariate Order Statistics Induced by Ordering Linear Combinations of Components of Multivariate Elliptical Random Vectors" of his Ph.D Thesis. Wang et al. (2012) proposed the SCAD-penalized GEE for analyzing longitudinal data with high-dimensional covariates. The SCAD-penalized selection procedures were illustrated in Xue et al. (2010) for generalized additive models with correlated data. To the best of our knowledge, variable selection problem is not attended in the GPLMM.

Here, we consider the GPLMM with longitudinal data by allowing for non-Gaussian data and nonlinear link functions. We develop simultaneous variable selection and estimation procedures in the framework of maximum likelihood esti-

mation based on the penalized estimating equation approach via B-spline regression to estimate the nonparametric components. We apply the penalty functions to the estimating equation objective function such that the proposed procedure can simultaneously estimate parameters and select the important variables. The proposed penelaized estimation involves the specification of the posterior distribution of the random effects, which cannot be evaluated in a closed form, and we use a Metropolis algorithm, which does not require the specification of the posterior distribution. We obtain consistency and asymptotic normality of the resulting estimators. To estimate the parameters, a computationally flexible iterative algorithm is developed.

The plan of this chapter is as follows. Section 2, formulates the model, discusses the approximation of the nonparametric function using splines and considers the estimation under the GEE framework. Section 3 discusses how to select the regularization parameters and the model selection procedure for assessing the fits of candidate models is also addressed. Moreover, asymptotic properties of the estimators and a Monte Carlo Newton–Raphson algorithm to implement the procedures is given. Section 4 includes model assessments via simulations and data analysis. Some concluding remarks are given in Sect. 5. The proofs of the main results are given in the Appendix.

2 Generalized PLMM

Consider a longitudinal study with n subjects and n_i observations over time for the ith subject ($i = 1, \ldots, n$). Let $\boldsymbol{u}_i$ be a $q \times 1$ vector of random effects corresponding to the ith subject, and y_{ij} be an observation of the ith subject measured at time t_{ij} for $i = 1, \ldots, n$ and $j = 1, \ldots, n_i$. Suppose that $y_{i1}, \ldots, y_{in_i}$ given $\boldsymbol{u}_i$ are conditionally independent and each $y_{ij}|\boldsymbol{u}_i$ is distributed as an exponential family distribution whose probability density function is given by

$$p(y_{ij}|\boldsymbol{u}_i, \boldsymbol{\beta}_n, \phi) = \exp\Big[\phi^{-1}\{y_{ij}\theta_{ij} - b(\theta_{ij})\} + c(y_{ij}, \phi)\Big], \tag{1}$$

where ϕ is a scale parameter, $c(.,.)$ is a function only depending on y_{ij} and ϕ, and θ_{ij} is the (scalar) canonical parameter. The conditional expectations and variances of y_{ij} given $\boldsymbol{u}_i$ are given by $\mu_{ij} = E(y_{ij}|\boldsymbol{u}_i) = b^{\cdot}(\theta_{ij})$ and $v_{ij} = var(y_{ij}|\boldsymbol{u}_i) = \phi b^{\cdot\cdot}(\theta_{ij})$, respectively, where $b^{\cdot}(\theta) = \frac{\partial b(\theta)}{\partial \theta}$ and $b^{\cdot\cdot}(\theta) = \frac{\partial^2 b(\theta)}{\partial \theta^2}$. In this chapter, we assume that the conditional mean μ_{ij} satisfies

$$g(\mu_{ij}) \triangleq \eta_{ij} = \boldsymbol{X}_{ij}^{\top}\boldsymbol{\beta}_n + \boldsymbol{Z}_{ij}^{\top}\boldsymbol{u}_i + f(t_{ij}), \quad i = 1, \ldots, n;\ j = 1, \ldots, n_i, \tag{2}$$

where $g(.)$ is a known monotonic link function, $\boldsymbol{X}_{ij}^{\top}$ is a $p_n \times 1$ vector of explanatory variables, $\boldsymbol{\beta}_n$ is a $p_n \times 1$ vector of unknown parameters of the fixed effects, $\boldsymbol{Z}_{ij}^{\top}$ is a $q \times 1$ vector of explanatory variables relating to the random effects, $f(.)$ is an

unknown smooth function which is continuous and twice differentiable function on some finite interval. The dimension of the covariates p_n is allowed to depend on the number of subjects n. To complete the specification, assume that the random effects $\boldsymbol{u} = \{\boldsymbol{u}_1, \ldots, \boldsymbol{u}_q\}$ independently follow the same distribution, depending on parameters $\boldsymbol{\Sigma}$ as

$$\boldsymbol{u}_i \sim p_{\boldsymbol{u}_i}(\boldsymbol{u}_i|\boldsymbol{\Sigma}). \tag{3}$$

The model defined in Eqs. (1)–(3) is referred to as generalized semiparametric mixed model (GPLMM).

2.1 Smoothing Spline Approximation

Following the most literature such as He et al. (2005) and Qin and Zhu (2009), the unspecified smooth function can be approximated sufficiently well by the following polynomial spline

$$f(t_{ij}) = \alpha_0 + \alpha_1 t_{ij} + \ldots + \alpha_d t_{ij}^d + \sum_{l=1}^{L_n} \alpha_{(d+1)+l}(t_{ij} - t_i^{(l)})_+^d = \boldsymbol{B}(t_{ij})^\top \boldsymbol{\alpha}_n,$$

where d is the degree of the polynomial component, L_n is the number of interior knots (which rate of L_n will be specified in Sect. 3.3., $t_i^{(l)}$ is referred as knots of the ith subject, $\boldsymbol{B}(t_{ij}) = \left(1, t_{ij}, \ldots, t_{ij}^d, (t_{ij} - t_i^{(1)})_+^d, \ldots, (t_{ij} - t_i^{(L_n)})_+^d\right)$ is a $h_n \times 1$ vector of basis functions, h_n is the number of basis functions used to approximate $f(t_{ij})$, $h_n = d + 1 + L_n$, $(a)_+ = \max(0, a)$, and $\boldsymbol{\alpha}_n = (\alpha_0, \ldots, \alpha_d, \alpha_{d+1}, \ldots, \alpha_{d+1+L_n})^\top$ is the spline coefficients vector of dimention h. Regression splines have some desirable properties in approximating a smooth function. It often provides good approximations with a small number of knots. The spline approach also treats a nonparametric function as a linear function with the basis functions as pseudo design variables, and thus this linearizes our regression model (2) so that our regression problem becomes

$$g(\mu_{ij}) \triangleq \eta_{ij} = \boldsymbol{X}_{ij}^\top \boldsymbol{\beta}_n + \boldsymbol{Z}_{ij}^\top \boldsymbol{u}_i + \boldsymbol{B}(t_{ij})\boldsymbol{\alpha}_n, \quad i = 1, \ldots, n; j = 1, \ldots, n_i. \tag{4}$$

For convenience, model (4) can take the form

$$g(\mu_{ij}) \triangleq \eta_{ij} = \boldsymbol{D}_{ij}^\top \boldsymbol{\theta}_n + \boldsymbol{Z}_{ij}^\top \boldsymbol{u}_i, \quad i = 1, \ldots, n; j = 1, \ldots, n_i,$$

where $\boldsymbol{D}_{ij} = \left(\boldsymbol{X}_{ij}^\top, \boldsymbol{B}_j(\boldsymbol{t}_i)^\top\right)^\top$ being a $(p_n + h_n) \times 1$ design matrix combining the fixed-effects and spline-effects design matrices for the jth outcome of the ith

subject, and $\boldsymbol{\theta}_n = (\boldsymbol{\beta}_n^\top, \boldsymbol{\alpha}_n^\top)^\top$ is a $(p_n + h_n) \times 1$ combined regression parameters vector that must be estimated.

According to the linearization of the GPLMM (2) using spline approach, any computational algorithm developed for the GMM can be used for the GSMM. We now formulate the linearization of GPLMM in the seamless form

$$\begin{aligned} p(y_{ij}|\boldsymbol{u}_i, \boldsymbol{\theta}_n, \phi) &= \exp\left[\phi^{-1}\{y_{ij}\theta_{ij} - b(\theta_{ij})\} + c(y_{ij}, \phi)\right], \\ \boldsymbol{u}_i &\sim f_u(\boldsymbol{u}_i|\boldsymbol{\Sigma}), \\ \mu_{ij} &= \mathrm{E}(y_{ij}|\boldsymbol{u}_i), \\ g(\mu_{ij}) \triangleq \eta_{ij} &= \boldsymbol{D}_{ij}^\top \boldsymbol{\theta}_n + \boldsymbol{Z}_{ij}^\top \boldsymbol{u}_i, \quad i = 1, \ldots, n;\ j = 1, \ldots, n_i, \end{aligned} \tag{5}$$

2.2 Estimation Procedure

For linearization of GPLMM defined in (5), the classical likelihood function can be defined as

$$L(\boldsymbol{\theta}_n, \boldsymbol{\Sigma}, \phi) = \prod_{i=1}^{n} \int p_{\boldsymbol{y}_i|\boldsymbol{u}_i}(\boldsymbol{y}_i|\boldsymbol{u}_i, \boldsymbol{\theta}_n, \phi) p_{\boldsymbol{u}_i}(\boldsymbol{u}_i|\boldsymbol{\Sigma}) d\boldsymbol{u}_i \tag{6}$$

where $\boldsymbol{y}_i = (\boldsymbol{y}_{i1}, \ldots, \boldsymbol{y}_{in_i})^\top$ and

$$p_{\boldsymbol{y}_i|\boldsymbol{u}_i}(\boldsymbol{y}_i|\boldsymbol{u}_i, \boldsymbol{\theta}_n, \phi) = \prod_{j=1}^{n_i} p(\boldsymbol{y}_{ij}|\boldsymbol{u}_i, \boldsymbol{\theta}_n, \phi).$$

For the maximum likelihood (ML) estimates of the parameters $\boldsymbol{\theta}_n$, ϕ and $\boldsymbol{\Sigma}$, one can maximize this likelihood function by using suitable numerical techniques. The EM algorithm is an attractive method to obtain the ML estimates, in presence of incomplete data, which avoids explicit calculation of the observed data log-likelihood. To set up the EM algorithm we consider the random effects, $\boldsymbol{u}_i$, to be the missing data. The complete data, is then $(\boldsymbol{y}_i, \boldsymbol{u}_i)$ and the complete data log-likelihood is given by

$$\ell(\boldsymbol{\theta}_n, \boldsymbol{\Sigma}, \phi) = \sum_{i=1}^{n} \ln p_{\boldsymbol{y}_i|\boldsymbol{u}_i}(\boldsymbol{y}_i|\boldsymbol{u}_i, \boldsymbol{\theta}_n, \phi) + \sum_{i=1}^{n} \ln p_{\boldsymbol{u}_i}(\boldsymbol{u}_i|\boldsymbol{\Sigma}). \tag{7}$$

Considering $\boldsymbol{u}_i$ to be the missing has an advantage that in the M-step, maximization can be accomplished with respect to the parameters $\boldsymbol{\theta}_n$ and ϕ only in the first term of (7). Thus, the M-step with respect to $\boldsymbol{\theta}_n$ and ϕ uses only the GLM part

of the likelihood function. Hence, the procedure is similar to a standard GLM computation assuming $\boldsymbol{u}_i$ is known. Therefore, maximizing with respect to $\boldsymbol{\Sigma}$, in the second term, can be handled by the maximum likelihood using the distribution of $p_{\boldsymbol{u}_i}(\boldsymbol{u}_i|\boldsymbol{\Sigma})$ after replacing sufficient statistics with the conditional expected values. The EM algorithm is a standard technique for LMM, but GLMs are usually fit with a Newton–Raphson or scoring algorithm. Number of numerical methods are available in the literature (McCulloch 1997). It thus makes sense to develop a simulation analogous to the Newton–Raphsona approach for fitting the GPLMM. Using this separation as in (7), the ML equations for $\boldsymbol{\theta}_n$ and $\boldsymbol{\Sigma}$ take the following forms

$$\mathrm{E}\left[\frac{\partial \ln p_{y_{ij}|\boldsymbol{u}_i}(y_{ij}|\boldsymbol{u}_i,\boldsymbol{\theta}_n)}{\partial \boldsymbol{\theta}_n}|y_{ij}\right]=\mathbf{0},$$
$$\mathrm{E}\left[\frac{\partial \ln p_{\boldsymbol{u}_i}(\boldsymbol{u}_i|\boldsymbol{\Sigma})}{\partial \boldsymbol{\Sigma}}|y_{ij}\right]=\mathbf{0}.$$

The ML estimates of $\boldsymbol{\theta}_n$ and $\boldsymbol{\Sigma}$ can be obtained by solving the preceding equations numerically. McCulloch (1997) developed a Monte Carlo Newton–Raphson (MCNR) algorithm for solving these estimating equations, and obtained approximate ML estimates of the parameters for the GMM. Motivated by his work and combining it with the GEE of Liang and Zeger (1986), the optimal estimating equation for $\boldsymbol{\theta}_n$ is given by

$$\mathrm{E}_{\boldsymbol{u}|\boldsymbol{y}}\Big[n^{-1}\sum_{i=1}^{n}\frac{\partial \boldsymbol{\mu}_i(\boldsymbol{\theta}_n,\boldsymbol{u}_i)}{\partial \boldsymbol{\theta}_n^{\top}}\boldsymbol{V}_i^{-1}(\boldsymbol{\theta}_n,\boldsymbol{u}_i)\big(\boldsymbol{y}_i-\boldsymbol{\mu}_i(\boldsymbol{\theta}_n,\boldsymbol{u}_i)\big)\Big]=\mathbf{0}, \tag{8}$$

where $\boldsymbol{\mu}_i(\boldsymbol{\theta}_n,\boldsymbol{u}_i)=(\mu_{i1},\ldots,\mu_{in_i})^{\top}$ and $\boldsymbol{V}_i(\boldsymbol{\theta}_n,\boldsymbol{u}_i)$ is the covariance matrix of $\boldsymbol{y}_i|\boldsymbol{u}_i$. In real applications the true intracluster covariance structure is often unknown. The GEE procedure adopts a working covariance matrix, which is specified through a working correlation matrix $\boldsymbol{R}(\boldsymbol{\rho})$: $\boldsymbol{V}_i(\boldsymbol{\theta}_n,\boldsymbol{u}_i)=\boldsymbol{A}_i^{\frac{1}{2}}(\boldsymbol{\theta}_n,\boldsymbol{u}_i)\boldsymbol{R}(\boldsymbol{\rho})\boldsymbol{A}_i^{\frac{1}{2}}(\boldsymbol{\theta}_n,\boldsymbol{u}_i)$, where $\boldsymbol{\rho}$ is a finite dimensional parameter and $\boldsymbol{A}_i(\boldsymbol{\theta}_n,\boldsymbol{u}_i)=\mathrm{diag}(v_{i1},\ldots,v_{in_i})$. Some commonly used working correlation structures include independence, autocorrelation (AR)-1, equally correlated (also called compound symmetry), or unstructured correlation, among others. For a given working correlation structure, $\boldsymbol{\rho}$ can be estimated using the residual-based method of moments. With the estimated working correlation matrix $\widehat{\boldsymbol{R}}\equiv\boldsymbol{R}(\widehat{\boldsymbol{\rho}})$, the estimating equations in (8) reduces to

$$\mathrm{E}_{\boldsymbol{u}|\boldsymbol{y}}\Big[n^{-1}\sum_{i=1}^{n}\boldsymbol{D}_i^{\top}\boldsymbol{A}_i^{\frac{1}{2}}(\boldsymbol{\theta}_n,\boldsymbol{u}_i)\widehat{\boldsymbol{R}}^{-1}\boldsymbol{A}_i^{-\frac{1}{2}}(\boldsymbol{\theta}_n,\boldsymbol{u}_i)\big(\boldsymbol{y}_i-\boldsymbol{\mu}_i(\boldsymbol{\theta}_n,\boldsymbol{u}_i)\big)\Big]=\mathbf{0}, \tag{9}$$

where $\boldsymbol{D}_i=(\boldsymbol{D}_{i1}^{\top},\ldots,\boldsymbol{D}_{in_i}^{\top})^{\top}$. We formally define the estimator as the solution $\widehat{\boldsymbol{\theta}}_n$ of the above estimating equations. For ease of exposition, we assume $\phi=1$ and $n_i=m<\infty$ in the rest of the article. Extension of the methodology to the cases of

unequal n_i is straightforward. We vary the dimension of $\boldsymbol{A}_i$ and replace $\widehat{\boldsymbol{R}}$ by $\widehat{\boldsymbol{R}}_i$, which is the $n_i \times n_i$ matrix using the specified working correlation structure and the corresponding initial parameter $\boldsymbol{\rho}$ estimator.

3 Regularization in the GPLMM

In order to select important covariate variables and estimate them simultaneously, the log-likelihood (8) is expanded to include the penalty term $\sum_{k=1}^{p_n} p_{\lambda_n}(|\beta_{nk}|)$ which yields the following penalized log-likelihood

$$\ell^p(\boldsymbol{\beta}_n, \boldsymbol{\alpha}_n, \boldsymbol{D}, \phi) = \sum_{i=1}^{n} \ln p_{\boldsymbol{y}_i|\boldsymbol{u}_i}(\boldsymbol{y}_i|\boldsymbol{u}_i, \boldsymbol{\theta}_n) + \sum_{i=1}^{n} p_{\boldsymbol{u}_i}(\boldsymbol{u}_i|\boldsymbol{\Sigma}) - n\sum_{k=1}^{p_n} p_{\lambda_n}(|\beta_{nk}|), \tag{10}$$

where $p_\lambda(|\beta_{nk}|)$ is any penalty function and λ_n is a tuning parameter that determines the amount of shrinkage. Since the coefficients $\boldsymbol{\theta}_n$ depends to the first and third terms of (10), we propose the penalized estimating equation

$$\boldsymbol{U}_n(\boldsymbol{\theta}_n) = \boldsymbol{S}_n(\boldsymbol{\theta}_n) - q_{\lambda_n}(|\boldsymbol{\beta}_n|)\text{sign}(\boldsymbol{\beta}_n),$$

where

$$\boldsymbol{S}_n(\boldsymbol{\theta}_n) = \text{E}_{u|y}\Big[\sum_{i=1}^{n} \boldsymbol{D}_i^\top \boldsymbol{A}_i^{\frac{1}{2}}(\boldsymbol{\theta}_n, \boldsymbol{u}_i)\widehat{\boldsymbol{R}}^{-1}\boldsymbol{A}_i^{-\frac{1}{2}}(\boldsymbol{\theta}_n, \boldsymbol{u}_i)\big(\boldsymbol{y}_i - \boldsymbol{\mu}_i(\boldsymbol{\theta}_n, \boldsymbol{u}_i)\big)\Big],$$

with $q_{\lambda_n}(|\boldsymbol{\beta}_n|) = \big(q_{\lambda_n}(|\beta_{n1}|), \ldots, q_{\lambda_n}(|\beta_{np_n}|)\big)^\top$ is a $p_n \times 1$ vector of penalty functions, $\text{sign}(\boldsymbol{\beta}_n) = \big(\text{sign}(\beta_{n1}), \ldots, \text{sign}(\beta_{np_n})\big)^\top$ with $\text{sign}(a) = I(a > 0) - I(a < 0)$ and $q_{\lambda_n}(|\beta_{nk}|) = p'_{\lambda_n}(|\beta_{nk}|)$.

Note that we assume the non parametric part contains significant contribution in the model and the proposed penalized estimating equation has been defined to shrink small components of coefficient $\boldsymbol{\beta}_n$ to zero not $\boldsymbol{\alpha}_n$. Thus the method performing variable selection for fixed effects, produces estimators of the nonzero components and the nonparametric component.

Among all penalty functions, the smoothing clipped absolute deviation (SCAD) penalty proposed by Fan and Li (2001) can be used to retain the good features of both subset selection and ridge regression, for producing sparse solutions, and to ensure continuity of the selected models. Therefore, we will use the SCAD penalty in our simulation and application studies. The SCAD penalty function is defined by

$$q_{\lambda_n}(|\beta_n|)=p'_{\lambda_n}(|\beta_n|)=\lambda_n\left\{I(|\beta_n|\leq\lambda_n)+\frac{(a\lambda_n-|\beta_n|)_+}{(a-1)\lambda_n}I(|\beta_n|>\lambda_n)\right\};\quad a>2,$$

where the notation $(.)_+$ stands for the positive part of $(.)$.

Our proposed estimator for $\boldsymbol{\theta}_n$ is the solution of $\boldsymbol{U}_n(\boldsymbol{\theta}_n)=\mathbf{0}$. Because $\boldsymbol{U}_n(\boldsymbol{\theta}_n)$ has discontinuous points, an exact solution to $\boldsymbol{U}_n(\boldsymbol{\theta}_n)=\mathbf{0}$ may not exist. We formally define the estimator $\widehat{\boldsymbol{\theta}}_n$ to be an approximate solution, i.e., $\boldsymbol{U}_n(\widehat{\boldsymbol{\theta}}_n)=o(a_n)$ for a sequence $a_n\to 0$. Alternatively, since the penalty function is singular at the origin, it is challenging to obtain the estimator of $\boldsymbol{\theta}_n$ by solving $U_n(\boldsymbol{\theta}_n)=\mathbf{0}$. Following Fan and Li (2001) we locally approximate the penalty function by a quadratic function. In the neighbourhoods of the true parameter values β_{n0k}, $|\beta_{n0k}|>0$, the derivative of the penalty function is well approximated by

$$q_{\lambda_n}(|\beta_{nk}|)\text{sign}(\beta_{nk})\approx\frac{q_{\lambda_n}(|\beta_{n0k}|)}{|\beta_{n0k}|}\beta_{nk}.$$

With the local quadratic approximation, we apply the Newton–Raphson method to solve $\boldsymbol{U}_n(\widehat{\boldsymbol{\theta}}_n)=o(a_n)$, and get the following updating formula

$$\widehat{\boldsymbol{\theta}}_n^{(m+1)}=\widehat{\boldsymbol{\theta}}_n^{(m)}+\left\{\boldsymbol{H}_n(\widehat{\boldsymbol{\theta}}_n^{(m)})+n\boldsymbol{E}_n(\widehat{\boldsymbol{\theta}}_n^{(m)})\right\}^{-1}\times\left\{\boldsymbol{S}_n(\widehat{\boldsymbol{\theta}}_n^{(m)})+n\boldsymbol{E}_n(\widehat{\boldsymbol{\theta}}_n^{(m)})\widehat{\boldsymbol{\theta}}_n^{(m)}\right\},\quad(11)$$

where

$$\boldsymbol{H}_n(\widehat{\boldsymbol{\theta}}_n^{(m)})=\text{E}_{u|y}\Big[\sum_{i=1}^{n}\boldsymbol{D}_i^{\top}\boldsymbol{A}_i^{\frac{1}{2}}(\boldsymbol{\theta}_n,\boldsymbol{u}_i)\widehat{\boldsymbol{R}}^{-1}\boldsymbol{A}_i^{\frac{1}{2}}(\boldsymbol{\theta}_n,\boldsymbol{u}_i)\boldsymbol{D}_i\Big],$$

$$`\boldsymbol{E}_n(\widehat{\boldsymbol{\theta}}_n^{(m)})=\text{diag}\Big\{\frac{q_{\lambda_n}(|\beta_{n1}|)}{\epsilon+|\beta_{n1}|},\ldots,\frac{q_{\lambda_n}(|\beta_{np_n}|)}{\epsilon+|\beta_{np_n}|},\mathbf{0}_{h_n}\Big\},$$

for a small numbers e.g. $\epsilon=10^{-6}$. Here, $\mathbf{0}_{h_n}$ denotes a zero vector of dimension h_n.

Note that, in general, the expectations in (11) cannot be computed in a closed form as the conditional distribution of $\boldsymbol{u}_i|\boldsymbol{y}_i$ involves the marginal distribution of $\boldsymbol{y}_i$, which is not easy to be computed explicitly. Similar to McCulloch (1997), here, we use an alternative method that produces random observations from the conditional distribution of $\boldsymbol{u}_i|\boldsymbol{y}_i$ by using a Metropolis algorithm where the specification of the density of $\boldsymbol{y}_i$ is not required.

In the Metropolis algorithm, $p_{\boldsymbol{u}}$ is chosen as the candidate distribution from which potential new draws are made; then we specify the acceptance function that provides the probability of accepting the new value (as opposed to retaining the previous value). In the forthcoming section we outline the computational procedure used for sample generation.

3.1 MCNR Algorithm

Let $\boldsymbol{U}$ denote the previous draw from the conditional distribution of $\boldsymbol{U}|\boldsymbol{y}$, and generate a new value u_k^* for the jth component of $\boldsymbol{U}^* = (u_1, \ldots, u_{k-1}, u_k^*, u_{k+1}, \ldots, u_{nq})$ by using the candidate distribution $p_{\boldsymbol{u}}$, accept $\boldsymbol{U}^*$ as the new value with probability

$$\alpha_k(\boldsymbol{U}, \boldsymbol{U}_*) = \min\left\{1, \frac{p_{u|y}(\boldsymbol{U}^*|\boldsymbol{y}, \boldsymbol{\theta}_n, \boldsymbol{D})\, p_u(\boldsymbol{U}|\boldsymbol{D})}{p_{u|y}(\boldsymbol{U}|\boldsymbol{y}, \boldsymbol{\theta}_n, \boldsymbol{D})\, p_u(\boldsymbol{U}^*|\boldsymbol{D})}\right\}. \tag{12}$$

otherwise, reject it and retain the previous value $\boldsymbol{U}$. The second term in brace in (11) can be simplified to

$$\begin{aligned}\frac{p_{\boldsymbol{u}|\boldsymbol{y}}(\boldsymbol{U}^*|\boldsymbol{y}, \boldsymbol{\theta}_n, \boldsymbol{D})\, p_u(\boldsymbol{U}|\boldsymbol{D})}{p_{\boldsymbol{u}|\boldsymbol{y}}(\boldsymbol{U}|\boldsymbol{y}, \boldsymbol{\theta}_n, \boldsymbol{D})\, p_u(\boldsymbol{U}^*|\boldsymbol{D})} &= \frac{p_{\boldsymbol{y}|\boldsymbol{u}}(\boldsymbol{y}|\boldsymbol{U}^*, \boldsymbol{\theta}_n)}{f_{\boldsymbol{y}|\boldsymbol{u}}(\boldsymbol{y}|\boldsymbol{U}, \boldsymbol{\theta}_n)} \\ &= \frac{\prod_{i=1}^n p_{\boldsymbol{y}_i|\boldsymbol{u}}(\boldsymbol{y}_i|\boldsymbol{U}^*, \boldsymbol{\theta}_n)}{\prod_{i=1}^n f_{\boldsymbol{y}_i|\boldsymbol{u}}(\boldsymbol{y}_i|\boldsymbol{U}, \boldsymbol{\theta}_n)}.\end{aligned}$$

Note that, the calculation of the acceptance function $\alpha_k(\boldsymbol{U}, \boldsymbol{U}_*)$ here involves only the specification of the conditional distribution of $\boldsymbol{y}|\boldsymbol{u}$ which can be computed in a closed form.

Algorithm 1 describes the Metropolis step into the Newton–Raphson iterative equation (11) for the Monte Carlo estimates of expected values.

3.2 Choice of Regularization Parameters

To implement the proposed method, several parameters need to be chosen appropriately. One needs to choose the knot sequence in the polynomial spline approximation, λ_n and a in the SCAD penalty function. It is important that the number of distinct knots h, must increase with the sample size n. On the other hand, too many knots would increase the variance of our estimators. Therefore, the number of knots must be properly chosen to balance the bias and variance. For computational convenience, we use equally spaced knots with the number of interior knots $L_n \approx n^{1/(2r+1)}$. A similar strategy for knot selection can also be found in He et al. (2002), Qin and Zhu (2007) and Sinha and Sattar (2015). To reduce the computational burden, we follow Fan and Li (2001) and set $a = 3.7$. Finally we need to choose λ_n.

First of all, define a fine grid of different values for the tuning parameter, $0 \leq \lambda_1 \leq \ldots \leq \lambda_L \leq \infty$. Next, the optimal tuning parameter is determined using one of the following techniques and finally, the whole data set is fitted again using the proposed method with λ_{opt} to obtain the final estimates the parameters of model. Selection criteria that have been used extensively include cross validation (CV), generalized cross-validation (GCV) and information criterion such as Akaike's

Algorithm 1 Monte Carlo Newton–Raphson (MCNR) algorithm

step 1. Set $m_k = 0$. Choose initial values $\boldsymbol{\theta}_n^0$ and $\boldsymbol{\Sigma}^0$.

step 2. Generate N observations $\boldsymbol{U}^{(1)}, \ldots, \boldsymbol{U}^{(N)}$ from the distribution $p_{\boldsymbol{u}|\boldsymbol{y}}(\boldsymbol{u}|\boldsymbol{y}, \boldsymbol{\theta}_n^{(m_k)}, \boldsymbol{\Sigma}^{(m_k)})$ using the Metropolis algorithm. Use these observations to find the Monte Carlo estimates of the expectations. Specially,

a) Compute $\boldsymbol{\theta}_n^{(m_k+1)}$ from the expression

$$\begin{aligned}\boldsymbol{\theta}_n^{(m_k+1)} &= \boldsymbol{\theta}_n^{(m_k)} + \Big\{\frac{1}{N}\sum_{k=1}^{N}\Big[\boldsymbol{H}_n\big(\widehat{\boldsymbol{\theta}}_n^{(m_k)}, \boldsymbol{U}^{(k)}\big)\Big] + n\boldsymbol{E}_n\big(\widehat{\boldsymbol{\beta}}_n^{(m_k)}\big)\Big\}^{-1} \\ &\quad \times\Big\{\frac{1}{N}\sum_{k=1}^{N}\Big[\boldsymbol{S}_n\big(\widehat{\boldsymbol{\theta}}_n^{(m_k)}, \boldsymbol{U}^{(k)}\big)\Big] - n\boldsymbol{E}_n\big(\widehat{\boldsymbol{\beta}}_n^{(m_k)}\big)\widehat{\boldsymbol{\beta}}_n^{(m_k)}\Big\},\end{aligned}$$

where

$$\boldsymbol{H}_n\big(\widehat{\boldsymbol{\theta}}_n^{(m_k)}, \boldsymbol{U}^{(k)}\big) = \sum_{i=1}^{n}\boldsymbol{D}_i^{\top}\boldsymbol{A}_i^{\frac{1}{2}}\big(\boldsymbol{\theta}_n^{(m_k)}, U_i^{(k)}\big)\widehat{\boldsymbol{R}}^{-1}\boldsymbol{A}_i^{\frac{1}{2}}\big(\boldsymbol{\theta}_n^{(m_k)}, U_i^{(k)}\big)\boldsymbol{D}_i,$$

$$\boldsymbol{S}_n\big(\widehat{\boldsymbol{\theta}}_n^{(m_k)}, \boldsymbol{U}^{(k)}\big) = \sum_{i=1}^{n}\boldsymbol{D}_i^{\top}\boldsymbol{A}_i^{\frac{1}{2}}\big(\boldsymbol{\theta}_n^{(m_k)}, U_i^{(k)}\big)\widehat{\boldsymbol{R}}^{-1}\boldsymbol{A}_i^{-\frac{1}{2}}\big(\boldsymbol{\theta}_n^{(m_k)}, U_i^{(k)}\big)\big(\boldsymbol{y}_i - \boldsymbol{\mu}_i\big(\boldsymbol{\theta}_n^{(m_k)}, U_i^{(k)}\big)\big).$$

b) Compute $\boldsymbol{\Sigma}^{(m_k+1)}$ by maximizing

$$\frac{1}{N}\sum_{k=1}^{N}\ln f_u\big(\boldsymbol{U}^{(k)}|\boldsymbol{\Sigma}\big).$$

c) Set $m_k = m_k + 1$.

step 3. Go to step 2 until convergence is achieved. Choose $\boldsymbol{\theta}_n^{(m_k+1)}$ and $\boldsymbol{\Sigma}^{(m_k+1)}$ to be the MCNR estimates of $\boldsymbol{\theta}_n$ and $\boldsymbol{\Sigma}$.

information criterion (AIC, Akaike 1973) and Bayesian information criterion (BIC, Schwarz 1978). Due to the lack of joint likelihood in the generalized model, to select the tuning parameter λ_n we use generalized cross validation (GCV) suggested by Fan and Li (2001) as defined by

$$\mathrm{GCV}_{\lambda_n} = \frac{\mathrm{RSS}(\lambda_n)/n}{(1 - d(\lambda_n)/n)^2},$$

where

$$\mathrm{RSS}(\lambda_n) = \frac{1}{N}\sum_{k=1}^{N}\Big[\sum_{i=1}^{n}\big(\boldsymbol{y}_i - \boldsymbol{\mu}_i\big(\widehat{\boldsymbol{\theta}}_n, U_i^{(k)}\big)\big)^{\top}\boldsymbol{W}_i^{-1}\big(\boldsymbol{y}_i - \boldsymbol{\mu}_i\big(\widehat{\boldsymbol{\theta}}_n, U_i^{(k)}\big)\big)\Big] \quad (13)$$

is the residual sum of squares, and

$$d(\lambda_n) = tr\Big[\Big\{\frac{1}{N}\sum_{k=1}^{N}\Big[\boldsymbol{H}_n\big(\widehat{\boldsymbol{\theta}}_n, \boldsymbol{U}^{(k)}\big)\Big] + n\boldsymbol{E}_n(\widehat{\boldsymbol{\theta}}_n)\Big\}^{-1} \times \Big\{\frac{1}{N}\sum_{k=1}^{N}\Big[\boldsymbol{H}_n\big(\widehat{\boldsymbol{\theta}}_n, \boldsymbol{U}^{(k)}\big)\Big]\Big\}\Big]$$

is the effective number of parameters. Then, λ_{opt} is the minimizer of the GCV_{λ_n}.

Note that $\boldsymbol{W}_i$ in (13) is an $n_i \times n_i$ covariance matrix of $\boldsymbol{y}_i$, that can be computed as $\boldsymbol{W}_i = \mathrm{E}_{u|y}\Big(\mathrm{var}(\boldsymbol{y}_i|\boldsymbol{u}_i)\Big) + \mathrm{var}_{u|y}\Big(\mathrm{E}(\boldsymbol{y}_i|\boldsymbol{u}_i)\Big)$, where

$$\begin{aligned}
\mathrm{E}_{u|y}\Big(\mathrm{var}(\boldsymbol{y}_i|\boldsymbol{u}_i)\Big) &= \mathrm{E}_{u|y}\Big(\boldsymbol{V}_i(\widehat{\boldsymbol{\theta}}_n, \boldsymbol{u}_i)\Big) = \frac{1}{N}\sum_{k=1}^{N}\Big[\boldsymbol{V}_i(\widehat{\boldsymbol{\theta}}_n, U_i^{(k)})\Big],\\
\mathrm{var}_{u|y}\Big(\mathrm{E}(\boldsymbol{y}_i|\boldsymbol{u}_i)\Big) &= \mathrm{var}_{u|y}\Big(\boldsymbol{\mu}_i(\widehat{\boldsymbol{\theta}}_n, \boldsymbol{u}_i)\Big)\\
&= \mathrm{E}_{u|y}\Big(\boldsymbol{\mu}_i(\widehat{\boldsymbol{\theta}}_n, \boldsymbol{u}_i)\Big)^2 - \mathrm{E}^2_{u|y}\Big(\boldsymbol{\mu}_i(\widehat{\boldsymbol{\theta}}_n, \boldsymbol{u}_i)\Big)\\
&= \frac{1}{N}\sum_{k=1}^{N}\Big[\boldsymbol{\mu}_i(\widehat{\boldsymbol{\theta}}_n, U_i^{(k)})\Big]^2 - \Big[\frac{1}{N}\sum_{k=1}^{N}\Big[\boldsymbol{\mu}_i(\widehat{\boldsymbol{\theta}}_n, U_i^{(k)})\Big]\Big]^2.
\end{aligned}$$

3.3 Asymptotic Properties

In this section, we study the asymptotic properties of the estimator $\widehat{\boldsymbol{\beta}}$ under the proposed penalized estimating equations. Consider the framework where the true value of $\boldsymbol{\beta}_0$ is partitioned as $\boldsymbol{\beta}_0 = (\boldsymbol{\beta}_{01}^\top, \boldsymbol{\beta}_{02}^\top)^\top$ and the corresponding design matrix into $\boldsymbol{X}_i = \big(\boldsymbol{X}_{i(1)}, \boldsymbol{X}_{i(2)}\big)$. In our study, the true regression coefficients are $\boldsymbol{\theta}_{n0} = (\boldsymbol{\beta}_{01}^\top, \boldsymbol{\beta}_{02}^\top, \boldsymbol{\alpha}_0^\top)^\top$, where $\boldsymbol{\alpha}_0$ is an h_n-dimensional vector depending on f_0. For technical convenience let $\boldsymbol{\theta}_0 = (\boldsymbol{\theta}_{01}^\top, \boldsymbol{\theta}_{02}^\top)^\top$ where $\boldsymbol{\theta}_{01} = (\boldsymbol{\beta}_{01}^\top, \boldsymbol{\alpha}_0^\top)^\top$ is $(s = s^* + h_n)$-dimensional vector of true values that the elements are all nonzero and $\boldsymbol{\theta}_{02} = \boldsymbol{\beta}_{02} = \boldsymbol{0}$. Here, s^* is the dimention of $\boldsymbol{\theta}_{01}$ and assume that only a small number of covariates contribute to the response i.e. $\jmath^* = \{1 \le j \le p; \beta_j \ne 0\}$ has cordiality $|s| = s^* < p$. Consequently, estimated values and the design matrix is re-partitioned as $\widehat{\boldsymbol{\theta}}_n = (\widehat{\boldsymbol{\theta}}_{n1}^\top, \widehat{\boldsymbol{\theta}}_{n2}^\top)^\top$, and $\boldsymbol{D}_i = \big(\boldsymbol{D}_{i(1)}^\top, \boldsymbol{D}_{i(2)}^\top\big)^\top$ which $\widehat{\boldsymbol{\theta}}_{n1} = (\widehat{\boldsymbol{\beta}}_{n1}^\top, \widehat{\boldsymbol{\alpha}}_n^\top)^\top$, $\boldsymbol{D}_{i(1)} = \big(\boldsymbol{X}_{i(1)}^\top, \boldsymbol{B}(\boldsymbol{t}_i)^\top\big)^\top$, $\widehat{\boldsymbol{\theta}}_{n2} = \widehat{\boldsymbol{\beta}}_{n2}$ and $\boldsymbol{D}_{i(2)} = \boldsymbol{X}_{i(2)}$.

Meanwhile, If Eq. (9) has multiple solutions, only a sequence of consistent estimator $\widehat{\boldsymbol{\theta}}_n$ is considered. A sequence $\widehat{\boldsymbol{\theta}}_n$ is said to be a consistent sequence, if $\widehat{\boldsymbol{\beta}}_n - \boldsymbol{\beta}_{n0} \to \boldsymbol{0}$ and $\sup_t |\boldsymbol{B}^\top(t)\widehat{\boldsymbol{\alpha}}_n - f_0(t)| \to \boldsymbol{0}$ in probability as $n \to \infty$.

The following regularity conditions are required for the main results.

(A.1) n_i is a bounded sequence of positive integers, and the distinct values of t_{ij} form a quasi-uniform sequence that grows dense on [0, 1], and the kth derivative of $\boldsymbol{f}_0(\boldsymbol{t}_i)$ is bounded for some $k \geq 2$;

(A.2) The unknown parameter $\boldsymbol{\beta}_n$ belongs to a compact subset $\mathcal{B} \subseteq \mathcal{R}^p$, the true parameter value $\boldsymbol{\beta}_{n0}$ lies in the interior of $\mathcal{B}$;

(A.3) There exist two positive constants, b_1 and b_2, such that

$$b_2 \leq \lambda_{\min}\left(n^{-1}\sum_{i=1}^{n}\boldsymbol{X}_i^\top \boldsymbol{X}_i\right) \leq \lambda_{\max}\left(n^{-1}\sum_{i=1}^{n}\boldsymbol{X}_i^\top \boldsymbol{X}_i\right) \leq b_3,$$

where $\lambda_{\min}$(resp. $\lambda_{\max}$) denotes the minimum (resp. maximum) eigenvalue of a matrix;

(A.4) The common true correlation matrix $\boldsymbol{R}_0$ has eigenvalues bounded away from zero and $+\infty$; the estimated working correlation matrix $\overline{\boldsymbol{R}}$ satisfies $\|\widehat{\boldsymbol{R}}^{-1} - \overline{\boldsymbol{R}}^{-1}\| = O_p(n^{-1/2})$, where $\overline{\boldsymbol{R}}$ is a constant positive definite matrix with eigenvalues bounded away from zero and $+\infty$; we do not require $\overline{\boldsymbol{R}}$ to be the true correlation matrix $\boldsymbol{R}_0$;

(A.5) Let $\boldsymbol{\epsilon}_i(\boldsymbol{\theta}_n, \boldsymbol{u}_i) = \big(\epsilon_{i1}(\boldsymbol{\theta}_n, \boldsymbol{u}_i), \ldots, \epsilon_{in_i}(\boldsymbol{\theta}_n, \boldsymbol{u}_i)\big)^\top = \boldsymbol{A}_i^{-1/2}(\boldsymbol{\theta}_n, \boldsymbol{u}_i)\big(\boldsymbol{Y}_i - \boldsymbol{\mu}_i(\boldsymbol{\theta}_n, \boldsymbol{u}_i)\big)$. There exists a finite constant $M_1 > 0$ such that $\mathrm{E}(\|\boldsymbol{\epsilon}_i(\boldsymbol{\theta}_{n0}, \boldsymbol{u}_i)\|^{2+\delta}) \leq M_1$, for all i and some $\delta > 0$; and there exist positive constants M_2 and M_3 such that $\mathrm{E}\Big[\exp\big(M_2|\epsilon_{ij}(\boldsymbol{\theta}_{n0}, \boldsymbol{u}_i)|\big)\big|\boldsymbol{X}_i\Big] \leq M_3$, uniformly in $i = 1, \ldots, n$, $j = 1, \ldots, m$;

(A.6) Let $B_n = \{\boldsymbol{\theta}_n : \|\boldsymbol{\theta}_n - \boldsymbol{\theta}_{n0}\| \leq \Delta\sqrt{p_n/n}$, then $\boldsymbol{\mu}^{\cdot}(\boldsymbol{D}_{ij}^\top\boldsymbol{\theta}_n)$, $1 \leq i \leq n$, $1 \leq j \leq m$, are uniformly bounded away from 0 and ∞ on B_n; $\boldsymbol{\mu}^{\cdot\cdot}(\boldsymbol{D}_{ij}^\top\boldsymbol{\theta}_n)$ and $\boldsymbol{\mu}^{(3)}(\boldsymbol{D}_{ij}^\top\boldsymbol{\theta}_n)$, $1 \leq i \leq n$, $1 \leq j \leq m$, are uniformly bounded by a finite positive constant M_2 on B_n;

(A.7) Assuming $\min_{1\leq k\leq s_n}|\theta_{n0k}|/\lambda_n \to \infty$ as $n \to \infty$ and $\lambda_n \to 0$, $(\log n)^2 = o(n\lambda_n^2)$, $(\log n)^6 = o(n^2\lambda_n^2)$ and $(\log n)^8 = o(n^2\lambda_n^4)$.

Under (A.1), the total sample size n is of the same order as the number of subjects m and there exists only local dependence in the sample. The smoothness condition on f_0 given by (A.1) determines the rate of convergence of the spline estimate $\widehat{f}(t) = \boldsymbol{B}(\boldsymbol{t})^\top\widehat{\boldsymbol{\alpha}}_n$. When $m = 1$ (i.e., each subject has only one observation), condition (A.3) is also popularly adopted in the literature on regression for independent data. Condition (A.4) is a similar assumption in the Liang and Zeger (1986), assumes that the estimator of the working correlation matrix parameter $\widehat{\boldsymbol{\tau}}$ satisfies $\sqrt{n}(\widehat{\boldsymbol{\tau}} - \boldsymbol{\tau}_0) = O_p(1)$ for some $\boldsymbol{\tau}_0$. Note that when a nonparametric moment estimator is used for the working correlation matrix, we have $\overline{\boldsymbol{R}} = \boldsymbol{R}_0$. The first part of condition (A.5) is similar to the condition in Lemma 2 of Xie and Yang (2003) and condition $(\tilde{N}_\delta)$ in Balan and Schiopu-Kratina (2005); the second part is satisfied for Gaussian distribution, sub-Gaussian distribution, and Poisson distribution, etc. Condition (A.6) requires $\mu_{ij}^{(k)}(\boldsymbol{D}_{ij}^\top\boldsymbol{\theta}_n)$, which denotes the kth derivative of $\mu_{ij}^{(k)}(t)$ evaluated at $\boldsymbol{D}_{ij}^\top\boldsymbol{\theta}_n$, to be uniformly bounded when $\boldsymbol{\theta}_n$ is in a local neighborhood

around $\boldsymbol{\theta}_{n0}$, $k = 1, 2, 3$. This condition is generally satisfied for the GEE. For example, when the marginal model follows a Poisson distribution, $\mu(t) = exp(t)$; thus $\mu_{ij}^{(k)}(\boldsymbol{D}_{ij}^{\top}\boldsymbol{\theta}_n) = exp(\boldsymbol{D}_{ij}^{\top}\boldsymbol{\theta}_n)$, $k = 1, 2, 3$, are uniformly bounded around $\boldsymbol{\theta}_{n0}$ on B_n.

Now, consider the following estimating equation

$$\overline{\boldsymbol{S}}_n(\boldsymbol{\theta}) = \mathrm{E}_{u|y}\Big[\sum_{i=1}^{n} \boldsymbol{D}_i^{\top} \boldsymbol{A}_i^{\frac{1}{2}}(\boldsymbol{\theta}, \boldsymbol{u}_i)\overline{\boldsymbol{R}}^{-1}\boldsymbol{A}_i^{-\frac{1}{2}}(\boldsymbol{\theta}, \boldsymbol{u}_i)\big(\boldsymbol{y}_i - \boldsymbol{\mu}_i(\boldsymbol{\theta}, \boldsymbol{u}_i)\big)\Big].$$

Let $\overline{\boldsymbol{M}}_n(\boldsymbol{\theta}_n)$ to be the covariance matrix of $\overline{\boldsymbol{S}}_n(\boldsymbol{\theta})$, then

$$\overline{\boldsymbol{M}}_n(\boldsymbol{\theta}) = \mathrm{E}_{u|y}\Big[\sum_{i=1}^{n} \boldsymbol{D}_i^{\top} \boldsymbol{A}_i^{\frac{1}{2}}(\boldsymbol{\theta}, \boldsymbol{u}_i)\overline{\boldsymbol{R}}^{-1}\boldsymbol{R}_0\overline{\boldsymbol{R}}^{-1}\boldsymbol{A}_i^{\frac{1}{2}}(\boldsymbol{\theta}, \boldsymbol{u}_i)\boldsymbol{D}_i\Big].$$

By the following Lemma 1, we approximate $f_0(t)$ by $\boldsymbol{B}(t)\boldsymbol{\alpha}_0$; then have

$$\eta_{ij}(\boldsymbol{\theta}_0) = g\big(\mu_{ij}(\boldsymbol{\theta}_0)\big) = \boldsymbol{X}_{ij}^{\top}\boldsymbol{\beta}_0 + \boldsymbol{B}(t_{ij})\boldsymbol{\alpha}_0 + \boldsymbol{Z}_{ij}^{\top}\boldsymbol{u}_i, \quad \boldsymbol{\theta}_0 = (\boldsymbol{\beta}_0^{\top}, \boldsymbol{\alpha}_0^{\top})_{(p_n+N)\times 1}^{\top}$$

Lemma 1 *Under condition (A.1), there exists a constant C such that*

$$\sup_{t\in[0,1]} |f_0(t) - \boldsymbol{B}(t)\boldsymbol{\alpha}_0| \le CL_n^{-r},$$

where $\boldsymbol{\alpha}_0$ *is a N-dimensional vector depending on* f_0.

The proof of this lemma follows readily from Theorem 12.7 of Schumaker (1981).

The following theorem shows under the regularity conditions, all the covariates with zero coefficients can be detected simultaneously with probability tending to 1, and the estimators of all the non-zero coefficients are asymptotically normally distributed.

Theorem 1 (Oracle Properties) *Assume conditions (A.1)–(A.7), if the number of knots* $L_n = O_p(n^{1/(2r+1)})$, *then* $\forall \boldsymbol{\xi}_n \in \mathcal{R}^p$ *such that* $\|\boldsymbol{\xi}_n\| = 1$, *we have*

$$(Sparsity) \qquad P(\widehat{\boldsymbol{\beta}}_{n2} = \boldsymbol{0}) \to 1$$

$$(Asymptoticnormality) \qquad \boldsymbol{\xi}_n^{\top}\overline{\boldsymbol{M}}_n^{*^{-1/2}}(\boldsymbol{\beta}_{n0})\overline{\boldsymbol{H}}_n^{*}(\boldsymbol{\beta}_{n0})(\widehat{\boldsymbol{\beta}}_{n1} - \boldsymbol{\beta}_{n01}) \xrightarrow{D} N(0, 1)$$

where

$$\overline{\boldsymbol{M}}_n^{*} = E_{u|y}\Big[\sum_{i=1}^{n} \boldsymbol{X}_i^{*^{\top}} \boldsymbol{A}_i^{\frac{1}{2}}(\boldsymbol{\theta}_n, \boldsymbol{u}_i)\overline{\boldsymbol{R}}^{-1}\boldsymbol{R}_0\overline{\boldsymbol{R}}^{-1}\boldsymbol{A}_i^{\frac{1}{2}}(\boldsymbol{\theta}_n, \boldsymbol{u}_i)\boldsymbol{X}_i^{*}\Big], \quad \boldsymbol{X}_i^{*}=(\boldsymbol{I} - \boldsymbol{P})\boldsymbol{X}_i$$

$$\boldsymbol{P} = \boldsymbol{B}(\boldsymbol{B}^{\top}\boldsymbol{\Omega}\boldsymbol{B})^{-1}\boldsymbol{B}^{\top}\boldsymbol{\Omega}, \ \boldsymbol{\Omega}=diag\{\boldsymbol{\Omega}_i\}, \ \boldsymbol{\Omega}_i=E_{u|y}\Big[\boldsymbol{A}_i^{\frac{1}{2}}(\boldsymbol{\theta}_n, \boldsymbol{u}_i)\overline{\boldsymbol{R}}^{-1}\boldsymbol{A}_i^{\frac{1}{2}}(\boldsymbol{\theta}_n, \boldsymbol{u}_i)\Big],$$

$$\overline{\boldsymbol{H}}_n^{*} = E_{u|y}\Big[\sum_{i=1}^{n} \boldsymbol{X}_i^{*^{\top}} \boldsymbol{A}_i^{\frac{1}{2}}(\boldsymbol{\theta}_n, \boldsymbol{u}_i)\overline{\boldsymbol{R}}^{-1}\boldsymbol{A}_i^{\frac{1}{2}}(\boldsymbol{\theta}_n, \boldsymbol{u}_i)\boldsymbol{X}_i^{*}\Big].$$

Theorem 1 is often referred to as the oracle properties of variable selection, that is, the procedure estimates the true zero coefficient as zero with probability approaching one and estimates the nonzero coefficients as efficiently as if the true model is known in advance.

From Algorithm 1, we obtain the following sandwich formula to estimate the asymptotic covariance matrix of $\widehat{\boldsymbol{\theta}}_n$:

$$\mathrm{Cov}(\widehat{\boldsymbol{\theta}}_n) \approx [\boldsymbol{H}_n(\widehat{\boldsymbol{\theta}}_n, \boldsymbol{u}_i) + n\boldsymbol{E}_n(\widehat{\boldsymbol{\theta}}_n)]^{-1}\boldsymbol{M}_n(\widehat{\boldsymbol{\theta}}_n, \boldsymbol{u}_i)[\boldsymbol{H}_n(\widehat{\boldsymbol{\theta}}_n, \boldsymbol{u}_i) + n\boldsymbol{E}_n(\widehat{\boldsymbol{\theta}}_n, \boldsymbol{u}_i)]^{-1},$$

where $\boldsymbol{H}_n$ and $\boldsymbol{E}_n$ are defined in Sect. 3, and

$$\boldsymbol{M}_n(\widehat{\boldsymbol{\theta}}_n, \boldsymbol{u}_i) = \sum_{i=1}^{n} \boldsymbol{D}_i^{\top} \boldsymbol{A}_i^{1/2}(\widehat{\boldsymbol{\theta}}_n, \boldsymbol{u}_i)\widehat{\boldsymbol{R}}^{-1}\left[\boldsymbol{\epsilon}_i(\widehat{\boldsymbol{\theta}}_n, \boldsymbol{u}_i)\boldsymbol{\epsilon}_i^{\top}(\widehat{\boldsymbol{\theta}}_n, \boldsymbol{u}_i)\right]\widehat{\boldsymbol{R}}^{-1}\boldsymbol{A}_i^{1/2}(\widehat{\boldsymbol{\theta}}_n, \boldsymbol{u}_i)\boldsymbol{D}_i^{\top}.$$

4 Numerical Studies

In this section, we consider some simulation studies to investigate the performance of the proposed penalized estimating equations. We also apply our proposed method to analyze a real longitudinal data set.

4.1 Simulation Studies

We conduct simulations to evaluate the performance of the proposed penalized GPLMM (P-GPLMM) procedure for both normal and poisson responses. Throughout our simulation study, the dimensionality of the parametric component is taken as $p_n = [4.5n^{1/4}]$, where $[a]$ stands for the largest integer no larger than a, where three sample size $n = 50, 100$ and 150 were considered. The predictor dimension p_n is diverging but the dimension of the true model is fixed to be 3. For each setup in the simulations, we generate 100 data sets and apply the iterative algorithm in Sect. 3 to estimate parameters. We select the tuning parameter λ_n in the SCAD penalty function using a GCV criterion. Performance of the proposed P-GPLMM procedure compared with the unpenalized GPLMM and the penalized GLMM (P-GLMM), where each simulated data set was fitted under these three methods.

For evaluating estimation accuracy, we report the empirical mean square error (MSE), defined as $\sum_{k=1}^{100} \|\widehat{\boldsymbol{\beta}}_n^k - \boldsymbol{\beta}_{n0}\|/100$ where $\widehat{\boldsymbol{\beta}}_n^k$ is the estimator of $\boldsymbol{\beta}_{n0}$ obtained using the k-th generated data set. The performance of variable selection is checked by (C, I), where "C" is the mean over all 100 simulations of zero coefficients which are correctly estimated by zero and "I" is the mean over all 100 simulations of nonzero coefficients which are incorrectly estimated by zero. To present a more comprehensive picture, we also use other criteria for variable selection performance

evaluation. "Under-fit" corresponds to the proportion of excluding any true nonzero coefficients. Similarly, we report the proportion of selecting the exact subset model as "Correct-fit" and the proportion of including all three important variables plus some noise variables as "Over-fit".

Example 1

The underlying model is the random intercept Poisson model so that the nonlinear function is set to a sinusoidal function;

$$y_{ij}|b_i \sim \text{Pois}(\mu_{ij}), \qquad i = 1, \ldots, n, \quad j = 1, \ldots, n_i,$$
$$\eta_{ij} = \log(\mu_{ij}) = \sum_{k=1}^{p} x_{ij}^{(k)} \beta_k + \sin(2\pi t_{ij}) + b_i,$$

where $i = 1, \ldots, n$, and $j = 1, \ldots, n_i$, and the number of observations per subjects is assumed to be fixed at $n_i = 5$. The true regression coefficient are $\boldsymbol{\beta} = (-1, -1, 2, 0, \ldots, 0)$ with the mutually independent covariates $\boldsymbol{X}_{ij}^{\top} = (x_{ij}^{(1)}, \ldots, x_{ij}^{(p)})$ drawn independently from the uniform distribution on $(-1, 1)$. The measurement time points t_{ij} are also drawn from the uniform distribution on $(0, 1)$. The random effect process b_i is taken to be a Gaussian process with mean 0 and variance $\sigma^2 = 0.25$.

The results of Table 1 summarize the estimation accuracy and model selection properties of the competitive models for three different values of sample size. In terms of estimation accuracy the penalized GPLMM procedure performs closely

Table 1 Simulation results for the Poisson response: comparison of the P-GPLMM, GPLMM, and P-GLMM with sample sizes $n = 50$, 100, and 150

	$n = 50$, $p = 11$					
Method	MSE	C(8)	I(0)	Under-fit	Correct-fit	Over-fit
GPLMM	0.116	0.09	0.00	0.00	0.00	1.00
P-GLMM	0.060	6.54	0.00	0.00	0.13	0.87
P-GPLMM	0.052	7.59	0.00	0.00	0.64	0.36
	$n = 100$, $p = 14$					
Method	MSE	C(11)	I(0)	Under-fit	Correct-fit	Over-fit
GPLMM	0.072	0.16	0.00	0.00	0.00	1.00
P-GLMM	0.041	10.52	0.00	0.00	0.61	0.39
P-GPLMM	0.036	10.70	0.00	0.00	0.77	0.23
	$n = 150$, $p = 15$					
Method	MSE	C(12)	I(0)	Under-fit	Correct-fit	Over-fit
GPLMM	0.060	0.26	0.00	0.00	0.00	1.00
P-GLMM	0.044	11.25	0.00	0.00	0.42	0.58
P-GPLMM	0.045	11.87	0.00	0.00	0.87	0.13

Table 2 Simulation results for the Poisson response: performance of the P-GPLMM with sample sizes $n = 50$, 100, and 150

		β_1	β_2	β_3
$n = 50$, $p = 11$	Bias	0.047	0.096	0.069
	SD1	0.092	0.085	0.113
	SD2	0.097	0.094	0.097
	CP	0.96	0.95	0.92
$n = 100$, $p = 14$	Bias	0.076	0.103	0.053
	SD1	0.071	0.067	0.084
	SD2	0.072	0.067	0.078
	CP	0.96	0.95	0.96
$n = 150$, $p = 15$	Bias	0.101	0.124	0.099
	SD1	0.060	0.059	0.070
	SD2	0.052	0.059	0.059
	CP	0.97	0.96	0.95

Bias absolute value of the empirical bias; *SD1* estimated standard deviation using the sandwich variance estimator; *SD2* sample standard deviation; *CP* the empirical coverage probability of the 95% confidence interval

to the penalized GLMM, whereas our proposed approach gives smallest MSE, and consistently outperforms its penalized GLMM counterpart. In terms of model selection we observe that the unpenalized GPLMM generally does not lead to a sparse model. Furthermore, the penalized GPLMM and the penalized GLMM successfully selects all covariates with nonzero coefficients (i.e., "I" rates are zero), but it is obvious that the proposed approach has slightly stronger sparsity (i.e., a fairly higher number of Cs) than the penalized GLMM. For the P-GPLMM, the probability of identifying the exact underlying model is about 80% and this rate grows by increasing the sample size, confirming the good asymptotic properties of the penalized estimators.

To further investigate the performance of the proposed method, Table 2 reports its bias, the estimated standard deviation (calculated from the sandwich variance formula), the empirical standard deviation, and the empirical coverage probability of 95% confidence interval for estimating β_1, β_2, and β_3. The estimated standard deviation is close to the empirical standard deviation, and the empirical coverage probability is close to 95%. These results all together demonstrate the good performance of the sandwich variance formula.

These observations suggest that considering partial part is important to modify the estimation accuracy and model selection when the growth curves of the data exhibit a nonlinear fashion over time, especially in a complicated manner. On the other hand, the P-GPLMM allows us to make systematic inference on all model parameters by representing a partially model as a modified penalized GLMM.

For proposed method, the estimated baseline function $f(t)$ is also evaluated through visualization. We plot and compare the estimated $f(t)$ and pointwise biases, for two sample size $n = 50$ and 100 when the number of parameters (p_n) are set to

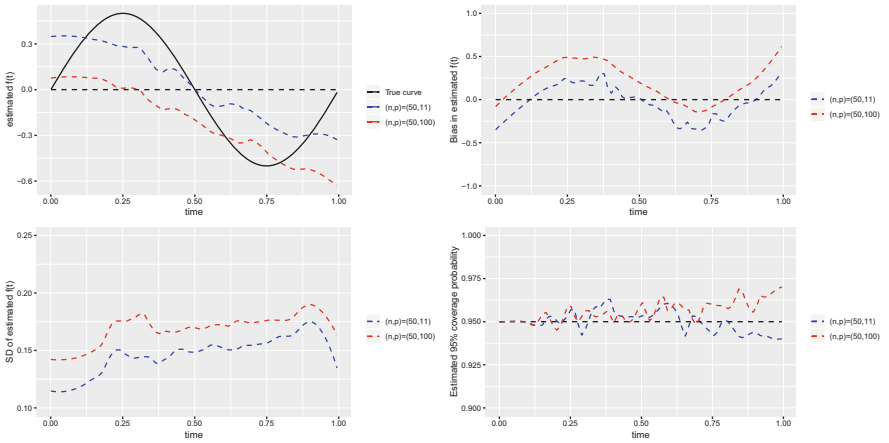

Fig. 1 Plots for estimated $f(t)$ in the $p_n < n$ and $p_n >> n$ cases (n=50) based on 100 samples. Plots top-left and top-right show the averaged fit and pointwise bias; plot bottom-left shows the standard deviation; and plot bottom-right plots the averaged coverage probability rates for 95% confidence intervals

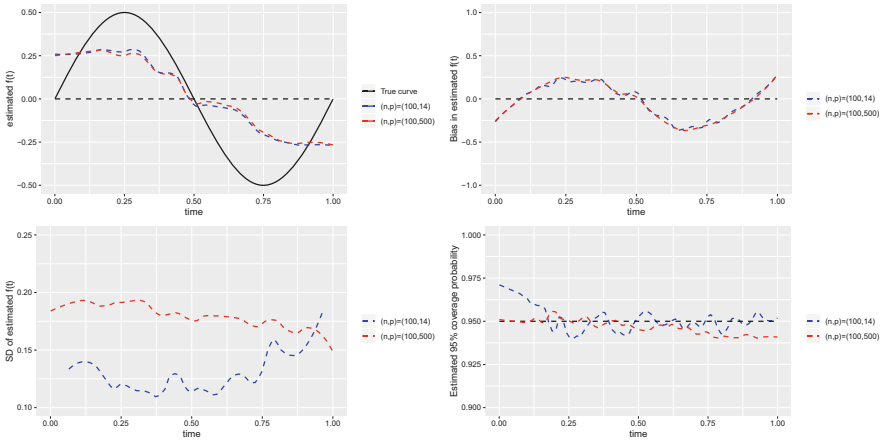

Fig. 2 Plots for estimated $f(t)$ in the $p_n < n$ and $p_n >> n$ cases (n=100) based on 100 samples. Plots top-left and top-right show the averaged fit and pointwise bias; plot bottom-left shows the standard deviation; and plot bottom-right plots the averaged coverage probability rates for 95% confidence intervals

be a small value and a relatively large. We also plot the pointwise standard deviations (calculated from the sandvich variance formula), and coverage probability of 95% confidence intervals. Figure 1 shows that when the p_n is small value, our approach yields smaller overall biases and standard deviations in comparing with the large p_n. Also, it can be seen that the empirical coverage probability for $f(t)$ is close to 95% for two cases. Figure 2 depicts the results for $n = 100$. As shown, larger sample size

modified the biases and the differences between two cases. Nevertheless, the case of small value of p_n has smaller standard deviation.

Example 2

The normal responses are generated from the model

$$y_{ij} = \sum_{k=1}^{p} x_{ij}^{(k)} \beta_k + \sin(2\pi t_{ij}) + b_i + \epsilon_{ij},$$

where the random errors $(\epsilon_{i1}, \ldots, \epsilon_{in_i})^\top$ are generated from the multivariate normal distribution with standard marginals (mean 0, variance 1) and $\boldsymbol{\beta} = (2, 1, 0.5, 0, \ldots, 0)$. The other components of the model are generated the same as in Example 1. Note that Example 2 is more challenging than Example 1 because of inclusion the small signal ($\beta_3 = 0.5$) in the nonzero coefficients.

The results for estimation accuracy and model selection properties of the normal response summarized in Table 3. We observe that the penalized method significantly improves the estimation accuracy of the unpenalized one. In terms of model selection, we observe that the unpenalized method does not lead to a sparse model. The P-GPLMM has small MSE, high C rate, and low I rate for variable selection in comparison to the P-GLMM. We also observe that the P-GLMM has higher chance ($I = 0.12$) to miss the small signal ($\beta_3 = 0.5$) in contrast to P-GPLMM ($I = 0.08$). In addition, estimation accuracy and model selection properties of

Table 3 Simulation results for the normal response: comparison of the P-GPLMM, GPLMM, and P-GLMM with sample sizes $n = 50$, 100, and 150

	$n = 50$, $p = 11$					
Method	MSE	C(8)	I(0)	Under-fit	Correct-fit	Over-fit
GPLMM	0.508	0.01	0.00	0.00	0.00	1.00
P-GLMM	0.219	7.77	0.40	0.12	0.49	0.39
P-GPLMM	0.202	7.84	0.35	0.10	0.55	0.35
	$n = 100$, $p = 14$					
Method	MSE	C(11)	I(0)	Under-fit	Correct-fit	Over-fit
GPLMM	0.339	0.01	0.00	0.00	0.00	1.00
P-GLMM	0.109	10.80	0.12	0.12	0.70	0.18
P-GPLMM	0.106	10.83	0.08	0.08	0.76	0.16
	$n = 150$, $p = 15$					
Method	MSE	C(12)	I(0)	Under-fit	Correct-fit	Over-fit
GPLMM	0.251	0.02	0.00	0.00	0.00	1.00
P-GLMM	0.087	11.93	0.12	0.12	0.82	0.06
P-GPLMM	0.079	11.93	0.08	0.08	0.84	0.07

Table 4 Simulation results for the normal response: performance of the P-GPLMM with sample sizes $n = 50$, 100, and 150

		β_1	β_2	β_3
$n = 50$, $p = 11$	Bias	0.014	0.022	0.181
	SD1	0.171	0.198	0.124
	SD2	0.175	0.222	0.258
	CP	0.95	0.96	0.97
$n = 100$, $p = 14$	Bias	0.027	0.035	0.096
	SD1	0.126	0.145	0.100
	SD2	0.120	0.167	0.212
	CP	0.95	0.98	0.98
$n = 150$, $p = 15$	Bias	0.006	0.002	0.143
	SD1	0.107	0.119	0.076
	SD2	0.114	0.142	0.174
	CP	0.94	0.97	0.96

Bias absolute value of the empirical bias; *SD1* estimated standard deviation using the sandwich variance estimator; *SD2* sample standard deviation; *CP* the empirical coverage probability of the 95% confidence interval

all competitive models improve by increasing the sample size. Tables 2, 3, and 4 report the bias, estimated standard deviation (calculated from the sandwich variance formula), empirical standard deviation, and empirical coverage probability of 95% confidence interval for estimating β_i, $i = 1, 2, 3$, when the P-GPLMM procedure is applied. The empirical coverage probabilities are close to 95%, the estimated standard deviation is also close to the empirical standard deviation for β_1 and β_2, and the estimated standard deviation is smaller in comparison to the empirical standard deviation, for the small coefficient β_3.

4.2 CD4 Data Analysis

In this section, to illustrate our method, we consider the longitudinal CD4 cell count data among HIV seroconverters. This dataset contains 2376 observations of CD4 cell counts on 369 men infected with the HIV virus; see Zeger and Diggle (1994) for a detailed description of this dataset. Figure 3 (top-left) displays the trajectories of 369 men for exploring the evolution of CD4 cell counts.

The first objective of this analysis is to characterize the population average time course of CD4 decay while accounting for the following additional predictor variables including AGE, SMOKE (smoking status measured by packs of cigarettes), DRUG (yes, 1; no, 0), SEXP (number of sex partners), DEPRESSION as measured by the CESD scale (larger values indicate increased depressive symptoms) and YEAR (the effect of time since seroconversion). Since there seems to exist a positive correlation among responses from the same patient, we need to incorporate

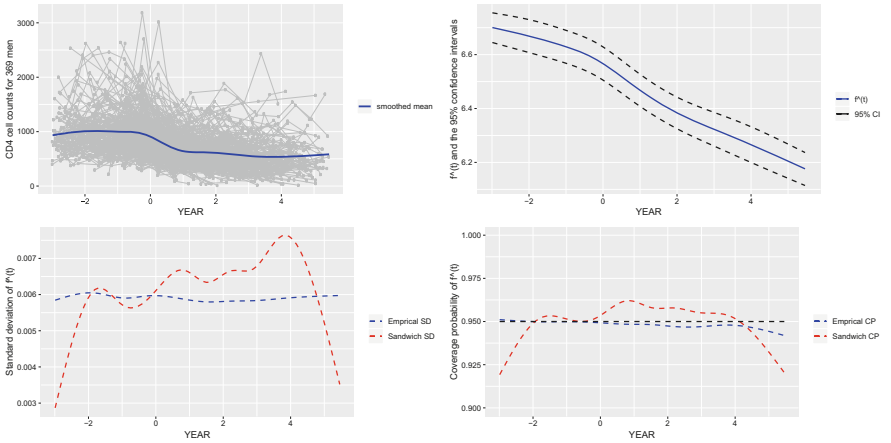

Fig. 3 Plots for estimated $f(t)$ for AIDS data based on P-GSMM. Plot top-left shows the trajectories plot for CD4 data. Observed evolution (in gray) of CD4 cell counts for 369 men against time (in YEAR). Solid (in thick blue) line show the smoothed mean profile of men. Plot top-right shows the estimated baseline function $f(t)$ (in thick blue) in the selected model of P-GSMM and the 95% confidence interval (dashed line) corresponding to the robust confidence interval. Plots bottom-left and bottom-right respectively, show the standard deviation and coverage probability rates for 95% confidence intervals based on empirical variance and sandwich formula

a correlation structure into the estimation scheme. Zeger and Diggle (1994) found that the compound symmetry covariance matrix fitted the data reasonably well. This data analyzed by many authors, e.g. Wang et al. (2005); Huang et al. (2007); Ma et al. (2013), among all. Their analyses was conducted on square root transformed CD4 numbers whose distribution is more nearly Gaussian. In our analysis, we fit our proposed GPLMM to the data, without considering any transformation on the CD4 data, by adopting the Poisson regression. To take advantage of flexibility of the partially linear model, we let YEAR be modeled in a nonparametric fashion. It is of interest to examine whether there are any interaction effects between the parametric covariates, so we included all these interactions in the parametric part. We further applied the proposed approach to select significant variables. We used the SCAD penalty, with the tuning parameter $\lambda = 0.45$. To compare the performance of our proposed method (P-GPLMM) with other two existing alternatives, the unpenalized GPLMM, and the penalized GLMM (P-GLMM), we use the standard error (SE). To best identify a model supported by the data, we adopt the Akaike information criterion (AIC; Akaike 1973) and the Bayesian information criterion (BIC; Schwarz 1978). They are defined as

$$\text{AIC} = 2m - 2\ell_{\max}, \qquad \text{BIC} = m \log n - 2\ell_{\max}, \tag{14}$$

where $\ell_{\max}$ is the maximized log-likelihood value, m is the number of free parameters in the model. Table 5 presents the summary of the results including

Table 5 Summary of parameter estimates along with standard errors (in parentheses) for the three fitted models, for the CD4 data

	GPLMM	P-GLMM	P-GPLMM
Variables	$\widehat{\beta}$(SE)	$\widehat{\beta}$(SE)	$\widehat{\beta}$(SE)
AGE	0.073 (0.039)	−0.092 (0.051)	0 (0)
$SMOKE$	0.188 (0.179)	0.888 (0.192)	0.079 (0.045)
$DRUG$	0.130 (0.143)	6.068(0.125)	0.142 (0.074)
$SEXP$	−0.049 (0.031)	0.672 (0.030)	0.017 (0.012)
$CESD$	−0.001 (0.011)	0 (0)	0 (0)
$AGE * SMOKE$	0.002 (0.014)	0.014 (0.004)	0 (0)
$AGE * DRUG$	−0.034 (0.024)	0.032 (0.035)	0 (0)
$AGE * SEXP$	−0.009 (0.003)	0 (0)	0 (0)
$AGE * CESD$	0.001 (0.002)	0 (0)	0 (0)
$SMOKE * DRUG$	0.009 (0.054)	−0.584 (0.150)	−0.014 (0.038)
$SMOKE * SEXP$	−0.010 (0.012)	−0.034 (0.010)	0 (0)
$SMOKE * CESD$	−0.006 (0.009)	0 (0)	0 (0)
$DRUG * SEXP$	−0.025 (0.019)	−0.598 (0.041)	−0.022 (0.012)
$DRUG * CESD$	0.006 (0.006)	0 (0)	0 (0)
$SEXP * CESD$	0.001 (0.003)	0 (0)	0 (0)
$\ell_{\max}$	8,463,007	7,529,158	8,624,429
AIC	−16,925,983	−15,058,286	−17,248,827
BIC	−16,925,924	−15,058,228	−17,248,769

the values of standard errors, together with $\ell_{\max}$, AIC, and BIC for the three named models.

Judging from Table 5, the P-GPLMM exhibits smaller standard errors compared to the GPLMM and P-GLMM, nevertheless this difference is not dramatic. Meanwhile, the values of AIC, BIC of our proposed model are smaller than those for the other two competing models, revealing that the P-GPLMM can provide better fit. By the P-GPLMM, SMOKE, DRUGS, SEXP, $SOMKE * DRUG$ and $DRUG * SEXP$ are identified as significant covariates. Note that when P-GLMM is used, $AGE * SMOKE$, $AGE * DRUG$, and $SMOKE * SEXP$ may also be significant. We also find some interactions among covariates which may be ignored according to Wang et al. (2005) and Huang et al. (2007). The nonparametric curve estimate using the P-GPLMM estimators is plotted in Fig. 3 for $YEAR$. The Results for nonparametric curve estimates using the P-GSMM estimators are plotted in Fig. 3 for $YEAR$. It shows the estimated nonparametric function $f(t)$, its 95% pointwise confidence bands, standard deviation, and 95% coverage probability given by the empirical and sandwich formula variance. We can see that the baseline function $f(t)$ has decreasing effect as time passing. Therefore, one can see that it is more reasonable to put it as a nonparametric component. We notice the disparity between the empirical and the sandwich formula standard deviation in the boundary positions and the sandwich formula standard deviations are smaller in which case the coverage probability recede from 95%.

5 Concluding Remarks

In general, when the number of covariates is large, identifying the exact underlying model is a challenging task, in particular when some of the nonzero signals are relatively weak. Here, we have developed a general methodology for simultaneously selecting variables and estimating the unknown components in the partially linear mixed effects model for non-normal longitudinal data. We approximate the nonparametric components using polynomial B-spline smoothing, propose a penalized estimating equation approach to do variable selection, and estimate both parametric and nonparametric components in the framework of maximum likelihood estimation. We apply the penalty functions to the estimating equation objective function such that the proposed procedure can simultaneously estimate parameters and select important variables. The procedure involves specification of the posterior distribution of the random effects, which cannot be evaluated in a closed form, and we use a Metropolis algorithm, which does not require the specification of the posterior distribution. To implement the procedure in practice, we designed a computationally flexible iterative algorithm. We further investigated the asymptotic normality of the resulting estimators. To investigate the performance of newly proposed approach, we analyzed and compared with the unpenalized generalized partially linear mixed effects model and penalized linear mixed effects model through a simulation study and CD4 data analysis. Obtained results demonstrated that the proposal works well, and can estimate the nonzero coefficients efficiently.

For the computation of the generalized linear mixed models, we constructed a Monte Carlo version of the EM algorithm, where we proposed a Monte Carlo Newton–Raphson algorithm. Another popular method to maximize GLMMs is the quasi likelihood (QL), which has been suggested by Breslow and Clayton (1993), Breslow and Lin (1995), and Lin and Breslow (1996). For future work, one can employ QL method and compare the performance of this approach with our utilized method. We also refer to Sutradhar (2010) and Sutradhar et al. (2008) for further studies. Another possible future direction is that our work can be extended to the case where the nonparametric components are regularized in an additive model; see Xue (2009) for details.

Appendix: Proof of the Main Result

We write $\overline{\boldsymbol{S}}_n(\boldsymbol{\theta}) = \left(\overline{S}_{n1}(\boldsymbol{\theta}), \ldots, \overline{S}_{np}(\boldsymbol{\theta}_n)\right)^\top$, where $\overline{S}_{nk}(\boldsymbol{\theta}_n) = \boldsymbol{e}_k^\top \overline{\boldsymbol{S}}_n(\boldsymbol{\theta})$, and $\boldsymbol{e}_k$ is a p dimensional basis vector with the kth element being one and all the other elements being zero, $1 \leq k \leq p$. we also use $\overline{D}_{nk}(\boldsymbol{\theta}_n) = -\frac{\partial}{\partial \boldsymbol{\theta}_n^\top} \overline{S}_{nk}(\boldsymbol{\theta}_n)$ and we have $\overline{D}_{nk}(\boldsymbol{\theta}_n) = \overline{H}_{nk}(\boldsymbol{\theta}_n) + \overline{E}_{nk}(\boldsymbol{\theta}_n) + \overline{G}_{nk}(\boldsymbol{\theta}_n)$ where $\overline{H}_{nk}$, $\overline{E}_{nk}$ and $\overline{G}_{nk}$ denotes the kth element of $\overline{\boldsymbol{H}}_n$, $\overline{\boldsymbol{E}}_n$ and $\overline{\boldsymbol{G}}_n$ and defined similarly to $\overline{S}_{nk}$. In the following, we first present some useful lemmas. The proofs are similar to those in Wang (2011).

To facilitate the Taylor expansion of the estimating function $\boldsymbol{S}_n(\boldsymbol{\theta}_n)$, we also use $\overline{\boldsymbol{D}}_n(\boldsymbol{\theta}_n) = \frac{\partial}{\partial \boldsymbol{\theta}_n^\top}\overline{\boldsymbol{S}}_n(\boldsymbol{\theta}_n)$ to approximate the negative gradient function $\boldsymbol{D}_n(\boldsymbol{\theta}_n) = \frac{\partial}{\partial \boldsymbol{\theta}_n^\top}\boldsymbol{S}_n(\boldsymbol{\theta}_n)$.

Lemma 2

$$\overline{\boldsymbol{D}}_n(\boldsymbol{\theta}_n) = \overline{\boldsymbol{H}}_n(\boldsymbol{\theta}_n) + \overline{\boldsymbol{E}}_n(\boldsymbol{\theta}_n) + \overline{\boldsymbol{G}}_n(\boldsymbol{\theta}_n), \tag{15}$$

where

$$\overline{\boldsymbol{H}}_n(\boldsymbol{\theta}_n) = -n^{-1}E_{u|y}\Big[\sum_{i=1}^{n}\boldsymbol{D}_i^\top \boldsymbol{A}_i^{\frac{1}{2}}(\boldsymbol{\theta}_n,\boldsymbol{u}_i)\overline{\boldsymbol{R}}^{-1}\boldsymbol{A}_i^{\frac{1}{2}}(\boldsymbol{\theta}_n,\boldsymbol{u}_i)\boldsymbol{D}_i\Big],$$

$$\overline{\boldsymbol{E}}_n(\boldsymbol{\theta}_n) = -(2n)^{-1}E_{u|y}\Big[\sum_{i=1}^{n}\boldsymbol{D}_i^\top \boldsymbol{A}_i^{\frac{1}{2}}(\boldsymbol{\theta}_n,\boldsymbol{u}_i)\overline{\boldsymbol{R}}^{-1}\boldsymbol{A}_i^{\frac{-3}{2}}(\boldsymbol{\theta}_n,\boldsymbol{u}_i)\boldsymbol{C}_i(\boldsymbol{\theta}_n,\boldsymbol{u}_i)\boldsymbol{F}_i(\boldsymbol{\theta}_n,\boldsymbol{u}_i)\boldsymbol{D}_i\Big],$$

$$\overline{\boldsymbol{G}}_n(\boldsymbol{\theta}_n) = (2n)^{-1}E_{u|y}\Big[\sum_{i=1}^{n}\boldsymbol{D}_i^\top \boldsymbol{A}_i^{\frac{1}{2}}(\boldsymbol{\theta}_n,\boldsymbol{u}_i)\boldsymbol{F}_i(\boldsymbol{\theta}_n,\boldsymbol{u}_i)\boldsymbol{J}_i(\boldsymbol{\theta}_n,\boldsymbol{u}_i)\boldsymbol{D}_i\Big],$$

with

$$\boldsymbol{C}_i(\boldsymbol{\theta}_n,\boldsymbol{u}_i) = \operatorname{diag}\Big(\boldsymbol{y}_{i1} - \boldsymbol{\mu}_{i1}(\boldsymbol{\theta}_n,\boldsymbol{u}_i),\ldots,\boldsymbol{y}_{im} - \boldsymbol{\mu}_{im}(\boldsymbol{\theta}_n,\boldsymbol{u}_i)\Big),$$

$$\boldsymbol{F}_i(\boldsymbol{\theta}_n,\boldsymbol{u}_i) = \operatorname{diag}\Big(\boldsymbol{\mu}^{\cdot\cdot}(\boldsymbol{D}_{i1}^\top\boldsymbol{\theta}_n + \boldsymbol{Z}_{i1}^\top\boldsymbol{u}_i),\ldots,\boldsymbol{\mu}^{\cdot\cdot}(\boldsymbol{D}_{im}^\top\boldsymbol{\theta}_n + \boldsymbol{Z}_{im}^\top\boldsymbol{u}_i)\Big),$$

$$\boldsymbol{J}_i(\boldsymbol{\theta}_n,\boldsymbol{u}_i) = \operatorname{diag}\Big(\overline{\boldsymbol{R}}_i^{-1}\boldsymbol{A}_i^{\frac{1}{2}}(\boldsymbol{\theta}_n,\boldsymbol{u}_i)\big(\boldsymbol{y}_i - \boldsymbol{\mu}_i(\boldsymbol{\theta}_n,\boldsymbol{u}_i)\big)\Big),$$

In above, for $a = (a_1,\ldots,a_{n_i})^\top$, $\operatorname{diag}(a_1,\ldots,a_m)$ *and* $\operatorname{diag}(\boldsymbol{a})$ *both denote an* $m \times m$ *diagonal matrix with diagonal entries* $(a_1,\ldots,a_m)$.

Lemma 3 *Assume conditions (A2)–(A7), then* $\forall\Delta > 0$, *for* $\boldsymbol{b}_n \in \mathcal{R}^p$, *we have*

$$\sup_{\|\boldsymbol{\theta}_n-\boldsymbol{\theta}_{n0}\|\le\Delta\sqrt{p_n/n}}\ \sup_{\|\boldsymbol{b}_n\|=1}\Big|\boldsymbol{b}_n^\top\big[\boldsymbol{D}_n(\boldsymbol{\theta}_n) - \overline{\boldsymbol{D}}_n(\boldsymbol{\theta}_n)\big]\boldsymbol{b}_n\Big| = O_p(\sqrt{n}).$$

Remark 1 The matrix $\boldsymbol{D}_n(\boldsymbol{\theta}_n) - \overline{\boldsymbol{D}}_n(\boldsymbol{\theta}_n)$ is symmetric. The above lemma immediately implies that

$$\sup_{\|\boldsymbol{\theta}_n-\boldsymbol{\theta}_{n0}\|\le\Delta\sqrt{p_n/n}}\Big|\lambda_{\min}\big[\boldsymbol{D}_n(\boldsymbol{\theta}_n) - \overline{\boldsymbol{D}}_n(\boldsymbol{\theta}_n)\big]\Big| = O_p(\sqrt{n}),$$

$$\sup_{\|\boldsymbol{\theta}_n-\boldsymbol{\theta}_{n0}\|\le\Delta\sqrt{p_n/n}}\Big|\lambda_{\max}\big[\boldsymbol{D}_n(\boldsymbol{\theta}_n) - \overline{\boldsymbol{D}}_n(\boldsymbol{\theta}_n)\big]\Big| = O_p(\sqrt{n}).$$

Furthermore, we can use the leading term $\overline{\boldsymbol{H}}_n(\boldsymbol{\theta}_n)$ in (15) to approximate the negative gradient function $\overline{\boldsymbol{D}}_n(\boldsymbol{\theta}_n)$. This result is given by Lemma 4 below. Lemma 5 further establishes an equicontinuity result for $\overline{\boldsymbol{H}}_n(\boldsymbol{\theta}_n)$.

Lemma 4 *Assume conditions (A2)–(A7), then* $\forall \Delta > 0$, *for* $\boldsymbol{b}_n \in \mathcal{R}^p$, *we have*

$$\sup_{\|\boldsymbol{\theta}_n - \boldsymbol{\theta}_{n0}\| \le \Delta\sqrt{p_n/n}} \sup_{\|\boldsymbol{b}_n\|=1} \left| \boldsymbol{b}_n^\top \left[\overline{\boldsymbol{D}}_n(\boldsymbol{\theta}_n) - \overline{\boldsymbol{H}}_n(\boldsymbol{\theta}_n) \right] \boldsymbol{b}_n \right| = O_p(\sqrt{n}).$$

Lemma 5 *Assume conditions (A2)–(A7), then* $\forall \Delta > 0$, *for* $\boldsymbol{b}_n \in \mathcal{R}^p$, *we have*

$$\sup_{\|\boldsymbol{\theta}_n - \boldsymbol{\theta}_{n0}\| \le \Delta\sqrt{p_n/n}} \sup_{\|\boldsymbol{b}_n\|=1} \left| \boldsymbol{b}_n^\top \left[\overline{\boldsymbol{H}}_n(\boldsymbol{\theta}_n) - \overline{\boldsymbol{H}}_n(\boldsymbol{\theta}_{n0}) \right] \boldsymbol{b}_n \right| = O_p(\sqrt{n}).$$

The asymptotic distribution of the proposed penalized estimator $\widehat{\boldsymbol{\theta}}_n$ is closely related to that of the ideal estimating function $\overline{\boldsymbol{S}}_n(\boldsymbol{\theta}_{n0})$. When appropriately normalized, $\overline{\boldsymbol{S}}_n(\boldsymbol{\theta}_{n0})$ has an asymptotic normal distribution, as shown by the following lemma.

Lemma 6 *Assume conditions (A1)–(A7), then* $\forall \boldsymbol{\xi}_n \in \mathcal{R}^p$ *such that* $\|\boldsymbol{\xi}_n\| = 1$, *we have*

$$\boldsymbol{\xi}_n^\top \overline{\boldsymbol{M}}_n^{-\frac{1}{2}}(\boldsymbol{\theta}_{n0}) \overline{\boldsymbol{S}}_n(\boldsymbol{\theta}_{n0}) \xrightarrow{D} N(0, 1).$$

Proof of Theorem 1

Proof of Sparsity We first show that the estimator $\widehat{\boldsymbol{\theta}}_n$ must possesses the sparsity property $\widehat{\boldsymbol{\theta}}_{n2} = 0$. To prove that the optimality is obtained at $\widehat{\boldsymbol{\theta}}_{n2} = 0$, it suffices to show that with probability tending to 1, as $n \to \infty$, for any $\widehat{\boldsymbol{\theta}}_{n1}$ satisfying $\|\widehat{\boldsymbol{\theta}}_{n1} - \widehat{\boldsymbol{\theta}}_{n10}\| = O_p(\sqrt{1/n})$, and $\|\widehat{\boldsymbol{\theta}}_{n2}\| \le C(\sqrt{1/n})$, $U_{nk}(\boldsymbol{\theta})$ have different signs for $\beta_k \in \left(-C(\sqrt{1/n}), C(\sqrt{1/n})\right)$, for $k = s+1, \ldots, p$. Note that

$$U_{nk}(\boldsymbol{\theta}) = S_{nk}(\widehat{\boldsymbol{\theta}}) + n q_{\lambda_n}(|\beta_k|)\text{sign}(\beta_k),$$

where $S_{nk}(\widehat{\boldsymbol{\theta}})$ denotes the kth element of $S_n(\widehat{\boldsymbol{\theta}})$. From $S_{nk}(\widehat{\boldsymbol{\theta}}) = O_p(\sqrt{1/n})$, we obtain

$$U_{nk}(\boldsymbol{\theta}) = n\lambda_n \left\{ \frac{q_{\lambda_n}(|\beta_k|)}{\lambda_n} \text{sign}(\beta_k) + O_p(\sqrt{1/n}) \right\}.$$

It is easy to see that the sign of β_k completely determines the sign of $U_{nk}(\boldsymbol{\theta})$. Hence, the desired result is obtained.

Proof of Asymptotic Normality First we show that $\boldsymbol{\xi}_n^\top \overline{\boldsymbol{M}}_n^{-\frac{1}{2}}(\boldsymbol{\theta}_{n0}) \overline{\boldsymbol{H}}_n(\boldsymbol{\theta}_{n0})(\widehat{\boldsymbol{\theta}}_{n1} - \boldsymbol{\theta}_{n01}) \xrightarrow{D} \text{N}(0, 1)$. We have

$$\boldsymbol{\xi}_n^\top \overline{\boldsymbol{M}}_n^{-\frac{1}{2}}(\boldsymbol{\theta}_{n0}) \overline{\boldsymbol{S}}_n(\boldsymbol{\theta}_{n0}) = \boldsymbol{\xi}_n^\top \overline{\boldsymbol{M}}_n^{-\frac{1}{2}}(\boldsymbol{\theta}_{n0}) \overline{\boldsymbol{H}}_n(\boldsymbol{\theta}_{n0})(\widehat{\boldsymbol{\theta}}_n - \boldsymbol{\theta}_{n0})$$

$$+ \boldsymbol{\xi}_n^\top \overline{\boldsymbol{M}}_n^{-\frac{1}{2}}(\boldsymbol{\theta}_{n0})[\boldsymbol{D}_n(\boldsymbol{\theta}_n^*) - \overline{\boldsymbol{H}}_n(\boldsymbol{\theta}_{n0})](\widehat{\boldsymbol{\theta}_n} - \boldsymbol{\theta}_{n0})$$
$$+ \boldsymbol{\xi}_n^\top \overline{\boldsymbol{M}}_n^{-\frac{1}{2}}(\boldsymbol{\theta}_{n0})[\overline{\boldsymbol{S}}_n(\boldsymbol{\theta}_{n0}) - \boldsymbol{S}_n(\boldsymbol{\theta}_{n0})].$$

By Lemma 6, $\boldsymbol{\xi}_n^\top \overline{\boldsymbol{M}}_n^{-\frac{1}{2}}(\boldsymbol{\theta}_{n0})\overline{\boldsymbol{S}}_n(\boldsymbol{\theta}_{n0}) \xrightarrow{D} N(0, 1)$. Therefore, to prove the theorem, it is sufficient to verify that $\forall \Delta > 0$,

$$\sup_{\|\boldsymbol{\theta}_n - \boldsymbol{\theta}_{n0}\| \le \Delta\sqrt{p_n/n}} |\boldsymbol{\xi}_n^\top \overline{\boldsymbol{M}}_n^{-\frac{1}{2}}(\boldsymbol{\theta}_{n0})[\boldsymbol{D}_n(\boldsymbol{\theta}_n) - \overline{\boldsymbol{H}}_n(\boldsymbol{\theta}_{n0})](\widehat{\boldsymbol{\theta}_n} - \boldsymbol{\theta}_{n0})| = o_p(1) \quad (16)$$

and

$$|\boldsymbol{\xi}_n^\top \overline{\boldsymbol{M}}_n^{-\frac{1}{2}}(\boldsymbol{\theta}_{n0})[\overline{\boldsymbol{S}}_n(\boldsymbol{\theta}_{n0}) - \boldsymbol{S}_n(\boldsymbol{\theta}_{n0})]| = o_p(1). \quad (17)$$

Then, the final result follows by some matrix algebra. We prove (17) first. Note that

$$\begin{aligned}
&\left[\boldsymbol{\xi}_n^\top \overline{\boldsymbol{M}}_n^{-\frac{1}{2}}(\boldsymbol{\theta}_{n0})[\overline{\boldsymbol{S}}_n(\boldsymbol{\theta}_{n0}) - \boldsymbol{S}_n(\boldsymbol{\theta}_{n0})]\right]^2 \\
&= \boldsymbol{\xi}_n^\top \overline{\boldsymbol{M}}_n^{-1/2}(\boldsymbol{\theta}_{n0})[\overline{\boldsymbol{S}}_n(\boldsymbol{\theta}_{n0}) - \boldsymbol{S}_n(\boldsymbol{\theta}_{n0})][\overline{\boldsymbol{S}}_n(\boldsymbol{\theta}_{n0}) - \boldsymbol{S}_n(\boldsymbol{\theta}_{n0})]^\top \overline{\boldsymbol{M}}_n^{-\frac{1}{2}}\boldsymbol{\xi}_n \\
&\le \lambda_{\max}\left(\overline{\boldsymbol{M}}_n^{-1}(\boldsymbol{\theta}_{n0})\right)\lambda_{\max}\left([\overline{\boldsymbol{S}}_n(\boldsymbol{\theta}_{n0}) - \boldsymbol{S}_n(\boldsymbol{\theta}_{n0})][\overline{\boldsymbol{S}}_n(\boldsymbol{\theta}_{n0}) - \boldsymbol{S}_n(\boldsymbol{\theta}_{n0})]^\top\right) \\
&\le \frac{\|\overline{\boldsymbol{S}}_n(\boldsymbol{\theta}_{n0}) - \boldsymbol{S}_n(\boldsymbol{\theta}_{n0})\|^2}{\lambda_{\min}\left(\overline{\boldsymbol{M}}_n(\boldsymbol{\theta}_{n0})\right)} \\
&\le \frac{\|\overline{\boldsymbol{S}}_n(\boldsymbol{\theta}_{n0}) - \boldsymbol{S}_n(\boldsymbol{\theta}_{n0})\|^2}{C\lambda_{\min}\left(\sum_{i=1}^n \boldsymbol{X}_i^\top \boldsymbol{X}_i\right)} = O_p(1/n) = o_p(1).
\end{aligned}$$

Then, (17) follows using the fact that $\lambda_{\min}\left(\overline{\boldsymbol{M}}_n(\boldsymbol{\theta}_{n0})\right) \ge C\lambda_{\min}\left(\sum_{i=1}^n \boldsymbol{X}_i^\top \boldsymbol{X}_i\right)$. Next, we prove (16). We have

$$\begin{aligned}
&\sup_{\|\boldsymbol{\theta}_n - \boldsymbol{\theta}_{n0}\| \le \Delta\sqrt{1/n}} |\boldsymbol{\xi}_n^\top \overline{\boldsymbol{M}}_n^{-\frac{1}{2}}(\boldsymbol{\theta}_{n0})[\boldsymbol{D}_n(\boldsymbol{\theta}_n) - \overline{\boldsymbol{H}}_n(\boldsymbol{\theta}_{n0})](\widehat{\boldsymbol{\theta}_n} - \boldsymbol{\theta}_{n0})| \\
&\le \sup_{\|\boldsymbol{\theta}_n - \boldsymbol{\theta}_{n0}\| \le \Delta\sqrt{1/n}} |\boldsymbol{\xi}_n^\top \overline{\boldsymbol{M}}_n^{-\frac{1}{2}}(\boldsymbol{\theta}_{n0})[\boldsymbol{D}_n(\boldsymbol{\theta}_n) - \overline{\boldsymbol{D}}_n(\boldsymbol{\theta}_n)](\widehat{\boldsymbol{\theta}_n} - \boldsymbol{\theta}_{n0})| \\
&+ \sup_{\|\boldsymbol{\theta}_n - \boldsymbol{\theta}_{n0}\| \le \Delta\sqrt{1/n}} |\boldsymbol{\xi}_n^\top \overline{\boldsymbol{M}}_n^{-\frac{1}{2}}(\boldsymbol{\theta}_{n0})[\overline{\boldsymbol{D}}_n(\boldsymbol{\theta}_n) - \overline{\boldsymbol{H}}_n(\boldsymbol{\theta}_n)](\widehat{\boldsymbol{\theta}_n} - \boldsymbol{\theta}_{n0})| \\
&+ \sup_{\|\boldsymbol{\theta}_n - \boldsymbol{\theta}_{n0}\| \le \Delta\sqrt{1/n}} |\boldsymbol{\xi}_n^\top \overline{\boldsymbol{M}}_n^{-\frac{1}{2}}(\boldsymbol{\theta}_{n0})[\overline{\boldsymbol{H}}_n(\boldsymbol{\theta}_n) - \overline{\boldsymbol{H}}_n(\boldsymbol{\theta}_{n0})](\widehat{\boldsymbol{\theta}_n} - \boldsymbol{\theta}_{n0})| \\
&= I_{n1} + I_{n2} + I_{n3}.
\end{aligned}$$

By the Cauchy–Schwarz inequality and Remark 1, we have $I_{n1} = o_p(1)$. By the same argument and Lemmas 4 and 5, we also have $I_{n2} = o_p(1)$ and $I_{n3} = o_p(1)$. This proves (16).

References

Akaike, H. (1973). Information theory and an extension of the maximum likelihood principle. In *2nd International Symposium on Information Theory* (pp. 267–281).

Balan, R. M., & Schiopu-Kratina, I. (2005). Asymptotic results with generalized estimating equations for longitudinal data. *Annals of Statistics, 32*, 522–541.

Bondell, H. D., Krishna, A., & Ghosh, S. K. (2010). Joint variable selection for fixed and random effects in linear mixed-effects models. *Biometrics, 66*, 1069–1077.

Breslow, N. E., & Clayton, D. G. (1993). Approximate inference in generalized linear mixed model. *Journal of the American Statistical Association, 88*, 9–25.

Breslow, N. E., & Lin, X. (1995). Bias correction in generalized linear mixed models with a single component of dispersion. *Biometrika, 82*, 81–91.

Cantoni, E., Flemming, J. M., & Ronchetti, E. (2005). Variable selection for marginal longitudinal generalized linear models. *Biometrics, 61*, 507–514.

Dziak, J. J. (2006). Ph.D Thesis. In *Penalized quadratic inference functions for variable selection in longitudinal research*. https://etda.libraries.psu.edu/paper/7084/

Fan, J. Q., Huang, T., & Li, R. (2007). Analysis of longitudinal data with semiparametric estimation of covarince function. *Journal of the American Statistical Association, 102*, 632–641.

Fan, J. Q., & Li, R. (2001). Variable selection via nonconcave penalized likelihood and its oracle properties. *Journal of the American Statistical Association, 96*, 1348–1360.

Fitzmaurice, G. M., Laird, N. M., & Ware, J. H. (2004). *Applied longitudinal analysis*. Hoboken: Wiley.

Frank, I. E., & Friedman, J. H. (1993). A statistical view of some chemometrics regression tools (with discussion). *Technometrics, 35*, 109–148.

Fu, W. J. (2003). Penalized estimating equations. *Biometrics, 59*, 126–132.

He, X. M., Fung, W. K., & Zhu, Z. Y. (2005). Robust estimation in generalized partial linear models for clustered data. *Journal of the American Statistical Association, 100*, 1176–1184.

He, X. M., Zhu, Z. Y., & Fung, W. K. (2002). Estimation in a semiparametric model for longitudinal data with unspecified dependence structure. *Biometrika, 89*, 579–590.

Huang, J. Z., Zhang, L., & Zhou, L. (2007) Efficient estimation in marginal partially linear models for longitudinal/clustered data using splines. *Scandinavian Journal of Statistics, 34*, 451–477.

Kurum, E., Li, R., Shiffman, S., & Yao, W. (2016). Time-varying coefficient models for joint modeling binary and continues outcome in longitudinal data. *Statistica Sinica, 29*, 979–1000.

Laird, N. M., & Ware, J. H. (1982). Random effects models for longitudinal data. *Biometrics, 38*, 963–974.

Liang, H. (2009). Generalized partially linear mixed-effects models incorporating mismeasured covariates. *Annals of the Institute of Statistical Mathematics, 61*, 27–46.

Liang, K. Y., & Zeger, S. L. (1986). Longitudinal data analysis using generalized linear models. *Biometrika, 73*, 13–22.

Li, Z., & Zhu, L. (2010). On variance components in semiparametric mixed models for longitudinal data. *Scandinavian Journal of Statistics, 37*, 442–457.

Lin, X., & Breslow, N. E. (1996). Bias correction in generalized linear mixed models with multiple components of dispersion. *Journal of the American Statistical Association, 91*, 1007–1016.

Ma, S., Song, Q., & Wang, L. (2013). Simultaneous variable selection and estimation in semiparametric modeling of longitudinal/clustered data. *Bernoulli, 19*, 252–274.

McCulloch, C. E. (1997). Maximum likelihood algorithms for generalized linear mixed models. *Journal of the American Statistical Association, 92*, 162–170.

McCullagh, P., & Nelder, J. A. (1989). *Generalized linear models*. London: Chapman and Hall (1989)

Ni, X., Zhang, D., & Zhang, H. H. (2010). Variable selection for semiparametric mixed models in longitudinal studies. *Biometrics, 66*, 79–88.

Pan, W. (2001). Akaike's information criterion in generalized estimating equations. *Biometrics, 57*, 120–125.

Qin, G. Y., & Zhu, Z. Y. (2007). Robust estimation in generalized semiparametric mixed models for longitudinal data. *Journal of Multivariate Analysis, 98*, 1658–1683.

Qin, G. Y., & Zhu, Z. Y. (2009). Robustified maximum likelihood estimation in generalized partial linear mixed model for longitudinal data. *Biometrics, 65*, 52–59.

Schumaker, L.L. (1981). *Spline functions*. New York: Wiley.

Schwarz, G. (1978). Estimating the dimension of a model. *The Annals of Statistics, 6*, 461–464.

Sinha, S. K., & Sattar, A. (2015). Inference in semi-parametric spline mixed models for longitudinal data. *Metron, 73*, 377–395.

Sutradhar, B. C. (2010). Inferences in generalized linear longitudinal mixed models. *The Canadian Journal of Statistics, 38*, 174–196.

Sutradhar, B. C., Jowaheer, V., & Sneddo, G. (2008). On a unified generalized quasi-likelihood approach for familial-longitudinal non-stationary count data. *Scandinavian Journal of Statistics, 35*, 597–612.

Tibshirani, R. (1996). Regression shrinkage and selection via the lasso. *Journal of the Royal Statistical Society: Series B (Methodological), 58*, 267–288.

Ueki, M. (2009). A note on automatic variable selection using smooth-threshold estimating equations. *Biometrika, 96*, 1005–1011.

Wang, L. (2011). GEE analysis of clustered binary data with diverging number of covariates. *The Annals of Statistics, 39*, 389–417.

Wang, L., & Qu, A. (2009). Consistent model selection and data-driven smooth tests for longitudinal data in the estimating equations approach. *Journal of the Royal Statistical Society, 71*, 177–190.

Wang, L., Zhou, J., & Qu, A. (2012). Penalized generalized estimating equations for high-dimensional longitudinal data analysis. *Biometrics, 68*, 353–360.

Wang, N., Carroll, R. J., & Lin X. (2005). Efficient semiparametric marginal estima- tion for longitudinal/clustered data. *Journal of the American Statistical Association, 100*, 147–157.

Xie, M., & Yang, Y. (2003). Asymptotics for generalized estimating equations with large cluster sizes. *The Annals of Statistics, 31*, 310–347.

Xu, P. R., Fu, W., & Zhu, L. X. (2012). Shrinkage estimation analysis of correlated binary data with a diverging number of parameters. *Science in China Series A: Mathematics, 56*, 359–377.

Xue, L. (2009). Consistent variable selection in additive models. *Statistica Sinica, 19*, 1281–1296.

Xue, L., Qu, A., & Zhou, J. (2010). Consistent model selection for marginal generalized additive model for correlated data. *Journal of the American Statistical Association, 105*, 1518–1530.

Zhang, D. (2004). Generalized linear mixed models with varying coefficients for longitudinal data. *Biometrics, 60*, 8–15.

Zeger, S. L., & Diggle, P. J. (1994). Semi-parametric models for longitudinal data with application to CD4 cell numbers in HIV seroconverters. *Biometrics, 50*, 689–99.

Zou, H. (2006). The adaptive Lasso and its oracle properties. *Journal of the American Statistical Association, 101*, 1418–1429.

Zou, H., & Hastie, T. (2005). Regularization and variable selection via the elasticnet. *Journal of the Royal Statistical Society: Series B (Statistical Methodology), 67*, 301–320.

Variable Selection of Interval-Censored Failure Time Data

Qiwei Wu, Hui Zhao, and Jianguo Sun

Abstract Variable selection is a commonly asked question in statistical analysis and has been extensively discussed under many contexts. In particular, many authors have investigated the problem under the survival analysis context. However, most of the existing methods for failure time data only deal with right-censored data and in this chapter, we will discuss the problem for regression analysis of interval-censored data, a more general type of failure time data, under the proportional hazards model. For covariate selection and estimation of covariate effects, a penalized estimation procedure is developed with the use of some commonly used penalized functions and the sieve approach. The simulation study suggests that it seems to work well for practical situations. In addition, an illustrative example is provided.

1 Introduction

Variable selection is a commonly asked question in statistical analysis and has been extensively discussed under many contexts (Dicker et al. 2013; Fan and Li 2001; Tibshirani 1996; Zou 2006). In particular, many authors have investigated the problem under the survival analysis context (Cai et al. 2009; Fan and Li 2002; Huang and Ma 2010; Martinussen and Scheike 2009). However, most of the existing methods for failure time data only deal with right-censored data and in practice, one may often face interval-censored data, a more general type of failure time data (Sun 2006; Sun et al. 2015). By interval-censored data, we usually mean that the failure time of interest is known or observed only to belong to an interval instead of being observed exactly. It is easy to see that among others, most of medical

Q. Wu · J. Sun (✉)
Department of Statistics, University of Missouri, Columbia, MO, USA
e-mail: sunj@missouri.edu

H. Zhao
School of Mathematics and Statistics & Hubei Key Laboratory of Mathematical Sciences, Central China Normal University, Wuhan, People's Republic of China

A. Bekker et al. (eds.), *Computational and Methodological Statistics and Biostatistics*, Emerging Topics in Statistics and Biostatistics,
https://doi.org/10.1007/978-3-030-42196-0_20

follow-up studies such as clinical trials will yield such data and interval-censored data include right-censored as a special case. In the following, we will consider regression analysis of interval-censored data with the focus on covariate selection.

There exist many methods for variable selection, especially under the context of linear regression, such as forward selection, backward selection and best subset selection. Among them, the penalized estimation procedure, which optimizes an objective function with a penalty function, has recently become increasingly popular and in particular, many penalty functions have been proposed. For example, one of the early work was given by Tibshirani (1996), who proposed the least absolute shrinkage and selection operator (LASSO) penalty for linear regression models, and Fan and Li (2001) developed the smoothly-clipped absolute deviation (SCAD) penalty. Also Zou (2006) generalized the LASSO penalty to the adaptive LASSO (ALASSO) penalty, and Lv and Fan (2009) and Dicker et al. (2013) proposed the smooth integration of counting and absolute deviation (SICA) penalty and the seamless-L_0 (SELO) penalty, respectively.

For covariate selection with failure time data, it is natural to generalize the methods discussed above, especially the penalized estimation procedures, once given a regression model. On the other hand, it is well-known that this is quite challenging or not straightforward due to the special structures of failure time data caused by censoring as well as truncation, the basic feature of the data. Among others, one of the most commonly used regression models for failure time data is the proportional hazards (PH) model and several authors have discussed the development of penalized estimation procedures for regression analysis of right-censored data under the model. For example, Tibshirani (1997), Fan and Li (2002) and Zhang and Lu (2007) discussed the generalizations of the LASSO, SCAD and ALASSO penalty-based procedures to the PH model situation, respectively, and more recently, Shi et al. (2014) extended the SICA penalty-based procedure.

In addition, some methods have also been proposed in the literature for covariate selection of right-censored failure time data under other regression models including the additive hazards model (Martinussen and Scheike 2009; Lin and Lv 2013) and the accelerated failure time model (Cai et al. 2009; Huang and Ma 2010). Two procedures have also actually been developed for the covariate selection of interval-censored failure time data under the PH model in Scolas et al. (2016) and Wu and Cook (2015). However, both procedures are parametric methods and in particular, Wu and Cook assumed that the baseline hazard function is a piecewise constant function. Also there is no theoretical justification given for both procedures. Note that for regression analysis of right-censored data with the PH model, a partial likelihood function is available (Kalbfleisch and Prentice 2002), which is free of the baseline hazard function and is the base for all of the existing penalized estimation procedures as it can be regarded as a parametric objective function. Also one main difference between right-censored data and interval-censored data is that the latter has a much more complex data structure and as one consequence, no partial likelihood function or a parametric objective function is available any more. In other words, one has to deal with both regression parameters and the baseline hazard

function together. In the following, we will develop a sieve penalized estimation procedure for interval-censored data under the PH model.

The remainder of the chapter is organized as follows. First we will begin in Sect. 2 with introducing some notation and assumptions that will be used throughout the chapter as well as describing the model and the resulting likelihood function. The proposed sieve penalized estimation approach will be presented in Sect. 3 and in the method, Bernstein polynomials will be employed to approximate the unknown baseline cumulative hazard function. For the implementation of the procedure, a coordinate decent algorithm will be described and it is faster and can be easily implemented than the EM algorithm given in Wu and Cook (2015). In addition, the proposed method can be applied with various penalty functions. Section 4 presents some results obtained from an extensive simulation study conducted for the assessment of the proposed method and suggest that it seems to work well for practical situations. An illustrative example is provided in Sects. 5 and 6 concludes with some discussion and remarks.

2 Notation, Assumptions and Likelihood Function

Consider a failure time study with T denoting the failure time of interest and suppose that there exists a p-dimensional vector of covariates denoted by $\underline{X}$. For the covariate effect, we will assume that T follows the PH model given by

$$\lambda(t; \underline{X}) = \lambda_0(t) \exp\{\underline{\beta}'\underline{X}\},$$

where $\lambda_0(t)$ denotes an unknown baseline hazard function and $\underline{\beta}$ is a vector of regression parameters. In the following, it will be supposed that the main goal is about inference on $\underline{\beta}$ with the focus on covariate selection.

For inference, we will assume that one only observes interval-censored failure time data given by $\{(L_i < T_i \leq R_i, \underline{X}_i), \ i = 1, \ldots, n\}$ from n independent subjects, where $(L_i, R_i]$ denotes the interval within which the failure time T_i belongs to. It is apparent that it will reduce to right-censored data if $L_i = R_i$ or $R_i = \infty$ for all i. In the following, we will assume that the mechanism generating the censoring intervals $(L_i, R_i]$'s is independent of the T_i's given covariates or non-informative (Sun 2006). Then the likelihood function has the form

$$L(\underline{\beta}, \Lambda_0) = \prod_{i=1}^{n} \left\{ \exp\left(-\Lambda_0(L_i)\, e^{\underline{\beta}'\underline{X}}\right) - \exp\left(-\Lambda_0(R_i)\, e^{\underline{\beta}'\underline{X}}\right) \right\}, \tag{1}$$

where $\Lambda_0(t) = \int_0^t \lambda_0(s)ds$ denotes the baseline cumulative hazard function. Note that the likelihood function above involves an infinite-dimensional function Λ_0 and this usually makes its maximization complicated and difficult. To address this, a sieve approach is commonly employed to approximate Λ_0 by some smooth

functions (Huang and Rossini 1997; Ma et al. 2015; Zhou et al. 2017). In the following, by following Zhou et al. (2017), we will use the Bernstein polynomial approximation.

More specifically, let $\Theta = \left\{ (\underline{\beta}, \Lambda_0) \in \mathscr{B} \otimes \mathscr{M} \right\}$ denote the parameter space of $(\underline{\beta}, \Lambda_0)$, where $\mathscr{B} = \left\{ \underline{\beta} \in \mathscr{R}^p, \ \|\underline{\beta}\| \leq M \right\}$ with M being a positive constant, and $\mathscr{M}$ is the collection of all bounded and continuous nondecreasing, nonnegative functions over the interval $[c, u]$. Here c and u are usually taken to be $\min(L_i)$ and $\max(R_i)$, respectively. Also define the sieve space $\Theta_n = \left\{ (\underline{\beta}, \Lambda_{0n}) \in \mathscr{B} \otimes \mathscr{M}_n \right\}$, where

$$\mathscr{M}_n = \left\{ \Lambda_{0n}(t) = \sum_{k=0}^{m} \phi_k B_k(t, m, c, u) : \sum_{0 \leq k \leq m} |\phi_k| \leq M_n, 0 \leq l\phi_0 \leq \phi_1 \leq \ldots \leq \phi_m \right\}$$

with $B_k(t, m, c, u)$ denoting the Bernstein basis polynomial defined as

$$B_k(t, m, c, u) = \binom{m}{k} \left(\frac{t-c}{u-c} \right)^k \left(1 - \frac{t-c}{u-c} \right)^{m-k}, \ k = 0, 1, \ldots, m .$$

In the above M_n is a positive constant and $m = o(n^v)$, denoting the degree of Bernstein polynomials, for some $v \in (0, 1)$. More discussion about m will be given below.

Note that by focusing on the sieve space Θ_n, the likelihood function given in (1) becomes

$$L(\underline{\beta}, \phi_k' s) = \prod_{i=1}^{n} \left\{ \exp\left(-\Lambda_{0n}(L_i)\, e^{\underline{\beta}' \underline{X}} \right) - \exp\left(-\Lambda_{0n}(R_i)\, e^{\underline{\beta}' \underline{X}} \right) \right\} . \tag{2}$$

Hence the use of Bernstein polynomials turns an estimation problem about both finite-dimensional and infinite-dimensional parameters into a problem that involves only finite-dimensional parameters with the constraint $0 \leq \phi_0 \leq \phi_1 \leq \ldots \leq \phi_m$. Note that this constraint can be easily removed by the reparameterization $\phi_0 = e^{\alpha_0}$ and $\phi_k = \sum_{i=0}^{k} e^{\alpha_i}$, $1 \leq k \leq m$. In other words, instead of $L(\underline{\beta}, \phi_k' s)$ given in (2), we can focus on the likelihood function $L(\underline{\beta}, \alpha_k' s)$, and in the next section, we will discuss the estimation of these parameters with the focus on covariate selection.

3 Sieve Penalized Estimation

Let $\underline{\beta} = (\beta_1, \ldots, \beta_p)'$ and $\underline{\alpha} = (\alpha_0, \ldots, \alpha_m)'$. To estimate $\underline{\beta}$ and $\underline{\alpha}$, we propose to use the sieve penalized maximum likelihood estimator $(\hat{\underline{\beta}}_n, \hat{\Lambda}_{0n}) = (\hat{\underline{\beta}}, \hat{\underline{\alpha}})$ defined as the values of $\underline{\beta}$ and $\underline{\alpha}$ that maximize the sieve penalized log likelihood function

$$Q_n(\underline{\beta}, \underline{\alpha}) = \log\left\{L(\underline{\beta}, \alpha_k' s)\right\} - n\sum_{j=1}^{p} p_\lambda(\beta_j)$$

$$= \sum_{i=1}^{n} \log\left\{\exp\left(-\Lambda_{0n}(L_i)\, e^{\underline{\beta}'\underline{X}_i}\right) - \exp\left(-\Lambda_{0n}(R_i)\, e^{\underline{\beta}'\underline{X}_i}\right)\right\} - n\sum_{j=1}^{p} p_\lambda(\beta_j)\,.$$

In the above, p_λ denotes a penalty function that depends on a tuning parameter $\lambda > 0$ and in the following, we will consider several commonly discussed penalty functions.

In particular, we will discuss the LASSO and ALASSO penalty functions with the latter defined as $p_\lambda(\beta_j) = \lambda\, w_j\, |\beta_j|$, where w_j is a weight for β_j. By following the suggestion of Zou (2006), in the following, we will set the weights as $w_j = 1/|\tilde{\beta}_j|$, where $\tilde{\beta}_j$ is the sieve maximum likelihood estimator of β_j based on the likelihood function $L(\underline{\beta}, \underline{\alpha})$. The above function $p_\lambda(\beta_j)$ will reduce to the LASSO penalty function with $w_j = 1$ for all j. Another penalty function to be investigated is the SCAD penalty function that has the form

$$p_\lambda(\beta_j) = \begin{cases} \lambda\,|\beta_j|\,, & |\beta_j| \le \lambda\,, \\ -(\beta_j^2 - 2a|\beta_j| + \lambda^2)/\left[2(a-1)\right]\,, & \lambda < |\beta_j| \le a\lambda\,, \\ (a+1)\,\lambda^2/2\,, & |\beta_j| \ge a\lambda\,, \end{cases}$$

where the constant a is set to be 3.7 to follow the suggestion of Fan and Li (2001). In addition, we will study the SICA and SELO penalty functions. The former is defined as

$$p_\lambda(\beta_j) = \lambda\, \frac{(\tau+1)\,|\beta_j|}{|\beta_j| + \tau}$$

with $\tau > 0$ being a shape parameter, while the latter has the form

$$p_\lambda(\beta_j) = \frac{\lambda}{\log(2)}\, \log\left(\frac{|\beta_j|}{|\beta_j| + \gamma} + 1\right)$$

with $\gamma > 0$ being another tuning parameter besides λ. In the numerical studies below, we will set $\tau = \gamma = 0.01$ (Dicker et al. 2013).

To maximize the sieve penalized log likelihood function $Q_n(\underline{\beta}, \underline{\alpha})$, we propose a two-step procedure that estimates $\underline{\beta}$ and $\underline{\alpha}$ alternatively. In particular, we will use the Nelder-Mead simplex algorithm to update the estimators of $\underline{\alpha}$ given the current estimators of $\underline{\beta}$ and then update the estimators of $\underline{\beta}$ by employing the coordinate decent algorithm while fixing $\underline{\alpha}$ (Fu 1998; Daubechies et al. 2004). The specific steps can be described as follows.

Step 1. Choose the initial values of $\underline{\beta}$ and $\underline{\alpha}$

Step 2. Given the current estimate of $\underline{\beta}$, update the estimate of $\underline{\alpha}$ by using the Nelder-Mead simplex algorithm.

Step 3. Given the current estimate of $\underline{\alpha}$, update the estimate of $\underline{\beta}$ by using the coordinate decent algorithm, and in particular, update each element of $\underline{\beta}$ by maximizing $Q_n(\underline{\beta}, \underline{\alpha})$ while holding the other elements of $\underline{\beta}$ fixed.

Step 4. Repeat steps 2 and 3 until convergence.

Note that the coordinate decent algorithm described above is essentially to conduct univariate maximization for each element of $\underline{\beta}$ vector repeatedly, and for each univariate maximization, one can use the golden-section search algorithm (Kiefer 1953). To check the convergency, a common way is to compare the summation of the absolute differences between the current and updated estimates of each component of both $\underline{\beta}$ and $\underline{\alpha}$. For the covariate selection, at the convergence, we will set the estimates of the components of β whose absolute values are less than a pre-specified threshold to be zero (Wang et al. 2007). For the numerical study below, we implement the Nelder-Mead simplex algorithm by using the R function *optim* and employ the R function *optimize* for the implementation of the golden-section search algorithm. Zeros are used as the initial values of $\underline{\beta}$ and $\underline{\alpha}$ and our numerical study suggests that it works well under various scenarios.

To implement the sieve penalized estimation procedure described above, it is apparent that we need to choose the tuning parameter λ as well as the degree m of Bernstein polynomials. For this, we propose to use the C-fold cross-validation. Specifically, let C be an integer and suppose that the observed data can be divided into C non-overlapping parts with approximately the same size. Also let $logL^c$ denote the observed log likelihood function based on the c^{th} part of the whole data set and $\hat{\underline{\beta}}^{-c}$ and $\hat{\underline{\alpha}}^{-c}$ the proposed sieve penalized estimates of $\underline{\beta}$ and $\underline{\alpha}$, respectively, obtained based on the whole data without the c^{th} part. For given λ and m, the cross-validation statistic can be defined as

$$CV(\lambda, m) = \sum_{c=1}^{C} \log L^c(\hat{\underline{\alpha}}^{-c}, \hat{\underline{\beta}}^{-c}),$$

and one can choose the values of λ and m that maximize $CV(\lambda, m)$. Note that other criteria can also be used to select the optimal λ and m, including AIC and BIC. We have briefly compared the performance between cross-validation and BIC and found that the latter is more aggressive and tended to choose a larger λ value that results in excluding more variables. AIC was not investigated since it does not include the sample size into consideration compared with BIC. In practice, one may perform grid search over possible ranges of λ and m and furthermore, may fix m to be the closest integer to $n^{0.25}$ to focus on the selection of λ.

4 A Simulation Study

An extensive simulation study was conducted to assess the performance of the sieve penalized estimation procedure proposed in the previous sessions. In the study, we considered several set-ups for covariates including $p = 8$ and $p = 100$ and generated covariates from either the normal distribution or Bernoulli distribution. For the true failure time, we assumed that the T_i's followed the Weibull distribution with the hazard function $\lambda(t|\underline{X}_i; \underline{\beta}) = k\,\eta\,(\eta t)^{k-1}\, e^{\underline{X}_i^T \underline{\beta}}$ with $k = 1$ and $\eta = -\log(0.05)$. To generate censoring intervals, we first generated the total number of examination time points for each subject from the zero-truncated Poisson distribution with mean μ, and given the number of examination time points, the examination times were generated from the uniform distribution over (0, 1). Then for subject i, the observed interval end points L_i and R_i were defined to be the largest examination time point before the true T_i and the smallest examination time point after T_i, respectively. The results given below are based on $n = 100$ or 500 with 100 replications.

Table 1 presents the results on the selection of the covariates with $n = 100$, $\underline{\beta}_0 = (0.8, 0, 0, 1, 0, 0, 0.6, 0)'$, $\mu = 10$ or 20, and $\underline{X}$ following the normal distribution with mean 0 and the correlation $\rho^{|j_1 - j_2|}$ between the two components X_{j_1} and X_{j_2} of $\underline{X}$ with $\rho = 0.5$. In the table, the MMSE and SD represent the median and the standard deviation of the MSE, respectively, given by $(\hat{\underline{\beta}} - \underline{\beta}_0)^T \Sigma (\hat{\underline{\beta}} - \underline{\beta}_0)$ among 100 data sets, where Σ denotes the covariance matrix of the covariates. The quantity TP denotes the averaged number of the correctly selected covariates whose true coefficients are not 0, and FP the averaged number of incorrectly selected covariates whose true coefficients are 0. Here we considered all five penalty functions, LASSO, ALASSO, SCAD, SICA and SELO, described above, set $m = 3$, the closest integer to $n^{0.25}$, and used the 5-fold cross-validation for the selection of λ based on the grid search. For comparison, we also investigated the method given in Wu and Cook (2015), referred to as WC method in the table, by the using the program provided in their paper. Note that their method assumed that the baseline hazard function is a piecewise constant function and the program only considered LASSO and ALASSO penalty functions with the four piecewise constant function.

One can see from Table 1 that the proposed method seems to perform well no matter which penalty function was used, especially in terms of the quantity TP, the measure of true positive selection. Based on the quantity FP, the measure of false positive selection, the method with ALASSO and SICA appears to give better selection results but there was no major difference among each other. Also the proposed method seems to give a little better and stable results than the WC method but again there was no significant difference. However, the study here did show that the proposed method converged much faster than the WC method as mentioned above. Table 2 gives the results on the selection of covariates with $n = 500$ and $p = 100$, and here we set the first and last five components of the true $\underline{\beta}$ being 0.5 and the remaining components equal to zero. All other set-ups were the same as with Table 1 except that we took $m = 5$, again the closest integer to $n^{0.25}$. It is apparent

Table 1 Results on the covariate selection with $n = 100$ and $p = 8$

Penalty	Method	MMSE (SD)	TP	FP
$\mu = 10$				
LASSO	WC method	0.1633 (0.1043)	3	1.5
	Proposed method	0.1547 (0.1008)	3	1.5
ALASSO	WC method	0.09511 (0.1576)	2.91	0.41
	Proposed method	0.06644 (0.09131)	2.95	0.07
SCAD	Proposed method	0.1049 (0.1559)	2.97	0.12
SICA	Proposed method	0.08234 (0.1278)	2.9	0.08
SELO	Proposed method	0.08246 (0.1125)	2.94	0.09
$\mu = 20$				
LASSO	WC method	0.1297 (0.09371)	3	1.63
	Proposed method	0.1288 (0.09323)	3	1.64
ALASSO	WC method	0.08182 (0.1601)	2.91	0.46
	Proposed method	0.06674 (0.1223)	2.97	0.09
SCAD	Proposed method	0.07405 (0.1363)	2.98	0.14
SICA	Proposed method	0.06286 (0.1295)	2.95	0.09
SELO	Proposed method	0.06214 (0.1253)	2.96	0.11

Table 2 Results on the covariate selection with $n = 500$ and $p = 100$

Penalty	Method	MMSE (SD)	TP	FP
$\mu = 10$				
LASSO	WC method	0.2679 (0.1783)	10	18.24
	Proposed method	0.3994 (0.1821)	10	11.29
ALASSO	WC method	0.05492 (0.05759)	10	0.12
	Proposed method	0.1322 (0.08613)	10	0
SCAD	Proposed method	0.06888 (0.1132)	9.93	0.58
SICA	Proposed method	0.05553 (0.05829)	9.94	0.13
SELO	Proposed method	0.06017 (0.06966)	9.94	0.06
$\mu = 20$				
LASSO	WC method	0.3118 (0.1059)	10	12.32
	Proposed method	0.3969 (0.1549)	10	9.72
ALASSO	WC method	0.05013 (0.04084)	10	0.09
	Proposed method	0.2234 (0.09529)	10	0.01
SCAD	Proposed method	0.06459 (0.1553)	9.93	0.35
SICA	Proposed method	0.05217 (0.05733)	9.98	0.03
SELO	Proposed method	0.05161 (0.05445)	9.98	0.04

that these results gave similar conclusions to those seen in Table 1 except that the proposed method with ALASSO, SCAD, SICA and SELO penalty functions seems to give much better performance than that with LASSO penalty function in terms of the FP.

Table 3 Results on the covariate selection with $n = 100$, $p = 8$ and different types of covariates

Penalty	Method	MMSE (SD)	TP	FP
$\mu = 10$				
LASSO	WC method	0.4309 (0.3941)	2.71	1.41
	Proposed method	0.4299 (0.3419)	2.7	2.13
ALASSO	WC method	0.4507 (0.4667)	2.52	0.68
	Proposed method	0.4301 (0.3476)	2.55	0.67
SCAD	Proposed method	0.4289 (0.5244)	2.39	0.52
SICA	Proposed method	0.4456 (0.4505)	2.51	0.45
SELO	Proposed method	0.4241 (0.5046)	2.55	0.59
$\mu = 20$				
LASSO	WC method	0.4073 (0.3237)	2.8	1.38
	Proposed method	0.3948 (0.3285)	2.75	2.05
ALASSO	WC method	0.4076 (0.4018)	2.53	0.55
	Proposed method	0.3914 (0.3306)	2.59	0.54
SCAD	Proposed method	0.4055 (0.4431)	2.41	0.54
SICA	Proposed method	0.3839 (0.3874)	2.51	0.33
SELO	Proposed method	0.3826 (0.3915)	2.56	0.42

Note that in the above set-ups, all of covariates were assumed to be continuous and we also investigated the situation where some of covariates are discrete. Table 3 presents some results on the selection of covariates similarly obtained as in Table 1 except that here only the first three covariates were generated as above. The other five covariates were assumed to take values 0 and 1 with $E(X_i) = 0.2$ and the correlation $\rho^{|j_1 - j_2|}$ among them with $\rho = 0.5$. The different types of covariates were supposed to be independent and all other set-ups were the same as in Table 1. They again indicate that the proposed method gave reasonable performance for the covariate selection and also gave similar conclusions as above in terms of different penalty functions and the comparison of the proposed method to that given by Wu and Cook (2015).

5 An Application

In this section, we will apply the methodology proposed in the previous sections to a set of interval-censored failure time data collected during the 2003 Nigeria Demographic and Health Survey on the childhood mortality in Nigeria (Kneib 2006). In the study, the children's survival information was obtained by interviewing their mothers and for the children who died within the first 2 months of birth, the survival times were collected exactly in days. However, for other survival times, they were all interval-censored. One goal of interest for the study is to determine or find the factors that had significant influence on the survival times or children's mortality. The factors of interest include the mother's age and body mass index

when giving birth, whether the baby was delivered in a hospital, the gender of the baby, whether mother received higher education, and whether the family lived in urban. In the following, we will focus on the data from the 5730 children with survival information and complete information about the factors above. The left-, interval- and right-censoring rates, based on the 5730 children, are 2%, 10% and 88%, respectively.

For the analysis, let T denote the survival time of the child and define X_1 and X_2 to be the mother's age (AGE) and body mass index (BMI) when giving birth, respectively, $X_3 = 1$ if the baby was delivered in a hospital and 0 otherwise (Hospital), $X_4 = 1$ if the baby is male and 0 otherwise (Gender), $X_5 = 1$ if the mother received a higher education and 0 otherwise (Education), and $X_6 = 1$ if the family lived in a urban area and 0 otherwise (Urban). Note that the first two covariates are continuous and the other are binary. For the analysis below, the first two were standardized. Table 4 gives the analysis results obtained by the proposed estimation procedure with the use of the penalty functions discussed above. Here we considered 100 candidate values for the grid search of λ and several values for m based on the 5-fold cross-validation. The table includes the estimated covariate effects and the estimated standard errors (SD) with $m = 12$ and 16. For comparison, we also obtained and include in the table the results given by the WC method with the four piecewise constant hazard function and the LASSO and ALASSO penalty functions.

One can see from Table 4 that both the proposed and WC methods with all penalty functions except LASSO selected the covariates Hospital, Education and Urban and suggested that the AGE, BMI and Gender were not related to the survival time of interest. As suggested by others and seen in the simulation study, the method with the LASSO penalty tends to have a higher false positive rate and to select more unimportant covariates than the other penalty functions. Furthermore, all procedures indicated that the covariates Hospital, Education and Urban had significant effects on the survival time and that the children would have higher mortality risk if the baby was not delivered in a hospital, the child's mother did not receive higher education, or the child's family was not living in urban area. In addition, the results are consistent with different m values and between the proposed and WC method.

6 Discussion and Conclusion Remarks

This chapter discussed the covariate selection problem when one faces interval-censored failure time data arising from the proportional hazards model and for it, a sieve penalized estimation procedure was developed. In the method, Bernstein polynomials were employed to approximate the unknown cumulative baseline hazard function and the method allows the use of various commonly used penalty functions. For the implementation of the proposed method, an iterative algorithm was presented with the use of the Nelder-Mead simplex algorithm and the coordinate

Table 4 The analysis results of children's mortality data

Penalty	AGE (SD)	BMI (SD)	Hospital (SD)	Gender (SD)	Education (SD)	Urban (SD)
Proposed method with $m = 12$						
LASSO	−0.001 (0.030)	0.008 (0.030)	−0.313 (0.106)	0.020 (0.060)	−0.196 (0.092)	−0.262 (0.093)
ALASSO	0	0	−0.326 (0.103)	0	−0.187 (0.092)	−0.287 (0.094)
SCAD	0	0	−0.356 (0.115)	0	−0.225 (0.101)	−0.314 (0.095)
SICA	0	0	−0.357 (0.132)	0	−0.219 (0.118)	−0.311 (0.103)
SELO	0	0	−0.356 (0.125)	0	−0.221 (0.114)	−0.313 (0.098)
Proposed method with $m = 16$						
LASSO	−0.003 (0.030)	0.011 (0.031)	−0.315 (0.106)	0.022 (0.060)	−0.200 (0.092)	−0.266 (0.094)
ALASSO	0	0	−0.340 (0.107)	0	−0.208 (0.094)	−0.296 (0.095)
SCAD	0	0	−0.353 (0.119)	0	−0.225 (0.110)	−0.314 (0.095)
SICA	0	0	−0.354 (0.157)	0	−0.216 (0.148)	−0.310 (0.125)
SELO	0	0	−0.354 (0.127)	0	−0.221 (0.116)	−0.313 (0.098)
WC method						
LASSO	0	0	−0.316 (0.104)	0.025 (0.061)	−0.196 (0.092)	−0.268 (0.094)
ALASSO	0	0	−0.356 (0.114)	0	−0.224 (0.106)	−0.315 (0.100)

decent algorithm as well as the cross-validation for the selection of the tuning parameter. In addition, the simulation study indicated that it works well for practical situations.

As mentioned above, several methods have been given in the literature for the problem discussed here when one observes right-censored failure time data, a special case of interval-censored data. However, it is not straightforward to generalize these to interval-censored data as the data structure for the latter is much more complicated than that for the former. Although two procedures have been developed for interval-censored data in the literature, they are fully parametric. It is also worth pointing out that the algorithm given here is also much faster and more efficient than the penalized EM algorithm developed in Wu and Cook (2015). This is partly because we directly maximized the penalized log-likelihood function, while they calculated the conditional expectation of the penalized log-likelihood function and maximized the penalized conditional expectation iteratively.

Throughout the whole chapter, it is assumed that the sample size n is larger than the number of covariates p. It is apparent that there exist situations when p is larger than n, such as in genetic or biomarker studies where there may exist hundreds of thousands genes or biomarkers. Although some literature has been developed for variable selection for high-dimensional right-censored data, it is quite difficult to directly generalize these methods to interval-censored data as mentioned above. In other words, more research is clearly needed to achieve variable selection for high-dimensional interval-censored data.

References

Cai, T., Huang, J., & Tian, L. (2009). Regularized estimation for the accelerated failure time model. *Biometrics, 65*(2), 394–404.

Daubechies, I., Defrise, M., & De Mol, C. (2004). An iterative thresholding algorithm for linear inverse problems with a sparsity constraint. *Communications on Pure and Applied Mathematics, 57*(11), 1413–1457.

Dicker, L., Huang, B., & Lin, X. (2013). Variable selection and estimation with the seamless-L0 penalty. *Statistica Sinica, 23*(2), 929–962.

Fan, J., & Li, R. (2001). Variable selection via nonconcave penalized likelihood and its oracle property. *Journal of the American Statistical Association, 456*(96), 1348–1360.

Fan, J., & Li, R. (2002). Variable selection for Cox's proportional hazards model and frailty model. *The Annals of Statistics, 30*(1), 74–99.

Fu, W. (1998). Penalized regressions: the bridge versus the lasso. *Journal of Computational and Graphical Statistics, 7*(3), 397–416.

Huang, J., & Ma, S. (2010). Variable selection in the accelerated failure time model via the bridge method. *Lifetime Data Analysis, 16*(2), 176–195.

Huang, J., & Rossini, A. (1997). Sieve estimation for the proportional-odds failure-time regression model with interval censoring. *Journal of the American Statistical Association, 439*(92), 960–967.

Kalbfleisch, J. D., & Prentice, R. L. (2002). *The statistical analysis of failure time data*. New York: Wiley.

Kiefer, J. (1953). Sequential minimax search for a maximum. *Proceedings of the American Mathematical Society, 4*(3), 502–506.

Kneib T. (2006). Mixed model-based inference in geoadditive hazard regression for interval-censored survival times. *Computational Statistics and Data Analysis, 51*(2), 777–792.

Lin, W., & Lv, J. (2013). High-dimensional sparse additive hazards regression. *Journal of American Statistical Association, 501*(108), 247–264.

Lv, J., & Fan, Y. (2009). A unified approach to model selection and sparse recovery using regularized least squares. *The Annals of Statistics, 6A*(37), 3498–3528.

Ma, L., Hu, T., & Sun, J. (2015). Sieve maximum likelihood regression analysis of dependent current status data. *Biometrika, 102*(3), 731–738.

Martinussen, T., & Scheike, T. (2009). Covariate selection for the semiparametric additive risk model. *Scandinavian Journal of Statistics, 36*(4), 602–619.

Scolas, S., El Ghouch, A., Legrand, C., & Oulhaj, A. (2016). Variable selection in a flexible parametric mixture cure model with interval-censored data. *Statistics in Medicine, 35*(7), 1210–1225.

Shi, Y., Cao, Y., Jiao Y., & Liu Y. (2014). SICA for Cox's proportional hazards model with a diverging number of parameters. *Acta Mathematicae Applicatae Sinica, English Series, 30*(4), 887–902.

Sun, J. (2006) *The statistical analysis of interval-censored failure time data*. New York: Springer.

Sun, J., Feng, Y., & Zhao, H. (2015). Simple estimation procedures for regression analysis of interval-censored failure time data under the proportional hazards model. *Lifetime Data Analysis, 21*(1), 138–155.

Tibshirani, R. (1996). Regression shrinkage and selection via the lasso. *Journal of the Royal Statistical Society, Series B, 58*(1), 267–288.

Tibshirani, R. (1997). The lasso method for variable selection in the Cox model. *Statistics in Medicine, 16*(4), 385–395.

Wang, H., Li, R., & Tsai, C. (2007). Tuning parameter selectors for the smoothly clipped absolute deviation method. *Biometrika, 94*(3), 553–568.

Wu, Y., & Cook, R. (2015). Penalized regression for interval-censored times of disease progression: Selection of HLA markers in psoriatic arthritis. *Biometrics, 71*(3), 782–791.

Zhang, H., & Lu, W. B. (2007). Adaptive lasso for Cox's proportional hazards model. *Biometrika, 94*(3), 1–13.

Zhou, Q., Hu, T., & Sun, J. (2017). A sieve semiparametric maximum likelihood approach for regression analysis of bivariate interval-censored failure time data. *Journal of the American Statistical Association, 518*(112), 664–672.

Zou, H. (2006). The adaptive lasso and its oracle properties. *Journal of the American Statistical Association, 476*(101), 1418–1429.

Flexible Modeling of Frailty Effects in Clustered Survival Data

Samuel Manda

Abstract Survival data that have a multivariate structure occur in many health sciences including biomedical research, epidemiology studies and, clinical trials. In most cases, an analysis of multivariate survival data deals with association structures among survival times within same subjects or clusters. Under the conditional (frailty) model approach, the baseline survival functions are modified using mixed effects that incorporates cluster-specific random effects. This approach can be routinely applied and implemented in several statistical software packages with tools to handle analyses of clustered survival data. The random cluster terms are typically assumed to be independently and identically distributed from a known parametric distribution. However, in most practical application, the random effects may change over time, and the assumed parametric random effect distribution could be incorrect. In such cases, nonparametric forms could be used instead. In this chapter, we develop and apply two approaches that assume (a) time dependent random effects and (b) nonparametric random effect distribution. For both approaches, full Bayesian inference using the Gibbs sampler algorithm is used for computing posterior parameter for the mixing distribution and regression coefficients. The proposed methodological approaches are demonstrated using real data sets.

1 Introduction

Modeling and analysis of clustered survival data complicate the estimation procedures since independence between the survival times can no longer be assumed. It has been proven that ignoring clustering effects when an analysis of such data

S. Manda (✉)
Biostatistics Research Unit, South African Medical Research Council, Pretoria, South Africa

Department of Statistics, University of Pretoria, Pretoria, South Africa

School of Mathematics, Statistics, and Computer Science, University of KwaZulu-Natal, Pietermaritzburg, South Africa
e-mail: samuel.manda@mrc.ac.za

A. Bekker et al. (eds.), *Computational and Methodological Statistics and Biostatistics*, Emerging Topics in Statistics and Biostatistics,
https://doi.org/10.1007/978-3-030-42196-0_21

is undertaken could lead to biased estimates of both fixed effect and variance parameters (Heckman and Singer 1984; Pickles and Crouchley 1995; Ha et al. 2001). Random effects models and marginal models are the two most common approaches to modeling clustered survival data. Marginal models focus on the population average of the marginal distributions of multivariate failure times, and the correlation is treated as a nuisance parameter to reduce the dependence of the marginal models on the specification of the unobservable correlation structure of clustered survival data. Parameters are often estimated using generalized estimating equations and the corresponding variance-covariance estimators are corrected properly to account for the possible dependence structure. An excellent overview, with examples, of the marginal approach is discussed in Lin (1994).

On the other hand, random effects models explicitly formulate the underlying dependence in the survival data using random effects. They provide insights into the relationship among related failure times. Conditional on the cluster-specific random effects, the failure times are assumed to be independent. A more general framework for incorporating random effects within a proportional hazards model is given in Sargent (1998) and Vaida and Xu (2000). Random effect survival models are commonly referred to as *shared frailty models* because observations within a cluster share the same cluster-specific effects (Clayton 1991). The nomenclature of frailty effect survival data has its roots from seminal work on univariate survival analyses developed by Vaupel et al. (1979). The frailty effect is taken to collectively represent unknown and unmeasured factors, which affect the cluster-specific baseline risk. The frailty effects can be nested at several clustering levels (Sastry 1997; Bolstad and Manda 2001).

Most of the methodological and analytical developments in the context of frailty models have been based on assuming that the random effects are independent and time-invariant. Within parametric Bayesian hierarchical models (see, for example, Gilks et al. 1996), the usual set-up uses first stage modeling in the observed outcomes. The second stage involves an exchangeable prior distribution on the unobservables (the random frailties), which parameterize the distribution for the observables. However, for some diseases, there may be an increase in the patient's frailty, especially after the first failure event. In such cases, there is need to accommodate the effect of past infection patterns as well as the possibility of time-dependent frailty, for example in recurrent event data. This first part is usually accomplished by a *monitoring risk* variable, which is introduced as a fixed effect covariate. This measures the effect of the deterministic time-dependent component of frailty which can be modeled by the number of prior episodes as in Lin (1994) and Lindsey (1995), or by the total time from study entry as in McGilchrist and Yau (1996) and Yau and McGilchrist (1998). A positive coefficient corresponding to a monitoring risk variable would imply that the rate of infection increases once a first infection has occurred and might indicate serial dependence in the patient's frailty. Alternatively, time-dependent frailty could be modelled using an autoregressive process prior. A simple model uses a stochastic AR(1) prior for the subject (cluster)-specific frailty and residual maximum likelihood estimation procedures have been used (Yau and McGilchrist 1998).

Perhaps a more restrictive assumption is on the parametric model for the frailty effects. For computational convenience, in many applications, the random frailty effects are usually assumed to be independent and identically distributed from a distribution of some known parametric family; in particular, under multiplicative frailty effects, the frailty distribution is from gamma or lognormal families. In practice, information about the distribution of the random effects is often unavailable, and this might lead to poor parameter estimates when the distribution is mis-specified (Walker and Mallick 1997). Furthermore, estimates of covariate effects may show changes in both sign and magnitude depending on the form of frailty distribution (Laird 1978; Heckman and Singer 1984). To reduce the impact of distributional assumptions on the parameter estimates, finite mixture models for frailty effects have been studied (Laird 1978; Heckman and Singer 1984; Guo and Rodriguez 1992; Congdon 1994). A more flexible approach uses nonparametric modelling of frailty effect terms, though this is not used widely in practice (Walker and Mallick 1997; Zhang and Steele 2004; Naskar 2008). Furthermore, asymptotic unbiasedness for estimates of frailty variance depend on the form of the frailty distribution (Ferreira and Garcia 2001). Thus, it is not correct to always assume that the random frailty effects are constant over the study period nor that they arise from a known parametric distribution with its restrictive unimodality and shape. It is important to choose the distribution of the frailty effects to be more flexible in order to account for arbitrary multimodality and unpredictable skewness types (Walker and Mallick 1997). These possibilities can be addressed when the frailty effects distribution is drawn from a large class of distributions. Such a large class could be formed by using nonparametric approaches to model the frailty effect distribution.

In this chapter, we develop methodologies for the analysis of clustered survival where frailty random terms are modelled as time-dependent and nonparametrically. For time-dependent random frailty effect, both the deterministic monitoring risk and stochastic AR(1) model are developed. For the nonparametric frailty model, a Dirichlet process prior is employed (Ferguson 1973). In both frailty effects constructions, parameters are estimated within full Bayesian framework by implementing the Gibbs sampling algorithm in WinBUGS, a statistical software package for Bayesian inference (Spiegelhalter et al. 2004). Both methodologies are applied to example data, and comparisons are made to the constant frailty model using the deviance information criteria (DIC) (Spiegelhalter et al. 2002). Further details on the methods described here could be found in Manda and Meyer (2005) and Manda (2011). We develop the methodology for the nonparametric frailty model. In Sect. 2, we describe the standard conditional survival model and possible extensions. The Dirichlet process prior for nonparametric modelling of the unknown distribution of the frailty effects is presented in Sect. 3, which also describes two constructions of the process: the *Polya urn scheme* and the *stick-breaking* construction. We also describe how the model can be computed using the Gibbs sampler. The child survival data and the resulting parameter estimates are given in Sect. 4. Section 5 presents the proposed time-dependent frailty model for recurrent event analysis, and in Sect. 5.1, we apply the proposed methodology to a data set from Fleming and Harrington (1991) on patients suffering from chronic granulomatous disease. The proposed methodologies are discussed in Sect. 6.

2 Conditional Frailty Survival Model

2.1 Basic Model and Notation

Following Andersen and Gill (1982) (see also Clayton (1991) and Nielsen et al. (1992)), the basic proportional hazards model is formulated using counting process methodology. A counting process $N(t)$ $t \geq 0$, is a stochastic process with $N(0) = 0$. The sample path of $N(t)$ is increasing, piecewise constant, with jumps of size 1 and right-continuous. Additionally, a stochastic process $Y(t)$ is defined to indicate *alive* and under observation at time t.

We extend the counting process methodology to account for clustered events data. The methodology could easily be adopted to work with recurrent-times data. Let J be the number of clusters and each has K_j subjects. For subject jk $(j = 1, \ldots, J;\ k = 1, \ldots, K_j)$, a process $N_{jk}(t)$ is observed, which is a cumulative count of observed events experienced by the subject by time t. In addition, a process $Y_{jk}(t)$, which indicates whether the subject was at risk for the event at time t is also observed. We also measure a possibly time-varying p-dimensional vector of covariates, $x_{jk}(t)$. Thus, for the $(jk)^{th}$ subject the observed data are $D = \{N_{jk}(t), Y_{jk}(t), x_{jk}(t);\ t \geq 0\}$, and are assumed independent. Let $dN_{jk}(t)$ be the increment of $N_{jk}(t)$ over an infinitesimal interval $[t,\ t + dt)$; i.e. $dN_{jk}(t) = dN_{jk}[(t + dt)^-] - dN_{jk}(t^-)$; ($t^-$ is time just before t). For right-censored survival data, the change dN_{jk} takes a value 1 if an event occurred at time t or 0, otherwise. Suppose F_{t-} is the available data just before time t. Then

$$E[dN_{jk}(t)|F_{t-}] = P(dN_{jk}(t) = 1|F_{t-}) = Y_{jk}(t)h_{jk}(t)dt$$

is the mean increase in $N_{jk}(t)$ over the short interval $[t,\ t + dt)$, where $h_{jk}(t)$ is hazard function for subject jk. The process $I_{jk}(t) = Y_{jk}(t)h_{jk}(t)$ is called the *intensity process* of the counting process. The effect of the covariates on the intensity function for subject jk at time t is given by the Cox proportional covariate effects function (Cox 1972)

$$I_{jk}(t|\lambda_0, \beta, x_{jk}(t), w_j) = Y_{jk}(t)\lambda_0(t)w_j e^{\beta^T x_{jk}(t)} \tag{1}$$

where β is a p-dimensional parameter vector of regression coefficients; w_j is the cluster-specific unobserved frailty, which captures the risk of the unobserved or unmeasured risk variables; and $\lambda_0(t)$ is the baseline intensity, which is unspecified and to be modelled nonparametrically. In the present study, the frailty effect w_j is assumed time-invariant, but this can be relaxed in certain situations (Manda and Meyer 2005). Under non-informative censoring, the (conditional) likelihood of the observed data D is proportional to

$$\prod_{j=1}^{J}\prod_{k=1}^{K_j}\prod_{t\geq 0}(I_{jk}(t|\lambda_0(t),\beta,x_{jk}(t),w_j))^{dN_{jk}(t)}e^{-I_{jk}(t|\lambda_0(t),\beta,x_{jk}(t),w_j)dt}. \quad (2)$$

This is just a Poisson likelihood taking the increments $dN_{jk}(t)$ as independent Poisson random variables with means $I_{jk}(t|\lambda_0,\beta,x_{jk}(t),w_j)dt = Y_{jk}(t)w_j\exp(\beta^T x_{jk}(t))d\Lambda_0(t)$, where $d\Lambda_0(t)$ is the increment in the integrated baseline hazard function in interval $[t,\ t+dt)$. We conveniently model the increment $d\Lambda_0(t)$ by a gamma $d\Lambda_0(t) \sim \text{gamma}(cdH_0(t), c)$ prior, where $H_0(t)$ is a known non-decreasing positive function representing the prior mean of the integrated baseline hazard function and c is the confidence attached to this mean (Kalbfleisch 1978; Clayton 1991). Mixtures of beta or triangular distributions could also be used to nonparametrically model the baseline hazard function (Perron and Mengersen 2001), but this is not done here.

2.2 *Prior on the Frailty Distribution*

In a nonparametric Bayesian hierarchical structure, prior uncertainty is at the level of the frailty distribution function F (Green and Richardson 2001). One such prior is the Dirichlet process, which models nonparametrically the distribution function F as a random variable. The use of the Dirichlet process prior to model a general distribution function arises from the work of Ferguson (1973). However, the resulting flexibility comes with higher cost due to increased computational complexity of the analysis. A number of algorithms have been proposed recently for fitting nonparametric hierarchical Bayesian models using Dirichlet process mixtures; namely Gibbs sampling, sequential imputations and predictive recursions. In a comparative analysis of these three algorithms using an example from multiple binary sequences, Quintana and Newton (2000) found the Gibbs sampler, though computational intensive, was more reliable. It is the algorithm of choice for studies involving the Dirichlet process mixture to model random effects distributions in linear models (Kleinman and Ibrahim 1998) and in multiple binary sequences (Quintana and Newton 2000).

The Dirichlet process has previously been successfully used by Escobar (1994) and Maceachern (1994) to estimate a vector of normal means. Recently, Dubson (2009) introduced many interesting applications of Bayesian nonparametric priors for inference in biomedical problems. A number of examples provide motivation for non-parametric Bayes methods in bio-statistical applications. These ideas have been expanded upon by (Muller and Quintana 2009) focussing more on inference for clustering. Naskar et al. (2005) and Naskar (2008) suggest Monte Carlo Conditional Expected Maximisation (EM), a hybrid algorithm to analyse HIV infection times in a cohort of females and recurrent infections in kidney patients, respectively, using a Dirichlet process mixing of frailty effects.

3 Nonparametric Dirichlet Frailty Process Frailty Model

3.1 Dirichlet Process Prior

Parametric Bayesian hierarchical modelling uses first stage modelling in the observed outcomes $dN_{11}(t), dN_{12}(t), \ldots, dN_{JK_J}(t);\ t \geq 0$, and the second stage uses an assumed exchangeable prior, F, usually a gamma or lognormal distribution, on the unobservable $w_1, w_2, \ldots, w_J$. Thus, we have

$$\text{Stage 1}: I_{jk}(t|\lambda_0, \beta, x_{jk}(t), w_j) = Y_{jk}(t)\lambda_0 w_j e^{\beta^T x_{jk}(t)}$$
$$\text{Stage 2}: w_j \sim F$$

A stage where F is allowed to be an unknown random variable is added. Thus, we have

$$\text{Stage 3}: F \sim \text{DP}(M_0, F_0(\gamma))$$

where $\text{DP}(M_0, F_0(.))$ is a Dirichlet process (DP) prior on the distribution function F. The DP prior has two parameters: the function $F_0(.)$, which is one's prior best guess for F, and the scalar M_0, which measures the strength of our prior belief on how well F_0 approximates F. The Dirichlet process prior for distribution function F stems from the work of Ferguson (1973). The property of the process is that for any finite partition $(A_1, \ldots, A_q)$ on the real line R^+, the random vector of prior probabilities $(F(A_1), \ldots, F(A_q))$ has a Dirichlet distribution with parameter vector $(M_0F_0(A_1), \ldots, M_0F_0(A_q))$. Using the moments of the Dirichlet distribution, the DP has prior mean $M_0F_0(0, .]/M_0F_0(0, \infty) = F_0(.)$ and variance $[M_0^2(1 - F_0(.))F_0(.)]/(M_0 + 1)$.

A number of useful constructive characterisations of the Dirichlet process (DP) have been proposed in the literature. For instance, Sethuraman (1994) (see also Ishwaran and James (2001)), proposed that the unknown distribution F could be represented as

$$F \sim \sum_{j=1}^{N} \pi_j \delta_{w_j} \tag{3}$$

a random probability measure with N components; $(w_1, w_2, \ldots, w_N)$ are independent and identically distributed random variables with a distribution F_0; $(\pi_1, \pi_2, \ldots, \pi_N)$ are random weights independent of $(w_1, w_2, \ldots, w_N)$. The random weights are chosen using a stick-breaking construction

$$\pi_1 = V_1 \text{ and } \pi_j = (1 - V_1)(1 - V_2)\cdots(1 - V_{j-1})V_j;\ j = 2, \ldots, N \tag{4}$$

where V_j's are independent Beta $(1,\ M_0)$ random variables. It is necessary to set $V_N = 1$ to ensure that $\sum_{j=1}^{N} \pi_j = 1$. In this paper, we use another important characterisatisation of the DP mixture model: the Polya urn and Gibbs sampling inference.

3.2 Polya Urn Sampling Scheme

The Dirichlet process is not very useful for sampling purposes. Blackwell and Macqueen (1973) presented the process as being generated by a Polya urn scheme. In this scheme, w_1 is drawn from F_0 and then the j^{th} subsequent cluster effect w_j is drawn from this mixture distribution:

$$p(w_j|w_1, \ldots, w_{j-1}) = \sum_{k=1}^{m_j} \frac{m^*_{k,j}}{M_0 + j - 1} \delta_{w^*_{k,j}} + \frac{M_0}{M_0 + j - 1} F_0(.)$$

where $\delta_{w^*_{k,j}}$ is a degenerate distribution giving mass 1 to the point $w^*_{k,j}$; $(w^*_{1,j} \ldots,$ $w^*_{m_j,j})$ are unique set of values in $(w_1, \ldots, w_{j-1})$ with frequency $(m^*_{1,j}, \ldots,$ $m^*_{m_j,j})$; *i.e.* $m^*_{1,j} + \ldots + m^*_{m_j,j} = j - 1$. Thus, if M_0 is very large compared to J, little weight is given to previous samples of w_j, implying that the Dirichlet process leads to a full parametric modelling of the random frailty effects by F_0. On the other hand, if M_0 is small, then the process leads to draws from the previous sampled frailty effect.

Polya urn scheme essentially generates samples of w_j from a finite mixture distribution where the components of the mixture are all prior draws $\{w_1, \ldots, w_{j-1}\}$ and $w_1 \sim F_0$ with probabilities described in the Polya urn scheme above. Polya urn sampling is a special case of what is known as a Chinese Restaurant Process (CRP), a distribution on partitions obtained from a process where J customers sit down in a Chinese restaurant with an infinite number of tables (Teh et al. 2005). The basic process specifies that the first customer sits at the first table, then the j^{th} subsequent customer w_j sits at table $w^*_{k,j}$, with probability proportional to the number $m^*_{k,j}$ of customers already seated at the table, otherwise the customer sits at a new table with probability proportional to M_0

Using this representation of the Dirichlet model, the joint prior distribution of $w = (w_1, \ldots, w_J)$ is given by

$$p(w) = \prod_{j=1}^{J} \frac{\sum_{l=1}^{j-1} \delta_{w^*_l} + M_0 f_0(w_j)}{M_0 + j - 1} \tag{5}$$

where δ_b is a degenerate distribution giving mass 1 to the point b, and $f_0(b) = dF_0(b)$.

The Polya urn sampling results in a discrete distribution for a continuous frailty effect by partitioning the J clusters into latent sub-clusters whose members have identical values of w distinct from members in other sub-clusters. The number of latent sub-clusters depends on the parameter value M_0 and the number of the frailty terms (Escobar 1994). This inherent property of partitioning a continuous sample space into discrete clusters, has often led to the Dirichlet process being criticized as selecting a discrete distribution for an otherwise continuous random variable.

3.3 Posterior Distribution Using Polya Urn Scheme

The marginal and joint posterior distributions of the model parameters given the data are obtained from the product of the data likelihood (2); the priors for Λ_0 , β, w and the hyperprior for γ. To overcome this computational difficulty, the Gibbs sampler (Tierney 1994), a Markov Chain Monte Carlo (MCMC) method, is used to obtain a sample from the required posterior distribution. The Gibbs sampler algorithm generates samples from the joint posterior distribution by iteratively sampling from the conditional posterior distribution of each parameter, given the most recent values of the other parameters. Let $\pi(.|.)$ denote the conditional posterior distribution of interest, $\Lambda_{0(-t)}$ and w_{-j} be the vectors Λ_0 and w, excluding the element t and j respectively.

The conditional of w_j: From Theorem 1 in Escobar (1994), conditional on the other w and the data, w_j has the following mixture distribution:

$$\pi(w_j|\beta, w_{-j}, N(t), Y(t)) \tag{6}$$
$$\propto \frac{\sum_{l\neq j} L(N_j(t), Y_j(t)|\Lambda_0, \beta, w_l)\delta_{w_l} + M_0 g_0(w_j|\gamma)L(N_j(t), Y_j(t)|\Lambda_0, \beta, w_j)}{M_0 \int L(N_j(t), Y_j(t)|\Lambda_0, \beta, w_j) f_0(w_j|\gamma)dw_j + \sum_{l\neq j} L(N_j(t), Y_j(t)|\Lambda_0, \beta, w_l)}$$

where $L(N_j(t), Y_j(t)|\Lambda_0, \beta, w_j)$ is the sampling distribution of the data in the jth cluster. We note that

$$\pi(w_j|\Lambda_0, \beta, \gamma, N_j(t), Y_j(t)) = f_0(w_j|\gamma)L(N_j(t), N_j(t)|\Lambda_0, \beta, w_j)/\pi(N_j(t), Y_j(t))$$

where $\pi(N_j(t), Y_j(t))$ is the marginal density of $(N_j(t), Y_j(t))$ which, typically, is evaluated by numerical integration. This can be costly when the number J of clusters is large. In order to ease the computational burden, the base measure F_0 is selected to be conjugate to the likelihood of the data. We chose F_0 to be a gamma distribution with mean 1 and variance $\sigma^2 = 1/\gamma$. The marginal distribution of the cluster-specific observed data $(N_j(t), Y_j(t))$ when w_j has the gamma f_0 prior is

$$\pi(N_j(t), Y_j(t)) \propto \int \prod_{k=1}^{K_j} \prod_{t\geq 0} \left[(w_j d\Lambda_0(t) e^{\beta^T x_j(t)})^{dN_j(t)} e^{-Y_j(t) w_i e^{\beta^T x_j(t)} d\Lambda_0(t)} \right]$$
$$w_j^{\gamma-1} e^{-\gamma w_j} dw_j$$

$$= \frac{\Gamma(\gamma + D_j)}{(\gamma + H_j)^{\gamma + D_j}} \prod_{t \geq 0} (d\Lambda_0(t) e^{\beta^T x_j(t)})^{dN_j(t)} \tag{7}$$

where D_j and $H_j = \sum_t Y_j(t) \exp(\beta^T x_j(t)) d\Lambda_0(t)$ are the total number of events and integrated hazard function for cluster j, respectively. Substituting (5) into (4), we have a two-component mixture for the posterior distribution of w_j, which is drawn in the following manner. Using probability proportional to

$$\prod_{k=1}^{K_i} \prod_{t \geq 0} (w_i d\Lambda_0(t) e^{\beta^T x_{ik}(t)})^{dN_{ik}(t)} \exp(-Y_{ik}(t) w_i e^{\beta^T x_{ik}(t)} d\Lambda_0(t))$$

the selection is made from δ_{w_i}, which means that $w_j = w_i$; and with probability proportional to $M_0 \pi(N_j(t), Y_j(t))$ we select w_j from its full conditional posterior distribution $\pi(w_j | \Lambda_0, \beta, \gamma, N_j(t), Y_j(t))$, which is given by

$$\begin{aligned} \pi(w_j | \Lambda_0, \beta, \gamma, N_j(t), Y_j(t)) &\propto F_0(w_j | \gamma) L(N_j(t), Y_j(t) | \Lambda_0, \beta, w_j) \\ &= \frac{(\gamma + H_j)^{\gamma + D_j}}{\Gamma(\gamma + D_j)} w_j^{\gamma + D_j - 1} e^{-(\gamma + H_j) w_j} \end{aligned}$$

a gamma$(\gamma + D_j, \gamma + H_j)$ distribution. This is a mixture of point masses and a gamma distribution. This process draws a new frailty term for cluster j more often from the sampled effects w_l, $l \neq j$ if the observed likelihood for the cluster conditional on the w_l's are relatively large; otherwise the draw is made from its conditional gamma distribution.

The conditional distribution of $d\Lambda_0(t)$ is

$$\pi(d\Lambda_0(t) | \Lambda_{0-t}, \beta, w, N(t), Y(t)) \propto d\Lambda_0(t)^{cdH_0(t) + dN_+(t) - 1} e^{-(c + R_+(t|\beta, w_i)) d\Lambda_0(t)}$$

where $dN_+(t) = \sum_j^J \sum_k^{K_j} dN_{jk}(t)$ and $R_+(t|\beta, w_i) = \sum_j^J \sum_k^{K_j} Y_{jk}(t) w_j \exp(\beta^T x_{jk}(t))$. This conditional is the gamma$(cdH_0(t) + dN_+(t), c + R_+(t|\beta, w_i))$ distribution, and will be sampled directly.

The conditional posterior distribution of β is

$$\begin{aligned} \pi(\beta | \Lambda_0, w, \gamma, N(t), Y(t)) \propto \pi(\beta) \prod_{j=1}^{J} \prod_{k=1}^{K_j} \prod_{t \geq 0} w_j (e^{\beta^T x_{jk}(t)})^{dN_{jk}(t)} \\ \exp(-Y_{jk}(t) w_j e^{\beta^T x_{jk}(t)} d\Lambda_0(t)) \end{aligned} \tag{8}$$

where $\pi(\beta)$ is a prior density for β, commonly assumed to be the multivariate normal distribution with mean zero and the covariance matrix having zero off-diagonal terms. This conditional does not simplify to any known standard density. The vector β can readily be sampled using a Metropolis-Hastings step with a

multivariate Gaussian density centred at the last draw (Tierney 1994). That is, at iteration m, a candidate β^* is generated from $\mathrm{N}(\beta^{m-1}, D_\beta)$, and with probability

$$\min\left\{\frac{\pi(\beta^*|\Lambda_0, w, \gamma, N(t), Y(t))}{\pi(\beta^{(m-1)}|\Lambda_0, \beta, w, \gamma, N(t), Y(t))}, 1\right\}$$

the draw $\beta^{(m)}$ is set to β^*, otherwise $\beta^{(m)} = \beta^{(m-1)}$. The covariance matrix D_β may be tuned to allow for an acceptance rate of around 50%.

We model the hyperparameter γ by a hyperprior gamma distribution with known shape κ_1 and scale κ_2. Its conditional distribution uses the $J' \leq J$ distinct values $w^* = (w_1^*, \ldots, w_{J'}^*)$, which are regarded as a random sample from F_0 (Quintana and Newton 2000). Subjects sharing a common parameter value in w^* have a common distribution and thus are in the same group. The conditional posterior density of γ is

$$\pi(\gamma|\beta, w^*, N(t), Y(t)) \propto \gamma^{\kappa_1-1}e^{-\kappa_2\gamma}\frac{\gamma^{J'\gamma}}{(\Gamma(\gamma))^{J'}}\prod_{j=1}^{J'}(w_j^*)^{\gamma-1}e^{-\gamma\sum_{j=1}^{J'}w_j^*} \quad (9)$$

$$\propto \frac{\gamma^{J'\gamma+\kappa_1-1}}{(\Gamma(\gamma))^{J'}}e^{-\gamma(sum_j-\log prod_j+\kappa_2)}$$

where $sum_j = \sum_{j=1}^{J'} w_j^*$ is the sum of the distinct frailty values, and $prod_j = \prod_{j=1}^{J'} w_j^*$ is their product. This conditional does not simplify to any standard distribution, thus requiring a non-standard method of sampling from it.

4 Application of the Model

4.1 Data

The example data concerns child survival collected in the 2000 Malawi Demographic and Health Survey. The data are hierarchically clustered in 559 enumeration areas (EAs); these form our community clustering units. We concentrate on all of the 11,926 births in the 5 years preceding the survey. The distribution of the number of births per community had a mean of 21 and median of 20 with an interquartile range of 16–26. The minimum and maximum number of births per community was 5 and 68, respectively. Infant and under-five mortality rates per 1000 live births were estimated to be 104 and 189, respectively (NSO 2001). These rates are still very high when compared to those around the world (56 and 82, respectively) (Bolstad and Manda 2001). We considered some standard explanatory variables used in the analysis of child mortality in sub-Saharan countries (Manda 1999). The distributions of the predictor variables are presented in Table 1.

Table 1 Descriptive statistics of explanatory variables used in the analysis

Variable	Frequency	Percent
Gender of child		
Male	5951	49.9
Female	5975	51.1
Preceding birth interval		
First birth	2924	24.5
<24 months	1514	12.7
24–36 months	3569	29.9
>36 months	3919	32.9
Maternal education		
No education	3547	29.7
Primary	7213	63.0
Secondary and higher	866	7.3
Residence		
Urban	2084	17.5
Rural	9842	82.5
Region		
Northern	1936	16.2
Central	4394	36.8
Southern	5596	46.9
Total	11,926	100.0
	Mean	*Median*
Birth order	3.4	3.0
Maternal age	25.8	24.3

4.2 Implementation and Results

In a previous analysis of childhood mortality using the 1992 Malawi Demographic Health Survey data, Manda (1999) found that the rate of death for children under five years was 0.0055 deaths per birth per month. Thus, we set the mean cumulative increment in the baseline child death rate as $dH_0(t) = 0.0055\,dt$, where dt denoted a one-month interval. Our prior confidence in the mean hazard function is reflected by assigning $c = 0.1$, which is weakly informative. We adopt a vague proper gamma $(1, 0.1)$ prior for the precision of the community frailty effect γ. This implies that *apriori* the community-specific frailty w_j has variance $1/10 = 0.1$, which we thought to be reasonable as the differences in risk are likely to be minimal because we have adjusted for some important community-level factors: region and type of residence. We do not have sufficient prior information on the prior precision and concentration parameter M_0, so we assigned it a gamma $(0.001, 0.001)$ prior implying a mean of 1, but with reasonable coverage across its space.

The computation of the parameter estimates was run in *WinBUGS* software (Spiegelhalter et al. 2004). For each model considered, three parallel Gibbs sampler chains from independent starting positions were ran for 50,000 iterations. All fixed

effects and covariance parameters were monitored for convergence. Trace plots of sample values of each of these parameters showed that they were converging to the same distribution. We formally assessed convergence of the three chains using the German-Rubin reduction factor, and it stabilised to 1.0 by 2000 iterations. However, for posterior inference, we used a combined sample of the last 30,000 iterations. Using the posterior samples of the parameters, we calculated 50% (median) and (2.5% 97.5%) (95% CI) percentiles for posterior summaries. We also performed limited model selection using the Bayesian Information Criterion (BIC). BIC is defined as BIC $= -2 * \log$ likelihood $+ P \log g$, where P is the number of unknown parameters in the model and g is the sample size. A better fitting model has a smaller BIC value. The parametric gamma and the nonparametric model had BIC values of 13,657.68 and 11,797.96, respectively, showing that the nonparametric approach to frailty was a better fitting model for the data.

Posterior summaries are presented in Table 2 for both the gamma frailty model and the Dirichlet process frailty model. For the fixed effects, the results are presented on the logarithm scale where no risk is represented by 0. The estimates of the fixed

Table 2 Posterior median and 95% credibility interval (CI) of the parameters for the Malawi child survival data

	The parametric frailty		The nonparametric frailty	
Parameter	Median	95% CI	Median	95% CI
Male child (0: No, 1: Yes)	0.095	−0.008, 0.200	0.091	−0.008, 0.186
Birth order	−0.025	−0.112, 0.066	−0.027	−0.133, 0.073
Birth order^2	0.003	−0.006, 0.010	0.002	−0.006, 0.010
Preceding birth interval				
<2 years	0	–, –		–, –
2–3 years	−0.383	−0.528, −0.243	−0.381	−0.522, −0.252
>2 years	−0.404	−0.555, −0.254	−0.406	−0.570, −0.254
Maternal age				
(Age-26)/10	0.009	−0.154, 0.174	0.019	−0.154, 0.189
((Age-26)/10)^2	0.123	0.018, 0.230	0.117	0.006, 0.227
Maternal education				
Secondary+ (0: No, 1: Yes)	−0.197	−0.472, 0.060	−0.206	−0.465, 0.052
Region of residence				
Northern region	0	–, –		
Central region	−0.101	−0.275, 0.077	−0.106	−0.278, 0.079
Southern region	0.014	−0.155, 0.184	0.013	−0.152, 0.190
Rural residence (0: No, 1: Yes)	0.305	0.142, 0.479	0.295	0.127, 0.457
Frailty effects				
No of risk classes			21	3, 79
Variance of sub-risk frailties			0.073	0.026, 0.379
DP precision (M_0)			4.172	0.454, 33.83
Variance of frailty effects	0.056	0.027, 0.101		

effects are largely the same between a fully parametric and a nonparametric model. Based on the 95% CI, not all of the fixed effects are significant; however, the median estimated effects of the modelled covariates support the findings in previous studies on child mortality in sub-Saharan Africa and other less developed countries (Sastry 1997; Manda 1999). A male child has slightly higher risk of death. Birth order has a decreasing risk effect. A long preceding birth interval greatly reduces the risk of death for the index child. The coefficient of the quadratic part of the age of the mother indicates a child born to a younger or older mother has higher risk. Maternal education is clearly an important factor: higher educational level is a surrogate for many positive economic and social factors. Living in rural areas has an increased risk. Region of residence is a risk factor, though not greatly pronounced.

The nonparametric Dirichlet mixing process has identified 21 classes into which the 559 communities can be separated according to their childhood mortality risk. The distinct latent risk values have a posterior median variance of 0.073, slightly larger than the variance of the frailty effects under the full parametric gamma frailty. The precision of the DP process has a median of 4, well below the total number of communities, indicating that distribution of the community effects is more likely multimodal and nonparametric.

5 Time Dependent Frailty

We have seen that in Sect. 3, stage 2 could be modelled conveniently, using a gamma distribution with mean one and unknown variance. However, apart from being restrictive, the gamma distribution has some undesirable properties in that it is not symmetric or scale-invariant; a property which ensures that the inference does not depend on the measuring units (Vaida and Xu 2000). We have shown how this frailty effect could be modeled nonparametrically. In here, we still use stage 2 modeling as in Sect. 3, where some flexibility is imposed on the random frailty effects by assuming it is time-dependent. Thus, the notation for subject frailty effect is slightly changed to depend on t. Thus, in the following, $w_{i(t)}$ is assumed to follow a first-order autocorrelated AR(1) process prior:

$$w_{i(t)}|w_{i(t-1)} = \phi w_{i(t-1)} + e_{i(t)}; \;\; i = 1, \ldots, I, \;\; t \geq 0 \tag{10}$$

where $w_{i(0)} \sim \text{Normal}(0, \sigma_w^2)$ and $e_{i(t)}$ are *i.i.d* random variables having a Normal$(0, \sigma_w^2)$ distribution. The parameter ϕ is constrained to lie between -1 and 1 and it measures the degree of serial correlation in the subject-specific frailty. The prior density of the frailty vector $w = (w_{1(t)}, \ldots, w_{I(t)})$ is given by

$$p(w|\phi, \sigma_w^2) \propto \prod_{i=1}^{I} \prod_{t \geq 0}^{c} (\sigma_W^2)^{-1/2} \exp\left(-\frac{1}{2\sigma_w^2} (w_{i(t)} - \phi w_{i(t-1)})^2 \right)$$

5.1 Example Data

The example data is taken from Fleming and Harrington (1991) and it describes a double-blinded placebo controlled randomised trial of gamma interferon (γ-IFN) in chronic granulomatous disease (CGD). The disease is a group of rare inherited disorders of the immune function, characterized by recurrent pyogenic infections. These infections result from the failure to generate microbicidal oxygen metabolites, within the phagocytes, to kill ingested micro-organisms. The disease usually presents early in life and may lead to death in childhood. There is evidence that gamma interferon is an important macrophage activating factor which could restore superoxide anion production and bacterial killing by phagocytes in CGD patients. A total of 128 patients were followed for about a year and 203 infections/censorings were observed, with the number of infections per patient ranging from 1 to 8. Of the 65 patients on placebo, 30 had at least one infection, but only 14 of the 63 patients on gamma interferon treatment had more than one infection. This resulted in 56 and 20 infections amongst the placebo and gamma interferon groups respectively.

The original data set is shown by treatment group in Table 3. The use of corticosteroid on entry is not sufficiently varied in the data (a very small proportion of the subjects were using it), hence it is not used in the present analysis. These data have previously been analysed using gap-times between infections and total times using the number of preceding events and a shared frailty model. In our analysis, we also use the logarithm of the number of previous infections plus 1 (labelled as *PEvents (t)*) as the deterministic time-dependent component of frailty. Its parameter ω measures the effect of past infections on the risk of the current infection. We used 5-day intervals for each patient, resulting in 88 such intervals.

Table 3 Baseline characteristics according to treatment group

Baseline characteristic	Placebo	Gamma interferon
No. of patients	65	63
Pattern of inheritance		
(0: autosomal recessive, 1: X-linked)	41 (63.1%)	45 (71.4%)
Age (in years)[a]	14.98 (9.64)	14.29 (10.12)
Height (in cm)[a]	140.55 (34.10)	139.57 (27.24)
Weight (in kg)[a]	42.30 (24.32)	38.76 (19.92)
Corticosteroid use (0: No, 1: Yes)	2 (3.1%)	1 (1.6%)
Prophylactic antibiotic use (0: No, 1: Yes)	55 (84.6%)	56 (88.9%)
Gender (0: male, 1: female)	12 (18.5%)	12 (19.1%)
Hospital region (0: USA, 1: Europe)	22 (33.8%)	17 (27.0%)

[a]Mean with standard deviation (SD) in parenthesis

5.2 *Prior Specification and Model Comparison*

In running the Gibbs sampling algorithm, the prior specifications were as follows: For both the baseline and fixed effect parameters, σ_0^2 was set to 1000, resulting in a normal distribution which is very uninformative. In specifying noninformativeness for the frailty variance σ_W^2, the hyperparameters κ_0 and ω_0 of the inverse-gamma prior are usually set to very low values, typically 0.001 is used in the WinBUGS software. However, κ_0 and ω_0 values near 0 can result in an improper posterior density. Moreover, when the true frailty variance is near 0, inferences become sensitive to choices of κ_0 and ω_0 (Gelman 2004). For numerical stability, we chose $\sigma_W^2 \sim$ inverse-gamma(1, 1). In specifying a Beta(ξ_0, φ_0) prior for ξ, the values of ξ_0 and φ_0 were set at 3 and 2. This centres ξ at 0.6 (and ϕ at 0.2), but is flat far away from this value.

We considered a number of competing models for these data and compared them using the Deviance Information Criterion (DIC) developed by Spiegelhalter et al. (2002). The DIC is defined as DIC $= \bar{D} + p_D$ where $\bar{D}$ is the posterior mean of the deviance (measures model *fit*) and p_D is the effective number of parameters in the model (measures model *complexity*). The parameter p_D is calculated using $p_D = \bar{D} - D(\bar{\psi})$, where $D(\bar{\psi})$ is the deviance evaluated at the posterior mean of the unknown parameters. The DIC is particularly useful in situations involving complex hierarchical models in which the number of parameters used is not known. It is a generalisation of the Akaike Information Criterion (AIC) and works on similar principles. The models we compared were:

- Model 1: $\eta_{i(t)} = \beta^T X_i(t) + \omega PEvents(t)$. This model allows for differences in the infection times that only depend on the measured risk variables including a deterministic time-dependent component of frailty; it does not allow for the random frailty component.
- Model 2: $\eta_{i(t)} = \beta^T X_i(t) + \omega PEvents(t) + W_i$. This model allows for differences depending on the covariates as well as the random frailty component for each patient. However, it assumes that the patient random frailty is constant over time. Thus, W_i can be considered as the frailty on entry for the ith patient and it does not change with time.
- Model 3: $\eta_{i(t)} = \beta^T X_i(t) + \omega PEvents(t) + W_{i(t)}$. Rather than assuming a constant model for the random subject frailty effect, Model 3 uses a time-dependent random frailty. This became our main model, which we suggest is better at explaining all the variation in the data.

For each model, the Gibbs sampler was run for 100,000 iterations and using trace plots of sample values, we found very rapid convergence for the baseline and fixed effect parameters, but a longer *burn-in* was required for the convergence of variance and correlation parameters. The first 50,000 iterations were discarded and the remaining 50,000 samples were used for posterior inference. The estimates of DIC and p_D for the three competing models are presented in Table 4. It should be noted that the use of DIC is not meant to show a true model, but rather to compare

Table 4 DIC parameters for model selection

Model I	$\bar{D}$	$D(\bar{\psi})$	p_D	DIC
Model I	812.00	803.04	8.96	821.33
Model II	783.24	750.14	33.10	816.74
Model III	724.74	651.11	73.62	798.36

different sets of models. Model choice is based on a combination of model fit, complexity and the substantive importance of the model. Starting with the fixed effect Model 1, the effective number of parameters p_D is 8.96, nearly equal to the correct number of parameters which is 10 (8 fixed effects, a longitudinal parameter and a constant baseline hazard). This model does not offer any meaningful insights into the variation in the data above that given by the observed covariates. Thus, we are motivated to consider random effects models, which are Models 2 and 3. For Models 2 and 3, the estimates of p_D are roughly 33 and 74 respectively. The number of unknown is 139 and 11,266 for Models 2 and 3, respectively. Thus, even though the number of unknown parameters in Model 3 is about 80 times larger than that in Model 2, its effective number of parameters is just a little over twice as large. This suggest that Model 3 is still quite sparse. Furthermore, it has the lowest goodness-of-fit as measured by $\bar{D}$. The effectiveness of Model 3 is further supported by its lowest DIC value, indicating that this model is best in terms of overall model choice criterion that combines goodness-of-fit with a penalty for complexity. In these circumstances, we prefer Model 3, as it is more effective and explains the variation in the data better.

5.3 Results

The posterior estimates from Model 1 are given in columns two and three in Table 5. The posterior distribution of the treatment effect has mean -0.875 and standard deviation (SD 0.276), showing that the (γ-IFN) treatment has the effect to reduce substantially the rate of infection in CGD patients. Other covariates that have an effect on the rate of infection include pattern of inheritance, age, the use of prophylactic at study entry, gender and hospital region. Height and weight were not significantly related to rate of infection. The results also show that the risk of recurrent infection significantly increases as the number of previous infections increases (mean 0.712 and SD 0.225). For comparison, the treatment and the longitudinal effects in Lindsey (1995), without controlling for the other covariates, were estimated at -0.830 (SD 0.270) and 1.109 (SD 0.227), respectively, using maximum likelihood estimation. When we left out the number of previous infections, the effect of treatment increases to -1.088; the same was also observed in Lindsey (1995) where it changed to -1.052. Thus, the effect of treatment is partially diminished by the inclusion of the number of previous infections.

Table 5 Posterior estimates of parameters using the Gibbs sampling

	Model 1		Model 2		Model 3	
Parameter	Mean	SD	Mean	SD	Mean	SD
γ-IFN	−0.875	0.276	−1.065	0.353	−0.889	0.283
Inheritance	−0.458	0.297	−0.542	0.393	−0.466	0.308
Age	−0.063	0.034	−0.073	0.045	−0.063	0.035
Height	0.004	0.010	0.008	0.015	0.005	0.011
Weight	0.001	0.016	0.005	0.022	0.009	0.017
Prophylactic	−0.541	0.323	−0.726	0.466	−0.561	0.336
Sex	−0.507	0.400	−0.536	0.520	−0.507	0.412
Hospital region	−0.553	0.312	−0.658	0.400	−0.556	0.319
ω	0.712	0.225	0.146	0.330	0.699	0.247
σ_W^2	–	–	0.788	0.459	0.879	0.507
ϕ	–	–	–	–	0.313	0.278

Next, we consider Model 2 which compares to analyses in McGilchrist and Yau (1996), Yau and McGilchrist (1998) and Vaida and Xu (2000) using (restricted) maximum likelihood estimation on inter-event times and the EM algorithm on the Cox model, respectively. The results are presented in columns four and five of Table 5. The posterior estimates of the risk variables are fairly close to those obtained under Model 1, except that the effect of the longitudinal parameter ω is now much reduced and no longer significant. Similar results were found in Vaida and Xu (2000), where the effect of the number of previous infections was reduced to a non-significant result when the random frailty term was included in the analysis. The variance of patient frailty effect is estimated with a posterior mean 0.788 and SD 0.459 and is significant. In comparison, the estimates of the frailty variance were 0.237 (SD 0.211) and 0.593 (SD 0.316) under ML and REML methods, respectively, in McGilchrist and Yau (1996) when the number of the previous infections was adjusted for, and 0.743 (SD 0.340) in Yau and McGilchrist (1998) without controlling for the number of previous infections. It appears that the number of previous infections explains most of the variation in the patient's frailty effects. However, we argue for the inclusion of both deterministic time-dependent and random components of frailty as they control for order and common dependence in recurrent-event times. Moreover, using a random frailty effect will also account for the effects of the missing covariates.

Finally, we examine the results from Model 3 and these are given in the last two columns of Table 5. Posterior means and SDs of the risk variables are in general agreement with those obtained in Models 1 and 2. The frailty correlation parameter ϕ is estimated with a posterior mean 0.313 and SD 0.278, indicating the presence of a positive serial correlation between the recurrent event times, but not sufficiently significant. The variance of frailty has posterior mean 0.879 and SD 0.507, showing that, apart from the serial dependence, the recurrent event times within a subject share a common frailty effect that partially summarizes the dependence within the subject.

The general criticism of using a normal model for the subject random effects is its susceptibility to outliers. Thus, we considered three other comparable models for the subject random effects: double exponential, logistic and t_d distributions for sensitivity analyses on the parameter estimates. Using a small d, say 4, the t_4 distribution can also be used as a robust alternative model for the subject random effects. We fitted each alternative model as in Model 3 with the same prior specification for β and the variance parameters. The fixed effects were essentially the same as those in Table 5. For instance the effect of treatment was estimated with posterior mean -0.909, -0.894 and -0.883 with SD 0.296, 0.284 and 0.281, respectively, for the double exponential, logistic and t_4 models. There was a slight sensitivity to the frailty variance estimate with mean and SD values 0.255 (0.093), 0.418 (0.112) and 0.349 (0.122) respectively. However, the overall conclusions that the frailty variance is significant is the same for the models and in general this application is insensitive and robust.

Our analyses yield posterior means and SDs of fixed effect parameters that are lower than those obtained by Yau and McGilchrist (1998) using either ML or REML estimation. However, we obtain an estimate of the frailty variance, which is larger than the ML estimate (0.200, SD 0.480), but similar to the REML estimate (0.735, SD 0.526). The Bayesian estimate of the correlation parameter is also lower than both the ML (0.729, SD 0.671) and REML (0.605, SD 0.325) estimates. It should be noted that they used total time since the first failure to define a deterministic time-dependent frailty, in addition to using inter-event times in their models, so these differences might be due to the modelling strategy of recurrent event times and the deterministic time-varying component of frailty.

6 Discussion

This chapter has introduced two flexible approaches to dealing with associations between survival times in a conditional model for the analysis of multivariate survival data. The two approaches were demonstrated using real data sets. Firstly, we assumed that frailty effect could be modelled nonparametrically using a Dirichlet process prior, which specifies prior uncertainty for random frailty effects at the level of the distribution function; this offers infinite alternatives. This could have practical benefits in many applications, where, often, the concern is grouping units into strata of various degrees of risk. In our analysis of the child survival data, the nonparametric approach allowed us to categorize the sample of the communities into 21 classes of risk of childhood mortality. Understanding that communities can be classified according to their risk of childhood mortality provides useful guidance on the effective use of resources for childhood survival and preventive interventions. The identified 21 sub-classes of risk could be administratively convenient and manageable for child health intervention programs.

We note that the model could be extended to have the covariate link function unspecified and modelled nonparametrically, for instance, by a mixture of beta or

triangular distributions (Perron and Mengersen 2001). Such an extension would make the proportional hazards model fully nonparametric in all parts of the model. A similar model involving minimal distributional assumptions on fixed and frailty effects was presented in Zhang and Steele (2004). However, implementation of such models would be computationally more complex and intensive, especially when there are many short intervals for the counting process.

For the data example, the estimates of the fixed effects and 95% confidence intervals were similar under both frailty model assumptions; thus substantive conclusions are not affected by whether or not we use a nonparametric form for the frailty effects. The fact that a seemingly more complex model produces similar results to those under a simpler model is irrelevant when we consider that there is no reason *aprior* to believe that a gamma shape is adequate for the distribution of the random frailties (Dubson 2009). A parametric gamma model would have been unable to model frailty adequately if the distribution of the frailties had arbitrary shapes and if there were interactions between the observed and the unobserved predictors. Thus, a nonparametric frailty model validates the parametric gamma model in this application.

In the second approach, we have shown that a model encompassing dependence through a time-varying longitudinal parameter with complex structure, that accounts for both intra-subject and order correlation, provides a better fit than other traditional models of dependence. It has also been shown for these data that only the deterministic time component of frailty is important. In the more complex models, using an AR(1) frailty model, the correlation and the random component show high positive dependence and variation, respectively, though with minimal significance since these estimates are marginally larger than their standard deviations. Despite this, we are satisfied that a model has been presented for consideration in the analysis of similar data structures, whether binary or count data.

References

Andersen, P. K., & Gill, R. D. (1982). Cox's regression models for counting processes. *The Annals of Statistics, 10*, 1100–1120.

Blackwell, D., & Macqueen, J. B. (1973). Ferguson distribution via Polya Urn schemes. *Annals of Statistics, 1*, 352–355.

Bolstad, W. M., & Manda, S. O. M. (2001). Investigating child mortality in Malawi using family and community random effects: a Bayesian analysis. *Journal of the American Statistical Association, 96*, 12–19.

Clayton, D. G. (1991). A Monte Carlo method for Bayesian inference in frailty models. *Biometrics, 47*, 467–485.

Congdon, P. (1994). Analysing mortality in London: Life-Tables with frailty. *Statistician, 43*, 277–308.

Cox, D. R. (1972). Regression and Life-Tables (with discussion). *Journal of the Royal Statistical Society, Series B, 34*, 187–220.

Dubson, D. P. (2009). Nonparametric Bayesian application to biostatistics. In N. Njort, C. Holmes, P. Muller, & S. Walker (Eds.), *Bayesian nonparametrics in practice* Cambridge: Cambridge University Press.

Escobar, M. D. (1994). Estimating normal means with a Dirichlet process prior. *Journal of the American Statistical Association, 89*, 268–277.
Ferguson, T. S. (1973). A Bayesian analysis of some non-parametric problems. *The Annals of Statistics, 1*, 209–230.
Ferreira, A., & Garcia, N. L. (2001). Simulation study for mis-specifications on frailty model. *Brazilian Journal of Probability and Statistics, 15*, 121–134.
Fleming, T. R, Harrington, D. P. (1991). *Counting processes and survival analysis*. New York: Wiley.
Gelman, A. (2004). Parameterization and Bayesian Modeling. *Journal of the American Statistical Association, 99*(466), 537–545. https://doi.org/10.1198/016214504000000458.
Gilks, W. R., Richardson, S., & Spiegelhalter, D. J. (1996). *Markov chain Monte Carlo in practice*. London: Chapman and Hall.
Green, P. J., & Richardson, S. (2001). Modelling heterogeneity with and without the Dirichlet process. *Scandanavian Journal of Statistics, 28*, 355–375.
Guo, G., & Rodriguez, G. (1992). Estimating a multivariate proportional hazards model for clustered data using the EM algorithm, with application to child survival in Guatemala. *Journal of the American Statistical Association, 87*, 969–979.
Ha, I. D., Lee, Y., & Song, J.-K. (2001). Hierarchical likelihood approach for frailty models. *Biometrika, 88*, 233–243.
Heckman, J., & Singer, B. (1984). A Method of minimising the impact of distributional assumptions in econometric models for duration data. *Econometrical, 52*, 231–241.
Ishwaran, H., & James, L. F. (2001). Gibbs sampling methods for stick-breaking priors. *Journal of the American Statistical Association, 96*, 161–173.
Kalbfleisch, J. D. (1978). Nonparametric Bayesian analysis of survival time data. *Journal of the Royal Statistical Society, Series B, 40*, 214–221.
Kleinman, K. P., & Ibrahim, J. G. (1998). A semiparametric Bayesian approach to the random effects model. *Biometrics, 54*, 921–938.
Laird, N. (1978). Nonparametric maximum likelihood estimation of a mixture distribution. *Journal of the American Statistical Association, 73*, 805–811.
Lin, D. Y. (1994). Cox regression analysis of multivariate failure time data: The marginal approach. *Statistics in Medicine, 13*, 2233–2247.
Lindsey, J. K. 1995. Fitting parametric counting processes by using log-linear models. *Applied Statistics, 44*, 201–212.
Maceachern, S. N. (1994). Estimating normal means by a conjugate style Dirichlet process prior. *Communications in Statistics, 23*, 727–741.
Manda, S. O. M. (1999). Birth intervals, breastfeeding and determinants of childhood mortality in Malawi. *Social Science and Medicine, 48*, 301–312.
Manda, S. O. M. (2011). A nonparametric frailty model for clustered survival data. *Communications in Statistics: Methods and Theory, 40*(5), 863–875.
Manda, S. O. M., & Meyer, R. (2005). Bayesian inference for recurrent events data using time-dependent frailty. *Statistics in Medicine, 24*, 1263–1274.
McGilchrist, C. A, & Yau, K. K. W. (1996). Survival analysis with time dependent frailty using a longitudinal model. *Australian Journal of Statistics, 38*, 53–60.
Muller, P., & Quintana,F. (2009). *More nonparametric Bayesian for biostatistics*. Available at www.mat.puc.cl/~quintana/mnbmfb.pdf. Accessed 21 May 2009.
Naskar, N. (2008). Semiparametric analysis of clustered survival data under nonparametric frailty. *Statistica Neerlandica, 62*, 155–172.
Naskar, N., Das, K., & Ibrahim, I. G. (2005). A semiparametric mixure model for analysing clustered competing risk data. *Biometrics, 61*, 729–737.
National Statistical Office (NSO). (2001). *Malawi demographic and health survey 2000*. Calverton, MD: National Statistical Office and Macro International Inc.
Nielsen, G. G., Gill, R. D., Andersen, P. K., & Sorensen, T. I. A. (1992). A counting process approach to maximum likelihood estimation in frailty models. *Scandinavian Journal of Statistics, 19*, 25–43.

Perron, F., & Mengersen, K. (2001). Bayesian nonparametric modeling using mixtures of triangular distributions. *Biometrics, 57*, 518–528.

Pickles, A., & Crouchley, R. (1995). A comparison of frailty models for multivariate survival data. *Statistics in Medicine, 14*, 1447–1461.

Quintana, F. A., & Newton, M. A. (2000). Computational aspects of nonparametric Bayesian analysis with applications to the modelling of multiple binary sequences. *Journal of Computational and Graphical Statistics, 9*, 711–737.

Sargent, D. J. (1998). A general framework for random effects survival analysis in the Cox proportional hazards setting. *Biometrics, 54*, 1486–1497.

Sastry, N. (1997). A nested frailty model for survival data, with application to study of child survival in Northeast Brazil. *Journal of American Statistical Association, 92*, 426–435.

Sethuraman, J. (1994). A constructive definition of Dirichlet priors. *Statistica Sinica, 4*, 639–650.

Spiegelhalter, D. J., Best, N. G., Carlin, B. P., van der Linde, A. (2002). Bayesian measures of model complexity and fit. *Journal of the Royal Statistical Society, Series B, 64*, 583–639.

Spiegelhalter, D. J., Thomas, A., Best, N. G., & Lunn, D. (2004). *BUGS: Bayesian inference using Gibbs sampling, version 1.4.1*. Medical Research Council Biostatistics Unit, Cambridge University.

Teh, Y. W., Jordan, M. I., Beal, M. J., & Blei, D. M. (2005). *Hierarchical Dirichlet Processes*. Technical Report 653. Department of Statistics, University of California at Berkeley.

Tierney, L. (1994). Markov chain for exploring posterior distributions. *Annals of Statistics, 22*, 1701–1762.

Vaida, F., & Xu, R. (2000). Proportional hazards model with random effects. *Statistics in Medicine, 19*, 1309–3324.

Vaupel, J. W., Manton, K. G., & Stallard, E. (1979). The impact of heterogeneity in individual frailty on the dynamics of mortality. *Demography, 16*, 439–454.

Walker, S. G., & Mallick, B. K. (1997). Hierarchical generalised linear models and frailty models with Bayesian nonparametric mixing. *Journal of Royal Statistical Society B, 59*, 845–860.

Yau, K. K. W., & McGilchrist, C. A. (1998). ML and REML estimation in survival analysis with time dependent correlated frailty. *Statistics in Medicine, 17*, 1201–1213.

Zhang, W., & Steele, F. (2004). A semiparametric multilevel survival model. *Journal of the Royal Statistical Society, Series C, 53*, 387–404.

Partitioned GMM Marginal Model for Time Dependent Covariates: Applications to Survey Data

Elsa Vazquez Arreola and Jeffrey R. Wilson

Abstract Addressing correlated observations in longitudinal studies is crucial as extra variation is crucial. In addition, there are usually time-dependent covariates that will affect the responses differently at different times. To estimate the regression coefficients for the time-dependent covariates in such cases require estimation methods other than maximum likelihood. In particular, GMM method is particularly useful. However, most GMM method are applied to combine all valid moment conditions to produce an averaged regression parameter estimate for each covariate. These methods usually assumed that the effect of each covariate on the response is constant at all measured periods. This assumption is not necessarily optimal. In this chapter, we depart from such assumption and instead use a Partitioned GMM model. This model allows one to provide regression coefficents for the data, reflecting effects at different periods. These extra regression coefficients are obtained using a partitioning of the moment conditions as they pertain to the different relationship based on the period. The Partitioned marginal GMM method exhibits benefits over previously proposed models with improved insight into the non-constant relationships realized. We demonstrate this fit using the *%PartitionedGMM* macro in SAS to survey data obtained from national studies.

1 Introduction

In a simple regression course, one was often exposed to the analysis of cross-sectional data. In that case, there is a response vector $\mathbf{Y}$ of length n representing the outcomes from n different units (sampling units). In addition, there is one predictor represented by the data matrix $\mathbf{X}$ of dimension $n \times 2$ corresponding to the n sampling units and $\boldsymbol{\beta}$ vector of the two coefficients, the constant and the slope. The regression model is $\mathbf{Y} = \mathbf{X}\boldsymbol{\beta} + \boldsymbol{\varepsilon}$ where $\boldsymbol{\beta} = (\beta_0, \beta_1)'$ is a two-dimensional

E. V. Arreola (✉) · J. R. Wilson
Arizona State University, Tempe, AZ, USA
e-mail: maria.vazquez@asu.edu; jeffrey.wilson@asu.edu

A. Bekker et al. (eds.), *Computational and Methodological Statistics and Biostatistics*, Emerging Topics in Statistics and Biostatistics,
https://doi.org/10.1007/978-3-030-42196-0_22

vector with β_0 denoting the constant and β_1 denoting slope, and $\boldsymbol{\varepsilon}$ is a vector of unexplained variation of dimension n.In this case, we examined how $\mathbf{X}$ impact $\mathbf{Y}$. We estimate $\boldsymbol{\beta}$ based on the normal equations such that $\mathbf{b} = (\mathbf{X}'\mathbf{X})^{-1}\mathbf{X}'\mathbf{Y}$ is an unbiased estimator of $\boldsymbol{\beta}$. This also follows from the method of moment based on the product of $\mathbf{X}'$ and the residual $\left(\mathbf{Y} - \hat{\mathbf{Y}}\right)$, where $\hat{\mathbf{Y}}$ is the predicted value, is zero. These are orthogonal vectors such that $\mathrm{E}\left[\mathbf{X}'\left(\mathbf{Y} - \hat{\mathbf{Y}}\right)\right] = 0$.

It is common in many fields, such as health and health related research, to observe subjects repeatedly measured over time. For example, in the Chinese Longitudinal Healthy Longevity Survey, there are four waves, with the first wave of data obtained in 1998. Such longitudinal studies have improved efficiency of estimates, as compared to cross-sectional, though the process of obtaining estimates are more involved. In addition, the longitudinal survey data provide accurate predictions of individual outcomes, as it pools the information, despite the creation of some complications in the statistical analysis. However, in longitudinal studies, there are opportunities for some potential interesting questions beyond what are asked in cross sectional data setting. A diagrammatical display with one predictor in $\mathbf{X}$ and one response in $\mathbf{Y}$ over four time-periods provides a demonstration, Fig. 1. In Fig. 1, we see different color lines representing a different relation between X and Y.

We know that when the covariate X and the response Y are in the same period the moments are always valid and can be used to obtain estimates of the corresponding regression coefficient. However, for the periods, other than cross-sectional ones, we must verify the moments are valid. Thus, in our example, we have four times of repeated measurement on X and Y. There are $4 + 3 + 2 + 1 = 10$ different situations (check the arrows in Fig. 1) to address relationships. Of these ten situations, we know that four of them provide valid moment conditions that can be used to obtain the estimates. In particular, they are the ones corresponding to cross sectional periods. In that case, we have (X_1, Y_1), (X_2, Y_2), (X_3, Y_3), (X_4, Y_4). However for one period lag we have (X_1, Y_2), (X_2, Y_3), (X_3, Y_4); for two-period lag we have (X_1, Y_3),

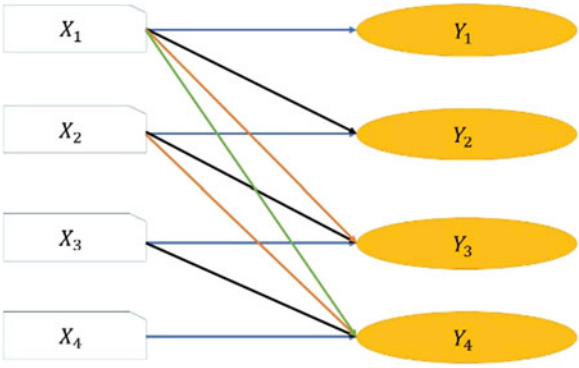

Fig. 1 Relationships between X and Y over time

(X_2, Y_4),; and for three-period lag we have (X_1, Y_4). We need to determine which of these periods $(3 + 2 + 1)$ i.e. other than cross sectional (horizontal lines), are valid to utilize to obtain regression coefficient estimates.

The correlation between repeated response measurements and covariates in longitudinal studies has been addressed using marginal models (models the mean response as a function of covariates), as in generalized estimating equations (GEE) (Zeger and Liang 1986). However, when there are longitudinal data with time-dependent covariates, Pepe and Anderson (1994) showed that the GEE approach is valid and provides consistent estimates only if the independent working correlation matrix is utilized. However, the GEE approach uses all of the cases (ten in our example) whether they are valid or not valid moment conditions.

Lai and Small (2007), Lalonde et al. (2014), Chen and Westgate 2017, Guerra et al. 2012, Zhou et al. 2014 among others have proposed generalized method of moments (GMM) models to address data with time-dependent covariates (Hansen 1982). These approaches present different methods of identifying valid moment conditions to be used in the estimation process. Despite this attempt to identify moments, these models do not distinguish the strength and type of the association between the responses and the covariates at different measured periods. Instead, these approaches combine all associations (all lines, Fig. 1) to provide one regression parameter estimate for each covariate. Thus, any varying strength of the association due to the covariate is masked.

In this chapter, we concentrate on the use of a Partitioned GMM model for time-dependent covariates. This method utilizes a partitioning of the moment conditions to distinguish between the varying relations for a covariate on the responses at different measured periods (Irimata et al. 2019). The approach presents a lower diagonal data matrix that allows the strength of the impact of the covariate to be measured. It represents a configuration of the original data matrix. Thus, we provide a model with additional regression coefficients rather than using a linear combination of the associations, which masks the true relation. These multiple regression coefficients provide a complete description of the relationship between the covariates and the response. It avoids the opportunity of averaging positive and negative, or strong and weak relationships into one value. In Sect. 2, we review some existing methods for longitudinal data, with an emphasis on GMM models. In Sect. 3, we outline the Partitioned GMM framework by revisiting Irimata et al. (2019). We give a step-by-step approach of the macro presented by Irimata and Wilson (2018). In Sect. 4, we demonstrate with survey data with applications to Chinese Longitudinal Healthy Longevity Survey, and Continuity and Change in Contraceptive Use study.

2 Marginal Regression Modeling with Time-Dependent Covariates

Marginal models with time-dependent covariates have addressed the challenges presented with the extra correlation (Guerra et al. 2012; Selig et al. 2012). Zhou et al. (2014) introduced a method using the modified quadratic inference function. Chen and Westgate (2017) provided a new GMM approach, which utilized a modified weight matrix based on linear shrinkage. However, most of these methods have the effect of each predictor on the response viewed as constant across periods of measurement. Müller and Stadtmuller (2005) introduced a generalized functional linear regression model where the predictor is a random function, which relied on dimension reduction using orthogonal expansion.

2.1 GMM Models with Covariate Classification

Let us denote the response y_{it} from subject i at time t, with marginal distribution to follow a generalized linear model, with J different covariates $\mathbf{x}_{\text{it.}} = (x_{it1}, \ldots, x_{itJ})$. Assume that the observations y_{is} and y_{kt} are independent when $i \neq k$ but not necessarily when subject $i = k$ and $s \neq t$. Thus, observations from different subjects are assumed independent, while observations from the same subject are not. Lai and Small (2007) used a marginal model for longitudinal continuous data with GMM to account for the time-dependent covariates. In obtaining estimates of the regression coefficients, Lai and Small (2007) made use of the moment conditions such that

$$\mathrm{E}\left[\frac{\partial \mu_{is}(\boldsymbol{\beta})}{\partial \beta_j}\left\{y_{it} - \mu_{it}(\boldsymbol{\beta})\right\}\right] = 0 \tag{1}$$

for appropriately chosen s, t, and j, where $\mu_{it}(\boldsymbol{\beta}) = \mathrm{E}[\{y_{it}|\,\mathbf{x}_{\text{it.}}\}]$ denotes the expectation of y_{it} based on the vector of covariate values $\mathbf{x}_{\text{it.}}$ associated with the vector of parameters $\boldsymbol{\beta}$ in the systematic component that describes the mean of the distribution of y_{it}. Their relation (1) is used to obtain valid moment conditions to be used in obtaining regression parameter estimates. However, the method combines the strength and direction of the relation between the response and the covariate. Such an assumption ignores differential effects as time progresses and provides an average estimate.

2.2 GMM Models with Ungrouped Moment Conditions

As an alternative to the grouping of moments based on covariate type, Lalonde et al. (2014) introduced a method to test the validity of each moment separately. In their approach to identify valid moments, they relied on a bivariate correlation to

determine the corresponding moment condition. All moments when the predictor and response are observed in the same time-period, $s = t$ are valid. We address the remaining $T(T-1)/2$ moment conditions individually for validity. The moment condition (1) is considered valid when $\rho_{x_t,e_s} = 0$, that is when the correlation between the residual observed at time s, denoted by e_s, and the covariate observed at time t, denoted by x_t where $s \neq t$ was zero. However, similar to the method of Lai and Small (2007), they grouped the valid moments to obtain an estimate of a single regression coefficient to represent the overall effect of a given covariate.

3 Partitioned Coefficients with Time-Dependent Covariates

We fit a Partitioned GMM for time-dependent covariates model. First, we identify the valid moment based on methods developed by Lalonde et al. (2014). However, instead of grouping all valid moment conditions to obtain an average effect of the covariate on the response, we partition the moment conditions and separate out the effects of the covariates on the responses across time. This partitioning, based on the lag between the covariate and the response, results in extra regression parameters for each covariate. It provides an insight into each of the period and any varying relationships inherent to longitudinal data.

3.1 Partitioned GMM Model

The Partitioned GMM model presents a relationship between the outcomes observed at time t, Y_t and the j^{th} covariate observed at time s, X_{js} for $s \leq t$. For each time-dependent covariate X_j measured at times 1, 2, ..., T; for subject i and the j^{th}covariate, the data matrix is reconfigured as a lower triangular matrix,

$$\mathbf{X_{ij}} = \begin{bmatrix} 1 & X_{ij1} & 0 & \dots & 0 \\ 1 & X_{ij2} & X_{ij1} & \dots & 0 \\ \vdots & \vdots & \vdots & \dots & \vdots \\ 1 & X_{iJT} & X_{ij(T-1)} & \dots & X_{ij1} \end{bmatrix} = \begin{bmatrix} \mathbf{1} & \mathbf{X_{ij}^{[0]}} & \mathbf{X_{ij}^{[1]}} & \dots & \mathbf{X_{ij}^{[T-1]}} \end{bmatrix}$$

where the superscript denotes the difference, $t - s$ in time-periods between the response time t and the covariate time s. Thus, the model,

$$\mathrm{g}\left(\mu_{it}\right) = \beta_0 + \beta_j^{tt} X_{ij}^{[0]} + \beta_j^{[1]} X_{ij}^{[1]} + \beta_j^{[2]} X_{ij}^{[2]} \cdots + \beta_j^{[T-1]} X_{ij}^{[T-1]} \tag{2}$$

depends on the regression coefficients $\boldsymbol{\beta}_{\mathrm{j}} = \left(\beta_0, \beta_j^{tt}, \beta_j^{[1]}, \beta_j^{[2]}, \ldots, \beta_j^{[T-1]}\right)$. The coefficient β_j^{tt} denotes the effect of the covariate X_{jt} on the response Y_t during the

t^{th} period, or in other words when the covariate and the outcome are observed in the same time-period. When $s < t$ we denote the lagged effect of the covariate X_{js} on the response Y_t by the coefficients$\beta_j^{[1]}, \beta_j^{[2]}, \ldots, \beta_j^{[T-1]}$. These additional coefficients allow the identification of the effect of the covariate on the response at different times in point. It avoids having to assume that the association is the same in strength and direction at different times. In particular, the coefficient $\beta_j^{[1]}$ denotes the effect of X_{js} on Y_t across a one time-period lag. Thus, each of the J time-dependent covariates yield a maximum of T partitions of β_j. Thus, for a model with J time-dependent covariates, the data matrix $\mathbf{X}$ will have a maximum dimension of N by $(J \times T) + 1$, and $\boldsymbol{\beta}$ is a vector of maximum length $(J \times T) + 1$.

However, the use of additional regression parameters produces reliable estimates when the number of clusters are large in comparison to the number of time-periods. This approach is similar to the use of parameter estimates in GEE models with correlated data and using the unstructured working correlation matrix. At times, they may not converge when the size of each cluster is large relative to the number of clusters. In such cases, certain working correlation structures may produce estimates (Stoner et al. 2010).

3.2 Partitioned GMM Estimates

Consider y_{it} for $i = 1, \ldots, N$; to be an independent and identically distributed random variable with mean μ_{it} at time t such that $\mathrm{E}(\mathbf{y}_{\mathrm{it}}) = \boldsymbol{\mu}_{\mathrm{it}} = \boldsymbol{\mu}_{\mathbf{it}}(\boldsymbol{\beta}_0)$ and let $\boldsymbol{\beta_0}$ denote the vector of regression parameters. These beta regression coefficients are estimated based on the methods of Irimata et al. (2019) and laid out in Appendix.

Logistic Regression Model: In the case of the logistic regression model, the mean is

$$\mu_{it}\left(\boldsymbol{\beta_0}\right) = \frac{\exp\left(\mathbf{x_{it.}}\boldsymbol{\beta}\right)}{1 + \exp\left(\mathbf{x_{it.}}\boldsymbol{\beta}\right)},$$

so, the valid elements in the function $\mathbf{g_i}$ each take the form:

$$\frac{\partial \mu_{is}\left(\boldsymbol{\beta_0}\right)}{\partial \beta_j^{[k]}}\left[y_{it} - \mu_{it}\left(\boldsymbol{\beta_0}\right)\right] = x_{isj}\mu_{is}\left(\boldsymbol{\beta_0}\right)\left[1 - \mu_{is}\left(\boldsymbol{\beta_0}\right)\right]\left[y_{it} - \mu_{it}\left(\boldsymbol{\beta_0}\right)\right].$$

Thus, for the asymptotic variance, in the case of logistic regression, each N_v x 1 vector $\frac{\partial \mathbf{g_i}(\boldsymbol{\beta})}{\partial \beta_l^{[k]}}$ in the matrix

$$\frac{\partial \mathbf{g_i}\left(\boldsymbol{\beta}\right)}{\partial \boldsymbol{\beta}} = \left[\frac{\partial \mathbf{g_i}(\boldsymbol{\beta})}{\partial \beta_j^{[1]}}, \ldots, \frac{\partial \mathbf{g_i}(\boldsymbol{\beta})}{\partial \beta_j^{[T-1]}}\right]$$

is obtained as

$$\frac{\partial\left\{\left[\frac{\partial\mu_{is}(\boldsymbol{\beta})}{\partial\beta_j^{[k]}}\right]\left[y_{it}-\mu_{it}\left(\boldsymbol{\beta}\right)\right]\right\}}{\partial\beta_l^{[m]}} = x_{isj}\mu_{is}\left(\boldsymbol{\beta}\right)\left[1-\mu_{is}\left(\boldsymbol{\beta}\right)\right]\left\{x_{isl}\left[1-2\mu_{is}\left(\boldsymbol{\beta}\right)\right]\right.$$
$$\left.\left[y_{it}-\mu_{it}\left(\boldsymbol{\beta}\right)\right]-x_{itj}\mu_{it}\left(\boldsymbol{\beta}\right)\left[1-\mu_{it}\left(\boldsymbol{\beta}\right)\right]\right\},$$

where $j=1,\ \ldots, J, l=1,\ \ldots J, k=1,\ \ldots, T-1$ and $m=1,\ \ldots, T-1$.

Normal distribution model: Similarly, for the normal error model, the moment conditions in $\mathbf{g}_\mathrm{i}$ take the form

$$\frac{\partial\mu_{is}\left(\boldsymbol{\beta_0}\right)}{\partial\beta_j^{[k]}}\left[y_{it}-\mu_{it}\left(\boldsymbol{\beta_0}\right)\right]=x_{isj}\left[y_{it}-\mu_{it}\left(\boldsymbol{\beta_0}\right)\right],$$

for the valid moment conditions. The asymptotic variance is computed using the $N_v \times J$ matrix

$$\frac{\partial\mathbf{g}_\mathrm{i}\left(\boldsymbol{\beta}\right)}{\partial\boldsymbol{\beta}}=\left[\frac{\partial\mathbf{g}_\mathrm{i}(\boldsymbol{\beta})}{\partial\beta_j^{[1]}},\ \ldots,\ \frac{\partial\mathbf{g}_\mathrm{i}(\boldsymbol{\beta})}{\partial\beta_j^{[T-1]}}\right],$$

where each of the $N_v \times 1$ vectors $\frac{\partial\mathbf{g}_\mathrm{i}(\boldsymbol{\beta})}{\partial\beta_j^{[k]}}$ is computed as

$$\frac{\partial\left\{\left[\frac{\partial\mu_{is}(\boldsymbol{\beta})}{\partial\beta_j^{[k]}}\right]\left[y_{it}-\mu_{it}\left(\boldsymbol{\beta}\right)\right]\right\}}{\partial\beta_l^{[m]}}=-x_{isj}x_{isl},$$

for $j=1,\ \ldots, J,\ l=1,\ \ldots J,\ k=1,\ \ldots,\ T-1$ and $m=1,\ \ldots,\ T-1$. We demonstrate the fit of these models and the estimates using the SAS macro.

3.3 SAS Macro for Partitioned GMM Model

The *%partitioned*GMM SAS macro (Irimata and Wilson 2018) allows the fit of a model for longitudinal binary and continuous outcomes. This macro first tests for valid moment conditions. It uses the valid moments to outline the partitioned data matrices for time-dependent covariates. Then, it fits the model with the new data matrix using a GMM model. It provides regression parameter estimates, along with their standard errors and associated p-values. We outline the steps in this macro to allow the reader to follow the process. The complete code for this macro is located at https://github.com/kirimata/Partitioned-GMM. However, the user needs to attend to the following code to fit a partitioned GMM model:

***%partitionedGMM*(file=, timeVar=, outVar=, predVarTD=, idVar=, alpha=0.05, predVarTI=, distr=bin, optim=NLPNRA, MC=LWY);**

There are ten arguments that users must specify when using this macro to fit a partitioned GMM model (Irimata and Wilson 2018). The ***file*** argument contains the name of the dataset to use. It can be a SAS dataset or a SAS file. The ***timeVar*** argument calls for the name of the variable listing the time points. The ***outVar*** argument calls for the name of the outcome or response variable. The ***predVarTD*** argument calls for all time-dependent covariates in the model. The ***idVar*** argument calls for the variable with subject's ID. The ***alpha*** argument calls for the level of significance for the correlation test to determine the valid moment, Lalonde et al. (2014). The ***predVarTI*** argument calls for the names of any time-independent covariates in the model; if none exists, the argument is blank. The ***distr*** argument is either binary if outcome is dichotomous or normal if outcome is continuous. The ***optim*** argument identifies a nonlinear optimization method to fit their model. The ***MC*** argument calls for selecting the method to test for valid moment conditions. The options are LWY for correlation test (Lalonde et al. 2014) and LS for hypothesis tests (Lai and Small 2007).

4 Numerical Examples

4.1 Contraceptive Use Data

The 2012–2014 Continuity and Change in Contraceptive Use study was originally collected by the Guttmacher Center for Population Research Innovation and Dissemination (Jones 2018). It assessed the contraceptive use in the United States for women aged 18–39. These data were obtained from a nationally representative probability sample through online surveys, every 6 months starting in 2012 in four waves. A sample of these data are given in Table 1. The columns are identified as

Caseid	Age	HHEAD	HHSIZE	HHINC	Wave	Income 100–299 PL	Income greater 299 PL
Col1	Col2	Col3	Col4	Col5	Col6	Col7	Col8

Some_college	Other_insurance	No_insurance	Ever_married	Hispanic	Black	USE_BC
Col9	**Col10**	Col**11**	**Col12**	**Col13**	**Col14**	**Col15**

We fit a partitioned GMM marginal logistic regression model with time dependent covariates to the 2012–2014 Continuity and Change in Contraceptive Use Study data. We wish to understand the relationship between women's sociodemographic characteristics and their use of contraceptive methods. This analysis used the first three waves as the fourth wave had incomplete information on some of the

Table 1 Sample of survey data continuity and change in contraceptive use

Col1	Col2	Col3	Col4	Col5	Col6	Col7	Col8	Col9	Col10	Col11	Col12	Col13	Col14	Col15
81	36	1	4	15	1	0	1	1	0	0	1	0	0	1
81	36	1	4	15	2	0	1	1	0	0	1	0	0	1
81	36	1	4	15	3	0	1	1	0	0	1	0	0	1
83	27	1	3	11	1	1	0	1	0	0	1	0	0	0
83	27	1	3	11	2	1	0	1	0	0	1	0	0	0
83	27	1	3	11	3	1	0	1	0	0	1	0	0	0
84	19	0	5	16	1	0	1	1	0	0	0	0	0	1
84	19	0	5	16	2	0	1	1	0	0	0	0	0	1
84	19	0	5	16	3	0	1	1	0	0	0	0	0	1
85	34	1	2	12	1	0	1	1	0	0	1	1	0	1
85	34	1	2	12	2	0	1	1	0	0	1	1	0	0
85	34	1	2	12	3	0	1	1	0	0	1	1	0	1
86	24	1	3	19	1	0	1	1	0	0	0	0	0	0
86	24	1	3	19	2	0	1	1	0	0	0	0	0	0
86	24	1	3	19	3	0	1	1	0	0	1	0	0	0

time-dependent covariates. The binary outcome is use of any contraceptive (pill, patch, ring, IUD, shot, implant) or none of above during the last 30 days. The time-independent covariate is race (black, Hispanic, white). The time-dependent covariates are income (100–299 poverty level, >299 poverty level vs <100 poverty level), marital status (ever been married vs never been married), household head status (yes vs no), insurance type (non-private insurance, no insurance vs private insurance) and education (high school diploma or GED or less vs at least some college). We created dummy variables for each categorical time-dependent covariate to be used in the %partitionedGMM macro.

We made use of 5028 observations from 1676 participants. First, we tested and identified for valid moment conditions between outcomes and lagged covariates using individual correlation tests (Lalonde et al. 2014). We considered four segments: cross sectional (immediate effect), one lag period (delayed effect), two-lag period (further delayed effect), and three lag period (furthermost delayed effect). The following code was used to fit the model.

$$\%\boldsymbol{partitionedGMM}\ (\textbf{file} = \text{birth\_control}, \textbf{timeVar} = \text{wave}, \textbf{outVar} = \text{use\_bc},$$
$$\textbf{predVarTD} = \text{hhead hhsize income2 income3 some\_college other\_insurance}$$
$$\text{no\_insurance ever\_married}, \textbf{idVar} = \text{caseid}, \textbf{alpha} = 0.05, \textbf{predVarTI} =$$
$$\text{hispanic black age}, \textbf{distr} = \textbf{bin}, \textbf{optim} = \textbf{NLPNRA}, \textbf{MC} = \textbf{LWY})\ ;$$

We found that race and age had a significant impact on the use of contraceptive methods, (($OR_{black} = 0.616, p = 0.002$) and ($OR_{age} = 0.931, p < 0.0001$)). Head of household status, household size, or income had no effect on contraceptive use.

Table 2 Partitioned GMM model results for contraceptive use

Covariate	OR	OR 95% CI		P-value
Hispanic	0.842	0.635	1.117	0.233
Black	0.616	0.455	0.835	0.002
Age	0.931	0.913	0.949	0.000
Head of household	1.047	0.824	1.329	0.709
Lag-1 head of household	0.936	0.772	1.134	0.498
Lag-2 head of household	1.002	0.844	1.189	0.982
Household size	1.004	0.936	1.077	0.910
Lag-1 household size	1.037	0.982	1.095	0.190
Lag-2 household size	0.954	0.907	1.003	0.063
Income 100%–299% PL	0.804	0.592	1.093	0.164
Lag-1 income 100%–299% PL	1.067	0.931	1.224	0.352
Lag-2 income 100%–299% PL	1.112	0.893	1.385	0.344
Income >299% PL	1.171	0.815	1.682	0.393
Lag-1 income >299% PL	0.854	0.671	1.085	0.196
Lag-2 income >299% PL	1.113	0.867	1.428	0.401
Some college	0.976	0.727	1.311	0.873
Lag-1 some college	1.321	1.033	1.690	0.026
Lag-2 some college	0.836	0.663	1.055	0.132
Other insurance	1.052	0.807	1.371	0.706
Lag-1 other insurance	0.699	0.518	0.944	0.019
No insurance	0.483	0.372	0.627	0.000
Lag-1 no insurance	0.868	0.655	1.150	0.323
Ever married	0.755	0.620	0.919	0.005
Lag-1 ever married	0.852	0.723	1.005	0.057
Lag-2 ever married	0.839	0.720	0.977	0.024

There was neither immediate, delayed nor later delayed effect on contraceptive use, Table 2. Education showed no immediate effect but after some time it showed some significant delay effect, ($OR_{lag1\ -\ some\ collge} = 1.321$, $p = 0.026$) on the use of contraceptive methods. Having no insurance had an immediate effect while those who had non-private insurance had a delayed effect on the use of contraceptive methods (($OR_{lag1\ -\ nonprivate\ insurance} = 0.699, p = 0.019$) and ($OR_{No\ insurance} = 0.483$, $p < 0.0001$)). Marital status had an immediate effect and a further delayed effect on the use of contraceptive methods. Those who been married were less likely to use contraceptive methods(($OR_{ever\ married} = 0.755, p = 0.005$) and ($OR_{lag\ -\ 2\ ever\ married} = 0.839, p = 0.024$)). Contraceptive use shows less likely to be used by blacks, younger women, little education, and no insurance.

A graphical representation of the impact of the time-varying socioeconomic factors on contraceptive use is provided in Fig. 2. Figure 1 contains odds ratio estimates with its 95% confidence intervals for these effects. It shows a relation of the effects of these socioeconomic factors on contraceptive use at the different periods.

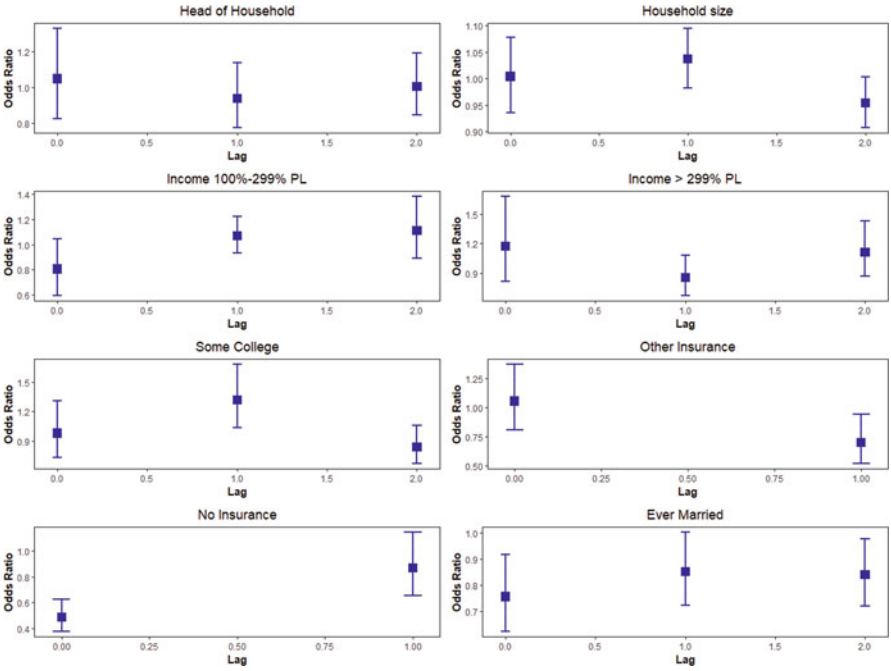

Fig. 2 Partitioned GMM model estimates for contraceptive use (OR and 95% confidence intervals)

4.2 Chinese Longitudinal Healthy Longevity Survey Data

The Chinese Longitudinal Healthy Longevity survey was designed to collect information on the elderly. The data obtained were used to identify social, behavioral, environmental and biological risk factors that affect healthy longevity and mortality in the oldest group of the population (Xiao et al. 2019). The dataset consisted of people aged 80 years or older, and resided in 22 of 31 provinces in China. The data were obtained four waves collected in 1998, 2000, 2002 and 2005. We fit a partitioned GMM logistic regression model with time-dependent covariates fit to identify the risk factors affecting diverse aspects of healthy longevity. A sample of the data is given in Table 3. In Table 3, Col1 denotes the ID; Col2 denotes wave, Col3 denotes "own decision", Col4 denotes "vegetables", Col5 denotes "dressing", Col6 denotes "visual difficulty", Col7 denotes "false teeth", Col8 denotes "*interviewer-rated health*", Col9 denotes "male", Col10 denotes "physical check".

We fit a partitioned GMM logistic regression model to the Chinese Longitudinal Healthy Longevity Study data to understand how determinants of healthy longevity affect participants' health and participants' ability to attend a physical check. There were initially 9093 individuals, but at each wave, the number of individuals

Table 3 Sample of survey data Chinese longitudinal healthy longevity survey

Col1	Col2	Col3	Col4	Col5	Col6	Col7	Col8	Col9	Col10
12,003,398	1	1	0	1	0	1	1	1	1
12,003,398	2	1	1	1	0	1	1	1	1
12,003,398	3	1	1	1	1	1	1	1	1
12,003,398	4	1	1	1	1	1	1	1	1
12,003,798	1	1	1	1	0	0	1	0	1
12,003,798	2	1	1	1	0	1	1	0	1
12,003,798	3	1	0	1	0	0	1	0	0
12,003,798	4	1	0	1	0	0	1	0	1
12,009,398	1	1	1	1	0	1	1	0	1
12,009,398	2	1	1	1	0	1	1	0	1
12,009,398	3	1	1	1	0	1	1	0	1
12,009,398	4	1	1	1	0	1	1	0	1
12,009,498	1	1	1	1	0	1	1	0	1
12,009,498	2	1	1	1	0	1	1	0	1
12,009,498	3	1	1	1	0	1	1	0	1
12,009,498	4	1	1	1	1	0	1	0	1
12,009,798	1	1	1	1	0	0	1	0	1
12,009,798	2	1	1	1	0	0	1	0	1
12,009,798	3	1	1	1	0	0	1	0	1

decreased due to either death or the inability to follow up. There were 1052 individuals remaining in the fourth wave. Of these only 732 individuals were interviewed in all four waves.

The variables of interest are binary with "whether interviewer considered participants' health good or very good (*interviewer-rated health*)" and "whether participants were able to attend for a physical check (*physical check*)". The interviewer rated health is rated on perception of participant's based on "surprisingly healthy" and "relatively healthy" versus "moderately ill" and "very ill". The interviewer rated whether participants were able to attend a physical check with a binary measure.

The binary time dependent covariates are: able to make their own decisions (*own decision*), whether they consumed vegetables frequently (*vegetables*), whether they were able to dress without assistance (*dressing*), whether they had any visual difficulty (*visual difficulty*) and whether they had false teeth (*false teeth*). Gender is a time-independent covariate. We used the method due to Lalonde et al. (2014) on individual correlation test to determine valid moment conditions for each of the lags present due to time-dependent covariates had for each outcome.

4.2.1 Interviewer Rated Health

A partitioned GMM model found that gender did not have a significant effect on interviewer rating of health (Table 4). We found that individuals' ability

Table 4 Partitioned GMM model results for interviewer-rated health

Covariate	OR	OR 95% CI		p-value
Male	0.992	0.695	1.415	0.964
Own decision	1.965	1.359	2.841	0.000
Lag −1 own decision	1.594	1.022	2.486	0.040
Lag-2 own decision	1.012	0.542	1.890	0.969
Lag-3 own decision	0.635	0.292	1.382	0.252
Vegetables	0.833	0.434	1.597	0.582
Lag-1 vegetables	0.286	0.143	0.575	0.000
Lag-2 vegetables	1.066	0.585	1.940	0.835
Lag-3 vegetables	0.657	0.234	1.842	0.424
Dressing	4.784	6.366	15.037	0.000
Lag-1 dressing	0.560	0.253	1.242	0.154
Lag-2 dressing	0.558	0.241	1.293	0.174
Lag-3 dressing	2.320	0.800	6.728	0.121
Visual difficulty	0.344	0.241	0.491	0.000
Lag-1 visual difficulty	1.330	0.791	2.237	0.283
Lag-2 visual difficulty	0.695	0.411	1.173	0.173
Lag-3 visual difficulty	0.616	0.346	1.095	0.099
False teeth	0.968	0.565	1.657	0.905
Lag-1 false teeth	1.285	0.740	2.229	0.373
Lag-2 false teeth	1.038	0.571	1.888	0.902

to make their own decisions had an immediate significant impact (cross sectional) on interviewers' health rating, ($OR_{\text{own decision}} = 1.965$, $p < 0.0001$). Frequently consuming vegetables had no immediate effect, though there was some significant delayed effect, ($OR_{\text{lag1 – vegetables}} = 0.286, p = < 0.0001$). The ability to dress oneself had an immediate effect on interviewer heath rating, ($OR_{\text{dressing}} = 4.784$, $p < 0.0001$). Individual's visual difficulty had immediate effect, ($OR_{\text{visual difficulty}} = 0.344, p < 0.0001$). The model suggests that participants' ability to make their own decisions and ability to dress oneself had a significant positive immediate impact on interviewer rated health. While having visual difficulty and vegetables had a significant negative immediate and delayed impact, respectively, on interviewer rated health.

Figure 3 presents the odds ratio estimates for the regression covariates with its confidence intervals for the impact of the time-dependent covariates on interviewer rated health at different periods. Figure 3 shows that the effects of the time-dependent covariates on interviewer rated health over different periods (Zeng et al. 2019).

4.2.2 Physical Check

We fit a partitioned GMM logistic regression model to determine what affected individuals' ability to complete a physical check, Table 5. Gender did not

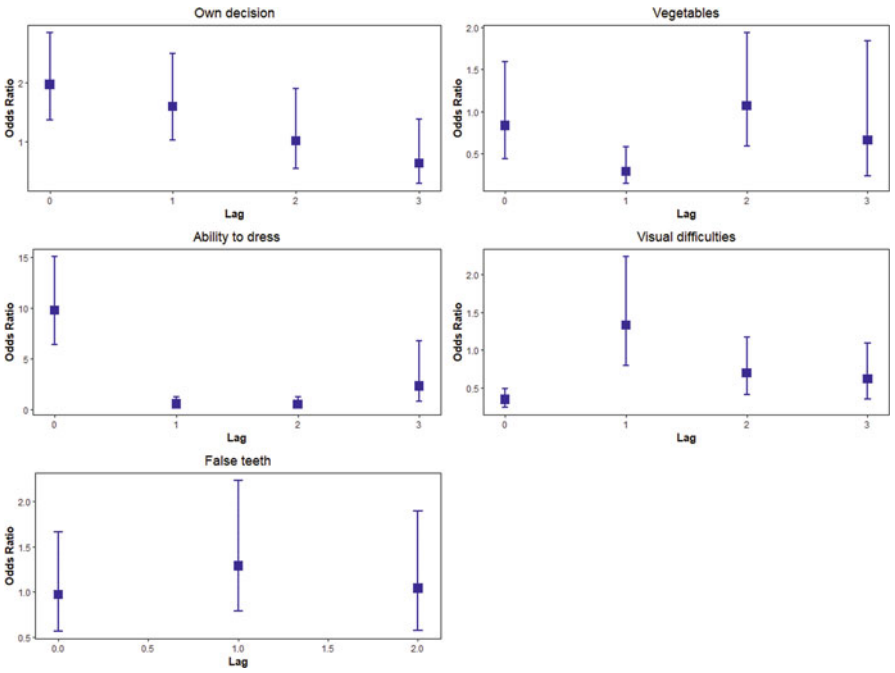

Fig. 3 Partitioned GMM model for interviewer-rated health in CLHLS (OR and 95% confidence intervals)

have a significant impact on participants' ability to complete a physical check. We found that individuals' ability to make their own decisions had an immediate significant impact (cross sectional) on interviewer's physical check, ($OR_{\text{own decision}} = 1.539$, $p = 0.013$). Frequently consuming vegetables had immediate effect, ($OR_{\text{vegetables}} = 2.033, p < 0.0001$). The ability to dress oneself had an immediate effect on interviewees' ability to complete a physical check, ($OR_{\text{dressing}} = 3.734$, $p < 0.0001$). Individuals having visual difficulties had immediate effect, ($OR_{\text{visual difficulty}} = 0.293, p < 0.0001$). The model suggests that participants' ability to make their own decisions, frequent vegetable consumption and ability to dress oneself had a significant positive impact on interviewer's view on completing a physical check. While having visual difficulty had a significant negative impact on interviewer's rating of completing physical check.

Figure 4 contains odds ratio estimates as well as their 95% confidence intervals for the impact of the time-dependent covariates on individuals' ability to complete a physical check. Figure 4 shows the relation from one period to the next.

Table 5 Partitioned GMM model results for physical check

Covariate	OR	OR 95% CI		P-value
Male	1.258	0.896	1.767	0.185
Own decision	1.539	1.095	2.163	0.013
Lag-1 own decision	0.731	0.396	1.349	0.316
Lag-2 own decision	0.930	0.435	1.988	0.851
Lag-3 own decision	1.451	0.812	2.591	0.209
Vegetables	2.033	1.473	2.805	0.000
Lag-1 vegetables	0.616	0.362	1.047	0.073
Lag-2 vegetables	0.792	0.439	1.431	0.440
Lag-3 vegetables	0.880	0.417	1.857	0.737
Dressing	3.734	4.119	9.637	0.000
Lag-1 dressing	0.771	0.430	1.383	0.383
Lag-2 dressing	1.610	0.792	3.270	0.188
Lag-3 dressing	1.128	0.527	2.412	0.756
Visual difficulty	0.293	0.216	0.398	0.000
Lag-1 visual difficulty	0.667	0.468	0.950	0.025
Lag-2 visual difficulty	1.128	0.504	2.527	0.769
Lag-3 visual difficulty	0.960	0.403	2.285	0.926
False teeth	1.337	0.814	2.195	0.252
Lag-1 false teeth	1.436	0.881	2.340	0.147
Lag-2 false teeth	1.254	0.622	2.528	0.527
Lag-3 false teeth	0.985	0.430	2.259	0.972

5 Discussion and Conclusions

Models are usually simpler in explanation when the observations are independent. However, when there are time-dependent covariates the explanation is usually complicated, as one has to decipher the cross sectional effects as opposed to effects identified due to lags. Measuring the sampling units repeatedly induces correlation among covariates that impact the efficiency of the estimates through the variance.

The fact that the longitudinal data have responses and covariates measure at different times, it is important to include valid moments in the computation of the regression coefficients. Including moments that are not valid or excluding valid moments are detrimental to the regression coefficients. The validity of the moment conditions is identified using the Lalonde et al. (2014) approach. However, if these valid moments are combined to obtain a single regression coefficient, then the true relationships may be distorted. Combining valid moments from different responses in one time-period with covariates in a different time-period mask the true relation and provide an average relation.

The partitioned and non-partitioned methods are utilizing different sets of information as they are using different sets of moment conditions. The non-partitioned models use an averaging of all information from the moments between the covariate and the response to produce a cross-sectional estimate. They assume

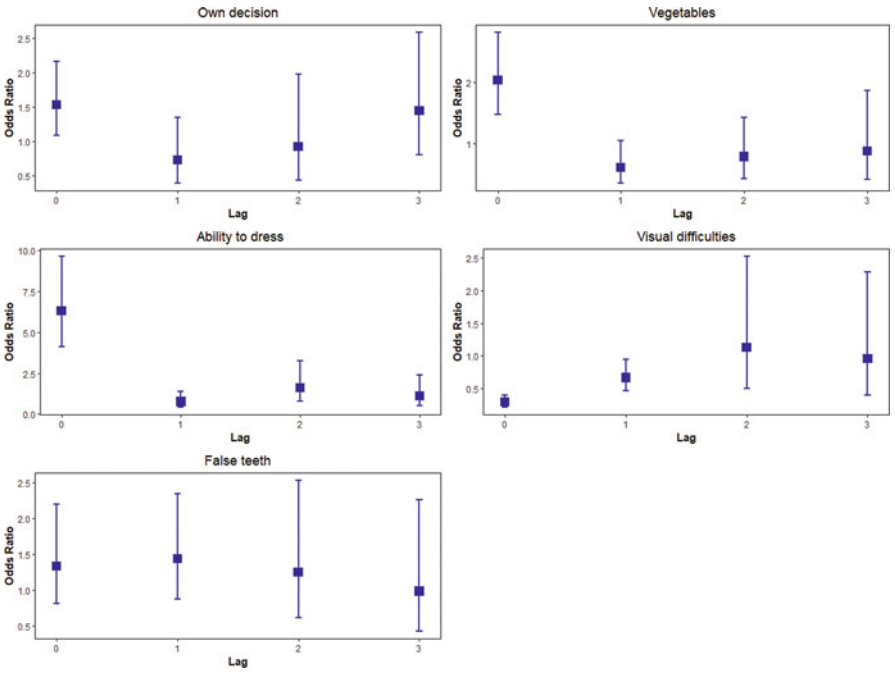

Fig. 4 Partitioned GMM model for ability to complete physical check in CLHLS (OR and 95% confidence intervals)

that the relationship between each covariate and the response remains the same over time.

The Partitioned GMM models separate the cross-sectional data and the lagged at different periods. The grouping of moment conditions force results in different periods in the estimation of each regression parameter to provide information pertaining to certain relationship.

Lai and Small (2007), Lalonde et al. (2014), and Zhou et al. (2014), among others, have presented models that do not distinguish between the cross-sectional and the lagged relationships but rather present an overall effect of the covariate on the responses. On the other hand, fitting a Partitioned GMM approach to data with a large number of time-periods may suffer from convergence issues. This limitation is similar to the restrictions for GEE models with an unstructured working correlations matrix. Overall, the Partitioned GMM provides a complete description of the effects of time-dependent covariates on outcomes.

Appendix

Let $\mathbf{T_j}$ be the $T \times T$ matrix, identifying moment conditions, which are valid for the j^{th} covariate. Thus, elements in $\mathbf{T_j}$ take on the value of one when there is valid moment condition (1) and takes a value of zero when the moment is not valid for the j^{th} covariate. The $\frac{1}{2}T\,(T-1)$ moments related to cases when $s > t$ are set to zero. The elements in $\mathbf{T_j}$ are partitioned into up to T separate $T \times T$ matrices denoted by $\mathbf{T_{jk}}$ for $k = 1, \ldots, T-1$. The information for the T moment conditions when $s = t$, occurring when the response and the covariate are observed in the same time-period, are contained in $\mathbf{T_{j0}}$, an identity matrix. Information for the moment conditions occurring when the response is observed one time-period after the covariate, $t - s = 1$ are contained in the matrix $\mathbf{T_{j1}}$.Each of the remaining matrices $\mathbf{T_{jk}}$ are created similarly. Let $\mathbf{T_{vjk}}$ be the reshaped 1 x T^2 vector of the elements in $\mathbf{T_{jk}}$. Concatenate the row vectors for all covariates and lagged effects to form the matrix $\mathbf{T_{shape}}$, which is of maximum dimension $(J \times T) \times T^2$. Let N_v be the number of ones in $\mathbf{T_{shape}}$, or equivalently the total number of valid moment conditions, Irimata et al. (2019). Thus, the fitted model to (3.1) is

$$\mu_{it}\left(\boldsymbol{\beta}\right) = \beta_0 + \beta_j^{tt} X_{ij}^{[0]} + \sum_{\mathbf{k=1}}^{\mathbf{T-1}} \beta_j^{[k]} X_{ij}^{[k]} \Bigg|_{\mathbf{valid\ moments}}$$

where $\mathbf{g_i}$ be an N_v x 1 vector composed of the values of all valid moment conditions for subject i, computed at the initial value $\boldsymbol{\beta_0}$. Each element in $\mathbf{g_i}$ is calculated as $\frac{\partial \mu_{is}(\boldsymbol{\beta_0})}{\partial \beta_j^{[k]}} \left[y_{it} - \mu_{it}\left(\boldsymbol{\beta_0}\right)\right]$ such that the corresponding element in $\mathbf{T_{jk}}$ takes value 1 for $k = 1, \ldots, T-1$. Let $\mathbf{G_n}$ be the N_v x 1 vector consisting the sample average of all valid moment conditions, such that

$$\frac{1}{N}\sum_{i=1}^{N} \mathbf{g_i} = \frac{1}{N}\sum_{i=1}^{N} \frac{\partial \mu_{is}\left(\boldsymbol{\beta_0}\right)}{\partial \beta_j^{[k]}} \left[y_{it} - \mu_{it}\left(\boldsymbol{\beta_0}\right)\right].$$

The optimal weight matrix $\mathbf{W_n}$ is computed as $\left(\frac{1}{N}\sum_{i=1}^{N} \mathbf{g_i}\mathbf{g_i}^{\mathrm{T}}\right)^{-1}$, which is of dimension $N_v \times N_v$. Then, the GMM regression estimator is

$$\hat{\boldsymbol{\beta}}_{\mathrm{GMM}} = \underset{\boldsymbol{\beta_0}}{\mathrm{argmin}} \mathbf{G_n}\left(\boldsymbol{\beta_0}\right)^{\mathrm{T}} \mathbf{W_n}\left(\boldsymbol{\beta_0}\right)\ \mathbf{G_n}\left(\boldsymbol{\beta_0}\right),$$

which is the argument minimizing the quadratic objective function. The asymptotic variance of the estimator $\hat{\boldsymbol{\beta}}_{\mathrm{GMM}}$ is

$$\left[\left(\frac{1}{N}\sum\nolimits_{i=1}^{N} \frac{\partial \mathbf{g_i}\left(\boldsymbol{\beta}\right)}{\partial \boldsymbol{\beta}}\right)^{\mathrm{T}} \mathbf{W_n}\left(\boldsymbol{\beta}\right) \left(\frac{1}{N}\sum\nolimits_{i=1}^{N} \frac{\partial \mathbf{g_i}\left(\boldsymbol{\beta}\right)}{\partial \boldsymbol{\beta}}\right)\right]^{-1},$$

evaluated at$\boldsymbol{\beta} = \hat{\boldsymbol{\beta}}_{\mathrm{GMM}}$.

References

Chen, I. C., & Westgate, P. M. (2017). Improved methods for the marginal analysis of longitudinal data in the presence of time-dependent covariates. *Statistics in Medicine, 36*, 2533–2546.

Guerra, M. W., Shults, J., Amsterdam, J., & Ten-Have, T. (2012). The analysis of binary longitudinal data with time-dependent covariates. *Statistics in Medicine, 31*, 931–948.

Hansen, L. P. (1982). Large sample properties of generalized method of moments estimators. *Econometrica, 50*, 1029–1054.

Irimata, K. M., Broatch, J., & Wilson, J. R. (2019). Partitioned GMM logistic regression models for longitudinal data. *Statistics in Medicine, 38*, 1–8.

Irimata, K.M.,Wilson, J.R. (2018). Using SAS to estimate lagged coefficients with the %partitioned GMM macro. *SAS Glob. Forum Proc. Presented at the SAS Global Forum, Denver*. April 8-11.

Jones, R. (2018). Continuity and Change in Contraceptive Use, United States, 2012–2014. https://doi.org/10.3886/ICPSR37067.v1. Accessed 1 December 2018.

Lai, T. L., & Small, D. (2007). Marginal regression analysis of longitudinal data. *Journal of the Royal Statistical Society, Series B (Statistical Methodology), 69*, 79–99.

Lalonde, T. L., Wilson, J. R., & Yin, J. (2014). GMM logistic regression models for longitudinal data with time-dependents covariates and extended classifications. *Statistics in Medicine, 33*, 4756–4769.

Muller, H. G., & Stadtmuller, U. (2005). Generalized functional linear models. *The Annals of Statistics, 33*, 774–805.

Pepe, M. S., & Anderson, G. L. (1994). A cautionary note on inference for marginal regression models with longitudinal data and general correlated response data. *Communications in Statistics: Simulation and Computation, 23*, 939–951.

Selig, J. P., Preacher, K. J., & Little, T. D. (2012). Modeling time-dependent association in longitudinal data: A lag as moderator approach. *Multivariate Behavioral Research, 47*, 697–716.

Stoner, J. A., Leroux, B. G., & Puumala, M. (2010). Optimal combination of estimating equations in the analysis of multilevel nested correlated data. *Statistics in Medicine, 29*, 464–473.

Zeng, Y., Vaupel, J.W., Xiao, Z., Liu, Y., &, Zhang, C. (2019). Chinese Longitudinal Healthy Longevity Survey (CLHLS), Community Datasets, 1998–2005. https://doi.org/10.3886/ICPSR37227.v1. Accessed 10 January 2019.

Zeger, S. L., & Liang, K. Y. (1986). Longitudinal data analysis for discrete and continuous outcomes. *Biometrics, 42*, 121–130.

Zhou, Y., Lefante, J., Rice, J., & Chen, S. (2014). Using modified approaches on marginal regression analysis of longitudinal data with time-dependent covariates. *Statistics in Medicine, 33*, 3354–3364.

A Family of Generalized Rayleigh-Exponential-Weibull Distribution and Its Application to Modeling the Progressively Type-I Interval Censored Data

(Din) Ding-Geng Chen and Yuhlong Lio

Abstract A family of three-parameter generalized Rayleigh-exponential-Weibull distribution (GREW), which unifies the families of two-parameter generalized Rayleigh distributions, two-parameter generalized exponential distributions, and two-parameter Weibull distributions, is considered to model the distribution of lifetimes for an example of 112 patients with plasma cell myeloma. A series of simulation studies are conducted to evaluate the three-parameter GREW modeling performance based on the type-I interval censored data similar to the data structure from these 112 patients. Parameter estimation, hypothesis testing, and model selection using the three-parameter GREW for these 112 patients are discussed.

1 The Generalized Rayleigh-Exponential-Weibull Distribution

The two-parameter generalized Rayleigh (GR) distribution, which is also known as the Burr type-X distribution, has probability density function (PDF) and cumulative distribution function (CDF) respectively given as follows,

$$f(t,\theta) = 2\alpha/\lambda^2 t\left(1-e^{-(t/\lambda)^2}\right)^{\alpha-1} e^{-(t/\lambda)^2} \tag{1.1}$$

D.-G. Chen (✉)
Department of Statistics, University of Pretoria, Pretoria, South Africa
e-mail: din.chen@up.ac.za

Y. Lio
Department of Mathematical Sciences, University of South Dakota, Vermilion, SD, USA

A. Bekker et al. (eds.), *Computational and Methodological Statistics and Biostatistics*, Emerging Topics in Statistics and Biostatistics,
https://doi.org/10.1007/978-3-030-42196-0_23

and

$$F(t,\theta) = \left(1 - e^{-(t/\lambda)^2}\right)^{\alpha}, \tag{1.2}$$

where $\theta = (\alpha, \lambda)$ are the two parameters with $\alpha > 0$ as the shape parameter and $\lambda > 0$ as the scale parameter. When $\alpha = 1$, the GR distribution defined above reduces to the conventional Rayleigh distribution. The GR distribution has been studied by many authors as seen in Sartawi and Abu-Salih (1991), Johnson et al. (1995), Jaheen (1995, 1996), Ahmad et al. (1997), Raqab (1998), Surles and Padgett (1998, 2001, 2004), Raqab and Kundu (2003), Kundu and Raqab (2005), and Lio et al. (2011). Similar to the generalized exponential distribution and Weibull distribution, the GR distribution has a closed form of CDF (1.2) and is very popular for dealing with censored data. Raqab and Kundu (2003) and Kundu and Raqab (2005) extensively discussed this distribution and compare it to other distributions.

On the other hand, the two-parameter generalized exponential (GE) distribution has PDF and CDF respectively given as follows,

$$f(t,\theta) = \alpha/\lambda \left(1 - e^{-(t/\lambda)}\right)^{\alpha-1} e^{-t/\lambda} \tag{1.3}$$

and

$$F(t,\theta) = \left(1 - e^{-(t/\lambda)}\right)^{\alpha}, \tag{1.4}$$

where $\theta = (\alpha, \lambda)$ are the two parameters with $\alpha > 0$ as the shape parameter and $\lambda > 0$ as the scale parameter. When $\alpha = 1$, the GE distribution defined above reduces to the conventional exponential distribution. The GE distribution was introduced by Mudholkar and Srivastava (1993) as an alternative to the commonly used gamma and Weibull distributions. Since then, the GE distribution has been studied by many authors, for example, in Gupta and Kundu (1999, 2001a, 2001b, 2002, 2003, 2007), Raqab and Ahsanullah (2001), Zheng (2002), Jaheen (2004), Raqab and Madi (2005), Sarhan (2007), and Chen and Lio (2010).

Another commonly used distribution is the two-parameter general Weibull (GW) distribution which has PDF and CDF respectively given as follows,

$$f(t,\theta) = \beta/\lambda(t/\lambda)^{\beta-1} e^{-(t/\lambda)^{\beta}} \tag{1.5}$$

and

$$F(t,\theta) = 1 - e^{-(t/\lambda)^{\beta}}, \tag{1.6}$$

where $\theta = (\beta, \lambda)$ are the two parameters with $\beta > 0$ as the shape parameter and $\lambda > 0$ as the scale parameter. Numerous research on lifetime modeling related to Weibull distribution has been conducted by, for example, Padgett and Sengupta

(1996), Nichols and Padgett (2006), Ng and Wang (2009) and Lio et al. (2012). When $\beta = 1$, the general Weibull distribution is reduced to conventional exponential distribution.

Unifying these three families of two-parameter distributions, a three-parameter generalized Rayleigh-exponential-Weibull (GREW) distribution is presented in this paper with the PDF and CDF given respectively as follows:

$$f(t,\theta) = \alpha\beta/\lambda^{\beta}(t/\lambda)^{\beta-1}e^{-(t/\lambda)^{\beta}}(1-e^{-(t/\lambda)^{\beta}})^{\alpha-1}, \tag{1.7}$$

$$F(t,\theta) = \left(1-e^{-(t/\lambda)^{\beta}}\right)^{\alpha} \tag{1.8}$$

where $\theta = (\alpha, \beta, \lambda)$, $\alpha > 0$ and $\beta > 0$ are the two shape parameters, and $\lambda > 0$ is the scale parameter. The GREW distribution is equivalent to the exponentiated Weibull distribution which was proposed by Mudholkar and Srivastava (1993) and also used by Mudholkar et al. (1995, 1996) except that the coefficient, λ^{β}, for t^{β} has been replaced by a new parameter for the exponentiated Weibull distribution. We continue to investigate the three-parameter GREW distribution that has many distributions as the special cases. When $\beta = 2$, the GREW distribution reduces to the GR distribution. When $\alpha = 1$ and $\beta = 2$, the GREW distribution reduces to Rayleigh distribution reported by Archer (1967). When $\beta = 1$, the GREW distribution reduces to the GE distribution mentioned above. When $\alpha = 1$, the GREW distribution reduces to the conventional two-parameter Weibull distribution described above. Furthermore, the GREW distribution reduces to conventional exponential distribution if $\alpha = 1$ and $\beta = 1$.

The rest of this chapter is organized as follows. Section 2 introduces the maximum likelihood estimators of the GREW distribution based on the progressively type-I interval censoring as well as the associated hypothesis testing. Section 3 gives the simulation results. Section 4 presents the application of the methods provided to discuss the modeling procedure for these 112 patients' lifetimes under the three-parameter GREW distribution family, and conclusions are given in Sect. 5.

2 Statistical Inferences Based on Progressively Type-I Interval Data

It is very often that participants under medical study, or, objects under lifetime test in industry, are lost or withdrawn before failure, or the lifetime is only known within an interval. Hence, the obtained sample is called a censored sample (or an incomplete sample). The most common censoring schemes are type-I censoring, type-II censoring, and progressively censoring. When the lifetime test ends at a pre-scheduled time, the lifetime test is known as the type-I censoring. For type-II censoring, the lifetime test ends whenever the number of lifetimes is reached. In both type-I and type-II censoring schemes, the tested subjects are allowed to

be withdrawn only at the end of lifetime testing. In the progressively censoring scheme, the tested subjects are allowed to be withdrawn at some other time before the end of the lifetime test. This is documented comprehensively in Balakrishnan and Aggarwala (2000), which showed progressively censoring combining with type-I or type-II and applications.

This paper focuses on progressively type-I interval censored data. To be consistent, the notations in Chen and Lio (2010) are continued. Suppose that there are n items to start the lifetime test (or n participants in medical studies) simultaneously at time $t_0 = 0$ and under inspection at m pre-specified times $t_1 < t_2 < \ldots < t_m$ where t_m is the time to end the experiment. As progressively type-I interval censored experiment at the ith time of inspection (i.e., t_i), we record the number of failures X_i within the interval of $(t_{i-1}, t_i]$ and randomly remove R_i subjects from the life testing. Therefore, the number of surviving subject Y_i is a random variable. As an example, given pre-specified percentage values, $p_1, \ldots, p_{m-1}$ and $p_m = 1$, for withdrawing at $t_1 < t_2 < \ldots < t_m$, the R_i can be calculated as $\lfloor p_i y_i \rfloor$ at each inspection time t_i where $i = 1, 2, \ldots, m$. Therefore, a progressively type-I interval censored sample can be generated as $\{X_i, R_i, t_i\}, i = 1, 2, \ldots, m$, where sample size $n = \sum_{i=1}^{m}(X_i + R_i)$. If $R_i = 0, i = 1, 2, \ldots, m-1$, then the progressively type-I interval censored sample is a type-I interval censored sample as $X_1, X_2, \cdots, X_m, X_{m+1} = R_m$.

2.1 Maximum Likelihood Estimation

Generally, let a progressively type-I interval censored sample, $\{X_i, R_i, t_i\}, i = 1, 2, \ldots, m$, of size n, be obtained from a general continuous lifetime distribution with CDF, $F(t, \theta)$, the general likelihood function can be constructed as follows,

$$L(\theta) \propto \prod_{i=1}^{m} [F(t_i, \theta) - F(t_{i-1}, \theta)]^{X_i} [1 - F(t_i)]^{R_i} . \tag{2.1}$$

This general likelihood function in Eq. (2.1) can be used to estimate parameters from the distributions of GR, GE, GW, and GREW and perform associated statistical inferences.

Specifically to GREW defined by Eq. (1.7), the likelihood function can be specified to be:

$$L(\theta) \propto \prod_{i=1}^{m} \left[\left(1 - e^{-(t_i/\lambda)^{\beta}}\right)^{\alpha} - \left(1 - e^{-(t_{i-1}/\lambda)^{\beta}}\right)^{\alpha} \right]^{X_i} \left[1 - \left(1 - e^{-(t_i/\lambda)^{\beta}}\right)^{\alpha}\right]^{R_i} \tag{2.2}$$

where $t_0 = 0$ and $0 < t_i$ is for $i = 1, 2, \ldots, m$. It can be seen easily that if $R_1 = R_2 = \cdots = R_{m-1} = 0$, the likelihood functions (2.2) reduces to the corresponding likelihood function for the conventional type-I interval censoring. By setting the

derivatives of the log likelihood function, $log(L(\theta))$, with respect to α, β and λ respectively equal to zero, the system of likelihood equations is established. It is obvious that the closed form of solution to this system of likelihood equations cannot be derived. Therefore, the maximum likelihood estimates (MLEs) of α, β and λ will be obtained by searching the solution through an iterative numerical method. In this paper, We make use of the typical numerical Newton-Raphson algorithm to obtain the estimates of θ iteratively as follows until its convergence:

$$\theta^{(k+1)} = \theta^{(k)} - \left[H\left(\theta^{(k)}\right)\right]^{-1} D\left(\theta^{(k)}\right) \tag{2.3}$$

where k indicates the kth iteration, $H\left(\theta^{(k)}\right)$ is the 3×3 Hessian matrix constructed by the second derivatives of negative log-likelihood function $-logL$ to θ evaluated at the $(k)th$ iteration $\theta^{(k)}$, and $D\left(\theta^{(k)}\right)$ is the 3×1 gradient vector constructed by the first derivatives of $-logL$ to θ evaluated at the $(k)th$ iteration $\theta^{(k)}$. Budhiraja et al. (2017) had proved in their Theorem 1 that the MLE, $\hat{\theta}$, from Eq. (2.3) were consistent and asymptotically normally distributed based on progressively type-I interval censored data under appropriate regularity conditions.

2.2 Hypothesis Testing

With the theorem from Budhiraja et al. (2017), we can establish the process of hypothesis testing based on the joint asymptotic normal distribution of MLE, $\hat{\theta}$. The null hypothesis can be $H_0 : \theta = \theta_0$ vs., the alternative hypothesis of $H_a : \theta \neq \theta_0$. This hypothesis testing can also be used for model selection.

Specifically, if

- the null hypothesis of $H_0 : \beta = 2$ is not rejected, the GREW distribution would be the GR distribution;
- the null hypothesis of $H_0 : \alpha = 1$ and $\beta = 2$ is not rejected, the GREW distribution would be the classical Rayleigh distribution;
- the null hypothesis of $H_0 : \beta = 1$ is not rejected, the GREW distribution would be the GE distribution;
- the null hypothesis of $H_0 : \alpha = 1$ and $\beta = 1$ is not rejected, the GREW distribution would be the exponential distribution;
- the null hypothesis of $H_0 : \alpha = 1$ is not rejected, the GREW distribution would be the Weibull distribution.

We illustrate the hypothesis testing by using the real data set regarding the 112 patients with plasma cell myeloma that was reported by Carbone et al. (1967) except the examination time schedule converted in terms of year.

3 Simulation Study

The purpose for simulation study is to investigate the convergence behavior of the proposed MLE estimation for GREW. To be prudent in generalizing distributions with multiple parameters, we are particularly interested in investigating whether there is any parameter confounding in estimation of the parameters uniquely for GREW as we observed in Chen and Lio (2009). In Chen and Lio (2009), we observed that there is the issue of parameter confounding when using the extended three-parameter generalized Gamma distribution to model the progressively type-II censored data. In dealing with the parameter confounding, a new re-parametrization has to be proposed to reformulate the generalized Gamma distribution to sustain the numerical stability in the search algorithm for the maximum likelihood estimation.

The simulation is conducted in R language (R Development Core Team 2006), which is a non-commercial, open source software package for statistical computing and graphics that was originally developed by Ihaka and Gentleman (1996). The R code can be obtained from the authors upon request.

3.1 Simulation Algorithm

The data generation is based on the algorithm proposed in Aggarwala (2001) which is a very general algorithm to simulate progressively type-I interval-censored data for any distributions. For example, the algorithm was used by Ng and Wang (2009) for Weibull distribution, Chen and Lio (2010) for GE distribution, and Lio et al. (2011) for GR distribution.

Given an initial sample of size n putting on life testing at time 0, the pre-specified inspection time schedules, $0 < t_1 < t_2 < \cdots < t_m$, and the percentages of withdrawn $p_i, i = 1, 2, \cdots, m-1$ and $p_m = 1.0$, the algorithm to generate a progressively type-I interval censored data, $(X_i, R_i, t_i), i = 1, \cdots, m$, from the GREW distribution which has distribution function (1.8) can be addressed as follows: let $t_{-1} < 0 = t_0$, $X_0 = 0$, $R_0 = 0$ and $\sum_{j=1}^{0}(X_j + R_j) = 0$. Then for $i = 1, 2, \cdots, m$,

$$X_i \mid X_{i-1}, \cdots, X_0, R_{i-1}, \cdots, R_0 \sim rBinom\left[n - \sum_{j=1}^{i-1}(X_j + R_j), \frac{F(t_i, \theta) - F(t_{i-1}, \theta)}{1 - \sum_{j=1}^{i-1}[F(t_j, \theta) - F(t_{j-1}, \theta)]}\right]. \quad (3.1)$$

and

$$R_i = \left[p_i \times \left(n - \sum_{j=1}^{i-1}(X_j + R_j) - X_i\right)\right]. \quad (3.2)$$

With GREW distribution function in (1.8), the above equations can be more specifically presented as

$$X_i \mid X_{i-1}, \cdots, X_0, R_{i-1}, \cdots, R_0 = rBinom\left[n - \sum_{j=1}^{i-1}(X_j + R_j), \frac{\left(1-e^{-(t_i/\lambda)^\beta}\right)^\alpha - \left(1-e^{-(t_{i-1}/\lambda)^\beta}\right)^\alpha}{1-\left(1-e^{-(t_{i-1}/\lambda)^\beta}\right)^\alpha} \right] \quad (3.3)$$

and

$$R_i = \left\lfloor p_i \times \left(n - \sum_{j=1}^{i-1}(X_j + R_j) - X_i \right) \right\rfloor \quad (3.4)$$

where $\lfloor x \rfloor$ returns the largest integer not greater than the argument x and $0 = t_0 < t_1 < \ldots < t_m < \infty$ are pre-scheduled times. Since $p_m = 1$, $R_m = n - \sum_{i=1}^{m-1}(X_i + R_i) - X_m$ in (3.4). Notice that if $p_1 = \cdots = p_{m-1} = 0$, then $R_1 = \cdots = R_{m-1} = 0$ and hence $X_1, \cdots, X_m, X_{m+1} = R_m$ is a simulated sample from the conventional type-I interval censoring.

3.2 Simulation Schemes and Cases

For simplicity, we consider the simulation setups parallel to the real data, given in Sect. 4, for the $m = 9$ pre-specified inspection times in terms of year, $t_1 = 5.5/12, t_2 = 10.5/12, t_3 = 15.5/12, t_4 = 20.5/12, t_5 = 25.5/12, t_6 = 30.5/12, t_7 = 40.5/12, t_8 = 50.5/12$, and $t_9 = 60.5/12$ which is the time to terminate the experiment. The simulation study also considered the same progressively type-I interval censoring schemes as the ones from Aggarwala (2001), Ng and Wang (2009), Chen and Lio (2010), and Lio et al. (2011). For simplicity, we report the simulation results for two progressively interval censoring schemes since the results are very similar. The two schemes are restated as follows:

- $P_{(1)} = (0, 0, 0, 0, 0, 0, 0, 0, 1)$
- $P_{(2)} = (0.25, 0, 0, 0, 0, 0, 0, 0, 1)$

which are the last two schemes considered in Aggarwala (2001), Ng and Wang (2009), Chen and Lio (2010), and Lio et al. (2011). The censoring scheme $P_{(1)}$ is the conventional type-I interval censoring where no removals prior to the experiment termination and the censoring in $P_{(2)}$ only occurs at the left-most and the right-most. To compare the performance, we consider two cases of parameter combinations of GREW distribution. Case 1 is the GREW distribution with parameters $\theta = (\alpha, \beta, \lambda) = (1, 1, 1)$ where all the GREW, GE and GW distributions are the same and all are reduced to the simplest exponential distribution with distribution function

as $F(t,\theta) = 1-e^{-t}$. However, in Case 1, the GR distribution has $F(t,\theta) = 1-e^{-t^2}$ which would be different from these three distributions. Case 2 is the GREW distribution with parameters $\theta = (\alpha, \beta, \lambda) = (1, 2, 2)$ where all the GREW, GR and GW distributions are the same with the CDF as $F(t,\theta) = 1 - e^{-(t/2)^2}$. However, in Case 2, the GE distribution is the same as an exponential distribution with distribution function $F(t,\theta) = 1-e^{-(t/2)}$ which would be different from these three distributions.

3.3 Simulation Results

Monte-Carlo simulation is conducted with 10,000 runs to report the average value of the 10,000 estimated parameters of $\theta = (\alpha, \beta, \lambda)$, their variance and mean squared error (MSE) for the two cases and two schemes which is summarized in Table 1.

For Case 1 as seen from Table 1, the parameters of $\theta = (\alpha, \beta, \lambda)$ in GREW distribution are estimated consistently and robustly with no biases, small variances and MSEs for both schemes. This pattern is the same for GE and GW distributions since all of these three families of distributions reduced to the simplest exponential distribution in Case 1. In this case, however, the GR distribution becomes $F(t,\theta) = 1 - e^{-t^2}$ which is different from these three distributions. This is why the estimated

Table 1 Summary of Monte-Carlo simulations for Case 1: $\alpha = \beta = \lambda = 1$

Scheme	Distribution	Parameter	True	Estimate	Variance	MSE
1	GREW	α	1	1.0056	0.0089	0.0090
		β	1	1.0012	0.0021	0.0021
		λ	1	1.0005	0.0061	0.0061
	GR	α	1	0.3048	0.0001	0.4833
		λ	1	2.1887	0.0009	1.4140
	GE	α	1	1.0004	0.0004	0.0004
		λ	1	0.9984	0.0017	0.0017
	GW	β	1	1.0003	0.0001	0.0001
		λ	1	0.9991	0.0010	0.0010
2	GREW	α	1	1.0006	0.0113	0.0113
		β	1	1.0022	0.0027	0.0027
		λ	1	1.0017	0.0079	0.0079
	GR	α	1	0.3082	0.0000	0.4787
		λ	1	2.1855	0.0012	1.4065
	GE	α	1	1.0006	0.0004	0.0004
		λ	1	0.9990	0.0011	0.0011
	GW	β	1	1.0003	0.0001	0.0001
		λ	1	0.9991	0.0010	0.0010

Note that the bias is not reported in the table since it can be implied by the "Estimate-True"

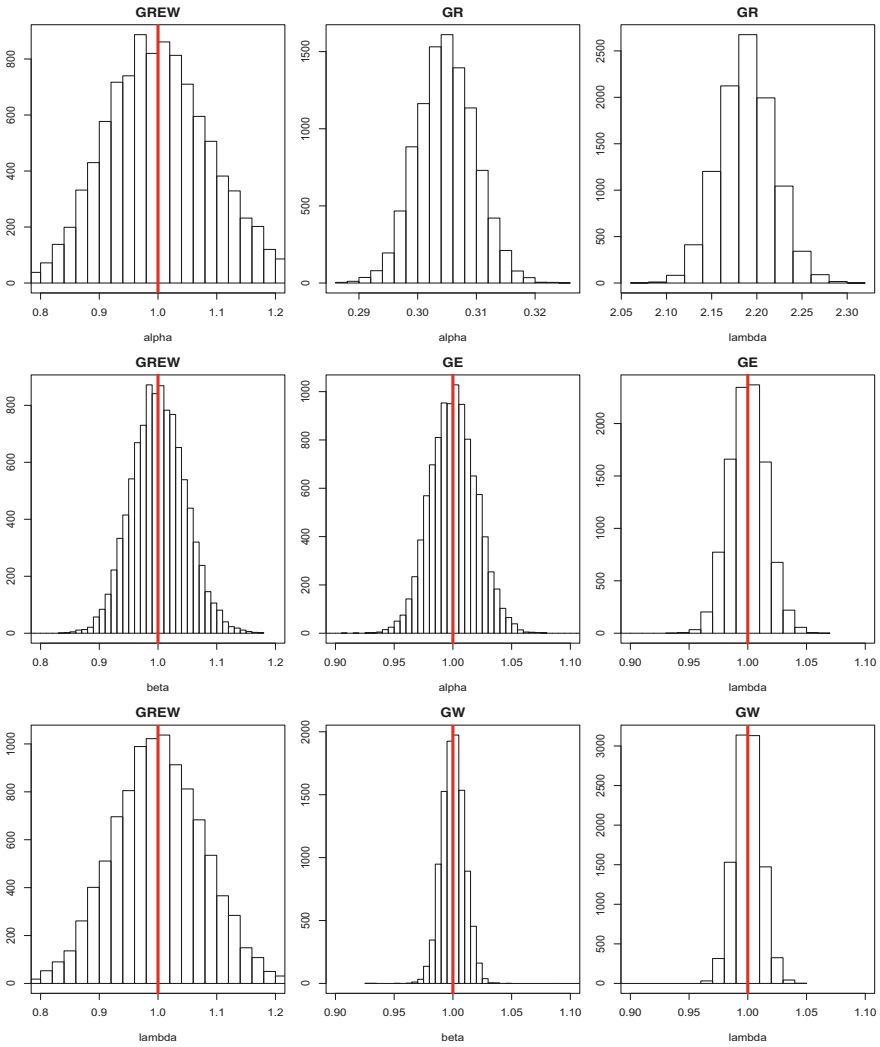

Fig. 1 Monte-Carlo sampling distributions for all parameters for GREW, GR, GE and GW distributions under Scheme 1 for Case 1

parameters of $\hat{\alpha}$ and $\hat{\lambda}$ in Table 1 are quite different from the true values of $\alpha = 1$ and $\lambda = 1$. However, the variances are still small, thus indicating consistency.

Figure 1 graphically summarizes all these observations. The left three figures are the sampling distributions for GREW distribution with the thick lines in the middle indicating the true parameters of $\alpha = \beta = \lambda = 1$. It can be seen that the three parameters from GREW distribution are unbiased estimated. This is the same

Table 2 Summary of Monte-Carlo simulations for Case 2: $\alpha = 1$ and $\beta = \lambda = 2$

Scheme	Distribution	Parameter	True	Estimate	Variance	MSE
1	GREW	α	1	1.0016	0.0027	0.0027
		β	2	2.0014	0.0036	0.0036
		λ	2	1.9998	0.0022	0.0022
	GR	α	1	1.0004	0.0002	0.0002
		λ	2	1.9999	0.0002	0.0002
	GE	α	1	3.7152	0.0049	7.3771
		λ	2	0.8870	0.0001	1.2388
	GW	β	2	2.0004	0.0003	0.0003
		λ	2	2.0001	0.0001	0.0001
2	GREW	α	1	1.0008	0.0031	0.0031
		β	2	2.0028	0.0045	0.0046
		λ	2	2.0006	0.0026	0.0026
	GR	α	1	1.0003	0.0002	0.0002
		λ	2	2.0000	0.0002	0.0002
	GE	α	1	3.5951	0.0052	6.7400
		λ	2	0.8962	0.0002	1.2186
	GW	β	2	2.0003	0.0003	0.0003
		λ	2	2.0001	0.0001	0.0001

for the GE distribution (the two figures at the right side at the second row) and GW distribution (the two figures at the right at the bottom row). The GR distribution is different as seen from the two figures at the top row since this distribution is totally different from the rest of the three distributions.

Similarly, for Case 2 as seen from Table 2, the parameters of $\theta = (\alpha, \beta, \lambda)$ in GREW distribution are estimated consistently with no biases, small variances and MSEs for both schemes. This pattern is the same for GR and GW distributions since for Case 2, all of these three families of distributions reduced to a special GR distribution with distribution function of $F(t, \theta) = 1 - e^{-(t/2)^2}$. In this case, however, the GE distribution becomes $F(t, \theta) = 1 - e^{-(t/2)}$ which is different from these three distributions. This is why the estimated parameters of $\hat{\alpha}$ and $\hat{\lambda}$ in Table 2 are quite different from the true values of $\alpha = 1$ and $\lambda = 2$. However, the variances are still small indicating consistency. Similarly Fig. 2 graphically summarizes all these observations in Table 2.

Based on this simulation study, we can conclude that there is no parameter confounding from the three-parameter GREW distribution which extends the three families of two-parameter distributions of GR, GE and GW.

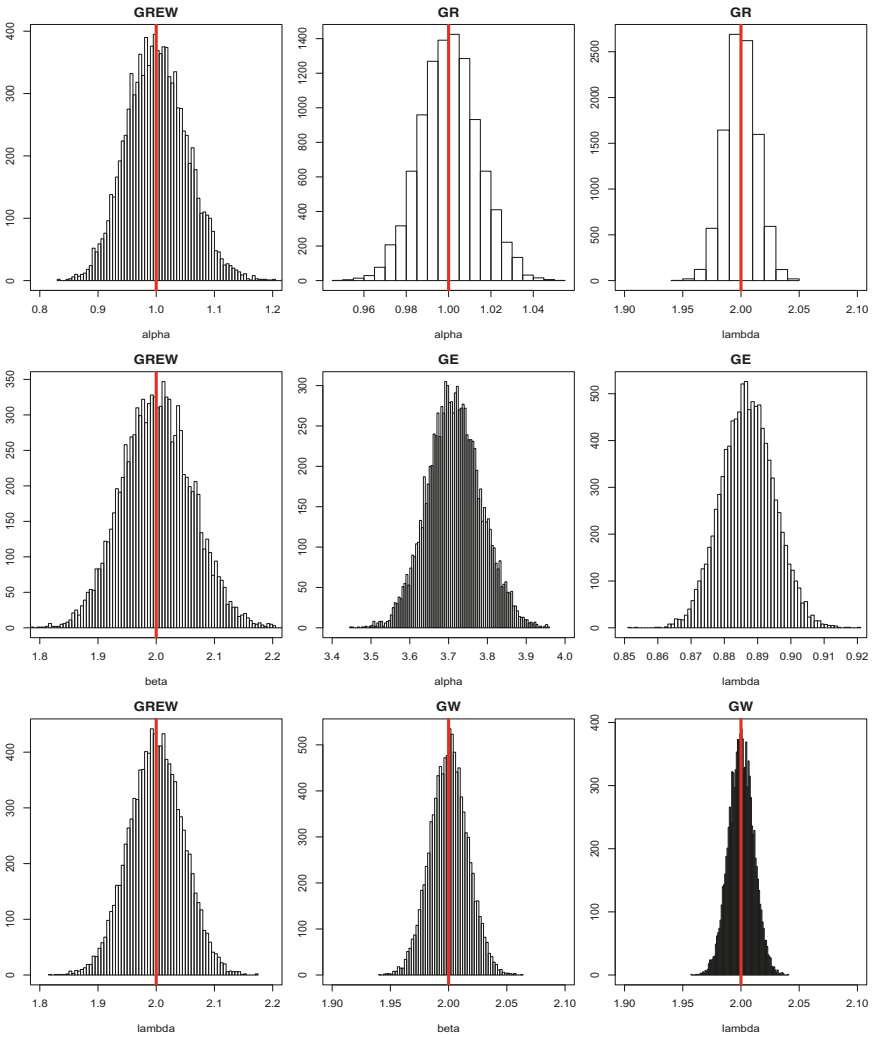

Fig. 2 Monte-Carlo sampling distributions for all parameters for GREW, GR, GE and GW distributions under Scheme 1 for Case 2

4 Analyzing the Plasma Cell Myeloma Data

The summary survival information for the 112 patients with plasma cell myeloma treated at the National Cancer Institute can be found in Carbone et al. (1967) and are given as follows: initially 112 patients were admitted for examination at initial time, labeled as $t_0 = 0$. The number of risks are 93, 76, 55, 45, 34, 25, 10, 3 and the numbers of withdrawals are 1, 1, 3, 0, 0, 1, 2, 3, 2 at inspection times $t_1 =$

Table 3 Summary of Maximum likelihood estimation and KS statistic

Distribution	$\hat{\alpha}$	$\hat{\beta}$	$\hat{\lambda}$	$-logL$	KS
GR	0.475	NA	2.932	231.006	0.171
GE	1.432	NA	1.459	230.470	0.162
GW	NA	1.230	1.924	230.340	0.157
GREW	0.979	1.245	1.952	230.339	0.157

$5.5/12$, $t_2 = 10.5/12$, $t_3 = 15.5/12$, $t_4 = 20.5/12$, $t_5 = 25.5/12$, $t_6 = 30.5/12$, $t_7 = 40.5/12$, $t_8 = 50.5/12$, respectively. These withdrawn patients are known to have survived at the right end of each time interval, but without further follow-up. Moreover, The number of deaths, $X_i, i = 1, 2, 3, \cdots, 9$, can be easily calculated to be $X = (18, 16, 18, 10, 11, 8, 13, 4, 1)$ from the numbers at risks and the numbers of withdrawals.

This progressively type-I interval censored data set was used by many papers to investigate different distributions, such as Lawless (1982), Ng and Wang (2009), Chen and Lio (2010), Lio et al. (2011). With this data, the parameter estimates, the associated values of the negative log-likelihood function and the Kolmogorov-Smirnov (KS) statistic are summarized in Table 3. It can be seen from this table that the values of negative log-likelihood function decrease from 231.006, 230.470, 230.340 to 230.339 and the KS statistic decrease from 0.171, 0.162, 0.157 to 0.157, respectively, for GR, GE, GW and GREW distributions. This results extend the results in Lio et al. (2011) to include the results of GREW and indicate that the model fit from GREW is the best among the four families of distributions.

Furthermore, in reviewing Table 3, the results from the GREW are very close to the results in the GW distribution due to the parameter estimate of $\hat{\alpha} = 0.979$. This estimate is very close to 1 indicating that the GW distribution may be a simpler choice for this data. To validate this observation, we perform hypothesis testing on $H_0, \alpha = 1$ vs. $H_a : \alpha \neq 1$. For GREW distribution, the estimated standard errors using hessian matrix from MLE are 0.697, 0.522 and 0.966, respectively for $\theta = (\alpha, \beta, \lambda)$. Therefore, the z-statistic to test the above null hypothesis can be calculated as $z = (0.979 - 1)/0.697 = -0.030$ and the associated p-value is 0.976 which indicates that the α parameter in GREW is not statistically significantly different from 1 and the null hypothesis can not be rejected. In this case, the simpler Weibull distribution is sufficiently enough for this data. The same hypothesis testing to GR and GE can yield the p-values of 0.148 and 0.639, respectively, for GR and GE distributions.

The data analysis is done with R and the interested readers can request the data and R code from the authors.

5 Conclusions

In this paper, a three-parameter family of GREW distribution, which unified the three two-parameter families of GR, GE and the GW distributions is proposed to model the lifetime distribution using the progressively type-I interval censored data obtained from the 112 patients with plasma cell myeloma. The parameter estimation and the associated hypothesis testing can be done from the theory of likelihood estimation. Simulation studies indicate that parameter estimations from MLE are well-behaved and consistent. The real data analysis using the progressively type-I interval censored data obtained from the 112 patients with plasma cell myeloma also indicates that this new family of GREW distribution can unify the three commonly used distribution families of GR, GE, and GW distributions.

We would like to mention that the GREW distribution in this paper is, in fact, a special distribution of the four-parameter generalized modified Weibull distribution proposed by Carrasco et al. (2008) where $F(t,\theta) = \left(1 - e^{\left(-\alpha' t^{\gamma'} exp(\lambda' t)\right)}\right)^{\beta'}$ in their original parametrization. We can re-parameterize this distribution as $F(t,\theta) = \left(1 - e^{-(t/\lambda)^{\beta} exp(\gamma t)}\right)^{\alpha}$ with additional parameter γ in $\theta = (\alpha, \beta, \gamma, \lambda)$ where $\alpha = \beta'$, $\beta = \gamma'$, $\lambda = \left(1/\alpha'\right)^{1/\beta'}$ and $\gamma = \lambda'$. The extra term $exp(\gamma t)$ is introduced in Carrasco et al. (2008) and therefore, if $\gamma = 0$, the generalized modified Weibull distribution would be the GREW distribution. Carrasco et al. (2008) only applied generalized modified Weibull distribution to complete data which is different from the progressively Type-1 censored data. We will further investigate this four-parameter distribution to progressively censored Type-I data.

Acknowledgements The authors would like thank to the co-editors and anonymous referees for their suggestions and comments, which significantly improved this manuscript.

This work is based upon research supported by the South Africa National Research Foundation (NRF) and South Africa Medical Research Council (SAMRC) (South Africa DST-NRF-SAMRC SARChI Research Chair in Biostatistics-Professor Ding-Geng Chen, Grant number 114613). Opinions expressed and conclusions arrived at are those of the author and are not necessarily to be attributed to the NRF and SAMRC.

References

Aggarwala, R. (2001). Progressively interval censoring: Some mathematical results with application to inference. *Communications in Statistics-Theory and Methods, 30*, 1921–1935.

Ahmad, K. E., Fakhry, M. E., & Jaheen, Z. F. (1997). Empirical Bayes estimation of $P(Y < X)$ and characterization of Burr-type X model. *Journal of Statistical Planning and Inference, 64*, 297–308.

Archer, C. O. (1967). *Some properties of Rayleigh distributed random variables and of their sums and products*. Technical Memorandum TM-67-15.

Balakrishnan, N., & Aggarwala, R. (2000). *Progressively censoring: Theory, methods and applications*. Boston: Birkhäuser. https://doi.org/10.1007/978-1-4612-1334-5

Budhiraja, S., Pradhan, B., & Sengupta, D. (2017). Maximum likelihood estimators under progressively Type-I interval censoring. *Statistics and Probability Letters, 123*, 202–209.

Carbone, P. P., Kellerhouse, L. E., & Gehan, E. A. (1967). Plasmacytic myeloma: A study of the relationship of survival to various clinical manifestations and anomalous protein type in 112 patients. *The American Journal of Medicine, 42*, 937–948.

Carrasco, J. M. F., Ortega, E. M. M., & Corderiro, C. M. (2008). A generalized modified Weibull distribution for life modelling. *Computational Statistics and Data Analysis, 53*, 450–462.

Chen, D. G., & Lio, Y. (2009). A note on the maximum likelihood estimation for the generalized gamma distribution parameters under progressively type-II censoring. *International Journal of Intelligent Technology and Applied Statistics, 2*(2), 145–152.

Chen, D. G., & Lio, Y. L.(2010). Parameter estimations for generalized exponential distribution under progressively type-I interval censoring. *Computational Statistics & Data Analysis, 54*, 1581–1591.

Gupta, R. D., & Kundu, D. (1999). Generalized exponential distributions. *Australian and New Zealand Journal of Statistics, 41*, 173–188.

Gupta, R. D., & Kundu, D. (2001a). Exponentiated exponential distribution: An alternative to gamma and Weibull distributions. *Biometrical Journal, 43*, 117–130.

Gupta, R. D., & Kundu, D. (2001b). Generalized exponential distributions: Different method of estimations. *Journal of Statistical Computation and Simulation, 69*, 315–338.

Gupta, R. D., & Kundu, D. (2002). Generalized exponential distributions: Statistical inferences. *Journal Statistic Theory Application, 1*, 101–118.

Gupta, R. D., & Kundu, D. (2003). Discriminating between Weibull and generalized exponential distributions. *Computational Statistics and Data Analysis, 43*, 179–196.

Gupta, R. D., & Kundu, D. (2007). Generalized exponential distribution: Existing results and some recent developments. *Journal of Statistical Planning and Inference, 137*, 3537–3547.

Ihaka, R., & Gentleman, R. (1996). R: A language for data analysis and graphics. *Journal of Computational and Graphical Statistics, 5*, 299–314.

Jaheen, Z. F. (1995). Bayesian approach to prediction with outliers from the Burr type X model. *Microelectronics Reliability, 35*, 45–47.

Jaheen, Z. F. (1996). Empirical Bayes estimation of the reliability and failure rate functions of the Burr type X failure model. *Journal Applied Statistical Science, 3*, 281–285.

Jaheen, Z. F. (2004). Empirical Bayes inference for generalized exponential distribution based on records. *Communications in Statistics-Theory and Methods, 33*, 1851–1861.

Johnson, N. L., Kotz, S., & Balakrishnan, N. (1995). *Continuous univariate distribution* (2nd ed., Vol. I). New York: Wiley.

Kundu, D., & Raqab, M. Z. (2005). Generalized Rayleigh distribution: Different methods of estimation. *Computational Statistics and Data Analysis, 49*, 187–200.

Lawless, J. (1982). *Statistical models and methods for lifetime data*. New York: Wiley.

Lio, Y. L., Chen, D.-G., & Tsai, T.-R. (2011). Parameter estimations for Generalized Rayleigh distribution under progressively type-I interval censored data. *American Open Journal of Statistics, 1*, 46–57.

Lio, Y. L., Tsai, T.-R., & Wu, S.-J. (2012). The designs of acceptance sampling for strength distributions with percentiles. *International Journal of Reliability, Quality and Safety Engineering, 19*, 1250004.

Mudholkar, G. S., & Srivastava, D. K. (1993). Exponential Weibull family for analyzing bathtub failure data. *IEEE Transactions on Reliability, 42*, 299–302.

Mudholkar, G. S., Srivastava, D. K., & Friemer, M. (1995). The exponentiated Weibull family: A reanalysis of the bus-motor-failure data. *Technometrics, 37*, 436–445.

Mudholkar, G. S., Srivastava, D. K., & Kollia, G. D. (1996). A generalization of the Weibull distribution with application to the analysis of survival data. *Journal of the American Statistical Association, 91*, 1575–1583.

Ng, H., & Wang, Z. (2009). Statistical estimation for the parameters of Weibull distribution based on progressively type-I interval censored sample. *Journal of Statistical Computation and Simulation, 79*, 145–159.

Nichols, M. D., & Padgett, W. J. (2006). A bootstrap control chart for Weibull percentiles. *Quality Reliability Engineering International, 22*, 141–151.

Padgett, W. J., & Sengupta, A. (1996). Performance of process capability indices for Weibull and lognormal distributions or autoregressive processes. *International Journal of Reliability, Quality and Safety Engineering, 3*, 217–229.

R Development Core Team. (2006). *A language and environment for statistical computing: R Foundation for Statistical Computing*, Vienna. ISBN 3-900051-07-0.

Raqab, M. Z. (1998). Order statistics from the Burr type X model. *Computational Mathematical Applications, 36*, 111–120.

Raqab, M. Z., & Ahsanullah, M. (2001). Estimation of the location and scale parameters of generalized exponential distribution based on order statistics. *Journal of Statistical Computation and Simulation, 69*, 109–124.

Raqab, M. Z., & Kundu, D. (2003). Burr type X distribution: Revisited. *Journal of Probability and Statistical Sciences, 4*, 179–193.

Raqab, M. Z., & Madi, M. T. (2005). Bayesian inference for the generalized exponential distribution. *Journal of Statistical Computation and Simulation, 75*, 841–852.

Sarhan, A. M. (2007). Analysis of incomplete, censored data in competing risks models with generalized exponential distributions. *IEEE Transactions on Reliability, 56*, 132–138.

Sartawi, H. A., & Abu-Salih, M. S. (1991). Bayes prediction bounds for the Burr type X model. *Communication in Statistics: Theory and Methods, 20*, 2307–2330.

Surles, J. Q., & Padgett, W. J. (1998). Inference for $P(Y < X)$ in the Burr type X model. *Journal Applied Statistical Science, 7*, 225–238.

Surles, J. Q., & Padgett, W. J. (2001). Inference for reliability and stress-strength for a scaled Burr type X model. *Lifetime Data Analysis, 7*, 187–200.

Surles, J. Q., & Padgett, W. J. (2004). Some properties of a scaled Burr type X model. *Journal Statisticsal Planning and Inference, 7*(2), 187–200.

Zheng, G. (2002). Fisher information matrix in type-II censored data from exponentiated exponential family. *Biometrical Journal, 44*, 353–357.